

Carbohydrate Nanoparticles for Peptide Delivery to the CNS

AIKATERINI LALATSA



June 2009

A Thesis submitted in partial fulfilment of the
requirement for the degree of Doctor of Philosophy

Department of Pharmaceutics
The School of Pharmacy, University of London
29-39, Brunswick Square, London, WC1N 1AX
United Kingdom



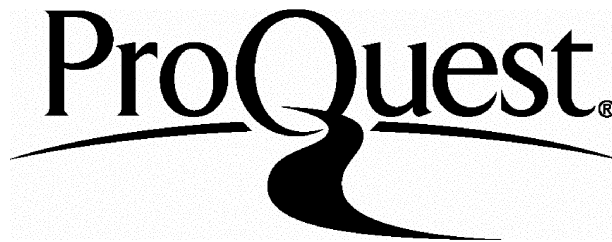
ProQuest Number: U507494

All rights reserved

INFORMATION TO ALL USERS

The quality of this reproduction is dependent upon the quality of the copy submitted.

In the unlikely event that the author did not send a complete manuscript and there are missing pages, these will be noted. Also, if material had to be removed, a note will indicate the deletion.



ProQuest U507494

Published by ProQuest LLC(2016). Copyright of the Dissertation is held by the Author.

All rights reserved.

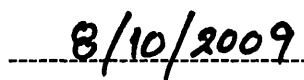
This work is protected against unauthorized copying under Title 17, United States Code.
Microform Edition © ProQuest LLC.

ProQuest LLC
789 East Eisenhower Parkway
P.O. Box 1346
Ann Arbor, MI 48106-1346

This thesis was conducted in The School of Pharmacy, University of London under the supervision of Professor Ijeoma F. Uchegbu. I certify that the research described is original and that any parts of the work that have been conducted by collaboration are clearly indicated. I also certify that I have written all the text herein and have clearly indicated by suitable citation any part of this dissertation that has already appeared in publication.

A handwritten signature in black ink, appearing to read "Zalat", written over a horizontal dashed line.

Signature

A handwritten date "8/10/2009" in black ink, written over a horizontal dashed line.

Date

Abstract

Many existing peptide pharmaceuticals are rendered ineffective or poorly absorbed after oral administration or are unable to cross the blood-brain barrier (BBB) mainly due to their hydrophilicity, size and charge. Leucine^[51]-Enkephalin (LENK) is an endogenous opioid neuropeptide with a blood half-life of approximately 3 minutes in man. The aim of this study is to evaluate the oral delivery potential of water soluble peptides such as LENK to the brain utilising two strategies: (i) lipidisation by creating a lipophilic bioreversible prodrug, palmitoylated Leucine^[51]-Enkephalin (TPLENK), comprising a cleavable ester bond susceptible to blood, liver and brain esterases and/or (ii) encapsulation in a carbohydrate central nervous system (CNS) bioavailability enhancer, Quaternary Ammonium Palmitoyl Glycol Chitosan (GCPQ). The lipophilic prodrug was converted into the LENK by plasma and liver esterases with apparent half-lives for the disappearance of the pro-drug of ~73 and ~44 minutes in homogenates respectively. The plasma half-life of LENK on intravenous (IV) administration was increased 1.4 fold when the nanoparticulate formulation was used and by 3.2 fold when TPLENK was administered with GCPQ. More importantly the brain area under the curve (AUC) of LENK was increased almost 2-fold by lipidisation of the peptide and encapsulation of the lipid prodrug within GCPQ aggregates after intravenous and oral administration, while maintaining analgesia in the tail-flick bioassay. We hypothesise that the increase in brain bioavailability following the strategy adopted is due to: (i) an increase in plasma levels of LENK leading to an increase in brain levels of LENK and (ii) the lipophilic prodrug promoting passage of the drug across the BBB, with GCPQ enabling the lipid prodrug to be transported in the blood to the BBB.

Acknowledgements

I would like to express my sincere and deepest gratitude to my supervisor and mentor, Prof. Ijeoma F. Uchegbu, for giving me the opportunity to work on this exciting project and has guided me and supported me throughout my studies. I want to thank her for coming out of this PhD more mature as a researcher but also as a person with valuable skills and experiences but more importantly a healthy optimism and passion for research that will be invaluable in anything I do in life. I also want to thank my second supervisor, Dr. Andreas Schätzlein, for his guidance, advice and help especially regarding my in vivo studies.

I need to thank Dr. Hang T. B. Le for welcoming me in this lab from the very first day we met and for sharing her experiences, expertise, and knowledge but above all a different way of thinking that influenced mine greatly. I owe a big thanks to my friend Adeline Siew for being there for me in good and difficult times throughout every step of my PhD and most importantly for putting up with me during the last 3 years. Finally, I am grateful for all my colleagues in the School of Pharmacy but also University of Strathclyde, especially Dr Kar Wai Chooi, that shared their everyday life in the lab, experiences, invaluable skills and knowledge.

I need to gratefully acknowledge the Engineering and Physical Sciences Research Council and the School of Pharmacy for funding me and this work. I also owe to thank Mr Steve Coppard for his help with the animal studies, Dr. Mire Zloh for his help with the conformational search, Dr. Alaine Martin for her help with peptide NMR characterisation, Dr Linda Thompson and Dr. John Malkinson for sharing their knowledge and skills in peptide synthesis, Mr. David McCarthy for his help the microscopic studies, and Dr Keith Jermyn for aiding me with the RIA studies.

Finally, I want to thank my family, and especially my mum and my dad, for being there for me all of these years that I am away, for their unconditional love and many sacrifices. A big thanks to my best friend, Maria Karampatsou, with whom I shared good and challenging moments in life and for always being there for me, and to my friends Hissham Bou Samra and Sophia Salta that believed in me and were like a second family for me in UK.

<u>TABLE OF CONTENTS</u>	<u>PAGE</u>
---------------------------------	--------------------

Abstract	3
-----------------	----------

Aknowledgements	4
------------------------	----------

Table of contents	5
--------------------------	----------

List of figures	11
------------------------	-----------

List of tables	18
-----------------------	-----------

List of equations	20
--------------------------	-----------

Abbreviations	21
----------------------	-----------

CHAPTER 1	INTRODUCTION	26
------------------	---------------------	-----------

1	Preface	26
----------	----------------	-----------

1.1	Barriers to oral peptide delivery	26
------------	--	-----------

1.1.1	Physical barriers to absorption	27
--------------	--	-----------

1.1.2	Enzymatic barriers to absorption	32
--------------	---	-----------

1.2	Strategies to increase Oral absorption of Peptides	36
------------	---	-----------

1.3	Blood-brain barrier and CNS peptide delivery	48
------------	---	-----------

1.4	Opioid receptors and Enkephalin	58
------------	--	-----------

1.5	Strategies available for BBB peptide (enkephalin) drug delivery	63
------------	--	-----------

1.5.1	Blood-brain barrier modulation	64
--------------	---------------------------------------	-----------

1.5.2	Physiological based strategies for BBB drug delivery	65
1.5.3	Pharmacological based strategies for BBB drug delivery	67
1.6	Aim and Objectives	83
CHAPTER 2	Peptide Synthesis and Characterisation	85
2.1	Solid Phase Peptide Synthesis	85
2.1.1	Variables of SPPS	88
2.1.2	Mass Spectroscopy (MS)	96
2.1.2.1	Electrospray Ionisation Mass Spectrometry (ESI-MS)	97
2.1.2.2	Tandem Mass Spectroscopy (MS-MS)	99
2.1.3	High-Performance Liquid Chromatography (HPLC)	100
2.1.4	Nuclear Magnetic Resonance (NMR) Spectroscopy	101
2.1.5	Fourier Transform Infrared Spectroscopy (FTIR)	103
2.1.6	Conformation Search, Molecular Modeling and Pharmacophores	105
2.2	Materials and Methods	108
2.2.1	Materials	108
2.2.2	Peptide Synthesis and Cleavage	109
2.2.3	Peptide Purification	113
2.2.4	Peptide Characterisation	113
2.2.4.1	Mass Spectrometry (MS)	113
2.2.4.2	Nuclear Magnetic Resonance (NMR)	114
2.2.4.3	Fourier Transform Infrared Spectroscopy (FTIR)	114
2.2.4.4	Analytical Reverse-Phase HPLC (RP-HPLC)	115
2.2.4.5	Transmission Electron Microscopy and Photon Correlation Spectroscopy	115
2.2.4.6	Scanning Electron Microscopy	116

2.2.4.7	X-Ray Powder Diffraction	116
2.2.4.8	Conformation Search and Molecular Modeling	116
2.3	Results	117
2.3.1	Mass Spectrometry (MS)	117
2.3.1.1	Electrospray Ionisation Mass Spectrometry (ESI-MS)	117
2.3.1.2	Tandem Mass Spectroscopy (MS-MS)	120
2.3.2	Nuclear Magnetic resonance (NMR) Spectroscopy	121
2.3.2.1	¹ H-NMR and ¹ H- ¹ H-Correlated Spectroscopy (COSY)-NMR	122
2.3.2.2	Nuclear Overhauser Effect Spectroscopy (NOESY)	124
2.3.3	Fourier Transform Infrared (FTIR) Spectroscopy	125
2.3.4	Reverse-Phase High Performance Liquid Chromatography (RP-HPLC)	125
2.3.4.1	Analytical Reverse-Phase HPLC (RP-HPLC)	125
2.3.4.2	Preparative Reverse-Phase HPLC (RP-HPLC)	126
2.3.5	Transmission Electron Microscopy and Photon Correlation Spectroscopy	127
2.3.6	Scanning Electron Microscopy	132
2.3.7	X-ray Powder Diffraction	133
2.3.8	Conformation Search and Molecular Modeling	134
2.4	Discussion-Conclusions	136
CHAPTER 3	GCPQ Synthesis and Formulation Characterisation	144
3	Introduction	144
3.1	Materials and Methods	146

3.1.1	Materials	146
3.1.2	Synthesis of Quaternary Ammonium Palmitoyl Glycol Chitosan	147
3.1.2.1	Acid Degradation of Glycol Chitosan	148
3.1.2.2	Palmitoylation of degraded Glycol Chitosan	149
3.1.2.3	Quaternisation of Palmitoyl Glycol Chitosan	149
3.1.3	Characterisation of Quaternary Ammonium Palmitoyl Glycol Chitosan and Formulation	150
3.1.3.1	¹ H and COSY NMR Spectroscopy	150
3.1.3.2	Fourier Transform Infrared Spectroscopy (FTIR)	150
3.1.3.3	Matrix-Assisted Laser Desorption Spectrometry (MALDI-MS)	151
3.1.3.4	Gel Permeation Chromatography (GPC) and Multi-angle Laser Light Scattering (MALLS)	152
3.1.3.5	Preparation of Self Assembled Polymer Aggregates	157
3.1.3.6	Particle Sizing	157
3.1.3.7	Transmission Electron Microscopy (TEM)	160
3.1.3.8	HPLC Analysis of Drug Loaded Polymers	161
3.1.3.9	Stability of wet and dry formulations of TPLENK	162
3.2	Results	164
3.2.1	Characterization of GCPQ	164
3.2.1.1	¹ H NMR spectroscopy	164
3.2.1.2	Fourier Transform Infrared Spectroscopy (FTIR)	169
3.2.1.3	Matrix-Assisted Laser Desorption Spectrometry (MALDI-MS)	170
3.2.1.4	Laser Light Scattering (LLS) and Gel Permeation Chromatography(GPC)	172
3.2.1.5	Preparation of Self-Assembled Polymer Aggregates	175

3.2.1.6	Particle sizing, TEM and HPLC analysis of Drug Loaded Polymers	176
3.3	Discussion-Conclusions	196
CHAPTER 4	<i>In Vitro</i> Assays	201
4	Preface	201
4.1	Enzymatic Assays	201
4.2	Esterases	205
4.3	Materials and Methods	209
4.3.1	Materials	209
4.3.2	<i>In vitro</i> stability in Simulated Gastric Fluid	210
4.3.3	<i>In vitro</i> stability in Simulated Intestinal Fluid	212
4.3.4	<i>In vitro</i> stability in Plasma, Liver, Brain Homogenate	213
4.3.4.1	Biological Media	213
4.3.4.2	<i>In vitro</i> Esterase Activity Studies	213
4.3.4.3	<i>In vitro</i> Prodrug Stability Studies	216
4.3.4.4	Analytical Methods	216
4.3.5	Statistical Analysis	217
4.4	Results	217
4.4.1	<i>In vitro</i> stability in Simulated Gastric Fluid	217
4.4.2	<i>In vitro</i> stability in Simulated Intestinal Fluid	219
4.4.3	<i>In vitro</i> stability in Plasma, Liver and Brain Homogenates	222
4.4	Discussion-Conclusions	228

CHAPTER 5	<i>In Vivo</i> Pharmacokinetic & Pharmacodynamic Studies	232
5	Introduction	232
5.1	Radioimmunoassays	235
5.2	Animal Models of Nociception & the Tail-Flick Bioassay	239
5.3	Materials and Methods	243
5.3.1	Animals	243
5.3.2	Formulations	224
5.3.3	Biological Sample Handling and Extraction	247
5.3.4	Radioimmunoassay	248
5.3.5	Tail-Flick Bioassay	249
5.3.6	Statistical Analysis	250
5.4	Results	250
5.4	Discussion-Conclusions	268
CHAPTER 6	Conclusions & Future Work	277
6	Conclusions	277
6.1	Future work	282
	Publications	285
	References	292

<u>List of Figures</u>	<u>Page</u>
Figure 1.1: The intestinal mucosa as a barrier	29
Figure 1.2 : Degradation and absorption processes of peptides and proteins in the intestine; Important brush-border membrane peptidases and their substrate requirements	34
Figure 1.3: Enzyme-mediated hydrolysis (top) and chemical modifications of the peptide bond leading to increased metabolic stability of peptide drugs against hydrolytic enzymes	38
Figure 1.4: Examples of peptide bonds replacements that resulted in metabolically stable peptidomimetics	39
Figure 1.5: 4-Imidazolidinone prodrugs of Methionine ^[5] -Enkephalin	40
Figure 1.6: Cyclic prodrug strategies. (A) Acyloxyalkoxy-based prodrug; (B) phenylpropionic acid-based prodrug; (C) coumarinic acid-based prodrug	40
Figure 1.7: Schematic diagram of the neurovascular unit/cell association forming the BBB	49
Figure 1.8: Molecular composition of endothelial tight junctions	50
Figure 1.9: Left: The choroid plexus (composed of fenestrated capillaries and an epithelial (ependymal) covering, which reverts from “tight” to “open” at the base)	52
Figure 1.10: Potential routes for transport across the BBB	54
Figure 1.11: Graph of <i>in vivo</i> log permeability coefficient of rat brain capillaries (cm/sec) for several solutes as a function of lipid solubility determined in an octanol/water partition system (LogPo/w)	56
Figure 1.12: Position of the opioid receptor in the cell membrane	59
Figure 1.13: Structural relationships among the prohormone, precursor forms of the 3 major branches of the opiate peptides	60
Figure 1.14: Left: Schematic of Leucine ^[5] -Enkephalin (1-4) β -turn. Right: General form of a β -turn. Ca or alpha carbon refers to the first carbon that attaches to a functional group (often a carbonyl)	62
Figure 1.15: Right: Structure of the nonpeptide δ -opioid ligands. Left: δ -opioid pharmacophore geometry determined from the best-fit superposition of 3 nonpeptide ligands	63
Figure 1.16: Cyclisations as examples to constrain the peptide backbone into a particular conformation. Cyclic peptides/peptidomimetics exhibit metabolic stability against exopeptidases due to protected C- and N-terminal ends	75
Figure 1.17: Left: Structure of DPDPE. Right: Structure of	76

Biphalin

Figure 2.1: Basic steps in Solid Phase Peptide Synthesis	85
Figure 2.2: Effect of yield per step on overall yield of synthesis (the “arithmetic demon”)	87
Figure 2.3: Acid sensitive 2-chlorotrityl chloride resin (polystyrene, 1%DVB)	89
Figure 2.4: Solid phase peptide synthesis utilising Fmoc amino acids	90
Figure 2.5: Mechanisms of racemisation	91
Figure 2.6: Top; Structure of common carbodiimides (DCC, DIPCDI). Bottom; Structure of HBTU & HOBt	92
Figure 2.7: Structures of BOP and PyBOP	94
Figure 2.8: Uronium reagents (e.g. HBTU, HATU) mechanism of peptide bond formation (B: Base)	95
Figure 2.9: Cleavage under strong (top) and weak (bottom) acidic conditions depending on the resin linkage used	95
Figure 2.10: Schematic of an ESI mass spectrometer and evaporation of solvent in ESI-MS and ion production	98
Figure 2.11: Peptide sequencing by Tandem Mass spectrometry-backbone cleavages	100
Figure 2.12: SPPS scheme from manual synthesis (top) or using a PS3 synthesizer (bottom) of Fmoc-LENK-2-Cl-Trt-resin	111
Figure 2.13: Palmitoylation of Fmoc protected Leucine ^[5] -Enkephalin using Palmitic acid N-hydroxysuccinimide ester	112
Figure 2.14: ESI-MS spectrum obtained for LENK-(tBu) or Y-(tBu)-GGFL	118
Figure 2.15: ESI-MS spectrum obtained for Leucine ^[5] -Enkephalin	119
Figure 2.16: ESI-MS spectrum obtained for TPLENK	119
Figure 2.17: Tandem MS-MS spectra obtained for [YGGFL+1] ⁺	120
Figure 2.18: ¹ H-NMR (top) and ¹ H- ¹ H COSY (bottom) (D ₂ O suppressed) spectrum of LENK-(tBu) (3.57 mM) in D ₂ O	122
Figure 2. 19: ¹ H-NMR (top) and ¹ H- ¹ H COSY (bottom) obtained for TPLENK in DMSO at a concentration of 5.35mM	123
Figure 2. 20: NOESY obtained for TPLENK in DMSO at a concentration of 5.35mM	124
Figure 2. 21: FTIR spectrum for TPLENK	125
Figure 2. 22: HPLC Chromatogram examples. A: Leucine ^[5] -Enkephalin and B: TPLENK	126
Figure 2. 23: Preparative HPLC Chromatogram examples. A: Leucine ^[5] -Enkephalin (LENK) and B: TPLENK	127
Figure 2. 24: TEM images of LENK (1mg ml ⁻¹) in H ₂ O (vortexed)	128
Figure 2. 25: PCS spectrum for LENK in H ₂ O (1 mg mL ⁻¹) only after vortexing for 4 minutes	128

Figure 2. 26: TEM images of TPLENK (2mg ml ⁻¹) in H ₂ O (vortexed)	129
Figure 2. 27: PCS spectrum for TPLENK in H ₂ O (2 mg mL ⁻¹) only after vortexing for 4 minutes	129
Figure 2. 28: TEM images of TPLENK (1mg ml ⁻¹) in H ₂ O (sonicated on ice for 2.5 min)	130
Figure 2. 29: PCS spectrum for TPLENK in H ₂ O (1mg mL ⁻¹) only after vortexing for 4 minutes and sonication	130
Figure 2. 30: Negative stained TEM images of an unfiltered aqueous dispersion of TPLENK (1mg mL ⁻¹) in Tris Buffer 100 mM pH 7.4 after vortexing	131
Figure 2. 31: PCS spectrum for TPLENK in Tris Buffer 100mM (pH 7.4) (1 mg mL ⁻¹) only after vortexing	131
Figure 2. 32: SEM images of TPLENK	132
Figure 2. 33: X-ray diffractogram of TPLENK	133
Figure 2. 34: Comparison of lower energy conformation for Leucine ^[5] -Enkephalin and the lipidic TPLENK with a proposed pharmacophore for the δ -opioid receptor	134
Figure 2. 35: Lower energy conformation in H ₂ O for 4 molecules of the lipidic peptide	135
Figure 2. 36: Lower energy conformation for 4 molecules of Leucine ^[5] -Enkephalin in the presence of H ₂ O	135
Figure 2. 37: Peptide-conjugate amphiphile composed of hydrophilic peptide with hydrophobic alkyl tail (palmitic tail)	140
Figure 2. 38: Schematic model for the formation of the various structures by aromatic homo-dipeptide (such as diphenylalanine and diphenylglycine)	140
Figure 2. 39: Model of the δ receptor	141
Figure 2. 40: Helical wheel for Leucine ^[5] -Enkephalin	143
 Figure 3.1: Synthetic scheme for Quaternary ammonium Palmitoyl Glycol Chitosan	 148
Figure 3.2: The MALDI ionization process	151
Figure 3.3: A: Scattering of incident light off a particle in solution or in vacuum B: Plane polarized light polarized in the z direction and incident on a small particle	154
Figure 3.4: Example of a Zimm plot	155
Figure 3.5: GPC-MALLS Set-up (left) and a schematic of MALLS measurement (right)	156
Figure 3.6: Light scattering and angle dependence	157
Figure 3.7: Cylinder on the left has an equivalent volume to the sphere on the right	159
Figure 3.8: ¹ H and ¹ H- ¹ H COSY NMR for degraded Glycol Chitosan (24 hours) (10mg) in D ₂ O (1mL)	166

Figure 3.9: ^1H and ^1H - ^1H COSY NMR for PGC (6.54mg) in Methanol-d ₄ 99.9% (0.4mL) and D ₂ O 99.9% (0.2mL) and Acetic Acid-d ₄ 99.9% (0.05mL)	167
Figure 3.10: ^1H and ^1H - ^1H COSY NMR for GCPQ (11.01mg) in Methanol-d ₄ 99.9% (1mL)	168
Figure 3.11: FTIR spectra for 24 hours degraded Glycol Chitosan (top) and Palmitoyl Glycol Chitosan (Palmitoylation: 18%) (bottom)	169
Figure 3.12: MALDI-TOF spectrum of GC. Matrix: Synapinic acid	170
Figure 3.13: MALDI-TOF spectrum of PGC (top) and GCPQ (bottom). Matrix: Synapinic acid	171
Figure 3.14: GPC-MALLS Chromatogram of degraded (24 hours) GC (5 mg mL ⁻¹)	172
Figure 3.15: GPC-MALLS Chromatogram of GCPQ (10.79 mg mL ⁻¹)	173
Figure 3.16: Example dn/dc curve of GC (GC031107) and GCPQ	173
Figure 3.17: Voltage Output versus time plots at increasing concentrations for 24 degraded GC (right) and GCPQ (left) and collective table of results for four batches of GCPQ	174
Figure 3.18: PCS spectrum for an unfiltered aqueous dispersion of GCPQ (2.3 mg mL ⁻¹) (Palmitoylation: 15%, Quaternisation: 11%) on sonication	175
Figure 3.19: Negative stained TEM images of polymeric dispersions of GCPQ in increasing concentrations (A: 2.3mg mL ⁻¹ , B: 5mg mL ⁻¹ , C: 8mg mL ⁻¹ , D: 10mg mL ⁻¹ , Palmitoylation: 15%, Quaternisation: 11%) and Leucine ^[5] -Enkephalin (1mg) after filtration through 0.45µm. Bottom Left: Volume Mean Distribution from PCS for the filtered samples. Bottom Right: Summary table of mean particle size measurements results.	176-8
Figure 3.20: Negative stained TEM images of polymeric dispersions of GCPQ in increasing concentrations (A: 5mg mL ⁻¹ , B: 10mg mL ⁻¹ , Palmitoylation: 15%, Quaternisation: 11%) and TPLENK (1mg) after filtration through 0.45µm. Sample appeared slightly opaque (A) and opaque (B). Bottom Volume Mean Distribution from PCS for the filtered samples (Left) and summary table of mean particle size measurements results (Right)	178-9
Figure 3.21: Top: Negative stained TEM images of polymeric dispersions of GCPQ in increasing concentrations (A: 2.3 mg mL ⁻¹ , B: 5mg mL ⁻¹ , C: 10mg mL ⁻¹ , Palmitoylation: 19.68 %, Quaternisation: 6.88 %) and TPLENK (1mg). Samples appeared slightly opaque (A) and opaque (B, C). Bottom: Volume Mean Distribution from PCS for the unfiltered samples (Left top) and summary tables of mean particle size measurements results for all three formulations	180-1

Figure 3.22: Negative stained TEM images of polymeric dispersions of TPLENK to GCPQ (1:2.3w/w) (1 mg mL ⁻¹). Letter A-C indicates the three triplicates (Wet Stability)	182-5
Figure 3.23: PCS spectra of polymeric dispersions of TPLENK : GCPQ (1 : 2.3 w/w) formulations in H ₂ O (1mg mL ⁻¹) after vortexing, sonication and filtration (0.22µm) (Wet stability studies)	186-7
Figure 3.24: PCS spectra of polymeric dispersions of TPLENK : GCPQ (1 : 2.3 w/w) formulations in H ₂ O (1mg mL ⁻¹) after vortexing, sonication and filtration (0.22µm) (Dry stability studies)	188
Figure 3.25: Negative stained TEM images of polymeric dispersions of TPLENK to GCPQ (1:2.3w/w) (1 mg mL ⁻¹). Letter A-C indicates the three triplicates (Dry Stability)	189-193
Figure 3.26: Stability of mean PCS particle size (left) and polydispersity index (right) of wet formulations (triplicates) versus time	193
Figure 3.27: Stability of mean PCS particle size (left) and polydispersity index (right) of dry (freeze-dried and reconstituted) formulations (triplicates) versus time	194
Figure 3.28: Percentage of TPLENK as quantified by RP-HPLC in wet (left) and dry (freeze-dried and reconstituted) (right) stability studies versus time (Mean of triplicates, *: p<0.05, Student's t-test)	195
Figure 4.1: Schematic representation of an enzymatic assay to illustrate its several components	202
Figure 4.2: Mechanism for the bioconversion of esters by esterases B	207
Figure 4.3: Stability of peptides in the presence of SGF with or without GCPQ. No statistical significant differences were observed (p > 0.05)	217
Figure 4.4: HPLC chromatograms of peptides in the presence of SGF with GCPQ	218
Figure 4.5: Bradford assay BSA calibration graph for quantifying the protein content in intestinal wash studies	219
Figure 4.6: Stability of peptides in intestinal washes with or without GCPQ	220
Figure 4.7: HPLC chromatograms of peptides in the presence of intestinal wash with GCPQ	221
Figure 4.8: Bradford assay BSA calibration graph for plasma, liver and brain homogenates studies	222
Figure 4.9: Stability of TPLENK in 50% Liver Homogenate and bioconversion to Leucine ^[5] -Enkephalin in the presence of liver esterases	223
Figure 4.10: HPLC chromatograms of TPLENK in 50% Liver Homogenate over time	224

Figure 4.11: Stability of TPLENK in 10% Plasma Homogenate and bioconversion to Leucine ¹⁵ I-Enkephalin in the presence of plasma esterases	225
Figure 4.12: HPLC chromatograms of TPLENK in 10% Plasma Homogenate over time	225
Figure 4.13: Stability of TPLENK in 50% Brain Homogenate	226
Figure 4.14: HPLC chromatograms of TPLENK in 50% Brain Homogenate over time	227
Figure 5.1: Competitive radioimmunoassay	236
Figure 5.2: Principles of Immunoassay	237
Figure 5.3: Skin and within temperature increase versus time and cutaneous receptors evoked by different temperatures	241
Figure 5.4: Vascularisation of the mouse tail	243
Figure 5.5: Top Right: Negative stained TEM images for L (5 mg mL ⁻¹), LG and PG (3 mg mL ⁻¹ , 1: 2.3 w/w peptide to GCPQ) in NaCl 0.9% (L & LG filtered through 0.22µm and PG through 0.8 µm). Top Left: Mean particle size of above formulations along with their mean distributions (red: intensity, blue: volume, green: number) from PCS after filtration (triplicates). Bottom: SEM images and macroscopic appearance of LG and PG unfiltered formulations for oral administration	251-2
Figure 5.6: Example of RIA standard curve plotted in Microsoft Excel used for extrapolation of concentrations of samples	254
Figure 5.7: Intravenous Study: A, B: Leucine ¹⁵ I-Enkephalin recovered as % of dose and concentration (ng 0.1mL ⁻¹) in plasma respectively. C, D: Leucine ¹⁵ I-Enkephalin recovered as % of dose and concentration (ng g ⁻¹) in brain respectively. E, F: Exponential decay (first order) fitted curves for calculation of Leucine ¹⁵ I-Enkephalin half-life in the absence and presence of GCPQ respectively	255
Figure 5.8: Intravenous study: A, B: Leucine ¹⁵ I-Enkephalin recovered as % of dose and concentration (ng 0.1mL ⁻¹) in plasma respectively. C, D: Leucine ¹⁵ I-Enkephalin recovered as % of dose and concentration (ng g ⁻¹) in brain respectively. E, F: Exponential decay (first order) fitted curves for calculation of Leucine ¹⁵ I-Enkephalin or TPLENK half-life in the presence of GCPQ respectively	257
Figure 5.9: Intravenous study: A, B: Leucine ¹⁵ I-Enkephalin recovered as % of dose and concentration (ng 0.1mL ⁻¹) in plasma respectively. C, D: Leucine ¹⁵ I-Enkephalin recovered as % of dose and concentration (ng g ⁻¹) in brain respectively. E, F: Exponential decay (first order) fitted curves for calculation of Leucine ¹⁵ I-Enkephalin or TPLENK half-life in the presence of GCPQ respectively	259

Figure 5.10: Oral Study: A, B: Leucine^[51]-Enkephalin recovered as % of dose and concentration (ng 0.1mL⁻¹) in plasma respectively. 261
C, D: Leucine^[51]-Enkephalin recovered as % of dose and concentration (ng g⁻¹) in brain respectively

Figure 5.11: Oral Study: A, B: Leucine^[51]-Enkephalin recovered as % of dose and concentration (ng 0.1mL⁻¹) in plasma respectively. 263
C, D: Leucine^[51]-Enkephalin recovered as % of dose and concentration (ng g⁻¹) in brain respectively

Figure 5.12: Tail Flick Bioassay; Top: Placebo/NaCl (black) Leucine^[51]-Enkephalin 14mg Kg⁻¹ (red), Leucine^[51]-Enkephalin: GCPQ 14mg Kg⁻¹ (1:2.3 w/w) (green), and Palmitoyl Tyrosyl Leucine^[51]-Enkephalin (TPLENK): GCPQ 20 mg Kg⁻¹ (blue) % Antinociception (Mean % MPE ± SEM) at equivalent doses after IV administration to CD-1 Mice (n=8), (ANOVA Statistically different groups: *:p<0.05 vs NaCl, +: p<0.05 vs Leucine^[51]-Enkephalin) 265

Figure 5.13: Tail Flick Bioassay; Placebo/H₂O (black) Leucine^[51]-Enkephalin 70mg Kg⁻¹ (red), Leucine^[51]-Enkephalin: GCPQ 70mg Kg⁻¹ (1:5 w/w) (green), and Tyrosyl Palmitate Leucine^[51]-Enkephalin (TPLENK): GCPQ 100 mg Kg⁻¹ (1:5 w/w) (blue) % Antinociception (Mean % MPE ± SEM) at equivalent doses after oral administration to CD-1 Mice (n=16), (ANOVA Statistically different groups: *:p<0.05 vs H₂O, +: p<0.05 vs Leucine^[51]-Enkephalin, #:p<0.05 vs Leucine^[51]-Enkephalin: GCPQ) 267

Figure 5.14: Quantal form and % of analgesic responders of tail-flick bioassay after IV (n=8) (left) and oral (n=16) (right) administration 267

Figure 5.15: Packing of particles when the volume fraction approaches the volume fraction maximum 273

Figure 5.16: Effect of predetermined cut-off time (left) and intensity of applied stimulus (right) on the % MPE calculated for the tail-flick test 275

<u>List of Tables</u>	<u>Page</u>
Table 1.1: Advantages and disadvantages of strategies to enhance CNS delivery	68
Table 1.2: Polarity, Hydrophobicity, pKa and Isoelectric point (IP) of Natural Amino Acids	70
Table 2.1: Materials for Peptide synthesis and characterisation	108
Table 2.2: Tandem MS-MS for Leucine ^[5] -Enkephalin	121
Table 2.3: X-ray diffraction results for TPLENK	133
Table 3.1: Materials for GCPQ synthesis and characterization	146
Table 3.2: Encapsulation efficiency of formulations used for wet & dry stability studies	194
Table 4.1: Classification System for Enzymatic Assay Methods	203
Table 4.2: Major Enzymes Involved in Bioconversion of Ester-Based Prodrugs	205
Table 4.3: Materials for <i>in vitro</i> stability experiments	209
Table 4.4: Stability of peptides in the presence of SGF	218
Table 4.5: Stability of peptides in intestinal washes with or without GCPQ	220
Table 4.6: <i>In vitro</i> enzymatic stability of peptide formulations in rat intestinal wash	220
Table 4.7: Plasma, Liver and Brain esterase stability studies summary	223
Table 4.8: Stability of lipidic pro-drug (TPLENK) in 50% Liver Homogenate	224
Table 4.9: Stability of lipidic pro-drug (TPLENK) in 10% Plasma Homogenate	226
Table 4.10: Stability of lipidic pro-drug (TPLENK) in 50% Brain Homogenate	227
Table 5.1: Sources of Artifacts in RIA Determinations of tissues and body tissues	239
Table 5.2: Study Design and Formulations for <i>in vivo</i> studies	245
Table 5.3: Formulations characterisation results for <i>in vivo</i> studies	253
Table 5.4: Summary of % of dose and concentration of Leucine ^[5] -Enkephalin recovered after IV administration (n=4) of L and LG (25mg kg ⁻¹) in plasma and brain samples quantified using RIA (Student's t-test, p-values significant: p≤0.05)	256

Table 5.5: Summary of % of dose and concentration of Leucine ^[5] -Enkephalin recovered after IV administration (n=4) of LG and PG (10mg kg ⁻¹) in plasma and brain samples quantified using RIA (Student's t-test, p-values significant: p≤0.05)	258
Table 5.6: Summary of % of dose and concentration of Leucine ^[5] -Enkephalin recovered after IV administration (n=4) of LG and PG (8.9 mg kg ⁻¹) in plasma and brain samples quantified using RIA (Student's t-test, p-values significant: p≤0.05)	260
Table 5.7: Summary of % of dose and concentration of Leucine ^[5] -Enkephalin recovered after oral administration (n=4) of L and LG (25 mg kg ⁻¹) and PG (37.5mg kg ⁻¹) in plasma and brain samples quantified using RIA (Student's t-test, p-values significant: p≤0.05)	262
Table 5.8: Summary of % of dose and concentration of Leucine ^[5] -Enkephalin recovered after oral administration (n=4) of L and LG (70mg kg ⁻¹) and PG (100mg kg ⁻¹) in plasma and brain samples quantified using RIA (Student's t-test, p-values significant: p≤0.05)	264
Table 5.9: Tail Flick Bioassay summary of % Antinociception and Standard Error for different time points after IV administration in CD-1 mice (n = 8 / arm)	265
Table 5.10: Tail Flick Bioassay summary of % Antinociception and Standard Error for different time points after oral administration in CD-1 mice (n = 16 / arm)	266

List of Equations

Page

Equation 3.1: Equation relating scattering of light to molecular weight	154
Equation 3.2: Equation for calculating K (an arbitrary constant used in Mw calculation)	154
Equation 3.3: Stokes-Einstein equation	158
Equation 3.4: Autocorrelation function	158
Equation 3.5: Relationship between the linewidth of the spectrum and the Diffusion coefficient	158
Equation 3.6: Equation for calculating the scattering vector q	158
Equation 3.7: Equation for calculating the particle radius	158
Equation 3.8: Calculation of the % Palmitoylation of GCPQ	164
Equation 3.9: Calculation of the % Quaternisation of GCPQ	165
Equation 4.1: Calculation of the Enzyme Units / mL of Enzyme	215
Equation 4.2: Calculation of the Esterase Specific Activities	215
Equation 5.1: Calculation of % Maximum Possible Effects	249
Equation 5.2: HPLC calibration curve for Leucine ^[5] -Enkephalin IV formulations	250
Equation 5.3: HPLC calibration curve for TPLENK IV formulations	251
Equation 5.4: Krieger-Dougherty equation	272
Equation 5.5: Calculation of % Maximum Possible Effects (Le Bars et. al. 2001)	274

Abbreviations

Page

A°	Angstrom
Ab	Antibody
Ab-Ag*	Radioactive Antibody-Antigen complex
ABC	ATP-binding cassette
ACN	Acetonitrile
AcOH	Acetic Acid
Act	Activator
ACTH	Adrenocorticotrophin Hormone
ADAMB	Na-amidino-Tyr-D-Arg-Phe-Meß-Ala-OH
ADP	Adenosine Diphosphate
Ag*	Radioactive Antigen
AIDS/HIV	Acquired Immunodeficiency Syndrome / Human Immunodeficiency Virus
AME	Absorptive Mediated Endocytosis
Amp	Ampule
AMT	Absorptive Mediated Transecytosis
amu	Atomic Molecular Unit
ANOVA	Analysis of variance
AP-N	Aminopeptidase N
ATP	Adenosine Triphosphate
BBB	Blood-Brain Barrier
BCRP	Breast Cancer Resistance Protein
BCS	Biopharmaceutics Classification System
Boc	Tert-butyloxycarbonyl
Bop	(Benzotriazol-1-yloxy) tris (dimethylamino) phosphonium hexafluorophosphate
BP	Boiling Point
BSA	Bovine Serum Albumin
Bzl	Benzyl
°C	Degrees Celsius
Ca / C-a	Alpha carbon
Caco-2	Human Caucasian Colon Adenocarcinoma cell line
CHCA	α-Cyano-4-hydroxycinnamic acid
CI	Chemical Ionisation
Cld-1	Claudin-1 isoform
Cld-2	Claudin-2 isoform
Cld-3	Claudin-3 isoform
cm	Centimeter(s)
CNS	Central Nervous System
CP A	Carboxypeptidase A

CPS	Convergent Peptide Synthesis
COSY	Correlated Spectroscopy
CS	Chitosan
CSF	Cerebrovascular Fluid
CV	Coefficient of Variation
CVO	Circumventricular Organs
CZE	Capillary zone electrophoresis
3D	Three Dimensional
d	Density
Da	Daltons
DADLE	H ₂ N-Tyr ⁵ -D-Ala ⁴ -Gly ³ -Phe ⁴ -Leu-OH
DCC	Dicyclohexylcarbodiimide
DCM	Dichloromethane
DCU	N, N'-Dicyclohexylurea
DHB	2,5 dihydrobenzoic acid
DIEA	Diisopropylethylamine
DIPCDI	Diisopropylcarbodiimide
DMAP	4-(Dimethylamino)pyridine
DMF	N, N-Dimethylformamide
DMSO	Methyl Sulfoxide/Dimethylsulfoxide
DNA	Deoxyribonucleic Acid
dn/dc	Differential refractive index increment
DPDPE	Tyr-c[D-Pen-Gly-Phe-D-Pen]-OH
D-Pen	D-Penicillamine
DPPIV	Dipeptidylaminopeptidase IV
DVB	Divinylbenzene
EDTA	Ethylenediaminetetraacetic acid
EI	Electrospray Ionisation
ESI-MS	Electrospray Ionisation Mass Spectrometry
eV	Electronvolt
FAB	Fast Atom Bombardment
Fmoc	9-Fluorenylmethoxycarbonyl
FTIR	Fourier Transform Infrared
GC	Glycol chitosan
GCPQ	Quaternary ammonium palmitoyl glycol chitosan
GI	Gastrointestinal
GIT	Gastrointestinal Tract
Gly/G	Glycine
GPC	Gel permeation chromatography
GPCR's	G Protein-Coupled Receptors
h	hour (s)
HABA	2-(4-Hydroxyphenylazo)benzoic acid

HAPyU	1-(1-pyrrolidiny-1 <i>H</i> -1,2,3-triazolo[4,5 <i>b</i>]pyridin-1-ylmethylene)pyrrolidinium hecafluorophosphate N-oxide
HATU	N-[(dimethylamino)-1 <i>H</i> -1,2,3-triazolo[4,5- <i>b</i>]pyridin-1-yl-methylene-N-methylmethanaminium hexafluoro-phosphate N-oxide
HBSS	Hank's Balanced Salt Solution
HBTU	O- (benzotriazol-1-yl)-N, N, N', N;-tetramethyluronium hexafluorophosphate
HF	Hydrogen Fluoride
HOBt	1-Hydroxybenzotriazole
HODhbt	1-Oxo-2-hydroxydihydrobenzotriazine
HONp	p-Nitrophenol
HOSu	Hydroxysuccinimide
hPepT1	Humeral proton-coupled oligopeptide transporter
HPLC	High-Performance Liquid Chromatography
IC ₅₀	Half maximal inhibitory concentration
ISF	Interstitial Fluid
Kcal	Kilocalories
kDa	Kilodaltons
L	Litre
LDL	Low Density Lipoprotein
LENK	Leucine ^[51] -Enkephalin/Leu ^[51] -Enkephalin
Leu/L	Leucine
LHRH	Luteinising Hormone Releasing Hormone
Log P	Logarithm of the Octanol-Water partition coefficient
IV	Intravenous
M	Molar
M cells	Microfold cells
MALDI	Matrix-Assisted Laser Desorption/Ionisation
MALLS	Multi-angle laser light scattering
MDR	Multidrug resistance receptor
MENK	Methionine ^[51] -Enkephalin/Met ^[51] -Enkephalin
mg	Milligram
min	Minute
μL	Microliter
μm	Milimeter
mM	Milimolar
mL	Milliliter
MPE	Maximum Possible Effects
MPR	Multidrug resistance-associated protein
MR	Maximum Response
MS	Mass Spectrometry

MSH	Melanocystic Stimulating Hormone
MW	Molecular Weight
m/z	Mass to charge ratio
Na / N-a	Apha Nitrogen
Na	Sodium
NAD	Nicotinamide Adeninde Dinucleotide Nicotinamide Adeninde Dinucleotide (reduced form)
NADH	
NCA	N-carboxyanhydrides
NHPA	N-hydroxysuccinimide palmitic acid
nm	Nanometers
NMM	N-Methylmorpholine
NMR	Nuclear Magnetic Resonance
NOE	Nuclear Overhouser Effect
NOESY	Nuclear Overhouser Effect Spectroscopy
4N	4-Nitrophenol
4NP	4-Nitrophenyl
Obt	Oxybenzotriazole
OMI	Oxymorphindole
PA	Palmitic Acid
PBCA	Poly(butylcyanoacrylate)
PCS	Photon correlation Spectroscopy
PEG	Poly(ethylene)glycol
PEP	Phosphoenolpyruvate
PGC	Palmitoyl glycol chitosan
P-gp	P-glycoprotein
Phe/F	Phenylaninine
Pi	Phosphoric Acid
PMT	Photomultiplier tube
PNPB	p-nitrophenyl butyrate
PO	(Per) Oral
Poly	Polydispersity Index
PON	Paraoxonase
PS	Polystyrene
PTLENK	Tyrosyl Palmitate Leucine ^[5] -Enkephalin (Benzotriazol-1-yloxy) tris (pyrrolidino) phosphonium hexafluorophosphate
PyBOP	
RES	Reticuloendothelial System
RIA	Radioimmunoassay
RMT	Receptor Mediated Transcytosis
RP-HPLC	Reverse-Phase HPLC
rpm	Rounds per minute
SA	Sinapinic acid
SAR	Structure-Activity Relationship

SD	Standard Deviation
SEM	Standard Error
SEM	Scanning Electron Microscopy
SGLT-1	Na ⁺ -dependent D-glucose transporter
SIOM	7-spiroindanyloxymorphone
SPPS	Solid-Phase Peptide Synthesis
TAN-67	2-methyl-4a- α -(3-hydroxyphenyl)- 1,2,3,4,4a,5,12,12a- α -octahydroquinolone[2,3,3,- g]isoquino-line
TAPA	H-Tyr-D-Arg-Phe- β -Ala-OH
TBTU	O- (benzotriazol-1-yl)-N, N, N', N'- tetramethyluronium tetrafluoroborate
tBu	Tert-butyl
TEER	Trans Epithelial Electric Resistance
TEM	Transmission Electron Microscopy
TFA	Trifluoroacetic acid
TFE	2,2,2,Trifluoroethanol
TMC	Trimethylated Chitosan
TMS	Tetramethylsaline
TOF	Time-of-flight
TPLENK	Tyrosine Palmitate Leucine Enkephalin
TRH	Thyrotropin-Releasing Hormone
Tyr/Y	Tyrosine
WSCDI	Water-soluble carbodiimide
w/w	Weight per weight
UV	Ultraviolet
V	Volt
v/v	Volume per volume
ZO	Zonula Occludens
Ω	Ohms

Chapter 1

Introduction

1.0 Preface

Recent advances in recombinant DNA technology and modern synthetic methodologies allow for the production of large quantities of structurally diverse peptides and proteins e.g. monoclonal antibodies, hormones, and vaccines possessing a broad spectrum of pharmacological effects (Pauletti et al. 1997). The 2006 Pharmaceutical Research and Manufacturers Association report “Biotechnology Medicines in Development” identifies 418 new biotechnology medicines for more than 100 diseases such as cancer, infectious diseases, autoimmune diseases, AIDS/HIV, which are in human clinical trials or under review by the Food and Drug Administration (Tauzin 2006). The clinical development of these potential drugs, however, has been restricted due to their very poor permeation across biological barriers (e.g. the intestinal mucosa, or blood-brain barrier) and their chemical and metabolic lability (Borchardt 1999). These characteristics generally lead to low oral bioavailabilities (<1-2%) and short *in vivo* half-lives (<30min) (Pauletti et al. 1996; Pauletti et al. 1997). Intravenous administration of pharmaceutical peptides / proteins is the most common route of administration with subcutaneous and intramuscular administration following. These routes are invasive and expensive, especially if one considers the frequency of administration required and not as acceptable to the patient as the oral route. However, the design of orally bioavailable peptide-based drugs will necessitate a compromise between incorporation of those structural features that optimise the pharmacological properties (e.g. receptor binding) and those structural features that optimise the biopharmaceutical properties (e.g. membrane permeability, clearance, metabolism) of the molecule (Pauletti et al. 1997).

1.1 Barriers to oral peptide delivery

Most peptides are large (in comparison to the large majority of non-peptide drugs), usually having molecular weights in excess of 500 Da, which makes diffusive transport across biological barriers slow resulting in poor absorption from the gastrointestinal

tract (GIT) to the blood stream. They are usually hydrophilic and have a significant potential to form hydrogen bonds in aqueous environments. Also, they often contain several ionisable groups and hence are typically charged at physiological pH. When taken in combination, these factors mean that unmodified peptides are likely to be very poor candidates for oral delivery.

After screening the physicochemical properties of over 2000 clinically used drugs Lipinski formulated the “rule of five” as a predictor of poor absorption or permeation (Lipinski et al. 2001). This rule states that poor absorption or permeation are more likely when the compound has more than 5 H-bond donors (expressed as the sum of OH and NH groups), a molecular weight greater than 500 Da, a calculated Log P (logarithm of the octanol-water partition coefficient) greater than 5, and more than 10 H-bond acceptors (expressed as the sum of N and O atoms (Lipinski et al. 2001). An exception to the rule will be a compound that is a substrate for biological transporters (Lipinski et al. 2001). Peptides which can potentially be employed as therapeutic targets routinely violate three (or all four) of these criteria. Unfortunately, the majority of a peptide’s undesirable physicochemical properties can be attributed to the presence of free amino and carboxyl termini, and amino acid residues with polar or charged side-chains which are vital for recognition by target proteins and receptors.

One of the physiological functions of the GIT is to digest dietary proteins into considerably smaller peptides or amino acids that can be absorbed across the epithelium into the blood, thus restricting intact absorption of peptides and proteins after oral administration.

1.1.1 Physical barriers to absorption

The organisation and architecture of the intestinal mucosa restricts peptides and proteins to either the paracellular or the transcellular route [Figure 1.1, Modified from: (Pauletti et al. 1996)]. The paracellular pathway is an aqueous, extracellular route across the epithelia. Translocation through the paracellular pathway is passive and the flux of the molecule (adequately hydrophilic) is driven by the electrochemical potential and hydrostatic pressure between the two sides of the epithelium (Cereijido et al. 1993). The main rate-limiting barrier to the paracellular diffusion of the molecules across the

intestinal epithelium is the region of the tight junctions or zonula occludens (Cereijido et al. 1981). The proteins that line the tight junctional channels were ultimately identified as occludins (Furuse et al. 1993) and claudins (Furuse et al. 1998). The presence of different isoforms of the claudins (Cld-1, Cld-2, and Cld-3) in the tight junction strands results in the formation of heterogeneous pores with a range of diameters and charges (Salamat-Miller and Johnston 2005). The dimensions of the paracellular space lies between 10 and 30-50 Å, suggesting that solutes with a molecular radius exceeding 15 Å (~3.5 kDa) will be excluded from this uptake route (Rubas et al. 1996). Paracellular permeability across Caco-2 cell monolayers for metabolically stable peptides bearing the same charge was found to be highly dependent on the molecular radius (Pauletti et al. 1997). Tight junctions are generally accepted as being negatively charged overall and therefore selective for positively charged permeants (Salamat-Miller and Johnston 2005). They maintain the apical/basolateral polarity in cell layers and inhibit the diffusion of lipid molecules from one cell to another, while regulating the passage of ions and molecules through the paracellular pathway (Salamat-Miller and Johnston 2005). Considering that the intestinal epithelium has more than 2×10^6 cm² of surface area, the corresponding values of the paracellular surface area which ranges from 200 to 2000 cm² should not be underestimated, especially when the absorption of even minute quantities (pM-nM range) of a polypeptide drug may be sufficient to exert their required biological effect (Salamat-Miller and Johnston 2005). Examples of peptide drugs that have been shown to permeate the intestinal mucosa via the paracellular route include octreotide (Drewe et al. 1993; Jaehde et al. 1994), vasopressin analogs (Lundin and Artursson 1990), thyrotropin releasing hormone (Thwaites et al. 1993), and salmon calcitonin (Lee and Sinko 2000).

The transcellular pathway (Figure 1.1) involves movement of the solute across the apical cell membrane, through the cytoplasm of the cell and across the basolateral membrane by passive diffusion, or by a carrier- or vesicle-mediated process. In general, with peptides, transcellular flux by passive diffusion is minimal (Conradi et al. 1996). The most important factors controlling passive transcellular absorption across the GIT epithelium are lipophilicity and size. Lipophilicity is commonly expressed in terms of Log P (partition coefficient). However, the Log P of a peptide drug does not necessarily

Barrier properties of the intestinal mucosa

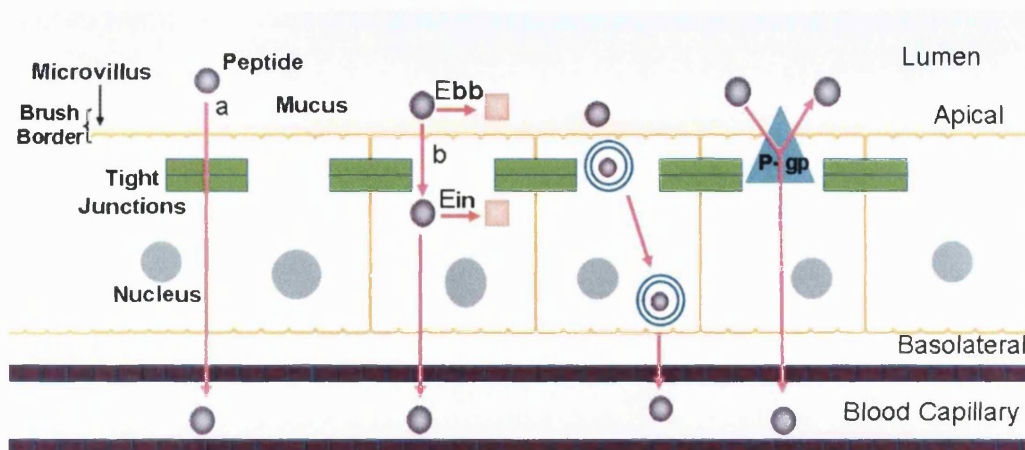


Figure 1.1: The intestinal mucosa as a barrier. The physical barrier limits peptide flux to (a) paracellular and (b) transcellular pathway. The biochemical barrier reduces transport of peptides through the intestinal mucosa by brush-border (Ebb: brush-border enzymes) and/or intracellular (Ein: intracellular enzymes) metabolism and by apically polarised efflux system.

predict permeability as with non-peptide drugs, due to their considerable hydrogen-bonding potential (amide bonds and side chains), which usually is a better predictor of peptide permeability (Conradi et al. 1991). For peptide passive absorption to take place, energy is required to break water-peptide hydrogen bonds in order for the solute to enter the cell membrane (Conradi et al. 1991). A high correlation was found for peptides with a reduced hydrogen bonding potential but not for lipophilicity as defined by Log P (Conradi et al. 1991). Passive diffusion within the lipid bilayer from the apical to the basolateral side is for many biologically active peptides inaccessible due to their relatively high hydrophilicity. However, for more hydrophobic derivatives, including peptide-mimetics and peptide prodrugs that reduce the number of H-bond donors, the lipid-soluble pathway may be a possible route for oral delivery (Pauletti et al. 1996).

Transport across the intestinal epithelium can also take place via various carriers and transporters. Carrier-mediated processes (e.g. using di- or tripeptide transporters) for the transport of peptides and peptidomimetics are fairly substrate-specific and do not contribute significantly to the transport of non-substrates although exceptions have been found (e.g. cephalosporins) (Pauletti et al. 1996; Pauletti et al. 1997). These

transporters are typically integral membrane proteins, and are primarily found on the apical membrane of epithelial cells, although some are found on basolateral membranes (Tsuji and Tamai 1996). One such transporter is the human proton-coupled oligopeptide transporter known as hPepT1, which is present mainly on epithelial cells in the duodenum and jejunum and displays unusually broad substrate specificity (Fei et al. 1994; Liang et al. 1995). PepT1-mediated uptake is electrogenic, independent of extracellular Na^+ , K^+ and Cl^- , and of membrane potential (Fei et al. 1994). A large variety of di- and tripeptides are transported, as are certain peptidomimetics such as β -lactam antibiotics (Franklin and Snow 1985; Palomo et al. 2007), angiotensin converting enzyme inhibitors, while peptides larger than tetrapeptides seem not to be transported (Tsuji and Tamai 1996). Other carriers and transporters potentially useful for peptide or peptidomimetic transport such as the bile acid, phosphate and monocarboxylic acid transporters or the Na^+ -dependent D-glucose transporter (SGLT-1) are more specific and require particular features for recognition (Tsuji and Tamai 1996).

Cellular internalisation of polypeptides by endocytosis is another important biological process for peptides that are too large to be absorbed by the di- or tripeptide transport systems (Pauletti et al. 1997). Fluid-phase endocytosis (pinocytosis) does not require any interaction between the polypeptide and the apical membrane (Pauletti et al. 1997). Pinocytosis is a non-specific process involving entrapment of extracellular fluid and possibly the peptide into a vesicle that then undergoes internalization into the cell (Wang 1996). In contrast, receptor-mediated or absorptive endocytosis involves the binding of peptides to the plasma membrane before being incorporated into endocytic vesicles (Pauletti et al. 1997). Finally, some polypeptides can be carried in endosomes directly to the basolateral side (i.e., bypassing the lysosomes), where they are released into the extracellular space (Pauletti et al. 1997). This process is known as transcytosis. However, more commonly the vesicle joins with a lysosome and its contents are metabolised (Oliyai and Stella 1993). Significant transcytosis of polypeptides has been described for M-cells (microfold cells), which are cells found in the follicle-associated epithelium of the Peyer's patches that have the unique ability to sample antigen from the lumen of the small intestine and deliver it via transcytosis to antigen presenting cells and lymphocytes located in a unique pocket-like structure on their basolateral side (Lee et al. 1991).

Efflux transporters can reduce intracellular accumulation and hence transcellular diffusion of many drugs including peptides transported across the intestinal epithelium. ATP-dependent efflux transporters such as P-glycoprotein [P-gp or multidrug resistance receptor (MDR) 1 or ATP-binding cassette (ABC) B1], multidrug resistance-associated protein 2 (MRP2 or ABCC2), and breast cancer resistance protein (BCRP or ABCG2) are also expressed on the apical membrane of intestinal epithelia in humans and rodents (Takano et al. 2006). P-gp is a 170-180 kDa membrane glycoprotein that acts as an ATP-dependent efflux pump recognising a variety of structurally and pharmacologically unrelated neutral and positively charged hydrophobic compounds (Mizuno et al. 2003; Chan et al. 2004). Peptides like cyclosporine (Ejendal and Hrycyna 2005), valinomycin, gramicidin D, and N-acetyl-leucyl-leucyl-norleucinal (Pauletti et al. 1996) are substrates for this efflux pumps. MRP2 transports relatively hydrophilic compounds, including the glucoronide, glutathione, and sulfate conjugates of endogenous and exogenous compounds (Suzuki and Sugiyama 2002; Chan et al. 2004). BCRP recognises relatively hydrophilic anticancer agents (Doyle and Ross 2003).

An additional factor that may hinder the passage of peptides through the intestinal mucosa is the mucus layer that coats the epithelial surfaces of the intestine with a thickness of 100-150µm. Mucus, in reality, is a constantly changing mix of many secretions, including exfoliated epithelial cells (Strous and Dekker 1992). The main determinants of the physical and functional properties of mucus secretions are high molecular weight glycoproteins, termed mucins (Strous and Dekker 1992). However, the role of the mucus layer as a physical barrier in the absorption of peptides from the gastrointestinal tract has not been well established (Pauletti et al. 1997). Peptides must diffuse through this mucus in order to reach the epithelial site of absorption, which can be limited by specific binding to the mucus components or by repulsion between charged species. Additionally, diffusion of lipophilic drug molecules is known to be slowed down by the mucous layer (Avdeef 2001).

The relative contribution of each of these transport processes to the overall absorption will vary depending on the various structural features of the compound, and its ability to act as a substrate for carrier systems. Overall uptake will be in most cases a combination of viable routes.

1.1.2 Enzymatic barrier to absorption

Enzymatic degradation of peptides starts immediately after oral ingestion. The enzymatic barrier is well designed to efficiently digest proteins by hydrolyzing peptide bonds to a mixture of amino acids and smaller peptide fragments consisting of 2 to 6 amino acid residues that can be absorbed by the enterocyte prior to their appearance in the portal circulation (Adibi and Mercer 1973). In normal individuals, 94-98% of the total protein is completely digested and absorbed (Langguth et al. 1997).

Peptides can be denatured or hydrolysed by the hostile acidic environment of the gastric juices and degraded by a family of aspartic proteinases called pepsins, which are most active at pH~3 (Lee et al. 1991). Pepsin, unlike some other endopeptidases, hydrolyses only peptide bonds. It does not hydrolyse non-peptide amide or ester linkages. Pepsins have very broad substrate-specificity, and can act at many sites on a target protein. Pepsin exhibits preferential cleavage for hydrophobic, preferably aromatic, residues (Sweeney and Walker 1993). Increased susceptibility to hydrolysis occurs if there is a sulfur-containing amino acid close to the peptide bond, which has an aromatic amino acid (Sweeney and Walker 1993). Pepsin will also preferentially cleave at the carboxyl side of phenylalanine and leucine and to a lesser extent at the carboxyl side of glutamic acid residues (Sweeney and Walker 1993). Pepsin will not cleave at valine, alanine, or glycine linkages (Sweeney and Walker 1993). Amidation of the C-terminal carboxyl group prevents hydrolysis by pepsin (Dixon and Webb 1979). Although they are capable of doing so, pepsins rarely degrade proteins to amino acids. However, on leaving the stomach pepsins become inactivated by a higher pH (above 5) (Lee et al. 1991)

The peptide fragments that result by partial digest in the stomach are then acted upon by pancreatic proteases in the duodenum and beyond. These proteases consist of trypsin, chymotrypsin, elastase, and carboxypeptidase A and B. The first three are endopeptidases (cleaving peptide bonds mid-chain), whereas the two latter are exopeptidases (cleaving terminal amino acids). The three endopeptidases have evolved to complement one another in cleaving almost all the internal peptide and proteins (Lee et al. 1991). A-chymotrypsin prefers to cleave peptide bonds near hydrophobic amino acids such as leucine, methionine, phenylalanine, tryptophan, and tyrosine (Lee et al.

1991). By contrast, trypsin preferentially cleaves peptide bonds near basic amino acids such as arginine, and lysine (Lee et al. 1991). Elastase complements the other two proteases by cleaving peptide bonds near alanine, glycine, isoleucine, leucine, serine, and valine; in other words, peptide bonds of amino acids bearing smaller, unbranched, nonaromatic side chains (Naughton and Sanger 1961). The smaller fragments produced by the endopeptidases may sequentially be further digested by exopeptidases. Carboxypeptidase A (CP A) is a well-characterised C-terminal exopeptidase (Whitaker et al. 1966). Substrates for this enzyme must meet two requirements: a free terminal carboxyl group and a C-terminal amino acid bearing a branched aliphatic or an aromatic group are particularly vulnerable to attack by this enzyme (Lee et al. 1991). For Carboxypeptidase B a free terminal carboxyl group and a C-terminal basic amino acid e.g. Arginine or Lysine are required (Langguth et al. 1997). Moreover, the nature of amino acids near the susceptible bond can modify the overall hydrolytic rate (Lee et al. 1991). All these proteases have an optimum functional pH of approximately 7 to 8 (Langguth et al. 1997). The products of these peptidases are typically fragments between 3 and 10 amino acid residues in length (Lee et al. 1991).

Although the pancreatic proteases are rather active against dietary proteins, their activity toward small peptides is very much restrained. (Lee et al. 1991) The bulk of luminal fluid activity against small peptides is derived from either the brush border or the cytoplasm or the lysosomes of the enterocyte (Silk et al. 1976). Luminal activity is less than 3% of cytosolic activity in the jejunum but rises to as high as 40% of brush border activity in the ileum (Silk et al. 1976). Overall, even when luminal degradation occurs, it constitutes normally less than 5%, and at best ~20% of the total degradation in a given intestinal segment (Adibi 1971; Crampton et al. 1973). The rest of the degradation occurs upon contact with the brush border or following cell entry (Lee et al. 1991). It appears that brush-border peptidases are active mainly against tri-, tetra- and higher peptides containing up to ten amino acid residues (Matthews and Payne 1980), while intracellular peptidases are active predominantly against dipeptides (Kim et al. 1972). The soluble enzymes of the cytoplasm consist mainly of dipeptidases, an aminotripeptidase, and the proline dipeptidases prolinase and prolidase, which serve to complete the intracellular hydrolysis of di- and tripeptides that are actively transported across the brush-border membrane by a proton-dependent carrier mechanism (Peters 1970; Adibi and Kim 1981). Besides the brush border and the cytosol, lysosomes and

other organelles are also potential sites of peptide degradation. Lysosomal peptidases seem to have their highest activities predominantly in the caecum (Bai 1994). Proteolytic degradation in the lysosomes is mainly catalysed by the cathepsins and may involve exo- as well as endopeptidase activity (Langguth et al. 1997). Most importantly though is the proteolytic activity of the abundant brush-border membrane peptidases (Figure 1.2). Aminopeptidase N (AP-N), an exopeptidase that hydrolyses peptides from the amino-terminal end, is a zinc-containing protein with a molecular weight of 120 kDa and is the most abundant peptidase in intestinal and renal microvilli but also in other tissues such as the brain, lung and nasal epithelium (Langguth et al. 1997). Aminopeptidase N has a broad specificity for L-configuration and a free α -amino group available, but peptides with D-amino acids or proline at the carboxy- or amino-terminus are relatively stable from enzymatic hydrolysis of this protease. Aminopeptidase P and W release the amino terminal amino acid from peptides when proline and tryptophan are in the penultimate position (Langguth et al. 1997). An

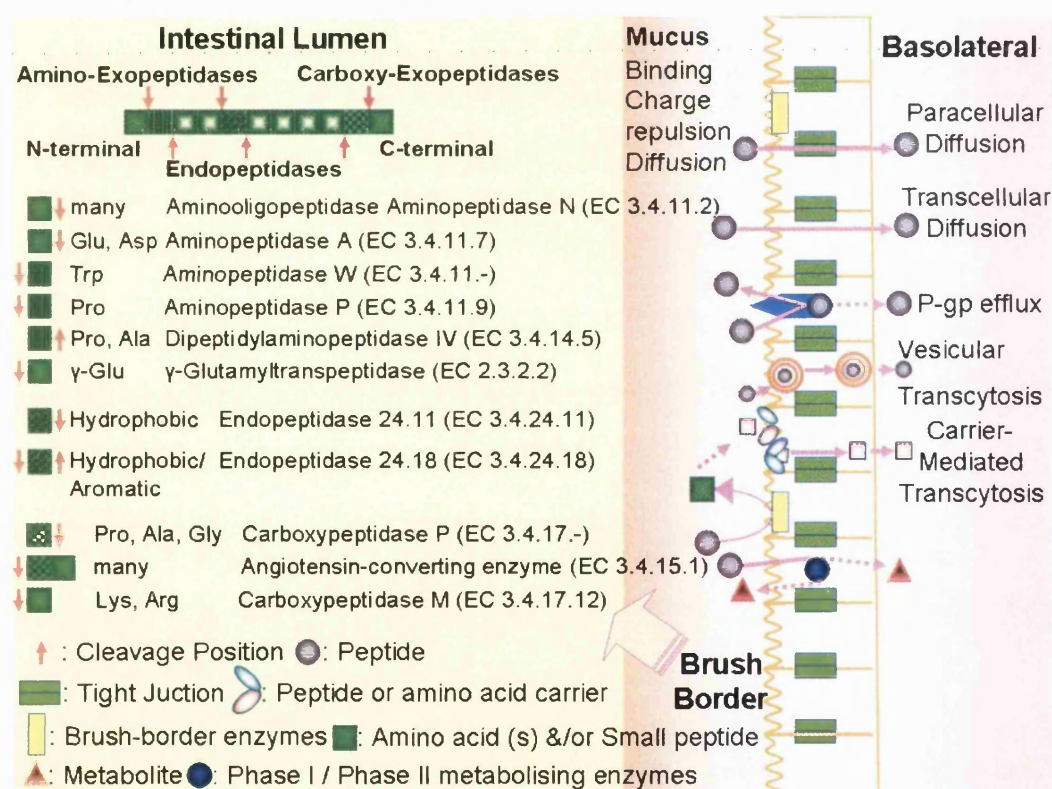


Figure 1.2: Degradation and absorption processes of peptides and proteins in the intestine: Important brush-border membrane peptidases and their substrate requirements. Squares are indicative of different amino acids. Modified from (Langguth et al. 1997).

amino dipeptidase is the serin protease dipeptidylaminopeptidase IV (DPP-IV) which cleaves the amino terminal dipeptide from peptides with proline in the penultimate position (Langguth et al. 1997). Finally γ -glutamyltranspeptidase catalyses the transfer of the γ -glutamyl group from the glutathione or other molecules with a γ -glutamyl group to the N-terminal of an amino acid or peptide acceptor to form a γ -glutamyl amino acid or peptide derivative (Langguth et al. 1997).

Among the brush border enzymes that hydrolyse peptides from the carboxy terminus is carboxypeptidase P, which releases C-terminal amino acids from polypeptides when proline is in the penultimate position (Langguth et al. 1997). It can also hydrolyse non-proline peptides, such as e.g. R-Ala-Tyr and R-Gly-Phe, however at slower rates (Langguth et al. 1997). Carboxypeptidase M hydrolyses C-terminal Lys and Arg residues from peptides (Langguth et al. 1997). Angiotensin-converting enzyme is a dipeptidyl carboxypeptidase which releases various unspecific dipeptides of the C-terminus (Yoshioka et al. 1987; Erickson et al. 1992), higher reaction rates are observed with proline residues in the C-terminal position (Langguth et al. 1997). Among the dipeptidases that have been reported to be present in the brush-border membrane are the microsomal dipeptidase responsible for the hydrolysis of glutathione and also of β -lactam antibiotics (Campbell et al. 1984). Other dipeptidases characterised involve Gly-Leu peptidase and the zinc-stable Asp-Lys peptidase (Langguth et al. 1997). Finally, two other important brush border endopeptidases are endopeptidase 24.11 or enkephalinase that hydrolyses the Gly³-Phe⁴ peptide bond in enkephalin opioid peptides and endopeptidase 24.18 with chymotrypsin-like activity (Langguth et al. 1997).

Microflora in the lower small and large intestine are capable of a number of metabolic reactions such as deglyuronidation, decarboxylation, reduction of double bonds, ester and amide hydrolysis and dehydroxylation reactions (Drasar and Hill 1974). Metabolism is extracellular and dependent on the dissolution of the peptide in the intestinal contents and transit time.

The lack of compliance, the difficulties associated with parenteral delivery, and poor oral bioavailability have lead to alternative routes to peptide delivery (Oliyai and Stella 1993). These include routes such as pulmonary (Quattrin 2006; Lee et al. 2009), ocular (Cortesi et al. 2006; Yenice et al. 2008), nasal (Veronesi et al. 2007; Doyle et al. 2008),

buccal (Bernstein 2008; Metia and Bandyopadhyay 2008), rectal (Liu et al. 2005), vaginal (Zhang et al. 2009) and transdermal (Badkar et al. 2007; Namjoshi et al. 2008). However, use of these alternative routes had limited success (Oliyai and Stella 1993) and are less convenient to the patient than the oral route.

1.2 Strategies to increase Oral Absorption of Peptides

For a peptide to be orally therapeutic it needs both a degree of metabolic stability and the ability to make use of a particular absorptive route across the intestinal mucosa. Strategies employed can be divided into two groups: (i) chemical modifications of the peptide structure and (ii) by formulating the peptide together with excipients that may reduce their presystemic degradation and increase permeability. Various strategies have been implemented to promote oral bioavailability of polypeptides, including supplemental administration of protease inhibitors (Ziv et al. 1987; Hussain et al. 1989; Lee 1990), use of absorption enhancers (Van Hoogdalem et al. 1988; Chiou and Chuang 1989), novel formulation strategies (Dange et al. 1990; Hutchinson and Furr 1990), and the employment of irreversible analogs (Morley 1980; Plattner et al. 1988) or reversible (prodrug) chemical modifications that may reduce their presystemic degradation and increase permeability (Wang et al. 2006).

Chemical modifications are directed at the creation of metabolically stable analogues by minimizing recognition of the analogue by families of peptidases in the GIT while retaining the original biological activity and receptor specificity of the native peptide. A promising approach to reducing metabolism is the substitution of L-amino acid with unnatural D-amino acids at either or both termini in order to prevent degradation. The amide bond between a naturally occurring L-amino acid and a D-amino acid is often not readily recognized as a substrate for proteolytic enzymes. The conformation of the peptide after modification does not allow binding into the enzyme's active site due to steric restrictions (Pauletti et al. 1997). 1-deamino-8-D-arginine vasopressin, a chemically modified analogue of arginine-vasopressin, showed slower degradation than the parent peptide in the intestinal content (intact for up to 35 minutes) and was shown to have enhanced bioavailability after oral administration when administered with lipid vehicles (Lundin et al. 1991; Fjellestad-Paulsen et al. 1995). D-Ala was substituted in

place of Gly² in Methionine^[5]-Enkephalin (Tyr-Gly-Gly-Phe-Met) and the analogue exhibited a longer half-life than the parent peptide, due to the inability of aminopeptidases to cleave the Tyr-D-Ala amide bond readily (Gesellchen et al. 1981). The analogue has been further modified by conversion of the C-terminal to an amide group (Tyr-D-Ala-Gly-Phe-Met-amide, or Tyr-D-Ala-Gly-Phe-N (CH₃)-Met-amide) with improved enzymatic stability (Lang et al. 1997). Other modifications, which have been used to prevent degradation by aminopeptidases, include N^α-acetyl, -formyl, and other N^α-alkylations (Pauletti et al. 1996). The use of a D-amino acid in place of an L-amino acid at the C-terminus can also inhibit carboxypeptidase-mediated degradation (Pauletti et al. 1996). In cases where D-amino acid replacement is not possible due to a loss of biological activity, other strategies have been used (e.g. conversion of the C-terminal amino acid residue into an ester or an amide). Some other modifications of the C-terminal end are converting the carboxy end to amino alcohols, methyl ketones, nitriles, tetrazoles, and decarboxy amino acids. The amino alcohol method was successful with enkephalin, where the C-terminal methionine was converted to a methionioyl residue (Pauletti et al. 1996). N-terminal modification of the dipeptide kyotorphin with a tert-butoxycarbonyl group increased its stability against intestinal aminopeptidases (Mizuma et al. 2000).

Cyclisation of a linear peptide by forming an amide bond between the N- and C-termini, between a side chain and the N- or C-terminus, or between two side-chains can confer increased stability to aminopeptidase as well as carboxypeptidases. In the case of a cyclic analogue between Asp⁵ and Lys¹⁰ of α -melanotropin, the half-life was 100 times greater than that of the parent linear peptide (Al-Obeidi et al. 1989). However, peptide cyclization can result in major structural and conformational changes that may affect the biological activity of the peptide (Pauletti et al. 1996).

The introduction of steric bulk in the form of an N-alkyl (usually methyl group) or C α -methylation (methylation of the α -carbon to generate quaternary amino acids) can slow the addition of an enzymatic nucleophile to a peptide bond (Figure 1.3) (Pauletti et al. 1997). N-methylation increases the incidence of the *cis* configuration of the amide bond, through steric interaction with the adjacent peptide residue and thus prevents the peptide substrate from binding tightly into the catalytic site of the enzyme, as well as slowing the formation of the tetrahedral transition intermediate, which is the first step in

peptide bond hydrolysis. N-methylation also results in a reduction in the hydrogen bonding potential of the peptide's backbone, which results in improved passive transcellular absorption and permeability (Pauletti et al. 1997). N-alkylation leads to only a small increase in lipophilicity (log P), suggesting that increased permeation is attributed to the reduction in hydrogen bonding potential (Conradi et al. 1991). An example could be the cyclic peptide cyclosporine that contains multiple N-methylated amino acids, which may contribute to its atypically high oral bioavailability (Lee et al. 1991)

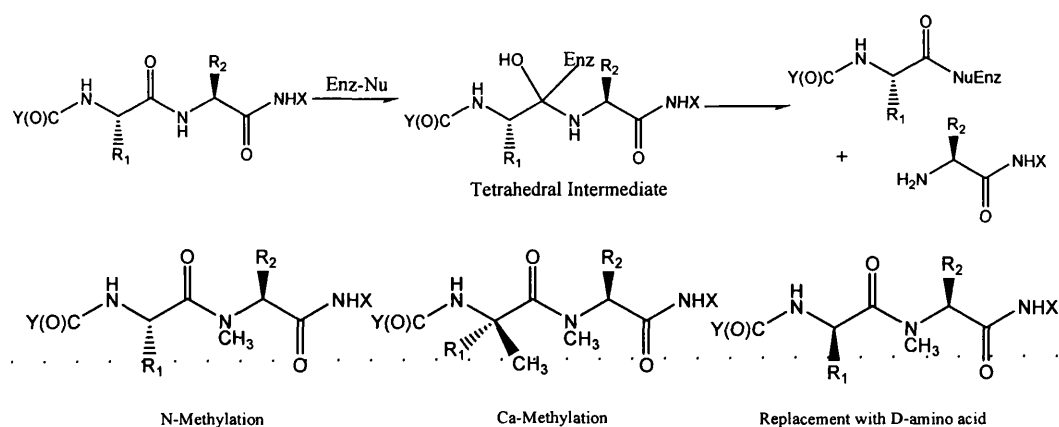


Figure 1.3: Enzyme-mediated hydrolysis (top) and chemical modifications of the peptide bond leading to increased metabolic stability of peptide drugs against hydrolytic enzymes (Pauletti et al. 1997)

A peptidomimetic is defined as a molecule that mimics the biological activity of a peptide but lacks traditional peptide structure as the labile peptide bonds being replaced with similar but enzymatically stable constructs such as reduced amides, hydroxyethylene, or hydroxyethylamino isosteres, or thioamides as many others (Figure 1.4) (Pauletti et al. 1997). Every surrogate of the peptide bonds, except the ester bond has been found to increase resistance toward enzymatic degradation, suggesting the there is recognition of the polar amide bond by most of the proteolytic enzymes; surrogate peptide bonds thus lead to enhanced stability of peptidomimetics (Spatola et al. 1986; Pauletti et al. 1997). For example, the [Gly³-Ψ-(CH₂-S)-Phe⁴-Leucine Enkephalin analog exhibited greater stability against enzymatic degradation, while the alkylidene amide surrogate (C=C) keeps the high double bond character of an amide bond (Shaw et al. 1982; Pauletti et al. 1996) (Figure 1.4). Modifications of the side-

chains of certain amino acids in the sequence (those not essential for binding) may also reduce recognition by some classes of peptidases (Oliyai and Stella 1993).

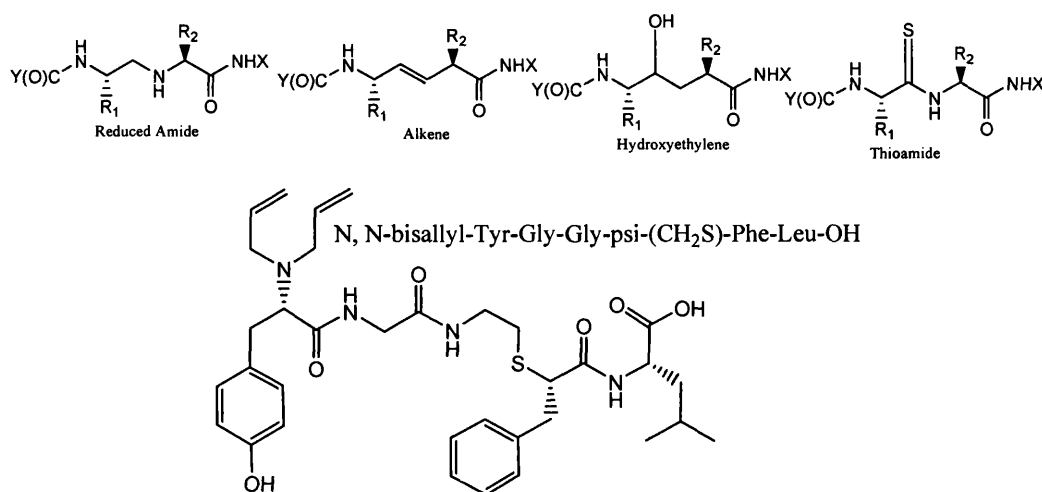


Figure 1.4: Examples of peptide bonds replacements that resulted in metabolically stable peptidomimetics. From: (Pauletti et al. 1997).

Prodrugs are chemically modified versions of the pharmacologically active agent that must undergo spontaneous or enzymatic transformation *in vivo* to release the active drug as a strategy to improve the physicochemical, biopharmaceutical or pharmacokinetic properties of pharmacologically potent agents (Rautio et al. 2008). An example is the pivalate ester prodrugs of desmopressin, a synthetic analog of the antidiuretic hormone, vasopressin (Kahns et al. 1993). Various prodrugs (N-alkoxycarbonyl derivatives) of TRH (thyrotropin releasing hormone) have been shown to be resistant to cleavage by enzymes (Bundgaard and Moss 1990; Rasmussen and Bundgaard 1991). Rasmussen and Bundgaard have developed aminopeptidase-resistant prodrugs of Leu-enkephalin and Met-enkephalin by condensing the enkephalins with various aldehydes and ketones to form a series of 4-imidazolidinone derivatives (Figure 1.5) (Rasmussen and Bundgaard 1991). In the presence of purified aminopeptidases, human plasma, and rabbit intestinal homogenates, the 4-imidazolidinone derivatives showed greater metabolic stability when compared to the parent enkephalin (Oliyai and Stella 1993). These derivatives are converted to the parent enkephalin via non-enzymatic hydrolysis with rates of conversion significantly influenced by the steric characteristics of the

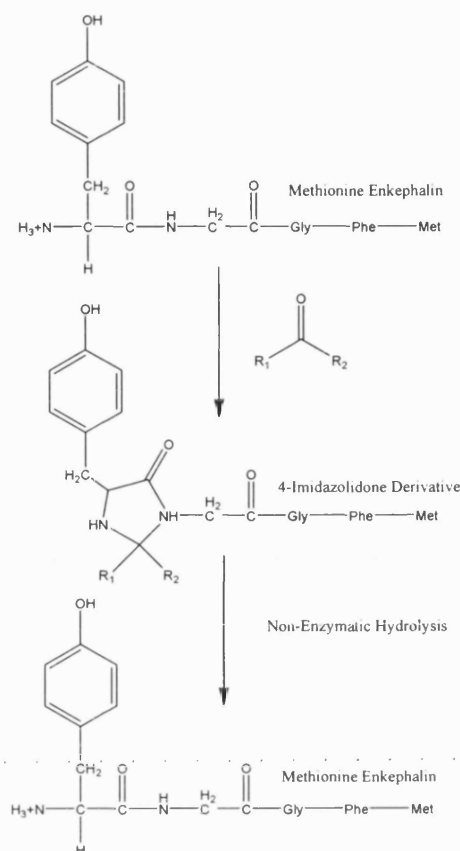


Figure 1.5: 4-Imidazolidinone prodrugs of Methionine^[51]-Enkephalin (Rasmussen and Bundgaard 1991)

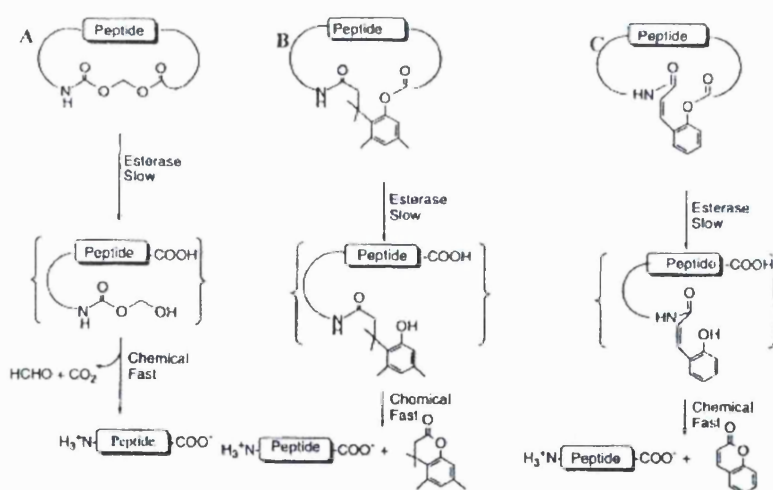


Figure 1.6: Cyclic prodrug strategies. (A) Acyloxyalkoxy-based prodrug; (B) phenylpropionic acid-based prodrug; (C) coumarinic acid-based prodrug (Borchardt 1999).

2-substituents (R_1 , R_2) on the terminal amino acid (Figure 1.5) (Oliyai and Stella 1993). Interestingly, the rate of conversion of these derivatives is significantly slower than the rate of systemic clearance of the parent peptides (Oliyai and Stella 1993). The potential therapeutic or pharmacodynamics implication of slower prodrug reversion rate compared to systemic clearance of the enkephalin is unknown (Oliyai and Stella 1993), but can be speculated to result in longer circulation times and prolonged pharmacodynamic effects.

Biodeversible cyclisation of the peptide backbone is one of the most promising new approaches in the development of peptide prodrugs (Pauletti et al. 1997). Cyclisation of the peptide backbone enhances the extent of intramolecular hydrogen bonding and reduces the potential for hydrogen bonding to aqueous solvents (Pauletti et al. 1997). As a consequence, the free energy for an amide bond decreased from 25.9 kJ/mol, when solvated, to 2.3 kJ/mol, if it is involved in an intramolecular bond (Roseman 1988). An example of this is delta sleep-inducing peptide that shows the unusual ability of passively diffusing across the blood-brain barrier (BBB) both *in vivo* (Banks et al. 1986) and *in vitro* (Raeissi and Audus 1989). The solution structure was shown to contain several intramolecular hydrogen bonds, resulting in an overall amphiphilic structure that may account for its unexpectedly high permeation characteristics (Gray et al. 1994). Conradi et al illustrated that a reduction in the number of potential hydrogen sites should increase the permeation characteristics of peptides across the intestinal mucosa (Conradi et al. 1992). Additionally, cyclisation of the backbone blocks the C-terminal carboxyl group and the N-terminal amino group, so that the peptide is less susceptible to enzymatic degradation mediated by amino- and carboxypeptidases (Oliyai and Stella 1993; Pauletti et al. 1997). A model esterase-sensitive prodrug strategy has been employed for H-Trp-Ala-Gly-Gly-Asp-Ala-OH using two different promoieties (Pauletti et al. 1997). These cyclic prodrugs were designed to be susceptible to esterase metabolism (slow step), leading to a cascade of chemical reactions resulting in the generation of the linear peptide (Figure 1.6) (Pauletti et al. 1997). Transport studies were conducted across monolayers of Caco-2 cells (Pauletti et al. 1997). In comparison to the linear hexapeptide, both cyclic prodrugs were found to be at least 70 times more able to permeate this *in vitro* cell culture model of the intestinal mucosa (Pauletti et al. 1997). Cyclic prodrug 1 appeared to be compact, due to intramolecular hydrogen bonding and the presence of a β -turn, probably due to reductions in the average

hydrodynamic radius of the molecule, thus increasing paracellular flux and/or increasing passive diffusion via the transcellular route because of reduction in the hydrogen bonding potential of the cyclic prodrug (Pauletti et al. 1997).

Co-administration of enzyme inhibitors with the peptide can lead to significant improvements in oral bioavailability of the pharmacologically active peptide (Jennewein et al. 1974; Bernkop-Schnurch 1998). The nonapeptide renin inhibitor Pro-His-Pro-Phe-His-Leu-Phe-Val-Phe was shown to cross the adult rabbit jejunum 90% intact in the presence of phosphoramidon, a metalloprotease inhibitor (Takaori et al. 1986). In the absence of the inhibitor, more than 55% of the nonapeptide was degraded within 5 minutes and none was left after 30 minutes (Takaori et al. 1986). Coadministration of aprotinin, a natural inhibitor of trypsin, with arginine vasopressin caused a substantial increase in the antidiuretic response of nearly 50% (Saffran et al. 1988; Pauletti et al. 1996). The target protease and its subcellular distribution will guide the selection of the peptidase inhibitor. Membrane-bound protease activity can be easily suppressed by co-administration of an effective inhibitor. It has to be noted though that the principal proteolytic activity is cytosolic, requiring the absorption of the inhibitor in the cell, which is challenging considering their large size and hydrophilic nature (Pauletti et al. 1996). Stabilisation of a peptide to intestinal proteases and metabolism may require a cocktail of inhibitors as more than one enzyme is normally active against a peptide, even though their metabolism maybe mainly attributed to a single enzyme (Pauletti et al. 1996). Furthermore, this strategy suggests that the enzymatic barrier is the major obstacle for absorption. Less than 3% of TRH is absorbed despite being metabolically stable in the gut, as it is absorbed through the upper intestinal regions (at least in the rat and dog) (Yokohama et al. 1984; Pauletti et al. 1996). Thus, even if a cocktail of peptidase inhibitors is used, the physicochemical properties of the peptide and the route of absorption (paracellular and/or transcellular) will have an impact on its overall absorption. However, disturbance of the digestion of nutritive proteins or causing an upregulation of protease synthesis raises toxicological questions (Bernkop-Schnurch 1998). Concerns are also raised on possible effects on the enterocyte (tight junctions changes) as well as on physiological processes following absorption into the systemic circulation (Pauletti et al. 1996). Prolonged usage of pancreatic enzyme inhibitors leads to both hypertrophy and hyperplasia of the pancreas (Bernkop-Schnurch 1998).

Absorption enhancers are defined as formulation additives whose purpose is to modify the barrier properties of the gastrointestinal epithelial cell layer (Fix 1996) and may promote both trans- and paracellular transport by interfering with the mucous layer, modulating tight junctions or affecting membrane components (Soares et al. 2007). Examples of such compounds are surfactants, salicylates, calcium chelating agents, bile salts, medium-chain fatty acids, phosphate esters, swellable polymers and cyclodextrins (van Hoogdalem et al. 1989; Muranishi 1990; Swenson et al. 1994; Soares et al. 2007). The intestinal absorption of the nonapeptide [1-desamino, D-Arg⁸]-vasopressin (dDAVP) was enhanced by medium-chain glyceride vehicles: (i) monohexanoin, (ii) mixed monoglycerides, diglycerides and triglycerides of hexanoic acid, (iii) and monoglycerides, diglycerides and triglycerides of octanoic and decanoic acids in an *in vivo* rat model with the former (monohexanoin) to enhance the oral bioavailability the highest (10 times that of control) (Lundin et al. 1997). No mucosal damage was observed after oral gavage of the lipid vehicle and the mechanism of this enhancement appeared to be related to protection against dDAVP degradation, the mucoadhesive properties of the vehicle and possibly an altered epithelial absorption pathway (Lundin et al. 1997). Three different chemical classes of absorption enhancers, namely, medium chain fatty acids (sodium caprylate and caprate), cyclodextrins (β -cyclodextrin, hydroxypropyl β -cyclodextrin) and bile salts (sodium cholate and deoxycholate) enhanced absorption of cyclosporine across the everted rat intestinal sac model from 2- to 27-fold (Sharma et al. 2005). Cyclodextrins were found to enhance the absorption of cyclosporine the most (~27-fold), followed by medium chain fatty acids (9- to 11-fold) and finally by bile salts (2-fold) (Sharma et al. 2005). However, cyclodextrins were found to be more toxic on this model than the other two types of enhancers tested (Sharma et al. 2005). However, the use of absorption enhancers with increased *in vitro* toxicity may raise toxicological issues, especially when considering chronic therapy, as they usually cause surface changes in the mucosa that include membrane component removal, cell loss and excessive mucus discharge (Soares et al. 2007). Histological or biochemical changes may occur locally or systemically if the additive is absorbed itself (Soares et al. 2007). Moreover, extended disruption of the barrier function of the GIT may allow the absorption of toxins or other chemicals that can lead to adverse side effects (Fix 1996).

Liposomes are well established particulate carrier systems that have been successfully employed for controlled release and site specific drug delivery consisting of one or more phospholipid bilayers separated by internal aqueous compartments (Gregoriadis 2006). The efficacy of liposomes as an oral delivery system of peptide drugs has not yet been established the main reason being instability of liposomes in GIT (Iwanaga et al. 1997). Liposomes were easily degraded by bile salts in GIT as they interact with liposomes as surfactants (Iwanaga et al. 1997). Surface coating of liposomes is used to avoid such interactions. In animal experiments, the attempt to improve the bioavailability of oral liposomal insulin by coating insulin-containing liposomes with PEG or mucin has successfully resulted in long-lasting lowering of glucose levels (Iwanaga et al. 1999). This is explained by the better interaction of polymer-coated liposomes with the mucus layer and better retention of insulin under the aggressive conditions of the stomach and GIT (Torchilin 2005). The efficiency of oral administration of liposomal insulin in liposomes of different phospholipid composition was also confirmed in rats (Kisel et al. 2001). However, high variability of effects caused by oral liposomal insulin was observed and still represents a challenge (Torchilin 2005). PEGylated liposomes provided the strongest and longest decrease in the glucose level, which supports the hypothesis that the hormone is slowly released from PEG liposomes and maintains a constant concentration in the blood for a long time (Torchilin 2005). Coating liposomal surface with biocompatible polymers such as polyethylene glycol (PEG) a protective layer is formed over the liposome surface that slows down liposome recognition by opsonins, and therefore clearance of liposomes (Torchilin 2005). Chitosan-coated insulin liposomes have been shown to produce hypoglycaemic effects in mice after oral administration (Wu et al. 2004). PEG liposomes have also been proposed for the oral delivery of recombinant human epidermal growth factor for gastric ulcer healing (Li et al. 2003). Hypocalcaemic effects of liposomal salmon calcitonin after oral delivery have also been demonstrated (Yamabe et al. 2003). Oral peptide bioavailability was improved for bee venom peptide after coating on alginate gel beads entrapped in liposomes targeted to the colon (Xing et al. 2003).

An established strategy to protein delivery consists of attaching the macromolecule to suitable particulate carrier systems, whereby the *in vivo* fate of the macromolecule is determined by the properties of the carrier system rather than those of the protein,

resulting in controlled and targeted release. Polymeric particulate systems used in drug delivery are larger than 1 μ m (microparticles) or submicron colloidal systems (nanoparticles). Polymeric particles will isolate the encapsulated peptide from the external medium therefore protecting the peptide from peptidases, allowing their uptake by enterocytes (Delie and Blanco-Prieto 2005). After absorption, polymeric particles will slowly degrade according to a kinetic profile depending on the nature of the polymer, thus providing a sustained and controlled release of the compound and prolonged *in vivo* half-lives (Delie and Blanco-Prieto 2005). Currently, the most prominent materials are biodegradable polyesters [e.g. poly(lactide) (PLA), poly(lactide-co-glycolide) (PLGA), poly- ϵ -caprolactone (PCL) and poly(ortho esters)] (Almeida and Souto 2007). The lactide/glycolide co-polymers are used in humans for parenteral (but not oral) delivery of peptides [luteinising hormone-releasing hormone (LHRH) analogues (Lupron Depot[®], Takeda Abbot; Decapeptyl Depot[®], Debiopharm], human growth hormone (Nutropin Depot[®], Genetech) and octreotide acetate (Sandostatin LAR[®], Novartis) (Almeida and Souto 2007). Research on the oral delivery potential of this biodegradable polymer has been shown to be successful for some peptides. Large porous PLGA microparticles loaded with insulin and coated with Eudragit L30D (0.03% w/v) resulted in pH responsive enteric coated particles that upon oral administration in alloxan diabetic rats produced a significant reduction (~63%) in blood glucose level in 2 hours with the effect continuing up to 24 hours (Naha et al. 2008). Positively charged salmon calcitonin hydrophobically ion paired to form physical complexes with sodium oleate and loaded on PLGA nanoparticles were administered via oral gavage into the stomach (pH neutralised with sodium bicarbonate) leading to an oral bioavailability of calcitonin of 0.4% (Sang Yoo and Gwan Park 2004). Polyanhydrides and solid lipids such as the physiologically cleavable medium and long chain diacylglycerols and triacylglycerols are also used for oral peptide delivery (Almeida and Souto 2007).

Chitosan has been extensively studied for oral delivery of peptides and proteins. Chitosan is a cationic polysaccharide composed of randomly distributed β -(1-4)-linked D-glucosamine (deacetylated unit) and N-acetyl-D-glucosamine (acetylated unit). It is produced via deacetylation of the naturally occurring chitin. The degree of deacetylation has a direct impact on the solubility of the polymer. The amine group of the polymer has a pKa in the range of 5.5-6.5. Therefore, chitosan is commonly insoluble at pH

values above 6.5 (Sugimoto et al. 1998). Chitosan refers to polymers of a broad range of molecular weight and different salts. Chitosan is capable of opening tight junctions and can therefore improve the oral uptake of hydrophilic drugs such as peptides (Dodane et al. 1999). Chitosan is a known mucoadhesive (Takayama et al. 1990) as ionic interactions occur between the cationic amino groups of chitosan and negative functional groups such as sialic acid of the mucus (Werle et al. 2008). Several chemical modifications of chitosan have been synthesised and evaluated for their oral peptide delivery potential. Chitosan is modified in order to improve the features of chitosan or to add additional properties. Trimethylated chitosan (TMC) has shown improved solubility of chitosan at neutral and slightly basic pH up to 9 (Kotze et al. 1997) and causes a reversible decrease of the transepithelial resistance (TEER) across Caco-2 cell monolayers (Werle et al. 2008). TMC has been found to increase the absorption of the peptide drugs busserelin and octreotide after intraduodenal or jejunal administration (van der Merwe et al. 2004). Another water soluble chitosan derivative (N-sulfonato-N,O-carboxymethyl-chitosan) has been shown to elevate anti-activated factor X levels to and above antithrombotic levels that were sustained for at least 6 hours, giving an 18.5-fold increase in the AUC of low molecular weight heparin in rats (Thanou et al. 2007). Thiolated chitosans exhibit increased mucoadhesive properties due to the ability of thiol groups to form disulfide bonds with the thiol groups of mucus leading to controlled release (Werle et al. 2008). Thiolated chitosan can cause a reversible opening of the tight junctions and is capable of inhibiting membrane bound efflux pumps (Werle et al. 2008). Chitosan-4-thiobutylamidine has been shown to increase the oral bioavailability of antide (decapeptide, LHRH antagonist), insulin and salmon calcitonin (Guggi et al. 2003; Krauland et al. 2004; Bernkop-Schnurch et al. 2005). Chitosan-enzyme inhibitor conjugates (chitosan-Bowman-Birk-Inhibitor, chitosan-pepstatin, and chitosan-elastinal) has been shown *in vivo* to enhance the bioavailability of insulin and salmon calcitonin (Guggi et al. 2003; Krauland et al. 2004). The covalent attachment of the enzyme-inhibitor to chitosan prevents the oral absorption of the inhibitor (Werle et al. 2008). Due to the mucoadhesive properties of chitosan, the peptide is released at the site where enzyme inhibition will take place and the polymeric matrix of chitosan reduces the contact time of the peptide with lumenally secreted proteases (Werle et al. 2008). Chitosan-succinate and chitosan-phthalate are soluble in alkaline pH as the carboxylic groups exist in nonionised form under acidic conditions. They release the majority of their contents (insulin) at physiologic pH and there is an increased hypoglycaemic effect

after oral administration (Ubaidulla et al. 2007; Ubaidulla et al. 2007). Coating of carriers with pegylated-chitosan has been shown to be beneficial versus the carrier alone after oral delivery of salmon calcitonin in rats (Prego et al. 2006). Pegylated chitosan was shown to be more stable in physiological conditions, have increased biocompatibility by significantly reducing positive charges of the nanoparticles (Quellec et al. 1998; Wu et al. 2005). Although weak, there is an interaction between the oxygen atom of PEG and the amino chitosan groups that affects nanoparticles formation producing looser, larger in size and irregular in shape nanoparticles (Wu et al. 2005).

Alginate micro- or nanoparticles have also been employed for the oral delivery of peptides with some success. Alginate is a naturally occurring copolymer of guluronic acid and manuronic acid (Ramadas et al. 2000). Fluorescent calcium alginate/chitosan microparticles, prepared using a spray-drying technique followed by crosslinking reactions with calcium ions and chitosan, were assayed *in vivo* for polymyxin B (PMB) oral toxicity, uptake by Peyer's patches and PMB oral absorption in rats (Coppi et al. 2008). Detectable antibiotic levels in Peyer's patches and urine as well as more constant PMB serum concentrations were provided by dosing PMB loaded in this microparticles, making the use of alginate/chitosan microparticles to target the lymphatic system possible and improving safety when administering PMB orally (Coppi et al. 2008). Nanospheres prepared with an alginate /dextran core matrix and complexed with chitosan and albumin have been used for the oral delivery of insulin in rats (Reis et al. 2008). Following oral delivery of insulin albumin-chitosan-coated alginate nanospheres blood glucose levels reduced to ~ 72% of basal values (Reis et al. 2008). Albumin served as an important enteric coating providing acid and protease protection (Reis et al. 2008). Microparticles of alginate and another mucoadhesive, lectin (wheat germ agglutinin) have also significantly decreased blood glucose levels in diabetic rats at 4 hours with an effect lasting 8 hours (Kim et al. 2005). Another study illustrated that insulin-loaded microparticles prepared with mucin and sodium alginate (1 part to 3 parts) caused a blood glucose reduction after 5 hours post-oral administration equal to the that of subcutaneously administered insulin (Builders et al. 2008). However, the encapsulation efficiency of alginate microparticles is low (Ramadas et al. 2000). Oral vaccination with alginate microspheres loaded with BCG (Bacille Calmette-Guerin, the attenuated live bovine tuberculosis bacillus) was possible in Balb/c mice yielding a

lower bacterial count after systemic infection with BCG preceded by oral vaccination compared to free BCG (Ajdary et al. 2007). Proliferative and delayed-type hypersensitivity (DTH) responses and IFN- γ (Interferon- γ) production were significantly higher in orally immunized mice with encapsulated BCG in comparison with results of mice immunized orally with free BCG (Ajdary et al. 2007).

Polymeric particulate delivery systems show promise in the oral delivery of peptide drugs and biopharmaceuticals as they are able to efficiently protect the peptide in the hostile environment of the gastrointestinal tract and enhance peptide absorption with a variable release profile that can be manipulated (sustained release, enteric coated, pH sensitive etc.). The use of biocompatible and biodegradable materials will ensure a low toxicity profile.

1.3 Blood-brain barrier and CNS peptide delivery

Despite enormous advances in brain research, neurological diseases associated with cancers, Alzheimer's disease, inborn errors of metabolism (e.g. lysosomal storage disease), pain, infectious diseases (e.g. HIV) and aging remain one of the world's leading cause of disability, morbidity and mortality. Many known neuroactive peptides hold promise as useful therapeutic agents, as neuroactive peptides play important biochemical roles in the CNS, for example as neurotransmitters and/or neuromodulators (Strand 1999). Delivery of this diverse range of peptides to the CNS provides many opportunities for therapeutic benefit. However, therapeutic intervention in many neurological diseases is thwarted by the physical obstacle formed by the blood-brain barrier (BBB) (Begley 2004). The BBB is a unique membranous barrier that tightly segregates the brain from the circulating blood and thus by regulating the constancy of the internal environment of the brain within very precise limits allows for neuronal functions of the CNS to optimally take place (Calvo et al. 2001). Thus, the same mechanisms that protect it against intrusive chemicals can also frustrate therapeutic interventions and these obstacles have to be overcome to provide useful treatments for neurological diseases.

The extracellular fluid compartments of the CNS comprise the brain and spinal cord parenchymal interstitial fluid (ISF) and the cerebrospinal fluid (CSF), contained within the ventricles of the brain and the cerebral and spinal subarachnoid spaces (Begley and Brightman 2003). The CNS consists of blood capillaries which are structurally different from the blood capillaries in other tissues. The BBB is not one single structure or membrane in the brain, but is rather formed at the level of the endothelial cells of the cerebral capillaries (Begley 1996) (Figure 1.7). The BBB is comprised of two plasma membranes in series, which are the luminal and the abluminal membranes of the brain capillary endothelium that are separated by about 0.3 μm of endothelial cytosol (Pardridge 1991). Anatomically, the endothelial cells of the BBB are distinguished from those in the periphery by increased mitochondrial content (Oldendorf et al. 1977), a lack of fenestrations (Fenstermacher et al. 1988), minimal pinocytotic activity (Sedlakova et al. 1999), and the presence of tight junctions (Kniesel and Wolburg 2000) (Hawkins and Davis 2005). These tight junctions between the cells of the capillaries [zonula

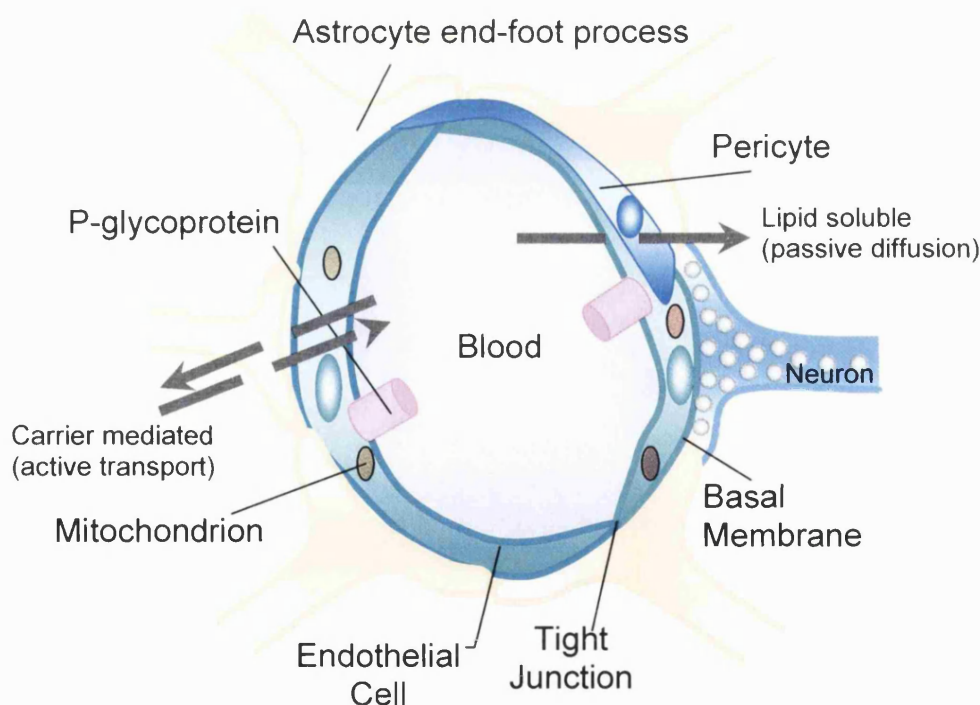


Figure 1.7: Schematic diagram of the neurovascular unit/cell association forming the BBB.

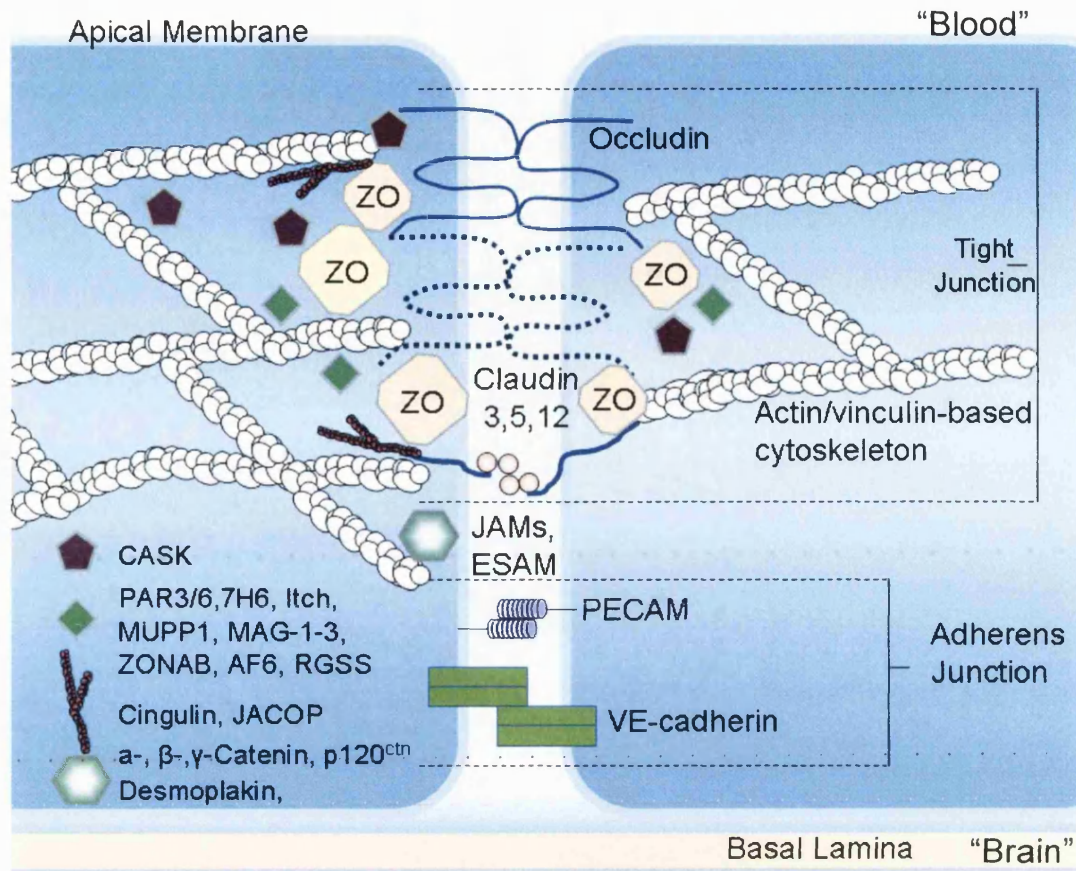


Figure 1.8: Molecular composition of endothelial tight junctions. Occludin is a 60-65 kDa protein that has four transmembrane domains with the carboxyl and amino terminals oriented to the cytoplasm and two extracellular loops that span the intercellular cleft of cerebral endothelial cells (Furuse et al. 1993). It increases electrical resistance in tight junctions containing tissues, a property mediated by the second extracellular loop domain (Wong and Gumbiner 1997). The junctional adhesion molecules (JAMs) and the endothelial selective adhesion molecule (ESAM) are members of the immunoglobulin superfamily and are believed to mediate the early attachment of adjacent cell membranes via homophilic interactions. Within the cytoplasm are many first-order adaptor proteins, including zonula occludens 1, 2, and 3 (ZO) and Ca^{2+} dependent serine protein kinase (CASK), that bind to the intramembrane proteins. Among the second-order adaptor molecules, cingulin is important, and junction-associated coiled-coil protein (JACOP) may also be present. Signaling and regulatory proteins include multi-PDZ-protein 1 (MUPP1), the partitioning defensive proteins 3 and 6 (PAR 3 / 6), MAGI-1-3 (membrane-associated guanylate kinase with inverted orientation of protein-protein interaction domains), ZO-1-associated nucleic acid-binding protein (ZONAB), afadin (AF6), and regulator of G-protein signalling 5 (RGS5). All of these adaptor and regulatory/signalling proteins control the interaction of the membranous components with the actin/vinculin-based cytoskeleton. In epithelial cells, tight and adherens junctions are strictly separated from each other, but in endothelial cells these junctions are intermingled. The most important molecule of endothelial adherens junctions is vascular endothelial cadherin (VE-cadherin). In addition, the platelet-endothelial cell adhesion molecule (PECAM) mediates homophilic adhesion. The chief linker molecules between adherens junctions and the cytoskeleton are the catenins, with desmoplakin and the p120 catenin (p120^{ctn}) also involved. Itch: E3ubiquitin protein ligase. Modified from (Wolburg et al. 2001; Hawkins and Davis 2005).

occludens, (ZO)]; (Brightman and Reese 1969) are produced by interaction of several transmembrane proteins that project into and seal the paracellular pathway (Figure 1.8). The interaction of these junctional proteins, especially occludin and claudin, is complex and effectively blocks an aqueous route of free diffusion for polar solutes from blood along these potential paracellular pathways denying free access to these solutes into the interstitial fluid (Begley 2004). Attached at irregular intervals to the abluminal membrane of the endothelium are pericytes, often divided into granular and filamentous subtypes (Tagami et al. 1990; Hawkins and Davis 2005). Pericytes and endothelial cells are ensheathed by the basal lamina, a membrane 30 to 40 nm thick composed of collagen type IV, heparin sulfate proteoglycans, laminin, fibronectin, and other extracellular matrix proteins (Farkas and Luiten 2001; Hawkins and Davis 2005). The basal membrane is contiguous with the plasma membranes of astrocyte end-feet, which ensheath cerebral capillaries (Hawkins and Davis 2005). Axonal endings from neurons are also present and contain vasoactive neurotransmitters and peptides. Microglial cells (perivascular macrophages), the resident immunocompetent cells of the brain, are part of the BBB and are derived from systemic circulating monocytes and macrophages. The endothelium is characterised by exhibiting a high transepithelial electrical resistance in the region of 1500-2000 $\Omega \text{ cm}^2$ (Butt et al. 1990). The BBB does not allow a free diffusional movement of solutes out of the CNS either, hindering free diffusion in a bidirectional way. Hence, the BBB formed by special endothelial cells sealed with tight junctions and a complete absence of pinocytic activity, restricts the movement of solutes to transcellular transport (passive diffusion, carrier transport) (Calvo et al. 2001).

Some regions within the CNS lack a BBB and the capillaries are fenestrated allowing the free movement of solutes between the circulating blood and the surrounding interstitial tissue. These areas around the ventricles of the brain are collectively known as the circumventricular organs (CVO) and comprise of the choroid plexus, the median eminence, the neurohypophysis, the pineal gland, the organum vasculosum of the lamina terminalis, the subfornical organ, the subcommisural organ and the area postrema (Begley 1996) (Figure 1.9). Capillaries in the choroid plexus and the CVO do not form tight junctions and the blood vessels are freely permeable (Begley 2004). The CVO possess specialised structures in the capillary wall termed fenestrae where the cytoplasm is attenuated and only the plasma membrane(s) form the diffusional barrier

(Figure 1.9) (Prescott and Brightman 1998). However, in the choroid plexus as in other CVO, the epithelial (ependymal) cells facing the CSF form tight junctions between adjacent cells, thus preventing diffusion of blood-borne solutes further into the brain (Brightman 1992) (Figure 1.9). Normally, ependymal cells do not form tight junctions elsewhere in the brain (Begley 2004). The origin as well as the mechanisms of the differentiating factors bringing about tight junction formation in the choroid plexus and in the ependymal cells near the CVO are unknown.

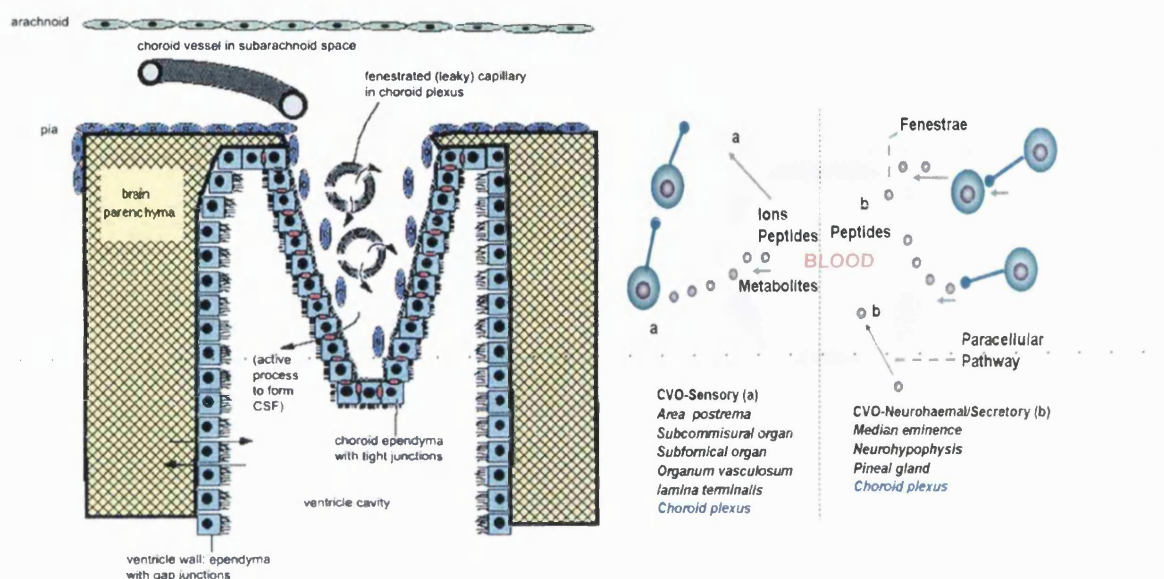


Figure 1.9: Left: The choroid plexus (composed of fenestrated capillaries and an epithelial (ependymal) covering, which reverts from “tight” to “open” at the base). From: (Washington 2009). Right: Organisation of a CVO.

The main functions of the choroid plexus are to secrete fresh CSF and to regulate the movement of solutes from blood to CSF and vice versa (further diffusion within the brain is limited by the tight junctions in the surrounding ependyma). The absence of tight junctions and the fenestrae ensure that the diffusional resistance of these capillaries is low and the extracellular fluid immediately surrounding the CVO can equilibrate with plasma and vice versa. Dendritic processes and receptors on neurons within this limited area can then interact with these blood-borne solutes and their nervous activity can be modulated (Begley 2004). These CVO-proximate neurons can then synaptically influence and initiate quite distant events elsewhere in the CNS depending on where their axons terminate (Begley 2004). This function of the CVO becomes vital due to the

creation of the BBB, and without their monitoring activity, the brain could not rapidly respond to many blood-borne signals (Begley 2004). The CVO can be divided into those that are primary sensory in function and those that are neurohaemal and comprise specialised regions allowing neurosecretion directly into the blood (Figure 1.9) (Begley 2004). The relative surface area of the permeable fenestrated capillaries of the circumventricular organ compared to the tight BBB capillaries is 1:5000 (Begley 1996). Given these considerations there is little possibility of these high permeability areas being able to influence the composition of the bulk of the brain extracellular fluid and the CVO do not form a realistic route for drug entry into the brain (Begley 1996).

The cells forming the avascular arachnoid membrane, which envelopes the whole CNS, also possess tight junctions that effectively seal the paracellular diffusional pathway between these cells (Begley 2004).

Despite the estimated total length of 650 km and total surface area of 12 m² of capillaries in human brain (Misra et al. 2003), the BBB is very efficient and makes the brain practically inaccessible for polar molecules and small ions. Thus, the endothelial cells are required to maintain a high level of expression of transport proteins for essential polar metabolites such as glucose and amino acids to facilitate their entry into the brain (Begley and Brightman 2003). Therefore, both receptor-mediated transcytosis (RMT) and nonspecific absorptive-mediated transcytosis (AMT) pathways exist across the cerebral endothelium transcytosis and are significant for the BBB transport of peptides (Begley and Brightman 2003). The RMT systems include the BBB insulin receptor and the transferrin (TfR) receptor and mediate the bidirectional movement of large endogenous peptide ligands between the blood and the brain.

The endothelial cells forming the BBB (as well as the CVO) exhibit a polarised expression of transport proteins in the luminal (part of cell's membrane facing the bloodstream) and abluminal (side exposed to the actual brain tissue) membranes of the endothelial cells, with some transporters expressed exclusively in one of these interfacial membranes and some in the other, whereas some are inserted into both membranes (Betz et al. 1980; Begley 1996; Mertsch and Maas 2002). As some transporters are unidirectional and some bi-directional in their transport of solutes

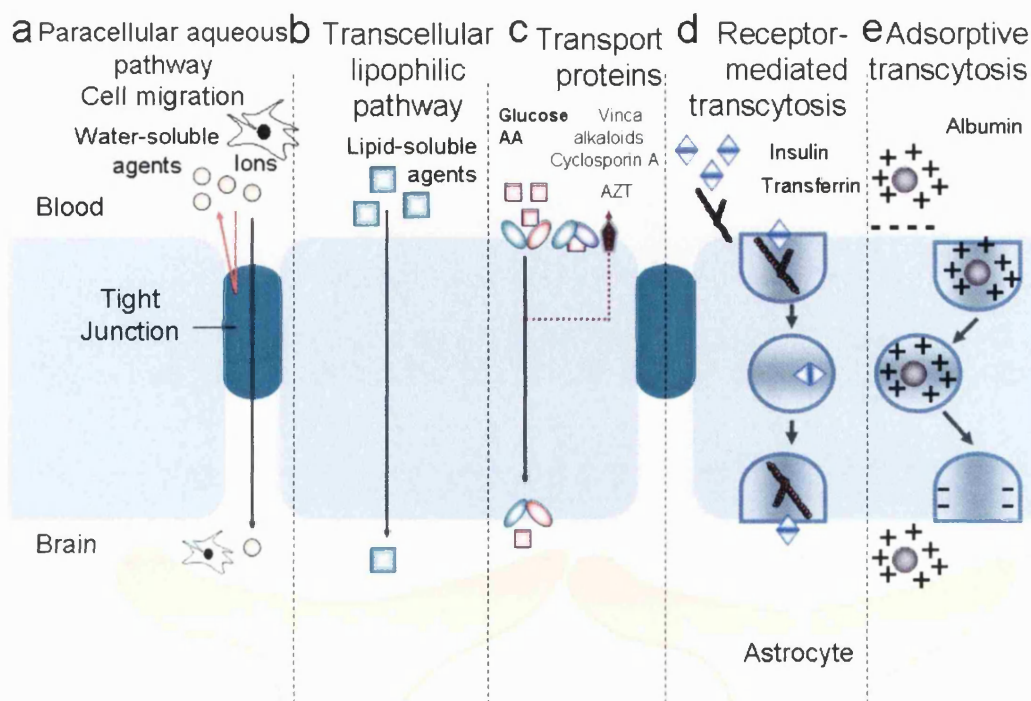


Figure 1.10: Potential routes for transport across the BBB. (a) Polar solutes transport across the paracellular pathway are severely restricted by the presence of tight junctions. Leukocytes and ions may cross the BBB adjacent to, or by modifying, the tight junctions. (b) Lipophilic or amphiphilic solutes may passively diffuse through the large surface of the lipid cell membrane and cross the endothelium. Greater lipid solubility favors this process. (c) Carrier-mediated influx, which may be passive or secondarily active, can transport many essential polar molecules such as glucose, amino acids, amines, monocarboxylates, choline and nucleosides into the CNS. Active efflux carriers may intercept some of these passively penetrating solutes and pump them out of the endothelial cell (e.g. AZT: Azidothymidine, Cyclosporine A, Vinca alkaloids). (d) Receptor-mediated transcytosis (RMT) can transport macromolecules such as peptides and proteins across the cerebral endothelium. Examples are Transferrin, Insulin, Leptin, Cytokines, Viruses (e.g. Herpes Simplex virus). (f) Adsorptive-mediated transcytosis (AMT) appears to be induced nonspecifically by positively charged macromolecules such as cationised albumin resulting in transport across the BBB. Drug delivery across the brain endothelium depends on making use of pathways b-e, while most CNS active agents enter via route b. Modified from (Begley and Brightman 2003; Abbott et al. 2006).

across the cell membrane, this polarization means that some solutes can be preferentially transported into the brain and some out of the brain. Thus, the transport of some solutes can be facilitated in either direction depending on whether the concentration gradient across the BBB is directed into, or out of, the CNS. This latter aspect can become important for some drugs with affinity for BBB transporters, when after systemic administration the pharmacokinetic profile can cause the concentration gradient to reverse across the BBB. It is thought that the formation of tight junctions between the endothelial cells may also act as a barrier in the cell membrane preventing both transport protein and lipid rafts in the membrane from exchanging between the

luminal and the abluminal membrane domains and therefore preserving the polarity of the BBB (Begley 2004). Potential routes across the BBB for drugs and other solutes are shown in Figure 1.10.

The BBB has about 1000 times more surface area than the choroid plexus and is the primary obstacle to delivery of therapeutic compounds to the CNS allowing only active transport of hydrophilic molecules such as peptides. However, lipophilic molecules readily transverse the BBB by passive transport or diffusion through the endothelial plasma membranes (Levin 1980). There is a well-established relationship between lipid solubility, either calculated or determined as an oil-water partition coefficient, with brain penetration, which increases with increasing lipid solubility (Figure 1.11) (Levin 1980; Bodor and Buchwald 2006). On the other hand, some lipid-soluble molecules do not enter the brain as readily as their lipophilicity solubility might suggest (Figure 1.11) (Bodor and Buchwald 2006). These substances and many of their metabolites are removed from the brain and the cerebral endothelium by active efflux transporters, which hydrolyse ATP and can move their substrates against a concentration gradient from blood to brain (Begley 2004; Begley 2004). These active transporters are generally ATP-binding cassette (ABC) transporters.

The polar surface area (PSA) is also an important descriptor for passive diffusion across the BBB (Kelder et al. 1999). Based on the inverse linear relationship between experimental data for penetration of the brain and the dynamic polar surface area of 45 drug molecules, it was found that most orally administered drugs that act on the CNS that cross the BBB by passive transcellular diffusion have a PSA below 60-70 Å² (Kelder et al. 1999; Lennernas and Lundgren 2004).

BBB penetration of a compound is thought to be dependent on its hydrogen-bonding potential, lipophilicity and size (Sorensen et al. 1997). Weak hydrogen-bonding potential, high lipophilicity, and small size are favorable to BBB penetration (Fu et al. 2004). Less than 2% of all small molecules cross the BBB in pharmacologically active amounts (Pardridge 2005). Cyclosporin A, a cyclic undecapeptide with a molecular weight of about 1200 Daltons (Da) and a log P (octanol/water) of 4.3 at room temperature (Lucangioli et al. 2003), is transported through the BBB at a much lower rate than its lipid solubility would predict. Such divergence between lipid solubility and

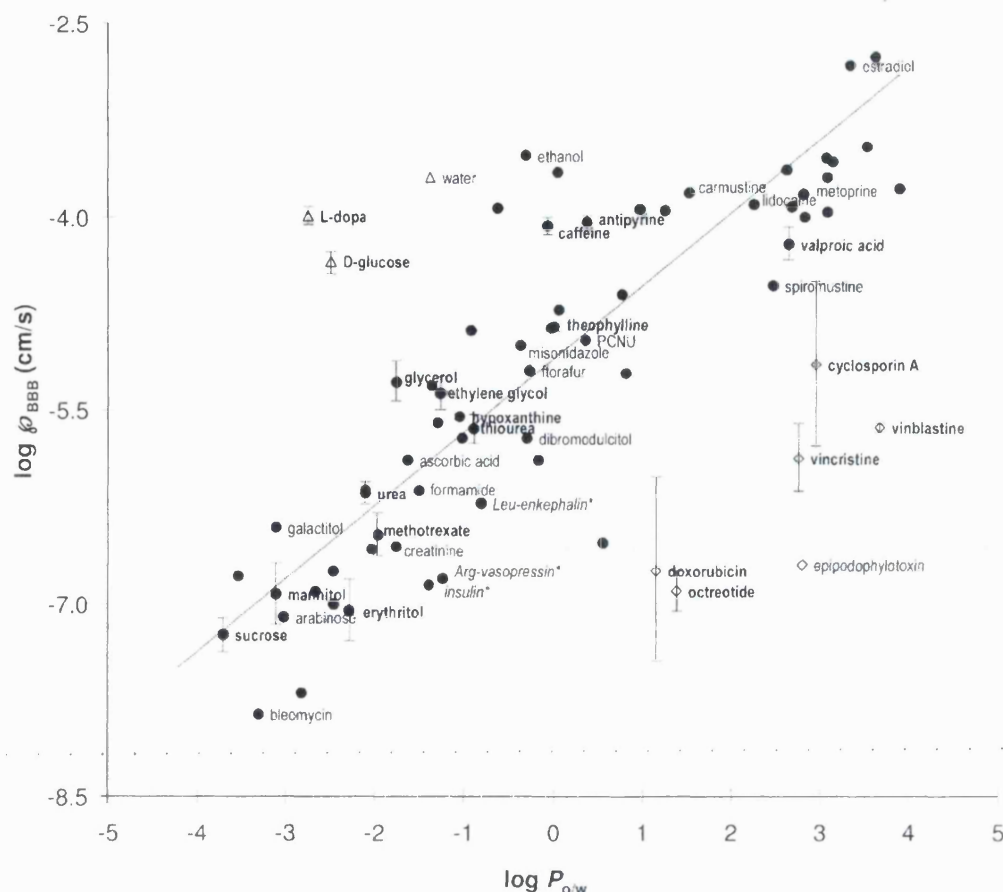


Figure 1.11: Graph of *in vivo* log permeability coefficient of rat brain capillaries (cm/sec) for several solutes as a function of lipid solubility determined in an octanol/water partition system ($\log P_{o/w}$). For many of these solutes (filled points), there is a clear correlation between lipid solubility and BBB penetration. There are several outliers shown as unfilled points. Glucose has a greater BBB penetration than its lipid solubility would suggest as the result of its facilitated transport across the cerebral endothelium. Strong deviants well below the regression line are all substrates for efflux transporters, principally P-glycoprotein. PCNU: 1-(2-chloroethyl)-3-(2,6-dioxo-1-piperidyl) 1-nitrosourea; *: Guinea pig; Compounds in italics: The Log distribution coefficient measured at physiological pH was used ($\log D_{o/w}$). (Reprinted with permission from: Blood-Brain Barriers: From Ontogeny to Artificial Interfaces. Edited by: R. Dermietzel, D. C. Spray, M. Nedergaard, Copyright© 2006 WILEY-VCH Verlag GmbH & Co. KGaA, Weinheim ISBN: 3-527-31088-6)

BBB permeation rates is probably due to steric hindrances and is common where the molecular weight of a compound exceeds 800-1000 Da. Peptide permeation of other cell monolayers has also been shown to be dependent on charge (Pauletti et al. 1997; Sorensen et al. 1997). Thus, the capacity of a peptide to cross the BBB and enter the brain is dependent upon several compositional factors, including size, flexibility, conformation, biochemical properties of amino acids, and the amino acids arrangement (Witt and Davis 2006).

Before peptides injected into the blood reach the CNS, they must withstand enzymatic degradation from the blood and brain capillary endothelium enzymes. The ability of the BBB, the choroid plexus, and the pericytes to transform and detoxify many substances entering the CNS has probably been underestimated in the past, as the transforming enzyme activity of the brain as a whole has usually been considered, which is low, rather than the activity of specific cell types or associations (Begley 2004). For several hydrolyzing and conjugating enzymes, the enzyme activity in the choroid plexus per unit weight of tissue is similar to that in the liver (Minn et al. 2000). BBB enzymes are known to degrade most naturally occurring neuropeptides (Brownless and Williams 1993; Witt et al. 2001).

Successful transcytosis of peptides to the BBB requires binding at the luminal side of the brain capillary endothelium, movement through the endothelial cytoplasm, and endocytosis at the abluminal of the BBB. However, peptides may bind to the luminal membrane of the brain capillary endothelium or undergo binding and endocytosis into the intracellular endothelial compartment without being transported into the CNS.

Peptide composition also determines, in part, the degree of protein binding, enzymatic stability, cellular sequestration, uptake into non-target tissue, clearance rate, and affinity for protein carriers (Witt and Davis 2006). Other aspects independent of peptide composition must also be considered, such as cerebral blood-flow, diet, age, sex, species (for experimental studies), dosing route, and effects of existing pathological conditions (Witt and Davis 2006). Each of these factors must be considered for a successful approach.

The BBB clearly changes in several brain diseases and a variety of pathological processes may either alter the quality of the barrier or contribute to the development of the disease process (Neuwelt 2004). Thus, the development of new drugs and drug-vectors must also contend with potential pathological conditions of the patient. Several disease states result in enhanced BBB permeability to fluid and/or solutes including hypoxia-ischaemia and inflammatory mechanisms involving the BBB in septic encephalopathy, HIV-induced dementia, multiple sclerosis and Alzheimer's disease. In Alzheimer's disease for example there is defective transport of amyloid- β by the BBB (Zlokovic 2004). In multiple sclerosis with active lesions an opening of the BBB can be

observed (Werring et al. 2000). Brain tumours affect the BBB integrity depending on the tumour type. It may appear normal and continuous with tight junctions or remain continuous but develop fenestrations or become discontinuous with or without fenestrations (Schlageter et al. 1999). Additionally, the robustness of the BBB may decline with age, although few studies are available (Preston 2001). The list of factors that may contribute to changes in drug bioavailability (changes in BBB cytoarchitecture, protein binding, receptor site, enzymes, etc.) during a pathological state is extensive and must be taken into account for appropriate drug design (Witt and Davis 2006). Specific changes at the BBB, such as opening/disruption of tight junctions, increased pinocytosis, changes in nutrient support, and pore formation may enhance/reduce drug uptake (Witt and Davis 2006).

It is obvious that currently existing drugs/biomacromolecules, especially peptides, are unable to overcome these structural and metabolic barriers to be delivered across the BBB in quantities sufficient to elicit a pharmacological response. Thus, there is a need for pharmaceutical formulations which can protect substances from degradation in the blood and in the BBB in sufficient amounts and at sufficient rates to be effective as well as generic strategies to modify the hydrophilic nature of compounds to allow transcytosis across the BBB.

1.4 Opioid receptors and Enkephalins

The opiate receptors contain seven transmembrane domains and belong to the family of the G protein-coupled receptors (GPCR) (Figure 1.12). They can be divided into μ -, δ -, κ - receptor sub-types (Deguchi et al. 2004). The N-terminal part of their protein chain is on the extracellular side of the membrane, the C-terminal part can be found inside the cell (Medzihradszky 2003). They are glycoproteins with the sugar components bound to asparagines residues as N-glycosides (Medzihradszky 2003). The C-terminal segment contains a palmitoyl chain, bound through a cysteine residue and submerged in the lipid layer. A cysteine residue binds the first and second extracellular loop (Medzihradszky 2003). Comparison of the structures of the three receptor types shows that the sequences of the transmembrane domains and of the intracellular loops are very similar, in some places even identical (Medzihradszky 2003). There are significant divergencies,

however, in the structures of the N- and C-terminal segments, and differences in chain length can also be found in these regions (Medzihradszky 2003). The longest is the μ -receptor (398 amino acids), shorter is the κ -receptor (380 amino acids), and the shortest is the δ -receptor (372 amino acids) (Medzihradszky 2003).

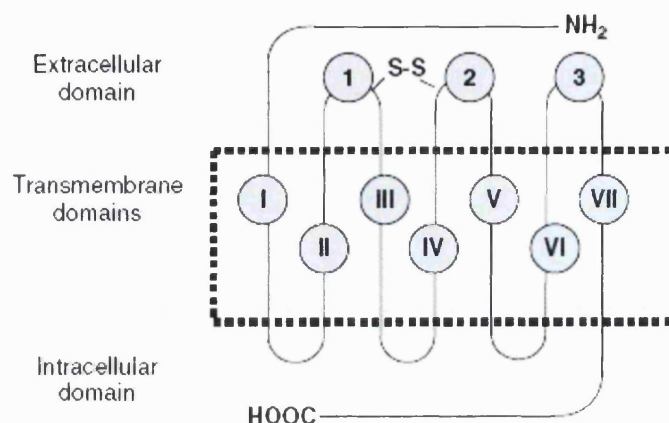


Figure 1.12: Position of opioid receptor in the cell membrane From: (Medzihradszky 2003)

The term “opioid” peptide has usually been applied to “naturally occurring peptides with opiate-like biological properties”. Opioid peptides have a direct effect on neurons via specific receptors, but also affect non-neural tissues and organs integrating brain and body functions. Neuropeptides may be divided into families with similar or identical genes that give rise to large precursor molecules, which after proteolytic cleavage produce several family members. The opiate family has 3 major branches: (i) the large precursor molecule, pro-opiomelanocortin (POMC) that contains three similar amino acid sequences of α -, β -, and γ -melanocyte-stimulating hormone (MSH), adrenocorticotrophic hormone (ACTH) and β -endorphin, (ii) the proenkephalin molecule that contains 6 copies of Methionine^[51]-Enkephalin and one of Leucine^[51]-Enkephalin, and (iii) the prodynorphin molecule that contains 3 Leucine^[51]-Enkephalin sequences (Figure 1.13) (Strand 1999). The opioid neuropeptides constitute a major subgroup of neuropeptides, composed of at least 20 neurotransmitter substances. Known members can be divided into five main groups: (i) the two pentapeptides, Methionine^[51]-Enkephalin and Leucine^[51]-Enkephalin (LENK) (Hughes et al. 1975), (ii) peptides that arise or are presumed to arise, from enkephalin precursors including 3 peptides arising from adrenal proenkephalin i.e. [Met]enkephaliny1-Arg-Phe, peptide E and the

presumed (not yet isolated) [Met]enkephaliny-Arg-Gly-Leu, and Dynorphin, α - and β -Neoendorphin and PH-8P, which may arise from other proenkephalins, (iii) β -Endorphin and the related α -, γ -, δ -endorphins, (iv) pronase-resistant peptides present in body fluids, e.g. β -Casomorphin-5 and -7 (in bovine milk) and possibly anodynin (in blood) and (v) various other peptides whose opiate-like properties do not arise from direct interaction with opiate or opiate-like receptors, e.g. kyotorphin, which seems to act via release of enkephalins and inhibition of enkephalin degradation (Morley 1983). They have three major characteristics in common; they are mostly inhibitory, they bind to opioid receptors of the postsynaptic membrane, and they serve as substance P agonists inducing analgesia (substance P is an 11 amino acids excitatory neuropeptide that acts as an important neurotransmitter in nociception) (Strand 1999).

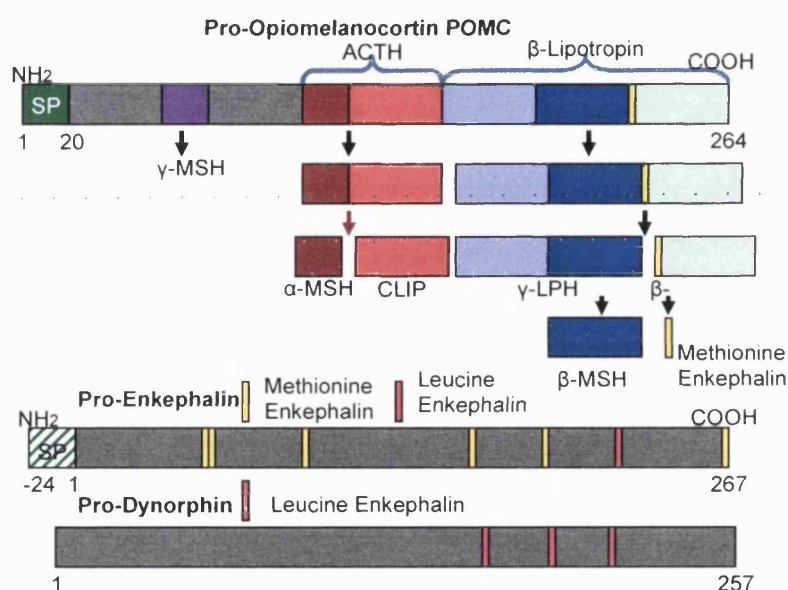


Figure 1.13: Structural relationships among the prohormone, precursor forms of the 3 major branches of the opiate peptides. The length in amino acid residues is indicated by the number at the corresponding C-terminus). SP: Substance P; MSH: Melanocyte-stimulating hormone; ACTH: Adrenocorticotrophic hormone Adapted from (Strand 1999).

The identification of the δ -opioid receptor followed the discovery of the first opioid receptor ligands, Methionine^[5]-Enkephalin [Tyr-Gly-Gly-Phe-Met] and Leucine^[5]-Enkephalin [Tyr-Gly-Gly-Phe-Leu] by Hughes and Kosterlitz and coworkers in 1975 (Hughes et al. 1975). It was shown that their pattern of agonist activity *in vitro* differed from that of the prototypical opioid ligands and naloxone, a nonselective opioid

antagonist, was less effective in blocking enkephalin-induced inhibition of the nerve-evoked contractions of the mouse vas deferens, compared with its antagonism of the response to normorphine (Lord et al. 1977; Corbett et al. 2006). They act as agonists at the opiate receptors and trigger a response cascade resulting in the relief of pain (Blomberg et al. 2006). The enkephalins are rapidly hydrolysed mainly *in vivo* (brain and periphery) by two well-defined enzymes, neutral endopeptidase and aminopeptidase N (Oliyai and Stella 1993).

Leucine^[51]-Enkephalin has been reported to be a δ -opioid selective peptide with an IC_{50} of 318 nM in the guinea pig ileum assay (GPI: rich in μ -receptors), an IC_{50} of 13 nM in the mouse vas deferens assay (MVD: rich in δ -receptors) [GPI/MVD (μ/δ) : 24] (Summers and Hayes 1981). Selective agonists of the δ -opioid receptor have potential advantages over the agonists that interact preferentially with the opioid μ - or κ -receptors, because the analgesia mediated through the δ -receptor does not appear to be accompanied with adverse side effects such as development of physical dependence, respiratory depression, constipation and others (Shenderovich et al. 2000). Thus, considerable effort has been made to find highly potent and selective ligands for the δ -opioid receptor. As a result, several attempts were made to create constrained analogs of the endogenous δ -opioid enkephalin peptides (Hughes et al. 1975).

Soon after the discovery of the two enkephalins X-ray crystallography revealed that Leucine^[51]-Enkephalin formed a (1-4) β -turn in the solid state (Smith and Griffin 1978). A beta-turn (β -turn) occurs where the polypeptide chain makes a sharp reversal by 180° within 4 residues. A turn is defined by 4 consecutive residues (i to i+3) if the Ca(i) to Ca(i+3) distance is less than 7 \AA and if the central 2 residues are not helical with an H-bond between the CO(i) and NH(i+3) (Figure 1.14) (Lewis et al. 1973; Wilmot and Thornton 1990). Based on this finding it was proposed that the flexible structures of the two enkephalins were stabilized in the bioactive conformation by forming an intermolecular hydrogen bond between the carbonyl oxygen atom in Tyr¹ and the amide NH in Phe⁴, thereby generating a β -turn conformation (Figure 1.14) (Aubry et al. 1989; Blomberg et al. 2006). Considerable efforts have been made to elucidate the bioactive conformation of the two ligands using spectral and computational techniques, including NMR spectroscopy in membrane mimicking environments (Behnam and Deber 1984;

Graham et al. 1992; Amodeo et al. 1998). However, in spite of all efforts a clear understanding of the bioactive conformation of the enkephalins has not yet been established (Blomberg et al. 2006).

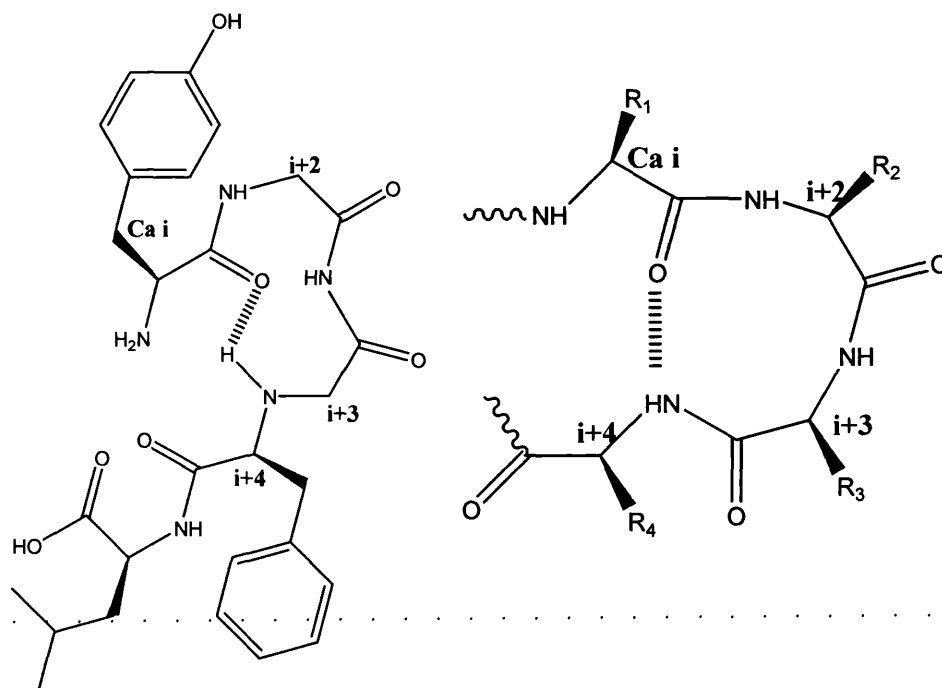


Figure 1.14: Left: Schematic of Leucine¹⁵-Enkephalin (1-4) β -turn. Right: General form of a β -turn. Ca or alpha carbon refers to the first carbon that attaches to a functional group (often a carbonyl).

A potent and highly selective cyclic peptide, DPDPE (Tyr-c[D-Pen-Gly-Phe-D-Pen]-OH), has been developed as a δ -opioid enkephalin peptide analog (Mosberg et al. 1983). Determination of the 3D pharmacophore of DPDPE remained a challenging problem due to an unconstrained mobility of the exocyclic N-terminal residue Tyr¹, and the Phe⁴ side chain group, that bear the main opioid pharmacophore groups (the α -amino group and the aromatic rings of Tyr¹ and Phe⁴), which assume quite different orientations depending on environmental conditions (Shenderovich et al. 2000). The presence of similar pharmacophore groups and the similar affinities of three non peptide ligands with high affinity for the δ -receptor, like 7-spiroindanyloxymorphone (SIOM), 2-methyl-4a- α -(3-hydroxyphenyl)-1,2,3,4,4a,5,12,12a- α octahydroquinolone [2,3,3,-g]isoquino-line (TAN-67) and oxymorbindole (OMI) allowed for the assumption that they might have a similar mode of binding to the opioid δ -receptor, and led to the determination of a 3D pharmacophore of the nonpeptide δ -opioid receptor ligands based

on the best fit conformation of the above mentioned 3 non-peptide ligands (Figure 1.15) (Shenderovich et al. 2000). Thus, the pharmacophore geometry is characterised by an average distance of 7.0 Å between two aromatic rings, by a distance of approximately 8.0 Å between the nitrogen atom and the second aromatic ring, and by the vector R1-R2-almost perpendicular to the plane N-R1-OH (Figure 1.15) (Shenderovich et al. 2000).

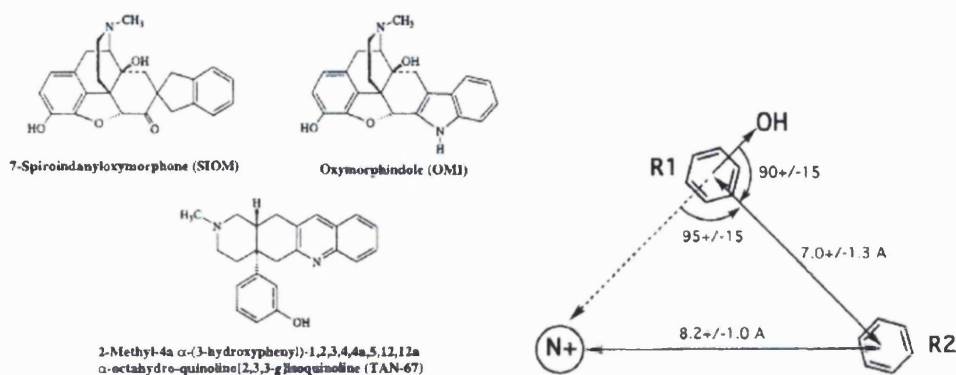


Figure 1.15: Right: Structure of the nonpeptide δ -opioid ligands. Left: δ -opioid pharmacophore geometry determined from the best-fit superposition of 3 nonpeptide ligands. From: (Shenderovich et al. 2000)

Finally, it has to be noted the β -turns are one such structural component that has been shown to enhance membrane permeability of peptides as they are more hydrophobic (Sorensen et al. 1997). Structural analyses of the cyclic aspartic acid containing hexapeptide (cyclo[Trp-Ala-Gly-Gly-Asn-Ala]) suggest that the existence of two β -turns explain its greater lipophilicity and increased transcellular flux across Caco-2 cells (Okumu et al. 1997). In another study, replacing an isoleucine residue with a glycine residue in a hydrophobic peptide, resulted in a β -turn that greatly enhanced membrane permeability across bovine brain microvessel endothelial cells (Sorensen et al. 1997).

1.5 Strategies available for BBB peptide (enkephalin) drug delivery.

Opioid peptide activity within the CNS is of particular interest for the treatment and management of pain, due to the elevated potency of peptides and the centrally mediated actions of pain processes (Witt and Davis 2006). However, peptides have seen limited use as clinically viable drugs for the treatment of pain mostly due to their poor

bioavailability due to low metabolic stability and high clearance by the liver. Furthermore, peptides as water-soluble compounds will not enter the CNS readily, via passive diffusion, due to the existence of the BBB. Delivery of therapeutic peptides to the CNS has seen varying levels of success and it can be divided into three general categories: (i) invasive procedures, (ii) physiologic-based strategies and (iii) pharmacologically-based approaches.

1.5.1 Blood-brain barrier modulation.

Invasive procedures, which include transient osmotic opening of the BBB (Kroll and Neuwelt 1998; Rapoport 2000), shunts (Alexander et al. 2000), and biodegradable implants (Emerich et al. 1999; Benoit et al. 2000) have been used for CNS delivery. Neurosurgical-based strategies include the opening of the BBB following intracarotid injection of hypertonic media (usually a 25% solution of mannitol infused into the carotid artery with a rate of 4-8mL/sec over 30 seconds) or the placement of intraventricular delivery catheters and continuous intraventricular drug infusion. These procedures often have a low therapeutic efficiency with substantial side-effects, while having the potential of being highly traumatic. Repetitive opening of the BBB with the injection of intracarotid hypertonic media has been associated with a high incidence of seizures as well as chronic neuropathologic changes in the brain (Neuwelt and Rapoport 1984; Salahuddin et al. 1988). The hypertonic solution is thought to osmotically pull water out of the endothelial cells, causing cell shrinkage, which may cause disengagement of the extracellular domains of the proteins forming and regulating the tight junctions (Begley 2004). The opening of the tight junctions of the BBB permits many undesirable substances even neurotoxic by-products of normal metabolic processes to cross the BBB along with the therapeutically beneficial molecule (Kroll and Neuwelt 1998).

The delivery of drugs by intraventricular infusion is complicated by the steep gradients of drug concentrations arising from the rapid bulk flow of CSF through the ventricular spaces and absorption into the peripheral circulation at the superior sagittal sinus, relative to the slow rates of peptide diffusion down into the brain parenchyma from the surface of the brain (Pardridge 1992). Thus, the limiting factor of invasive delivery strategies is that they rely on diffusion for drug penetration into the brain from the depot

site. Solute diffusion decreases with the square of the diffusion distance (Pardridge 2005). Therefore, the concentration of drug decreases logarithmically with each millimeter of brain tissue that is removed from the injection site, in the case of intracerebral implantation, or from the ependymal surface of the brain, in the case of intracerebroventricular infusion (Pardridge 2005) limiting peptide distribution beyond the surface of the brain. So, for example, the CSF compartment in the human brain contains approximately 140 ml and is turned over every four hours by absorption at the arachnoid granulations into the superior sagittal sinus and peripheral blood stream. Conversely, diffusion rates are relatively slow. For example, given a peptide with a molecular weight of 10,000 and a diffusion coefficient (D) of $1 \times 10^{-6} \text{ cm}^2 \text{ sec}^{-1}$, it may be calculated that it takes this peptide 2.9 days to diffuse 5 mm (Pardridge 1992). Thus, the peptide is more likely to exit the brain into the peripheral circulation following release into the ventricular compartment than it is to diffuse down into the brain parenchyma, where it is subject to sequestration by the cells in brain, thus impeding its further diffusion into brain parenchyma (Pardridge 1992).

While the risks involved with these invasive procedures are acceptable for life-threatening conditions, they are generally not justified for long-term or recurrent conditions that are less dramatic. Hence, less invasive, non-mechanical and safer strategies are required to enable therapeutic substances to transverse the BBB.

1.5.2 Physiological based strategies for BBB drug delivery.

Exploitation of the various nutrient, peptide and non-peptide hormones, and transport proteins carrier systems at the BBB (Begley 1996; Tsuji and Tamai 1999; Begley 2004; Tsuji 2005; Witt and Davis 2006) is a potential strategy that can be utilized for controlling the delivery of drugs into the brain. Eight separate transport systems have been identified and characterised in experimental animals and to a lesser extent in clinical studies, which are the following: (a) a hexose transport system that regulates the supply of D-glucose (GLUT-1); (b) a monocarboxylic transport system that is activated during starvation or other conditions leading to increased blood ketones in order to provide other nutrients (acetoacetic acid and beta-hydroxybutyric acid) in place of glucose and thereby maintain cerebral metabolism; (c) the choline transport system,

which has not been completely characterised but seems to be important in brain neurotransmitter metabolism; (d) the adenine transport system, which also regulates the entry of neurotransmitters into the brain, since it transports purine bases such as guanine and adenine; (e) the purine nucleosides and uridine that enter the brain by the nucleoside transport system; (f) the amino acids (AA) arginine, lysine, and ornithine that are transported by the basic amino acid transport system, an important system in normal protein metabolism; (g) the acidic AA transport system that, unlike the above carrier transport systems that operate in both directions across the BBB, actively pumps excitatory neurotransmitters out of the extracellular space of the brain into the blood; and (h) the neutral amino acid transport system that moves 14 AA from blood to brain (Pollay 1987; Neuwelt and Frenkel 1989).

Peptidomimetics must have a molecular structure mimicking the endogenous nutrient to enable the drug to be transported by one or more of the inwardly directed nutrient carriers. The first example is levodopa, a lipid insoluble precursor of dopamine that has been used for the treatment of Parkinson's disease, because it contains the carboxyl and α -amino groups that allow it to compete for transport across the BBB by the large neutral amino acid carrier (Witt and Davis 2006). Chemical groups could be designed in a way to be able to attach to specific pharmacologically active compounds rendering them substrates for carriers. Biphalin, a unique enkephalin analog ($\text{H}_2\text{N-Tyr}^1\text{-D-Ala}^2\text{-Gly}^3\text{-Phe}^4\text{-NH-NH-Phe}^{4'}\text{-Gly}^{3'}\text{-D-Ala}^{2'}\text{-Tyr}^{1'}$, Mouse vas deferens assay IC_{50} : 27 nM for Biphalin (Mollica et al. 2006) and 13 nM for Leucine^[5]-Enkephalin (Kane et al. 2006)) containing 2 enkephalin sequences linked by a hydrazide bridge has been shown to use the neutral amino acid carrier (Thomas et al. 1997). The hexose and large neutral amino acid carriers have the highest capacity and presently are the best candidates for delivery of substrates to the brain (Witt and Davis 2006). Peptides, which generally require low concentrations to induce effects can also utilise lower capacity carriers (Witt and Davis 2006). Targeting peptides to a specific nutrient transporter will require though good knowledge of both the peptide and the transporter. Nevertheless, these transport mechanisms may also be advantageous targets for prodrug and vector-mediated approaches to enhance peptide delivery to the brain (Witt and Davis 2006).

1.5.3 Pharmacological based strategies for BBB drug delivery.

Pharmacologically-based strategies aim to increase the passage through the BBB by increasing specific biochemical attributes of a compound. Peptide drug modification can be broadly divided into several categories: lipidisation, structural modification to enhance stability, glycosylation, increasing affinity for nutrient transporters, prodrugs, vector-based, cationisation, and polymer conjugation/encapsulation (Witt and Davis 2006). Additionally, modification of drug structure and/ or addition of constituents (i.e. lipophilicity enhancers, polymers, antibodies, etc.) may enhance drug concentration within the CNS while maintaining a reduced toxic profile. Table 1.1 provides a listing of these strategies to increase peptide uptake into the CNS, with associated advantages and limitations (Witt and Davis 2006).

Lipid solubility is a key factor in determining the rate at which a drug passively crosses the BBB. Heroin, a diacyl derivative of morphine, is a notorious example that crosses the BBB about 100 times more easily than its parent drug just by being more lipophilic (Misra et al. 2003). Peptide lipidisation involves the blocking of polar functional moieties on the peptide backbone with groups that greatly enhance the lipid solubility of the peptide. The presence of hydroxyl groups on peptides tends to promote hydrogen bonding with water leading to a concomitant decrease in the partition coefficient (i.e. lipophilicity) and resultant decrease in membrane permeability (Chikhale et al. 1994). Peptide drugs generally contain polar functional groups that impart an acidic or basic character based on the amino acids composition (Table 1.2) (Florence and Attwood). The overall balance of polar to nonpolar groups within a molecule can be reduced either by removal of a polar group or addition of a nonpolar group (Habgood et al. 2000). In addition, the relative positioning of polar to nonpolar amino acids (i.e., whether polar/nonpolar groups are at the centre or ends of a given peptide) will also determine the capability of a peptide to transport across a biological membrane (Habgood et al. 2000).

Table 1.1 Advantages and disadvantages of strategies to enhance CNS delivery (Witt and Davis 2006)

Strategy	Advantages	Limitations
Lipidisation	Increases membrane permeability	Increases plasma protein binding Intracellular sequestration Increased hepato-biliary elimination Non-specific targeting Receptor interference Increased size of molecule may counter membrane permeability enhancement
Structural modification to enhance stability	Increases stability Potential increase in mebrane transport Potential increase in receptor affinity	Potential decrease in membrane transport Potential decrease in receptor affinity
Glycosylation	Increases membrane permability Increases stability Increases serum-half life	Non-specific targeting Receptor interference
Nutrient trasport enhancement	Drug entry not dependent upon passivediffusion Potentially specific targeting	Limited capacity of carriers Potential interference with endogenous substrate of carrier Specificity of carrier Similarity of carrier mechanisms throughout body may reduce specificity of targeting

Table 1.1 Advantages and disadvantages of strategies to enhance CNS delivery (Witt and Davis 2006)

Strategy	Advantages	Limitations
Prodrug	Increases membrane permeability and/or pharmacokinetics	Kinetics of drug release must be precise
	Potential target specificity based on design of cleavable linker and/or enhancer moiety	Requires optimisation of linker and drug attachment
	"Redox" prodrugs lock drug in tissue	Charged "Redox" prodrugs are rapidly eliminated from body
Vector-based	Specific membrane targeting	Delivery to brain is directly limited to the transporter concentration
	Linker strategies may be incorporated to enhance stability and detachment of vector portion	Potential down-regulation of transporters with continual dosing
		Potential interference with endogenous substrate of carrier/transporter
		Requires optimisation of linker and drug attachment
		Altered pharmacokinetic profile
Cationisation	Increases membrane permeability	Increase plasma protein binding
	Increases serum-half-life	Immune complex formation
		Non-specific targeting
		Rapid elimination of charged moiety
Polymer conjugation/ Encapsulation	Increases stability	Hydrophobic polymers reduce membrane permeability
	Increases serum half-life	Decrease receptor binding with improper selection or placement of polymer
	Decreases elimination rate	Non-specific targeting
	Decreases immunogenicity / toxicity	
	Decreases protein binding	
	Potential for controlled release design	

Table 1.2 : Polarity, Hydrophobicity, pKa and Isoelectric point (IP) of Natural Amino Acids (Florence and Attwood; Jmol 2008)

	Side Chain	Log P	Hydrophobic Character	pK ₁ (COOH)	pK ₂ (NH ₃ ⁺)	pK ₃	IP
Most Hydrophobic							
Isoleucine	I CH ₃ CH ₂ CH(CH ₃)-	-1.7	1.83	2.36	9.68	-	6.02
Leucine	L CH ₃ CH(CH ₃)CH ₂ -	-1.52	1.8	2.36	9.6	-	5.98
Phenylalanine	F C ₆ H ₅ CH ₂ -	-1.38	1.69	1.83	9.13	-	5.48
Tryptophan	W C ₆ H ₄ -NH-CH=C-CH ₂ -	-1.05	1.35	2.38	9.39	-	5.89
Valine	V CH ₃ CH(CH ₃)-	-2.26	1.32	2.3	9.62	-	5.96
Methionine	M CH ₃ -S-CH ₂ CH ₂ -	-1.87	1.1	2.28	9.21	-	5.74
Proline	P HN-(CH ₂) ₃ -	-2.54	0.84	1.99	10.96	-	6.3
Cysteine	C HSCH ₂ -	-2.49	0.76	1.96	8.18	10.28 (SH)	5.07
Tyrosine	Y HOC ₆ H ₅ CH ₂ -	-2.26	0.39	2.2	9.11	10.07 (OH)	5.66
Alanine	A CH ₃ -	-2.85	0.35	2.34	9.69	-	6
Glycine	G -	-3.21	0	2.34	9.6	-	5.97
Threonine	T CH ₃ CH(OH)-	-2.94	-0.27	2.71	9.62	-	6.16
Serine	S HOCH ₂ -	-3.07	-0.63	2.21	9.15	-	5.68
Histidine	H HN-CH=N-CH=C-CH ₂ -	-3.32	-0.65	1.82	6	9.17 (NH ₃ ⁺)	7.59
Glutamine	Q H ₂ NCOCH ₂ CH ₂ -	-3.64	-0.93	2.17	9.13	-	5.65
Asparagine	N H ₂ NCOCH ₂ -	-3.82	-0.99	2.02	8.8	-	5.41
Lysine	K H ₃ N ⁺ -CH ₂ CH ₂ CH ₂ CH ₂ -	-3.05	-1.54	2.18	8.95	10.53 (ε-NH ₃ ⁺)	9.74
Glutamic Acid	E HOOCCH ₂ CH ₂ -	-3.69		2.19	4.25	9.67 (NH ₃ ⁺)	3.22
Aspartic Acid	D HOOCCH ₂ -	-3.89	-3.38	1.88	3.65	9.6 (NH ₃ ⁺)	2.77
Arginine	R H ₂ N-C(NH)NH-(CH ₂) ₃ -	-4.2					
Least Hydrophobic							

Addition of methyl groups has been shown to reduce hydrogen bonding potential. Dimethylation of the tyrosine on the opioid peptide DPDPE ($\text{H}_2\text{N-Tyr}^1\text{-D-Pen}^2\text{-Gly}^3\text{-Phe}^4\text{-D-Pen}^5\text{-OH}$) resulted in a 10-fold increase in the potency over the nonmethylated DPDPE at the delta opioid receptor and a 35-fold increase in potency at the μ -opioid receptor, while substantial delta receptor selectivity was maintained (Hansen et al. 1992; Witt and Davis 2006). Thus, methylation elicited a peptide with enhanced bioavailability and analgesic potency. In another study, trimethylation of the phenylalanine of DPDPE resulted in enhanced lipophilicity and BBB permeability while also reduced the P-gp affinity and thus efflux of the peptide (Witt et al. 2000). The metabolism and analgesic properties of the modified peptide were altered and dependent on the diastereoisomer configuration of the nonaromatic methyl group (Witt et al. 2000). Therefore, the stereoselectivity of the peptide needs also to be assessed for optimal bioavailability and receptor binding affinity.

Halogenation of peptides such as DPDPE (Weber et al. 1991; Weber et al. 1993), DPLPE (Gentry et al. 1999) and biphalin (Abbruscato et al. 1996) has been shown to significantly enhance lipophilicity and BBB permeability in a manner dependent upon the conjugated halogen (Cl, Br, F, I) (Witt and Davis 2006). Addition of chlorine on the Phe^4 residue of DPDPE led to significant increase in BBB permeability which was further increased by addition of 2 chlorine atoms in both *in vivo* and *in vitro* studies (Weber et al. 1991; Weber et al. 1993). Similarly, chlorinated biphalin possessed increased BBB permeability both *in situ* and *in vitro* (Abbruscato et al. 1996). However, fluorine addition to DPDPE did not increase the lipophilicity, while fluorine addition to biphalin greatly diminished BBB permeability.

Acylation or alkylation of the N-terminal amino acid has been shown to increase lipophilicity and membrane permeability while minimally interfering with receptor binding. Acyl derivatives of DADLE ($\text{H}_2\text{N-Tyr}^5\text{-D-Ala}^4\text{-Gly}^3\text{-Phe}^2\text{-Leu-OH}$) (Bak et al. 1999; Uchiyama et al. 2000), DPDPE (Bundgaard and Moss 1990), thyrotropin-releasing hormone (TRH) (Bundgaard and Moss 1990; Yamamoto 1998) and insulin (Asada et al. 1995) synthesised by creating of an amide bond in the C- or N-terminal or the free amine of a lysine residue have also shown improved absorption through artificial and biological membranes and enhanced enzymatic stability, while retaining

pharmacological activity. Addition of a palmitic tail to Bowman-Birk protease inhibitor has been achieved via a disulfide bond and has been shown to increase the *in vitro* uptake 140-fold into Caco-2 cells (Ekrami et al. 1995). Increased chemical and enzymatic stability was shown for phenolic esters of a Leucine^[5]-Enkephalin analog (Tyr-D-Ala-Gly-Phe-Leu-NH₂) with the O-pivaloyl ester having enhancing transport properties across Caco-2 monolayers (Fredholt et al. 2000). Furthermore, the hypoglycaemic effect of the mono palmitoylated derivative of insulin was more prolonged *in vivo* after IV administration (Hashimoto et al. 1989)

Point modifications of a BBB-impermeable polypeptide, horseradish peroxidase (HRP), with lipophilic (stearoyl) or amphiphilic (Pluronic block copolymer) moieties considerably enhance the transport of this polypeptide across the BBB and accumulation of the polypeptide in the brain *in vitro* and *in vivo*, while maintaining its enzymatic activity (Batrakova et al. 2005). The modifications of the HRP with amphiphilic block copolymer moieties through degradable disulphide links resulted in the most effective transport of the HRP across *in vitro* brain microvessel endothelial cell monolayers and efficient delivery of HRP to the brain (Batrakova et al. 2005). Stearoyl modifications of HRP improved its penetration by about 60% but also increased clearance from blood (Batrakova et al. 2005). Pluronic modifications increased penetration of the BBB and had no significant effect on clearance so that uptake by brain was almost doubled (Batrakova et al. 2005).

Increase of lipophilicity has been shown to be impaired by the chemical modification with other more bulky moieties. Subcutaneous administration of a 1-aminoadamantane hydrochloride DADLE analog via ester, amide or carbamate bonds has been shown to elicit a statistical significant increase in antinociception as measured by the tail pressure test (Tsuzuki et al. 1991). Another lipophilic prodrug of DADLE created by esterification of the free C-terminal with cholesterol and by amidation of the free N-terminus with the 1,4-dihydrotrigonellinate redox targetor (retrometabolic design) (Bodor et al. 1992) was documented to gain access to the brain via passive nonsaturable processes *in vivo*. The modified peptide enters the brain due to its increased lipophilicity. Then, the targetor moiety undergoes an enzyme-mediated oxidation that converts the dihydrotrigonellinate to the hydrophilic, membrane-impermeable trigonellinate ion, trapping the prodrug behind the BBB

(Bodor et al. 1992). Increased antinociception was shown for this prodrug approach after IV administration of a formulation of the prodrug in a vehicle (mixture of dimethylsulfoxide, ethanol, and 50% aqueous 2-hydroxypropyl- β -cyclodextrin solution) (Bodor et al. 1992). Retrometabolic design was also applied to another centrally active thyrotropin-releasing hormone with success (Prokai et al. 1994).

The oral bioavailability of a dermorphin tetrapeptide analog (N^{α} -1-iminoethyl-Tyr-*D*-Met-O²-Phe-Me β Ala-COOH) was improved by increasing its lipophilicity by esterification of the C-terminal carboxyl group and/or acylation of the phenolic hydroxyl group on tyrosine (Ogawa et al. 2003). Dermorphin, is a natural opiate tetrapeptide that was isolated from the skin of the South American frog. It binds selectively to the μ opioid receptor, with a potency 30-40 times that of morphine (Broccardo et al. 1981). Dermorphin tetrapeptide analogues are known to be highly stable against enzymatic degradation, attributing their low oral bioavailability to low intestinal absorption (Sasaki et al. 1985; Marastoni et al. 1987; Chaki et al. 1990; Ogawa et al. 2003). Derivatives with acylation of the phenolic hydroxyl group on Tyr¹ showed better results than derivatives with esterification of the C-terminal carboxyl group (Ogawa et al. 2003) by the tail pressure test (which is sensitive to μ - as well as κ -receptor agonists unlike the tail-flick test).

A reversible aqueous lipidisation (REAL) strategy has been used to deliver small peptides like Leucine^[5]-Enkephalin (LENK) and salmon calcitonin orally (Wang et al. 2003; Wang et al. 2006). This strategy involved in the case of Leucine^[5]-Enkephalin (LENK) lipidising the free N-terminus of the peptides with an amine reacting lipophilic dimethylmaleic anhydride analog 3, 4-bis (decylthiomethyl)-2,5-furandione (Wang et al. 2006). It is well known that while the C-terminal of LENK tolerates certain structural modifications, the free α -amino group at the N-terminal of LENK is absolutely required for binding to opioid receptors. Removal of the α -amino group or irreversible capping by acylation abolishes or greatly compromises its receptor binding affinity and thus reduces its pharmacological activity (Buscher et al. 1976; Bewley and Li 1983; Uchiyama et al. 2000). However, bioconversion by small intestine mucosal and liver homogenates and rapid hydrolysis in acidic conditions was shown for this prodrug (Wang et al. 2006). REAL-LENK (the produced lipidised pro-drug) demonstrated that significantly higher and sustained plasma peptide levels were

detected up to 24h and enhanced antinociception in the hind paw formalin pain model following oral administration. The authors concluded that the antinociception is elicited by peripheral opioid receptors and that brain uptake of [¹²⁵I]-REAL-LENK was low and not statistically different from that of [¹²⁵I]-LENK indicating limited CNS penetration (Wang et al. 2006).

Lipidisation with these and other strategies still poses certain limitations. Since highly soluble drugs may be extensively plasma protein-bound, there is the potential for a reduction in the amount of free or exchangeable drug in the plasma, therefore compromising brain uptake (Audus et al. 1992). *In vivo* studies of BBB permeability can differ from *in vitro* studies due to clearance, serum protein binding, and tissue sequestration that can influence *in vivo* results. Lipophilic modifications are known to increase the ability of compounds to cross the BBB while decreasing the amount of compound accumulated by brain (Batrakova et al. 2005). This paradoxical effect occurs because lipophilic modifications increase unspecific uptake reducing the amount of the compound available for transport across the BBB. If the decrease in the amount of compound available for transport exceeds the increase in transport rate, the net effect is to decrease the amount of compound taken up by the brain (Batrakova et al. 2005). The site of modification or attachment of substances/molecules to increase lipophilicity must also be taken into account, as receptor binding affinity may be diminished if alterations are within the pharmacophore region, thus reducing biological activity (Witt and Davis 2006). On the other hand, enhancement of lipophilicity alone may not necessarily improve BBB transport. Factors such as size, stability, intracellular sequestration, nontarget organ uptake, efflux rates and P-glycoprotein (P-gp) efflux activity must also be considered (Witt and Davis 2006).

Structural changes aimed in reducing enzymatic degradation *in vivo* involve simple additions that chemically protect the targeted bond from attack, to its replacement altogether, to global changes that, instead, modify the peptide conformation in such a way that is no longer recognised by the protease concerned (Pauletti et al. 1997). These modifications require extensive analytical investigation to define the site of enzymatic cleavage and the proteolytic enzymes that act upon a specific peptide (Pardridge 1991). However, even modest structural changes near the scissile peptide bond can result in significant conformational changes (Pauletti et al. 1997). The

introduction of steric bulk in the form of an N-alkyl (usually methyl group) or quaternary amino acid can slow the addition of an enzymatic nucleophile to a peptide bond (Figure 1.3) (Pauletti et al. 1997). Care must be taken as such modifications may result in reduced biological activity. Opioid peptides require the amino terminus to be free for effective receptor binding (Bewley and Li 1983; Chaturvedi et al. 2000).

Sometimes, conformation changes and altering chirality of amino acids rather than the replacement of a functional group by a less labile structure can be the driving force behind peptidomimetic design (Pauletti et al. 1997). Since smaller peptides can occupy a large portion of conformational space, it is likely that different global conformations might be responsible for interactions at different macromolecule targets, including protease enzymes (Pauletti et al. 1997). Constraining the peptide backbone into a particular conformation to mimic secondary structure such as a β -turn has been used as one of these strategies (Pauletti et al. 1997). Cyclisation of peptides may reduce hydrogen bonding, increase lipophilicity, and reduce the hydrodynamic radius in solution, thereby enhancing membrane permeability (Knipp et al. 1997; Borchardt 1999; Wang et al. 1999). A simple and effective strategy is to cyclise the peptide using a covalent linkage; possible attachments include the amide nitrogen, the α -carbon or a side chain (Toniolo 1990). Figure 1.16 illustrates some approaches utilised to mimic the β -turn peptide secondary structure.

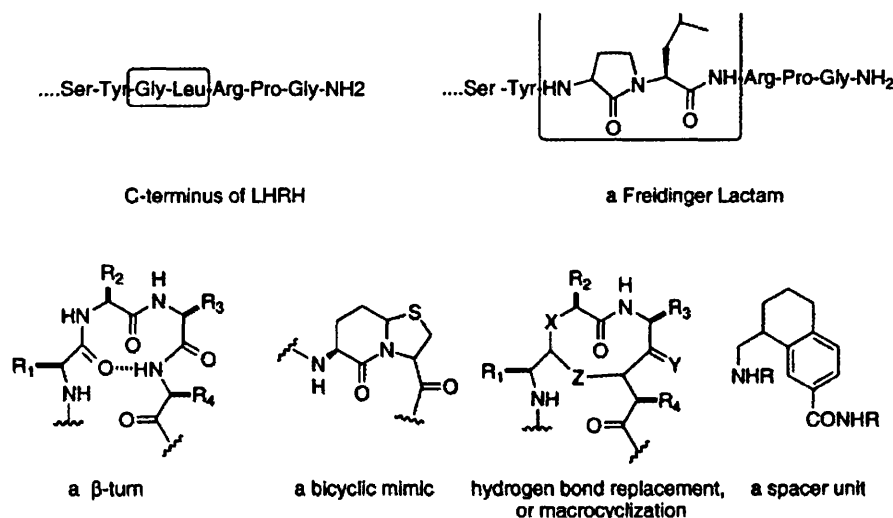


Figure 1.16: Cyclisations as examples to constrain the peptide backbone into a particular conformation. Cyclic peptides/peptidomimetics exhibit metabolic stability against exopeptidases due to protected C- and N-terminal ends (Pauletti et al. 1997).

A subtler introduction of chemical bulk would entail the use of a D-amino acid or a residue containing an unnatural side chain, in the hope that the peptidase (aminopeptidase) would not tolerate moving steric bulk from one face of the enzyme to the other. Substitution of the L-Glycine (L-Gly²) residue in the second position in the structure of Methionine^[5]-enkephalin with a D-Alanine (D-Ala²) residue, and amidation of its C-terminus, produce greater enzymatic stability (Roemer and Pless 1979). Similarly, the substitution of D-Ala² and D-Leucine⁵ (D-Leu⁵) DADLE has been shown to significantly increase half-life by reducing enzymatic proteolysis (Uchiyama et al. 1998). Modifications of amino acids or attachment of secondary structures onto peptides within these regions may also reduce enzyme degradation (Witt and Davis 2006).

The use of a disulphide bridge constrained peptide analogs has been shown also to significantly reduce enzymatic degradation (Weber et al. 1991; Weber et al. 1992) with the potential advantage of enhanced specificity for receptor subtypes. In the case of the linear Methionine^[5]-enkephalin, the conversion into the cyclic analog DPDPE (Figure 1.17) resulted in a δ -opioid-specific peptide (Knapp et al. 1991) with a saturable mode of transport at the BBB (Kalyanasundaram and Thomas 1977; Liao et al. 1998; Eggleton and Davis 1999). Due to the incorporation of 2 D-penicillamine (D-Pen) residues and conformational restriction by a disulphide bridge, DPDPE is enzymatically stable (Weber et al. 1992; Brownson et al. 1994).

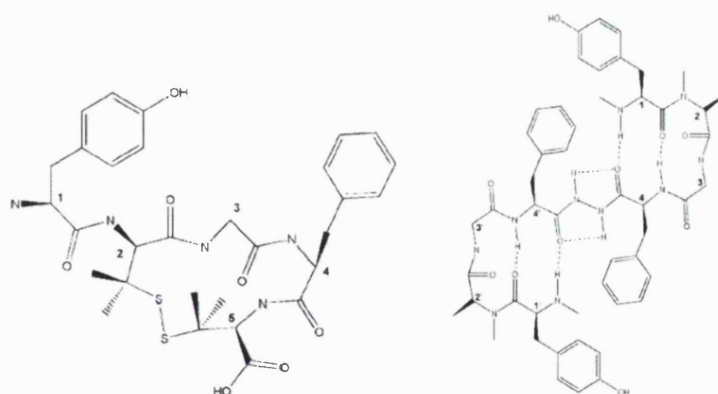


Figure 1.17: Left: Structure of DPDPE. Right: Structure of Biphalin

Biphalin (H₂N-Tyr¹-D-Ala²-Gly³-Phe⁴-NH-NH-Phe^{4'}-Gly^{3'}-D-Ala^{2'}-Tyr^{1'}) (Figure 1.17) possess two biologically active pharmacophores with affinity for both μ - and δ -

opioid receptors (Lipkowski et al. 1982; Lipkowski et al. 1982; Romanowski et al. 1997). Administered intracerebroventricularly in mice, biphalin was 6.7- and 257-fold more potent than etorphine or morphine, respectively, in eliciting analgesia (Horan et al. 1993). Biphalin is protected from aminopeptidase activity by D-Ala residues in the 2 and 2' positions and is protected from carboxypeptidase activity by the hydrazide bridge (Witt and Davis 2006).

Glycosylation (i.e the addition of carbohydrate moieties to a peptide) induces changes in the molecular structure of a peptide that alter dramatically their pharmacodynamic and/or pharmacokinetic properties (Lis and Sharon 1993). Glycosylation of enkephalins increases their BBB penetration and results in pharmacologically active glycopeptide analogs (Witt and Davis 2006). Different sugar moieties have been investigated, including glucose and xylose, exhibiting variations in BBB permeability (Egleton et al. 2000). Analgesia enhancement of opioid glycopeptides may be due to increased bioavailability of glycopeptides via higher metabolic stability (Powell et al. 1993), reduced clearance (Fisher et al. 1991), and improved BBB transport (Egleton et al. 2000). An enhanced analgesic profile has also been shown for glycosylated deltorphin (Tomatis et al. 1997; Negri et al. 1999), cyclised Methionine^[51]-enkephalin analogs (Polt et al. 1994; Egleton et al. 2000), and linear leucine enkephalin analogs (Bilsky et al. 2000). The glycosylated Leucine^[51]-enkephalin amide [H₂N-Tyr-D-Thr-Gly-Phe-Leu-Ser(βD-Glc)-CONH₂] elicits analgesic effects similar to morphine (even when administered peripherally) with reduced dependence as indicated by naloxone-precipitated withdrawal studies (Egleton et al. 2000). The mode of enhanced transport for glycopeptides is still not known, but it is thought to be unrelated to increased lipophilicity as octanol/saline distribution studies indicated that the addition of glucose significantly reduced lipophilicity, thereby reducing passive diffusion (Egleton et al. 2000). Glycosylated analogues of Methionine^[51]-Enkephalin are transported via the hexose transporter GLUT-1 (Polt et al. 1994; Tsuji and Tamai 1999) and endocytotic mechanisms have been shown to transport glycosylated peptides (Broadwell et al. 1988; Witt and Davis 2006). However, producing amphipathic glycopeptides (possessing one hydrophilic and one highly lipophilic part) is not adequate to enhance systemic delivery and BBB permeability. The glycopeptide sequence must be capable of assuming a water-soluble random coil conformation (i.e.

“biousian” activity), comparable to micelle formation, and the barrier between the 2 states must be low enough for rapid interconversion between the 2 states (Egleton et al. 2005; Witt and Davis 2006). It was proposed that some glycopeptides promote a negative membrane curvature leading to an increased rate of endocytosis, which in turn results in enhanced BBB transport (Egleton et al. 2005; Witt and Davis 2006).

A disadvantage of glycosylation is a reduction in μ -opioid receptor, while there is virtually no effect on δ binding or efficacy (Elmagbari et al. 2004; Witt and Davis 2006). This finding is consistent with Schwyzer’s membrane compartment theory (Sargent and Schwyzer 1986), which suggests that the μ -opioid receptor binding site resides in a more hydrophilic environment than the binding site for the δ -opioid receptor (Kane et al. 2006; Witt and Davis 2006). This is important because, the primary analgesic action of opioid-based drugs is thought to be regulated through the μ -opioid receptor (Witt and Davis 2006).

.....

The rationale for prodrug design is to optimise the structural requirements necessary to target the receptor of interest by conjugating the pharmacologically active moiety to a known transporter or a lipophilic enhancer that can be cleaved to yield the active drug. Ideally a prodrug is enzymatically stable in the blood, but rapidly degraded to the active parent compound when it reaches the site of action. Esterification is a promising strategy for prodrug design due to the abundance of endogenous esterases in the brain. Esterification or amidation of amino, hydroxyl, or carboxylic acid-containing drugs may greatly enhance lipophilicity, and thus brain permeability (Ghosh and Mitra 1992; Lambert et al. 1995). Hydrolysis of the ester or amide bond releases the active compound once the prodrug enters the brain. Both aromatic benzoyl esters (Ghosh and Mitra 1992) and branched chain tertiary butyl esters (Greig et al. 1990) have shown stability in plasma, while still remaining adequately cleaved within the CNS (Witt and Davis 2006). The addition of a Phenylalanine (lipophilic) amino acid as a cleavable unit to DPDPE at the amino terminal resulted in enhanced permeability at the BBB (Greene et al. 1996). Chains of nonpolar amino acids could further enhance lipophilicity, although the balance between molecular size and degree of lipophilic enhancement must be assessed individually (Witt and Davis 2006).

Another prodrug approach used the redox system (Bodor et al. 1975; Prokai et al. 2000), in which a lipophilic attachment (e.g., 1, 4-dihydrotrigonelline) is converted to the hydrophilic quaternary form, effectively “locking” the drug in the tissue (Bodor and Buchwald 1999). The drug is conjugated to a methyl dihydropyridine carrier and subsequently oxidised by NADH-linked dehydrogenases in the brain resulting in quaternary ammonium salt, which cannot cross back through the BBB endothelium (Brewster et al. 1988). This strategy has been applied to a wide variety of drugs, such as steroids, antivirals, neurotransmitters, anticonvulsants, and peptides (Leucine^[5]-Enkephalin analog) (Bodor and Buchwald 1999; Witt and Davis 2006). Disadvantages of this strategy include the non-specificity and the rapid elimination of the charged salt form (Witt and Davis 2006), while careful choice of the cleavable moieties and point of their attachment to the active pharmacophores is required for an optimised pharmacokinetic profile.

Cationisation of peptides is a method to increase membrane permeability via absorptive-mediated endocytosis (AME) (Vehaskari et al. 1984; Hardebo and Kahrstrom 1985; Pardridge et al. 1995; Deguchi et al. 2004; Abbott et al. 2006) as the BBB endothelium possesses anionic sites that attract cationic substances to the membrane surface (Chakrabarti and Sima 1990). Ebitatide, an adrenocorticotrophic hormone (ACTH) analog and a dynorphin-like analgesic peptide, E-2078 are polycationic peptides at physiologic pH that are transferred across the BBB via AME (Terasaki et al. 1989; Terasaki et al. 1992; Yu et al. 1997). The μ -selective [D-Arg²]-demorphin tetrapeptide analogs H-Tyr-D-Arg-Phe-Sar-OH, and H-Tyr-D-Arg-Phe- β -Ala-OH (TAPA) were developed (Ukai et al. 1995), showing potent analgesic activity with low physical and psychological dependence (Paakkari et al. 1993). TAPA was reported to cross the BBB via AME triggered by binding of the peptides to negatively charged sites on the surface of brain capillary endothelial cells (Deguchi et al. 2003). However, two additional [D-Arg²]-demorphin analogs were designed (N α -amidino-Tyr-D-Arg-Phe- β -Ala-OH (ADAB) and N α -amidino-Tyr-D-Arg-Phe-Me β -Ala-OH (ADAMB) that exhibited a slower degree of analgesic onset due to the parallel decrease in AME across the BBB (Deguchi et al. 2004). AME is not very specific, but the higher capacity of AME, compared to receptor-mediated transcytosis, could be a

favourable property for the delivery of peptides to the brain (Tsuji and Tamai 1999; Pardridge 2001).

Cationised albumin displayed a longer serum half-life and a general selectivity to the brain (Bickel et al. 2001). Additionally, when cationised albumin was conjugated to β -Endorphin, it yielded increased uptake into isolated brain endothelial cells, as compared to β -Endorphin alone by AME (Kumagai et al. 1987; Pardridge et al. 1990). However, cationised albumin has been shown to be significantly cleared by the kidney and liver, posing a potential toxicological threat as well (Bergmann et al. 1984; Pardridge et al. 1989; Bickel et al. 2001; Witt and Davis 2006). This approach is also non-specific when compared to tissue uptake, unless additionally coupled to a selective vector (Witt and Davis 2006).

Unfortunately, cationised proteins have been shown to induce immune complex formation with membranous nephropathy (Adler et al. 1983; Feng et al. 2004), and increased cerebral and peripheral vascular permeability (Nagy et al. 1983; Vehaskari et al. 1984; Hardebo and Kahrstrom 1985), limiting the therapeutic applications of this strategy.

Polymer conjugations are used to increase peptide stability, reduce elimination, and reduce immunogenicity (Witt and Davis 2006). Chemical modification of peptides with macromolecular polymers, such as poly(ethylene glycol) (PEG) (So et al. 1999; Tsutsumi et al. 2000) and poly(styrene maleic acid) (Duncan 1992; Mu et al. 1999) is a promising strategy. PEG linear or branched chains conjugated to a peptide alter its pharmacokinetic profile, while maintaining theoretically its pharmacological activity. PEG conjugation masks the peptide's surface and increases the molecular size, thus reducing the immune response to the peptide (by shielding immunogenic epitopes), enzymatic degradation, toxicity, and renal ultrafiltration (Reddy 2000). Pegylation of the opioid peptide DPDPE with a 2 kDa PEG moiety on the terminal tyrosine decreased clearance, reduced plasma protein binding, and first-pass elimination while increasing the analgesic effect following intravenous administration (Witt et al. 2000; Witt et al. 2001). BBB permeability of the pegylated form was not significantly different when compared with the native form, despite enhanced hydrophilicity conferred by the PEG moiety, possibly due to an association with the saturable

mechanism observed at the BBB (Kalyanasundaram and Thomas 1977) or a reversal of P-gp affinity (Chen and Pollack 1998) of the native compound (Witt and Davis 2006). The principle disadvantages of pegylation of peptides regarding CNS focused delivery is the potential loss of activity with improper choice of PEG (length, branching), choice of linker and choice of attachment site followed by the enhanced hydrophilicity and molecular size of the peptide (Witt and Davis 2006).

Encapsulation of hydrophilic drugs in liposomes or polymeric nanoparticles could be a useful alternative for their brain targeting as the entrapped drug is protected from the administration site to the CNS, where it can be released and / or transported across the BBB.

Liposomes are composed of a phospholipid bilayer that may act as a carrier for both hydrophilic and hydrophobic drugs. The beneficial attributes of liposomes are enhanced plasma half-life, decreased clearance, and decreased toxicity of associated drugs (Reddy 2000). One such liposome formulation is the pluronic copolymer P85, a self-forming micelle preparation that encapsulates a drug. The P85 formulation has been shown to enhance the delivery of digoxin into the brain (Batrakova et al. 2001), and to enhance the analgesic profile of Biphalin, DPDPE, and morphine (Witt et al. 2002) with the mechanism of action hypothesised to be the inhibition of P-gp activity, yet may also result in undesired responses within the endothelium (Batrakova et al. 2004). However, loading of hydrophilic compounds in liposomes is poor (< 25%) in the majority of formulations (Lutsiak et al. 2002).

Nanoparticulate delivery of peptides involves formulations that peptides can be bound in the form of a solid solution or dispersion, or they can be absorbed to the surface of the particle or chemically attached (Kreuter 2001). Polymeric nanoparticles used for brain delivery successfully have been coated with surfactants. It is known that the surfactant contact angle may be indicative in predicting the body distribution of the coated nanoparticles (Troster and Kreuter 1988). A series of poloxamers (Pluronic[®]) (poloxamer 188, 407, 184, 338, and poloxamine 908), polysorbates (Tween[®]) (polysorbate 20, 60 and 80), and Brij[®] 35, were used as coating material to poly(methyl methacrylate) (PMMA) nanoparticles of 131 +/-30 nm in size to investigate the possible correlation between the nanoparticle surface properties and

their *in vivo* biodistribution (Troster et al. 1990). The results indicated that: (i) no correlation exists between the body distribution pattern and the contact angle of the nanoparticle coating materials; (ii) although all used surfactants decreased the liver uptake and increased the uptake in other organs and tissues, poloxamer 338 and poloxamine 908 were the most powerful surfactants in enhancing nanoparticle blood levels and in increasing the spleen uptake while reducing the liver uptake; (iii) P80 and poloxamer 184 yielded the highest accumulation in the heart, muscles, kidneys, and the brain. Thus, it was thought that polysorbates and poloxamers could be useful for specific targeting to non-reticuloendothelial organs (Troster et al. 1990). The total nanoparticulate brain amount was increased with all surfactants up to 24 hours, especially by polysorbates 60 and 80, poloxamers 407, 184, and 338 and poloxamine 908 (Troster et al. 1990).

Poly (butylcyanoacrylate) [PBCA] nanoparticles represent the only successful example of *in vivo* delivery of peptides to the brain. This polymer has the advantage of being biodegradable. Dalargin (Tyr-D-Ala-Gly-Phe-Leu-Arg), a Leucine^[5]-Enkephalin analogue peptide, which exhibits potent analgesic activity after intracisternal administration, but not after IV administration, induced a prolonged central analgesia by the IV route when loaded onto polybutylcyanoacrylate (PBCA) nanoparticles of a size around 250 nm overcoated with polysorbate 80 (hydrophilic surfactant) as demonstrated by the hot plate and the tail-flick test (Alyautdin et al. 1995; Kreuter et al. 1995; Kreuter et al. 1997; Olivier et al. 1999; Kreuter 2001). However, less than 1% w/v of poly(methylmethacrylate) nanoparticles coated with polysorbate 80 were found to be in the brain (including brain vessels and parenchyma) after IV administration, most of them ending up in the lung, the liver and the spleen, due to their uptake by the mononuclear phagocyte system (Olivier et al. 1999). The high dose of PCBA nanoparticles used (200mg/kg body weight) although close to the lethal dose 50% (LD50 = 230mg/kg (Kante et al. 1982) was well tolerated with only rare events of death which could be attributable to faulty injection technique (Kreuter et al. 2003). However, there was a study that highly criticised these outcomes and reported higher death occurrences of dalargin loaded polysorbate 80-coated PCBA nanoparticles at a PCBA nanoparticle dose of 166 mg/kg (Olivier et al. 1999). Polysorbate 80 was necessary for dalargin entry to the CNS: dalargin-loaded PBCA nanoparticles without polysorbate 80 were ineffective after IV administration

(Olivier et al. 1999). Later on it was shown that overcoating with polysorbate-80 leads to the adsorption of apolipoprotein E from the blood plasma onto the nanoparticle surface (Gessner et al. 2001; Kreuter et al. 2002; Das and Lin 2005). The particles are thought to mimic low density lipoprotein (LDL) and interact with the LDL receptor leading to their uptake by the endothelial cells lining the BBB (Das and Lin 2005). Enhanced transport of these nanoparticles may also involve tight junction modulation (Kreuter 2001) or P-gp inhibition (Woodcock et al. 1992). A recent attempt was successful in delivering orally Dalargin loaded PBCA nanoparticles surface coated with polyoxyethylene sorbitan monoolate (Tween-80) and PEG 20,000 in varying concentrations of up to 2% each (Das and Lin 2005). PEG was added for protecting the peptide-loaded nanoparticles in the GI environment, while also enhancing plasma half-life due to the dysopsonic action of long PEG chains (Das and Lin 2005). Nevertheless, it is important to note that coating with surfactants may prevent or retard the rapid removal of particles by the reticuloendothelial system (RES) (Kreuter 2001).

The investigation of the *in vivo* fate of nanoparticles coated with different surfactants further confirmed the P80 effectiveness at enhancing brain drug uptake (Blasi et al. 2007). The intravenous injection of polysorbates 20, 40, 60, or 80 was able to induce analgesia in mice. Other surfactants such as poloxamers 184, 188, 338, 407, poloxamine 908, Cremophor[®] EZ, Cremophor[®] RH40, and Brij[®] 35 were totally or almost inactive (Blasi et al. 2007). P80 enabled the highest induction of analgesia after an intravenous dose of dalargin (Blasi et al. 2007).

The major limiting factor for the systemic use of nanoparticles is their rapid clearance by the reticuloendothelial system (Blasi et al. 2007). The extent of this uptake depends mainly on particle size, surface charge, and surface properties (Hoet et al. 2004; Borm et al. 2006).

1.6 Aim and Objectives:

From all the above it is obvious that delivering peptides and biopharmaceuticals orally to the central nervous system in sufficient therapeutic amounts is challenging. The

aim of this project is to attempt to achieve oral delivery of a hydrophilic opioid neuropeptide, Leucine^[5]-Enkephalin, to the central nervous system. The working hypothesis for enhancing the brain activity of this peptide involved two strategies: (i) a combination of a lipidisation and prodrug strategy and (ii) the use of a central nervous system carbohydrate amphiphilic bioavailability enhancer, quaternary ammonium palmitoyl glycol chitosan (GCPQ). Synthesis of a novel lipidic Leucine^[5]-Enkephalin prodrug was achieved by acylation of the phenolic hydroxyl group via an ester bond in order to improve its lipophilicity and therefore its permeation across biological barriers. The choice of the ester linkage to anchor the lipophilic moiety to the hydrophilic parent peptide was preferred as ester bonds can be cleaved in the body by available esterases (plasma, liver, brain). Esterifying the hydroxyl group of the tyrosine of Leucine^[5]-Enkephalin elicited the lipidic prodrug, Tyrosyl Palmitate Leucine^[5]-Enkephalin (TPLENK or PTLENK). Quaternary ammonium glycol chitosan (GCPQ), an amphiphilic carbohydrate polymer, has been shown to significantly enhance drug bioavailability of propofol by 10-fold when compared to the commercial formulation (Qu et al. 2006), while also significantly increasing oral bioavailability of cyclosporin, a cyclic undecapeptide BCS class IV drug, when compared to a commercial cyclosporin formulation (Le and Uchegbu 2006). Thus, the delivery potential of GCPQ as a carrier system for the delivery of hydrophilic compounds will be evaluated. Specifically, the objectives of this work were:

- (i) to synthesise, purify and characterise Leucine^[5]-Enkephalin and the novel lipidic pro-drug of this neuropeptide, TPLENK
- (ii) to assess the *in vitro* stability of both peptides in simulated gastrointestinal fluids in the presence and absence of GCPQ
- (iii) to create and characterize the particulate peptide formulations with GCPQ and assess their stability
- (iv) to assess the *ex-vivo* stability of the lipidic prodrug (TPLENK) in the presence of biological fluids (plasma, liver and brain homogenates) as well as its potential to regenerate to the parent hydrophilic peptide
- (v) to study the *in vivo* pharmacokinetics and pharmacodynamics.

Chapter 2

Peptide Synthesis and Characterisation

2.1 Solid Phase Peptide Synthesis

The basic steps of solid-phase peptide synthesis are outlined in Figure 2.1. Conceptually, the unique feature of this approach was the use of a polymeric support to assist in the synthesis of another polymeric compound. The process required a solid, insoluble support / resin to hold the first amino acid residue and the subsequent stages of the peptide as it was lengthened. A preference for a covalent attachment at

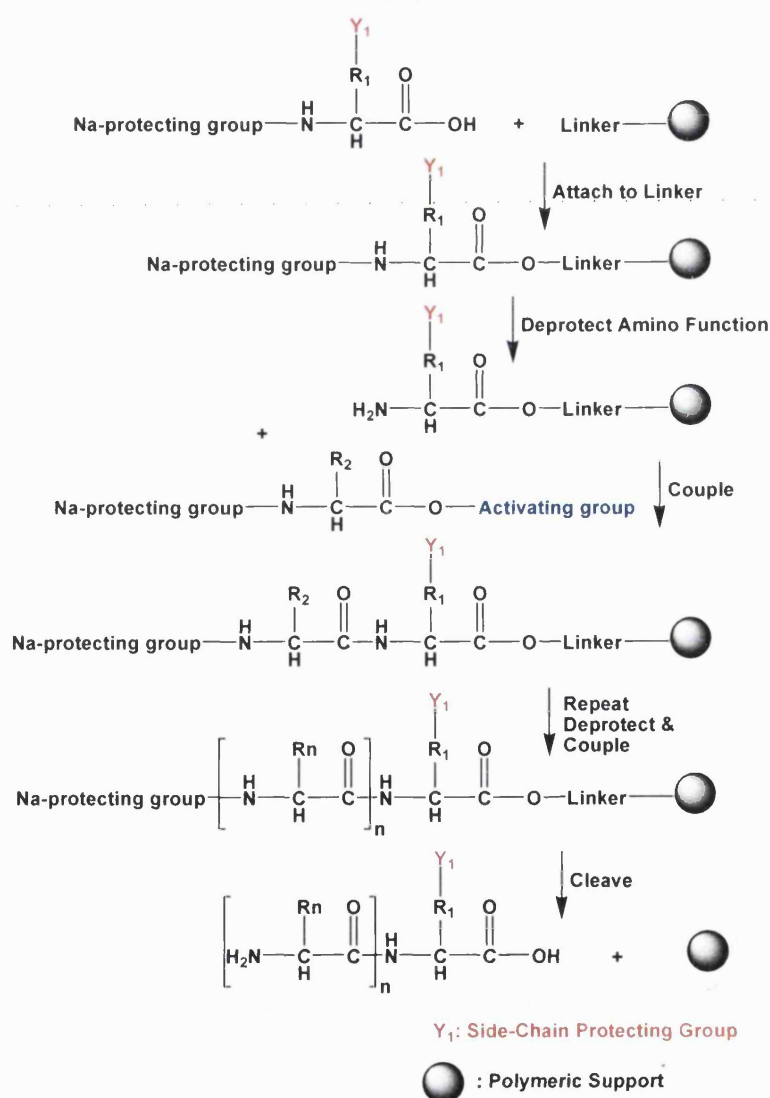


Figure 2.1: Basic steps in Solid Phase Peptide Synthesis

the carboxyl end is important for avoiding cleavage of the synthesised sequence from the resin before completion (Merrifield 1997). An N- α -derivatised amino acid is attached to an insoluble support via a linker. The amino acid may be attached directly to the linker-support or first attached to the linker, with subsequent attachment of the amino-acid linker to the support (Fields and Noble 1990). After washing with solvent, the N- α -protecting group is then removed (deprotected) and the amino acid-linker-support is then washed again thoroughly with solvent. It is then necessary to activate the next N-protected amino acid for coupling to the growing peptide chain. The next N- α -protected amino acid is then coupled to the amino acid-linker support as either a preactivated species (i.e. symmetrical anhydride, active ester) or directly (*in situ*) in the presence of an activator (Fields and Noble 1990). These three steps, deprotection, neutralisation, and coupling, would be repeated until the desired sequence is assembled (Merrifield 1997). Finally, the peptide-linker-support would be cleaved and the peptide liberated into solution either as a free acid or amide depending on the chemical nature of the linker (Fields and Noble 1990). Ideally, the cleavage reagent also removes the amino acid side chain protecting groups, which are stable to the deprotection reagent (Fields and Noble 1990). Because the growing peptide was in the solid phase throughout the synthesis, the process was given the name solid-phase peptide synthesis.

Coupling may also be carried out using peptides (fully characterised and homogenous protected segments) instead of single amino acids, where the peptide is N- α - and side chain protected (Fields and Noble 1990). Protected peptide coupling is referred to as fragment (or segment) condensation or convergent peptide synthesis (CPS) (Fields and Noble 1990; Barlos and Gatos 1999). The size of the peptide usually determines the strategy, and peptides up to 5 amino acids in length are generally manufactured by a linear strategy (i.e. stepwise addition of each amino acid in the sequence until the entire sequence has been assembled), while for longer peptides a convergent strategy (i.e. synthesis of small segments or fragments that are subsequently assembled to give the final sequence) is more suitable (Andersson et al. 2000). This is mainly due to the “arithmetic demon” (Ireland 1969), by which the overall yield in a multistep process is critically dependent on the yield per step (Figure 2.2) (Andersson et al. 2000).

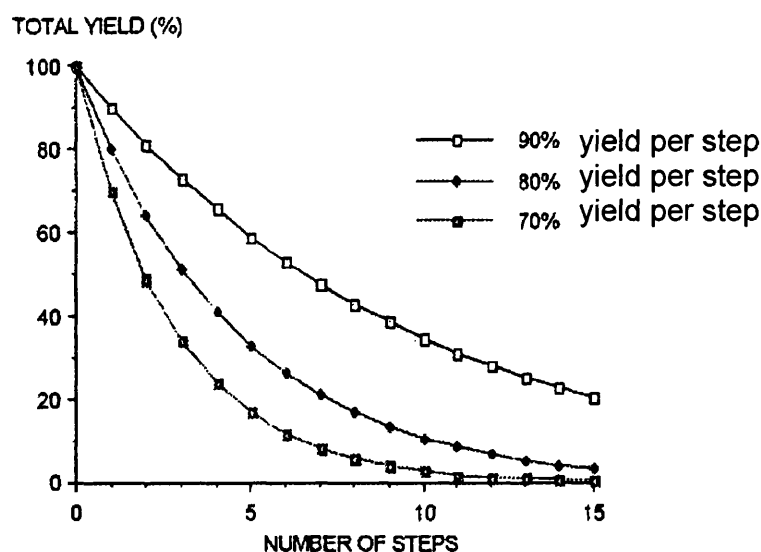


Figure 2.2: Effect of yield per step on overall synthetic yield (the “arithmetic demon”).
From: (Lloyd-Williams et al. 1997; Andersson et al. 2000)

SPPS is normally carried out in the C to N direction by sequential incorporation of Naurethane-protected amino acids, followed by removal of the protecting group. (Lloyd-Williams et al. 1997). Today, the reverse (N to C) direction is possible, with the advantage of being able to directly generate C-terminal modified peptides (which are abundant in nature) (Thieriet et al. 2000).

The potential advantages of SPPS appeared to be speed, simplicity, and yield (Merrifield 1997). Once the support containing the first amino acid is placed in a suitable reaction vessel or a packed column it would not have to be transferred or removed until the end of the synthesis (Merrifield 1997). If the solid support were completely insoluble in all solvents used, the peptide would also be insoluble, and it could be readily filtered and washed without transfer to other containers and the usual physical losses would be avoided (Merrifield 1997). The coupling reaction could be driven to completion by molar excess and a high concentration of the protected amino acid (Merrifield 1997). Thorough washing by large volumes of solvents would be efficiently remove excess reagents and soluble by-products and thereby effect a rapid partial purification at each step without the need for difficult and time-consuming isolation and crystallisation procedures after each synthetic cycle (Merrifield 1997). Incomplete reactions and the gradual build-up of insoluble side reaction by-products

were recognised as obvious potential disadvantages (Merrifield 1997). No purification is possible until after cleavage of the fully assembled peptide from the solid support, when most of the by-products accumulated during the synthesis were simultaneously cleaved (Andersson et al. 2000). Another main disadvantage of SPPS is the problem of nonquantitative yield of the amino acid coupling and N- α -deprotection steps (Barlos and Gatos 1999). Additionally, it is not possible to retain absolutely the optical integrity of the amino acids during the coupling reaction (Barlos and Gatos 1999).

2.1.1 Variables of SPPS

The choice of solid support has a large influence on the outcome of solid-phase synthesis, in particular when the synthesis becomes more difficult or chemically demanding (Meldal 1997). The majority of SPPS schemes utilise a solid support of polystyrene, crosslinked (1%) with m-divinylbenzene (DVB). 1% crosslinked polystyrene beads swell in DCM to approximately five times their dry volume (Gutte and Merrifield 1971). Good swelling of the resin is important to avoid limiting the growth of the peptide chain, and was achieved by using low cross-linking and good swelling apolar solvents such as dichloromethane, or dimethylformamide (Merrifield 1997). Better swelling of the resin in organic solvents is crucial, especially if taken into consideration that this copolymer can become highly solvated and swollen, and can reach a volume 50-fold greater than the dry-bead (Merrifield 1997). The solvent (apolar) apart from ensuring swelling of the peptide resin, it aids potentially the disaggregation of intermolecularly H-bonded aggregates (Schwyzer et al. 1955; Merrifield 1997).

With some minor modifications the 1% crosslinked Merrifield resin together with the Sheppard's polyamide resins (Atherton et al. 1975) have been used extensively and only during the last decades have new, improved resins based on composite polymers appeared. In general, the resins used for organic synthesis should be compatible with strongly acidic and basic conditions, with radical, carbene, carbanion, and carbenium ion chemistry, with reducing or oxidizing conditions, or with conditions of nitrations and halogenations (Deshpande 1994; Rinova and Lebl 1996; Meldal 1997).

While solid-phase methods are usually employed for the manufacture of supplies during the early stages of a product's development, scale-up of the method is commonly thought to be difficult or impossible, especially if the original Merrifield method, using tert-butyloxycarbonyl (BOC) strategy, is employed, due to the use of strongly acidic reagents, such as liquid hydrogen fluoride, to detach the peptide from the resin (Andersson et al. 2000). However, with the introduction of new resins, such as the 2-chlorotrityl chloride (Figure 2.3) (Barlos et al. 1989) and SASRIN resins (Mergler et al. 1988), it is now possible to synthesise protected peptides and fragments that can be detached from the resin with the protecting groups intact.

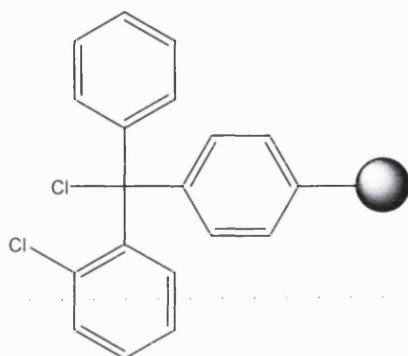


Figure 2.3: Acid sensitive 2-chlorotrityl chloride resin (polystyrene, 1% DVB)

Ideally, the cleavage reagent removes the amino acid side chain protecting groups, which are stable to deprotection reagent, during cleavage from the insoluble support. The tert-butyloxycarbonyl (Boc)/benzyl (Bzl) strategy depends on graduated acid lability (Albericio 2000). Thus, while the Boc group is removed with trifluoroacetic acid (TFA), Bzl, and related protecting groups are removed at the end of the synthetic strategy with strong acids such as liquid hydrogen fluoride (HF) or trifluoromethanesulfonic acid (Albericio 2000). However, long exposure of the peptide chain to TFA in the removal of the Boc group can cause also premature removal of the benzyl protecting group (Albericio 2000). Furthermore, conditions for the removal of Bzl groups will always remove the Boc group (Albericio 2000). Thus, an alternative strategy was required, which was based on the *orthogonal* concept, i.e. a strategy that involves two protecting groups belonging to independent classes that are removed by different mechanisms in any order and in presence of all other classes (Fields and Noble 1990; Albericio 2000). The alternative 9-fluorenyl-methoxycarbonyl groups (Fmoc)/ tert-butyl (tBU) strategy involves removal of the Fmoc protecting group usually by using 20% piperidine

(secondary base) in dimethylformamide through a β -elimination reaction with the absence of side reactions (Wellings and Atherton 1997), while tBU is removed by acidolysis with TFA (Figure 2.4). Orthogonal protection schemes are milder, because the selective deprotection is governed by alternative cleavage mechanisms rather than by reaction rates (Albericio 2000). On the other hand, the Boc strategy forms volatile byproducts during the deprotection step, while the Fmoc deprotection byproducts lack volatility and the dibenzofulvene formed is highly reactive.

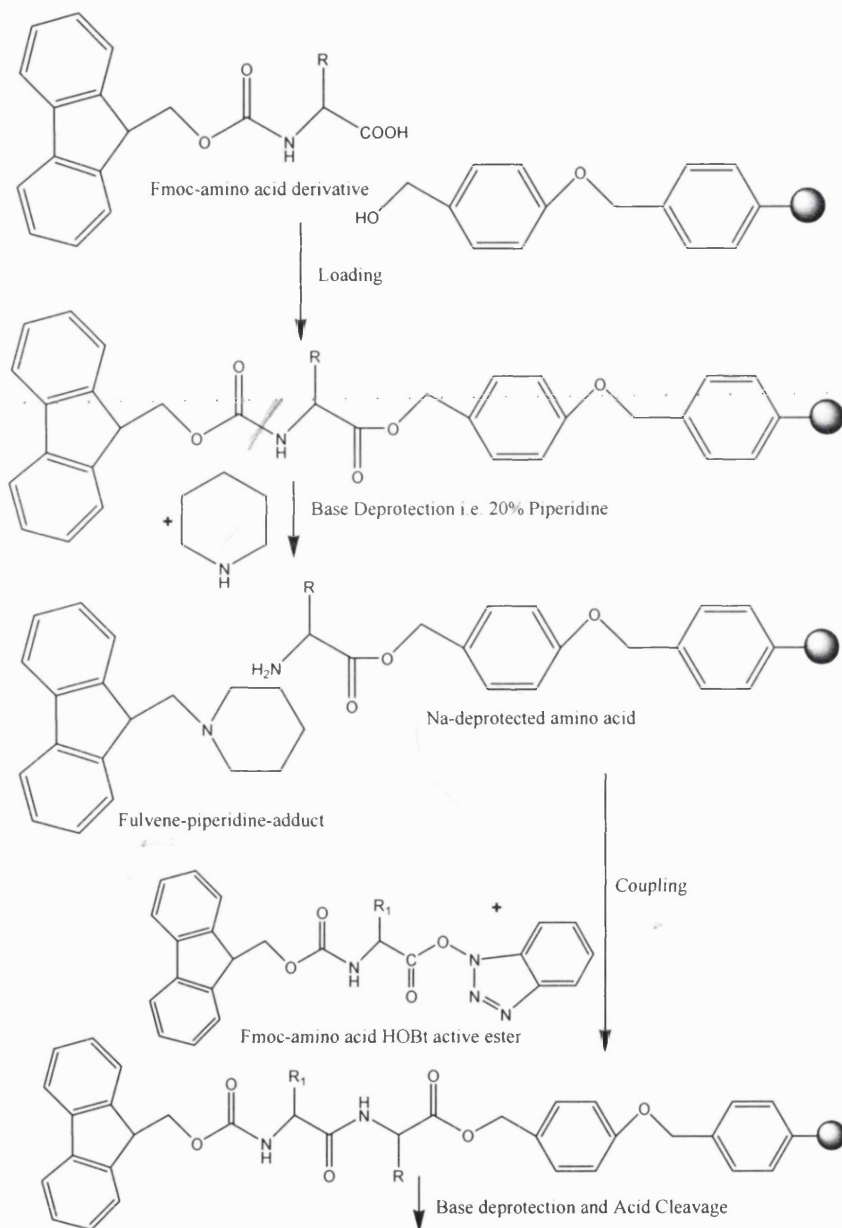
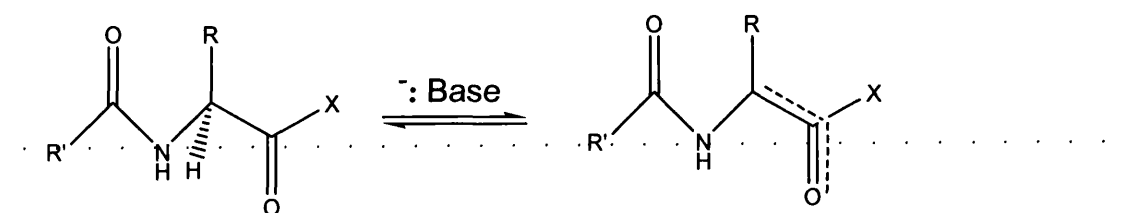


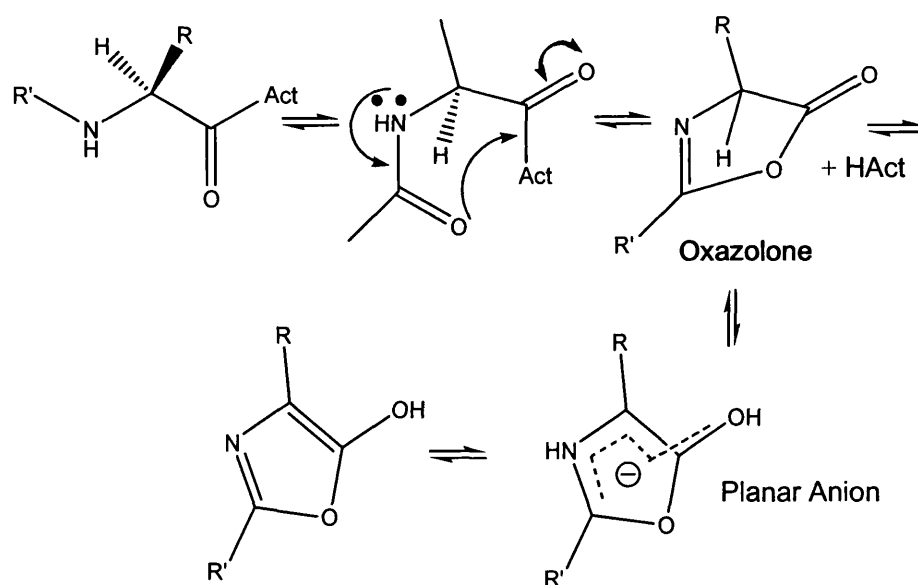
Figure 2.4: Solid phase peptide synthesis utilising Fmoc amino acids

The controlled formation of peptide bonds (coupling reaction) between two amino acids requires activation of the carboxyl group of one for facile reaction with the amino group of the other (Albericio and Carpino 1997). An essential feature of all coupling methods is that, in addition to giving the peptide bond in good yield, the configurational integrity of the carboxylic component must be maintained, which is difficult to achieve, because the best methods usually involve conversion of the acid to a derivative bearing a good leaving group (Albericio and Carpino 1997). Such leaving groups tend to increase the acidity of the α -proton and favour formation of an oxazolone (Sheehan and Hess 1955; Albericio and Carpino 1997). Loss of configuration is especially prominent if oxazolone formation occurs, but it also can occur at the stage of the activated carboxyl derivative (Figure 2.5) (Albericio and Carpino 1997).



X: Leaving group

Base catalysed proton abstraction from an activated species



Oxazolone formation

Figure 2.5: Mechanisms of racemisation (Act: Activator).

In stepwise SPPS the problem of racemisation is less dramatic than for other strategies (Albericio and Carpino 1997). The N_α -protecting group of the amino acid to be coupled (the one with the carboxylic function activated) is normally a urethane function such as Fmoc or Boc (Albericio and Carpino 1997). The presence of an alkoxy group in these carbamates reduces the tendency to give an oxazolone, and if formed such oxazolones are less sensitive to racemisation (Albericio and Carpino 1997). Furthermore, an important feature of the solid-phase approach is the general use of a large excess of reagents (coupling reagents, protected-amino acids). The coupling reactions are therefore generally faster than in solution, thus minimising loss of configuration. A variety of coupling methods are available today from mixed carboxylic-carbonic anhydrides, carbodiimides [e.g. dicyclohexylcarbodiimide (DCC) (Figure 2.6) (Albericio and Carpino 1997)], water-soluble carbodiimide (WSCDI) and urothane reagents [e.g. o- (benzotriazol-1-yl)-N, N, N', N'-tetramethyluronium tetrafluoroborate (TBTU), o- (benzotriazol-1-yl)-N, N, N', N'-tetramethyluronium hexafluorophosphate (HBTU) (Figure 2.6) (Andersson et al. 2000)]. In addition to these methods, commercially available preactivated amino acids derivatives, such as active esters [e.g. hydroxysuccinimide (HOSu) and p-nitrophenol (HONp) esters] and N-carboxyanhydrides (NCAs), may be used. The most widely used coupling reagents are carbodiimides, on the one hand, and phosphonium and aminium salts, on the other hand.

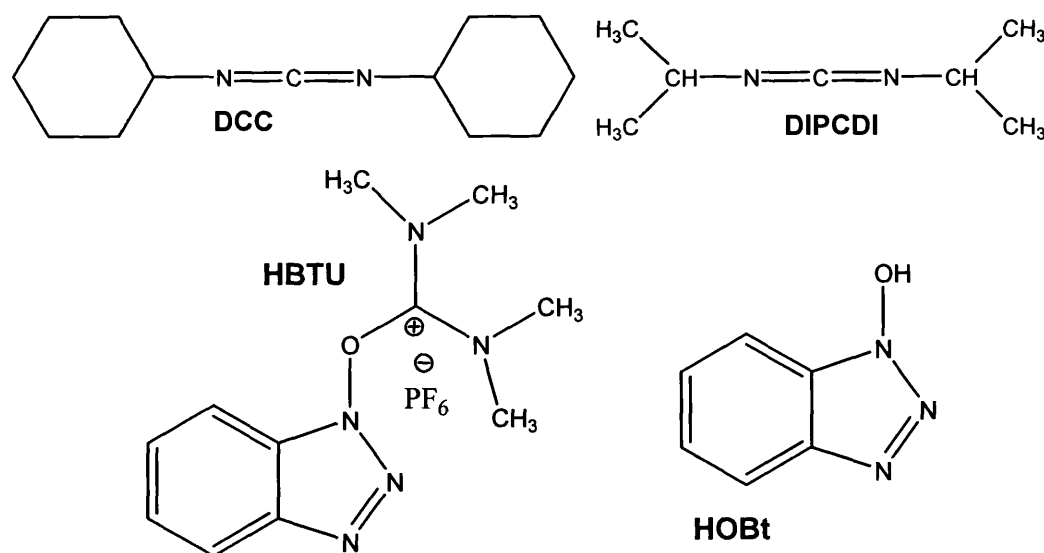


Figure 2.6 Top; Structure of common carbodiimides (DCC, DIPCDI). Bottom; Structure of HBTU & HOBt.

Reaction of the protected carboxylic acid with a carbodiimide is believed to involve a labile *O*-acylisourea, which reacts with the amino component to give the corresponding amide (Albericio and Carpino 1997). If two equivalents of carboxylic acid are used, the intermediate *O*-acylisourea reacts with the second equivalent of acid to give the corresponding symmetric anhydride (Albericio and Carpino 1997). If the activation process is carried out in the presence of a hydroxylamine derivative [e.g. 1-hydroxybenzotriazole (HOBt) (Figure 2.6), or 1-oxo-2-hydroxydihydrobenzotriazine (HODhbt)] an active ester is obtained (Albericio and Carpino 1997). Any one of the three active species, *O*-acylisourea, symmetric anhydride, or active ester, is an excellent acylating reagent (Albericio and Carpino 1997). The main advantage of using *N*-hydroxy compounds as additives is to reduce loss of configuration at the carboxylic acid residue (Albericio and Carpino 1997).

For carrying out SPPS by the Boc/Bzl strategy, among carbodiimides the *N*, *N*'-dicyclohexyl derivative (DCC) (Figure 2.6) is the most widely used, as the by-product *N*, *N*'-dicyclohexylurea (DCU) can be eliminated from the reaction vessel owing to its solubility during removal of the Boc group with TFA (Albericio and Carpino 1997). The high solubility in *N*, *N*-dimethylformamide (DMF) of the urea derived from the *N*,*N*'-diisopropylcarbodiimide (DIPCDI) (Figure 2.6) makes it the carbodiimide of choice when the Fmoc/tBU strategy is used (Albericio and Carpino 1997). In fact use of DCC is not possible in the latter case, as DCU would plug the frit of either the reaction vessel or the column in the case of batch or continuous-flow synthesis, respectively (Albericio and Carpino 1997).

Carbodiimide-mediated couplings are usually carried out with pre-activation of the protected amino acid, at either 25°C or 4°C (Albericio and Carpino 1997). If desired, after filtration of DCU and evaporation of DCM, DMF may be used as a coupling medium. The activation process is slower in DMF and for this reason it is not used during coupling (Albericio and Carpino 1997). For large-scale synthesis (~10 mmol of peptide), it is mandatory to pre-activate at 4°C, because the exothermic nature of the reaction increases the risk of racemisation, even when urethane-type protecting groups are used (Albericio and Carpino 1997).

Although Kenner and co-workers (Gawne et al. 1969) were the first to describe the use of acylphosponium salts as coupling reagents, these species have only been widely adopted after the extensive studies of Castro and Coste (Castro et al. 1975; Coste et al. 1990), who described the applicability of (benzotriazol-1-yloxy) tris (dimethylamino) phosphonium hexafluorophosphate (BOP) (Figure 2.7) and (benzotriazol-1-yloxy) tris (pyrrolidino) phosphonium hexafluorophosphate (PyBOP) (Figure 2.7) (Albericio and Carpino 1997). These coupling reagents incorporate in their structure an equivalent of HOBT, and the final reactive species are the corresponding oxybenzotriazole (Obt) esters (Albericio and Carpino 1997). Formation of the Obt ester is achieved in the presence of an equivalent of a tertiary base such as N, N-diisopropylethylamine (DIEA) or N-methylmorpholine (NMM) (Castro et al. 1977). The presence of an extra equivalent of HOBT can accelerate the coupling process. The precise nature of the intermediates involved in the use of the BOP reagent is not known (Albericio and Carpino 1997).

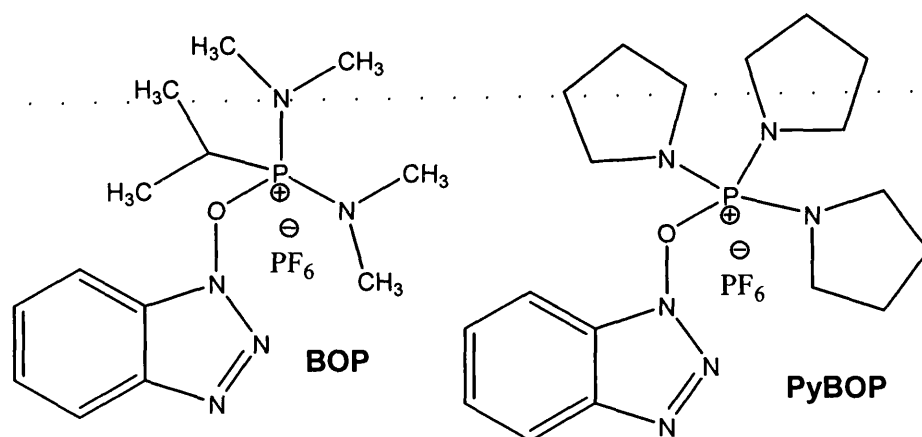


Figure 2.7: Structures of BOP and PyBOP.

The preparation and use in peptide synthesis of analogs of phosphonium salts such as N-[(1*H*-benzotriazol-1-yl)(dimethylamino)methylene]-N-methylmethanaminium hexafluorophosphate N-oxide (HBTU) (Figure 2.8) and N-[(dimethylamino)-1*H*-1,2,3-triazolo[4,5-*b*]pyridin-1-yl-methylene-N-methylmethanaminium hexafluorophosphate N-oxide (HATU) bearing a positive carbon atom in place of the phosphonium residue have also been reported (Albericio and Carpino 1997). Although initially assigned a uronium-type structure, presumably by analogy with the corresponding phosphonium salts, more recently it has been determined by X-ray analysis that HBTU, HATU, and 1-(1-pyrrolidinyl)-1*H*-1,2,3-triazolo[4,5-*b*]pyridin-1-ylmethylene) pyrrolidinium hecafluorophosphate N-oxide (HAPyU) crystallise as aminium salts (guanidinium N-

oxides) rather than the corresponding uronium salts (Figure 2.9) (Albericio and Carpino 1997).

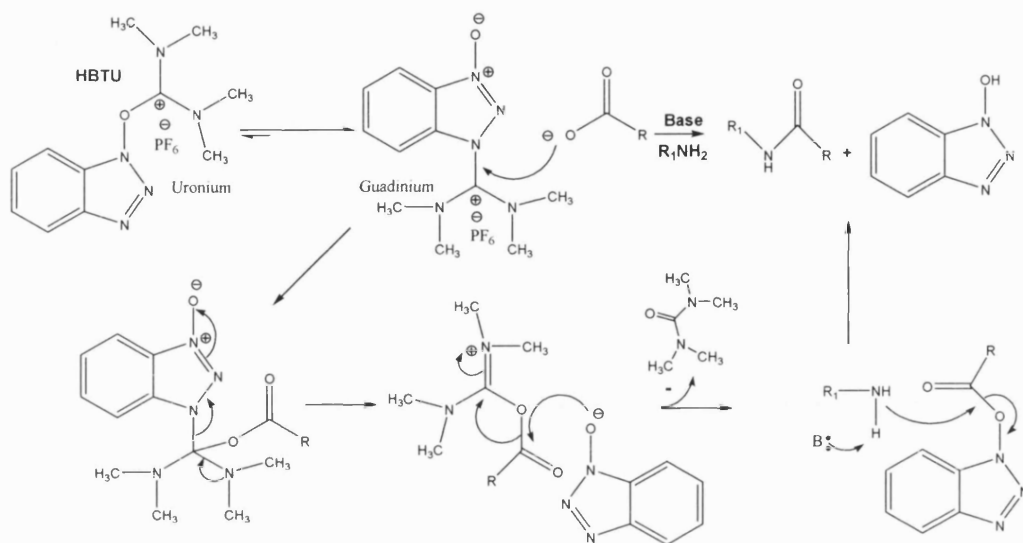


Figure 2.8: Uronium reagents (e.g. HBTU, HATU) mechanism of peptide bond formation (B: Base).

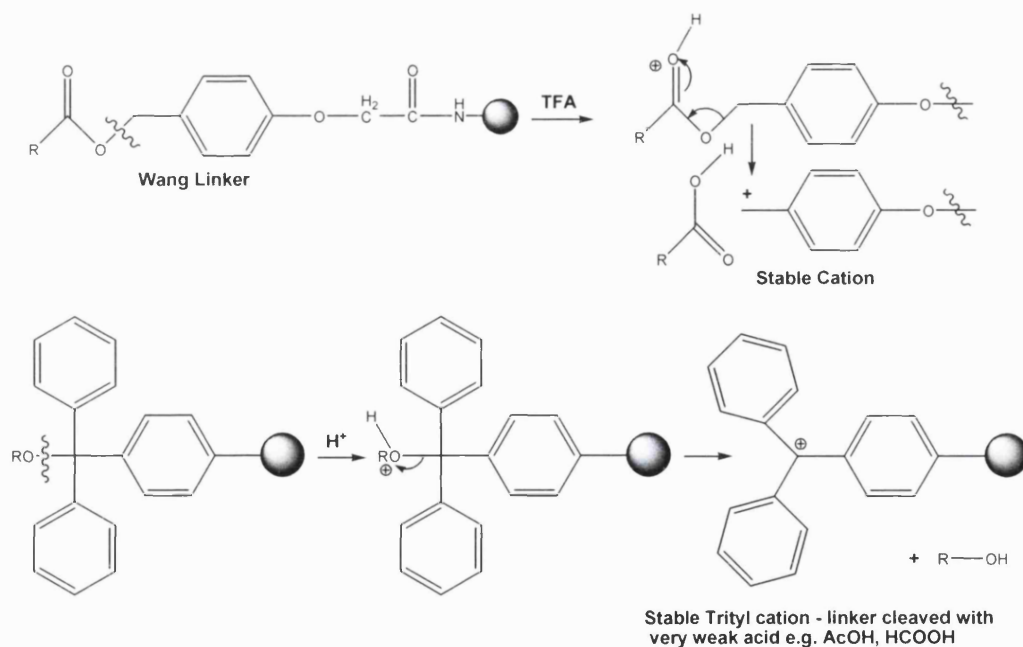


Figure 2.9: Cleavage under strong (top) and weak (bottom) acidic conditions depending on the resin linkage used.

Detachment of the peptide from the resin after assembly, often with simultaneous removal of side-chain protecting groups, is a critical step, during which many side products can be formed (Andersson et al. 2000). Optimisation of this step is important to the yield and purity of the final product. Fmoc SPPS is primarily designed for acidolysis of the bond between the peptide residue and the linker that attaches it to the polymeric support. Since non-acidic conditions are used for N- α -amino group deprotection, acidolysis can be used for cleavage and side chain deprotection (Fields and Noble 1990). The majority of the linkers and side chain protecting groups for Fmoc SPPS are thus designed to be labile to strong but also weak acid if strong acid interferes with the final product in any way (Figure 2.9) (Fields and Noble 1990; Crooks and Charles 2000). Alternate cleavage conditions, such as alkali, photolysis, fluoride ion, or hydrogenation, are used primarily for peptide isolation with intact side chain protecting groups or to produce a unique peptide carboxyl terminus (Fields and Noble 1990; Andersson et al. 2000).

2.1.2 Mass Spectrometry (MS)

Mass spectrometry (MS) is the most direct and efficient analytical tool for structure verification and elucidation of synthesised peptides due to the introduction and development of techniques such as fast atom bombardment (FAB) (Seifert and Caprioli 1996), matrix-assisted laser desorption/ionisation (MALDI) (Stults 1995) and electrospray ionisation (ESI) (Mann and Wilm 1995) that are capable of directly ionising involatile, labile biomolecules (Beranova-Giorgianni and Desiderio 1997). Confirmation of proper synthesis by high performance liquid chromatography (HPLC) retention time requires a peptide standard for comparison (Burdick and Stults 1997). However, molecular mass measurement provides data only on the composition of a peptide. Isomeric compounds (e.g. rearrangements, swaps of amino acids due to synthesizer / operator error) are not distinguished (Burdick and Stults 1997). Fortunately, these types of synthetic errors are normally minor (Burdick and Stults 1997). When there is a question on the sequence, tandem MS can be used to determine the sequence (Burdick and Stults 1997).

The mass spectrometer is designed to vaporise compounds of widely varying volatility, to produce ions from the resulting gas-phase molecules (except where the volatilisation

process directly produces ions rather than neutrals) and to separate ions according to their mass-to-charge ratios (m/z), and subsequently detect and record them (Williams and Fleming 1995). Since multiply charged ions are produced only rarely relative to singly charged ions, z can normally be taken as one (Williams and Fleming 1995). As the charge of one electron is constant, then the m/z can give the mass of the ion (Williams and Fleming 1995). Almost always sufficient vibrational energy is put into the ion to fragment to some extent to produce new ions with loss of neutrals or even further decompositions of the produced ions (Williams and Fleming 1995). When the array of ions has been separated and recorded, the output is known as a mass spectrum which is a record of the abundance of each ion (plotted vertically) against its m/z value (plotted horizontally) (Williams and Fleming 1995). The most abundant ion is arbitrarily assigned a value of a hundred per cent and it is known as the base peak. Negative-ion spectra, although less commonly used than positive-ion spectra, may also be obtained (Williams and Fleming 1995).

2.1.2.1 Electrospray Ionisation Mass Spectrometry (ESI-MS)

Electrospray produces ions from molecules in solution by spraying the solution from a sharp tip in the presence of a high electric field at atmospheric pressure (Burdick and Stults 1997). The small flow of liquid (generally $1\text{--}10\ \mu\text{L min}^{-1}$) is passed through a capillary needle when a potential difference of 3–6 kV is typically applied between the end of the capillary and a cylindrical electrode located 0.3–2 cm away (Figure 2.10) (Williams and Fleming 1995). The liquid leaving the capillary does not leave as a drop, but rather as a spray, or fine mist. Rapid desolvation and charge-induced breakup of the droplets leads to droplets of submicron size (Burdick and Stults 1997). The spray consists of highly charged liquid droplets, positively or negatively charged depending on the voltage applied to the capillary (Williams and Fleming 1995). The ions move from atmospheric pressure to the high vacuum of the mass spectrometer usually through a series of capillaries, nozzles, and/or skimmers (Burdick and Stults 1997). During this transfer process into the high vacuum, the ions experience collisions with residual gas molecules at an intermediate pressure that provides sufficient energetic excitation to remove residual solvent molecules, yet retain the covalent bonds until the ions are detected (Burdick and Stults 1997). Another characteristic of the ions is their propensity

to acquire multiple charges (Burdick and Stults 1997). The charges normally attached are protons in the positive mode (Burdick and Stults 1997). For peptides the number of added protons (charges) is roughly correlated with the number of basic sites on the molecule and its size, but there is frequently a distribution of charge number that may vary with instrument settings and solution pH (Burdick and Stults 1997).

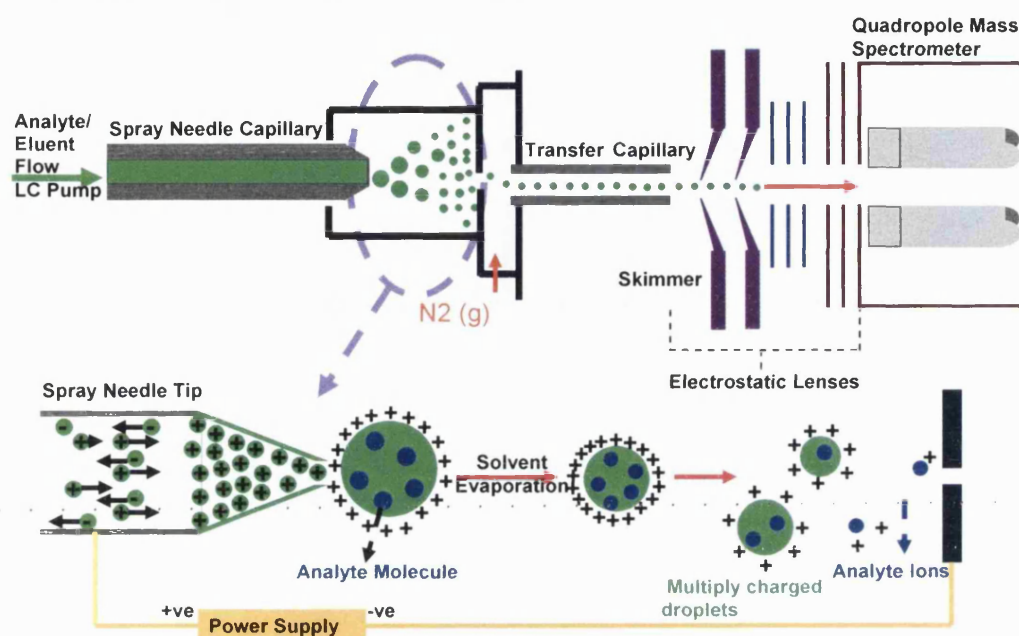


Figure 2.10: Schematic of an ESI mass spectrometer and evaporation of solvent in ESI-MS and ion production. Modified from (Williams and Fleming 1995).

The mass of a synthetic peptide is an excellent indication of the peptide composition with differences from the expected mass arising from incomplete removal of protecting groups (Burdick and Stults 1997).

One of the limitations of ESI-MS is its extremely limited tolerance of nonvolatile solution components. Sodium, even in small amounts ($>0.01\text{mM}$) will also act as a charge carrier and may lead to extra peaks at + 22 units (Burdick and Stults 1997). At higher concentrations ($>10\text{mM}$), sodium or other ionic species may totally suppress analyte ionisation (Burdick and Stults 1997).

2.1.2.2 Tandem Mass Spectrometry (MS-MS)

Tandem mass spectrometry (MS-MS) is used to produce structural information about peptides by fragmenting specific sample ions inside the mass spectrometer and identifying the resulting fragment ions generating structural information regarding the intact molecule (Ashcroft 2008). Tandem mass spectrometry also enables specific compounds to be detected in complex mixtures on account of their specific and characteristic fragmentation patterns (Ashcroft 2008). One common combination of analysers is quadrupole and time of flight. The first analyser is used to select user-specified sample ions, usually the molecular-related (i.e. $(M+H)^+$ or $(M-H)^-$) ions (daughter-ion scanning) (Ashcroft 2008). These selected ions pass into the collision cell, are bombarded by the gas molecules, which cause fragment ions to be formed, and these fragment ions are then separated according to their mass to charge ratios by the second analyser (Ashcroft 2008). As all the fragment ions arise directly from the precursor ions specified in the experiment, a fingerprint pattern specific to the compound investigated is produced (Ashcroft 2008). This is particularly useful for generating peptide sequence information.

Peptides fragment in a reasonably well-documented manner along their peptide backbone (and also exhibit some side-chain fragmentation) (Ashcroft 2008). There are 3 different types of bonds that can fragment along the amino acid backbone: the NH-CH, CH-CO, and the CO-NH bonds (Ashcroft 2008). Breakage of each bond will yield a neutral and a charged species, of which only the charged species will be monitored by the mass spectrometer. The charge can remain on either of the two fragments depending on the proton affinity of the two species, eliciting in total 6 possible fragment ions for each amino acid residue (labelled as a, b and c ions having the charge on the N-terminal fragment and the x, y, and z ions having the charge retained on the C-terminal fragment (Figure 2.11) (Ashcroft 2008). The most common cleavage sites are at the CO-NH bonds giving rise to the b and/or the y ions. The mass difference between two adjacent b or y ions is indicative of a particular amino acid residue. Quadrupole and time of flight mass spectrometers generate low energy fragmentations with fewer types of side-chain fragmentations.

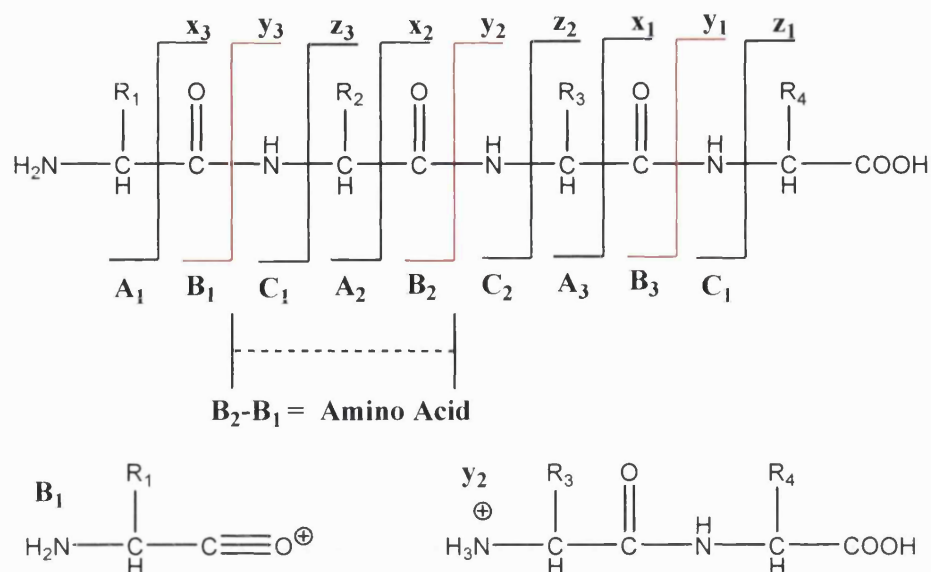


Figure 2.11: Peptide sequencing by Tandem Mass spectrometry-backbone cleavages.

Each amino acid residue leads to a diagnostic immonium ion, with the exception of the two pairs leucine (L) and iso-leucine (I) and lysine (K) and glutamine (Q), which produce immonium ions with the same m/z ratio (m/z 86 for L and I and m/z 101 for K and Q) (Ashcroft 2008). Immonium ions appear in the very low m/z range of the MS-MS spectrum and are helpful for detecting and confirming many of the amino acid residues in a peptide, although no information regarding the position of these amino acid residues in the peptide sequence can be ascertained (Ashcroft 2008).

2.1.3 High-Performance Liquid Chromatography (HPLC)

HPLC techniques are particularly suited to the purification of a single peptide from the kind of complex peptide mixtures encountered following solid-phase peptide synthesis, where impurities are usually closely related to the peptide of interest (deletion, terminated, or chemically modified peptides), perhaps missing only one amino acid residue, and hence, may be difficult to separate (Mant et al. 1997). In reverse-phase high-performance liquid chromatography (RP-HPLC), the column substrate can separate mixtures of polar components in an aqueous solution with the most polar components to be eluted first (Williams and Fleming 1995). The later-eluted hydrophobic components are often eluted by gradually increasing the concentration of acetonitrile (organic phase) in the otherwise aqueous developing solvent (Williams and

Fleming 1995). The availability of volatile mobile phases makes it ideal for both analytical and preparative separations (Mant et al. 1997). Although excellent resolution of peptide mixtures may be obtained at acidic or neutral pH, it is common to carry out RP-HPLC below pH = 3.0 to take advantage of acidic volatile mobile phases (particularly aqueous TFA/acetonitrile (ACN) systems) (Mant et al. 1997). Acidic pH values prevent non-specific ionic interactions between positively charged residues and any underivatised silanol groups (negatively charged above pH values of about 3-4) on silica-based packings (Meek 1980; Mant et al. 1997).

RP-HPLC offers great versatility in the choice of mobile-phase and stationary-phase characteristics to improve peptide separations. (Mant et al. 1997) Such manipulations may include varying the ion-pairing reagent, functional groups on the stationary phase, pH, packing support, and temperature (Mant et al. 1997). Even if only the gradient rate or flow rate is simply changed can have a dramatic effect on peptide resolution (Sereda et al. 1995).

2.1.4 Nuclear Magnetic Resonance (NMR) Spectroscopy

Nuclear magnetic resonance is currently the only experimental tool that can yield high resolution structural information on peptides and proteins in solution without the need of a crystal structure and it depends upon the magnetic features exhibited by atomic nuclei and electrons (Williams and Fleming 1995). NMR relies on atomic nuclei with nonzero nuclear spin (I) of $\frac{1}{2}$ (or $\frac{3}{2}$ etc.) such as ^1H and ^{13}C that in the presence of an applied magnetic field can behave like bar magnets and orient themselves in $2I + 1$ ways (Williams and Fleming 1995). ^1H and ^{13}C both have spins of $\frac{1}{2}$ and can take up one of only two orientations, a low energy orientation aligned with the applied field and a high energy orientation opposed to the applied field (Williams and Fleming 1995).

Transfer energy from a radio frequency applied to the nuclei located in the magnetic field is known as resonance, which causes a change in spin orientation of the nuclei or change in the spin populations in the higher energy levels (Williams and Fleming 1995). The resonance frequency is dependent, therefore, upon both the applied field strength and the nature of the nucleus examined (Williams and Fleming 1995). After the pulse is over, the magnetisation returns to its original equilibrium via the emission of energy or

by the transfer of energy to the surrounding molecules and the receiver coil picks up the response (Williams and Fleming 1995). Normally the difference between the two energetic states is very small causing NMR to be a relatively insensitive technique. Thus, the higher the applied field strength, the greater the difference (with more electrons achieving the higher energy state) allowing for an increased sensitivity (Williams and Fleming 1995).

Samples are dissolved in a solvent that does not itself give rise to signals in the NMR spectrum such as CCl_4 , CDCl_3 , C_6D_6 , d_6 -DMSO [$(\text{CD}_3)_2\text{SO}$], and D_2O , the choice of solvent being largely determined by the sample solubility. Chemical shift of the test compound (δ) is the difference between the resonance frequency of the sample peak and the reference peak of an internal reference compound, usually tetramethylsilane (TMS, $(\text{CH}_3)_4\text{Si}$), which are arbitrarily assigned a shift of $\delta = 0$ ppm (Claridge 2009).

The circulation of electrons surrounding a nucleus creates a secondary magnetic field opposed to the applied field at the nucleus causing nuclei in a region of high electron density to experience a field proportionately weaker than those in a region of low electron density, and a higher field has to be applied to bring them into resonance (shielded) (Williams and Fleming 1995; Claridge 2009). In the presence of an electronegative group which withdraws electron density from neighbouring protons, the deshielded proton will require less applied magnetic field to change the direction of its spin resulting in a downfield shift (i.e. to the left of a spectrum) compared to the more shielded protons which are surrounded by circulating electrons (Claridge 2009).

Chemical bonds (regions of high electron density) create anisotropic fields affecting the chemical shift of nearby nuclei (Claridge 2009). The π -bonds are especially effective in influencing the chemical shift of nearby atoms to higher δ values. Carbonyl carbons have similar effects and resonate at the lowest field position normally found in organic structures, since they suffer the combined effects of the induced anisotropic field and a nearby electronegative oxygen (Williams and Fleming 1995). The inductive and anisotropic effects are more or less additive (Williams and Fleming 1995). In a hydrogen bond, the electrons of the hydrogen atom involved are shared between two electronegative elements, and thus it is deshielded and it will come into resonance at a

low field (Williams and Fleming 1995; Claridge 2009). Finally, it has to be mentioned that the relative areas under the principle signal are proportional to the numbers of protons giving rise to the signal.

In all two dimensional NMR, multiple-pulse sequences are applied, so that in one kind of pulse sequence (Correlated Spectroscopy, COSY) magnetisation is transferred between nuclei that are spin-spin coupled, or in another (Nuclear Overhauser Effect Spectroscopy, NOESY) magnetisation is transferred between nuclei that undergo mutual dipolar relaxation (Williams and Fleming 1995; Claridge 2009). All peaks that are mutually spin-spin coupled are shown by cross-peaks which are symmetrically placed about the diagonal created by plotting two identical chemical shift (with different resolution) axes orthogonally (Williams and Fleming 1995; Claridge 2009). Similarly to the COSY spectrum, in a NOESY spectrum the cross-peaks indicate protons that are close in space (i.e. evidence of through-space, rather than through-bond, interactions). Large molecules (>1000 Da or more, or >500 in viscous solvents as d₆-DMSO) normally give much more intense NOE cross peaks (Williams and Fleming 1995; Claridge 2009). The NOE is due to mutual dipolar relaxation of protons and the intensity of the cross-peaks falls off rapidly with increasing internuclear separation of protons (Williams and Fleming 1995).

2.1.5 Fourier Transform Infrared Spectroscopy (FTIR)

FTIR spectroscopy for the qualitative and quantitative analysis of compounds has increased in importance for the analysis of solid and liquid compounds as it is rapid and non-destructive. Infrared radiation is passed through a sample, some of which is absorbed by the sample and some is transmitted resulting in a unique molecular fingerprint of the sample. Absorption in the infrared region results in changes in vibrational and rotational status of the molecules (Amand and Tullin). The absorption frequency depends on the vibrational frequency of the molecules, whereas the absorption intensity depends on how effectively the infrared photon energy can be transferred to the molecule, and this depends on the change in the dipole moment that occurs as a result of molecular vibration (Amand and Tullin). As a consequence, a molecule will absorb infrared light only if the absorption causes a change in the dipole moment. FTIR instruments utilise an interferometer that divides the incoming infrared

beam encompassing all of the infrared frequencies into two. A path difference between the beams is introduced (as one beam travels a fixed length and the other is constantly changing as its mirror moves constantly) whereupon they are allowed to recombine at the beamsplitter. The intensity of the output beam from the interferometer can be monitored as a function of path difference using an appropriate detector and the interferogram signal is Fourier transformed to yield a frequency spectrum (Amand and Tullin).

A macromolecule has a large number of vibrational modes that are associated with the vibrations of individual bonds or functional groups (localised vibrations as stretching, bending, rocking, twisting, or wagging that appear above 1500 cm^{-1}) and others of the whole molecule giving rise to a series of absorption bands at low energy below 1500 cm^{-1} that are characteristic of the molecule (fingerprint region) (Williams and Fleming 1995). Intensities in the infrared are frequently recorded and are usually expressed subjectively as strong (s), medium (m) and weak (w) (Williams and Fleming 1995). Because there needs to be a relative scale for the absorption intensity, a background spectrum must also be measured (measurement with no sample in the beam) that is used to determine the percent transmittance, resulting in a spectrum which has all of the instrumental characteristics removed.

In attenuated total reflection (ATR) FTIR, the changes that occur in a totally internally reflected infrared beam, when the beam comes into contact with a sample, are measured (Sciences 2005). An infrared beam is directed onto an optically dense crystal with a high refractive index (zinc selenide or germanium) at a certain angle (Sciences 2005). This internal reflectance creates an evanescent wave that extends beyond the surface of the crystal into the sample held in contact with the crystal (Sciences 2005). This evanescent wave protrudes only a few microns ($0.5\text{--}5\text{ }\mu$) beyond the crystal surface and into the sample requiring good contact between the crystal and the sample (Sciences 2005). In regions of the infrared spectrum, where the sample absorbs energy, the evanescent wave will be attenuated or altered (Sciences 2005).

2.1.6 Conformation Search, Molecular Modeling, and Pharmacophores

Molecular modelling is a collective term that refers to theoretical methods and computational techniques to calculate the structure and energy of molecules based on nuclear motions. The Born-Oppenheimer approximation of the Schrödinger equation states that nuclei are much heavier and move much more slowly than electrons, which will find their optimum, distribution once the positions of the nuclei are known, thus nuclear motions, vibrations and rotations, can be studied separately (Dixon and Harden 2008). To picture this, molecular modelling considers a molecule as a collection of weights connected with springs, where the weights represent the nuclei and the springs represent the bonds (Dixon and Harden 2008).

A force field is used to calculate the energy and geometry of a molecule, which is a collection of atom types that defines the molecule, parameters such as bond lengths and angles and equations that will aid in calculating the energy of a molecule (Dixon and Harden 2008). The total energy of the molecule is divided into several parts called force potentials, or potential energy equations that are calculated independently and are summed to give the total energy of the molecule (Dixon and Harden 2008). Bond stretching, bond bending, torsional strain, stretch-bend interactions, van der Waals interactions, dipole interactions are examples of force field potentials that will define the potential energy surface of a molecule (Dixon and Harden 2008).

Thus, when studying a biomolecular system, four choices need to be made on (i) which atomic or molecular degrees of freedom are explicitly considered in the model, (ii) which force field is used to describe the energy of the system as a function of the chosen degrees of freedom, (iii) how these degrees of freedom are to be sampled, and (iv) how the spatial boundaries and external forces are to be sampled (van Gunsteren et al. 2006).

The Optimised Potential for Liquid Simulations of Amino Acids (OPLS-AA) force field is probably the best one available for condensed phase simulations of peptides (Jorgensen et al. 1996; Macromodel 1999). Comparisons to *ab initio* calculations and experiment illustrate that OPLS-AA reproduces conformational energies well for systems for which it has been specifically parameterised (Macromodel 1999). Convergence, the problem resulting from the inability of conformational search

methods to cope with structures with more than a dozen rotatable bonds, can be one of the major errors in modeling (Macromodel 1999). It is wise to carry out multiple searches with different starting geometries to verify that the same final structures are found. Dynamics calculations are also problematic as the time periods necessary for adequate coverage of conformational space is often much longer than appreciated (Macromodel 1999). However, simulations of (un)folding equilibria of polypeptides in solution using a thermodynamically calibrated force field and an explicit representation of the solvent molecules have shown that the unfolded or denatured state of these polypeptides contains much fewer conformations significantly populated at equilibrium than there are possible polypeptide conformations (van Gunsteren et al. 2006). The difference is due to the presence of hydrogen-bond donor and acceptor atoms in polypeptides, which restrict (through favourable hydrogen bonding) the conformational space accessible to the molecule at the given temperature. In the absence of hydrogen-bond donors, this restriction is not present and the number of relevant conformations grows linearly with time (van Gunsteren et al. 2006). When a realistic force field is used, most of the configuration space will have a very high energy, which indicates that the configuration space to be searched or sampled to predict the most stable fold of a polypeptide or protein does not grow exponentially with the system size or chain length (van Gunsteren et al. 2006). The Monte Carlo / Stochastic Dynamics mixed-mode procedure is proposed to alleviate the problem of convergence. Monte Carlo methods are step methods generating a new configuration of the complete system from previous configuration with the step direction taken at random and the step size limited by the Boltzmann acceptance criterion (average energy of a system is equal to the Boltzmann energy average determined by Boltzmann distribution law at thermal equilibria) (van Gunsteren et al. 2006). In Stochastic Dynamics simulations a random component is added to the force, the size of which is determined by the temperature of the system and the atomic masses and friction coefficients (van Gunsteren et al. 2006).

It has to be noted that the solvent medium can have a major effect on molecular structures and energies. While for small organic molecules with only one polar functional group, solvation does not appear to be a major determinant of conformational energies, for molecules having several polar functional groups, the effect of the solvent can be dramatic since the electrostatically least stable structures are typically the most heavily solvated and thus stabilised in a polar solvent (Macromodel 1999). While using

explicit solvent molecules is one solution to the problem, solution calculations run much more slowly due to the increased number of particles, especially if converged energies are required. MacroModel ® adopts a more practical alternative in which solvent is treated as a statistical continuum, providing both energies and derivatives analytically (so it can be used in a molecular mechanics force field) and giving small-molecule hydration energies of comparable accuracy to those obtained from free energy perturbation methods but at only a fraction of the computational expense (Still et al. 1990).

A pharmacophore is the ensemble of steric and electronic features that is necessary to ensure the optimal supramolecular interactions with a specific biological target structure and to trigger (or to block) its biological response (Wermuth 2006). A pharmacophore can be derived either in a structure-based manner by determining complementarities between a ligand and its binding site, or in a ligand-based manner, by flexibly overlaying a set of active molecules and determining those conformations that are able to be overlaid in such a way that a maximum number of important chemical features geometrically overlap (Wolber et al. 2008). A pharmacophore can be used to search for similarities between binding situations or even for similarities between molecules (Wolber et al. 2008) and can serve as a template to screen compounds till the desired ligand can be identified. The pharmacophore encompasses a prevailing assumption in drug design that ligand binding is due primarily to the interaction of some features of the ligand to “complementary” features of the receptor, with the rest of the ligand atoms merely providing a scaffold for holding the pharmacophore features in their spatial positions (Lavalle et al. 2000). Thus, comparing conformation search results with proposed pharmacophores of receptors can give information on the ability of analogues to bind to the required biological receptor.

2.2 Materials and Methods

2.2.1 Materials

Table 2.1 Materials for Peptide synthesis and characterisation

Chemical Name	Name	Purity	Company
✓ Acetic Acid (Glacial)	AcOH	99-100%	Riedel-de Haen
✓ Acetonitrile HPLC grade	ACN	≥99.9%	Fischer Scientific
✓ Dichloromethane	DCM	≥99.0%	Fischer Scientific
✓ Diethylether	Ether	≥99.5%	VWR International
✓ N,N'-Dimethylformamide	DMF	≥99.0	FLUKA / Univ. of London
✓ Ethanol (Absolute)	Eth	≥99.0	Univ. of London
✓ Fmoc-Gly-OH	G		Novabiochem
✓ Fmoc-Leu-OH	L		Novabiochem
✓ Fmoc-Phe-OH	F		Novabiochem
✓ Fmoc-Tyr-OH	Y	≥97.0%	FLUKA
Fmoc-Tyr-(OtBU)-OH	Y-(OtBU)		Novabiochem
H-Leu-2-Cl-Trt-Resin (0.86mmole/g)-1G			Novabiochem
✓ Leucine ^[5] -Enkephalin	LENK	≥96.0%	FLUKA
✓ H-Phe-2-Cl-Trt-Resin (75- 150um)			FLUKA
✓ O-(Benzotriazol-1-yl)-N, N, N', N'-tetramethyluronium hexafluorophosphate	HBTU		FLUKA / Novabiochem
Hexane		HPLC grade	Univ. of Strathclyde / London
✓ Methanol HPLC grade	MEOH	≥99.8%	FLUKA / Fisher
✓ 4-Methylmorpholine	NMM	≥99.5%	FLUKA
✓ Ninhydrin, ACS reagent		≥98.0%	FLUKA
Palmitic Acid N- hydroxysuccinimide ester	NHPA	98.00%	SIGMA
✓ Phenol SIGMAULTRA	Phenol	≥99.5%	SIGMA-ALDRICH
✓ Piperidine, biotech grade	PIP	99.5+%	SIGMA
✓ Potassium Cyanide	KCN	≥98.0%	FLUKA
2,2,2-Trifluoroethanol	TFE	≥99.0%	FLUKA

methanol
ethanol

Chemical Name	Name	Purity	Company
Trifluoroacetic acid	TFA	≥99.5%	FLUKA
Triethylamine	TIEA	≥99.0%	SIGMA
Deuterium Oxide 99.9 atom %D	D ₂ O	99.90%	ALDRICH
Methyl Sulfoxide 0.75mls amp. d:1.19g/ml, MW: 84.18, BP: 55°C/5mmHG	DMSO-d ₆	99.9%	ALDRICH

2.2.2 Peptide Synthesis and Cleavage.

Peptide synthesis of Leucine^[5]-Enkephalin-(tBu) (LENK-tBu) and of a novel lipidic Leucine^[5]-Enkephalin analogue, Tyrosine Palmitate Leucine^[5]-Enkephalin (TPLENK, or PTPLENK) was carried out by standard solid phase methodology employing a Zinsser Analytic (UK) Raikin PS3 peptide synthesizer (0.1mmol per batch) or manually (0.5mmol per batch). Fmoc chemistry was used with DMF as the solvent. All peptides were made on the pre-coupled with Leucine H₂N-Leu-2-Chlorotrityl resin. Stepwise addition of Fmoc-orthogonally protected amino acid derivatives (four equivalents when synthesised using the peptide synthesizer and five equivalents when prepared manually) on the pre-coupled peptide support was employed with equivalent HBTU in the presence of 4.45 v/v % 4-Methylmorpholine (NMM) in DMF. For manual synthesis each amino acid was coupled twice before proceeding to the next addition. The coupling steps were 45-min long employing HBTU as the coupling reagent when the synthesiser was used and 25-min long performed twice employing HBTU as a coupling reagent. Glycine was double-coupled. Deprotection of the Fmoc protecting group was performed twice for 10 minutes each using 20% (v/v) piperidine in DMF when done manually or for a total of 20 minutes and performed once when the synthesiser was used before the next coupling took place.

The Kaiser test was performed when the peptide was synthesised manually to ensure a successful coupling before proceeding to deprotection of the Fmoc moiety and further amino acid couplings especially after the addition of the first amino acid to the pre-loaded resin. All solutions were freshly prepared (Solution A: Phenol, ~80% w/v in absolute ethanol, Solution B: Potassium Cyanide 2% v/v of 1 mM aqueous solution in pyridine and Solution C: Ninhydrin, 6% w/v in ethanol). A small amount of the resin

beads (without washing away the reaction mixture with DMF) were transferred into a small glass test tube, washed with DCM: Methanol (1:1) and when dried under vacuum one drop of solution A, 2 drops of solution B, and one drop of solution C were added. The suspension was mixed well and heated with the aid of a heating block at 120°C for 5 minutes. Dark blue colouration of the resin beads and the solution is indicative of the presence of primary amine, while when the colour of the resin beads turns slightly orange and the solution remains yellow there is no free primary amine indicative of a successful coupling.

After the synthesis was completed, the resin was washed with copious amounts of DMF, followed by copious amounts of DCM and then by a mixture of DCM/Methanol (1:1). The resin was dried under vacuum and then transferred to a pre-weighted glass container and left in a dessicator under vacuum. After 4 hours, the resin was stored in the fridge until required for further use.

For Leucine¹⁵¹-Enkephalin, Fmoc deprotection was achieved with 20% (v/v) piperidine in DMF. The cleavage of the peptide from the 2-chlorotrityl resin was achieved with 1mL of AcOH/TFE/DCM (2:2:6 v/v/v) for 2 hours (Barlos et al. 1991) or utilising Reagent P [Phenol/TFA 5/95 (w/v), prepared by adding 0.5g of Phenol crystals to 9.5mL of TFA and protected from light] for each 0.1g of dry resin for 2 hours at room temperature. If the tBu protection on tyrosine was required only the former cleavage mixture based on acetic acid was used, as TFA can also cleave the side-chain protecting group as well as the 2-chlorotrityl resin. Evaporation and removal of acetic acid as an azeotrope with hexane or evaporation of TFA resulted in reduced volume of a suspension containing the crude peptide. The crude peptide (LENK) was precipitated with (frozen, -20°C) diethyl ether, collected with centrifugation (1500 rpm at 4°C for 45minutes) performed three times (with syringing and discarding the supernatant and further washing with frozen diethyl ether after the first two centrifugations), dried with nitrogen, dissolved in water and lyophilised. The overall yield of the reaction was between 92-99%.

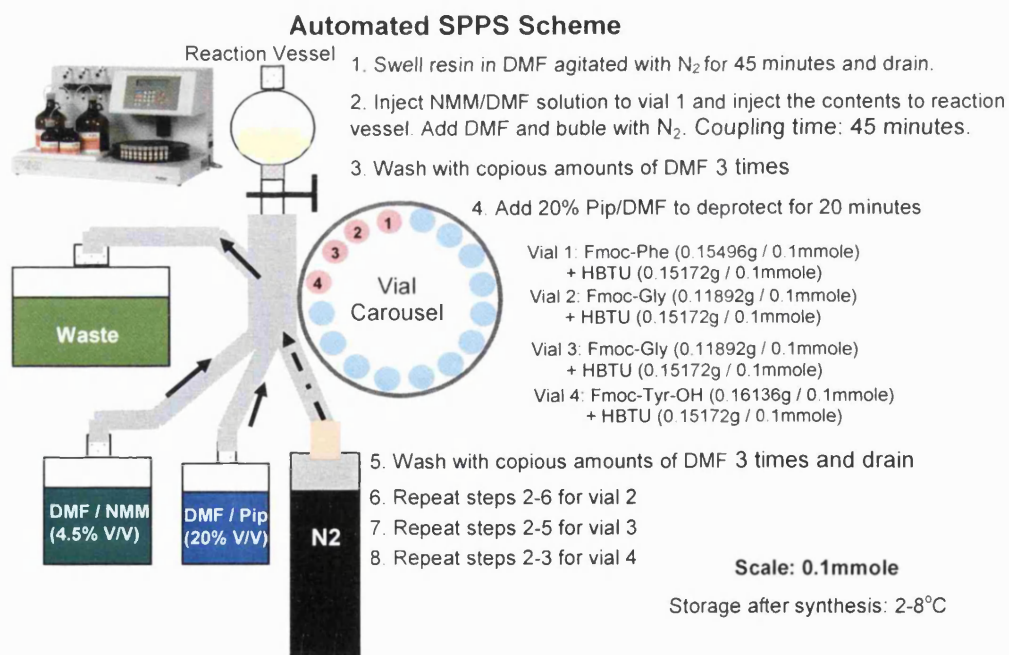
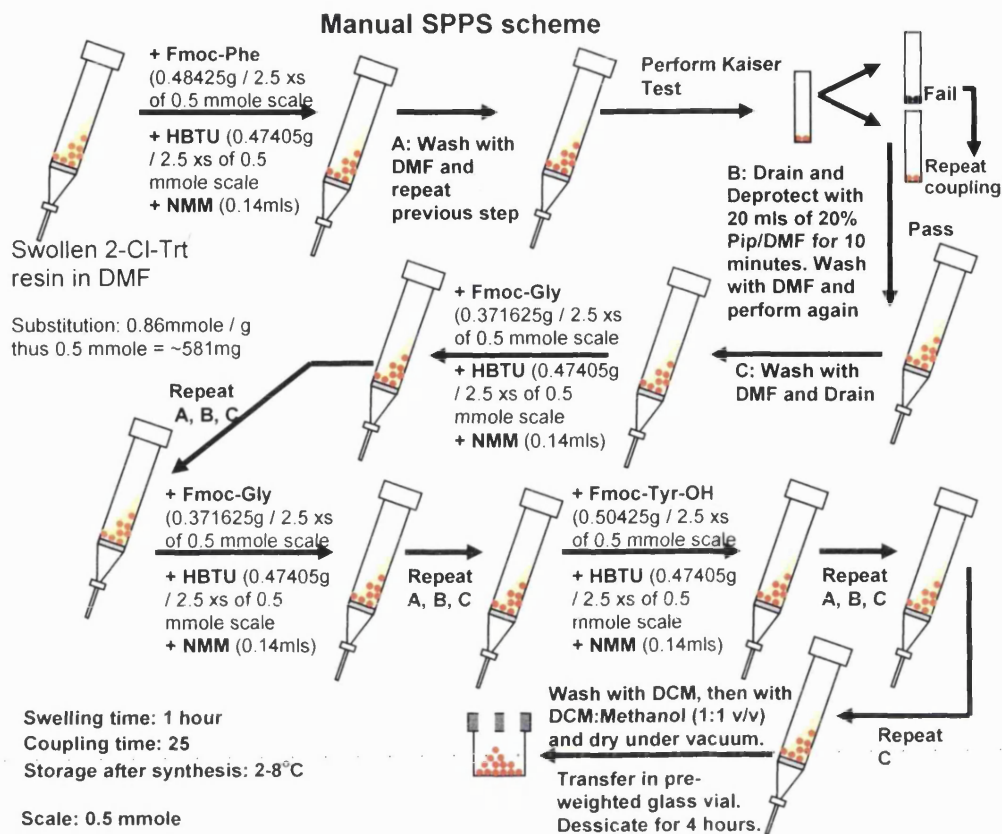


Figure 2.12 SPPS scheme from manual synthesis (top) or using a PS3 synthesizer (bottom) of Fmoc-LENK-2-Cl-Trt-resin.

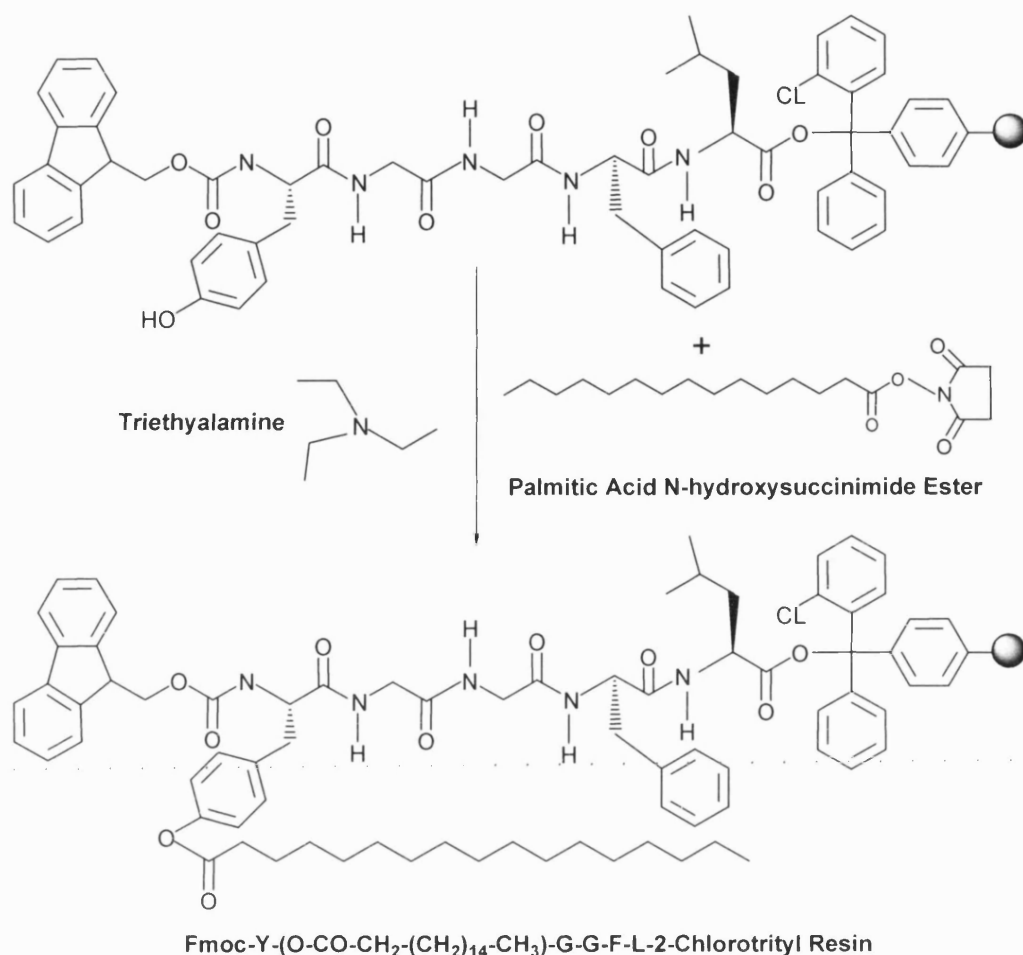


Figure 2.13 Palmitoylation of Fmoc protected Leucine^[5]-Enkephalin using Palmitic acid N-hydroxysuccinimide ester.

Triethylamine (350 μL , 2.5 mmol) was added to a solution of Fmoc-Tyr-(OH)-Gly-Gly-Phe-Leu-2-Cl-Trt-Resin (0.1 mmol) preswelled in DMF (8 mL) and the resultant suspension was reacted with the N-hydroxysuccinimide ester of palmitic acid (176.75mg, 0.5 mmol) in DMF (5 mL) at 25°C (constant temperature room or using a Grant OLS 200 waterbath, Sherpeth, UK) for 24 h, during which time the suspension was agitated (120 rpm). The mixture was then concentrated in vacuo to remove volatile products and then was redissolved in DMF (4 mL). Figure 2.13 illustrates the synthetic process. The redissolved product still on the resin was filtered and washed with copious amounts of DMF. The product bound to the resin was treated with 20% piperidine in DMF (20 mL) for 20-25 minutes. After washing with DMF and filtration, cleavage of the peptide chain from the resin was performed with the acetic acid cleavage mixture

(AcOH/TFE/DCM (2:2:6 v/v/v) for 2 hours (Barlos et al. 1991) at room temperature as stated above. Then, the crude peptide (TPLENK) was precipitated with cold purified water (4°C, pH 7.0), collected with centrifugation (2500 rpm at 4°C for 30 minutes) performed three times (with syringing and discarding the supernatant and further washing with cold water after the first two centrifugations) and lyophilised. The overall yield was between 55-75%.

2.2.3 Peptide Purification

Semi-preparative reverse-phase HPLC (RP-HPLC) was employed for the purification of the crude lyophilised Leucine^[5]-Enkephalin and TPLENK. A Waters HPLC system comprising of a Waters TM 515 HPLC pump connected to a Water TM 717 plus Autosampler with a Jones Chromatography Column Heater Model 7971 and a Waters TM 486 Tunable Absorbance Detector was used. The peptides were eluted on a semi-preparative Waters Spherisorb ODS2 C18 10x250mm with a pore size of 10µm with a flow rate of 4ml/min at 35°C. The mobile phase consisted of 82% 25mM ammonium bicarbonate buffer and 18% acetonitrile. Unless otherwise indicated, samples were detected at 280 nm. The injection volume was set to 250µL, which was the maximum for the autosampler's fitted injection. The retention time was 7.1 for Leucine^[5]-Enkephalin and 8.3 for TPLENK. Sample concentration of 15 mg ml⁻¹ was used. Collected fractions (4ml each) were freeze-dried to evaporate the ammonium bicarbonate and mass spectrometry was carried out to identify which fractions to select for pooling.

2.2.4 Peptide Characterisation.

2.2.4.1 Mass Spectrometry (MS)

Electrospray ionisation (positive) mass spectrometry was performed by either Finnigan Mat LcQ (ion trap) or a Finnigan Mat TSQ7000 (triple quadrupole) mass spectrometer to verify peptide masses. Samples (1mg) were dissolved in acetonitrile or methanol (1:1 ratio, 1ml) and infused into a TSQ 7000 mass spectrometer operated in the EI mode at a rate of 1mL h⁻¹, with needle voltage of 4.46kV and capillary temperature of 250°C. Mass of peptides (expected mass, in Daltons): Leucine^[5]-Enkephalin-(tBu) (LENK-

tBu): 611.37, Leucine^[51]-Enkephalin (LENK): 555.27, Tyrosine Palmitate-Leucine^[51]-Enkephalin (TPLENK): 794.51.

Tandem mass spectrometry for the identification of amino acid composition of the synthetic peptide was performed once for every batch of Fmoc-Tyr-(OH)-Gly-Gly-Phe-Leu-2-Cl-Trt-Resin synthesised in the form of Leucine^[51]-Enkephalin or TPLENK. Spectra were acquired with a Micromass Q-ToF Ultima GLOBAL (Micromass, Manchester, UK), consisting of a quadrupole (Q) mass analyzer, a quadrupole collision cell, and a second-stage time-of-flight (TOF) analyzer and operated in the positive mode. Sample was prepared in Acetonitrile / 0.1% TFA in H₂O (1:1) and was run using proxenon borosilicate tip with a capillary of 1.8 kV, cone voltage of 35 V and a collision energy of 30 eV. All parameters (e.g., aperture to the TOF, transport voltage, offset voltages) were optimized to achieve maximum sensitivity and a mass resolving power of 10,000 (full width at half-maximum).

2.2.4.2 Nuclear Magnetic Resonance (NMR)

All NMR spectra were recorded on a Bruker AMX400MHz NMR spectrometer. ¹H NMR, ¹H-¹H COSY, and analysis were performed on all peptides on a Bruker AMX 400 MHz spectrometer, Bruker Instruments, U.K. Leucine^[51]-Enkephalin-(tBu) (LENK-tBu) and Tyrosine Palmitate Leucine^[51]-Enkephalin were analysed in deuterated water (D₂O, 0.6ml) and methyl sulfoxide (DMSO, 0.6mL) respectively. The concentrations of the peptide samples were in the range of 3-6mM; (Leucine^[51]-Enkephalin-(tBu): 3.57mM, Tyrosine Palmitate- Leucine^[51]-Enkephalin: 5.84mM). The analysis was performed at a temperature of 45°C or 50°C.

2.2.4.3 Fourier-Transformed Infrared Spectroscopy (FTIR)

The infrared absorption spectrum for the sample were obtained using a Nicolet Avatar 360 FT-IR ESPTH spectrophotometer (Nicolet Instruments, UK) equipped with a Thermo Nicolet SMART OMNI-Sampler accessory to perform Horizontal Attenuated Total Reflectance (HATR) and a germanium crystal (4000 to 675 cm⁻¹) and EZ Omnic IR software (maximum resolution is 1 cm⁻¹) averaging 512 scans at 2 cm⁻¹ resolution. The spectra were viewed with EZ Omnic Version 5.0 computer IR analysis program

(Nicolet Instruments, UK). A background spectrum was recorded on a clean germanium spectral window before a sample spectrum was recorded.

2.2.4.4 Analytical Reverse-Phase HPLC (RP-HPLC)

The peptides were analysed by reversed phase high-performance liquid chromatography on two reverse-phase Merck KGaA Cromolith columns (5 μ m, 4.6mm X 100mm x 2) with a total length of 250mm, using a Waters TM 515 HPLC pump connected to a Water TM 717 plus Autosampler with a Waters TM 486 Tunable Absorbance Detector. The mobile phase consisted of 82% 200mM phosphate buffer and 18% acetonitrile (pH 8.8). Unless otherwise indicated, samples were detected at 214nm. The flow rate was set at 1mL/min at 35°C for analytical runs and the injection volume at 40 μ L. The retention time was 6.8 for Leucine^[5]-Enkephalin and 7.8 for TPLENK and the lowest detection limit is 0.1 μ g/ml and 10 μ g/ml respectively. Empower software I was utilised for obtaining the results.

2.2.4.5 Transmission Electron Microscopy and Photon Correlation Spectroscopy

A drop of solution was placed on Formvar[®]/Carbon Coated Grid (F196/100 3.05mm, Mesh 300, Tab Labs Ltd, England). Excess sample was filtered off with No. 1 Whatman Filter paper and negatively stained with 1% aqueous Uranyl Acetate. Imaging was carried out under a FEI CM120 BioTwin Transmission Electron Microscope (TEM) (Ex. Philips, Eindhoven, Netherlands). Digital Images were captured using an AMT (digital) camera.

Peptide dispersions (1mg mL⁻¹, 2mg mL⁻¹) of Leucine^[5]-Enkephalin (LENK) [1mg] or Palmitoylated Leucine^[5]-Enkephalin (TPLENK) [1 or 2mg] were prepared by vortexing for 5 minutes and filtered if specified (Millipore Millex-HA, 0.45 μ m filter pore size) and the particle size determined by photon correlation spectroscopy (PCS) (Malvern Zetasizer 3000HS, Malvern Instruments, UK) at 25°C at a wavelength of 633nm and the data analysed using the Contin method of data analysis. Polymer solutions were left for 15 min at room temperature (25°C) before particle sizing was done. Measurements were performed in triplicate.

2.2.4.6 Scanning Electron Microscopy

The electron micrograph studies were carried out in a Philips XL 30 Microscope, School of Pharmacy, University of London. This technique was used to provide visual information regarding the morphological properties of the modified peptide such as surface porosity, roughness, and texture as well as size, size distribution and degree of agglomeration of the particles within the test sample. Dry powder TPLENK (PT24D) sample was mounted on a standard SEM sample holder and fixed on a brass/aluminium stub using double sided carbon impregnated adhesive discs. The sample was then sputtered coated with a conducting gold-palladium (10nm, 60% gold-palladium) coating using a SEM coating system for 2 minutes at 30 mA (Emitech K550 Sputter Coater, Emitech Limited, Ashford, UK, Deposition range: 0-50mA, Deposition rate: 0-25nm/min, Sputter timer: 0-4 min, Vacuum Pump: 85lit/min, room temperature) before viewed and photographed under a range of magnifications under high vacuum using Philips XL 30 ESEM FEG scanning electron microscope.

.....

2.2.4.7 X-Ray Powder Diffraction

X-ray diffraction measurements were performed on dry TPLENK using a Phillips X-ray Diffractometer (PW 1381/30, XRA66) and calculations of d-spacings and intensity values were made using the X'PERT data collector software. It utilises Cu K α radiation that has a wavelength of 1.5406 Å. Irradiation conditions were 45kV and 30mA x-ray tube voltage, a 0.04° soller slit, 1° divergence and antiscatter slits, and a 1/2° receiving slit for the scanning of diffraction angle 2 θ between 5° and 40°. The total number of collected reflections was 1750.

2.2.4.8 Conformation Search and Molecular Modelling

Initial structures of peptide and lipidic peptide were built using Maestro v 7.5 (Schrödinger), atom and bond types were adjusted and minimized with the OPLS2005 force field parameters (Mohamadi et al. 1990). The Generalised Born Solvent Accessibility (GB/SA) continuum solvent model for H₂O (Mohamadi et al. 1990), implemented in MacroModel, was used to simulate a solvent environment, with a

constant dielectric function ($\epsilon = 1$). An extended non-bonded cutoff (van der Waals: 8 Å, electrostatics: 20 Å) was used (Mohamadi et al. 1990).

A systematic conformational search on each molecule was performed. Monte Carlo conformational analysis 200 steps was carried out on optimised structures. The energy cut-off was generally set to $\Delta E = 30 \text{ kJ mol}^{-1}$ above the lowest energy conformation.

2.3 Results

2.3.1 Mass Spectrometry (MS)

2.3.1.1 Electrospray Ionisation Mass Spectrometry (ESI-MS)

Mass of synthesised peptides (expected mass, in Daltons) is: Leucine^[51]-Enkephalin - (tBu): 611.37, Leucine^[51]-Enkephalin: 555.27 and TPLENK: 794.51.

Leucine^[51]-Enkephalin-(tBu) (1mg) were dissolved in acetonitrile (1:1 ratio, 1ml) and infused into a Finnigan Mat TSQ 7000 (triple quadrupole) mass spectrometer operated in the positive EI mode at a rate of 1 mL h^{-1} , with needle voltage of 4.46 kV and capillary temperature of 250°C . The base peak ion observed in the ESI-MS spectrum for Leucine^[51]-Enkephalin-(tBu) correlates well with the molecular ion of the side-chain protected analog with the addition of a proton (i.e. $611+1 \sim 612.2 \text{ amu}$) (Figure 2.14). In the same spectra a second peak is observed that correlates for Leucine^[51]-Enkephalin (YGGFL^+ , $555+1 \sim 556 \text{ amu}$). However, apart from the molecular ion with a proton, the protected side-chain analog of Leucine^[51]-Enkephalin is also recorded as an adduct with Na (+23 amu). It is possible also to observe the dimer $(2\text{M}+\text{H})^+$ ($611 \times 2 + 1 \sim 1223.3 \text{ amu}$) and trimer $(3\text{M}+2\text{H})^+$ ($611 \times 3 + 2 \sim 1835.3 \text{ amu}$) of Leucine^[51]-Enkephalin-(tBu).

Leucine^[51]-Enkephalin (1mg) were dissolved in methanol (1:1 ratio, 1ml) and infused into a TSQ 7000 mass spectrometer operated in the positive EI mode at a rate of 1 mL h^{-1} , with needle voltage of $9.72 \times 10^8 \text{ V}$ and capillary temperature of 250°C . The base peak ion observed in the ESI-MS spectrum for Leucine^[51]-Enkephalin correlates well with the molecular ion with the addition of a proton (i.e. $555.27+1 \sim 556.3 \text{ amu}$) (Figure 2.15).

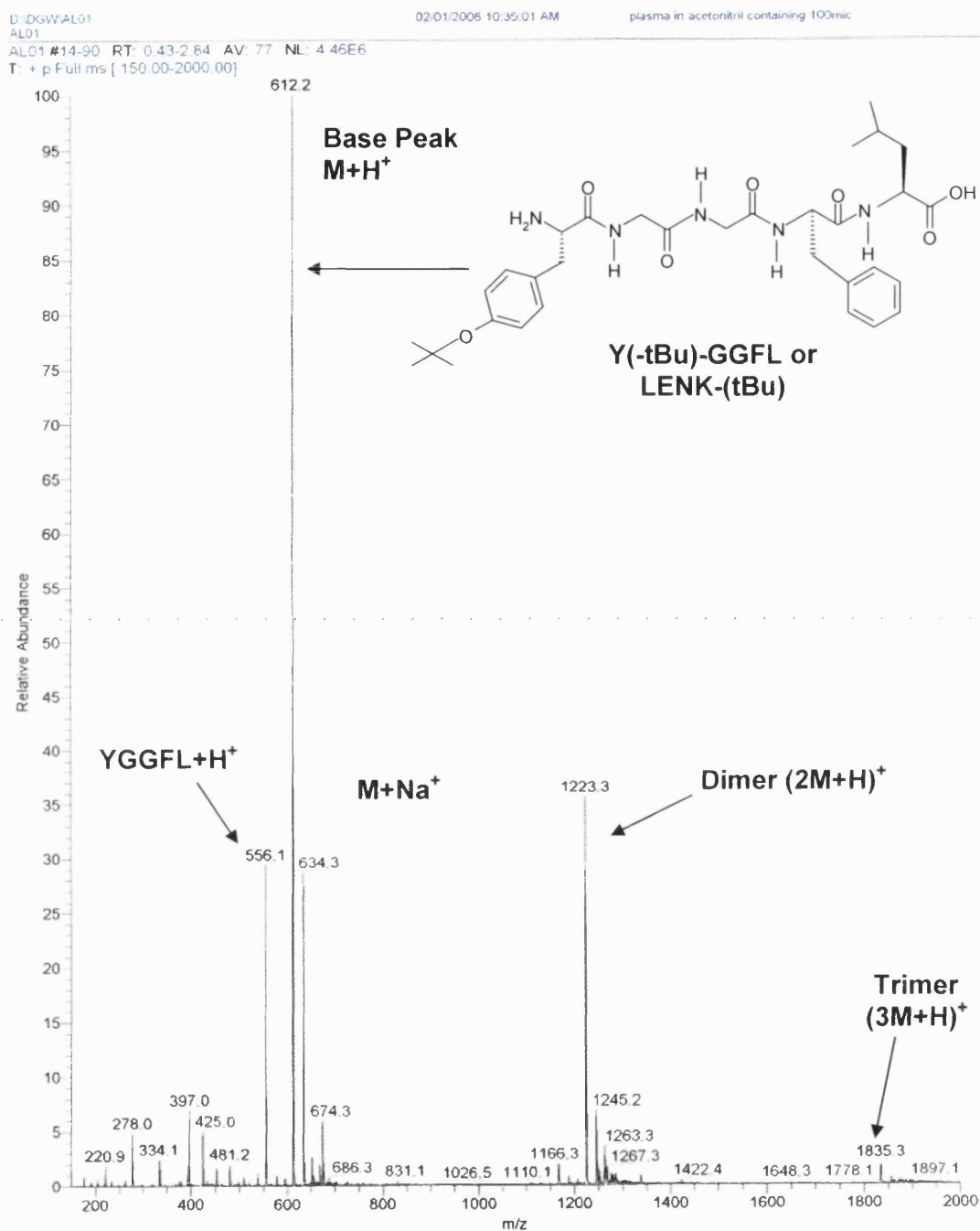


Figure 2.14: ESI-MS spectrum obtained for LENK-(tBu) or Y-(tBu)-GGFL.

lcq_3485 #2-12 RT: 0.02-0.13 AV: 11 NL: 9.72E8
F: + c ms [150.00-700.00]

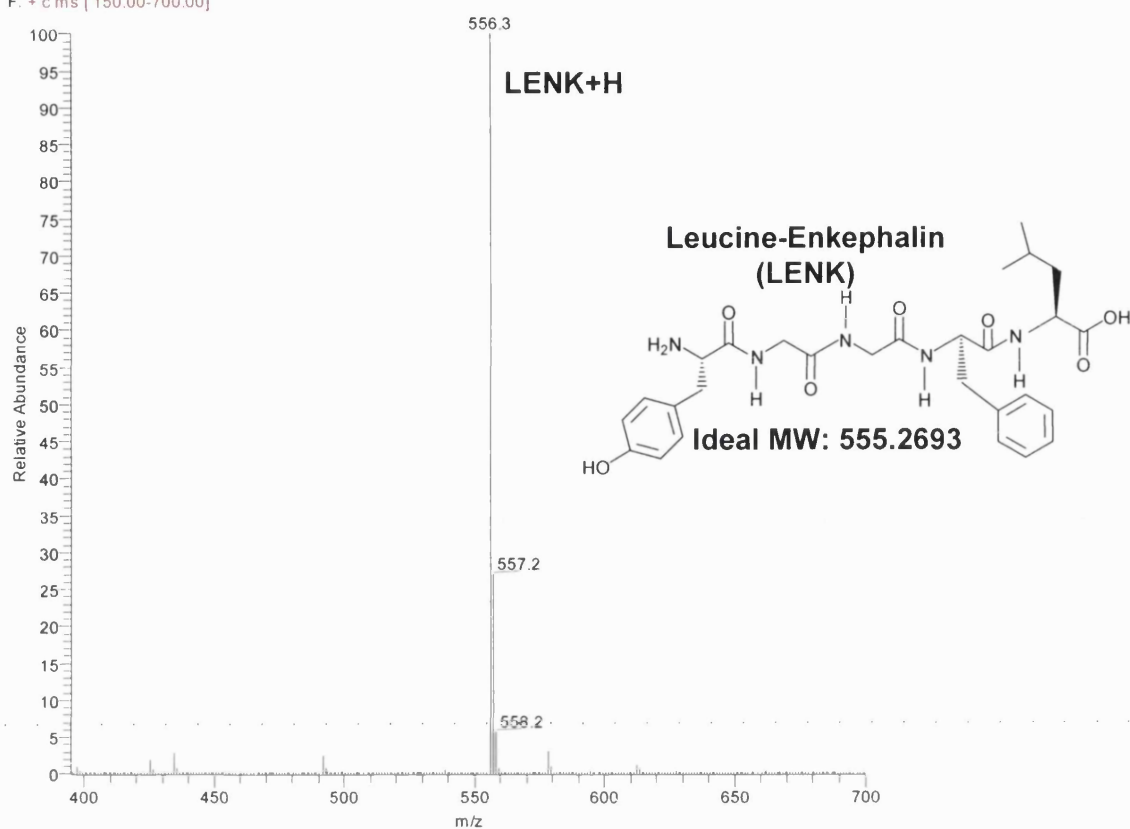


Figure 2.15: ESI-MS spectrum obtained for Leucine^[51]-Enkephalin.

Sample identification: pl 21
Acquired on 16-Mar-2007 at 12:39:50
(07/03/2007 24:03:40.51) C:\113\251

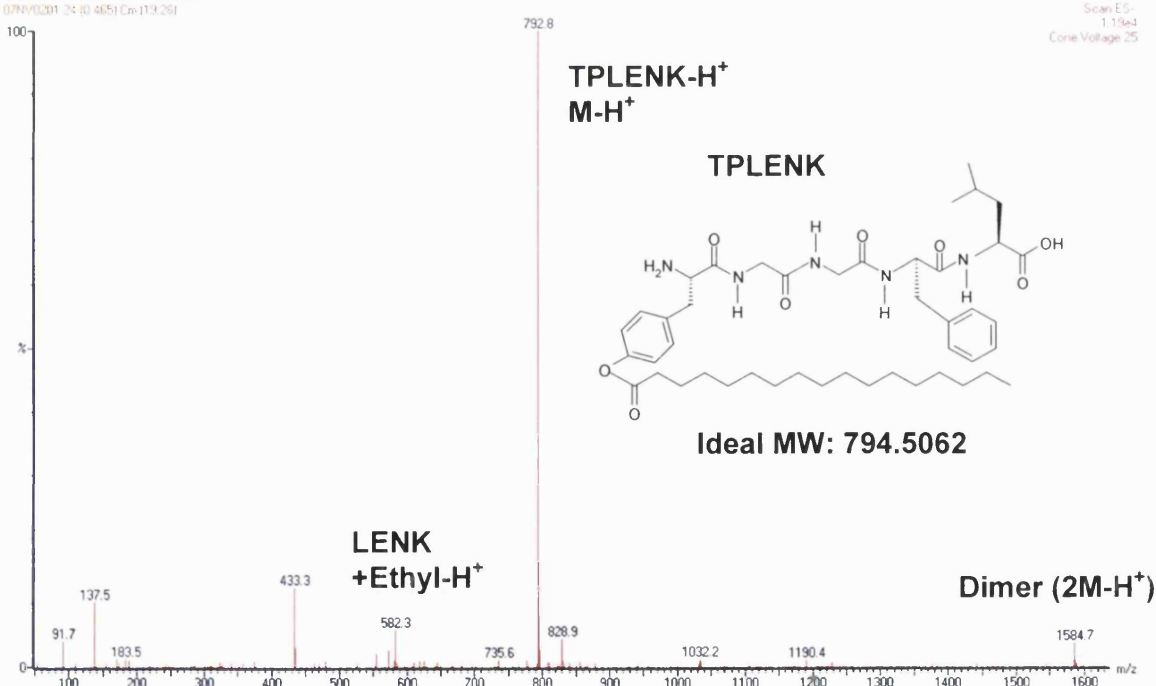


Figure 2.16: ESI-MS spectrum obtained for TPLENK.

Palmitoylated Leucine¹⁵-Enkephalin (TPLENK) (1mg) were dissolved in methanol (1:1ratio, 1ml) and infused into a TSQ 7000 mass spectrometer operated in the negative EI mode at a rate of 1mL h⁻¹, with cone voltage of 25 V and capillary temperature of 250°C. The base peak ion observed in the ESI-MS spectrum for TPLENK correlates well with the molecular ion with the addition of a proton (i.e. 794.51-1~792.8amu). In the same spectra a second peak is observed that correlates for Leucine⁵-Enkephalin (YGGFL⁻¹ + Ethyl, 555.27+28-1~582.3 amu). It is possible also to observe the dimer (2M-H)⁺ (792.8 x 2 -1~1584.7amu).

2.3.1.2 Tandem Mass Spectrometry (MS-MS)

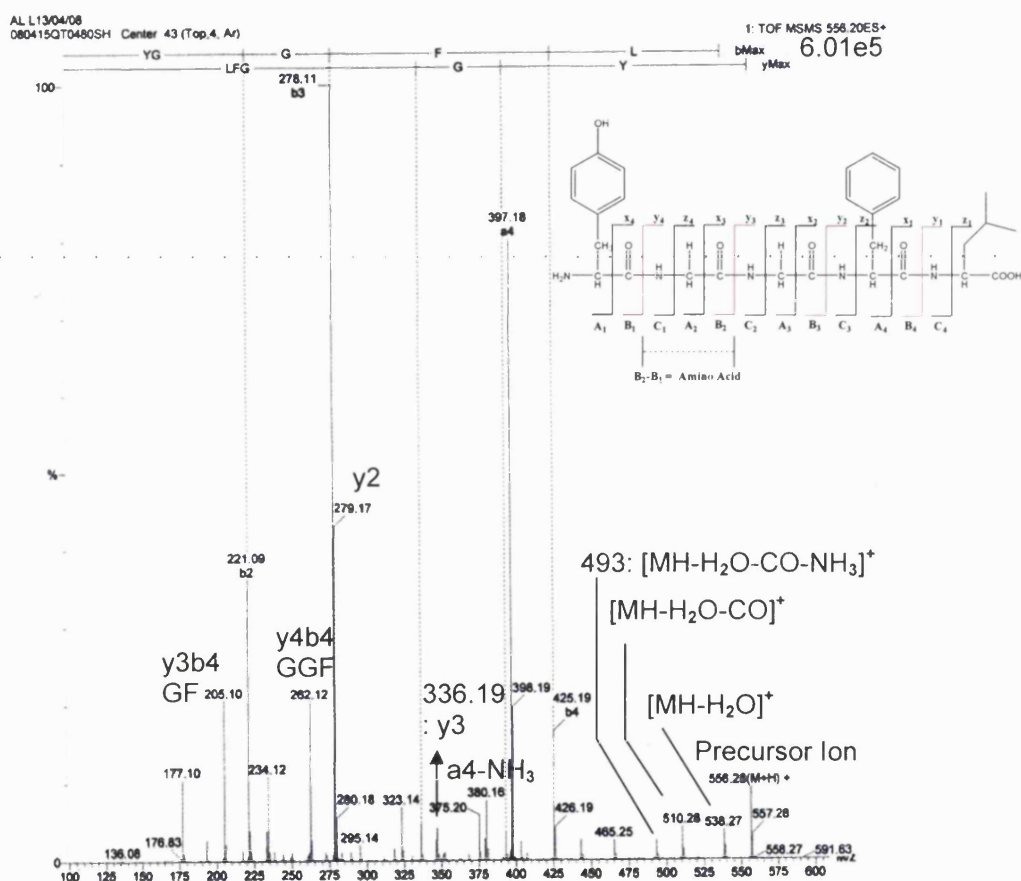


Figure 2.17: Tandem MS-MS spectra obtained for [YGGFL+1]⁺.

Tandem MS-MS confirmed the correct sequence after peptide synthesis (Figure 2.17). The most prevalent fragment ions present were the y ions (having the charge on the C-terminal).

Table 2.2 Tandem MS-MS for Leucine^[5]-Enkephalin**Predicted Fragment ions:****Monoisotopic / Average M/Z ratios with 1 positive charge(s)****Ions**

a	136.08	193.1	250.12	397.19	---
b	164.07	221.09	278.11	425.18	---
c	181.1	38.12	295.14	442.21	---
i	136.08	30.03	30.03	120.08	86.1
	1	2	3	4	5
	Tyr (Y)	Gly (G)	Gly (G)	Phe (F)	Leu (L)
	5	4	3	2	1
x	---	419.19	362.17	305.15	158.08
y	---	393.21	336.19	279.17	132.1
z	---	376.19	319.17	262.14	115.08

Residues**M/Z**

GG	115.05
GF	205.1
GGF	262.12

Observed Fragment ions-Precursor ion charge state: 1

a	136.08	193.1	250.12	397.19	510.27
	---	-0.00	-0.00	0.01	---
b	164.07	221.09	278.11	425.18	538.27
	---	-0.00	-0.00	-0.00	---
	Tyr (Y)	Gly (G)	Gly (G)	Phe (F)	Leu (L)
y	556.28	393.21	336.19	279.17	132.1
	---	-0.00	-0.00	---	---
z	539.25	376.18	319.16	262.14	115.08
	---	---	---	0.02	---

Key: Reducing colour intensity of fragment ions indicates reducing abundance after fragmentation.

2.3.2 Nuclear Magnetic resonance (NMR) Spectroscopy

¹H NMR spectra for both peptides were labelled with the aid of COSY as illustrated on each individual spectrum. In the case of TPLENK, NOESY were also performed, but due to the low concentration of the sample, the resulted spectra only assisted as further confirmation of the accuracy of assignments.

2.3.2.1 ^1H -NMR and ^1H - ^1H -Correlated Spectroscopy (COSY)-NMR

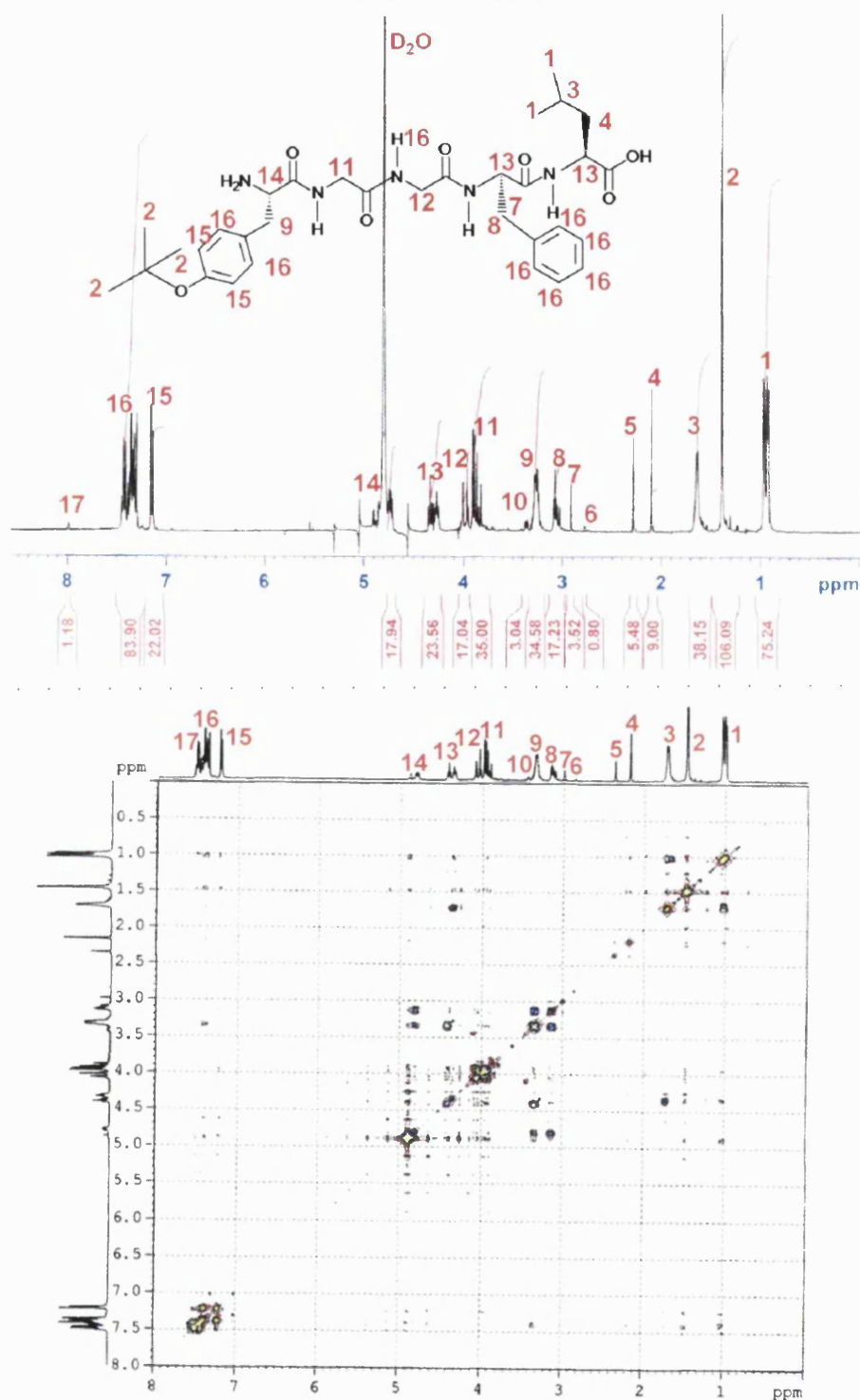


Figure 2.18: ^1H -NMR (top) and ^1H - ^1H COSY (bottom) (D_2O suppressed) spectrum of LENK-(tBu) (3.57 mM) in D_2O . Peaks 5,6,10, 17: Could not be assigned

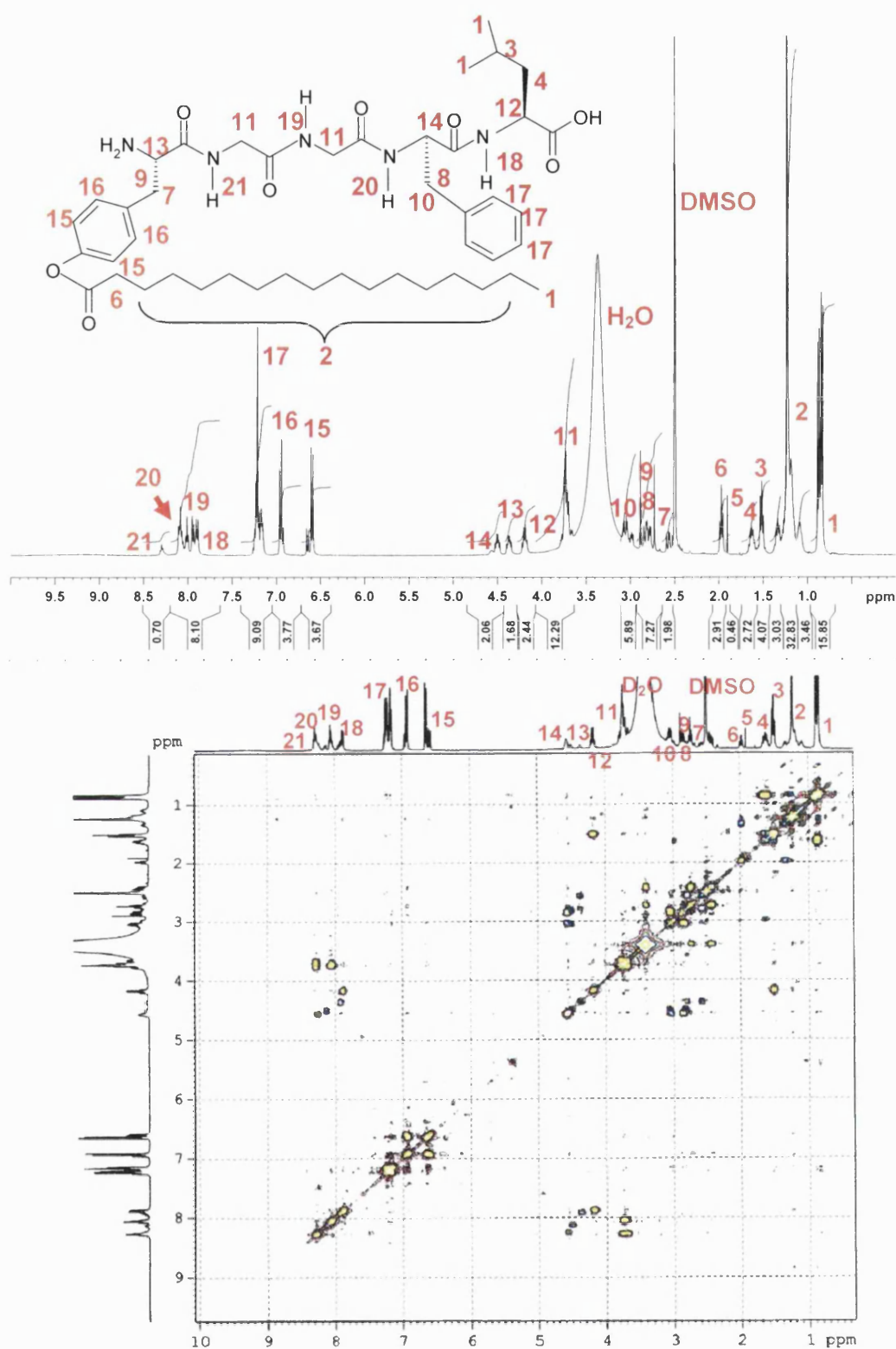


Figure 2.19: ^1H -NMR (top) and ^1H - ^1H COSY (bottom) obtained for TPLENK in DMSO at a concentration of 5.35mM. Peak 5: Impurity-possibly acetic acid.

2.3.2.2 Nuclear Overhauser Effect Spectroscopy (NOESY)

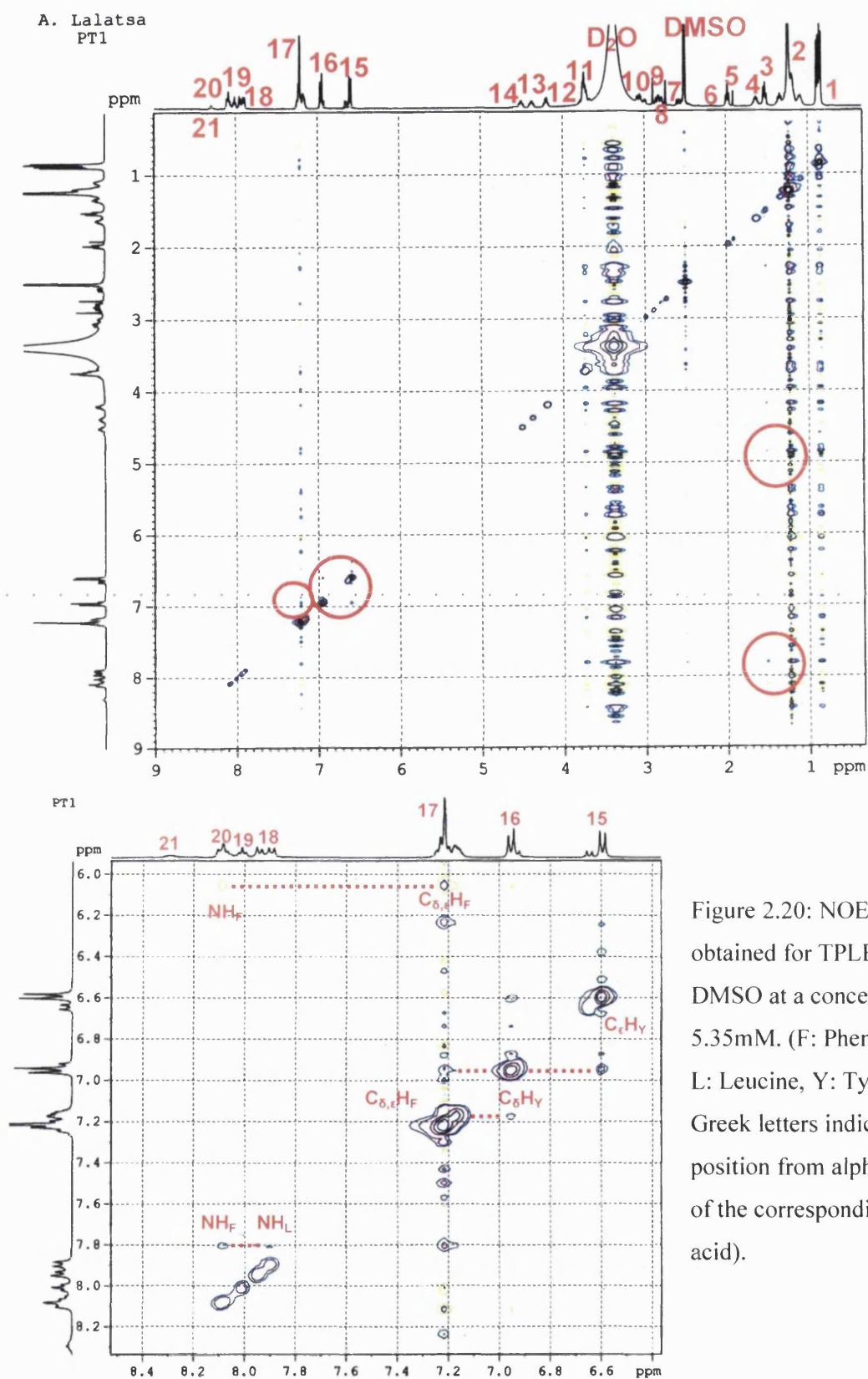


Figure 2.20: NOESY obtained for TPLENK in DMSO at a concentration of 5.35mM. (F: Phenylalanine, L: Leucine, Y: Tyrosine. Greek letters indicate the position from alpha carbon of the corresponding amino acid).

2.3.3 Fourier Transform Infrared (FTIR) Spectroscopy

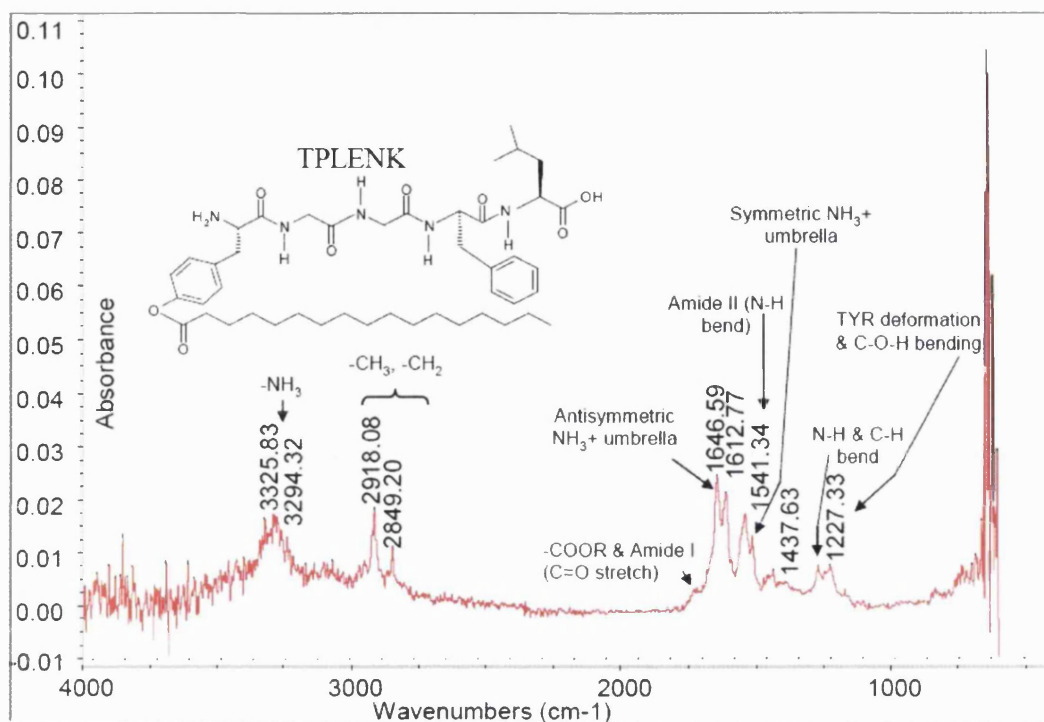


Figure 2.21: FTIR spectrum for TPLENK

The infrared absorption spectrum for the sample obtained shows the following significant bands, expressed in reciprocal wave numbers (cm^{-1}): 3326 (s), 3294 (s), 3241(s), 3173 (w), 3072(w), 2918 (s), 2849(s), 1727 (m), 1647 (s), 1613 (s), 1541 (s), 1526 (s), 1438 (m), 1277(s), 1227 (s), 700 (s), 686 (s), 667 (s), 658 (s), 647 (s), 638 (s), 626 (s), 618 (s), 607 (s). The error margin for all absorption bands of FTIR is $\pm 2\text{cm}^{-1}$. The intensities of the absorption bands are indicated as follows: (w): weak, (m): medium and (s): strong

2.3.4 Reverse-Phase High Performance Liquid Chromatography (RP-HPLC)

2.3.4.1 Analytical Reverse-Phase HPLC (RP-HPLC)

The calibration graph ($y = 4 \times 10^7 x$, $r^2 = 0.9988$) was created based on the concentration of the standards of Leucine¹⁵¹-Enkephalin and retained linearity between concentration of 100 ng ml^{-1} to 1.5 mg ml^{-1} . The calibration graph ($y = 190.88x + 2821.9$, $r^2 = 0.98724$)

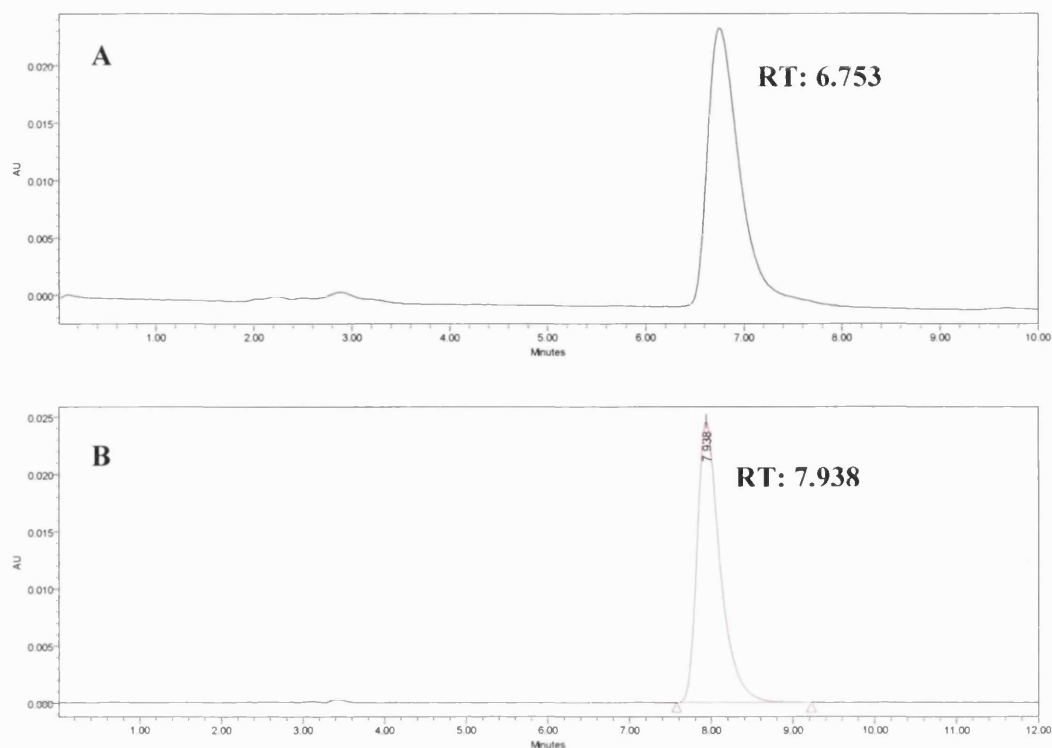


Figure 2.22: HPLC Chromatogram examples. A: Leucine^[51]-Enkephalin and B: TPLENK.

was created based on the concentration of the standards of TPLENK and retained linearity between concentration of $10 \mu\text{g ml}^{-1}$ to 1.0 mg ml^{-1} . Impurities present in the mixture would be detected at 214 nm if present. Absorbance could also be monitored at 280 nm where the phenolic moiety of the tyrosine residue in both the parent peptide (LENK) as well as the analog (TPLENK) absorb. The samples of LENK synthesised have retention times that correlate well with the standards obtained from a commercial supplier (Figure 2.22). The retention time for TPLENK differs from that of LENK for almost a minute indicating a more hydrophobic compound that would be retained more strongly on a reverse-phase column and elute later.

2.3.4.2 Preparative Reverse-Phase HPLC (RP-HPLC)

Fractions 6 (e.g. retention time between 6 and 7 minutes) and 7 (8 ml in total) were pooled for Leucine^[51]-Enkephalin (Retention time: 7.13) and fractions 8 to 9 were pulled for TPLENK (Retention time: 8.3) (Figure 2.23). Peptide purity was identified to be 95% (HPLC) for LENK and 90% (HPLC) for TPLENK. Leucine^[51]-Enkephalin was

found as an impurity occasionally due to the close retention time of the two peptides but it was always less than 5% of the total lipidic peptide. Yield of the purification procedure was 58% (54- 61%) for LENK and ~40% (29-53%) for TPLENK.

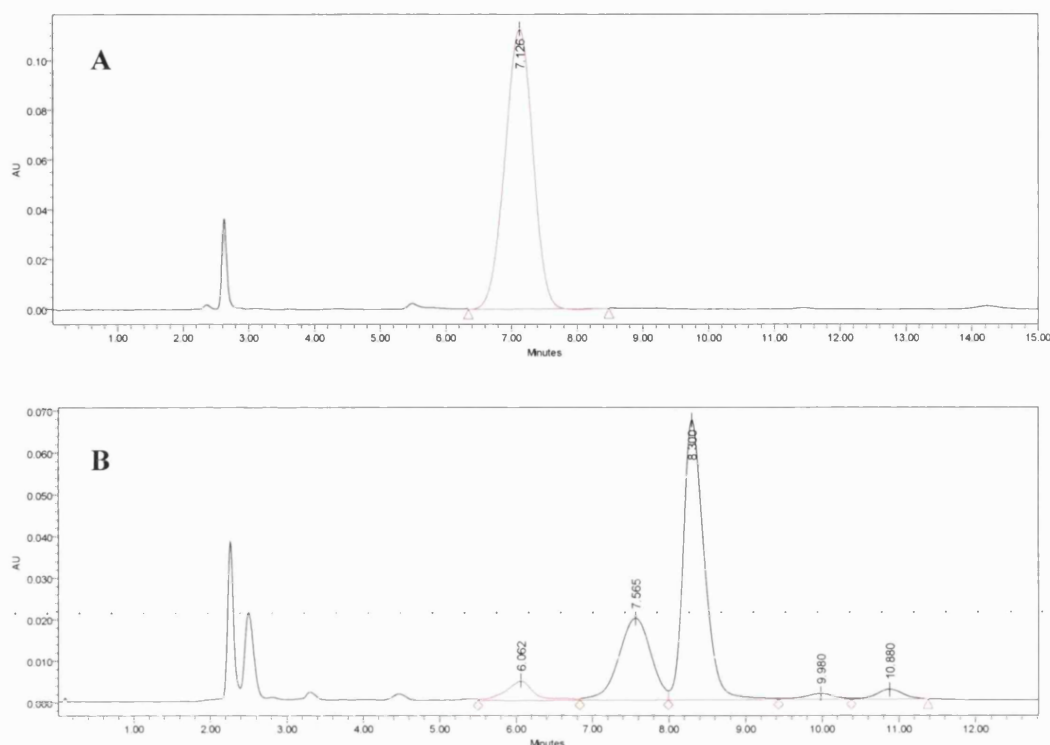


Figure 2.23: Preparative HPLC Chromatogram examples. A: Leucine^[5]-Enkephalin (LENK) and B: TPLENK.

2.3.5 Transmission Electron Microscopy and Photon Correlation Spectroscopy

Unfiltered negative stained solutions of LENK and TPLENK were examined with the aid of TEM. The clear LENK solution (1 mg ml⁻¹) gave a PCS mean size of ~370 nm which correlated well with the aggregates observed with TEM. The micrographs illustrated that the peptide amphiphile (TPLENK) in aqueous media appears to have morphology similar to small amyloid-like fibrils (longer than 0.4-1 μm in length and between 10-15 nm in diameter) with a mean size between ~400-700 nm. Sonication seems to disrupt mesh formation leading to formation of more compact aggregates (mean size of ~1 μm).

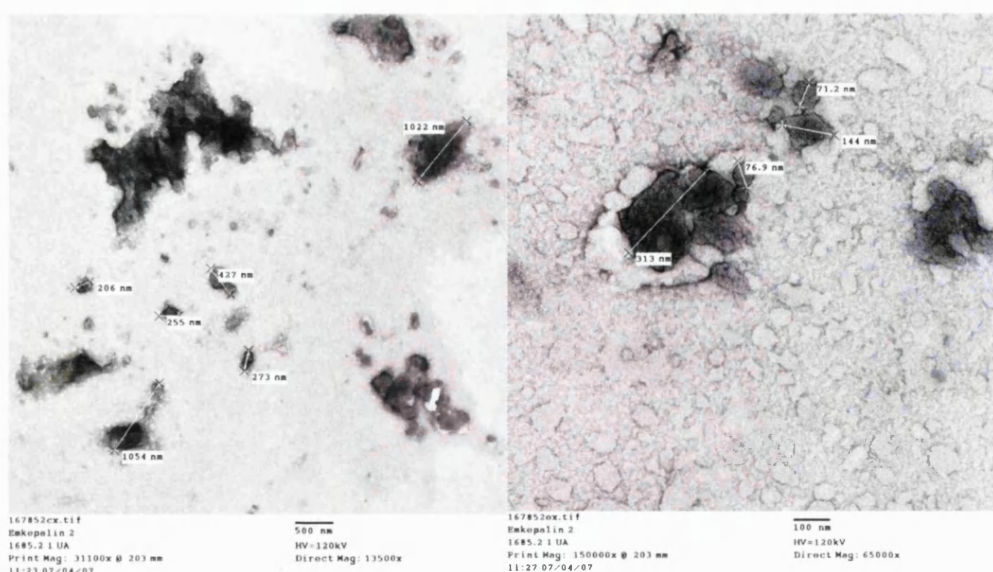


Figure 2.24: TEM images of LENK (1 mg mL^{-1}) in H_2O (vortexed,unfiltered). Bar: 500 nm (left) and 100 nm (right).

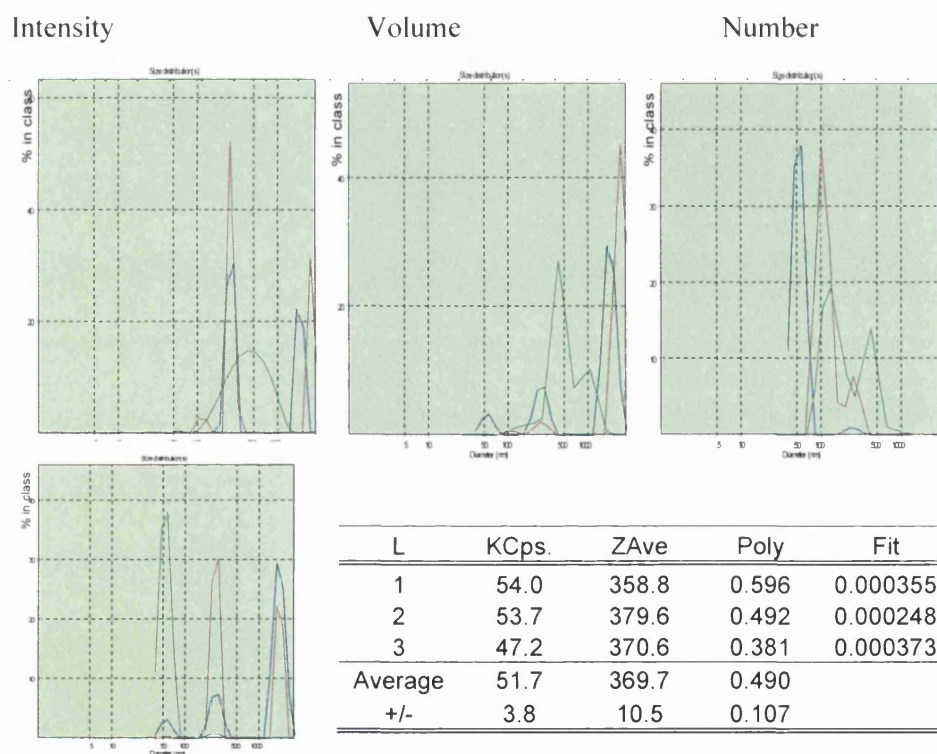


Figure 2.25: PCS spectrum for LENK in H_2O (1 mg mL^{-1}) only after vortexing for 4 minutes. Sample appeared clear. On top from left to right are the size distributions by intensity, volume, and number for triplicate runs (Run 1: red; 2:green; 3:blue). On the bottom, the size distribution combined by intensity (red), volume (green) and number (blue) along with a summary table of results.

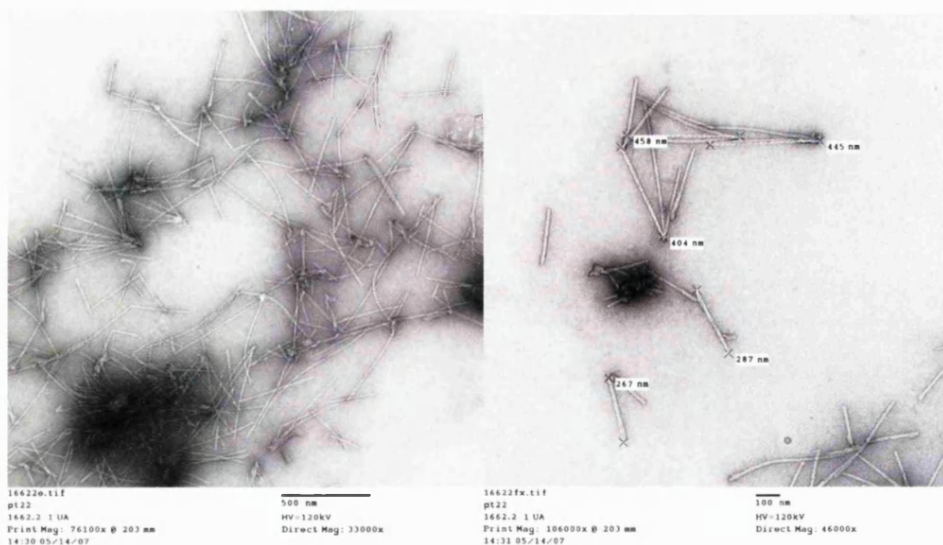


Figure 2.26: TEM images of TPLENK (2mg ml^{-1}) in H_2O (vortexed, unfiltered).

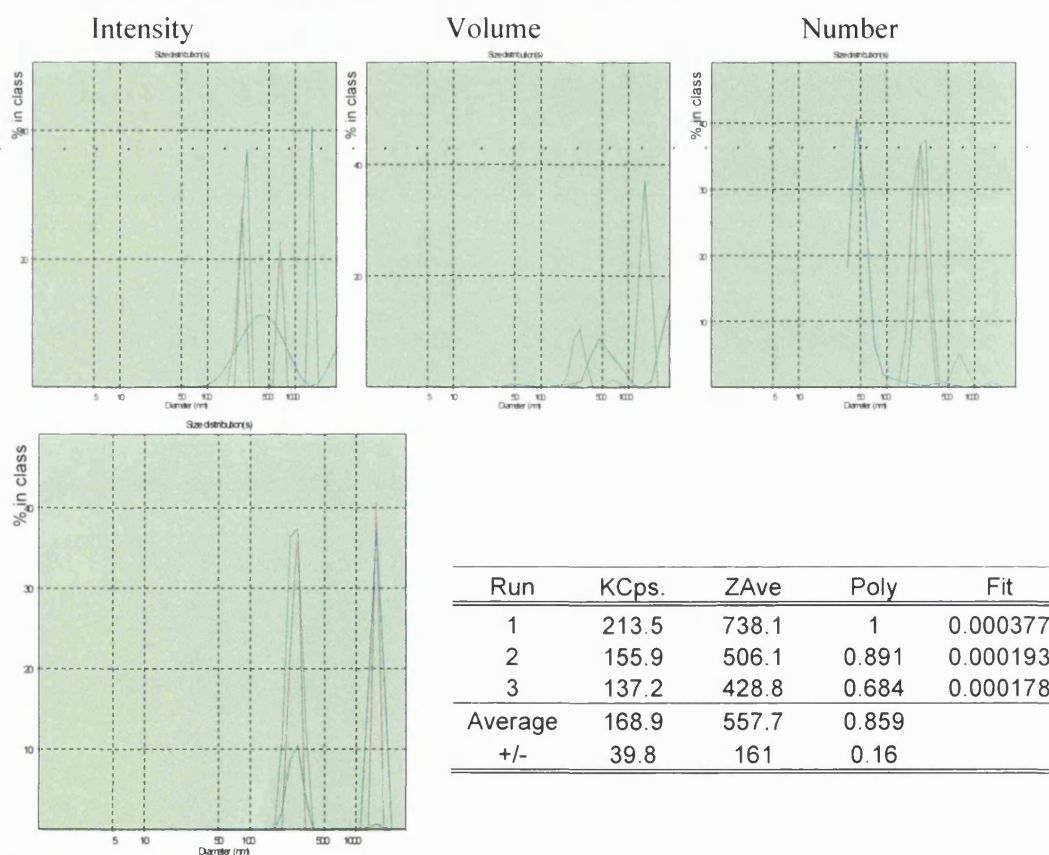


Figure 2.27: PCS spectrum for TPLENK in H_2O (2 mg mL^{-1}) only after vortexing for 4 minutes. Sample appeared translucent. On top from left to right are the size distributions by intensity, volume, and number for triplicate runs (Run 1: red; 2:green; 3:blue). On the bottom, the size distribution combined by intensity (red), volume (green) and number (blue) along with a summary table of results.

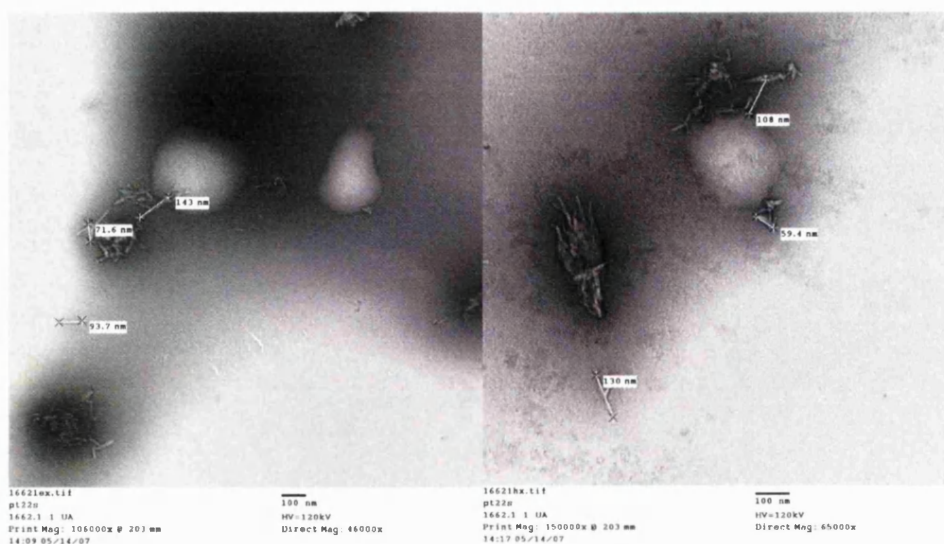


Figure 2.28: TEM images of TPLENK (1mg mL^{-1}) in H_2O (sonicated on ice for 2.5 min)

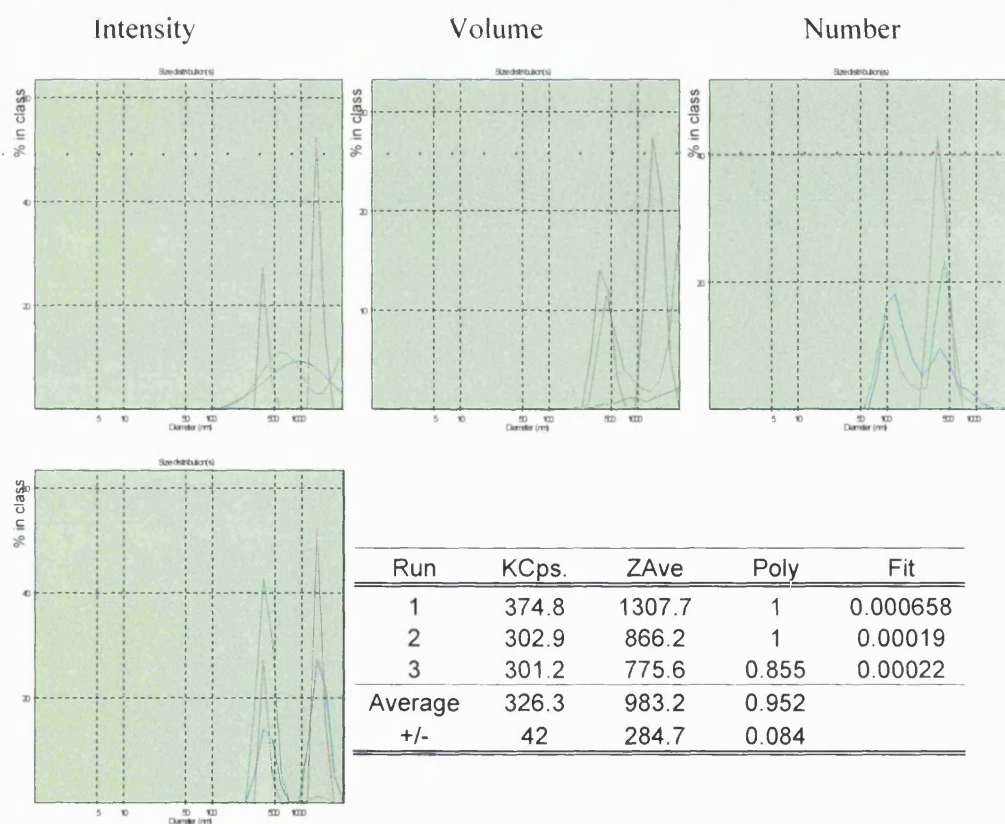


Figure 2.29: PCS spectrum for TPLENK in H_2O (1mg mL^{-1}) only after vortexing for 4 minutes and sonication. Sample appeared translucent. On top from left to right are the size distributions by intensity, volume, and number for triplicate runs (Run 1: red; 2:green; 3:blue). On the bottom, the size distribution combined by intensity (red), volume (green) and number (blue) along with a summary table of results.

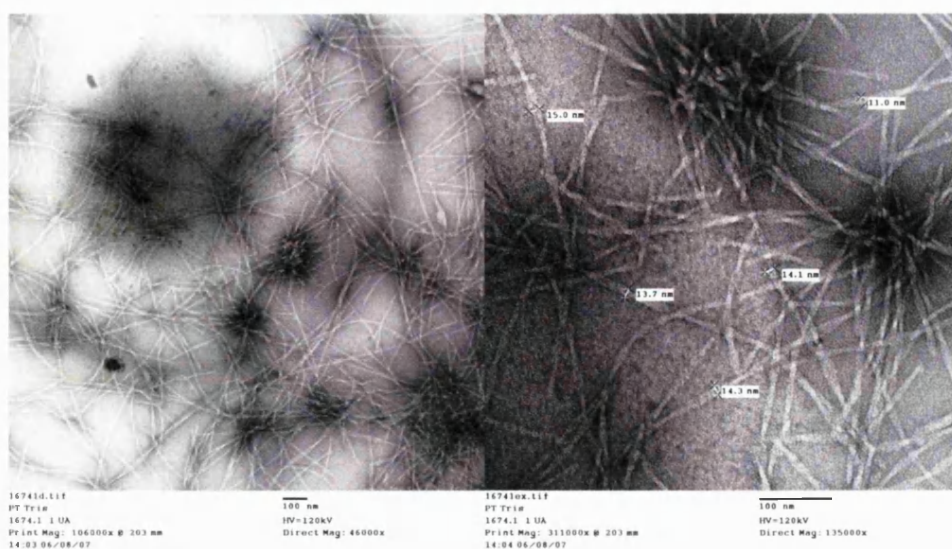


Figure 2.30: Negative stained TEM images of an unfiltered aqueous dispersion of TPLENK (1mg mL⁻¹) in Tris Buffer 100 mM pH 7.4 after vortexing. Bar: 100 nm.

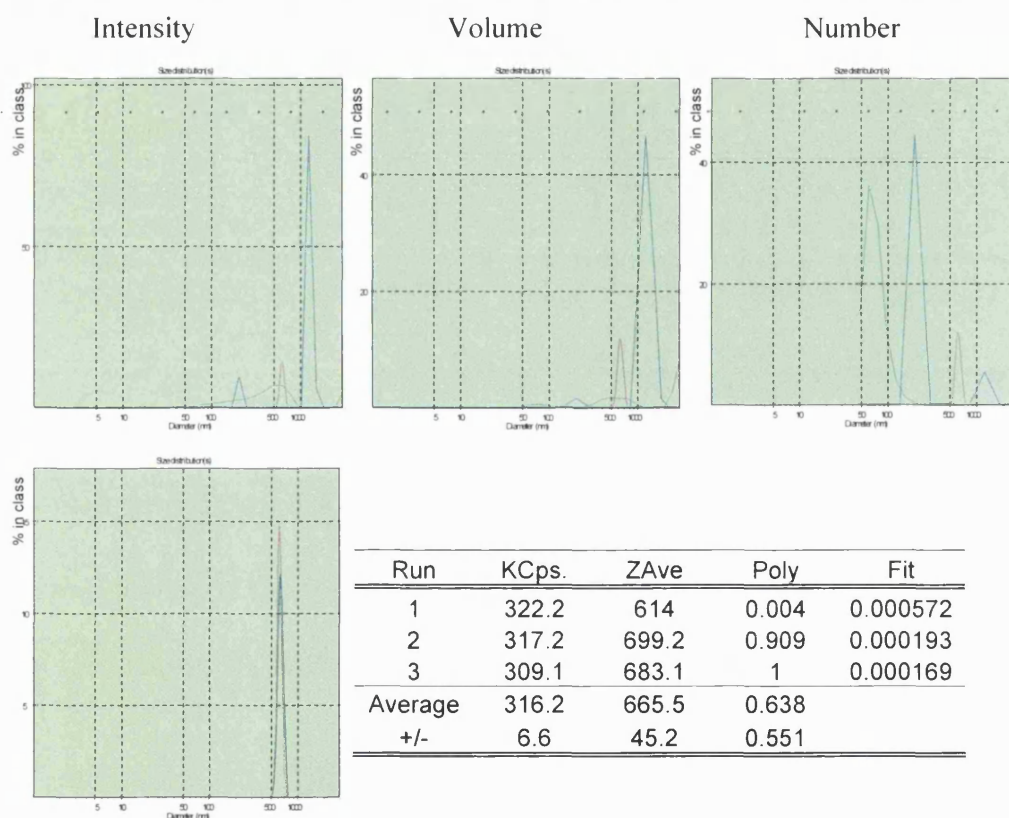


Figure 2.31: PCS spectrum for TPLENK in Tris Buffer 100mM (pH 7.4) (1 mg mL⁻¹) only after vortexing. Sample appeared translucent. On top from left to right are the size distributions by intensity, volume, and number for triplicate runs (Run 1: red; 2:green; 3:blue). On the bottom, the size distribution combined by intensity (red), volume (green) and number (blue) along with a summary table of results.

2.3.6 Scanning Electron Microscopy

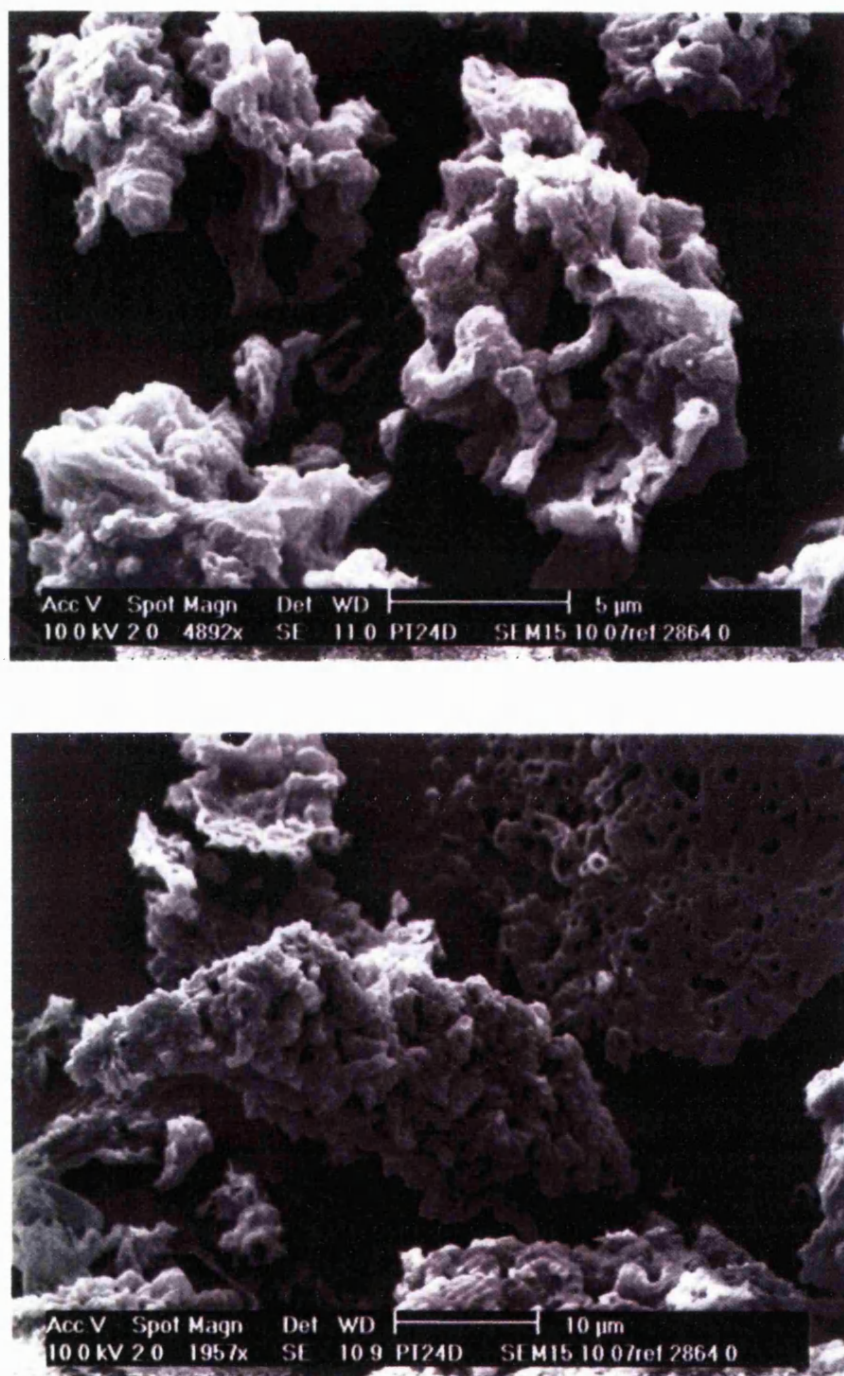


Figure 2.32: SEM images of TPLENK.

TPLENK has a porous interwoven structure which a high degree of porosity and rough, uneven edges based on the SEM micrographs.

2.3.7 X-ray Powder Diffraction

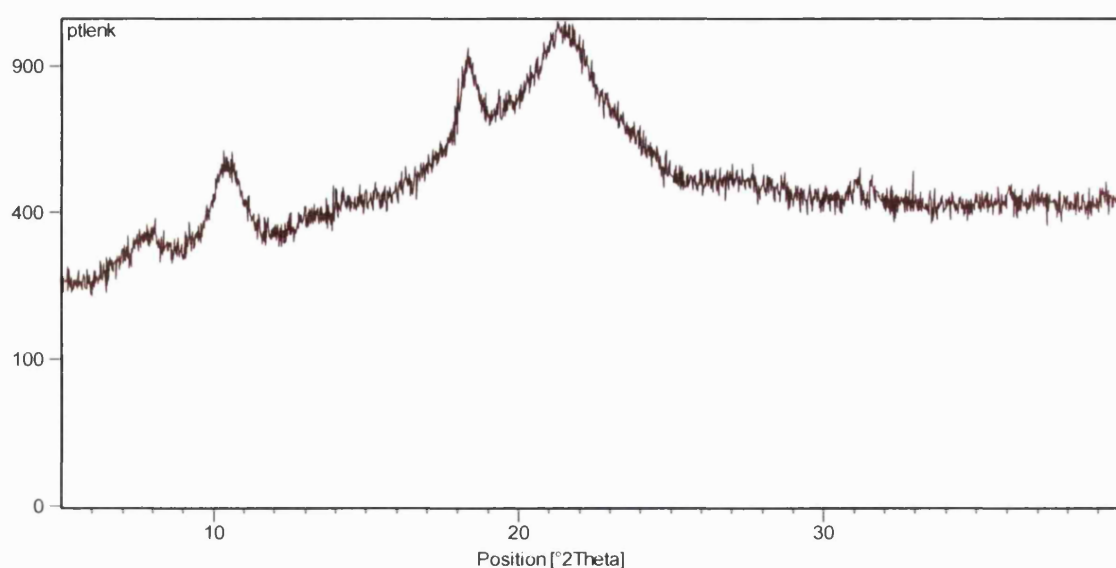


Figure 2.33: X-ray diffractogram of TPLENK

Table 2.3: X-ray diffraction results for TPLENK

No.	Pos. [°2Th.]	d-spacing [Å]	Rel. Int. [%]	FWHM [°2Th.]	Area [cts*°2Th.]	Backgr.[cts]	Height [cts]
1	8.0176	11.02755	21.79	0.1574	9.78	285	62.95
2	10.4506	8.46508	73.81	0.7085	149	323	213.2
3	14.0137	6.31978	24.24	0.0394	2.72	400.18	70.03
4	16.3213	5.43108	6.47	0.1574	2.9	481.56	18.69
5	18.357	4.83314	99.72	0.1574	44.74	641.7	288.05
6	21.3983	4.15259	100	0.3149	89.72	758	288.84
7	24.8367	3.58495	15.05	0.059	2.53	532.33	43.48
8	26.9601	3.30723	7.94	0.7872	17.81	475	22.93
9	28.6686	3.1139	9.15	0.1574	4.11	453	26.43
10	31.119	2.87407	17.39	0.1968	9.75	431	50.22
11	31.5998	2.83143	20.77	0.1181	6.99	428.51	59.98
12	33.4948	2.67323	16.25	0.072	4.51	417	46.94
13	33.656	2.663	17.26	0.059	2.9	417	49.85
14	36.0905	2.48876	17.22	0.1968	9.66	419	49.75
15	37.1155	2.42235	7.64	0.4723	10.28	420	22.07

During x-ray diffraction analysis, x-ray beams are reflected off the parallel atomic layers within a compound over a range of diffraction angles (Geology 2002). Because the x-ray beam has a specific wavelength, for any given d-spacing (distance between adjacent atomic planes) there are only specific angles at which the exiting rays will be “in phase” and therefore, will be picked up by the detector producing a peak on the

diffractogram (Geology 2002). Every compound has its own unique set of diffraction peaks that can be used to identify it (Geology 2002).

Peaks were observed for TPLENK at 2θ 8° , 10° , 14° , 18° , and 21° (Table 2.3). TPLENK diffraction pattern reveals a partially amorphous structure.

2.3.8 Conformation Search and Molecular Modeling

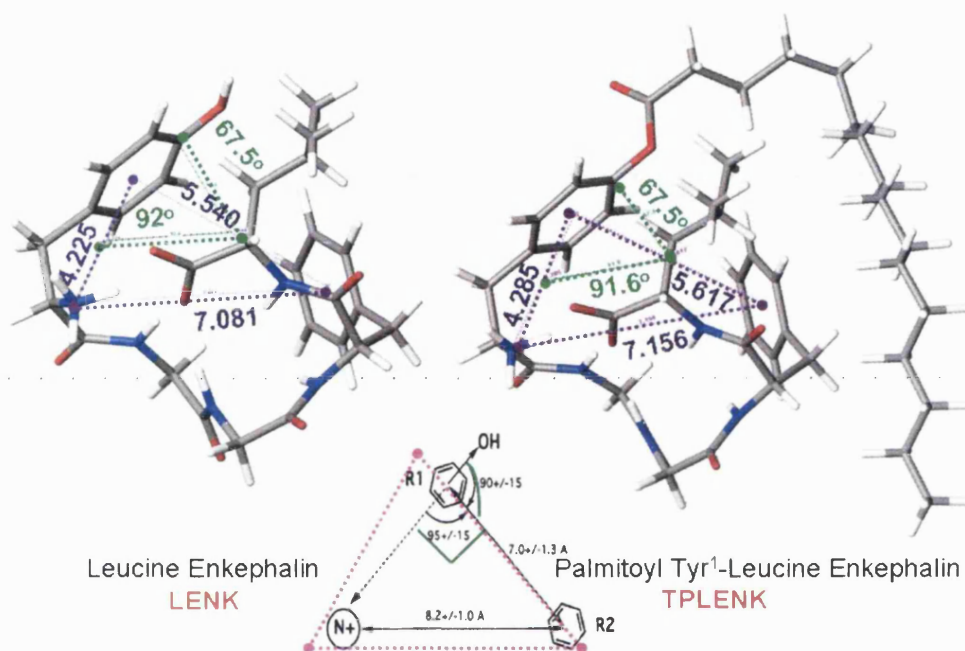


Figure 2.34: Comparison of lower energy conformation for Leucine^[51]-Enkephalin and the lipidic TPLENK with a proposed pharmacophore for the δ -opioid receptor.

Based on our conformation search, the β -turn structure of Leu-Enkephalin was retained after lipidisation of peptide, therefore addition of a hydrophobic tail on the phenolic –OH of Tyrosine has not altered dramatically the conformation of Leucine^[51]-Enkephalin required for binding to the opioid receptor and thus, activity (Figure 2.34). Repeating the conformation search with the same conditions but for 4 molecules of Leucine^[51]-Enkephalin illustrated some H-bonding potential between only 3 of the molecules, while TPLENK has shown a higher potential for hydrophobic interactions and has a higher propensity for aggregation in presence of H_2O (Figures 2.35, 2.36).

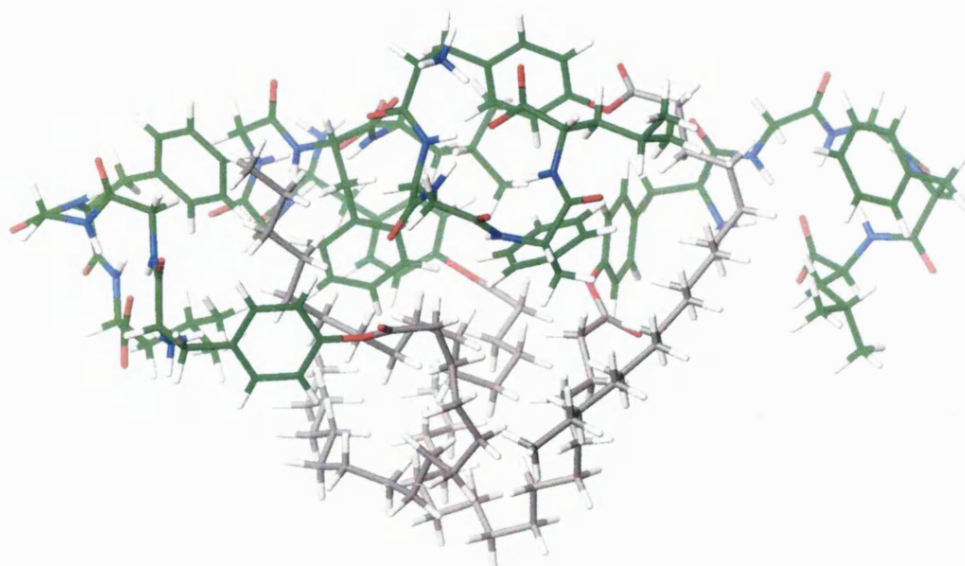


Figure 2.35: Lower energy conformation in H₂O for 4 molecules of the lipidic peptide.

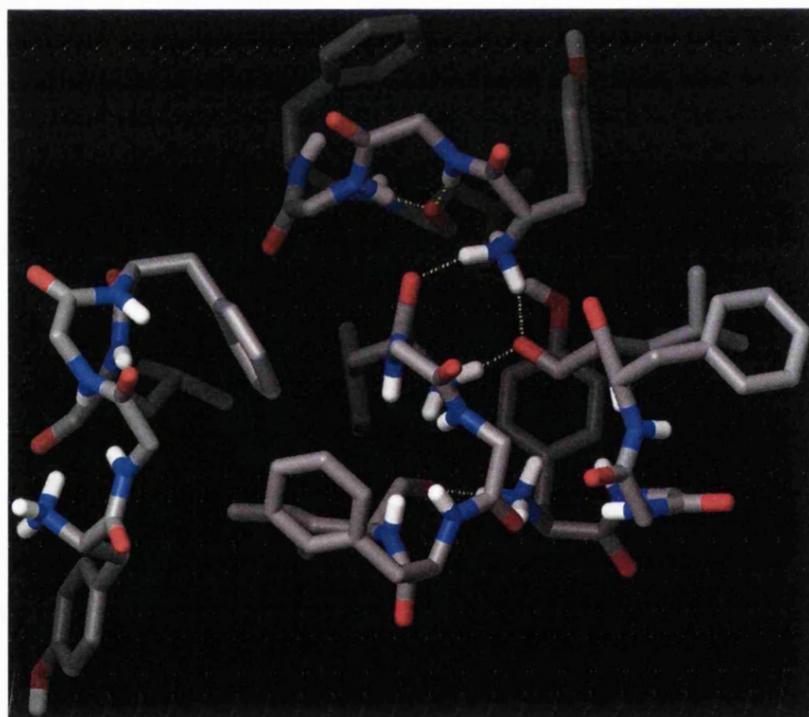


Figure 2.36: Lower energy conformation for 4 molecules of Leucine^[5]-Enkephalin in the presence of H₂O.

2.4 Discussion-Conclusions

Since the discovery of endogenous peptides with opiate activity, many potential roles have been identified for these substances. Possible therapeutic applications could extend from treatment of opiate dependence to numerous other CNS-mediated dysfunctions. Opioid peptides are implicated in mediating neuroendocrine activity, behavioral stress responses, eating disorders, alcoholism, schizophrenia and in modulating memory function, sexual behaviour and development (Bodor and Buchwald 1999). However, analgesia remains their best-known role, and is commonly used to evaluate endogenous opioid peptide activity (Bodor and Buchwald 1999).

A novel analog of Leucine^[5]-Enkephalin (LENK), an endogenous opioid neuropeptide, was synthesised by esterification of the phenolic hydroxy moiety of Tyrosine. The hydroxyl moiety was preferred for esterification compared to the free C-terminal of Leu⁵, as the latter is shown to be crucial for eliciting opioid activity (Uchiyama et al. 2000). Short linear chain (up to butyl) derivatives with acylation of the phenolic hydroxyl group of tyrosine showed better results than derivatives with esterification of the C-terminal carboxyl group (Ogawa et al. 2003). Additionally, esters have shown particular promise in prodrug design for targeting the brain due to the abundance of endogenous esterases in the CNS. Incorporation of labile lipid motifs (palmitoylation) into LENK will enhance the lipophilic character of the neuropeptide and contribute to cellular uptake with minimal alteration of the native sequence. The increase in molecular weight of the endogenous peptide remains small (from 555 to 794 in the case of LENK and TPLENK), which is still within the range of molecular weights (150-800 Da) of compounds found to be useful for the treatment of CNS diseases.

The synthetic approaches used to synthesise the tyrosine palmitate Leucine^[5]-Enkephalin (TPLENK) involved the already activated ester of palmitic acid in the presence of base. Although higher temperatures and shorter reaction times have been used for completion of palmitoylation reactions (e.g. 37 °C or 50°C), 24 hours at room temperature has proven adequate (Ekrami et al. 1995; Tsai et al. 1997).

The 2-chloro-trityl resin was used as the solid-support for the synthesis. The prominent advantages of this resin include negligible perturbation of the attached chain/group and high loading with ease of acid-mediated cleavage. The resin can be cleaved off either with TFA (95% TFA, 5% Phenol as a scavenger) or with a mixture of acetic acid, trifluoroethanol and dichloromethane (2:2:6 v/v/v) (Barlos et al. 1991). The latter cleavage mixture allows for cleavage of the resin while not cleaving off any side-chain protecting groups (e.g. -tBu). Therefore, it allows flexibility in the synthetic process. Furthermore, cleavage with acetic acid instead of TFA:Phenol (95:5) was preferred to cleave TPLENK from the 2-chloro-trityl resin because peptide fragmentation or more likely cleavage of the ester bond between the added palmitic tail and the hydroxy moiety of tyrosine was observed when TFA:Phenol (95:5) was used using ESI-MS (results not shown) as neither the parent peptide (LENK) or the analog (TPLENK) was evident. Thus, acetic acid based cleavage mixtures were used for cleavages, which proved to be effective resulting in an intact palmitoylated tyrosine unaffected as demonstrated with ESI-MS, MALDI-TOF and NMR.

.....

The synthesis of the lipidic peptide can be easily scaled up manually by reacting the Fmoc-protected peptide residue on the solid support with 5-8 molar excess of the palmitic acid N-hydroxysuccinimide ester (in the presence of 30-48 molar excess of triethylamine) directly in the reaction vessel that will be left shaking at the end of the synthesis for 24 hours at room temperature. After completion of the reaction, deprotection and cleavage can follow in the reaction vessel, and the filtrate collected in a round bottom flask will then be rotaevaporated, precipitated, centrifuged and freeze-dried according to the existing protocol. Scaling up thus from 0.1mmole scale to 1 mmole scale can easily take place using a “1g” reaction vessel (for up to 0.5 mmole scale as the weight of 0.5 mmole pre-loaded resin: ~ 1g) or a “2g” reaction vessel (for processes between 0.5-1 mmole scale) that will allow adequate swelling of the solid support. The synthesis can easily also be performed with an automated peptide synthesizer (by addition of the dissolved active ester of palmitic acid in DMF as an extra amino acid and modifying the reaction time) and can also be monitored by directly assaying the reaction mixture with UV or HPLC.

Mass spectrometry was used routinely to screen batches of synthesised peptide after purification. ESI-MS was preferred due to the small molecular weight of the peptides

and as fragmentation of the peptides was not proven to be a problem with Leucine^[5]-Enkephalin or TPLENK being the precursor ion. Tandem mass spectrometry (MS) was conducted on every batch of synthesised peptide and confirmed correct amino acid sequence after peptide synthesis. In the case of Leucine^[5]-Enkephalin, the spectra obtained correlate well with the expected fragmentation pattern for this peptide (Figure 2.17 and Table 2.2). Leucine^[5]-Enkephalin was preferred for tandem MS as the fragmentation pattern is well documented compared to that of TPLENK. However, as the same batch of Fmoc-YGGFL-2-Cl-Trt-resin was used for synthesis of both LENK and TPLENK, tandem MS of LENK is adequate to prove the amino acid sequence of TPLENK as well.

Apart from MS, NMR further provided evidence for the esterification of the phenolic –OH. The concentration of sample used was not adequate to provide a better resolved spectrum that could be used to extrapolate conformation parameters of TPLENK (NOESY). However, it was adequate to allow assignment of the ¹H NMR peaks with confidence using COSY. Nuclear Overhauser Effect (NOE) is caused by dipolar coupling between nuclei that is, the total field at one nucleus is affected by the presence of another nucleus. The intensity of the interactions is a function of the distance between the nuclei (according to the following equation: $I = A (1 / r^6)$, where I is the intensity of the signal, A is a scaling constant and r is the distance between nuclei). Cross peaks of higher intensity that are most likely to appear would be between: NH_i to NH_{i+1}, CαH_i to CαH_{i+1} and CβH_i to NH_{i+1}. The cross peaks indicated in Figure 2.20 (bottom) illustrate protons that are close in space (<5 Å), and are indicative of an interaction between the protons of the aromatic ring of tyrosine (Cδ_{1,2} and Cε_{1,2}) and phenylalanine (Cδ_{1,2} and Cε_{1,2} that overlap as peak 17). Simulation studies of neutral and zwitterionic LENK in DMSO and in water, respectively, have suggested that the pentapeptide has a tendency to form a compact bent structure through salt bridge formation between the peptide termini (van der Spoel and Berendsen 1997) while more recent molecular dynamics simulation studies also support a bent model with close head to tail arrangement and a 2 to 5 hydrogen bond at neutral pH (Aburi and Smith 2002; Chandrasekhar et al. 2006). Thus, the interaction of the aromatic rings is proof of their close proximity in space, possibly that of a 1-4 β-turn. A higher sample concentration (~20-30 mM) in a mixture of 90:10 D₂O:H₂O (to prevent loss of signals of amide protons from exchange with solvent deuterons) would have been more appropriate to

repeat the experiment in order to study further the conformation of TPLENK using NMR. D₆-DMSO was selected in this experiment due to the solubility needs of the peptide in combination with the fact that medium-sized molecules (500-1000) have weak NOE cross peaks unless they are studied in a more viscous solvent such as d₆-DMSO. d₆-DMSO has a smaller dielectric constant than water, is a more effective hydrogen bond acceptor and is 3.5 times more viscous than water.

FTIR spectroscopy provided further evidence for the successful synthesis of TPLENK with two strong bands at 2918 and 2849 cm⁻¹ along with a medium band at 1727 cm⁻¹ indicative of C=O stretch of an ester bond. X-ray crystallography showed a partially amorphous structure. However, it is difficult to combine the X-ray d-spacings with the NOESY spectra due to the lack of a crystallised structure for TPLENK. Linear peptides are not easy to crystallize, mainly because of their tendency to exist in several quasi-isoenergetic conformations (Meirovitch and Meirovitch 1996) and opioid peptides are particularly difficult, owing to the presence of the G-G motif in most of the sequences (Spadaccini and Temussi 2001).

TEM studies revealed that TPLENK can act as an amphiphile and has the ability to form a dense network of fibres in excess of 1µm long and a diameter of 10-15 nm (Figure 2.26, 2.30). Thus, dissolving TPLENK in water and placing it on a surface that is allowed to dry (e.g. directly on a TEM grid) are adequate to drive molecular self-assembly. It seems obvious that the presence of the palmitic tail is long enough to favour thermodynamically the extensive formation of nanofiber networks. The self-assembly process is mediated through weak intermolecular bonds, such as van der Waals bonds, electrostatic interactions, hydrogen bonds and stacking interactions. These low energy interactions are combined together to form intact and well-ordered supramolecular structures. A parallel molecular direction for the self-assembly of nanoscale peptide structures was reported by Stupp and co-workers and was based on the conjugation of single hydrophilic peptide motif with hydrophobic alkyl tail to form amphiphilic peptides (Figure 2.37). Peptide-based tubular structures can also self-assemble from linear peptides such as bolamphiphiles peptides synthesised by Matsui et al. by conjugating two hydrophilic peptides through a hydrophobic peptide linker. The intermolecular association of the hydrophobic moieties in the aqueous solution to form ordered structures similar to a micellization process was proposed as the driving force.

However, the exact mechanism that leads to self-assembly of polypeptides into ordered fibrils *in vitro* (and *in vivo*) is not fully elucidated.

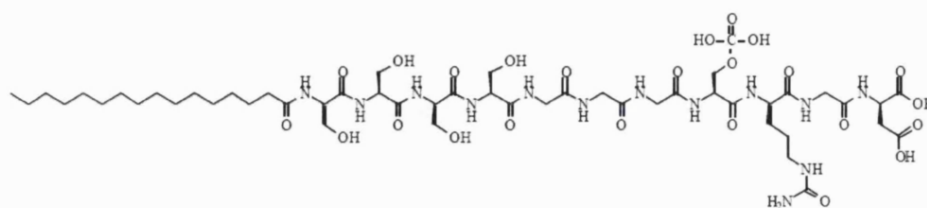


Figure 2.37: Peptide-conjugate amphiphile composed of hydrophilic peptide with hydrophobic alkyl tail (palmitic tail). From: (Reches and Gazit 2006).

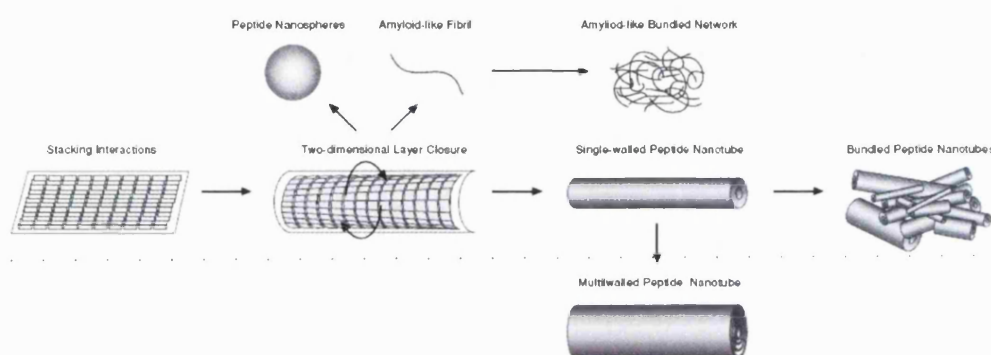


Figure 2.38: Schematic model for the formation of the various structures by aromatic homo-dipeptide (such as diphenylalanine and diphenylglycine). The specific organisation could lead to tubular (single walled or multi-walled), spherical or fibrillar structures. Due to geometrically-restricted interactions of the aromatic moieties and their complex hydrophobic and electrostatic nature, various changes in the electronic environment of the aromatic system in the context of very small peptide, can significantly affect the organisation of the assembled formed (Reches and Gazit 2006).

The importance of the phenylalanine residue in amyloid fibrils formation by a minimal amyloid-forming fragment of islet amyloid polypeptide was demonstrated, as substitution of phenylalanine by an alanine abolished the ability of the fragment to form amyloid fibrils *in vitro* (Reches and Gazit 2006). Based on this observation and the remarkable occurrence of aromatic residues in other short amyloid related sequences, stacking of aromatic residues was suggested to play a role in acceleration of the process of amyloid fibrils formation (Reches and Gazit 2006) (Figure 2.38). The presence of phenylalanine in TPLENK along with the addition of a long hydrophobic tail on the N-

terminal and a Leucine (hydrophobic) residue on the C-terminal can potentially work synergistically leading to TPLENK self-assembly.

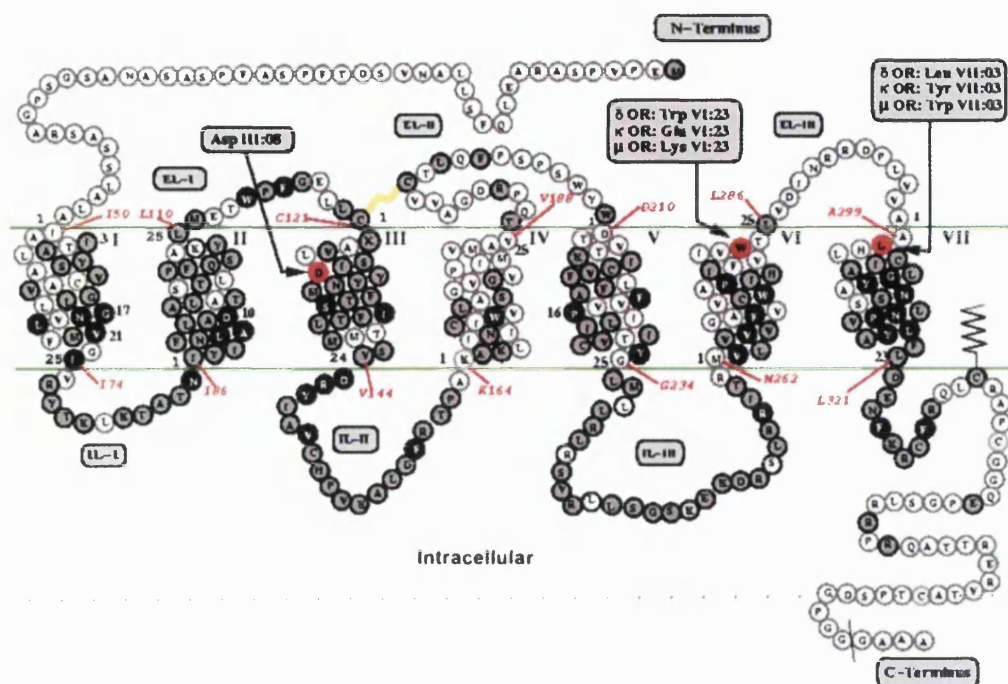


Figure 2.39: Model of the δ receptor. Circles contain the 1-letter code for the given amino acid. Green lines indicate the beginning and ends of the helices. The gray circles indicate the residues that are conserved among all 3 receptor types (μ , δ and κ), while the black circles indicate the residues that are highly conserved among the rhodopsin subclass of G-protein coupled receptors. Each transmembrane (TM) domain is indicated by a roman numeral. At the beginning and end of each helix there are Arabic numbers starting with 1 and ending at 25 (variable, depending on helix length). These numbers correspond to the position of the residue within the helix. For example, the Asp in TM III is denoted as III:08. Asp indicates aspartate; EL: extracellular loop; Glu: glutamine; IL: intracellular loop; Leu: Leucine; Lys: Lysine, OR: Opioid receptor; Trp: Tryptophan; Tyr: Tyrosine (Kane et al. 2006)

Because opioid receptors do not have a crystal structure, sequence analysis methods have been important in revealing many of the receptors' general characteristics and classifying them into class A G-protein coupled receptors (GPCR) resembling rhodopsin (Figure 2.39) (Knapp et al. 1995; Kane et al. 2006). These membrane-bound

proteins contain an extracellular N-terminus, 7 transmembrane helices, and an intracellular C-terminus. The helices are bundled in a counter-clockwise fashion and connected intra-and extracellularly by loops that vary in size and composition (Kane et al. 2006). The “message-address” concept states that ligands contain different recognition elements that are responsible for their differential binding activities (Kane et al. 2006). Their shared, or universal, portion represents the “message” while their unique, or variable portion represents the “address” (Kane et al. 2006). For opiates, Beckett and Casy proposed a crude receptor model that encompassed these characteristics: the tyramine moiety (the amine, which is expected to be protonated at physiological pH, and phenol) which represents the message and a third which is a hydrophobic region that further stabilises the ligand to the receptor site (Beckett and Casy 1954). Comparison of opiates to the catecholamines suggested that binding occurs within conserved regions of the transmembrane helices, specifically via a salt bridge between the free amine and the carboxylate of a Asp (Asp III:08) and hydrogen bonding of the phenolic –OH of a His (His VI:17) (Kane et al. 2006). Furthermore, sequence analysis revealed that a cluster of conserved hydrophobic residues existed approximately halfway down transmembrane helices III to VI (Trp IV:10, Phe V:13, Phe VI:09 and Trp VI:13) (Attwood and Findlay 1994). For the δ receptor specifically hydrophobic stabilisation involves residues unique to the δ receptor found at the top of transmembrane VI and VII (Trp VI:23, Leu VII:04, Ala VII:-01) (Kane et al. 2006). This pocket of the δ receptor can accommodate larger hydrophobic ligand domains compared to the one present in the μ receptor due to steric bulk created by the presence of Trp VII:03 residue (instead of a Ala, Leu, or Lys), which can act as a differentiating factor for δ -selective agonists (Kane et al. 2006).

Many structural proteins contain amphipathic helices, which consist of hydrophobic, non-polar residues on one side of the helical cylinder and hydrophilic and polar residues on the other side, resulting in a hydrophobic moment. In this way, they aggregate with other hydrophobic surfaces and serve for example as pores or channels in the cell membrane. A helical wheel (Figure 2.40) provides a possibility to visualise an amphipathic helix. Considering the esterification of the phenolic –OH with a long hydrophobic tail, an increase amphipathicity of TPLENK can be hypothesised.

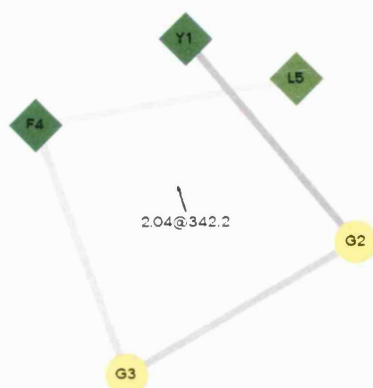


Figure 2.40: Helical wheel for Leucine¹⁵-Enkephalin. By default the output presents the hydrophilic residues as circles, hydrophobic residues as diamonds, potentially negatively charged as triangles, and potentially positively charged as pentagons. Hydrophobicity is color coded as well: the most hydrophobic residue is green, and the amount of green is decreasing proportionally to the hydrophobicity, with zero hydrophobicity coded as yellow. Created using: (Armstrong and Zidovetzki 2004).

Recently a study done with (4-Carboxamido) Phenylalanine instead of a Tyrosine moiety has shown increased δ selectivity for the δ -opioid receptor and has challenged the long-standing belief that a phenolic residue is required for high affinity binding (Wang et al. 2007). This study also revealed a structure in aqueous solution of a single-bend packed state stabilised by an intramolecular hydrogen bond from Leu⁵-NH to Gly²-CO (Wang et al. 2007), which was also observed in our conformation search. Enkephalins are very flexible and a highly constrained tyrosine derivative of enkephalin can have an increased opioid selectivity (especially δ) by binding of /stabilising the lipidic tail via hydrophobic interactions to the unique residues of the δ opioid receptor that create a hydrophobic pocket (Kane et al. 2006).

To summarise, a novel lipidic ester analog of Leucine¹⁵-enkephalin was synthesised purified and characterised. Addition of the palmitic tail although it increased the amphipathicity of the molecule, did not alter significantly the required pharmacophore for binding to the δ opioid receptor.

Chapter 3

GCPQ Synthesis & Formulation Characterisation

3.0 Introduction

Administering drugs orally is by far the most widely used and preferable route of administration. However, it is not feasible generally for peptide and protein drugs. Although peptides and proteins have become the drugs of choice for the treatment of numerous diseases as a result of their incredible selectivity and their ability to provide effective and potent action (Frokjaer and Otzen 2005), they possess low oral bioavailability due to presystemic enzymatic degradation and poor penetration of the intestinal membrane. Oral peptide delivery would not only be non-invasive and relatively free from complications arising from the need for sterile techniques usually occurring with parenteral formulations, but would also be convenient, easily dosed with low preparation costs, all of which would encourage patient compliance.

Recently, polymer nanoparticles have been widely investigated as a carrier for drug delivery (Gref et al. 1994). Briefly, nanoparticles have been used as oral drug carriers for several reasons: i) improvement of the bioavailability of drugs with poor absorption characteristics, (ii) prolongation of the residence time of drugs in the intestine, (iii) high dispersion at the molecular level and consequently increase in absorption, (iv) delivery of vaccine antigens to gut-associated lymphoid tissue (v) control of the release of the drugs, (vi) targeting of therapeutic agents to a particular organ and thus reducing toxicity, (vii) reduction of gastrointestinal irritation caused by drugs and (viii) assurance of the stability of drugs in the gastrointestinal tract (Pinto Reis et al. 2006). Polymeric nanoparticles have a special role in targeted drug delivery in the sense that they have all the advantages of liposomes including small size (Wu et al. 2005). But unlike liposomes, polymeric nanoparticles have a long shelf life, can entrap more drugs and have greater stability in biologic fluids as well as during storage. (Wu et al. 2005; Pinto Reis et al. 2006; Qu et al. 2006). Nanoparticles cross the gastric and intestinal epithelium in greater extent than microspheres ($>1\mu\text{m}$) (Desai et al. 1996; Behrens et al. 2002; Lin et al. 2009). Polymer nanoparticles from biodegradable and biocompatible

polymers are good candidates for drug carriers to deliver drugs, because they are expected to be absorbed in an intact form in the gastrointestinal tract after oral administration (Florence et al. 1995; Behrens et al. 2002).

Chitosan (CS) is the second most abundant polysaccharide and a cationic polyelectrolyte present in nature (Wu et al. 2005). Chitosan has shown favorable biocompatibility characteristics (Hirano et al. 1989) as well as the ability to increase membrane permeability, both *in vitro* (Lehr et al. 1992; Aspden et al. 1997; Chornet and Dumitriu 1998) and *in vivo* (Takeuchi et al. 1996; Le and Uchegbu 2006), and be degraded by lysozyme in serum (Wu et al. 2005). It has the potential of serving as an absorption enhancer across the intestinal epithelium for its mucoadhesive and permeability enhancing property (Janes et al. 2001). It has been proved that CS can enhance insulin and other peptide drugs absorption across human intestinal epithelial (Caco-2) cells without injuring them permanently (Artursson et al. 1994; Schipper et al. 1996; Schipper et al. 1997; Schipper et al. 1999; Thanou et al. 2001; Thanou et al. 2001). CS has been used in preparing films, beads, intragastric floating tablets, microspheres, and nanoparticles in the pharmaceutical field (Wu et al. 2005). However, nanoparticulate formulations possessed advantages over microparticulate formulations ($>1\mu\text{m}$) (McClellan et al. 1998). With their easy accessibility in the body, nanoparticles can be transported via the circulation to different body sites prolonging the duration of the therapeutic effect while delivering the drug to specific sites.

Quaternary Ammonium Glycol Chitosan (GCPQ), a carbohydrate polymer, has been shown to enhance significantly drug bioavailability of propofol measured as an increase in sleeping time up to 10 times after intravenous injection of the anaesthetic when compared to commercial formulations (e.g. Fresenius or Diprivan[®]) *in vivo* (Qu et al. 2006). Thus, this evidence of delivery of a centrally active drug across the blood-brain barrier with significant increase in bioavailability is demonstrating that GCPQ may prove beneficial for CNS delivery. The mechanism by which these carbohydrate amphiphiles improve drug delivery to the CNS is not fully understood. However, the particle size ($< 0.45\mu\text{m}$, filtered) and particle size distribution of the commercial propofol formulation is larger than that seen with the GCPQ micellar clusters ($< 0.45\mu\text{m}$, filtered) (Qu et al. 2006). On the other hand, recent data suggest that GCPQ is significantly increasing oral bioavailability of cyclosporin, a cyclic undecapeptide BCS

class IV drug, when compared to a commercial cyclosporin formulation (Neoral[®]) (Le and Uchegbu 2006). Only a handful of peptides have been studied for their oral delivery potential utilising nanocarriers (such as insulin, octreotide, somatostatin, vasopressin, luteinizing hormone releasing hormone and cyclosporine (Pinto Reis et al. 2006)) and from them only a single study using poly (butylcyanoacrylate) nanoparticles double coated with polysorbate 80 and poly(ethylene) glycol 20,000 was successful in delivering an analgesic peptide orally to the central nervous system as shown solely by pharmacodynamic studies (Das and Lin 2005). Thus, the potential use of a biocompatible chitosan polymer for the oral delivery of bioactive peptides that are CNS active is explored.

3.1 Materials and Methods

3.1.1 Materials

Table 3.1 Materials for GCPQ synthesis and characterization

Chemical Name	Name	Purity	Company
Acetic Acid		AnalaR	VWR international
Acetonitrile HPLC grade	ACN	≥99.99%	Fischer Scientific
Amberlite IRA-96, free base, 20-50mesh			FLUKA CHEMIKA
Fomvar / Carbon Support Film, Copper Grid 3.05mm, 300 mesh,			School of Pharmacy, University of London
Deuterium Oxide 99.9 atom %D	D ₂ O	99.90%	ALDRICH or Goss Scientific Instruments Ltd.
Dialysis Tubing-Visking Size Size 6 Inf. Dia. 27/32"-21.5mm:30M MWCO:12-14000 Daltons			Medicell International Ltd. , London
Diethylether	Ether	≥99.5%	BDH or Fischer Scientific
Ethanol (Absolute)	Ethanol	99%	School of Pharmacy, University of London
Glycol Chitosan, ≥60% (colloidal titration), crystalline	GC		SIGMA
Hydrochloric Acid	HCL	36.5-38%	VWR International

Chemical Name	Name	Purity	Company
Iodomethane, Reagent Plus		99%	SIGMA-ADRIK
Latex Beads, Polystyrene, 0.1µm mean particle size	LB		SIGMA
Methanol-d4	CD ₃ OD	99.80%	Cambridge Isotope Laboratories, Inc.
1-Methyl-2-pyrrolidone, A.C.S. reagent		99+%	SIGMA-ADRIK
Methyl Sulfoxide 0.75mls amp d:1.19g/ml, MW: 84.18, BP: 55°C/5mmHG	DMSO-d6	99.96%	ALDRICH
Palmitic Acid N-hydroxysuccinimide ester	NHPA	98.00%	SIGMA
Pyrene, puriss, p.a for fluorescence			FLUKA CHEMIKA
Sodium Bicarbonate		≥99.5%	FLUKA CHEMIKA
Sodium Hydroxide		99.13%	Fischer Scientific
Sodium Acetate anhydrous		≥99.0%	SIGMA-ADRIK
Sodium Acetate trihydrate ACS reagent		99+%	SIGMA-ADRIK
Sodium Dihydrogen Phosphate Monohydrate		99.5%	FLUKA CHEMIKA
Sodium Iodide, puriss, p.a		≥99.5%	FLUKA CHEMIKA
Sodium Phosphate dibasic heptahydrate ACS reagent		99%	Riedel-de Hæn
Trifluoroacetic acid, for biochemistry	TFA	99.5%	Acros Organics, Fischer Scientific
Water Deionised	H ₂ O		Millipore Elix –Progaard 2
Water Double Deionised	H ₂ O	<18 µΩ.cm	Millipore Synergy-Simpak 1

3.1.2 Synthesis of Quaternary Ammonium Palmitoyl Glycol Chitosan (GCPQ)

A schematic representation of the synthetic pathway is illustrated in Figure 3.1 (Uchegbu et al. 2001)

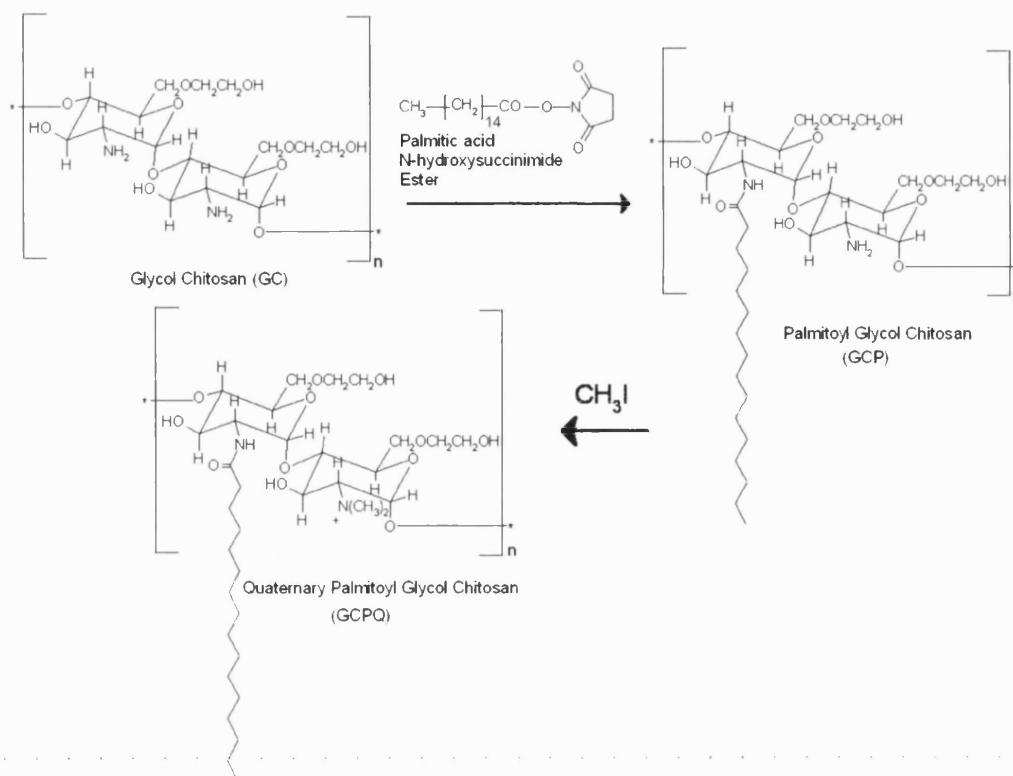


Figure 3.1: Synthetic scheme for Quaternary ammonium Palmitoyl Glycol Chitosan (Uchegbu et al. 2001)

3.1.2.1 Acid Degradation of Glycol Chitosan

The acid degradation of glycol chitosan was carried out as described earlier (Uchegbu et al. 2001). Glycol chitosan (2 g) was dissolved in hydrochloric acid (4 M, 150 mL) and the solution filtered to remove insoluble impurities (if required). The (filtered) solution was placed in a preheated water bath at 50°C. At 24 hours the reaction was stopped and the product was removed from the water bath. The molecular weight was controlled by the degradation time i.e. increasing the acid degradation time decreased the molecular weight of the resulting polymer (Wang et al. 2001). Previous work has shown that a molecular weight of 26,000 Da was obtained after 24 hours of acid hydrolysis of glycol chitosan with a starting molecular weight of approximately 250,000 Da (Wang et al. 2001). The product was purified by exhaustive dialysis (Visking seamless cellulose tubing, molecular weight cutoff 12-14,000 Da for cytochrome C) against deionised water (5 L) with six changes over 24 hours. The dialysate at the end of the dialysis procedure (neutral pH) was subsequently freeze-dried, and the product was recovered as

a cream-colored cotton-wool-like material. The degradation yielded 1.06 g (i.e. 53%) of degraded glycol chitosan.

3.1.2.2 Palmitoylation of degraded Glycol Chitosan

The synthesis of palmitoyl glycol chitosan was carried out as described earlier (Noble et al. 1999; Qu et al. 2006). Briefly, degraded glycol chitosan (500 mg) and sodium bicarbonate (376 mg, ~ 0.045 M) were dissolved in a mixture of absolute ethanol (24 mL) and deionised water (76 mL). To this glycol chitosan solution was added drop wise a solution of palmitic acid N-hydroxysuccinimide (NHPA) (792 mg, ~ 2.24 mmole) dissolved in absolute ethanol (150 mL), with continuous stirring over a period of 1 hour. The mixture was then stirred for 72 hours and the product isolated by evaporating off most of the ethanol and extracting 3 times the remaining aqueous phase (~ 100 mL) with diethylether (each time twice the volume of the aqueous phase i.e. 200 mL was used). The aqueous mixture of the polymer was exhaustively dialysed (Visking seamless cellulose tubing, molecular weight cutoff 12 – 14,000 Da for cytochrome C) against deionised water (5 L) with 6 changes over a 24 hour period and the resultant product freeze-dried to give a denser, white cotton-like solid.

3.1.2.3 Quaternisation of Palmitoyl Glycol Chitosan

Quaternisation was carried out using essentially the same method as reported by Domard and others (Domard et al. 1986; Uchegbu et al. 2001) with modifications (Qu et al. 2006). Briefly palmitoyl glycol chitosan (300 mg) was dispersed in N-methyl-2-pyrrolidone (25 mL) overnight for 12 hours at room temperature. Sodium hydroxide (40 mg, 1 mmole as an ethanolic solution 0.057 M), methyl iodide (1.0 g, d: 1.275 g mL^{-1} , ~ 0.44 mL) and sodium iodide (45 mg, as an ethanolic solution ~ 0.05 M) were added and the reaction stirred under a stream of nitrogen at 36°C for 3 hours.

The quaternary ammonium product was precipitated with diethylether (400 mL), filtered and washed twice more with copious amounts of diethyl ether (twice with 300 mL) to give a light brown hygroscopic solid. The quaternised product was dissolved in water (100 mL) to give a yellow solution. The resultant solution was passed through a

column (1 x 6 cm) packed with Amberlite IRA-96 Cl⁻. The column was packed with one volume of the resin (30 mL) and subsequently washed with hydrochloric acid solution (90 mL, 1 M) followed by deionised water (10 L) to give a neutral pH. The clear eluate from the column was exhaustively dialysed against water (5 L) with six changes over a 24 h period and the product freeze-dried to give GCPQ as a transparent fibrous solid. The synthetic yield of GCPQ is between 115-134 mg (i.e. 38.3 - 44.6%).

3.1.3 Characterisation of Quaternary Ammonium Palmitoyl Glycol Chitosan (GCPQ)

3.1.3.1 ¹H and COSY NMR spectroscopy

¹H NMR and COSY (Bruker AMX 400 MHz spectrometer, Bruker Instruments, UK) were performed on acid degraded glycol chitosan in D₂O (range c.a. 10.00 mg mL⁻¹ to 15.82 mg mL⁻¹), on palmitoyl glycol chitosan (range c.a. 8.33 mg mL⁻¹ to 19.18 mg mL⁻¹) in D₂O / CD₃OD mixtures (1:2) or neat DMSO-d₄ and GCPQ solutions (range c.a. 11.01 mg mL⁻¹ to 14.27 mg mL⁻¹) in CD₃OD. The level of palmitoylation was calculated by comparing the ratio of palmitoyl methyl protons (δ = 0.89 ppm) to sugar protons (δ = 3.5 - 4.5 ppm) and the level of quaternisation calculated by comparing the ratio of quaternary ammonium (δ = 3.45 ppm) to sugar protons (Uchegbu et al. 2001).

3.1.3.2 Fourier Transform Infrared Spectroscopy (FTIR)

The infrared absorption spectrum for degraded GC and PGC was obtained using a Nicolet Avatar 360 FTIR equipped with a Thermo Nicolet SMART OMNI-Sampler accessory to perform Horizontal Attenuated Total Reflectance (HATR) and a germanium crystal (4000 to 675 cm⁻¹) and EZ Omnic IR software (maximum resolution is 1 cm⁻¹) that also identified the attachment of the palmitic tail to the degraded GC.

3.1.3.3 Matrix-Assisted Laser Desorption Spectrometry (MALDI-MS)

Mass spectrometry (MS) is a powerful instrument method in which molecules are ionized, separated, and finally detected based on their mass to charge ratio. Polymers are inherently different in molecular structure and properties with generally high molecular weight, non-volatile compounds that are often thermally unstable. Mass spectrometers used for polymer analysis must be able to efficiently detect ions over a wide mass range due to high molecular weights that are possible, and often probable, of polymers. Mass spectrometry techniques for analyzing polymers can be divided into two categories: (i) degradation characterization and (ii) direct analysis of molecular ions. Up to the late 1980's, pyrolytic introduction systems were used to introduce the degradation products of a polymer into a mass spectrometer. Matrix-Assisted Laser Desorption Ionisation (MALDI) is a novel soft ionization technique that was initially developed for the analysis of large biomolecules, but was later shown that it could be used to analyse polymers over $100,000 \text{ g mol}^{-1}$. Today, the method is used to determine average molecular weights and molecular weight distributions of narrow polydispersity polymers. It can also be used to acquire structural information of end-groups, repeat units, and chemical modifications of polymer systems.

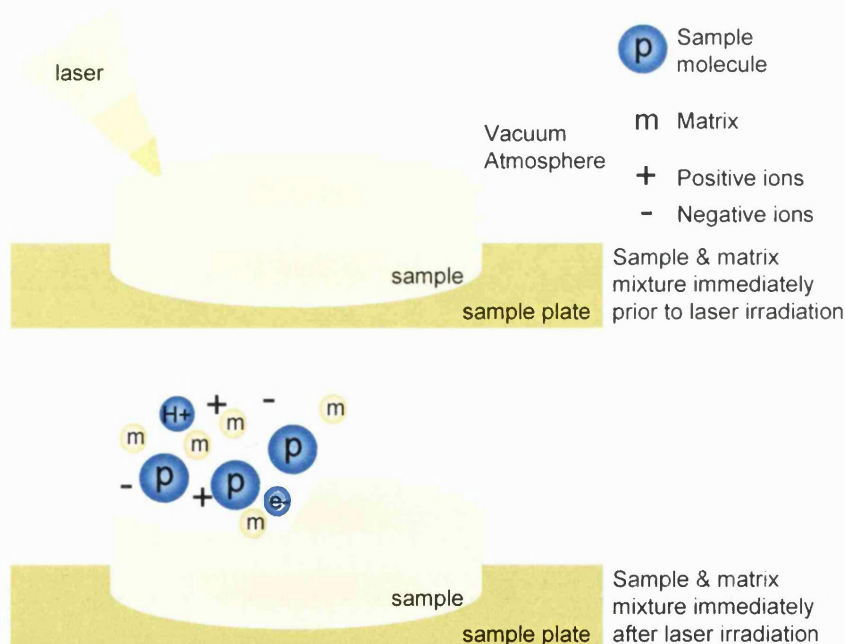


Figure 3.2: The MALDI ionization process.

MALDI is a laser desorption technique in which a sample within a matrix is irradiated using a laser beam of energy between 10 to 10000 nJ, which generally produces power densities between 2.12×10^7 to 2.12×10^8 W cm⁻² at the surface of the sample. Many polymers alone are either not affected by irradiation by a laser beam, or are destroyed by the laser. Combining a matrix material with polymer sample, however, creates a mixture that can absorb at the laser wavelength (337nm) and then ionize the polymer sample indirectly. In this case the matrix material absorbs most of the energy supplied by a laser and the energy in the mixture is then transferred to the polymer. The polymer is then ionized and volatilized, being released from the matrix/analyte mixture (Figure 3.2). Common matrix materials include indole, acrylic acid, and nicotinic acid which was the first material to be used as a matrix in a MALDI experiment. After ionization the analyte is placed in an electric field and accelerated towards the detector. By calculating the speed of the analyte and magnitude of the electric field, the mass/charge ratio can be determined.

All of the MALDI-MS measurements were performed on an ABI Voyager DE-PRO™ matrix-assisted laser desorption ionization time of flight mass spectrometer (Applied Biosystems, UK) equipped with a pulsed nitrogen laser (337 nm for 1 minute) and a delayed extraction ion source. MALDI mass spectra were observed in the positive ion mode using sinapinic acid (SA) as a matrix reagent (10 mg mL⁻¹, 50% methanol with 0.1% TFA) for determining the molecular weight of the carbohydrate polymers. 20 µL of sample (1 mg mL⁻¹) were premixed with 20 µL of prepared SA and applied directly to the sample plate. Once the sample is applied to the sample support (plate), the sample is allowed to air evaporate without heating it.

3.1.3.4 Gel Permeation Chromatography (GPC) and Multi-angle Laser Light Scattering (MALLS)

Gel permeation chromatography or size-exclusion chromatography is a separation technique based on the hydrodynamic volume, molecular weight, and viscosity of polymers. Molecules with large hydrodynamic radii cannot diffuse into the pores of the gel filtration medium and elute first from the column, while smaller molecules that diffuse inside the pores, elute later from the column based on their size. Thus, the smallest molecular weight compounds will elute last from the column. The selectivity of

the technique relies heavily on the pore size distribution of the gel filtration material used to pack the columns.

Although GPC provides good separation of molecules by their hydrodynamic radius, traditionally it has been necessary to calibrate GPC columns using standard samples of known molar mass in order to determine the molar mass of an unknown sample (Wyatt 1998). However, appropriate standards having the same composition and conformation as the unknown specimen are often not available (Wyatt 1998). If the value of dn/dc (differential refractive index increment) or the total mass of eluting solute is known, light scattering measurements can provide an absolute measurement of molar mass when used in series with a concentration-sensitive detector such as a refractive index (RI) detector (Wyatt 1998). Measurement of dn/dc is essential for the absolute characterization of the molar mass, since it is a term used in the molar mass calculation and is easily measured by injecting them into the refractive index detector. Software normally is used to calculate the dn/dc based on the signal strength from the RI (dn) at each concentration (dc). Polymers with larger values of dn/dc scatter more light at the same mass than those having smaller values (Wyatt 1999). Therefore, knowing dn/dc permits the deduction of molar masses from the light scattering data (Wyatt 1999). Because dn/dc changes with wavelength, it is vital to measure it at the same wavelength as the light scattering apparatus (Wyatt 1999). Moreover, it is also advantageous to measure dn/dc off line since determining this quantity on-line makes numerous assumptions about the total mass which has eluted (Wyatt 1999). Thus, light scattering can provide a continuous measurement of molar mass, if sample concentrations are high enough to provide adequate signals (Wyatt 1998).

Light scattering can be used in molecular weight determinations as incident light scatters in all different directions with an intensity that depends on the polarisability, which depends on molecular weight (Figure 3.3). Because the intensity of scattered light depends on the molecular weight of the particle, light scattering will depend on weight-averaged molecular weight (M_w). Besides molecular weight dependence, light scattering also has a direct dependence on particle size and can be used to measure the mean square radius of gyration.

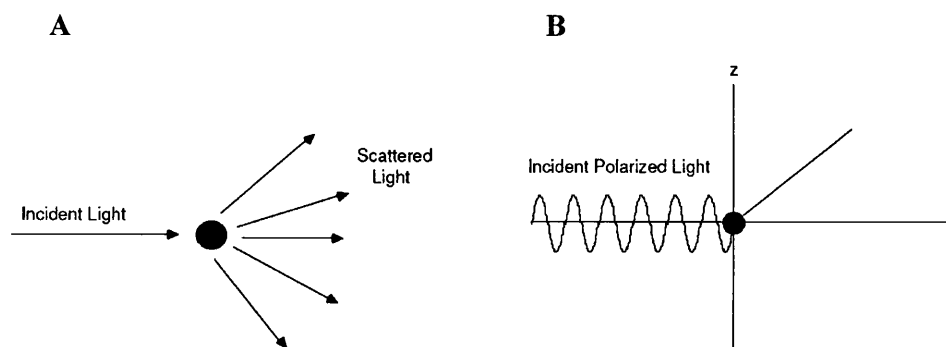


Figure 3.3: A: Scattering of incident light off a particle in solution or in vacuum B: Plane polarized light polarized in the z direction and incident on a small particle

When a parallel beam of light passes through a transparent system, a small part of light is scattered elastically (Rayleigh scattering). The scattering arises because of optical discontinuities in the medium. For solutions of polymer molecules, additional scattering arises from the presence of the solute molecules, and this may be shown to be a function of the concentration of the polymer molecules, as well as their size and shape. When measurements are made of the differences in intensity of the scattered light between the solvent and a series of dilute polymer solutions, then it is possible to determine the averaged size of polymer solutes and hence their molecular weights. The theoretical basis of light scattering from polymer solutions was first established by Zimm in the 1940's. The equation relating scattering of light to molecular weight is given as:

$$K_c / R_\theta = 1 / M_w + 1 / M_w (16 \pi^2 / 3 \lambda^2) \sin^2 (\theta / 2) (\langle r^2 \rangle_z)^2 + A_2 c \quad (\text{Equation 3.1})$$

where c is polymer concentration; R_θ , the Rayleigh ratio, i.e. the excess intensity of scattered light at the angle θ ; M_w , the weight-averaged molecular weight; λ , the wavelength of light; θ , π , the scattering angle; $\langle r^2 \rangle_z$, the z-averaged mean radius of gyration, i.e., the molecular size in solution; and A_2 , the second virial coefficient, which quantifies the interaction between the macromolecule and the solvent (Wang 2006). K_c is given by the equation:

$$K_c = 2 \pi^2 n^2 (dn/dc)^2 / N_0 \lambda^4 \quad (\text{Equation 3.2})$$

where N_0 is the Avogadro's number; n , the refractive index of the solvent, and dn/dc , the refractive index increment of the solute, i.e., the change in refractive index per unit change in polymer concentration (a constant for a polymer-solvent combination at a particular temperature) (Wang 2006).

In order to determine M_w , $\langle r^2 \rangle$, and A_2 , the scattering intensities of various dilute polymer solutions of differing concentrations are determined at various scattering angles (typically from 35°C to 150°C). R_θ is then calculated and K_c / R_θ plotted against $(\sin^2(\theta/2) + kc)$, where k is an arbitrary constant chosen to produce a reasonable spread of data points. This plot is termed a Zimm plot (Figure 3.4). Using this method, M_w is obtained as the inverse of the value of the intercept (K_c / R_θ) as shown in Figure 3.4. From the equation 3.1, $\langle r^2 \rangle$ and A_2 are estimated from the slopes of the $c = 0$ and $\theta = 0$ lines, respectively.

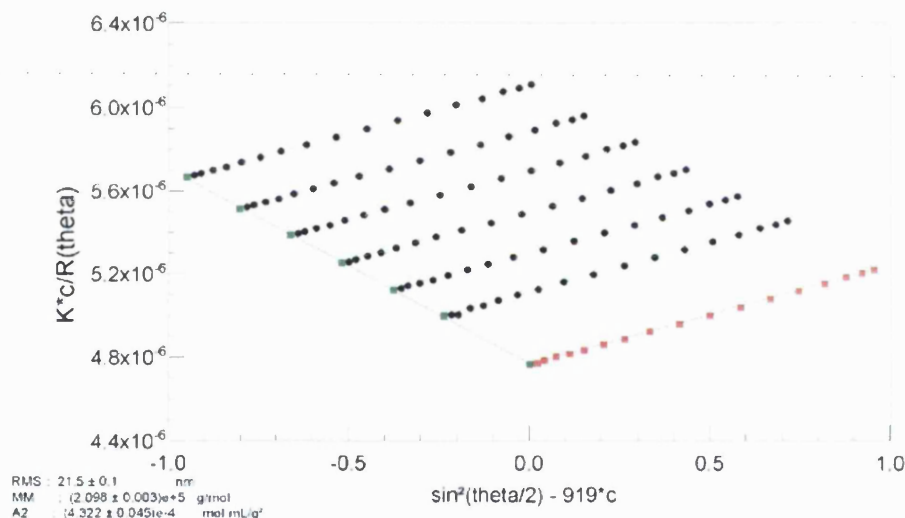


Figure 3.4: Example of a Zimm plot.

The molecular weight of Glycol Chitosan (GC) and Quaternary Ammonium Glycol Chitosan (GCPQ) was determined by GPC-MALLS equipped with DAWN[®] EOS[™] MALLS ($\lambda=690\text{nm}$), Optilab DSP Interferometric Refractometer ($\lambda=690\text{nm}$) and QELS detectors (Wyatt Technology Corporation, USA) (Figure 3.5), using as mobile phase an acetate buffer (0.3M CH_3COONa (anhydrous)/0.2M CH_3COOH , pH4.5) for GC and a mixture of acetate buffer (0.3M CH_3COONa (anhydrous) / 0.2M CH_3COOH , pH4.5) / HPLC grade Methanol (35:65) for GCPQ. Filtered samples (0.2 μm , 200 μL) were

injected using a Waters 717 plus Autosampler into a POLYSEPTM-GFC-P guard column (35 x 7.8mm, Phenomenex, UK) attached to a POLYSEP TM-GFC-P 4000 column (300 x 7.8 mm, exclusion limit for PEG = 200,000Da, Phenomenex, UK) at a loading concentration of 4-11 mg mL⁻¹. Measurements in quadruplicates were performed at room temperature with a mobile phase flow rate of 1 mL min⁻¹ (GC measurements) and 0.7 mL min⁻¹ (2 GCPQ measurements) or 0.4 mL min⁻¹ (1 GCPQ measurement) (Jasco PU-2080 Plus or a Waters 515c HPLC pump both attached to a Jones Chromatography 7600 series D-Gasser). The data were processed using ASTRA for Windows version 4.90.08 software (Wyatt Technology Corporation, USA). Toluene and BSA were used for DAWN used for DAWN[®] EOS[™] MALLS calibration and normalisation, respectively.

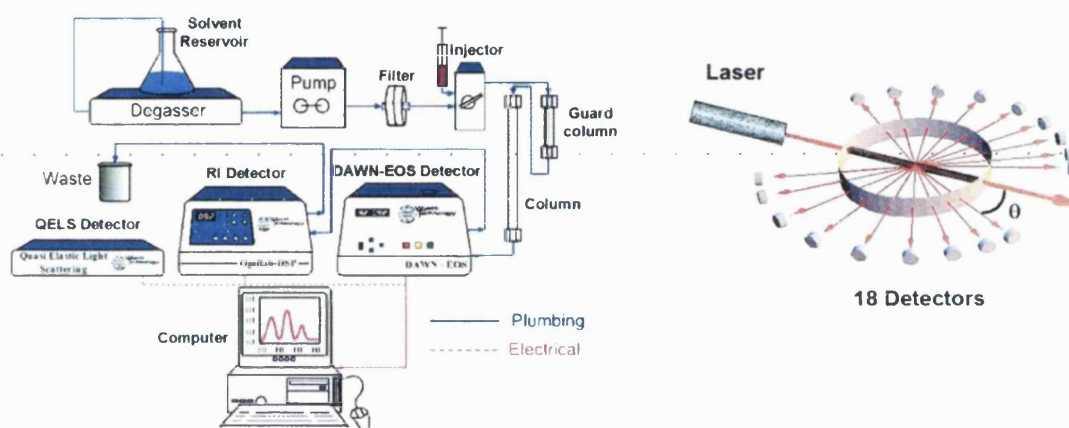


Figure 3.5: GPC-MALLS Set-up (left) and a schematic of MALLS measurement (right) (Wyatt 1998)

The specific refractive index increment (dn/dc) of GC and GCPQ was measured in triplicates in their respective solvents (as above) at 40°C with an Optilab DSP Interferometric Refractometer ($\lambda=690\text{nm}$). Filtered samples (0.2 μm , 33mm Millex GP syringe driven filter unit, PES membrane for sterilisation of aqueous solutions) of 5 or 6 different concentrations ranging from 0.1-0.6 mg mL⁻¹ were manually injected using an Injection System (Wyatt Technology Corporation, USA) at a pump flow rate of 0.3ml min⁻¹. The data were processed utilising DNDC for Windows version 5.90.03 software (Wyatt Technology Corporation, USA).

3.1.3.5 Preparation of Self Assembled Polymer Aggregates

Self assembled polymer amphiphiles of different concentrations were prepared by vortexing (WhirliMixer, Fisherbrand) in double-deionised water for 5 minutes and then by probe sonication (MSE Soniprep 150, MSE instruments, UK) for 8 -15 minutes with the instrument set at 50-75% of its maximum output.

3.1.3.6 Particle Sizing

Photon correlation spectroscopy (also known as dynamic light scattering or quasi-elastic light scattering) can be used to study the hydrodynamic diameter of particles in a fluid. Brownian motion describes the movement of particles suspended in a liquid medium. When a laser beam is directed through this liquid, the particles scatter light. When an incident light encounters a big particle, the scattering of light has a smaller angle than when it hits a smaller particle (Figure 3.6).

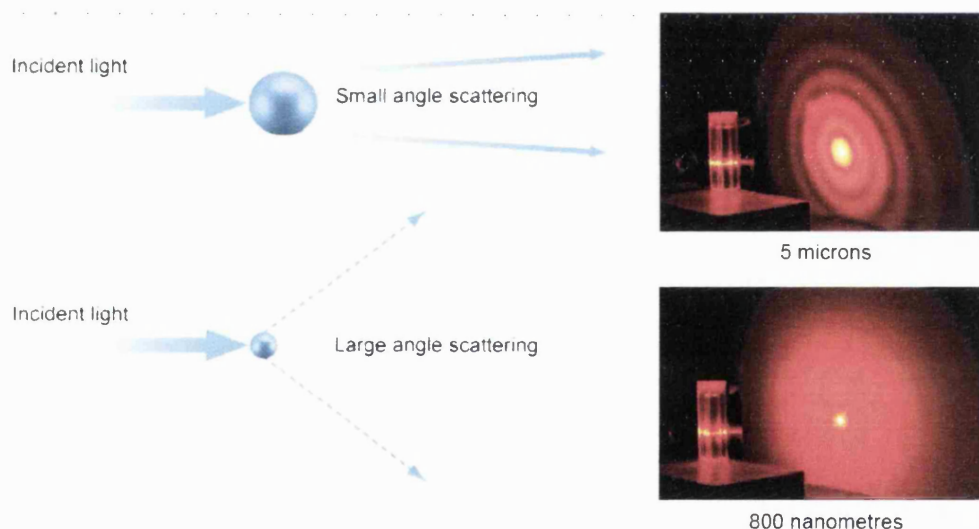


Figure 3.6: Light scattering and angle dependence (Virden 2008).

In light scattering experiments, the electric field of the incident light imparts an oscillating polarisation on the particles in the sample (Williams 1998). Those particles whose polarity differs from the surroundings scatter the incident light (Williams 1998). Within the sample, the particles are in constant motion, and it is the movement of particles that causes fluctuations in the detected intensity signal (Williams 1998). The

duration of the fluctuations can provide information about the size of the particles (Williams 1998). Diffusivity of a particle suspended in a liquid is opposed by the liquid's viscosity, so that the particles spread throughout the liquid more slowly as the viscosity of the liquid increases (Williams 1998). For small motion, laminar or steady-state flow is a good assumption. The Stokes-Einstein equation for the diffusivity of particles in a liquid defines the diffusion coefficient, D , of the particles as

$$D = k T / 6\eta\pi r \quad (\text{Equation 3.3})$$

where K is the Boltzmann's constant, T is the temperature in Kelvin, η is the viscosity of the liquid in which particles are suspended, and r is the radius of the particles. Since the fluctuation of the intensity signal is caused by the motion of particles, those particles that diffuse more quickly are characterised by a smaller fluctuation time (Williams 1998). Also, as the diffusion coefficient is inversely proportional to the size of the particles, the smaller the particle, the shorter the fluctuation time (Williams 1998). Using an autocorrelation function

$$[g_i(t) = I(t)I(t + t) = \exp(-t\Gamma)] \quad (\text{Equation 3.4})$$

the correlation or relationship between the measurements of a fluctuating signal can be identified (Williams 1998). For monodisperse systems in Brownian motion, the diffusion of the particles in erratic motion causes the intensity autocorrelation equation to decay exponentially, where Γ , the linewidth of the spectrum, is related to the diffusion coefficient by

$$\Gamma = D q^2 \quad (\text{Equation 3.5}),$$

and the scattering vector q , is given by

$$q = 4\pi n \sin (\theta/2) / \lambda_0 \quad (\text{Equation 3.6})$$

in which n is the index of refraction of the liquid medium, θ is the scattering angle and λ_0 is the laser wavelength in air (Williams 1998). Geometrically, the scattering vector is defined as the difference between the scattered wave vector and the incident wave vector (Williams 1998). Combining the above equations,

$$r = K T q^2 / 6 \eta \pi \quad (\text{Equation 3.7}).$$

Photon correlation spectroscopy digitally measures the intensity fluctuations of a signal at the level of the photon and multiple measurements are taken of the number of photons that reach a detector in a sample time (Williams 1998). For each sample time, the autocorrelation function is computed by an automated correlator (Williams 1998). When the logarithm of the autocorrelation function is graphed versus time, the slope of

the resulting line is the linewidth, Γ (Williams 1998). Finally, using the latter equation the size of the scattering particles can then be determined.

It has to be noted that the particle size measured by PCS refers to spheres of equivalent volume, therefore measurements of non-spherical particles can be challenging and interpretation of particle size need to be done with this in mind (Figure 3.7). Using TEM could give an indication of the particle shape that can aid in better understanding of the particle size. Furthermore, major errors in size measurement arise through poor sampling and dispersion (more important for smaller than 1 μm particles) (Virden 2008).

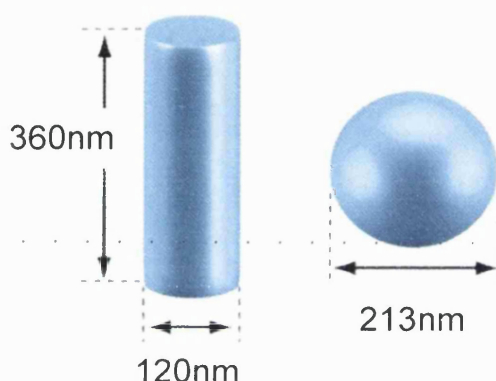


Figure 3.7 Cylinder on the left has an equivalent volume to the sphere on the right (Virden 2008).

Freshly prepared polymer dispersions (2mg mL^{-1} , 5mg mL^{-1} , 8mg mL^{-1} , 10mg mL^{-1}) with Leucine^[5]-Enkephalin (LENK) [1mg mL^{-1}] or Palmitoylated Leucine^[5]-Enkephalin (TPLENK) [1mg mL^{-1}] were prepared by vortexing for 8 minutes and filtered if specified (Millipore Millex-HA, $0.45\mu\text{m}$ filter pore size). Furthermore, unfiltered polymeric dispersions (2mg mL^{-1} , 5mg mL^{-1} , 10mg mL^{-1}) with TPLENK (1mg mL^{-1}) were prepared by vortexing for 5-10 minutes prior to probe sonication for 15 minutes (MSE Soniprep 150) with the instrument set at 50% of its maximum output for 15 minutes on ice. The particle size and distribution determined by photon correlation spectroscopy (PCS) (Malvern Zetasizer 3000HS, Malvern Instruments, UK) at 25°C at a wavelength of 633 nm and the data analysed using the *Contin* method of data analysis. Polymer solutions were left for 15 min at room temperature (25°C) before particle sizing was carried out. The accuracy of the instrument was assessed periodically using on drop of latex beads (polystyrene, mean size: $0.1\mu\text{m}$, Sigma Co., UK) in 50 mM sodium chloride (dispersed phase). All measurements were performed in triplicate.

3.1.3.7 Transmission Electron Microscopy (TEM)

The transmission electron microscope involves an evacuated metal cylinder (the column) about 2 meters high with the source of illumination, a tungsten filament (the cathode), at the top (Center 2008). When the filament is heated and a high voltage (the accelerating voltage) of between 40,000 to 100,000 volts is passed between it and the anode, the filament will emit electrons (Center 2008). These negatively charged electrons are accelerated to an anode (positive charge) placed just below the filament, some of which pass through a tiny hole in the anode, to form an electron beam which passes down the column with a speed that depends on the amount of accelerating voltage present (Center 2008).

Electromagnets, placed at intervals down the column, focus the electrons, mimicking the glass lenses on the light microscope (Center 2008). The double condenser lenses focus the electron beam onto the specimen, which is clamped into the removable specimen stage, usually on a specimen grid (Center 2008). As the electron beam passes through the specimen, some electrons are scattered whilst the remainder are focused by the objective lens either onto a phosphorescent screen or photographic film to form an image (Center 2008). Unfocussed electrons are blocked out by the objective aperture, resulting in an enhancement of the image contrast (Center 2008). The contrast of the image can be increased by reducing the size of this aperture (Center 2008). The remaining lenses on the TEM are the intermediate lens, which is used to control magnification, and the projector lens, that corresponds to the ocular lens of the light microscope and forms a real image on the fluorescent screen at the base of the microscope column (Center 2008).

The resolving power of the TEM is approximately three orders of magnitude (1,000) greater than that of the light microscope. The very short wavelength of electrons and modern technology makes it easy to obtain a resolution of 0.5 nm on a TEM and a magnification higher than 200,000 times.

The greatest obstacle with the electron microscope is the unphysiological conditions to which specimens must be exposed. Since the material must be exposed to a very high vacuum (10^{-5} to 10^{-8} Torr) when being examined, it must be dried at some stage in its

preparation. The specimen must be stabilized (or fixed) so that its ultrastructure is as close to that in the wet condition when exposed to the vacuum.

Furthermore, the limited penetrating power of electrons means that the specimens must be very thin or must be sliced into thin sections (50 - 100 nm) to allow electrons to pass through. Contrast in the TEM depends on the atomic number of the atoms in the specimen; the higher the atomic number, the more electrons are scattered and the greater the contrast. Biological molecules are composed of atoms of very low atomic number (carbon, hydrogen, nitrogen, phosphorus and sulphur). Thin sections of biological material are made visible by selective staining. Negative staining is applied in TEM to enhance the contrast of the observed sample exposing it to salts of heavy metals such as uranium (uranyl acetate), lead (lead citrate), phototungstic acid, and osmium, which are electron opaque. Due to the high electron density from nuclei of the heavy atoms, electron beams are scattered out of the optical path resulting in a dark image, while the sample appears lighter in colour as undeflected electron beams pass through low electron intensity areas (sample) and observed as fluorescent on the screen (Watt 1997)

The morphological examination of the nanoparticles was studied with TEM. A drop of unfiltered solution X was placed on Formvar[®]/Carbon Coated Grid (F196/100 3.05mm, Mesh 300, Tab Labs Ltd, England). Excess sample was filtered off with No. 1 Whatman Filter paper and negatively stained with 1% aqueous Uranyl Acetate. Imaging was carried out under a FEI CM120 BioTwin Transmission Electron Microscope (TEM) (Ex. Philips, Eindhoven, Netherlands). Digital Images were captured using an AMT (digital) camera.

3.1.3.8 HPLC Analysis of Drug Loaded Polymers

Polymer solutions with Leucine^[5]-Enkephalin (LENK) or Palmitoylated Leucine^[5]-Enkephalin (TPLENK) were filtered (0.45µm filter pore size, Millex GP Syringe Driven Filter Unit, PES, Sterile, 33mm) and dissolved in mobile phase and analysed by HPLC. Sonicated polymeric dispersion of TPLENK and GCPQ were filtered after TEM analysis (0.8µm, 13mm, Acrodisc Syringe Filter, Supor Low Protein Binding Non-Pyrogenic Membrane, PALL Life Sciences) and dissolved in mobile phase and analysed by HPLC. Samples were analysed using an HPLC system equipped with a Waters TM

515 HPLC pump connected to a Water TM 717 plus Autosampler with a Waters TM 486 Tunable Absorbance Detector. Two reverse phase Cromolith (Merck KGaA, Germany) columns (C18, 4.6 x 100 mm, total length: 260mm) or a reversed phase Waters Sunfire C18 column (5 μ m, 4.6mm X 250mm) with a guard column attached [Waters Sunfire C18 (5 μ m, 4.6mm X 10mm)] (used only for the sonicated TPLENK and GCPQ samples) were used maintained at 30°C with a Jones Chromatography Column Heater model 7971. The mobile phase consisted of acetonitrile / water /dilute (1/1000 v/v, pH 2) aqueous trifluoroacetic acid solution (180/819.5/0.5 v/v) (for Cromolith columns) or 82% 50mM acetate buffer and 18% acetonitrile (for Sunfire columns) with a final pH of 5.8. Unless otherwise indicated, samples were detected at 214nm. The flow rate was set at 1 mL min⁻¹ at 30°C for analytical runs and the injection volume at 50 μ L. The retention time was 6.8 and 11.5 min for Leucine^[5]-Enkephalin and 7.8 and 14.0 for TPLENK with the Cromolith columns and the Sunfire column respectively. The lowest detection limit is 1 μ g mL⁻¹ for LENK and 10 μ g mL⁻¹ for TPLENK. Empower software I was utilised for obtaining the results.

3.1.3.9 Stability of wet and dry formulations of TPLENK

Polymer solutions were prepared in triplicate (Formulation A, B, C) containing 6 mg of TPLENK and 13.8 mg of GCPQ (1 : 2.3 w/w ratio) for the wet (n = 3) and 7 mg of TPLENK and 16.1 mg of GCPQ (1 : 2.3 w/w ratio) for the dry formulations (n = 3) with a final concentration of TPLENK of 1 mg mL⁻¹. The level of palmitoylation and quaternisation for GCPQ used was 18.7% and 8.3% for the wet formulations and 19.7% and 6.9% for the dry formulations respectively. The suspensions were vortexed (WhirliMixer, Fisherbrand) for 5 to 10 minutes prior to probe sonication for 15 minutes (MSE Soniprep 150) with the instrument set at 50% of its maximum output for 15 minutes on ice. The formulations were left for 2 hours to settle and then were filtered (Millipore Millex-HA, 0.22 μ m filter pore size). The clear eluate was collected in a glass vial (wet formulations studies) that was stored in the fridge for that point on and in 6 glass vials each containing 0.9 mL of eluate that would be freeze-dried and then stored in -20°C till they would be reconstituted with 0.9 mL of double-deionised 0.22 μ m filtered water (sterile, pH 6.4) for further analysis. PCS particle size analyses, TEM and

analytical HPLC of the wet and dry (reconstituted) formulations were carried out after each week for 6 weeks and after 1 month for 6 months respectively.

The particle size of the formulations was measured by PCS (Malvern Zetasizer 3000HS_A, Malvern Instruments, UK) at 25°C at a wavelength of 633nm (He-Ne laser, 10mW, detection angle 90°) and the data analysed using the *Contin* method of data analysis. Polymer solutions were left for 30 min at room temperature before particle sizing was done. Measurements were performed in triplicate. Results are expressed as Zave, the mean hydrodynamic diameter ($\langle R_h \rangle = \frac{1}{2} Zave$) along with their polydispersity index. The morphological examination of the nanoparticles in both the wet and reconstituted formulations was studied with TEM as described above (3.1.3.7, p 161).

The formulations were filtered (0.45µm filter pore size, Millex GP Syringe Driven Filter Unit, PES, Sterile, 33mm) and their peptide content analysed by reversed phase high-performance liquid chromatography on two reverse phase a reversed phase Waters Sunfire C18 column (5µm, 4.6mm X 250mm) with a guard column attached [Waters Sunfire C18 (5µm, 4.6mm X 10mm)], using a Waters TM 515 HPLC pump connected to a Water TM 717 plus Autosampler with a Waters TM 486 Tunable Absorbance Detector. The mobile phase consisted of 82% 50 mM acetate buffer and 18% acetonitrile (pH 5.8). Unless otherwise indicated, samples were detected at 280nm. Flow rate was set at 1mL min⁻¹ at 35°C for analytical runs and the injection volume at 40µL. The retention time was 11.5 for Leucine^[5]-Enkephalin and 14.0 for TPLENK and the lowest detection limit is 1 µg ml⁻¹ and 10 µg ml⁻¹ respectively. Empower software I was utilised for obtaining the results.

3.2 Results

3.2.1 Characterization of GCPQ

3.2.1.1 ^1H NMR spectroscopy

Protons assignments for degraded GC (Figure 3.8) are δ 2.03 = CH_3 (acetyl-glycol chitosan); δ 2.73-3.13 = CH (sugar proton, glycol chitosan), δ 3.39-4.3 (sugar protons, glycol chitosan); δ 4.70 = D_2O (water protons) and δ 5.03-5.20= (anomeric sugar proton). The synthesis of palmitoyl glycol chitosan (PGC) was confirmed by ^1H NMR (Figure 3.9). Protons assignments for PGC δ 0.878 = CH_3 (palmitoyl); δ 1.163-1.262 = CH_2 (palmitoyl); δ 1.53 = CH_2 (palmitoyl deshielded by carbonyl); δ 1.93 = CH_3 (acetyl-glycol chitosan); δ 2.08-2.25 = CH_2 (adjacent to carbonyl protons); δ 2.73-3.13 = CH (sugar protons, glycol chitosan); δ 3.37-4.60 = (sugar protons); δ 3.21 = CD_3OD (methanol protons); and δ 4.8 = D_2O (water protons); δ 5.03-5.20= (anomeric sugar proton). The synthesis of quaternary ammonium palmitoyl glycol chitosan (GCPQ) was confirmed by ^1H and ^1H ^1H COSY NMR (Figure 3.10). For GCPQ, the protons assignments are δ 0.78-0.82 = CH_3 (palmitoyl); δ 1.19 = CH_2 (palmitoyl); δ 1.53 = CH_2 (palmitoyl deshielded by carbonyl); δ 1.93 = CH_3 (acetyl-glycol chitosan); δ 2.08-2.25 = CH_2 (adjacent to carbonyl protons); δ 2.73-3.13 = CH_3 (dimethyl amino); δ 3.27 = CH_3 (trimethyl amino); δ 3.37-4.60 = (sugar protons); δ 3.21 = CD_3OD (methanol protons); and δ 4.8 = D_2O (water protons); δ 5.03-5.20= (anomeric sugar proton)

Based on the ^1H -NMR spectra, palmitoylation levels were estimated by comparing the chemical shift δ of the methyl peak at δ = 0.79 ppm over the chemical shift of the sugar protons at δ = 3.37-4.6 ppm. As the chemical shift of the methyl peak represent 3 protons ($-\text{CH}_3$) and the sugar peak represents 9 protons, palmitoylation value is calculated as illustrated with equation (3.8) if the spectrum of GCPQ 050107 (Figure 3.10) is used as an example:

Equation (3.8):

$$\% \text{ Palmitoylation} = \frac{\delta \text{ of methyl protons on palmitoyl} / 3 \text{ protons}}{\delta \text{ of sugar chain protons} / 9 \text{ protons}} \times 100\%$$

$$= \frac{9 \times \delta \text{ methyl}}{3 \times \delta \text{ sugar}} \times 100\% = \frac{900 \times 2.13}{3 \times 51.20} = \sim 12.48\%$$

Quaternisation levels are calculated by comparing the chemical shift of protons of the trimethyl group of the quaternary amine (representing 9 protons) to the chemical shift of the sugar chain protons (representing 9 protons) as above. Using equation (3.9) if the spectrum of GCPQ 050107 (Figure 3.10) is used as an example, the quaternisation level of GCPQ 050107:

Equation (3.9):

$$\begin{aligned} \% \text{ Quaternisation} &= \frac{\delta \text{ of trimethyl group protons of quaternary amine} / 9 \text{ protons}}{\delta \text{ of sugar chain protons} / 9 \text{ protons}} \times 100\% \\ &= \frac{9 \times \delta \text{ methyl}}{9 \times \delta \text{ sugar}} \times 100\% = \frac{5.12 \times 100}{51.20} = \sim 10.00\% \end{aligned}$$

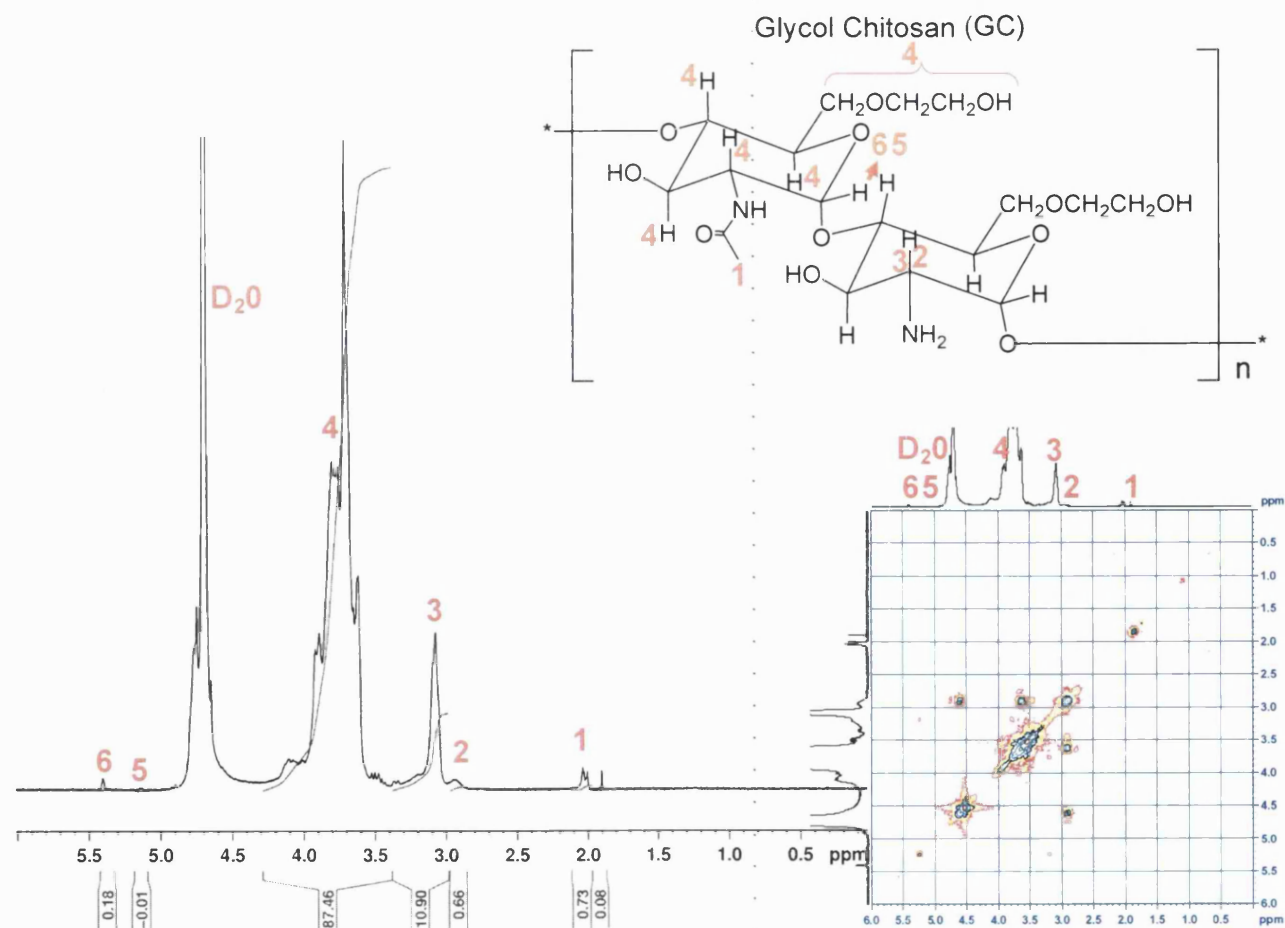


Figure 3.8: ¹H and ¹H-¹H COSY NMR for degraded Glycol Chitosan (24 hours) (10mg) in D₂O (1mL).

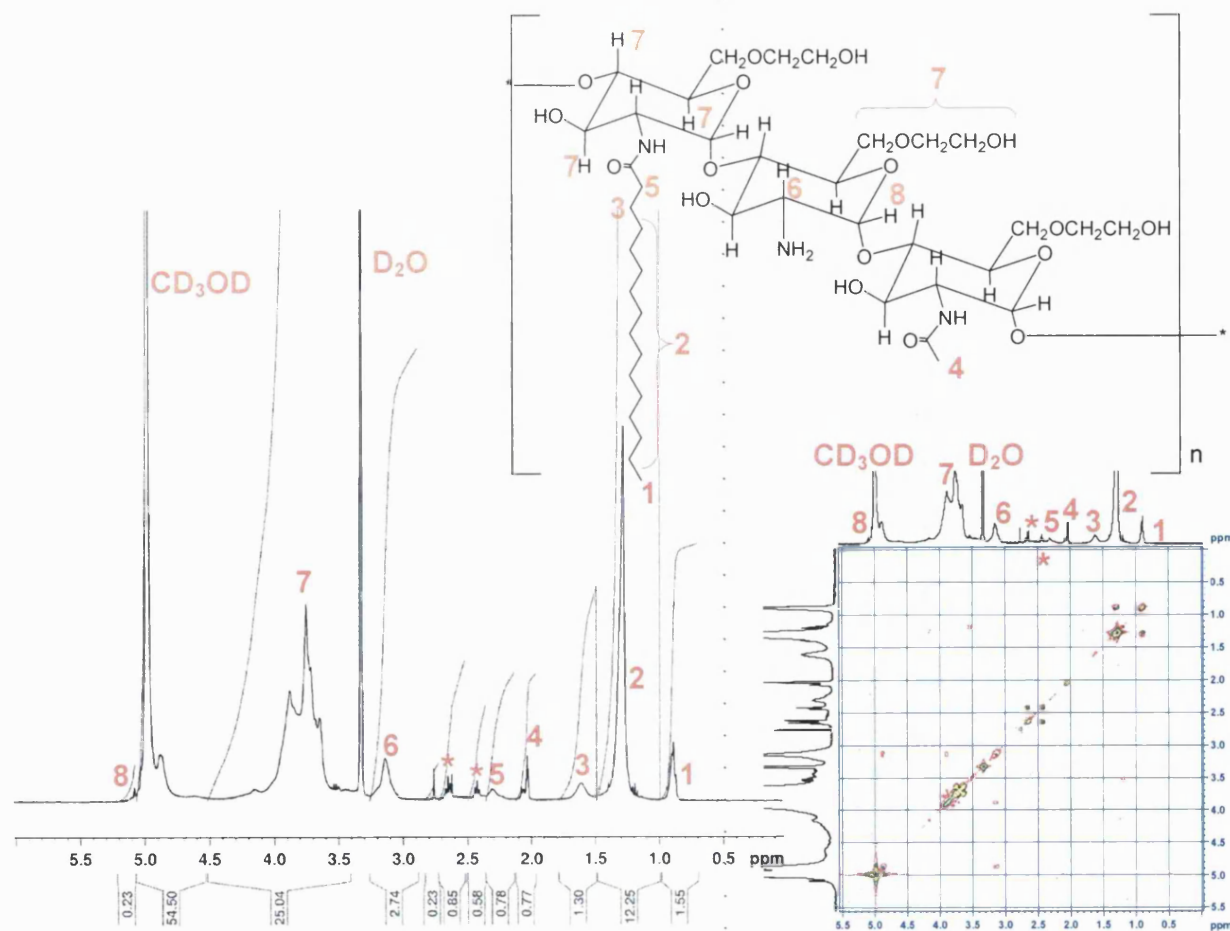


Figure 3.9: ^1H and ^1H - ^1H COSY NMR for PGC (6.54mg) in Methanol- d_4 99.9% (0.4mL) and D_2O 99.9% (0.2mL) and Acetic Acid- d_4 99.9% (0.05mL) (* : indicates an impurity probably succinimide).

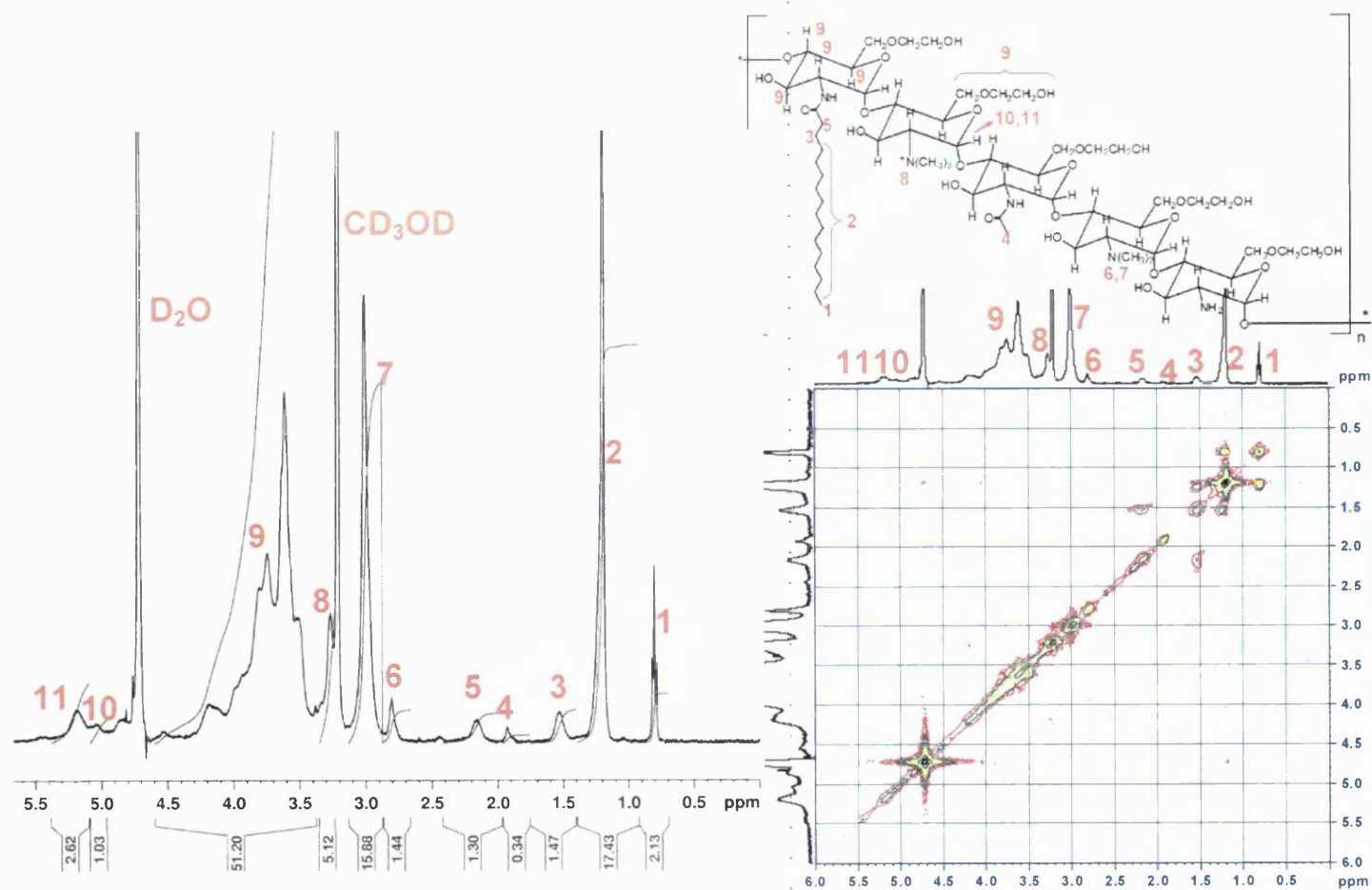


Figure 3.10: ^1H and ^1H - ^1H COSY NMR for GCPQ (11.01 mg) in Methanol- d_4 99.9% (1 mL).

3.2.1.2 Fourier Transform Infrared Spectroscopy (FTIR)

The spectrum obtained for the degraded GC (Figure 3.11) shows the following significant bands, expressed in reciprocal wave numbers (cm^{-1}): 3500-3250 (m), 2870 (m), 1611 (m), 1519 (m), 1375 (w), 1067 (vs), 653 (vs). Similarly, the spectrum obtained for PGC shows the following significant bands: 3381 (m), 3342 (m), 3309 (m), 2918 (vs), 2850 (vs), 1738 (m), 1654 (m), 1560 (m), 1467 (m), 1377 (m), 1069 (vs), 720 (w), 684 (w), 662 (w), 652 (w), 639 (vs), 632 (w), 622 (w). The error margin for all absorption bands of FTIR is $\pm 2\text{cm}^{-1}$. The intensities of the absorption bands are indicated as follows: (w): weak, (m): medium, (s): strong, (vs): very strong. The increase of the two separate peaks at 2850 and 2918 cm^{-1} is indicative of attachment of the palmitic tail on the GC molecule along with an increase in the absorbance of the amide I and II band (1648 and 1563 cm^{-1}).

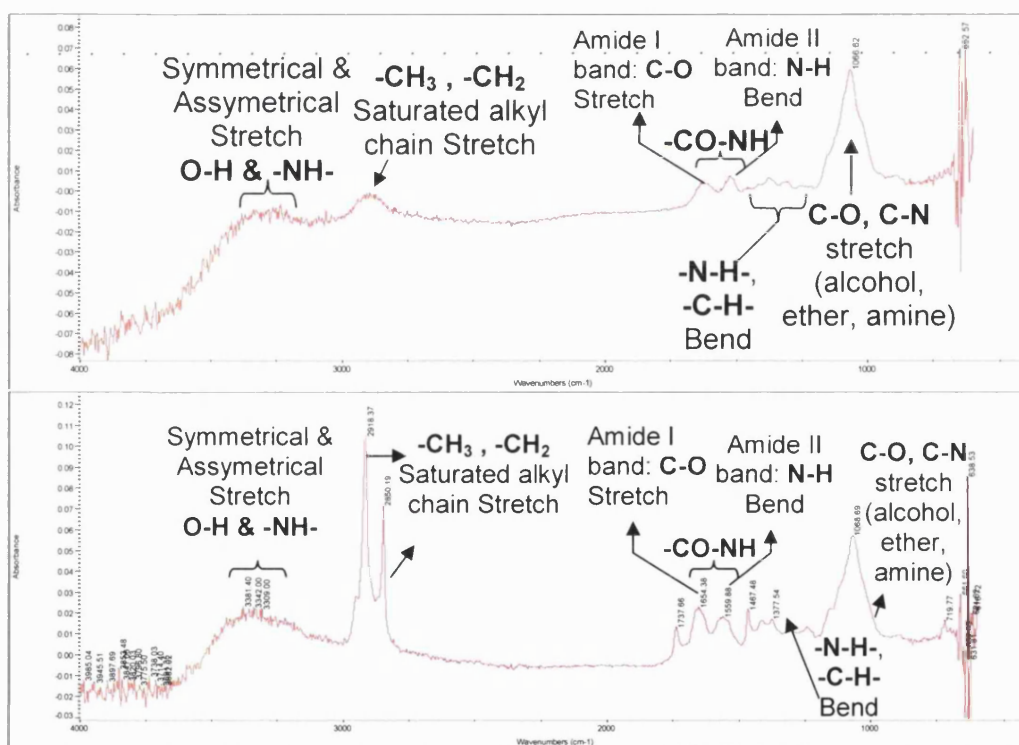


Figure 3.11: FTIR spectra for 24 hours degraded Glycol Chitosan (top) and Palmitoyl Glycol Chitosan (Palmitoylation: 18%) (bottom).

3.1.3.3 Matrix-Assisted Laser Desorption Spectrometry (MALDI-MS)

The GC spectra (Figure 3.12) correlates well with the GPC-Malls results obtained for the same batch of degraded GC (GC030107, Figure 3.13). The precursor peak is the peak of a double-charged ion which translates to a molecular weight of approximately $4824.66 \times 2^{-2}: 9647.32$ Da (GPC-Malls; Mn: 9422, Mw:11480, Mz: 15680). However, the ionisation of the PGC (Figure 3.13) and GCPQ (Figure 3.13) samples was not as efficient, making it difficult to separate the different peaks and provide a good baseline. One reason for this could be the increase of polydispersity due to grafting with palmitoyl and quaternary ammonium groups combined with the presence of multiple charged molecular ions.

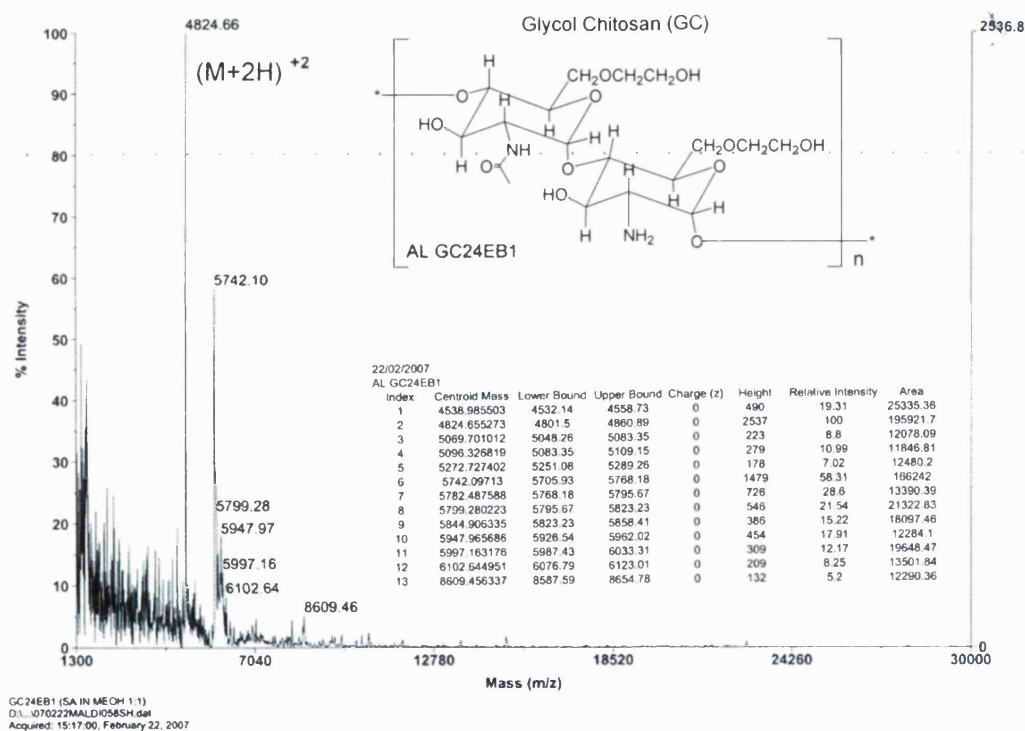
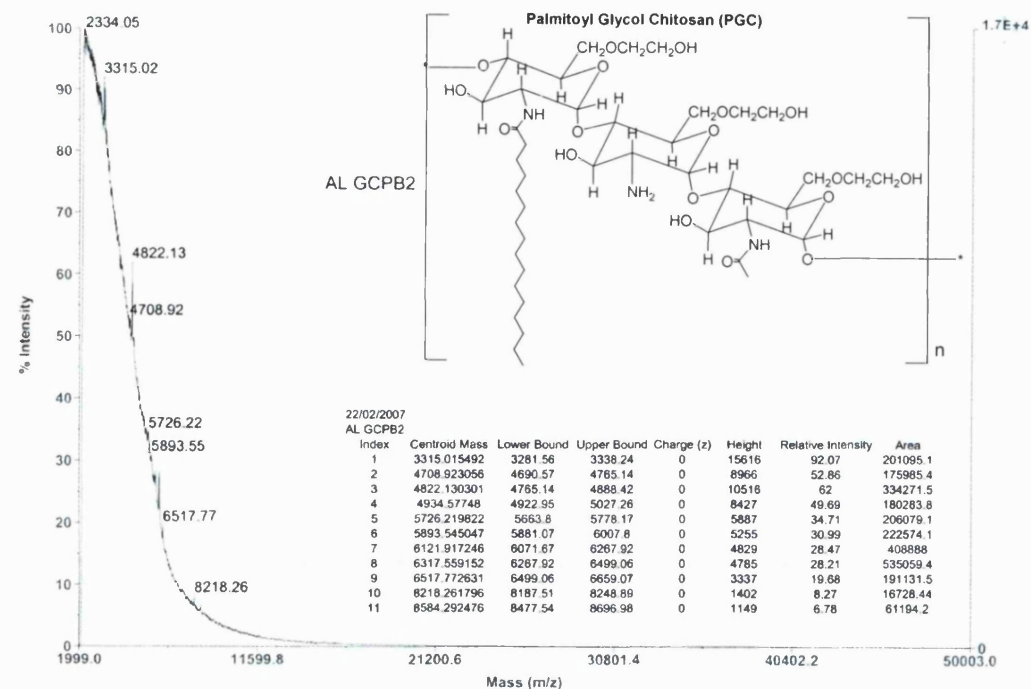
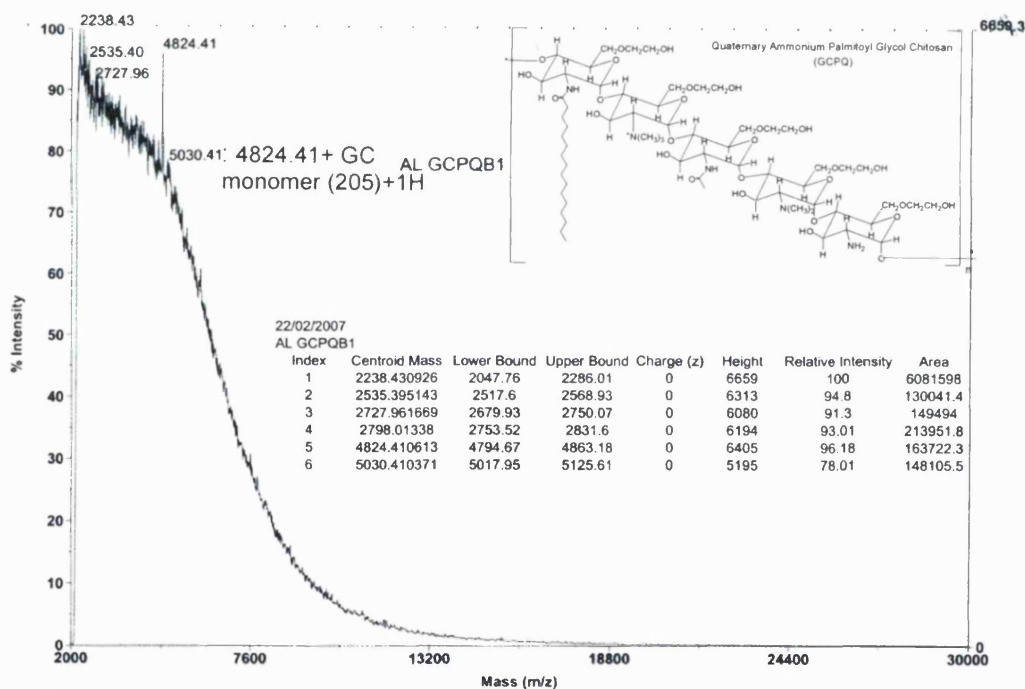


Figure 3.12: MALDI-TOF spectrum of GC. Matrix: Synapinic acid.



AL GCPB2
D:\1-070222MALDI059SH.dai
Acquired: 17:22:00, February 22, 2007



AL GCPQB1
D:\1-070222MALDI061SH.dai
Acquired: 17:48:00, February 22, 2007

Figure 3.13: MALDI-TOF spectrum of PGC (top) and GCPQ (bottom). Matrix: Synapinic acid.

3.2.1.4 Laser Light Scattering (LLS) and Gel Permeation Chromatography(GPC)

Figure 3.14 and 3.15 are example chromatograms for degraded GC and GCPQ respectively and Figure 3.16 illustrates example dn/dc curves obtained. The mean calculated molecular weight for the GCPQ measured by GPC-MALLS correlated well with the calculated molecular weight expected from grafting based on the NMR calculated percentages of palmitoylation and quaternisation (Figure 3.17). The dn/dc of GC and GCPQ was calculated for each sample separately by injecting a number of concentrations varying from 0.1 to 0.8 mg mL⁻¹ diluted in mobile phase (Figure 3.16). The average molecular weight (M_n) of GCPQ ($n=4$) was ~ 12400 g mole⁻¹ and the mean polydispersity (M_w/M_n) was 1.79. The high polydispersity can be attributed to the randomness of the palmitoylation and quaternisation reaction as well by the 24 hour degradation of GC in hydrochloric acid which was shown to increase the molecular weight distribution with increases in degradation time (Wang et al. 2001).

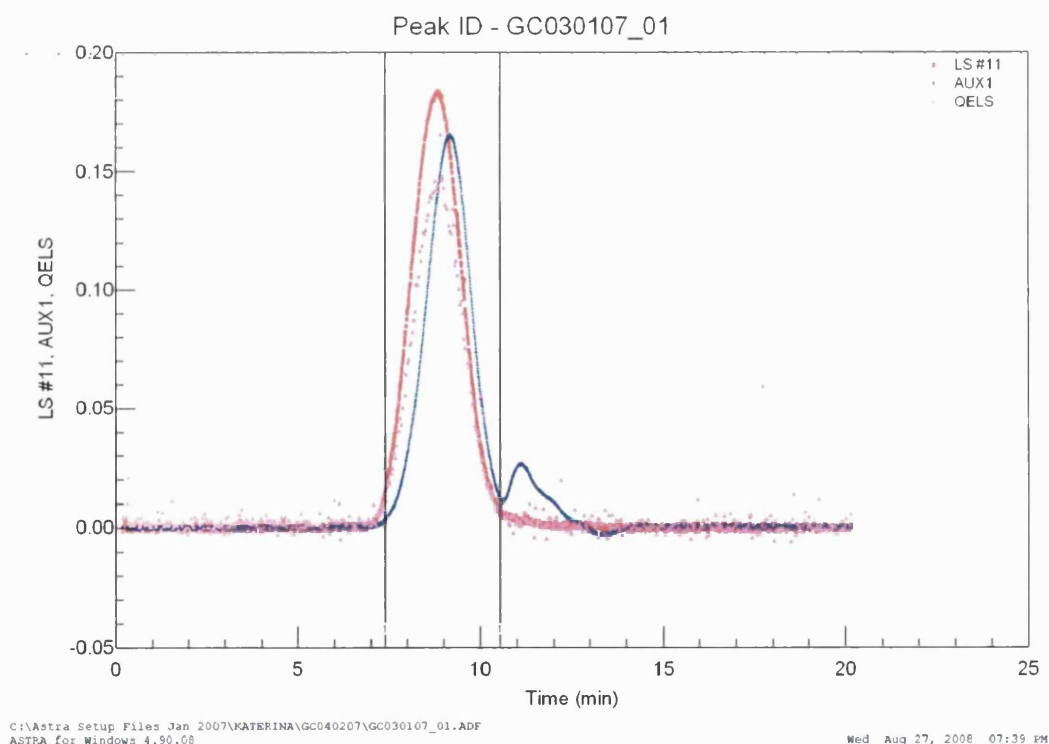


Figure 3.14: GPC-MALLS Chromatogram of degraded (24 hours) GC (5 mg mL⁻¹). Key: LS#11: Static Light Scattering detector (θ : 90°C), AUX 1: Refractive Index detector, QUELS: Quasi-elastic Light Scattering detector.

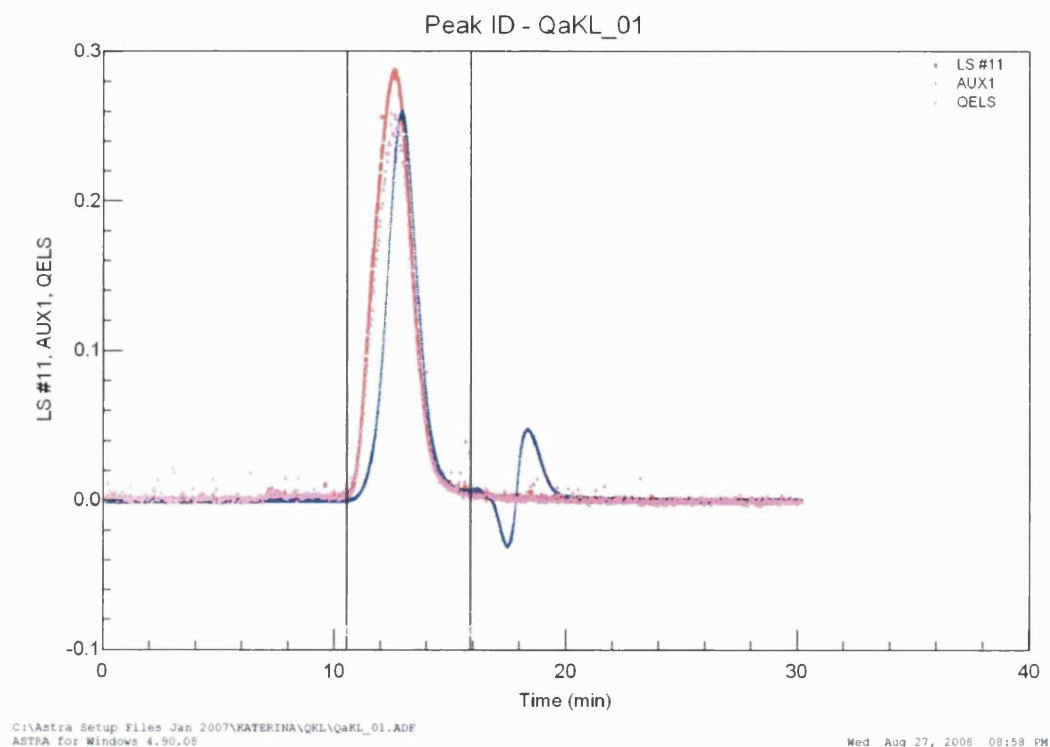


Figure 3.15: GPC-MALLS Chromatogram of GCPQ (10.79 mg mL^{-1}). Key: LS#11: Static Light Scattering detector ($\theta: 90^\circ\text{C}$), AUX 1: Refractive Index detector, QUELS: Quasi-elastic Light Scattering detector.

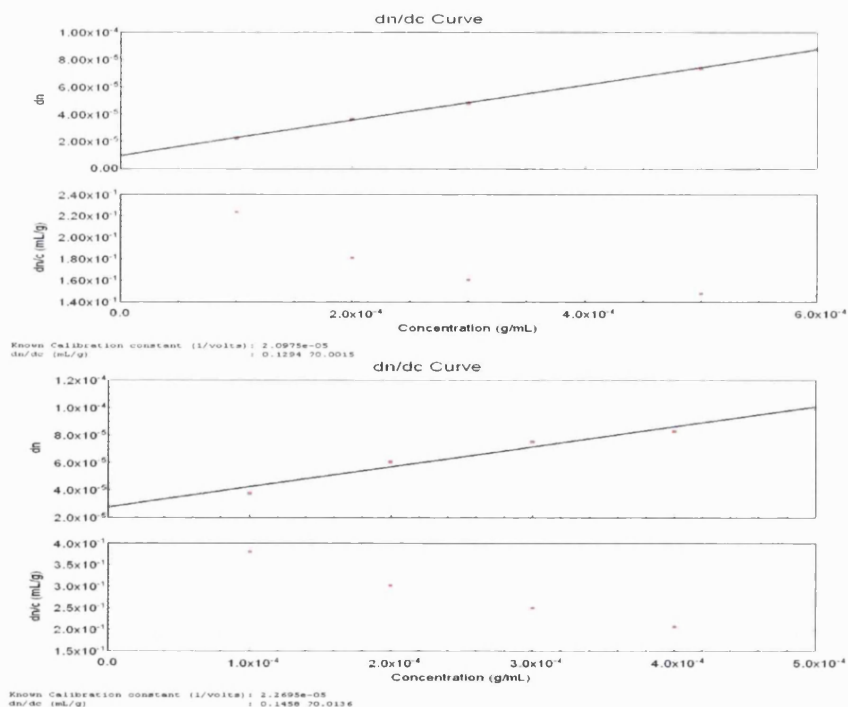
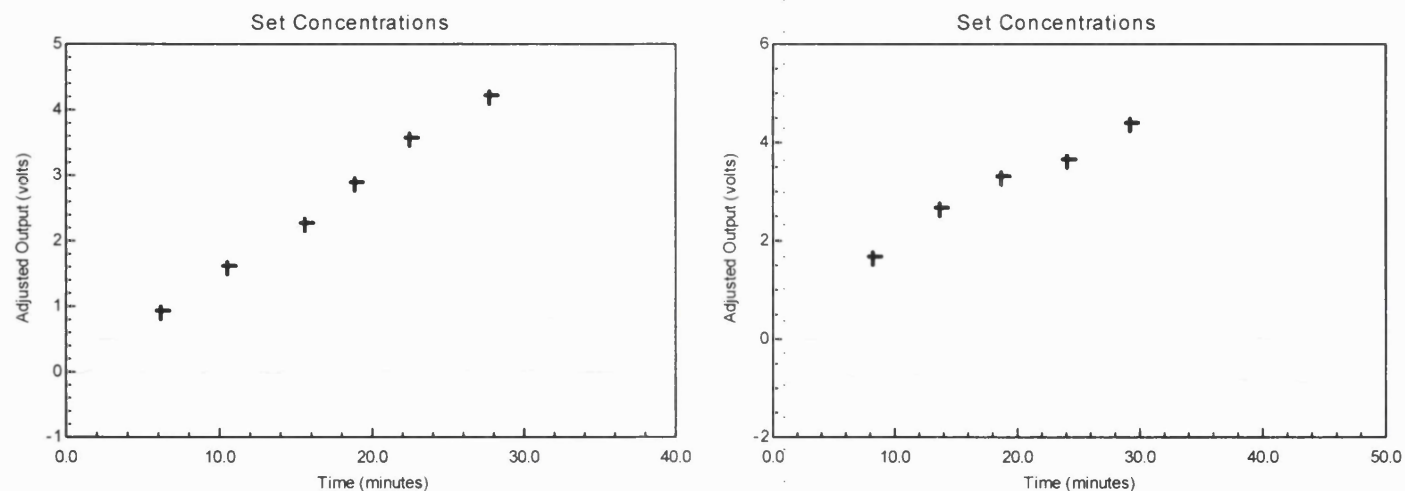


Figure 3.16: Example dn/dc curve of GC (GC031107) and GCPQ.



Batch	GC GPC- MALLS MN	GC dn/dc	GC Mono- mer (Da)	Mono- mers (n)	% P	Addition by CH ₃ - (CH ₂) ₁₄ - CO-	MW added by P	% Q	Addition by -(CH ₃) ₃	MW added by Q	Calculated Total MW	GCPQ dn/dc	GPC- MALLS MN	MW/MN
GC030107	9422	0.1296	205	45.96	14.286	239	1569.24	5.269	43	104.139	11095.378	0.2308	9955	1.34
GC040707	13420	0.1257	205	65.46	10.635	239	1663.89	9.094	43	255.997	15339.884	0.1964	17380	1.07
GC031107	9373	0.1294	205	45.72	13.095	239	1430.93	10.607	43	208.533	11012.464	0.1458	11110	1.55
GC011207	9182	0.137	205	44.79	22.086	239	2364.23	7.281	43	140.223	11686.456	0.304	11120	3.18
Mean	10349	0.1304	205	50.48	15.025	239	1757.07	8.0627	43	177.223	12283.545	0.2193	12391.3	
SD	2049.8	0.0047		9.999	4.9463		415.923	2.3059		68.0588	2059.5395	0.0664	3370.49	

Figure 3.17: Voltage Output versus time plots at increasing concentrations for 24 degraded GC (right) and GCPQ (left) and collective table of results for four batches of GCPQ. MN: Number average molecular weight, n: Number of monomers, MW: Weight average molecular weight, P: Palmitoylation, Q: Quaternisation, MW/MN: Polydispersity.

3.2.1.5 Preparation of Self-Assembled Polymer Aggregates

All produced vesicles were in the colloidal range. The majority of the vesicles (as described by the volume and number) are between 10 and 100 nm in size. Filtration reduced the mean average particle size in half and reduced the polydispersity index. TEM images illustrates micelles and clusters of particles.

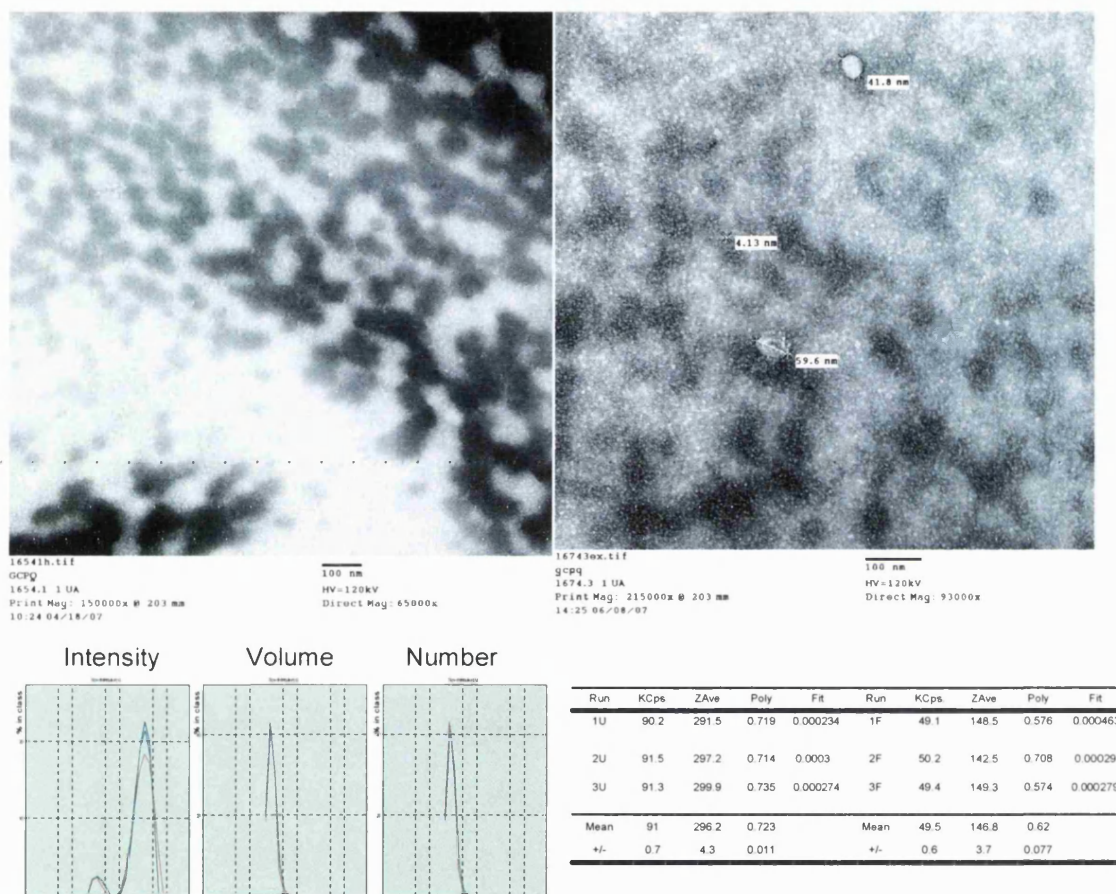
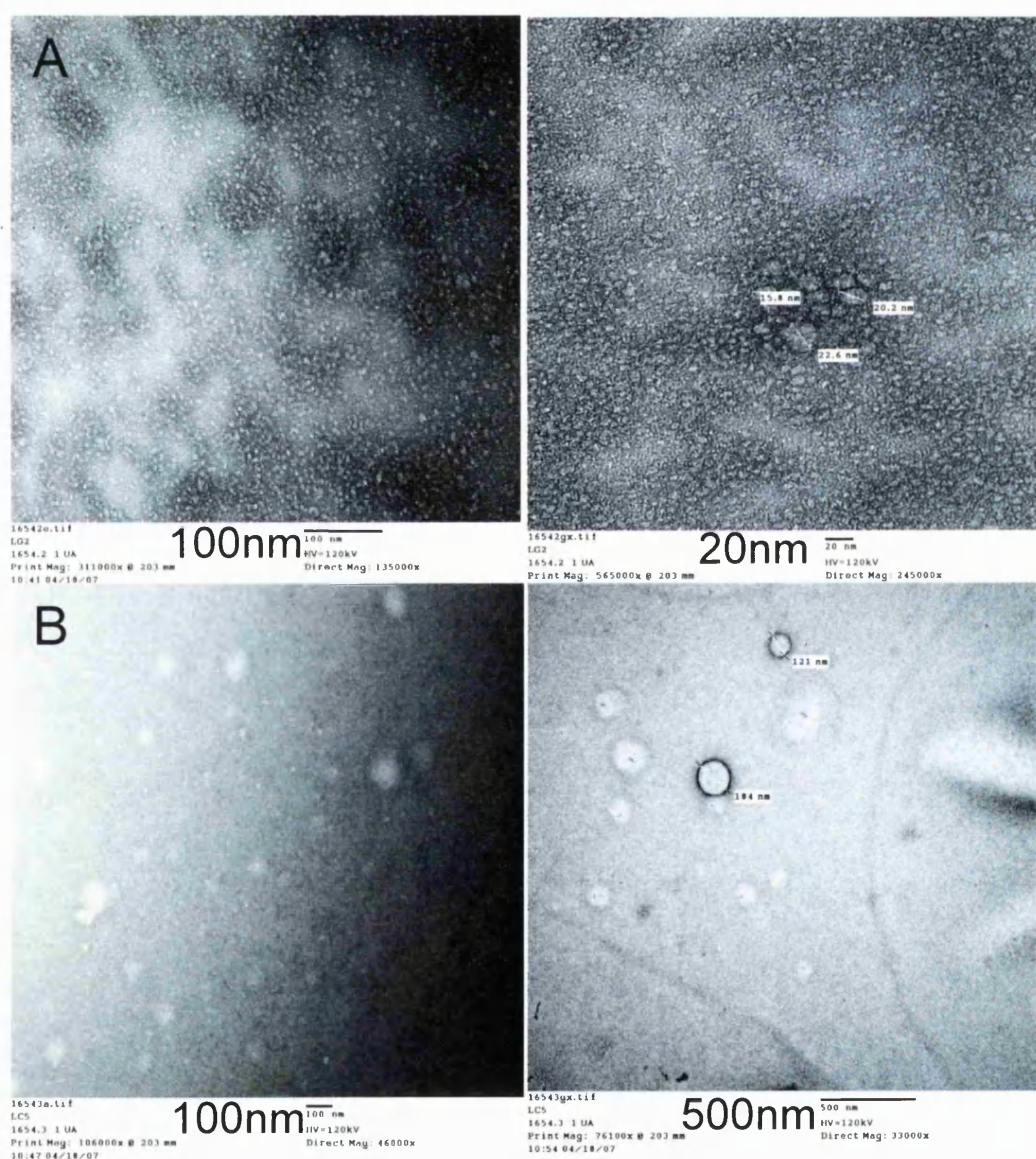
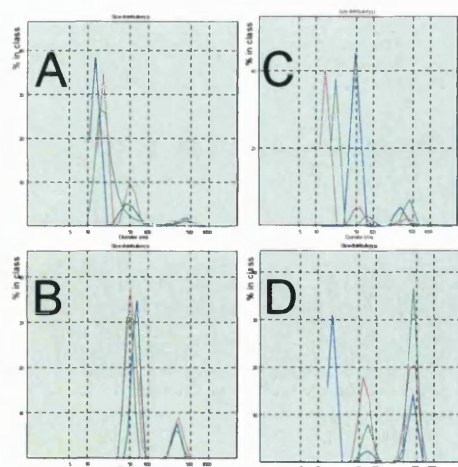
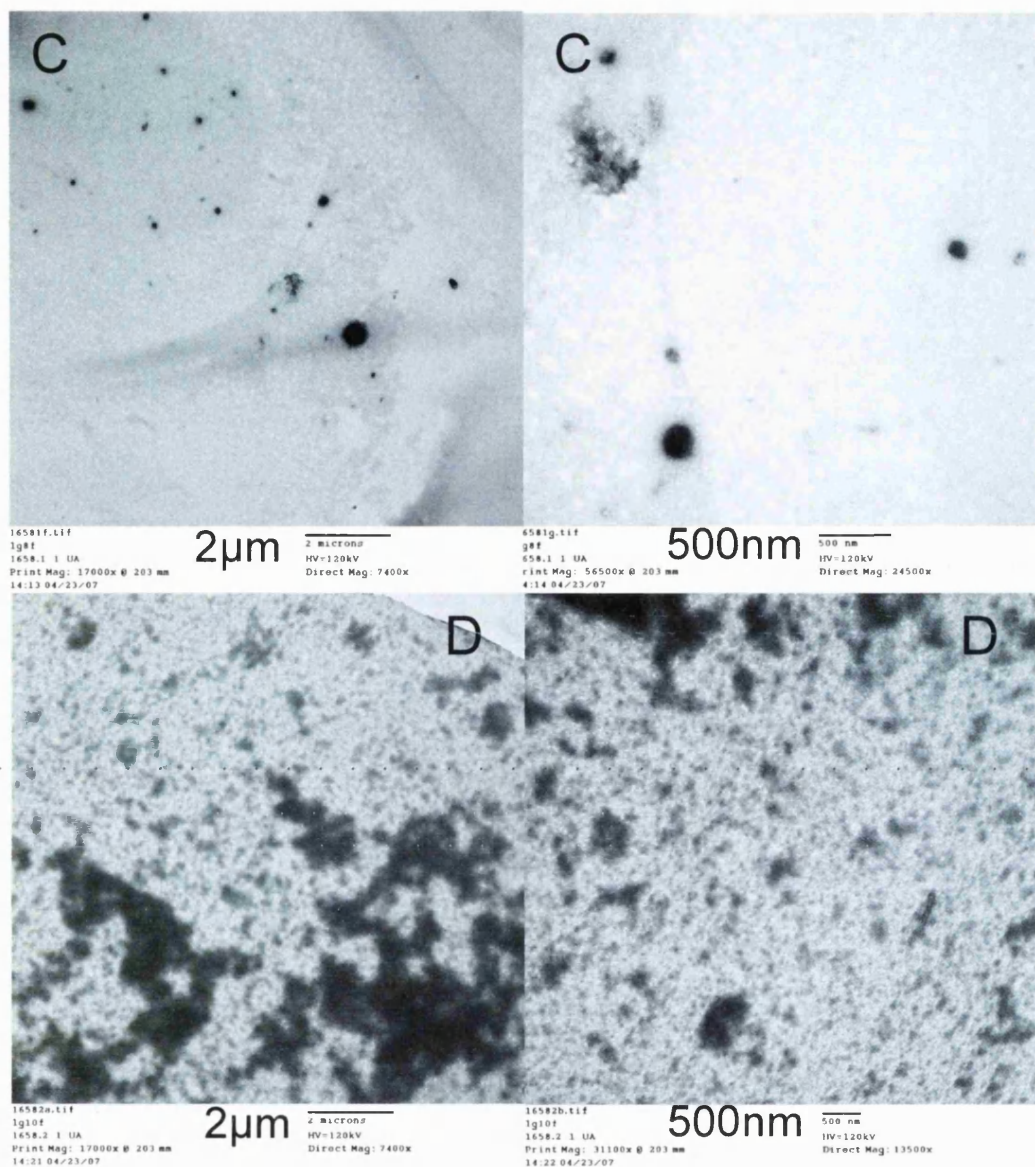


Figure 3.18: PCS spectrum for an unfiltered aqueous dispersion of GCPQ (2.3 mg mL^{-1}) (Palmitoylation: 15%, Quaternisation: 11%) on sonication. Sample appeared clear. Top: Negative stained TEM images of an unfiltered aqueous dispersion of GCPQ (Right Image: 2.3 mg mL^{-1} , Left Image: 5 mg mL^{-1}) (Palmitoylation: 15%, Quaternisation: 11%) on probe sonication. Bar: 100nm. Bottom: Size distributions by intensity, volume, and number for triplicate runs (Run 1: red; 2: green; 3: blue) and a summary table of results for the unfiltered compared to the results for the same sample after filtration ($0.45 \mu\text{m}$) (U: Unfiltered, F: Filtered).

3.2.1.6 Particle sizing, TEM and HPLC analysis of Drug Loaded Polymers

Based on HPLC quantitation, the encapsulation efficiency was 0.25%, 21.28%, 29.07% and 34.04% (LENK calibration curve: $y=330403x - 283168$, $r^2=0.9982$) for vortexed and filtered polymeric dispersions (2.3mg mL^{-1} , 5mg mL^{-1} , 8mg mL^{-1} , 10mg mL^{-1}) and LENK (1mg) respectively. For the lipidic peptide (TPLENK, 1mg) the encapsulation efficiency was 12.24% and 29.44% (TPLENK calibration curve $y=21416x+49213$, $r^2=0.9867$) for $0.45\mu\text{m}$ filtered polymer solutions (5mg mL^{-1} , 10mg mL^{-1}) respectively. The low encapsulation efficiency can be attributed to adsorption of the peptide with the filter used.

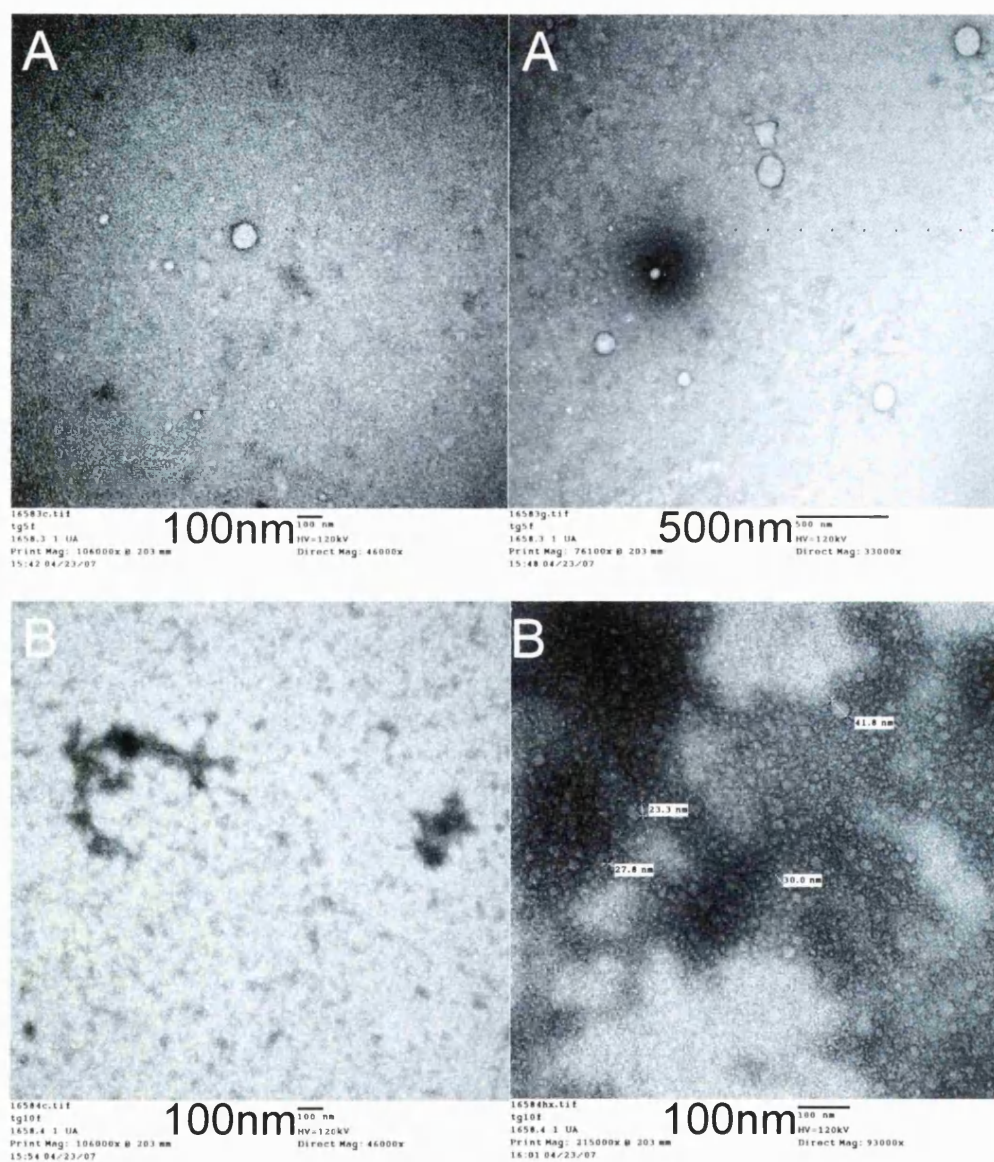




Sample	KCps.	ZAve (nm)	Poly
A	42.2 ±0.9	144.1 ±6.5	0.644 ±0.088
B	139.2 ±4.2	177.8 ±9.5	0.685 ±0.094
C	106.1 ±1.4	169.7 ±6.4	0.684 ±0.118
D	184.9 ±3.1	204 ±3.4	0.864 ±0.008

Figure 3.19: Negative stained TEM images of polymeric dispersions of GCPQ in increasing concentrations (A: 2.3mg mL^{-1} , B: 5mg mL^{-1} , C: 8mg mL^{-1} , D: 10mg mL^{-1} , Palmitoylation: 15%, Quaternisation: 11%) and Leucine^[5]-Enkephalin (1mg) after filtration through $0.45\mu\text{m}$. Bottom Left: Volume Mean Distribution from PCS for the filtered samples. Bottom Right: Summary table of mean particle size measurements results.

The mean particle size remained for polymeric dispersions of LENK between 140 and 200 nm with a small increase with the increase of polymer concentration. The majority of particles remained less than 100 nm, while a second population of larger aggregates varied between 250 and 750 nm (Figure 3.19). Two populations were



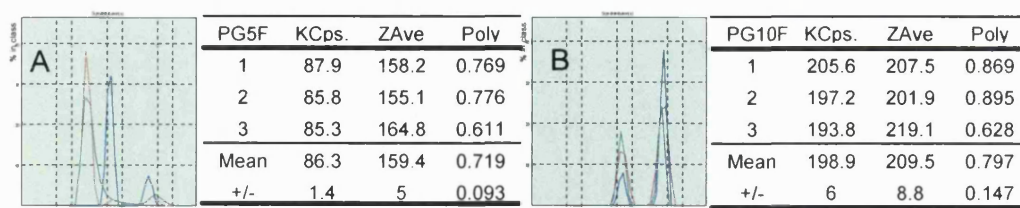
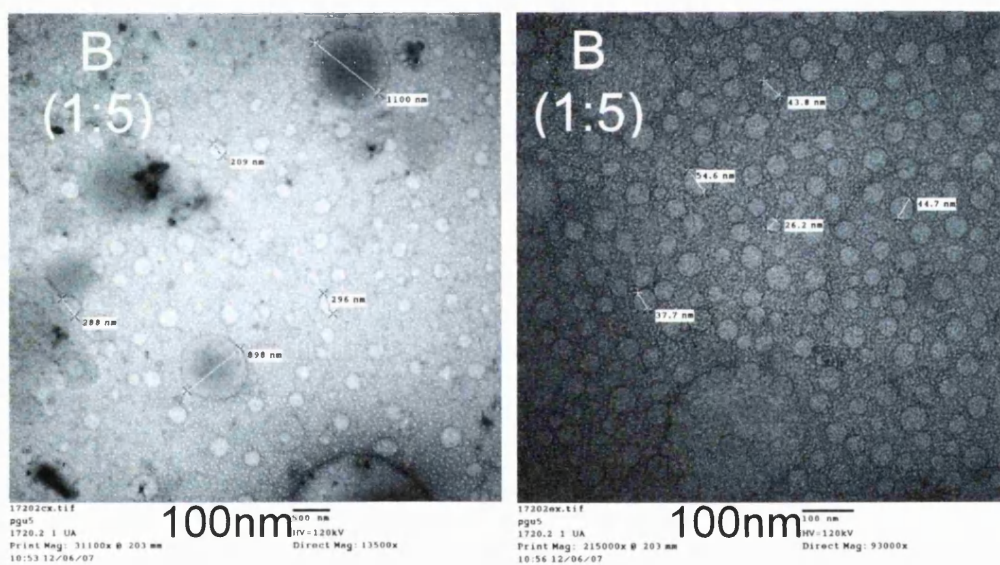
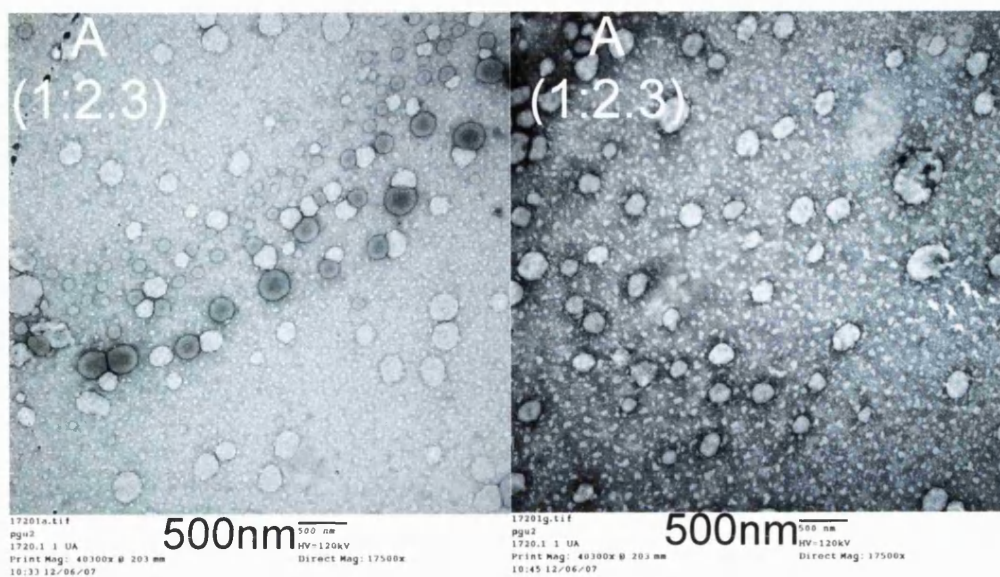


Figure 3.20: Negative stained TEM images of polymeric dispersions of GCPQ in increasing concentrations (A: 5mg mL⁻¹, B: 10mg mL⁻¹, Palmitoylation: 15%, Quaternisation: 11%) and TPLENK (1mg) after filtration through 0.45µm. Sample appeared slightly opaque (A) and opaque (B). Bottom Volume Mean Distribution from PCS for the filtered samples (Left) and summary table of mean particle size measurements results (Right).

observed for polymeric dispersions of TPLENK; one of small aggregates below the 100 nm range and one that ranged between 250 and 900 nm. In the case of TPLENK dispersions the larger aggregates were greater in number as the polymer concentration increased.

The encapsulation efficiency of the lipidic peptide after filtration (0.8µm) was 44%, 57% and 38% (TPLENK calibration curve $y=20089x + 42156$, $r^2=0.9811$) prepared with vortexing and sonication of 3 different ratios of GCPQ (2.3 mg mL⁻¹, 5mg mL⁻¹, 10mg mL⁻¹) and TPLENK (1mg mL⁻¹) respectively. The mean particle size remained for polymeric dispersions of TPLENK under 1µm as a single population of particles but increased with increasing concentration of polymer (Figure 3.21). Polydispersity of the dispersions also increased with increasing polymer concentration. TEM sizes do not correlate well with the mean particle size obtained from PCS, probably indicative of the presence of a small number of larger aggregates causing an overestimation of the mean particle size. Particle size as measured by PCS (> 0.8 µm) can explain the reduced encapsulation efficiency for formulation C (1:10 w/w ratio) as measured by HPLC (as all formulations were filtered through a 0.8 µm before HPLC analysis).



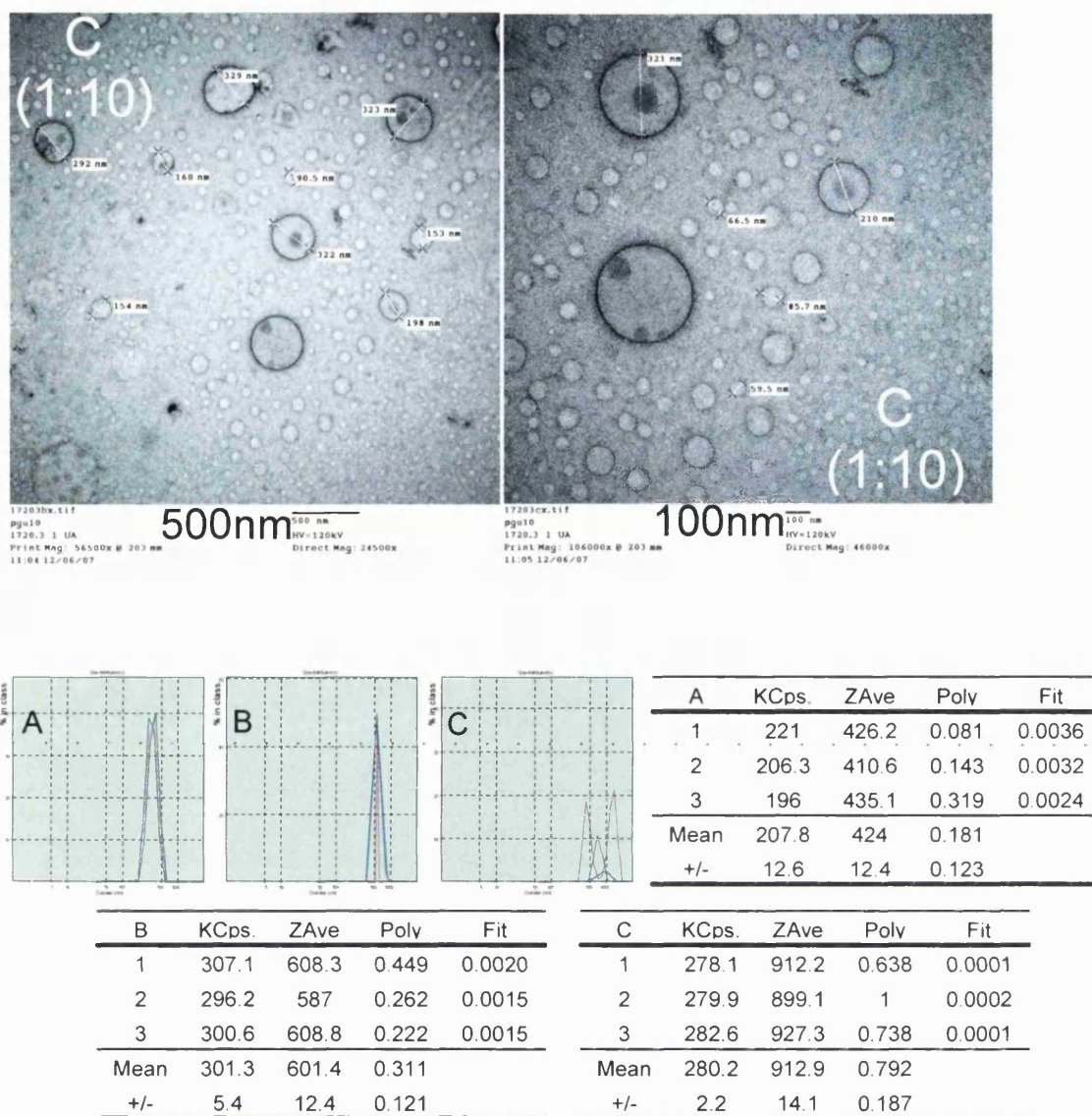


Figure 3.21: Top: Negative stained TEM images of polymeric dispersions of GCPQ in increasing concentrations (A: 2.3 mg mL⁻¹, B: 5mg mL⁻¹, C: 10mg mL⁻¹, Palmitoylation: 19.68 %, Quaternisation: 6.88 %) and TPLENK (1mg). Samples appeared slightly opaque (A) and opaque (B, C). Bottom: Volume Mean Distribution from PCS for the unfiltered samples (Left top) and summary tables of mean particle size measurements results for all three formulations.

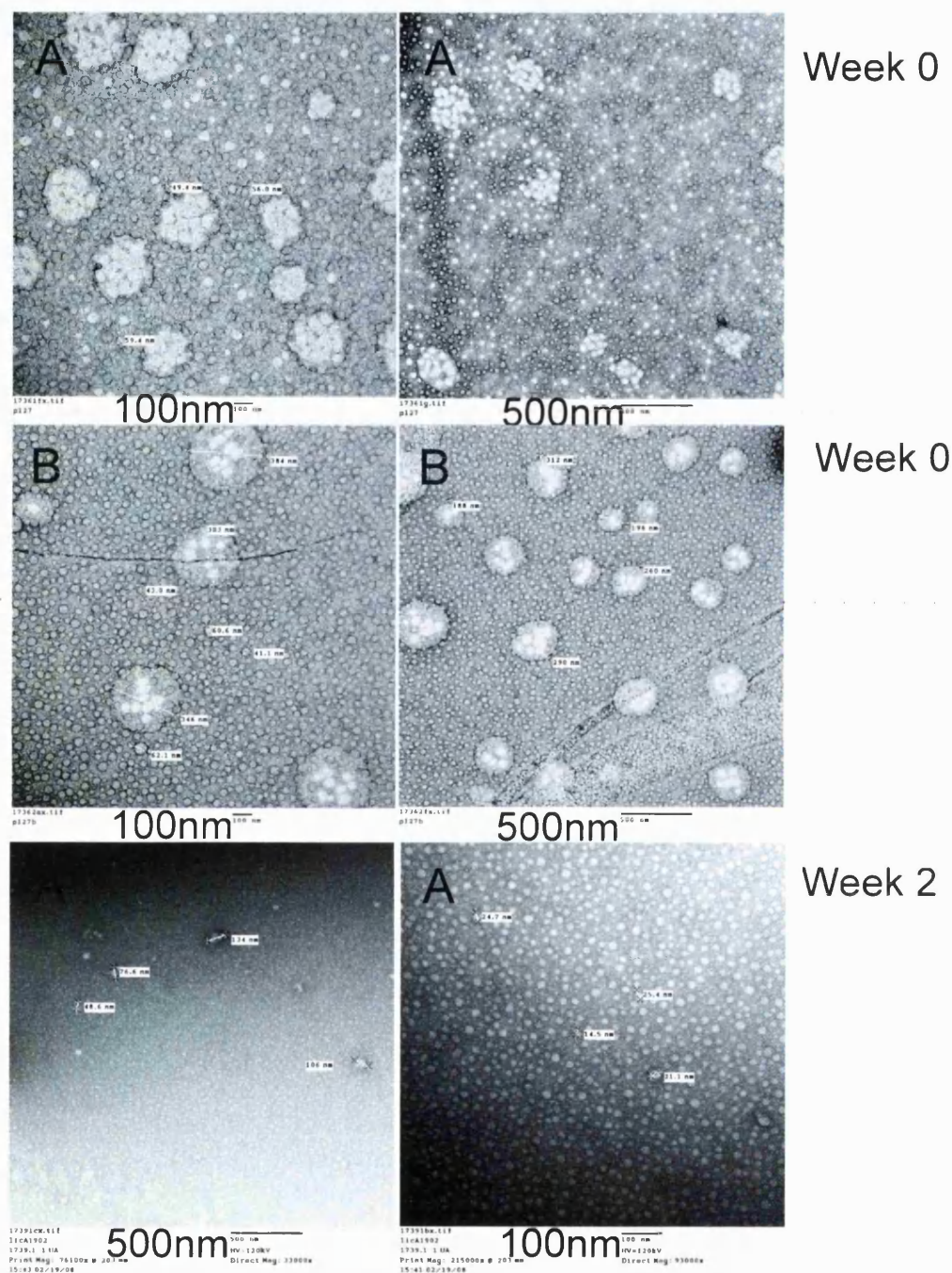


Figure 3.22: Negative stained TEM images of polymeric dispersions of TPLENK to GCPQ (1:2.3w/w) (1 mg mL⁻¹). Letter A-C indicates the three triplicates (Wet Stability). (Week 1 could not be analysed due to TEM failure). GCPQ Palmitoylation: 18.7%, Quaternisation: 8.3% for all three formulations.

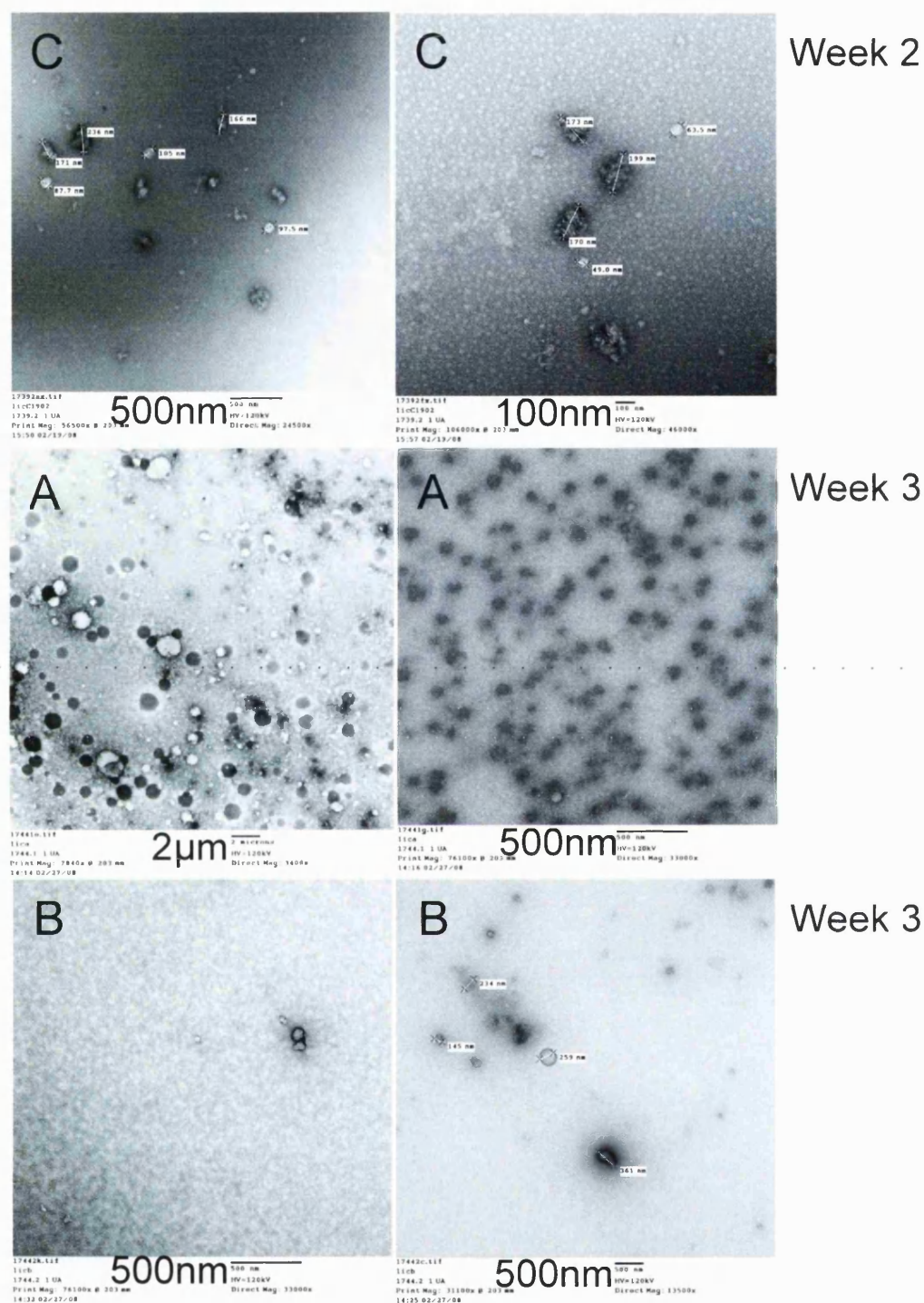


Figure 3.22: Negative stained TEM images of polymeric dispersions of TPLENK to GCPQ (1:2.3w/w) (1 mg mL⁻¹). Letter A-C indicates the three triplicates (Wet Stability). (Week 1 could not be analysed due to TEM failure). GCPQ Palmitoylation: 18.7%, Quaternisation: 8.3% for all three formulations.

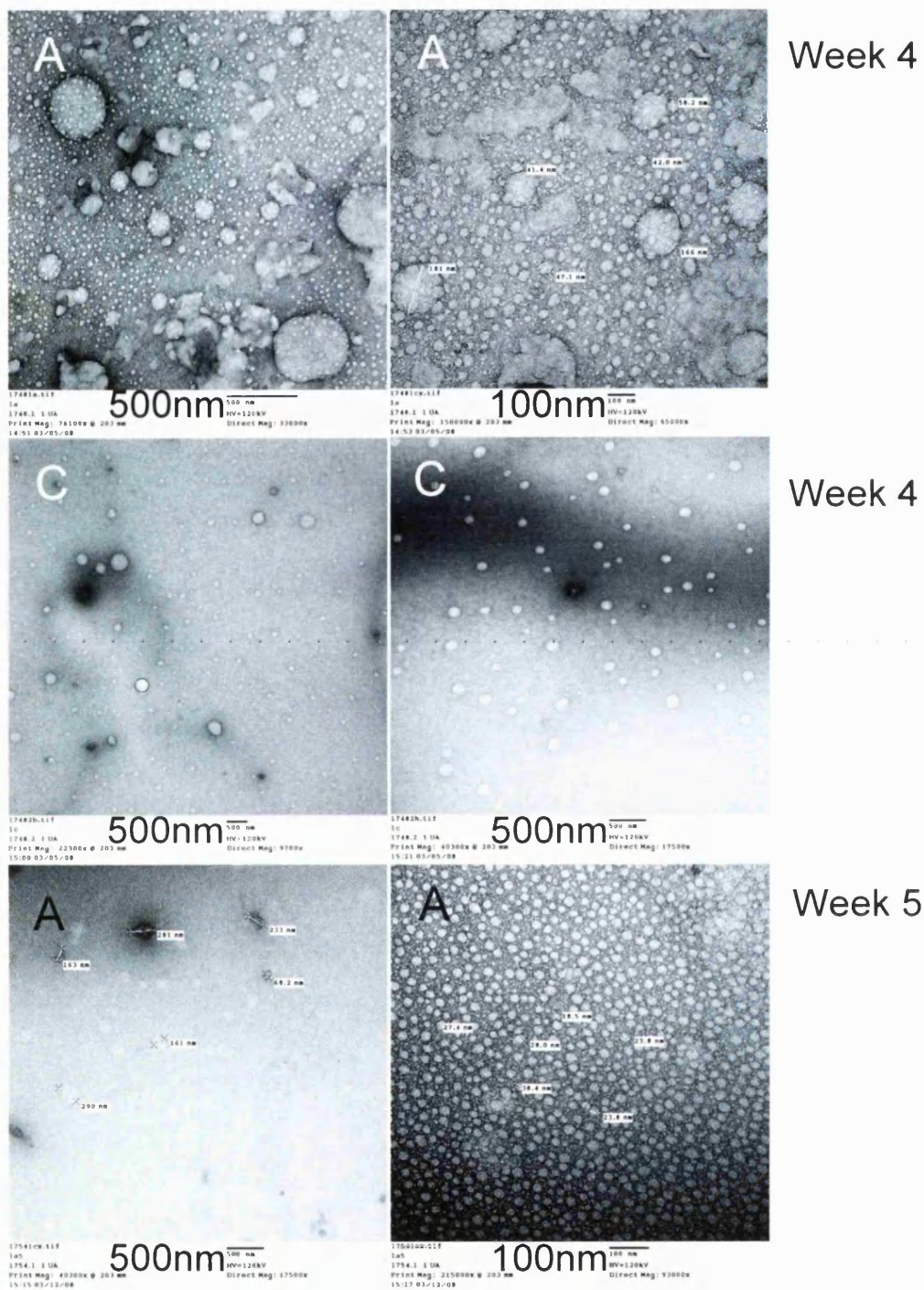


Figure 3.22: Negative stained TEM images of polymeric dispersions of TPLENK to GCPQ (1:2.3w/w) (1 mg mL^{-1}). Letter A-C indicates the three triplicates (Wet Stability). (Week 1 could not be analysed due to TEM failure). GCPQ Palmitoylation: 18.7%, Quaternisation: 8.3% for all three formulations.

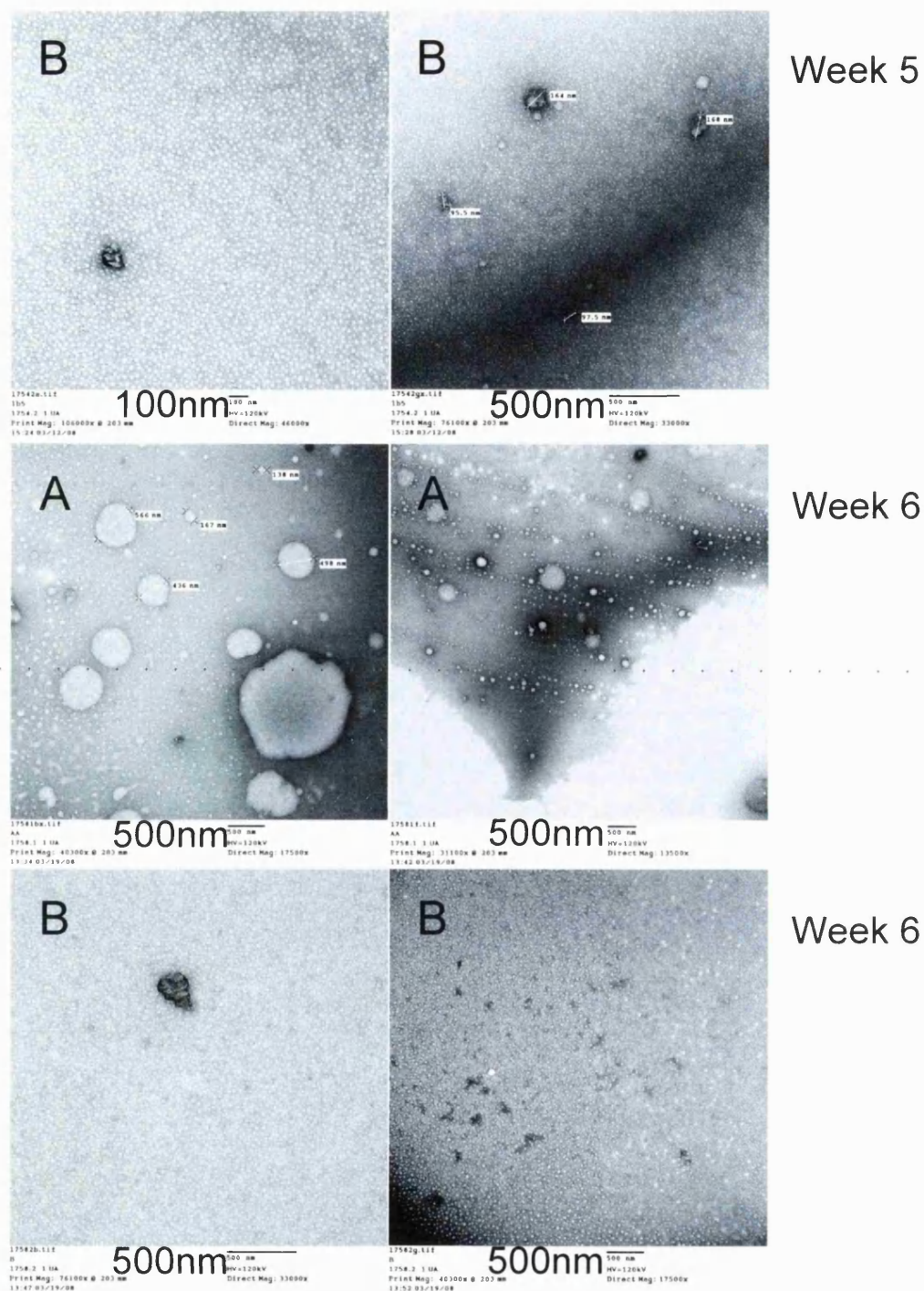


Figure 3.22: Negative stained TEM images of polymeric dispersions of TPLENK to GCPQ (1:2.3w/w) (1 mg mL^{-1}). Letter A-C indicates the three triplicates (Wet Stability). (Week 1 could not be analysed due to TEM failure). GCPQ Palmitoylation: 18.7%, Quaternisation: 8.3% for all three formulations.

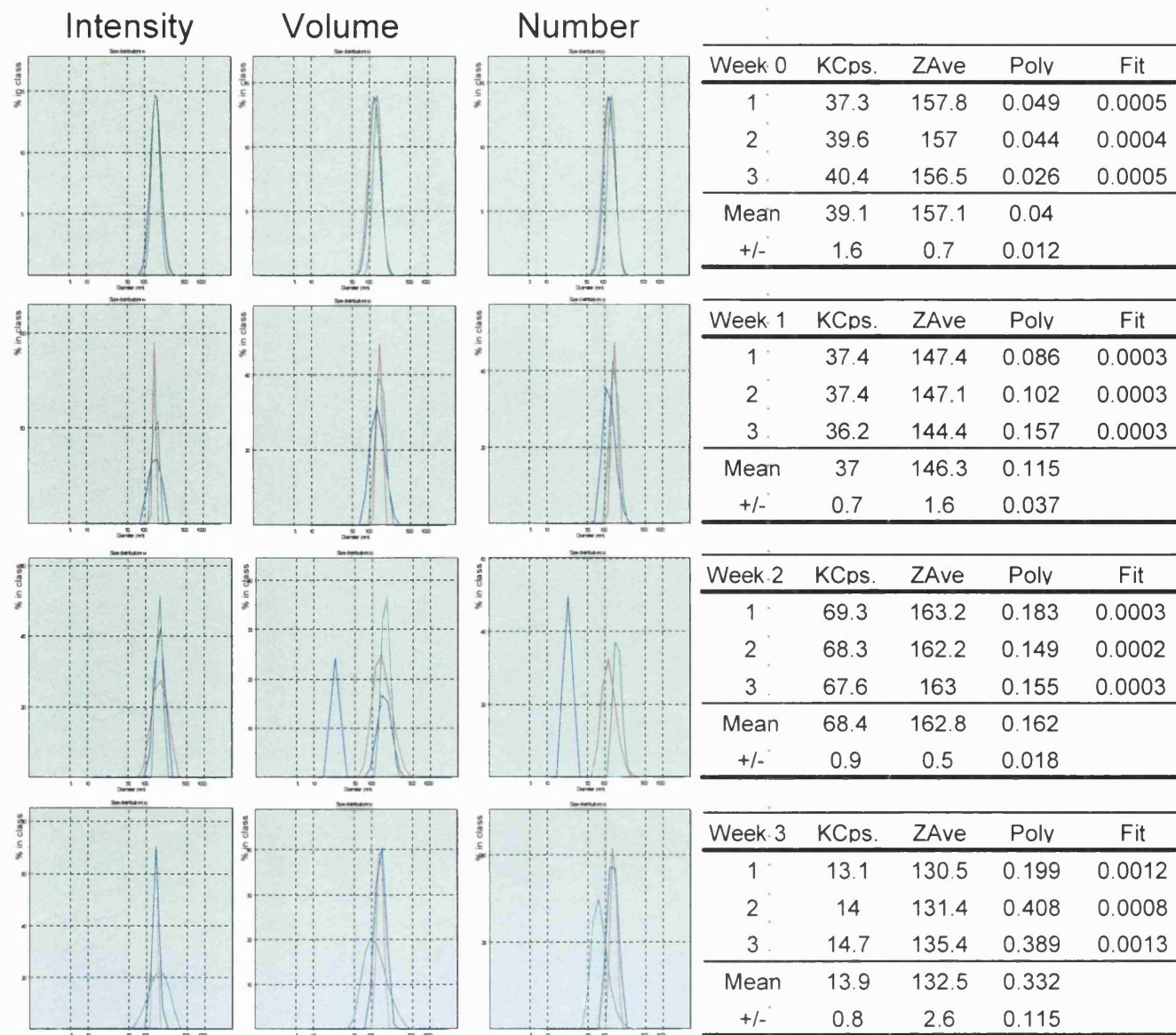


Figure 3.23: PCS spectra of polymeric dispersions of TPLENK : GCPQ (1 : 2.3 w/w) formulations in H₂O (1mg mL⁻¹) after vortexing, sonication and filtration (0.22µm) (Wet stability studies). Samples were clear throughout the stability experiment. From left to right, the size distribution by intensity, volume and number and a summary table of results (Z average, polydispersity index) appear for each week examined from top to bottom for 1 of the triplicates (Formulation A).

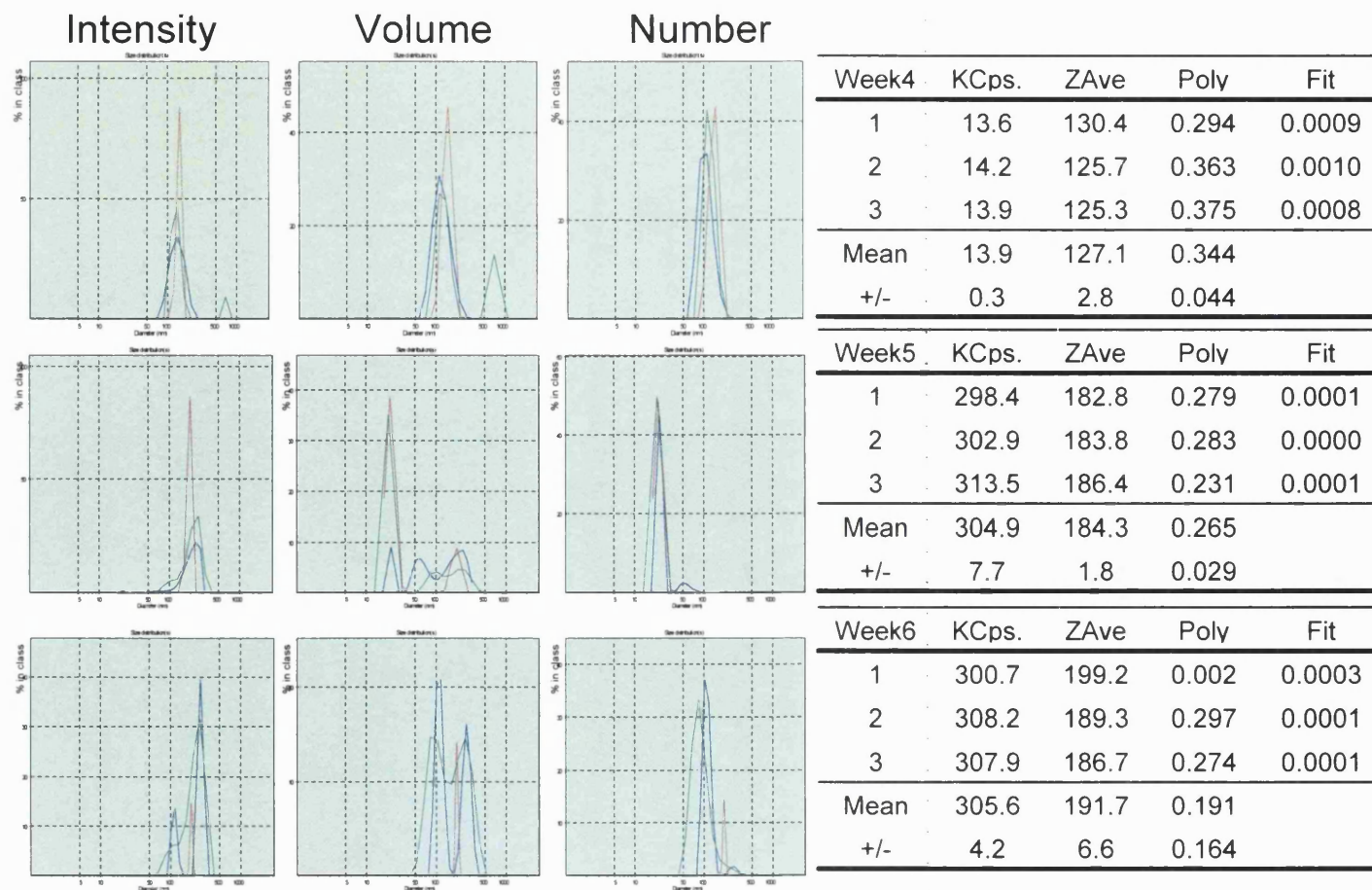


Figure 3.23: PCS spectra of polymeric dispersions of TPLENK : GCPQ (1 : 2.3 w/w) formulations in H₂O (1mg mL⁻¹) after vortexing, sonication and filtration (0.22µm) (Wet stability studies). Samples were clear throughout the stability experiment. From left to right, the size distribution by intensity, volume and number and a summary table of results (Z average, polydispersity index) appear for each week examined from top to bottom for 1 of the triplicates (Formulation A).

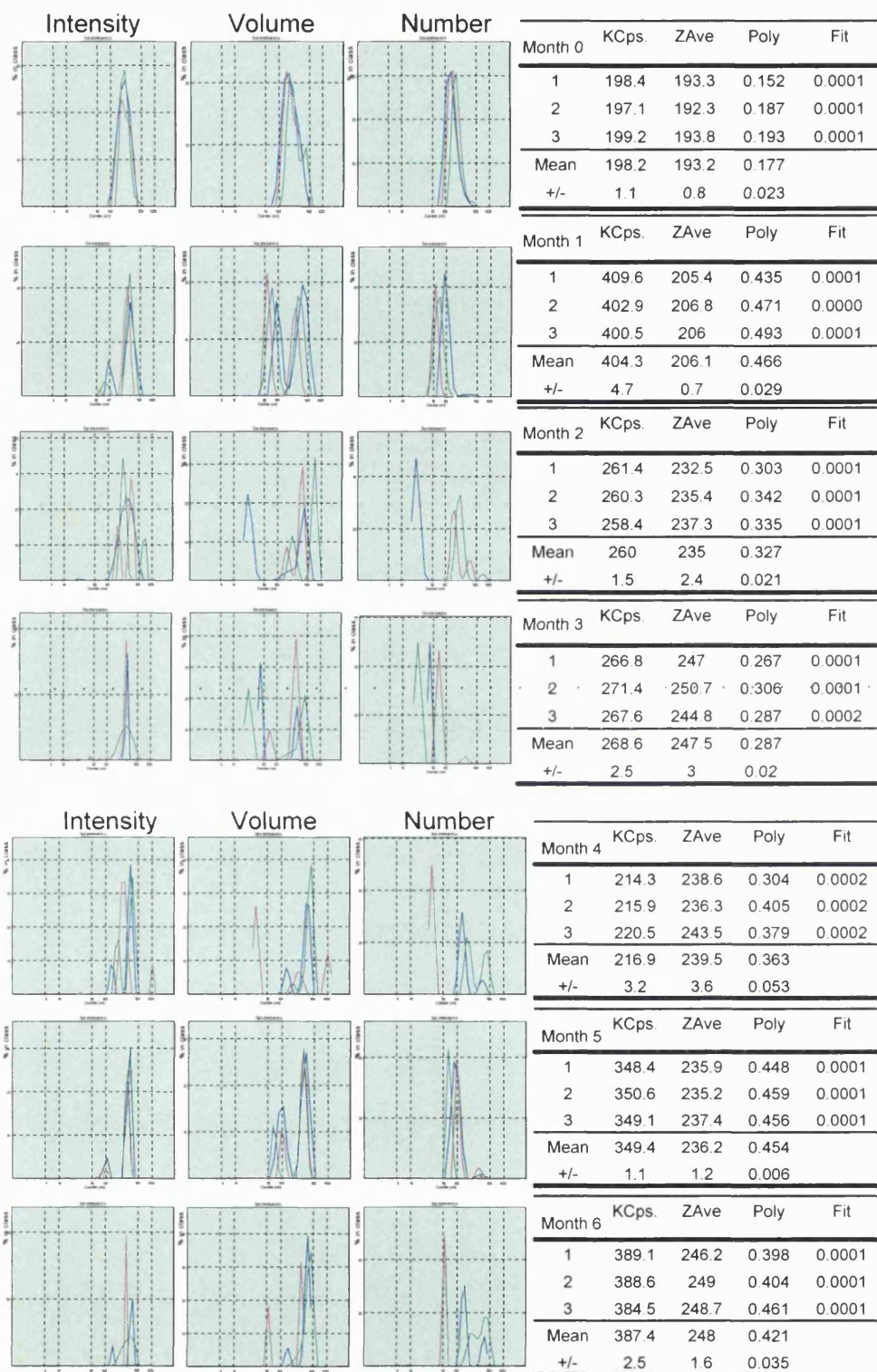


Figure 3.24: PCS spectra of polymeric dispersions of TPLENK : GCPQ (1 : 2.3 w/w) formulations in H₂O (1mg mL⁻¹) after vortexing, sonication and filtration (0.22 μ m) (Dry stability studies). Samples were clear throughout the stability experiment. From left to right, the size distribution by intensity, volume and number and a summary table of results (Z average, polydispersity index) appear for each week examined from top to bottom for 1 of the triplicates (Formulation C).

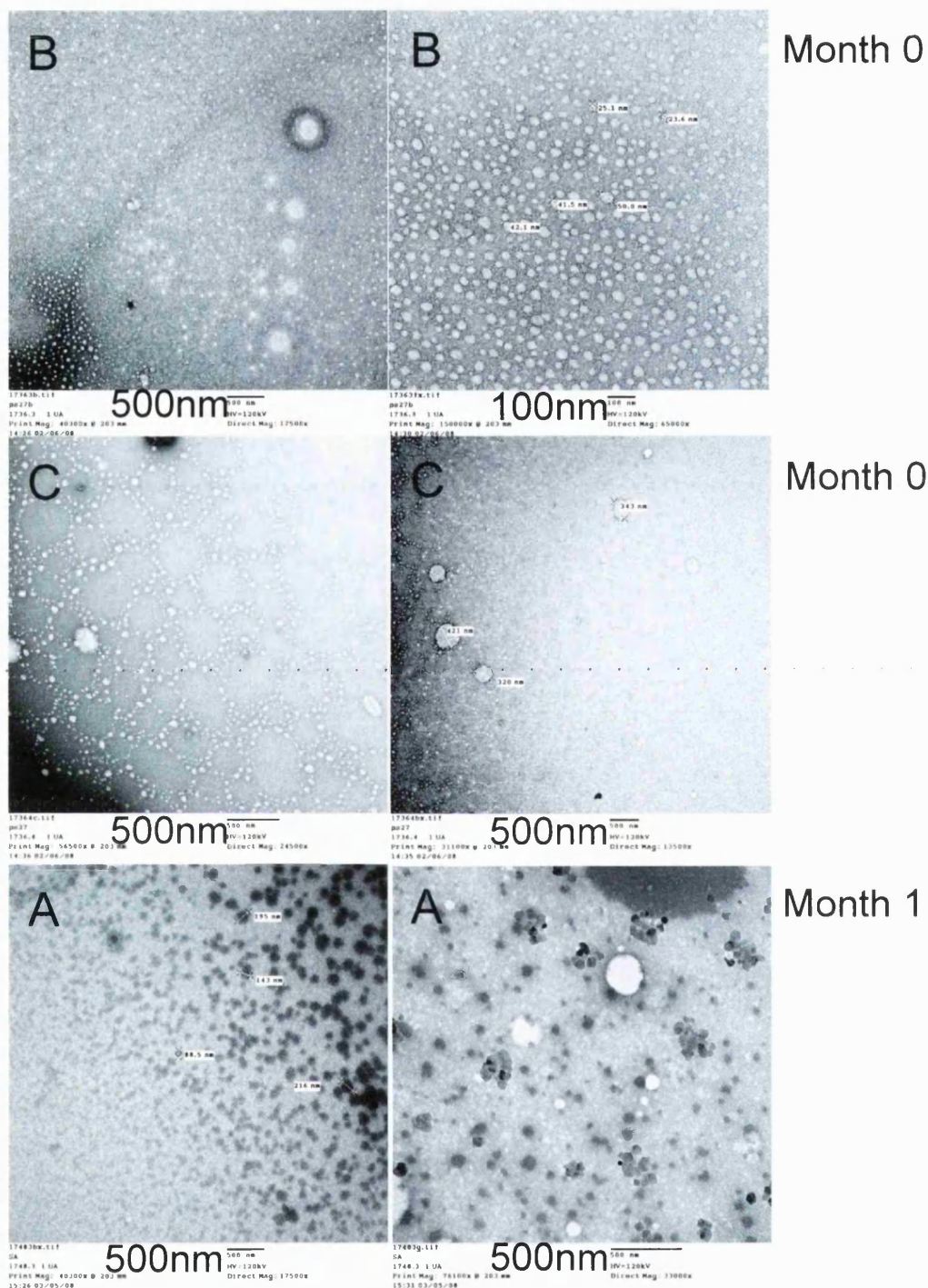


Figure 3.25: Negative stained TEM images of polymeric dispersions of TPLENK to GCPQ (1:2.3w/w) (1 mg mL^{-1}). Letter A-C indicates the three triplicates (Dry Stability). GCPQ Palmitoylation: 19.7%, Quaternisation: 6.9% for all three formulations.

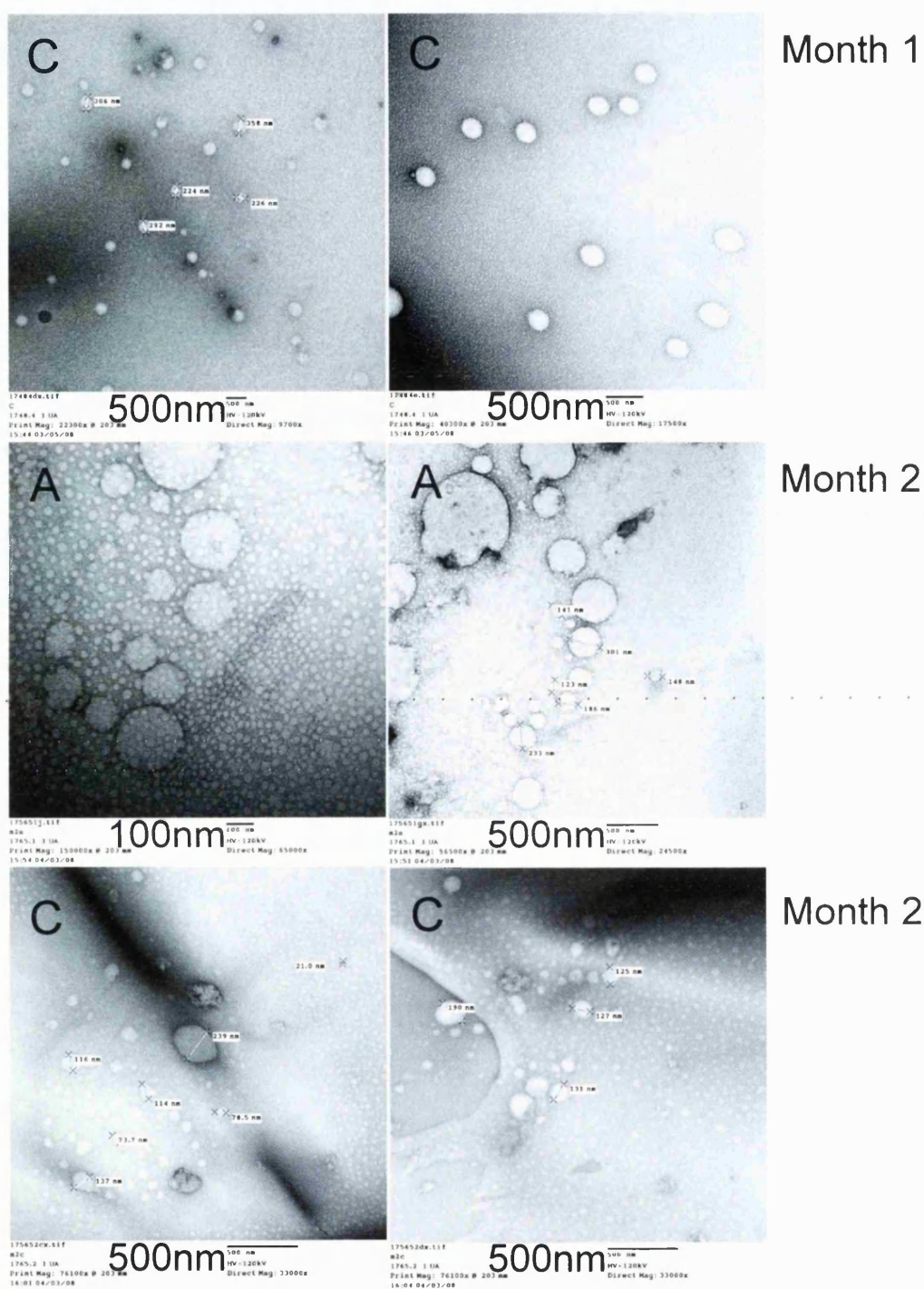


Figure 3.25: Negative stained TEM images of polymeric dispersions of TPLENK to GCPQ (1:2.3w/w) (1 mg mL^{-1}). Letter A-C indicates the three triplicates (Dry Stability). GCPQ Palmitoylation: 19.7%, Quaternisation: 6.9% for all three formulations.

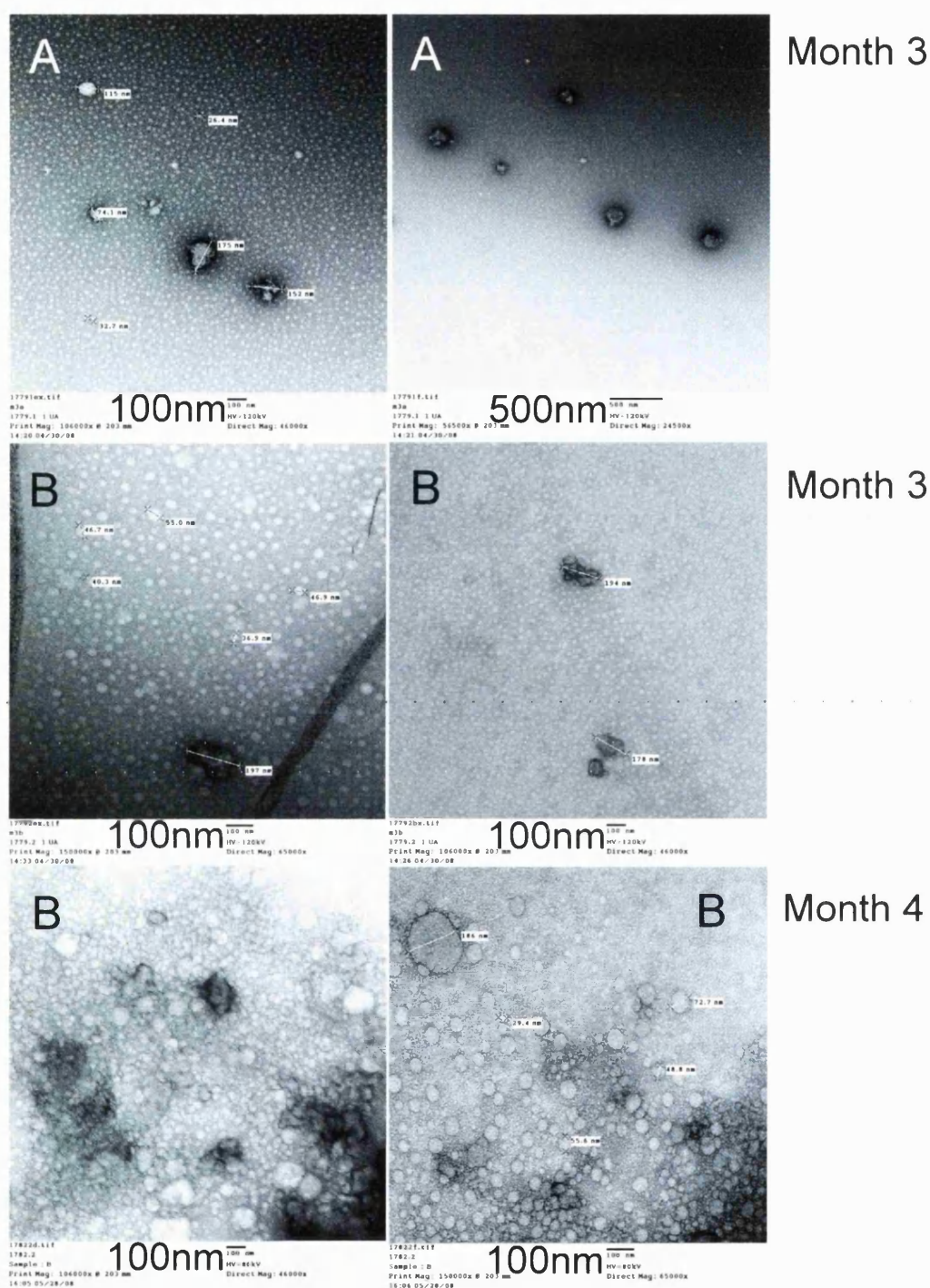


Figure 3.25: Negative stained TEM images of polymeric dispersions of TPLENK to GCPQ (1:2.3w/w) (1 mg mL⁻¹). Letter A-C indicates the three triplicates (Dry Stability). GCPQ Palmitoylation: 19.7%, Quaternisation: 6.9% for all three formulations.

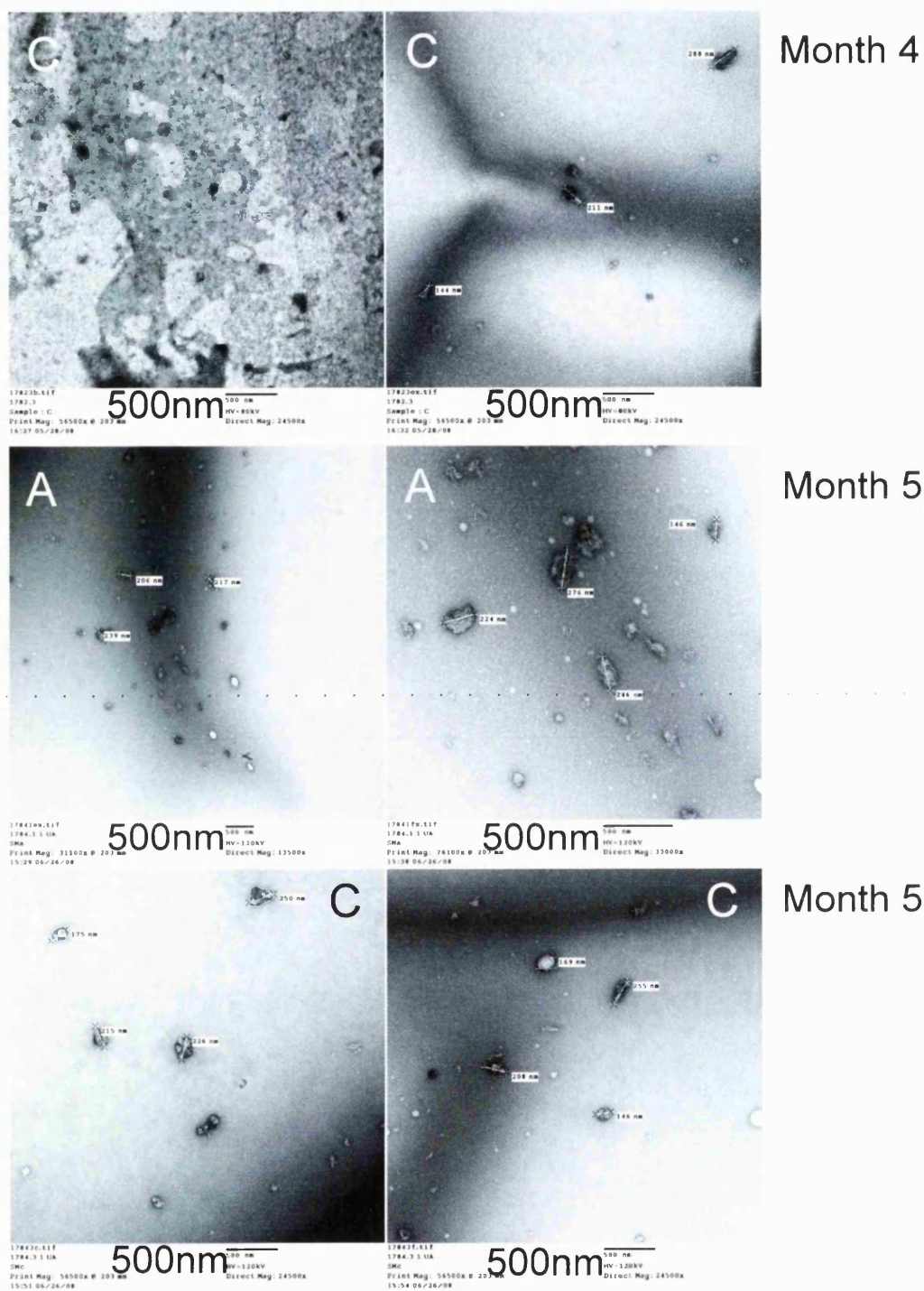


Figure 3.25: Negative stained TEM images of polymeric dispersions of TPLENK to GCPQ (1:2.3w/w) (1 mg mL^{-1}). Letter A-C indicates the three triplicates (Dry Stability). GCPQ Palmitoylation: 19.7%, Quaternisation: 6.9% for all three formulations.

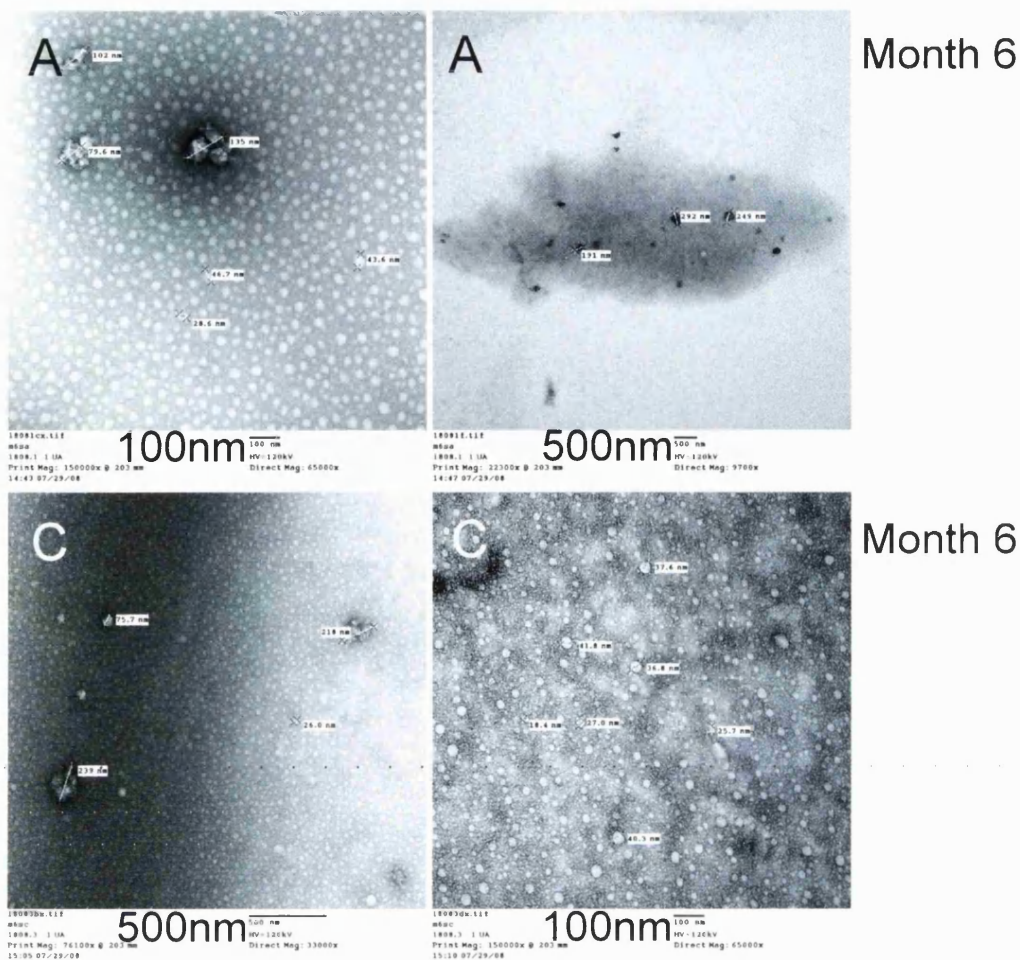


Figure 3.25: Negative stained TEM images of polymeric dispersions of TPLENK to GCPQ (1:2.3w/w) (1 mg mL^{-1}). Letter A-C indicates the triplicates (Dry Stability). GCPQ Palmitoylation: 19.7%, Quaternisation: 6.9% for all three formulations.

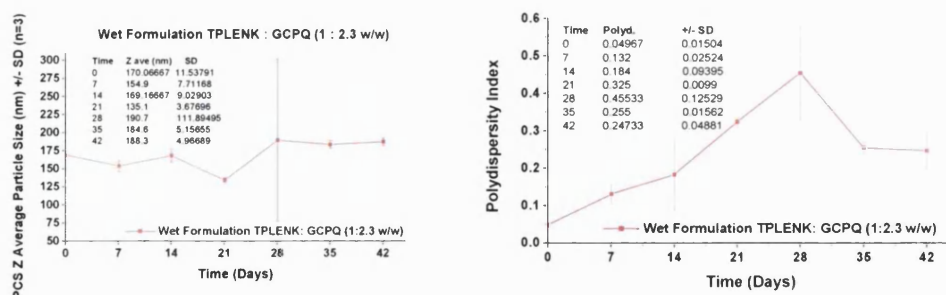


Figure 3.26: Stability of mean PCS particle size (left) and polydispersity index (right) of wet formulations (triplicates) versus time.

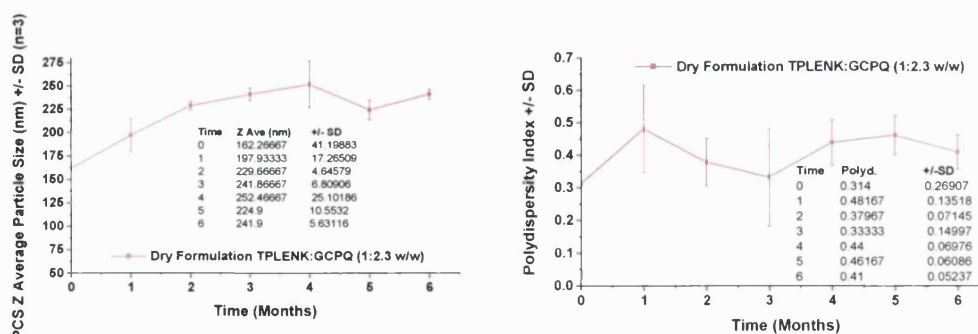


Figure 3.27: Stability of mean PCS particle size (left) and polydispersity index (right) of dry (freeze-dried and reconstituted) formulations (triplicates) versus time.

Table 3.2: Encapsulation efficiency of formulations used for wet & dry stability studies.

Batch	TPLENK (mg mL ⁻¹)	GCPQ (mg mL ⁻¹)	GCPQ P% / Q%	Processing	Storage	E (mg mL ⁻¹)	E %	
A (Wet)	5.97	13.73	18.7	8.3	V & S	2-8 °C	5.38	90.15
B (Wet)	5.85	13.46	18.7	8.3	V & S	2-8 °C	5.38	92.05
C (Wet)	5.79	13.32	18.7	8.3	V & S	2-8 °C	5.11	88.18
A (Dry)	6.93	15.94	19.7	6.9	V, S, FD, R	-20 °C	6.28	90.56
B (Dry)	6.7	15.41	19.7	6.9	V, S, FD, R	-20 °C	5.55	82.87
C (Dry)	6.91	15.9	19.7	6.9	V, S, FD, R	-20 °C	6.23	90.12

Key: TPLENK: Palmitoyl Tyrosyl Leucine Enkephalin, GCPQ: Quaternary Ammonium Glycol Chitosan, P%: Palmitoylation Percentage, Q%: Quaternisation Percentage, V: Vortexing, S: Probe Sonication 15 minutes on ice (50% output), FD: Freeze-Drying for 24 hours, R: Reconstitution with 1mL 0.22µm filtered H₂O, E: Encapsulation, E%: Encapsulation Efficiency

TEM images of the original polymeric dispersions prepared for the wet stability studies illustrate clusters of loaded micelles (30-60 nm) of 300-400 nm (Figure 3.22). The mean particle size was 157 nm with a narrow polydispersity index (± 0.04) as measured by PCS. Same particle size distribution is observed for the samples after two weeks storage in the fridge (2-8°C). However, at 3 and 4 weeks the distribution is wider ranging from under 50 nm to 500 nm, showing the presence of some larger aggregates. At weeks 5 and 6, two population of particles sizes are present with one just under 50 nm till 200 nm and one ranging from 200 nm till 500 nm. Although the mean particle size remained fairly constant (Student's t-test, $p > 0.05$) throughout the stability

experiment (Figure 3.26), the polydispersity of the samples shows an increasing trend and it is statistically different even after 1 week of storage (Student's t-test, $p: 0.014$). Similarly to the wet studies, TEM images of the initial fresh polymeric dispersions prepared for the dry stability studies illustrated clusters of loaded particles of 300-400 nm (Figure 3.25), which remained visible up to 6 months. The initial mean particle size was 193 nm with a narrow polydispersity index (± 0.177) as measured by PCS. The distribution of particle sizes of all freeze-dried samples after reconstitution for the whole duration of the experiment appeared as two populations, one between 30 to 150 nm and larger aggregates of 150 nm to 1 μm (Figure 3.24). The mean particle size and the polydispersity remained constant (Student's t-test, $p > 0.05$) throughout the whole duration of the experiment (Figure 3.27).

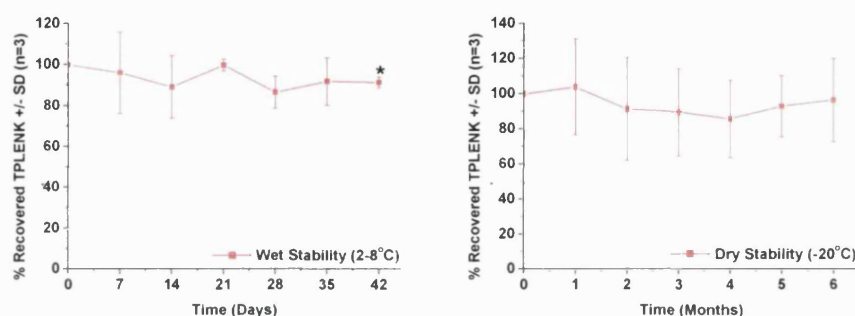


Figure 3.28: Percentage of TPLENK as quantified by RP-HPLC in wet (left) and dry (freeze-dried and reconstituted) (right) stability studies versus time (Mean of triplicates, *: $p < 0.05$, Student's t-test).

The stability of the lipidic peptide in the formulation was assessed using HPLC as well during the wet and dry stability studies (TPLENK calibration curve $y = 20089x + 42156$, $r^2 = 0.9811$). There is no statistical difference in the amount of peptide recovered in all freeze-dried samples after 6 months of storage in -20°C , while the peptide content remained stable up to 5 weeks in the formulation stored in the fridge ($2-8^\circ\text{C}$) with 91% recovered at 6 weeks ($p: 0.04634$, Student's t-test) compared to the original amount of peptide at the onset of the experiment (time 0) (Figure 3.28). The bigger error bars obvious in the dry stability experiments were due to formulation A, that had a consistently a higher level of peptide content, which could be attributed most likely to a dilution error of the stock solution of the formulation before splitting the formulation in separate containers and freeze-drying.

3.3 Discussion-Conclusions

In recent years, chitosan has attracted a lot of attention as a potential bioavailability enhancer for peptide drugs across mucosal epithelia due to its mucoadhesive properties and improvement of peptide transport across epithelial barriers (van der Merwe et al. 2004). Glycol chitosan compared to chitosan polymers possesses better solubility at neutral and basic pH, which in combination with a small molecular weight increases its aqueous solubility and avoids precipitation at physiological pH and slightly basic pH. At higher pH, due to charge loss in neutral and basic environments, chitosan polymers precipitate from solution and exist in a coiled configuration, which renders the polymer unsuitable as an absorption enhancer (Artursson et al. 1994). Quaternisation increases aqueous solubility and at low levels (<12%) was shown not to have an effect on the TEER (Trans Epithelial Electric Resistance) of intestinal epithelial Caco-2 cell monolayers at pH 6.2 and 7.4 (Kotze et al. 1999). Molecular weight and degree of acetylation are important factors for absorption enhancing properties as well as toxicity, with a low degree of acetylation and a low molecular weight being more efficacious (van der Merwe et al. 2004).

GCPQ, a low molecular weight amphiphilic carbohydrate polymer, was successfully synthesised and characterised comprising of repeating GC units (low degree of acetylation <15%) and a controllable number of pendant hydrophobic groups. Soluble polymers bearing pendant hydrophobic groups are able to form intramolecular micelles usually several per molecule and their solubilisation capacity is not lost on dilution making them especially useful as solubisers (Uchegbu et al. 2001).

Synthesis of GCPQ was confirmed using ^1H NMR and COSY-NMR. Palmitoylation levels varied between 10.6 - 26.9 %, while quaternisation levels varied between 5.3 - 14.0 % for different batches quantified by NMR. The hydrophobicity index (HI) can be calculated for the synthesised batches to help rank the polymers, with the more hydrophilic polymers having a higher value. It is calculated by dividing the molar fraction of quaternary ammonium groups / monomer (Q) to the molar fraction of palmitoyl groups / monomer (P) (i.e. $\text{HI} = \text{Q} / \text{P}$). HI varied between 0.33 (Palmitoylation: 22.086%, Quaternisation: 7.281%) to 0.86 (Palmitoylation: 10.635%,

Quaternisation: 9.094%). This index was used as it best estimates the balance between the hydrophilic and hydrophobic modifications of the synthesised carbohydrate amphiphiles (Qu et al. 2006).

Attenuated total reflection FTIR spectroscopy provided evidence for the successful grafting of the degraded GC. Although it was only used for qualitative purposes, ATR-FTIR can also be used quantitatively. The quantitation is based on calibration of Beer's Law by transmission FTIR measurements. If the effect of spectral distortion and penetration depth dependence of radiation wavelength due to ATR sampling is evaluated and corrected for before quantitation experiments, it is possible to identify the percentage of palmitoyl chain grafting by comparing the peak area ratios of two peaks e.g. 2918 or 2850 cm^{-1} to 1067 cm^{-1} [Figure 3.11 (bottom), p.: 169].

GPC-MALLs was used to elucidate the molecular weight of the synthesised polymers. The results obtained correlated with the calculated value based on the initial GC molecular weight and taking into account the percentage of grafting for every batch (Figure 3.17). Measurement of the dn/dc of every sample increased the accuracy of the measurements and the calculation of the absolute molecular weight. GCPQ had a low mean molecular weight of ~ 12400 Da. Low polymer molecular weight has been correlated to a reduced vesicle size, primarily due to an increased solubility in aqueous environments and secondly an increased hydration of the hydrophilic headgroup (GC backbone), that leads to an increased hydrophilic head group area and in turn a decreased vesicle size by increasing the vesicle curvature (Wang et al. 2001).

MALDI-MS was employed in order to provide further verification of the accuracy of molecular weight determinations by GPC. The matrix and conditions used in these experiments (Figure 3.13) were not able to separate adequately the molecular weight distribution of PGC and GCPQ, although it worked relatively well for GC. The advantage of developing a MALDI technique would be the avoidance of the presence of polymer aggregates which cannot be ruled out unless the samples are eluted in the absence of an aqueous environment. Two possible reasons are postulated. Firstly, the wide polydispersity ($M_w/M_n > 1.1$) molecular weight distribution of the grafted polymers versus GC is more likely to account for the ionisation problem (GCPQ molecular weight distribution is wider than that of PGC as observed, Figure 3.13) and

secondly the choice of matrix. Palmitoylation and alkylation with methyl iodide increases the polydispersity of the polymers, an indication that some polymer chains are derivatised to a greater degree than others (Uchegbu et al. 2001; Wang et al. 2001). The possibility of chain cleavage during the strong alkaline conditions of the quaternisation reaction can also be a reason. With MALDI-MS of synthetic polymers, mass discrimination occurs with a widely polydisperse polymer sample such that the high molecular weight components are hard to detect and, as a result the molecular weight distribution is not obtained accurately (Okamoto 2008). Because sample molecules of synthetic polymers are usually less easy to ionise by protonation than those of biopolymers in the MALDI process, the addition of a cationising agent can aid the ionisation in sample preparations (Okamoto 2008). In general, most synthetic polymers having heteroatoms such as polyethers, polyacrylates, polyesters, and polyamides are easy to ionise by the simple addition of sodium or potassium salts (Okamoto 2008) such as sodium iodide (Kawachi et al. 2001). Use of various matrices and dilutions could aid in optimising the conditions. As a last resort, size-exclusion chromatography can separate the sample to monodisperse ($M_w/M_n < 1.1$) fractions that can be analysed using MALDI-MS.

The formulations examined were created via self-assembly of the polymeric amphiphiles in water and entrapment of peptides (Figure 3.18, 3.19, 3.20, 3.21). Based on the results from the encapsulation efficiency, better formulations were obtained after sonication for 15 minutes on ice and filtration with a 0.8 μm low protein binding filter with a ratio of peptide to polymer of 1:5 w/w (Figure 3.21). Particle size of the unfiltered formulations (peptide to polymer ratio of 1:2.3 and 1:5 w/w) were lower than the filter's pore size (0.8 μm) justifying the increase in encapsulation efficiency. However, at high polymer concentration (10 mg mL^{-1}) the particle size increased and the formulation was prone to forming aggregates close to 1 μm in size (Figure 3.21). The rigidity and steric hindrance due to the size of the modified sugar backbone leads to formation of an interchain network that is likely to be responsible for the increase in the hydrodynamic radius of the aggregates. Similarly, increasing the concentration of polymer to 10 mg mL^{-1} also increased the viscosity of the observed samples. Although the 1:2.3 w/w ratio, encapsulated less peptide, it was less viscous, clear, while still able to encapsulate a significant amount of the lipidic peptide, and was considered optimal for intravenous administration. The mean particle size of all formulations with

Leucine^[5]-Enkephalin remained ≤ 200 nm (Figure 3.18). The low encapsulation efficiency for both peptides can be explained due to their exceptional acid-base properties. The pKa values of the carboxylic groups lie in a small range around 2.2, so at a pH above pH 3.5 these groups are entirely in their carboxylate form. All α -amino acids have pKa values near 9.4 and are almost completely in the ammonium ion form below pH 8.0. Thus, in the physiological pH range both the carboxylic acid and amino groups of peptides and proteins are completely ionised, resulting in a zwitterionic molecule, making them more hydrophilic than many other biologically active molecules (Couvreur and Puisieux 1993). Most processes for nanoencapsulation are based on the affinity of the compound for the lipophilic phase of an emulsion or for the polymer. As a result, drug loading is usually less than 10%, especially with the solvent evaporation process (Couvreur and Puisieux 1993). Thus, although the encapsulation efficiency of different formulations varied, in all cases is higher than that achieved with majority of available nanoparticulate formulations and can compete with best published levels for small hydrophilic peptides (Liang et al. 2008; Simone et al. 2009).

Polymeric aqueous dispersions of drug molecules are not normally stable over a long period of time (Tewa-Tagne et al. 2006). Problems encountered include microbiological contamination, non-enzymatic polymer hydrolysis, and physicochemical instability due to particle agglomeration (Tewa-Tagne et al. 2006). The wet formulations were stable for up to 5 weeks in 2-8 °C, as the particle size and peptide content remained statistically not different from initial values, even though the polydispersity of the samples increased significantly after 7 days indicative of aggregation processes (Figures 3.26, 3.28). Polymeric formulations have a tendency to intra- or intermolecularly associate creating bigger aggregates, decreasing the stability of the overall formulation. Stability of aqueous formulations of self-associated peptide drugs is even more problematic. Stability not greater than 7 days at 25°C for peptide loaded phospholipid nanomicelles has been reported. (Lim et al. 2008), precluding their storage before clinical use. Lyophilisation has been proposed as method to prolong shelf-life of peptide loaded nanocarriers (Lim et al. 2008). The freeze-dried formulations (dry stability studies) appeared as a fluffy, porous network with the peptide being dispersed in the polymer matrix. No shrinkage was observed from the sides of the container and the reconstitution with sterile water (pH 6.4) was almost instantaneous providing a

clear, colourless polymeric dispersion before analysis. The freeze-dried formulations remained stable for up to 6 months at least in terms of mean particle size, polydispersity and peptide content (Figures 3.27, 3.28). GCPQ was reported to be able to form a stable non-covalently cross-linked network of chitosan by the grafted palmitoyl groups on the degraded GC backbone similar to a hydrogel (Noble et al. 1999). As ice is sublimated, the polymer retains its architecture created by these non-covalent interactions maintaining the structure of complexes. GCPQ could be acting as a “cryoprotectant”, by hydrogen bonding to the hydrophilic parts of TPLENK (i.e. glycol moieties in GC disaccharide repeating unit, or free amine groups of GC to the C-terminal of the peptide), and by hydrophobic interactions also with the palmitic tail of the amphiphilic peptide.

The freeze-dried formulations were more stable in all three parameters examined i.e. shape of particles, particle size and polydispersity as well as peptide content and thus, would be preferred for long-term stability of the formulation. However, a stability parameter that we have not studied thoroughly is whether there is an increase in the formation of aggregates of the lipidic peptide after freeze-drying in the formulation, although we were not able to detect a statistical difference in size with PCS. Filtration was used to remove unencapsulated peptide or peptide molecules leaking out possibly from ruptured polymeric structures, which is important as they have a higher propensity to self-aggregate in an aqueous environment. However, a limitation of this method is that smaller aggregates than the filter’s cut-off can pass through even if they are not encapsulated. Finally, higher concentrations of peptide or other ratios of peptide to polymer were not studied as well as the effect of adjusting the final pH of the formulation closer to a physiologic pH preferably with a combination of two weak buffers.

In order to summarise, a low molecular weight carbohydrate amphiphilic polymer was synthesised and characterised for the delivery of hydrophilic and amphiphilic peptide molecules. Different ratios of polymer to peptide were explored and characterised and the stability of a selected formulation was studied over time.

Chapter 4

In vitro assays

4.0 Preface

Various strategies have been implemented to promote oral bioavailability of peptides, including supplemental administration of protease inhibitors, use of absorption enhancers, novel formulation strategies, and irreversible or reversible (prodrug) chemical modifications (Oliyai and Stella 1993). Increasing lipophilicity with a prodrug strategy is the most successful application of prodrugs with many prodrugs featuring the addition of a hydrophobic group in order to increase their lipid solubility that usually leads in increase in systemic bioavailability (Wu et al. 2005). Due to the presence of a wide variety of esterases in various body tissues, it is not surprising that esters are the most common prodrugs used to improve gastrointestinal absorption (Wu et al. 2005). By appropriate esterification of molecules containing a carboxylic acid or hydroxyl group, it is possible to obtain derivatives with almost any desirable hydrophilicity, lipophilicity, and *in vivo* lability (Wu et al. 2005). It should be noted that enzymatically catalysed ester hydrolysis is more likely to be influenced by steric than electronic effects and experimental determination to evaluate the rate of cleavage under incubation with plasma or homogenate from the intended tissue or organ where the prodrug would be activated should be performed (Wu et al. 2005). Permeation across the intestinal mucosa of prodrugs will depend on the mechanism and site of conversion and stability of the prodrug in contact with gastrointestinal fluids which can be assessed with stability studies performed under conditions mimicking closely the gut (study duration of at least 1 hour in gastric fluid and 3 hours in intestinal fluid) (FDA 2000).

4.1 Enzymatic Assays

Enzymatic activity assays are composed of several discrete steps of events (Figure 4.1). The first is preparation of both the reaction mixture and the enzyme. The reaction mixture usually contains such components as the buffer used to establish the correct pH, the substrate, and any cofactors such as metals that may be required for catalysis

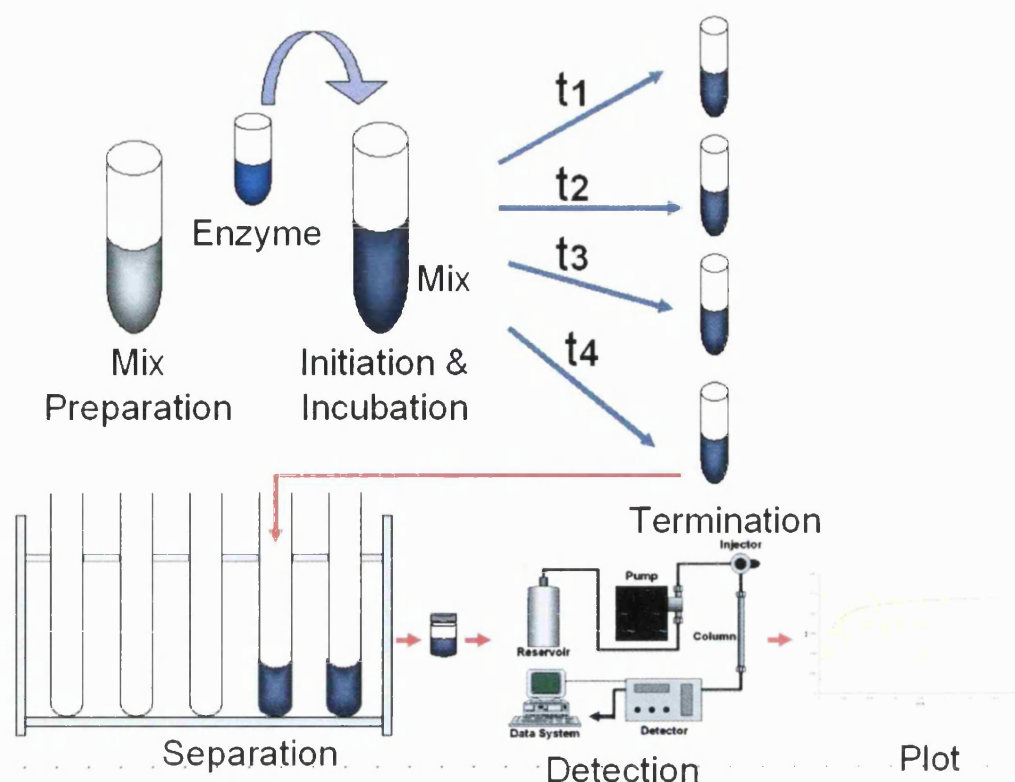


Figure 4.1: Schematic representation of an enzymatic assay to illustrate its several components. The reaction mixture is prepared (Mix Preparation) and the reaction can be started (Initiation) by the addition of the enzyme. During the reaction (Incubation), samples are removed at intervals labeled t_1 , t_2 , t_3 , and t_4 , and the reaction is stopped (Termination) by inactivating the enzyme. The incubation mixture is fractionated (i.e. using a traditional chromatographic column), and the product is isolated from the substrate (Separation). A UV detector and high performance liquid chromatography (HPLC) can be used for the detection. The results finally are plotted to illustrate the reaction kinetics.

(Rossomando 1987). Preparation of the reaction mixtures involves mixing these ingredients in a test tube or, for some assay methods, a cuvette (Rossomando 1987). Incubation of the reaction mixture to the required temperature prior to initiation of the reaction is sometimes required. The enzyme must also be prepared, and characterisation of the protein and enzyme content is required if the biological media used is a mixture in order to adjust the ratio of the enzyme to the peptide/substrate of interest. The second step in the assay is initiation, which involves the addition of the enzyme preparation to the substrate in the reaction mixture or vice versa (Rossomando 1987). This step is considered the start of the reaction ($t = 0$), and all subsequent time points are related to this time. Many reactions require termination, which is the step that brings about the cessation of catalysis and thus stops the reaction (Rossomando 1987). Several ways may

be utilized for termination, all of which usually involve inactivation of the enzyme. Termination is often followed by separation of the components in the reaction mixture by isolating the substrate from the reaction product (Rossomando 1987). The next step is detection, which refers to that process by which the amount of product formed by the enzyme during a specific incubation interval is determined (Rossomando 1987) followed by data analysis and determination of initial rates as well as kinetic constants.

The methods in use for the assay of enzymatic activities may be divided into three groups. These will be referred to as (1) continuous, (2) coupled, and (3) discontinuous methods (Table 4.1) (Rossomando 1987).

Table 4.1: Classification System for Enzymatic Assay Methods (Rossomando 1987)

Assay Method	Characteristics	Example
Continuous	Separation of substrate(s) from product(s) not required	4NP → 4N + Pi
	Samples not taken	colourless → yellow
Coupled	Separation not required for detection	PEP + ADP → pyruvate + ATP
	Samples not taken	pyruvate + NADH → lactate + NAD
Discontinuous	System for separation of substrate(s) from product(s) required for detection	Ab + Ag* + Ag → (Ab - Ag*) + Ag + Ag*
	Samples taken	

Key: 4NP (4-Nitrophenyl), 4N (4-Nitrophenol), Pi: Phosphoric acid, PEP (Phosphoenolpyruvate), ADP (Adenosine diphosphate), ATP (Adenosine triphosphate), NADH (Nicotinamide adenine dinucleotide-reduced form), NAD (Nicotinamide adenine dinucleotide), Ab (antibody), Ag* (Radioactive antigen), Ag (antigen), Ab-Ag* (Radioactive antibody-antigen complex)

Continuous methods do not require a separation step prior to detection. The substrate and product differ in some property such that either one may be measured directly in the incubation solution (Rossomando 1987). An example would be determining the activity of an enzyme catalysing the conversion of 4-nitrophenyl (4NP), a colorless compound, to 4-nitrophenol (4N), which is yellow and has an absorption maximum at 510 nm. Since the substrate does not absorb in this region of the spectrum, the reaction can be carried out directly in a cuvette, and the amount of product formed may be determined continuously by measuring the change in optical density with time at this wavelength. In coupled assay methods, activity is measured indirectly (Rossomando 1987). In this method, two reactions are involved. The first is of the type $A \rightarrow B$ and the second

converts $B \rightarrow C$ and might be referred to as an indicator reaction, not only because it utilises the product of the first reaction (i.e. B) as a substrate, but also because the formation of C may be assayed by a continuous method, that is without a separation step (Rossomando 1987).

Discontinuous methods require separating the products from the substrate in order to measure activity. Normally, the substrate and product are separated, and usually the amount of product formed is measured. Assays utilizing radiochemicals are normally in this group, since radiochemical detectors are unable to differentiate between the radiolabel of the substrate and that of the product.

An HPLC method would be a discontinuous method, since a separation step is part of the procedure. However, because termination can be accomplished by injecting the sample directly onto the column, the HPLC detection is usually carried out continuously with separation, an HPLC method can be considered a continuous method (Rossomando 1987). HPLC offers the potential to monitor multiple reaction components as it can separate with the use of suitable conditions (mobile phase, flow rate, column length, wavelength of detection and temperature) all or almost all reaction compounds providing simultaneously quantitative information for each time point during the course of the reaction. However, it is imperative to be able to adapt the reaction conditions developed for the assay in such a way as to be aligned with the HPLC method. Sufficient volume of the reaction mixture is normally required to allow the withdrawal of multiple samples over a variety of time points, unless dilutions can be made after sampling without comprising the detection efficiency (Rossomando 1987).

Termination of the reaction prior to injection in the HPLC column e.g. by using acids as TFA can reduce the pH of the sample. Since differences between the pH of the sample and the mobile phase can produce discrepancies in chromatographic profiles, the reduction in pH brought about by the termination may cause problems in interpretation (Rossomando 1987), unless a buffer with capacity to maintain the required chromatographic pH is used. Termination increases the possibility of producing a precipitate, which will have to be removed before sample can be injected into the column, to prevent clogging the column. Terminating the reaction by freezing (-20°C)

and thawing or by addition of HPLC mobile phase can be useful alternatives if they are suitable to achieve enzyme catalysis termination.

4.2 Esterases

Conversion to the parent drug at the target site is critical for the prodrug approach to be successful. The most important esterases that catalyse hydrolyses of prodrugs include carboxylesterase, acetylcholinesterase, butyrylcholinesterase, paraoxonase, and arylesterase (Table 4.2). One problem with ester prodrugs is the difficulty in predicting their rates of bioconversion and, thus, their pharmacological or toxicological effects, which can make difficult any prediction of the prodrugs bioconversion in humans based on animal data (Liederer and Borchardt 2005). Apart from species differences, gender, disease and age differences can affect bioconversion rates leading to wide bioavailabilities and varied toxicity profiles (Liederer and Borchardt 2006).

Table 4.2: Major Enzymes Involved in Bioconversion of Ester-Based Prodrugs (Liederer and Borchardt 2006)

Type	EC Number	Localisation
Hydrolytic Enzymes		
Esterases A		
Paraoxonase	3.1.8.1	Plasma, liver, brain, kidney, lung
Esterases B		
Carboxylesterase	3.1.1.1	Blood, liver, brain, kidney, lung, muscle, intestine, stomach, skin, heart, breast, ovary, cervix, testis, bladder, saliva, pancreas, thyroid, nasal/ respiratory/ adipose tissue, placenta, thymus, tumor
Acetylcholinesterase	3.1.1.7	Plasma, liver, brain, muscle, nerve, kidney, intestine, retina, placenta, thymus
Cholinesterase	3.1.1.8	Plasma, liver, brain, muscle, kidney, intestine, retina, placenta
Oxidative Enzymes		
Cytochrome P450s		Liver, brain, kidney, lung, intestine, adrenal, testis, skin, spleen, placenta, olfactory mucosa, ocular tissue, tumor

The International Union of Biochemistry and Molecular Biology (NC-IUBMB 2008) divides enzymes into six main categories according to the reactions they catalyse, with most enzymes involved in prodrug bioconversion belonging to class 3 (Hydrolases) such as Carboxylesterases (Enzyme Commission number EC 3.1.1.1) (Table 4.2) ((NC-IUBMB) 2008). The subsequent numbers identify the specific reactions being catalysed (e.g. 3.1 indicated hydrolysis of ester bonds, whereas 3.1.1 indicates hydrolysis of carboxylic ester bonds) (Liederer and Borchardt 2006; (NC-IUBMB) 2008). However, as esterases have an extremely wide and overlapping substrate specificities and are not limited only to the catalytic reaction of one substrate, making it difficult to classify accurately different enzymes (Liederer and Borchardt 2006).

A more general classification system arranged esterases into 3 groups (A, B and C esterases) based on substrate specificity (Aldrige 1952; Bergmann et al. 1957). Type A esterases (e.g. paraoxonase) are not inhibited by organophosphates such as paraoxon and diisopropyl phosphorofluoridate, but hydrolyse them (Liederer and Borchardt 2006). Similarly, type C esterases (e.g. acetylcholinesterase) are also not inhibited by organophosphates, while type B esterases (e.g. carboxylesterases) are inhibited by organophosphates.

Paraoxonase (PON) (EC 3.1.8.1) is one of the most important esterase A group of enzymes. The three members of this family PON1, PON2, and PON3 catalyse the hydrolysis of a broad spectrum of compounds such as the aromatic carboxylic acid esters, organophosphates (only PON1), organophosphinates, lactones, and cyclic carbonates (La Du 1992). Tawfik et al. postulate based on their recent elucidation of the structure of a variant of PON1 that the catalytic site is composed of a calcium ion, a phosphate ion, and a His-His dyad (Harel et al. 2004; Liederer and Borchardt 2006). When activated by His₁₁₅, His₁₃₅ deprotonates a water molecule, leading to the formation of a hydroxide anion that attacks the carbonyl atom of the substrate (Liederer and Borchardt 2006). The generated oxyanionic tetrahedral intermediate stabilised by the positively charged calcium atom then breaks down, regenerating the active enzyme and releasing the product (Liederer and Borchardt 2006). However, the exact mechanism of catalysis is not fully elucidated yet. Human PON1 appears to be localized predominantly in blood where it is associated with high-density lipoprotein (HDL) and the microsomal fraction of the liver (Liederer and Borchardt 2006). In contrast to

mammalian PON1, human PON1 has not been detected in various other tissues (e.g. brain, lung, kidney, heart etc.) (Liederer and Borchardt 2006). PON3 is found primarily in the liver, but is also present in serum. PON2 appears to be widely distributed and expressed in many tissues but not in plasma (Liederer and Borchardt 2006). Inactivation of esterases A can be elicited by EDTA (ethylenediaminetetraacetic acid), metals (e.g., Cu, Ba), and mercurial compounds [e.g. phenyl mercuric acetate, para-chloromercuribenzoate] (Gonzalvo et al. 1997).

Esterases B such as carboxylesterase, acetylcholinesterase, and butylcholinesterase act as an effective biological barrier to limit the distribution of substrates that might be toxic and facilitate their elimination by turning them into more polar molecules (Sato and Hosokawa 1998; Sogorb and Vilanova 2002). They are referred to as serine esterases, since serine is essential to their catalytic activity and their mechanism of action is analogous to serine proteases such as chymotrypsin (Liederer and Borchardt 2006). Thus, although these enzymes have remarkable substrate specificities, they share a catalytic triad consisting of three hydrogen bond-connected amino acid residues (Ser₂₀₃, Glu₃₃₅, and His₄₄₈) (Liederer and Borchardt 2006). In a first step (Figure 4.2), the nucleophilic serine oxygen activated by the histidine residue, which in turn is stabilized by the glutamate residue, attacks the carbonyl carbon of the substrate, leading to the formation of an acyl-enzyme intermediate (Liederer and Borchardt 2006). Then, water activated in the same manner as Ser by His and Glu (general base catalysis) in the previous step then attacks the carbonyl atoms of the substrate again (Liederer and Borchardt 2006). Cleavage of the ester bond generates the final product (e.g. acid, alcohol, etc.) and regenerates the enzyme. Unlike esterases A, esterases B do not require a cofactor such as inorganic ions and are inhibited by organophosphates (e.g., paraoxon) due to irreversible covalent bond formation (Liederer and Borchardt 2006).

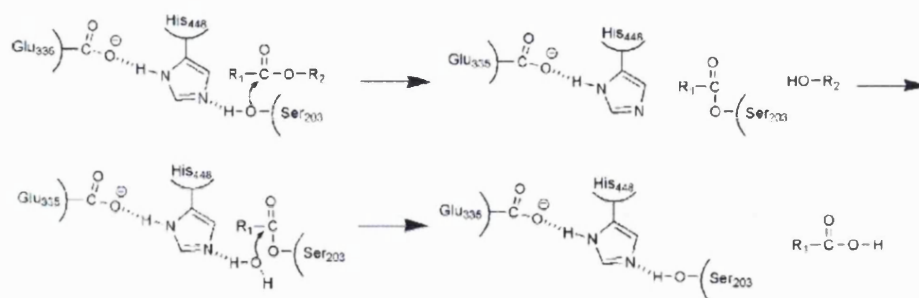


Figure 4.2: Mechanism for the bioconversion of esters by esterases B.

Carboxylesterases (EC 3.1.1.1) are ~60 kDa glycoproteins important for the metabolism of drugs and endogenous compounds as palmitoyl-CoA and have been successfully employed for the activation of many ester and amide prodrugs (Liederer and Borchardt 2006). Carboxylesterases have wide and overlapping substrate specificities with carboxylic acid esters as thioesters to be known substrates, while they show arylesterase, acetylerase, amidase, and lipase activity and are involved in transesterification (Bourland et al. 1997; White and White 1997; Liederer and Borchardt 2006). It is postulated that they possess a large and flexible binding pocket that facilitates the formation of multiple binding interactions (predominantly hydrophobic, van der Waals, and hydrogen bonding) allowing for wide substrate specificities (Bencharit et al. 2003). Although carboxylesterases show differing activity and substrate specificity, depending on species and location, they are present virtually throughout the body (e.g. intestine, blood, brain, skin, tumor, etc.) with their highest activity in the liver (Liederer and Borchardt 2006). Species differences need to be appreciated as for example carboxylesterases are part of the human BBB but not the rat's BBB, which can play a role in limiting cell membrane permeation of drug molecules (Liederer and Borchardt 2006).

Acetylerase (EC 3.1.1.7) (~80 kDa, glycoprotein) is one of the fastest enzymes known, and the hydrolysis of its characteristic substrate acetylcholine approaches the maximum possible rate, the diffusion-controlled limit (Quinn 1987). It attacks certain esters, amides, and anilides and has been shown to be involved in activation of prodrugs (Liederer and Borchardt 2006). It is more specific than carboxylesterase, which could be at least partly attributed to a smaller catalytic gorge which allows limited interaction of the bound substrate with only two aromatic residues of the acetylerase compared to the multiple interactions with several hydrophobic residues of carboxylesterase (Bencharit et al. 2003; Liederer and Borchardt 2006). It is mainly located in brain and blood or at neuromuscular junctions (Bencharit et al. 2003).

Most types of esterases can be found in the blood, liver, intestine, and many other biological fluids and tissues of various animal species including human (Table 4.2) (Liederer and Borchardt 2006). Their major subcellular location is in microsomes, cytosol, and lysosomes. Independent of animal species, the liver generally has the highest enzyme activity and is the organ chiefly responsible for drug metabolism and

prodrug activation (Liederer and Borchardt 2006). Species differences need to be taken into account carefully, if ester prodrugs activated exclusively at the target site is the aim. For example, the human brain appears to have 30 types of carboxylesterases, but the human liver only 5 (Liederer and Borchardt 2005; Liederer and Borchardt 2006). The rat liver possesses 19 forms of carboxylesterases of which only 1 could be detected in kidney, lung or adipose tissue (Liederer and Borchardt 2005; Liederer and Borchardt 2006). For most drugs, different animal species show different *in vitro* and *in vivo* enzymatic stability profiles. Furthermore, many examples have shown very rapid bioconversion rates for drugs in rodents such as rats, which can lead to an underestimation of the stability of the drug and wrongly discourage further development.

The aim of this *in vitro* studies is to assess the stability of Leucine^[5]-Enkephalin as well as the lipophilic prodrug, TPLENK, in the presence or absence of GCPQ in simulated gastric and intestinal fluid as an indicator of the amounts of peptides available for transport across the gastrointestinal mucosa. Furthermore, *ex vivo* stability studies were conducted in the presence of the most relevant biological media for oral brain delivery of the prodrug, while assessing the bioconversion of TPLENK to the parent peptide Leucine^[5]-Enkephalin.

4.3 Materials and Methods:

4.3.1 Materials

Table 4.3: Materials for *in vitro* stability experiments

Chemical Name	Name	Purity	Company
Acetonitrile HPLC grade	ACN	≥99.99%	Fischer Scientific
Acetic Acid	AcOH		VWR International
Albumin, Bovine Serum Fraction V, Low Heavy Metals (<0.5ppm)		98%	Calbiochem
Bradford Reagent			Sigma
Deuterium Oxide 99.9 atom %D	D ₂ O	99.90%	Goss Scientific Instruments Ltd.

Chemical Name	Name	Purity	Company
Diethyl p-nitrophenyl phosphate (ampule of 100mg)	Paraoxon		Supelco
Dimethylsulphoxide CHROMASOLV Plus, HPLC grade	DMSO	≥99.7 %	Riedel- de-Haën
Guanidine hydrochloride solution (~8M in water), BioChemika			Fluka Chemika
Hank's Balanced Salt Solution (Sterile filtered, Endotoxin tested), With Sodium bicarbonate, without phenol red, calcium chloride and magnesium sulphate) (pH 7.4)	HBSS		Sigma
Hydrochloric Acid	HCL	36.5-38%	VWR International
Ortho-Phosphoric Acid puriss. p.a. for HPLC 85-90%		85-90%	Fluka Chemika
p-Nitrophenyl Butyrate, BioChemika	PNPB	≥98.0%	Fluka Chemika
Paraoxon [O,O-Diethyl O-(4-nitrophenyl) phosphate]	Par		Supelco
Sodium Acetate trihydrate ACS reagent		99+%	Sigma-Aldrich
Sodium Carbonate	Na ₂ CO ₃	≥99.0%	Sigma-Aldrich
Sodium Dihydrogen Phosphate Monohydrate		99.5%	Fluka Chemika
Sodium Phosphate dibasic heptahydrate ACS reagent		99%	Riedel-de Häen
Trifluoroacetic acid, for biochemistry	TFA	99.5%	Acros Organics
Vacutainer (glass) NH 85 I.U. 5ml 13x75mm (Heparin)			BD
Water Deionised	H ₂ O		Millipore Elix – Progaard 2
Water Double Deionised	H ₂ O	<18 μΩ.cm	Millipore Synergy-Simpak 1

4.3.2 *In vitro* stability in Simulated Gastric Fluid

The simulated gastric fluid (SGF) was prepared according to the British Pharmacopoeia 2007 (Volume IV, Appendix 1A, page A61)(BP) 2007). It consisted of sodium chloride and diluted hydrochloric acid (1M) and was prepared by adding NaCl (2g) and HCL (80mL, 1M) and made up with double de-ionised water to 1000mL (pH 1.2). 3.6 mM (2 mg mL⁻¹, 80μL) Leucine^[5]-Enkephalin or 15.1 mM (12 mg mL⁻¹, 80μL) of TPLENK

were suspended to a total of 1.3mL of pre-incubated SGF at 37°C for 15 minutes. The mixtures were maintained at $37 \pm 0.1^\circ\text{C}$ and agitated at 130 cycles per minute (Grant OLS 200 water shaking bath, Cambridge Ltd, Herts, UK). Peptides were incubated in the presence and absence of GCPQ (1:5 w/w) in SGF for a maximum of 3 hours. Peptides (1 mg for LENK and 6mg for TPLENK) and polymer (5 mg for LENK or 30 mg for TPLENK formulations) were mixed with 0.5 mL of double de-ionised water, vortexed (WhirliMixer, Fisherbrand) and probe sonicated (MSE Soniprep 150) with the instrument set at 50% of its maximum output for 7 minutes on ice and were left to settle in the fridge for 3 hours after which they were left to come to room temperature and then incubated with SGF. 3.6 mM (2 mg mL^{-1} , 80 μL) Leucine^[5]-Enkephalin or 15.1 mM (12 mg mL^{-1} , 80 μL) of TPLENK were suspended to a total of 1.3mL of pre-incubated mixture at 37°C for 15 minutes of SGF with sodium carbonate (Na_2CO_3) (ratio 1: 0.65 v/v) to account for the time where no digestion took place (time: 0). Aliquots from the SGF, peptide with or without polymer reaction mixture (100 μL) were removed at specific time points and Na_2CO_3 (65 μL , 0.1M, pH 11) was added followed by the addition of HPLC mobile phase (35 μL) to increase the pH to above 8. Samples of reaction aliquots in mobile phase / Na_2CO_3 (20 μL) were then quantified by HPLC. Samples were analysed using an HPLC system equipped with a Waters TM 515 HPLC pump connected to a Water TM 717 plus Autosampler with a Waters TM 486 Tunable Absorbance Detector. A Waters OD₂ Spherisorb column (C18, 4.6 x 250 mm, 5 μm , Waters, UK) was used maintained at 30°C with a Jones Chromatography Column Heater model 7971. The mobile phase consisted of acetonitrile / 200 mM Phosphate Buffer (Monosodium Phosphate Monohydrate and Disodium Phosphate Heptahydrate, pH 8) (18/82 v/v) with a final pH of 8. Unless otherwise indicated, samples were detected at 214nm. The flow rate was set at 1 mL min^{-1} at 30°C for analytical runs and the injection volume at 20 μL . The retention time was 3.1 min for Leucine^[5]-Enkephalin and 4.7 for TPLENK and the lowest detection limit is $1 \mu\text{g mL}^{-1}$ and $10 \mu\text{g mL}^{-1}$ respectively. Empower software I was utilised for obtaining the results. Each set of experiments was conducted in triplicate.

4.3.3 *In vitro* stability in Simulated Intestinal Fluid

The protocol for studying peptide stability in intestinal fluid was adapted with modifications from a published report (Cheng et al. 2006). Male Wistar rats (n=3) weighing ~250g [Specialist Services Unit, Pharmacology Department, School of Pharmacy, University of London, London, U.K., or Harlan (Oxon, U.K.)] were fasted for 24 hours before they were euthanised. An abdominal incision was made to expose the intestine, and 30-40 cm of small intestine, starting from the duodenum, was excised from each rat. The lumen of each intestinal segment was immediately flushed with 7.5 - 9.0 mL of ice-cold PBS buffer (50mM, pH 6.6). The washings from all the intestinal segments were pooled, centrifuged at 4,000 rpm for 30 minutes (Hemle Z323 centrifuge, Hemle Laborteschnik GmbH, VWR, U.K.) and the supernatant stored in -20°C until it was used. The protein content was determined using the Bradford assay with bovine serum albumin (BSA) as a standard (BSA calibration graph in the linear range 0.1 – 1.4 µg/ml at λ_{max} : 595nm using a UV1650, Shimadzu, Buckinghamshire, UK). The degradation experiments were initiated by incubating Leucine^[5]- Enkephalin or TPLENK (10 mM) with intestinal fluids at a final intestinal protein concentration of ~46 µg mL⁻¹ in the absence or presence of GCPQ (ratio of peptide to polymer 1:5 w/w). Peptides (8.33 mg for LENK and 12.05 mg for TPLENK) and polymer (41.65 mg for LENK or 60.25 mg for TPLENK formulations) were mixed with 1.48 mL of PBS buffer (50mM, pH 6.6), vortexed (WhirliMixer, Fisherbrand) and probe sonicated (MSE Soniprep 150) with the instrument set at 50% of its maximum output for 7 minutes on ice and were left to settle in the fridge for 3 hours after which they were left to come to room temperature and then incubated with the intestinal washings (20 µL). The mixtures were shaken at 135 cycles per minute in a water bath at 37°C (\pm 0.1°C, Grant OLS 200, UK). At specific time points, aliquots (150µL) of the incubation mixture were withdrawn and the enzyme reaction was quenched by adding 10µL of acetic acid. The amount of peptide was quantified by HPLC. Samples were analysed using an HPLC system equipped with a Waters TM 515 HPLC pump connected to a Water TM 717 plus Autosampler with a Waters TM 486 Tunable Absorbance Detector. Two reverse phase Cromolith (Merck KGaA, Germany) columns (C18, 4.6 x 100 mm, total length: 260mm) were used maintained at 30°C with a Jones Chromatography Column Heater model 7971. The mobile phase consisted of acetonitrile / water /dilute (1/1000 v/v, pH 2) aqueous trifluoroacetic acid solution (180/819.5/0.5 v/v) with a final pH of 5.8.

Unless otherwise indicated, samples were detected at 214nm. Flow rate was set at 1mL min⁻¹ at 30°C for analytical runs and the injection volume at 40μL. The retention time was 5.4 min for Leucine^[5]-Enkephalin and 5.9 for TPLENK and the lowest detection limit is 1μg mL⁻¹ and 10μg mL⁻¹ respectively. Empower software I was utilised for obtaining the results. Each set of experiments was conducted in triplicate.

4.3.4 *In vitro* stability in Plasma and Liver Homogenate

4.3.4.1 Biological Media

Rat blood was obtained from male Wistar rats (n = 3) [Specialist Services Unit, Pharmacology Department, School of Pharmacy, University of London, London, U.K., or Harlan (Oxon, U.K.)]. Fresh blood was centrifuged immediately at 3000 rpm and 4°C for 15 min using a Hermle Z323K centrifuge (Hemle Z323 centrifuge, Hemle Laborteschnik GmbH, VWR, U.K.). Aliquots (approximately 0.5-2mL) of the separated rat plasma were frozen and kept at -80°C until used for stability studies. All samples were stabilized with heparin. Before each stability experiment, the plasma was quickly thawed and diluted to 90% (v/v) with HBSS, pH 7.4, to maintain the pH of the solution during the experiment. Rat livers and brains were obtained from male Wistar rats (n = 3) [Specialist Services Unit, Pharmacology Department, School of Pharmacy, University of London, London, U.K., or Harlan (Oxon, U.K.)]. The tissues were blotted to dryness, weighed, sliced into small pieces, and homogenized on ice with ice-cold HBBS (1mL/g of tissue) using a 3mL glass homogenizer (15 strokes, Jencons-PLS, England). Aliquots (approximately 1.5mL) of the homogenates were frozen and kept at -80°C until used. Prior to using these samples for experiments, the homogenates were quickly thawed and re-homogenised on ice with an equal volume of ice-cold HBSS. Cell debris and nuclei were removed by centrifugation (MSE, MicroCentaur, U.K.) for 10 minutes at 10,000 rpm. The supernatants were used for activity and stability studies.

4.3.4.2 *In vitro* Esterase Activity Studies

The total esterase activity (n = 3) in biological media was assessed at pH 7.4 and 25°C using p-nitrophenyl butyrate (PNPB) as a substrate (Liederer and Borchardt 2005).

Esterase activities were expressed as units per milligram of protein. One unit represents the amount of enzyme that catalyses the formation of 1 μ mol *p*-nitrophenol per minute in HBSS, pH = 7.4 at 25°C (Ouyang et al. 2002). *p*-Nitrophenol, the final product of this enzymatic reaction, was quantified spectrophotometrically at $\lambda = 420$ nm using a Shimadzu UV – 1650PC UV-Vis double-beam spectrophotometer (Shimadzu, UK). Conditions of linearity for the enzymatic hydrolysis of PNPB were maintained for 300s between 0.02-2 U/ml (Ouyang et al. 2002). To determine the amount of esterase B versus esterases A/C in various biological media, the total esterase activity ($n = 3$) was assessed in the presence and absence of paraoxon. Since paraoxon inhibits only the enzymatic hydrolysis of PNPB by esterase B, the remaining esterase activity can be attributed to esterases A and/or C (Liederer and Borchardt 2005).

Briefly, 5 μ L of diluted biological samples were added to a 4mL cuvette containing 30 μ L of PNPB (100mM in DMSO) and 2.965 mL of HBSS (pH 7.4) with a blank control containing 5 μ L of HBSS, 30 μ L of PNPB (100mM in DMSO) and 2.965 mL of HBSS (pH 7.4) and the difference in absorbance at 420 nm was measured using the UV Probe software Kinetics mode over 5 minutes. Reaction mixtures were mixed by cuvette inversion. Measurements were performed in triplicates and the mean was used for calculation of esterase activities. When measurements were performed in the presence of paraoxon to quantify the amount of A/C esterases, 5 μ L of diluted biological samples were added to a 4mL cuvette containing 3 μ L of 1mM of paraoxon, 30 μ L of PNPB (100mM in DMSO) and 2.962 mL of HBSS (pH 7.4) with a blank control containing 5 μ L of HBSS, 3 μ L of 1mM of paraoxon, 30 μ L of PNPB (100mM in DMSO) and 2.962 mL of HBSS (pH 7.4) and the difference in absorbance at 420 nm was measured using the UV Probe software Kinetics mode over 5 minutes. Reaction mixtures were mixed by cuvette inversion. Measurements were performed in triplicates and the mean was used for calculation of esterase activities.

The total protein concentration ($n = 3$) in the biological media was determined using the Bradford protein assay with bovine serum albumin (BSA) as a standard. The Bradford assay is based on the observation that the absorbance maximum for an acidic solution of Coomassie Brilliant Blue G-250 shifts from 465nm to 595nm when binding to protein occurs. Both hydrophobic and ionic interactions stabilise the anionic form of the dye, causing a visible color change. For peptide / protein samples of unknown

concentrations, it is necessary to prepare a calibration graph of known BSA concentration of 0.1 to 1.4 mg mL⁻¹ (linear range for Bradford reagent according to supplier) and ensure the concentration of the unknown samples falls within this range. To construct the calibration curve, a total of 100µL of standard in D₂O was added to 3mls of Bradford reagent and incubated at room temperature for 5 minutes before absorbance measurements at λ = 595 nm. Biological samples of 10µl was further diluted further with 90µl of D₂O and 3mls of Bradford reagent were added and incubated at room temperature for 5 minutes before absorbance measurements at λ = 595 nm using a Shimadzu UV – 1650PC UV-Vis double-beam spectrophotometer.

For the calculations the following equations were used:

Equation (4.1):

$$\text{Units / mL Enzyme} = \frac{(\Delta A_{420\text{nm}} / 5 \text{ minutes Test} - \Delta A_{420\text{nm}} / 5 \text{ minutes Blank}) \times 3 \times \text{df}}{14.775 \times 0.1}$$

where:

ΔA_{420nm} : is the absorbance difference at 420 nm for the test sample or blank used

5 minutes: the duration of the assay

3: the total volume (in millilitres) of assay

df: dilution factor

14.775: Millimolar extinction coefficient of p-nitrophenol sodium salt at 400 at pH 7.25 (Quinn et al. 1982)

0.1: volume (in millilitre) of enzyme used

The esterase specific activities were calculated as follows:

Equation (4.2):

$$\text{Esterase Specific Activity} = \frac{\text{Total Esterase Activity [Units / mL Enzyme]}}{\text{Protein Concentration [mg Protein / mL Enzyme]}}$$

[Units/mg Protein]

The esterase specific activities were expressed as units per milligram of protein, where one unit (U) represents the amount of enzyme that catalyses the formation of 1µmol p-nitrophenol per min in HBSS, pH 7.4, at 25°C.

4.3.4.3 *In vitro* Prodrug Stability Studies

The enzymatic stabilities of TPLENK were determined in triplicate in various rat biological media [(plasma (diluted to 90% with HBSS), liver and brain homogenates (diluted to 50% with HBSS) in the absence of paraoxon. TPLENK was incubated at a final concentration of 750 μ M (0.6 mg TPLENK in 0.99 mL of diluted biological samples) with the respective biological matrix containing 1 % DMSO (10 μ L). The samples were maintained at 37 °C for at least two half-lives in a temperature-controlled shaking water bath (60 rpm). At various time intervals, aliquots of 100 μ L were removed. The enzyme activity of these samples was immediately quenched by adding an ice-cold, freshly prepared 6N guanidium hydrochloride solution in acidified HBSS containing 0.01% (v/v) ortho-phosphoric acid, and then keeping the samples at -80°C until further use. Prior to high performance liquid chromatography (HPLC) analysis, the samples were thawed at room temperature and centrifuged at 3000 rpm for approximately 20 minutes at 4 °C.

.....

4.3.4.4 Analytical Methods

For *in vitro* stability studies the disappearance of TPLENK in biological media was monitored by reversed phase high-performance liquid chromatography (RP-HPLC) utilising a Waters isocratic system consisting of Waters TM 515 HPLC pump connected to a Water TM 717 plus Autosampler with a Waters TM 486 Tunable Absorbance Detector. Two Merck KGaA 100mm x 4.6mm columns were used joined together via a linker (total length 250mm) for the plasma and liver homogenate studies or a reversed phase Waters Sunfire C18 column (5 μ m, 4.6mm X 250mm) with a guard column attached [Waters Sunfire C18 (5 μ m, 4.6mm X 10mm) for the brain homogenate studies and the samples were eluted using a mobile phase that consisted of 82% 50mM Acetate Buffer (pH 5.6): 18% Acetonitrile to give a final pH of mobile phase of 5.9 (\pm 0.05) at 32 °C (controlled using a Model 7971 Column Heater by Jones Chromatography). Samples were detected at 280 nm with a flow rate of 1ml min⁻¹ and an injection volume of 40 μ L out of a total 180 μ L sample. The retention time was 4.5 min for Leucine^[5]-Enkephalin and 5.6 for TPLENK for the plasma and liver homogenate studies while the retention time was 7.9 for Leucine^[5]-Enkephalin and 8.9 for TPLENK for the brain

homogenate studies. The lowest detection limit is $1\mu\text{g mL}^{-1}$ and $10\mu\text{g mL}^{-1}$ respectively. Empower software I was utilised for obtaining the results. Each set of experiments was conducted in triplicate.

4.3.5 Statistical Analysis

All results were expressed as mean \pm standard deviation (SD). The Student's t-test (Microsoft Excel) was used to assess any statistically difference among the means of % peptide remaining of the same group at different time points compared to time 0 or when only two arms of a study were compared. A p-value less than 0.05 was considered as a representation of significant difference. If more than 2 groups were compared in a stability study, a one-way ANOVA test using Minitab 16 was done to assess any statistically difference among the means of % peptide remaining for the different arms of the study. A post-hoc analysis (Tukey's Test) was performed to determine the groups, which show significant difference. In each case, a p-value less than 0.05 was considered as a representation of significant difference. Plasma and liver half-life calculations were performed by assuming exponential decay in Origin 6.

4.4 Results

4.4.1 *In vitro* stability in Simulated Gastric Fluid

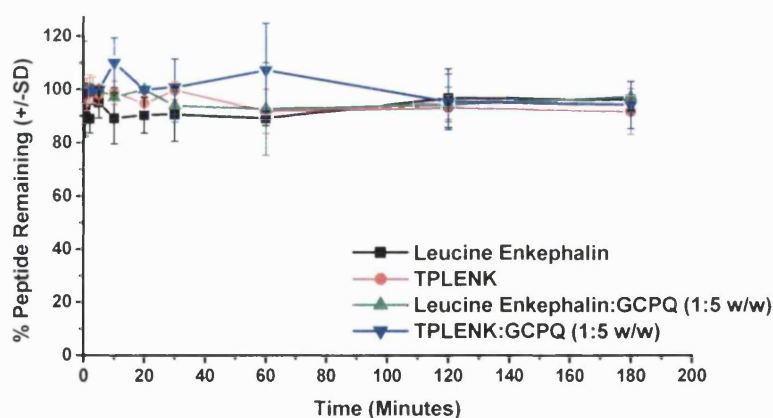


Figure 4.3: Stability of peptides in the presence of SGF with or without GCPQ. No statistically significant differences were observed ($p > 0.05$).

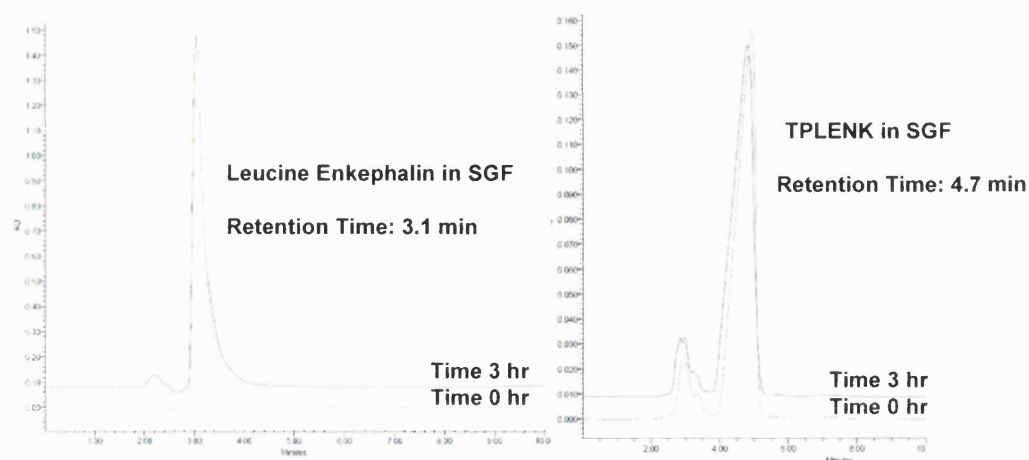


Figure 4.4: HPLC chromatograms of peptides in the presence of SGF with GCPQ.

Leucine¹⁵¹-Enkephalin calibration curve was $y = 2 \times 10^7 X + 10^6$ ($r^2 = 0.9953$) and $y = 6 \times 10^7 X + 8 \times 10^6$ ($r^2 = 0.9517$) for TPLENK, where y is the area under the curve (AUC) and X is the concentration in $\mu\text{g mL}^{-1}$. Both peptides are stable for up to 3 hours in SGF in the absence of pepsin (acidic pH) with the presence or absence of GCPQ with at least 92% of the peptides remaining at all times (Table 4.4, Figure 4.3). No statistical significant differences were detected ($p > 0.05$) for all time points within the four different groups.

Table 4.4: Stability of peptides in the presence of SGF

Time (Minutes)	Leucine Enkephalin (L) %	SD L	TPLENK %	SD TPLENK	Leucine Enkephalin : GCPQ (LG) %	SD LG	TPLENK : GCPQ (PG)	SD PG
0	100.0	18.1	100.0	4.6	100.0	0.1	100.0	0.2
0.5	91.7	9.2	98.1	2.7	94.1	5.7	--	--
1	--	--	98.2	6.3	--	--	--	--
2	89.0	5.3	100.8	5.1	96.1	7.0	--	--
3	--	--	99.9	5.1	--	--	--	--
5	95.0	5.7	98.2	4.0	97.2	1.0	--	--
10	89.1	9.5	99.1	4.4	95.7	7.8	110.2	9.3
20	90.3	6.7	94.9	2.9	--	--	--	--
30	90.6	10.1	99.9	3.4	94.0	6.3	100.9	10.7
60	89.1	2.7	92.1	8.3	92.8	17.4	107.4	17.7
120	96.7	11.0	93.3	4.3	94.4	6.5	95.4	10.4
180	96.2	4.2	91.9	8.6	97.2	5.7	94.2	8.9

Key; --: Sample was not analysed for this time point, SD: Standard Deviation of mean of triplicates

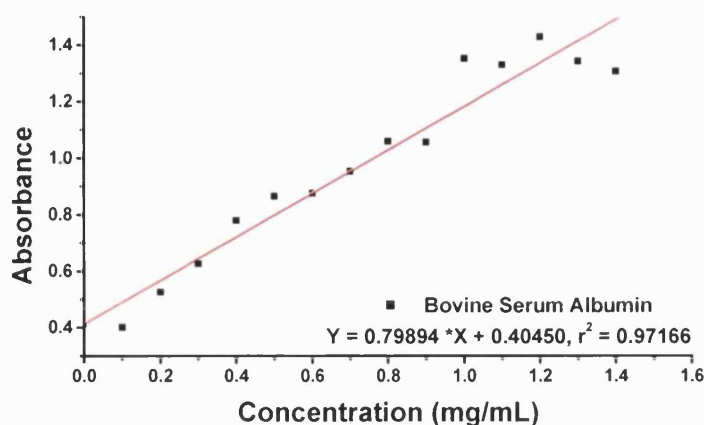
4.4.2 *In vitro* stability in Simulated Intestinal Fluid

Figure 4.5: Bradford assay BSA calibration graph for quantifying the protein content in intestinal wash studies.

The protein content ($\sim 0.775 \text{ mg mL}^{-1}$) of the intestinal wash was determined using the Bradford assay with bovine serum albumin (BSA) as a standard (BSA calibration graph in the linear range (λ_{max} : 595nm, 0.1 – 1.4 $\mu\text{g/mL}$: $Y = 0.79894 X_1 + 0.40450$, $r^2 = 0.97166$, where Y is the absorbance and X_1 is the protein concentration in mg mL^{-1} , Figure 4.4). Leucine^[51]-Enkephalin calibration curve was $y = 3 \times 10^7 X + 3 \times 10^6$ ($r^2 = 0.9954$) and $y = 2 \times 10^6 X + 189393$ ($r^2 = 0.9922$) for TPLENK where y is the area under the curve (AUC) and X is the concentration in $\mu\text{g mL}^{-1}$. Stability of the lipidic prodrug TPLENK as well as Leucine^[51]-Enkephalin in rat intestinal wash was greatly enhanced by the addition of GCPQ with $66.46 \pm 0.89\%$ of TPLENK and $84.49 \pm 0.76\%$ of Leucine^[51]-Enkephalin recovered after 4 hours in the presence of GCPQ compared to $17.77 \pm 0.66\%$ and $54.11 \pm 1.71\%$ respectively in the absence of GCPQ. In the presence of GCPQ statistical significant (Student t-test, $p < 0.05$) changes in the mean % of peptides remaining was observed after 4 hours of incubation of the peptide formulations in intestinal wash, while in the polymer absence statistical significant changes were obvious after 15 minutes and 30 minutes of incubation of TPLENK and Leucine^[51]-Enkephalin in the intestinal washings. Addition of GCPQ increased the half-life -if a first order exponential decay is hypothesized, by 1.5-fold and 2.5 fold for the parent peptide and pro-drug respectively (Table 4.6).

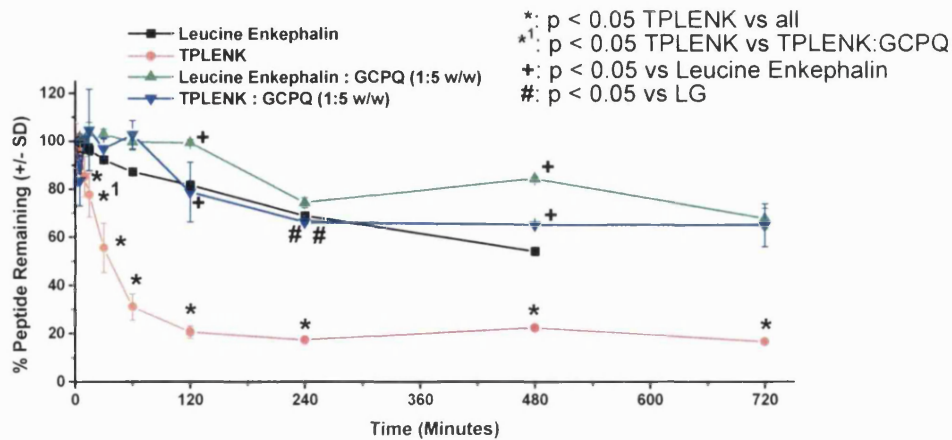


Figure 4.6: Stability of peptides in intestinal washes with or without GCPQ.

Table 4.5: Stability of peptides in intestinal washes with or without GCPQ

Time (Minutes)	Leucine Enkephalin		TPLENK %	SD TPLENK	Leucine Enkephalin : GCPQ (LG)		TPLENK : GCPQ (PG)	
	(L) %	SD L			%	SD LG	(PG)	SD PG
1	100	1.8	100	7.8	100	0.3	100	0.5
5	97.6	2.3	95.5	8.1	101.8	0.9	83.7	10.5
10	96.9	1.9	85.7	8.4	100.1	0.5	100.6	1.6
15	96.5	2.2	78.0	9.1	103.7	4.4	104.8	16.9
30	92.2	1.0	56.0	10.2	103.1	2.1	97.0	4.4
60	87.2	1.3	31.5	5.4	99.8	3.3	102.9	5.9
120	81.7	1.8	21.0	2.6	99.6	1.3	79.0	12.4
240	68.9	1.6	17.8	0.7	74.5	2.1	66.5	0.9
480	54.1	1.7	22.7	1.3	84.5	0.8	65.2	0.5
720	--	--	16.9	0.7	67.8	4.2	65.0	8.9

Key; --: Sample was not analysed for this time point, SD: Standard Deviation of mean of triplicates

Table 4.6: *In vitro* enzymatic stability of peptide formulations in rat intestinal wash

Formulations	Half-life $t^{1/2}$ (h)	SD	r^2 -First order Exponential Decay
Leucine ^[5] -Enkephalin	3.5	0.74	0.994
Leucine ^[5] -Enkephalin: GCPQ (1:5 w/w)	5.28	2.86	0.842
TPLENK	0.4	0.06	0.953
TPLENK: GCPQ (1:5 w/w)	1.01	0.16	0.974

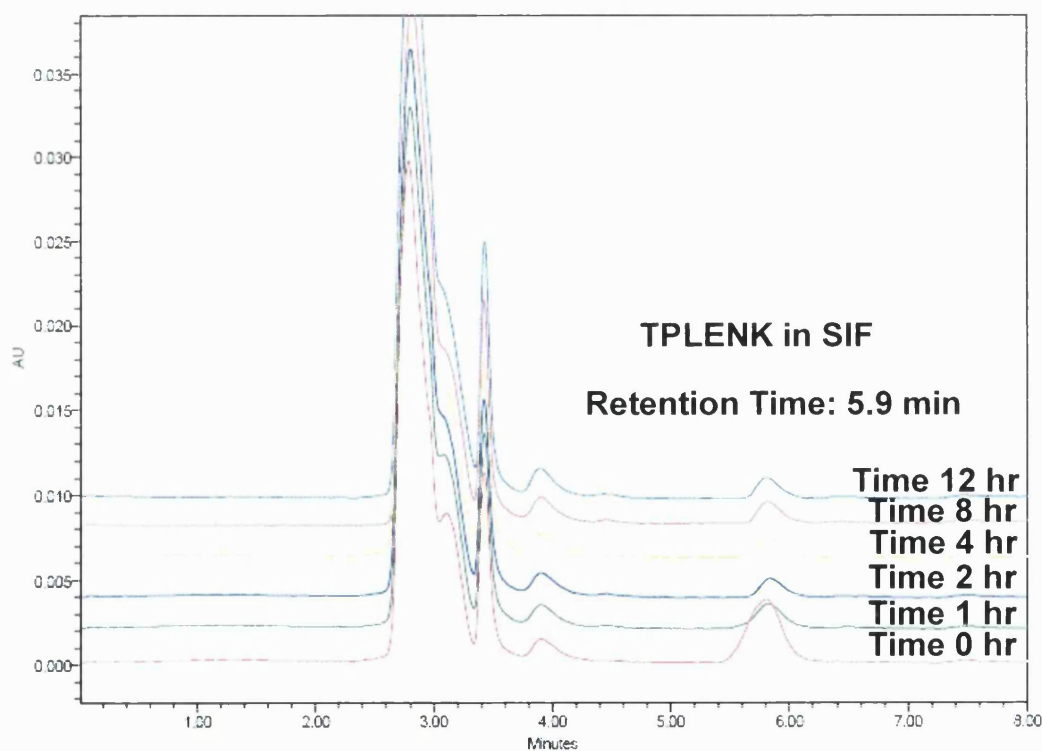
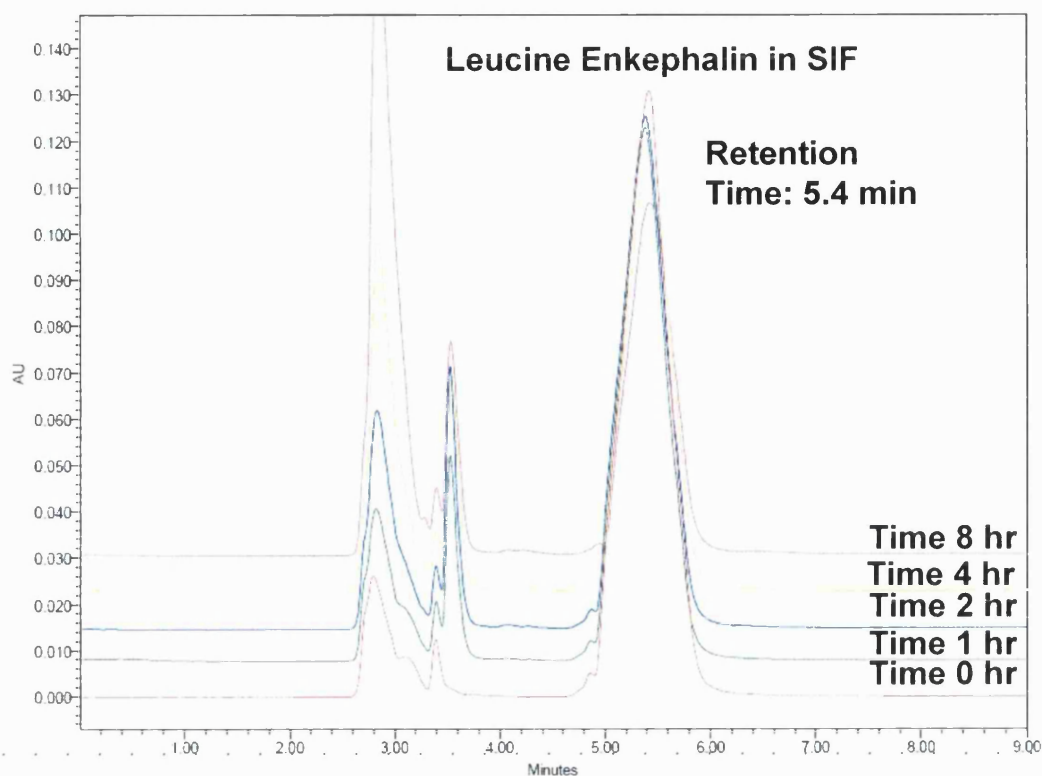


Figure 4.7: HPLC chromatograms of peptides in the presence of intestinal wash with GCPQ.

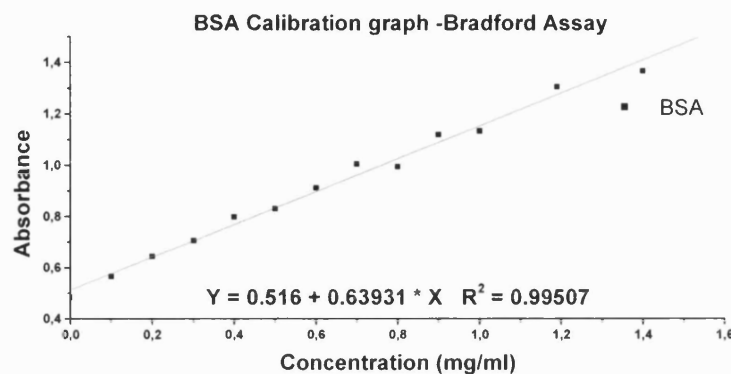
4.4.3 *In vitro* stability in Plasma, Liver and Brain Homogenates

Figure 4.8: Bradford Assay BSA calibration graph for plasma, liver and brain homogenates studies.

The protein content for rat plasma homogenates (10%) ($n = 3$), rat liver homogenate (50%) ($n = 3$) and for rat brain homogenate (50%) ($n=3$) was found to have a mean of 8.76 mg mL^{-1} (SD: ± 0.10), 24.15 mg mL^{-1} (SD: ± 6.75) and 54.53 mg mL^{-1} (SD: ± 17.35) respectively as extrapolated from the Bovine Serum Albumin Bradford assay calibration graph. The total amount of esterases was $734.1 \text{ Units mg}^{-1}$ of protein in the plasma homogenate (10%), 189.4 Units /mg of protein in the liver homogenate (50%) and $36.3 \text{ Units mg}^{-1}$ of protein in the brain homogenate (50%) and of which only $18.1 \text{ Units mg}^{-1}$ of protein were not inhibited by paraoxon (Type A/C esterases) in the plasma homogenate, $11.1 \text{ Units mg}^{-1}$ of protein in the liver homogenate and $23.36 \text{ Units mg}^{-1}$ of protein in the brain homogenate (Table 4.7).

Leucine^[5]-Enkephalin calibration curve was $y = 3 \times 10^7 X + 3 \times 10^6$ ($r^2 = 0.9954$) and $y = 2 \times 10^6 X + 189393$ ($r^2 = 0.9922$) for TPLENK for the plasma and liver homogenate studies and $y = 2303.2 X$ ($r^2 = 0.9891$) and $y = 13.048 X$ ($r^2 = 0.9841$) for TPLENK for the brain homogenate studies, where y is the area under the curve (AUC) and X is the concentration in $\mu\text{g mL}^{-1}$ (Table 4.7). The degradation of ester prodrugs in plasma involves type B esterases as the half-lives are increased when paraoxon, an inhibitor of type B esterases, is added to the plasma (Fredholt et al. 2000). The lipidic prodrug is converted *ex vivo* to Leucine^[5]-Enkephalin (Figure 4.10, 4.12, p;224, 225). Apparent half-lives ($t_{1/2}$) for the disappearance of the lipophilic pro-drug were ~ 73 and ~ 44

minutes approximately in plasma and liver homogenates respectively as calculated from pseudo first-order rate constants obtained by linear regression of log drug concentration versus time plots ($y = 6.29674 + 80.27412^{-2.73252} T$, $r^2 = 0.96504$ for plasma and $y = 52.00779^{-0.94672} T$, $r^2 = 0.97502$ for liver) (Table 4.7). It was not possible to calculate the apparent half-life for the disappearance of TPLENK in brain homogenates as no statistical significant degradation ($p > 0.05$) was observed under the experimental conditions used (Figure 4.13 and 4.14, p: 226, 227) although two sets of triplicates were tested.

Table 4.7: Plasma, Liver and Brain esterase stability studies summary

	Plasma 10%	Liver 50%	Brain 50%
Protein Content (mg mL ⁻¹ ± SD)	8.76 ± 0.1	24.15 ± 6.75	54.53 ± 17.35
Total Esterases (Units mg ⁻¹ of protein)	734.1	189.4	36.3
Type A/C Esterases (not paraoxon inhibited) (Units mg ⁻¹ of protein)	18.1	11.1	23.36
LENK HPLC calibration curve	$y = 3 \times 10^7 X + 3 \times 10^6$, $r^2 = 0.9954$		$y = 2303.2 X$, $r^2 = 0.9891$
TPLENK HPLC calibration curve	$y = 2 \times 10^6 X + 189393$, $r^2 = 0.9922$		$y = 13.048 X$, $r^2 = 0.9841$
TPLENK $t_{1/2}$ (minutes)	~73	~44	-----
1 st order kinetics	$y = 6.29674 + 80.27412^{-2.73252} T$, $r^2 = 0.96504$	$y = 52.00779^{-0.94672} T$, $r^2 = 0.97502$	-----

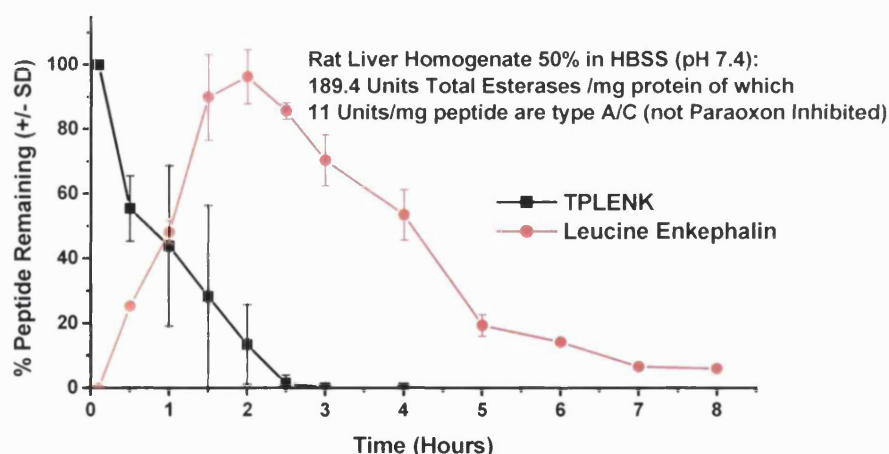


Figure 4.9: Stability of TPLENK in 50% Liver Homogenate and bioconversion to Leucine^[5]-Enkephalin in the presence of liver esterases

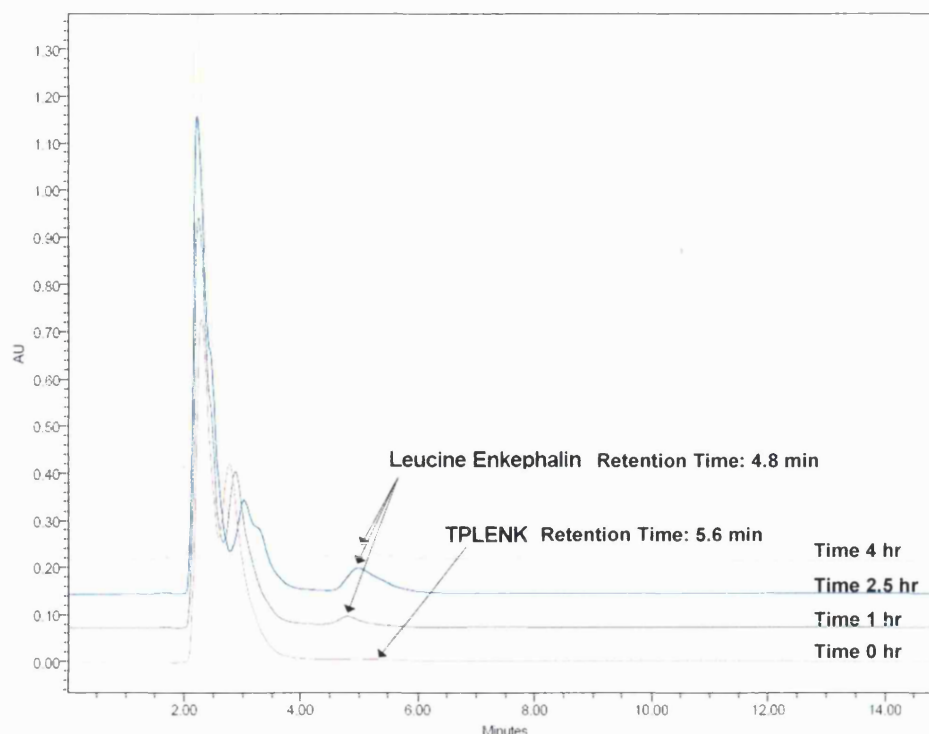


Figure 4.10: HPLC chromatograms of TPLENK in 50% Liver Homogenate over time

Table 4.8: Stability of lipidic pro-drug (TPLENK) in 50% Liver Homogenate

Time (Hours)	TPLENK %	SD TPLENK	Leucine ^[5] - Enkephalin (L) %	SD L
0.1	100	0	0	0.24
0.5	55.40	10.12	25.53	0.50
1	43.84	24.78	48.27	3.75
1.5	28.24	28.11	90.14	13.32
2	13.40	12.26	96.54	8.44
2.5	1.43	2.47	85.82	2.56
3	0.02	0.03	70.66	7.90
4	0	0	53.80	7.79
5			19.51	3.33
6			14.40	0
7			6.73	0
8			6.12	0

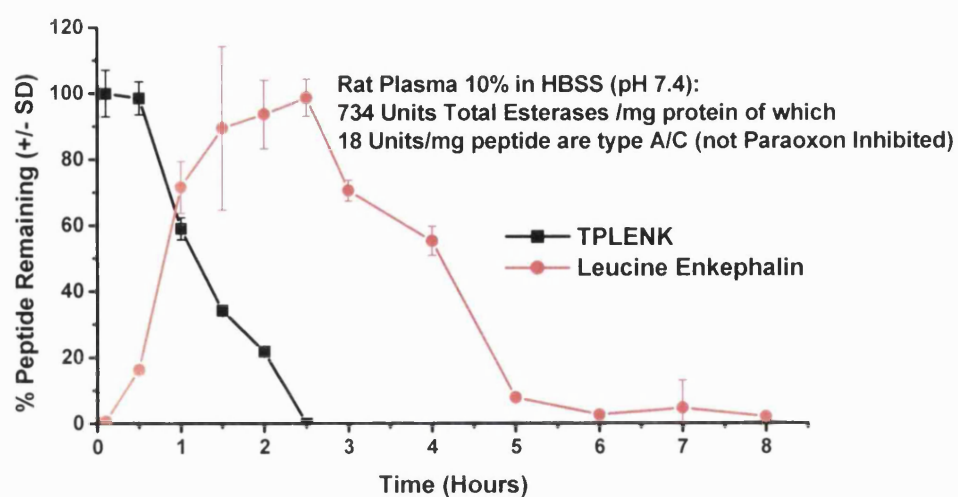


Figure 4.11: Stability of TPLENK in 10% Plasma Homogenate and bioconversion to Leucine^[5]-Enkephalin in the presence of plasma esterases

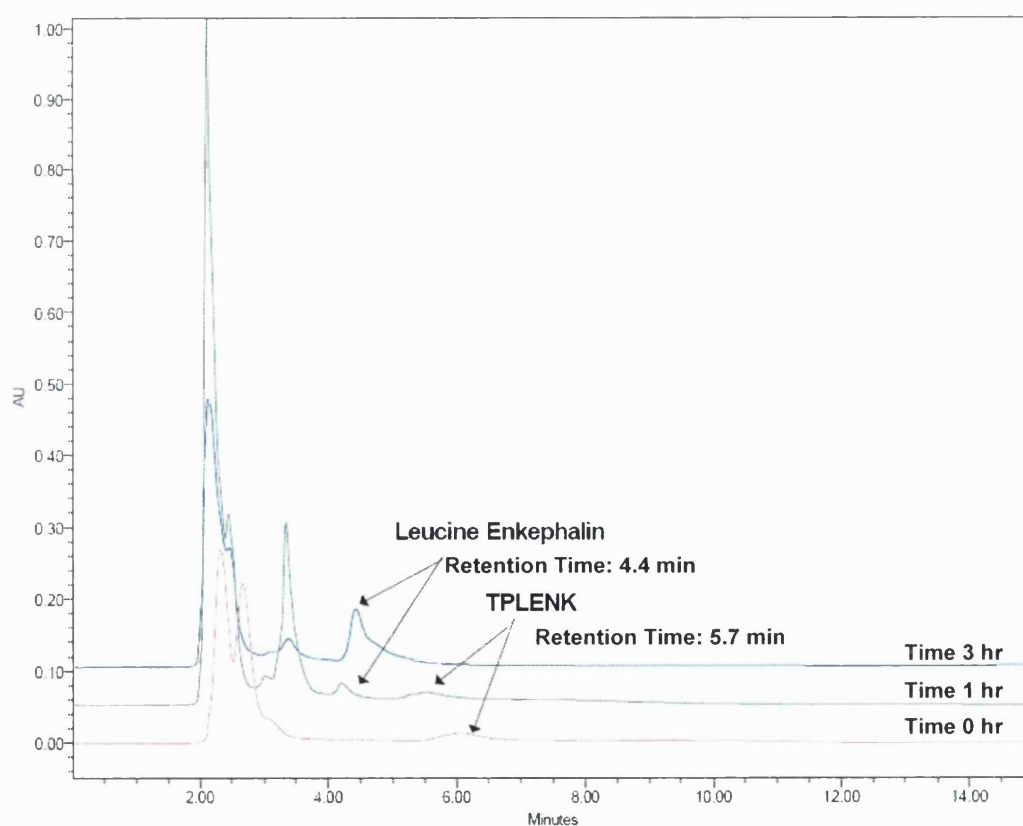


Figure 4.12: HPLC chromatograms of TPLENK in 10% Plasma Homogenate over time

Table 4.9: Stability of lipidic pro-drug (TPLENK) in 10% Plasma Homogenate

Time (Hours)	TPLENK %	SD TPLENK	Leucine ^[5] - Enkephalin (L) %	SD L
0.1	100	7.12	0.83	1.45
0.5	98.51	5.02	16.46	1.52
1	58.97	3.39	71.81	7.86
1.5	34.11	0.39	89.68	24.77
2	21.80	1.41	93.87	10.40
2.5	0	0	98.87	5.66
3			70.76	3.13
4			55.51	4.42
5			8.04	1.39
6			2.80	0.48
7			4.84	8.38
8			2.18	0.38

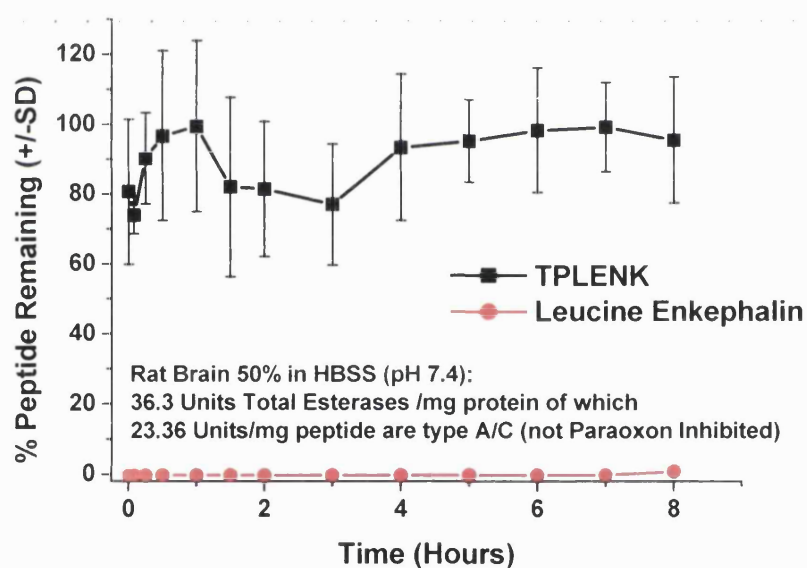


Figure 4.13: Stability of TPLENK in 50% Brain Homogenate

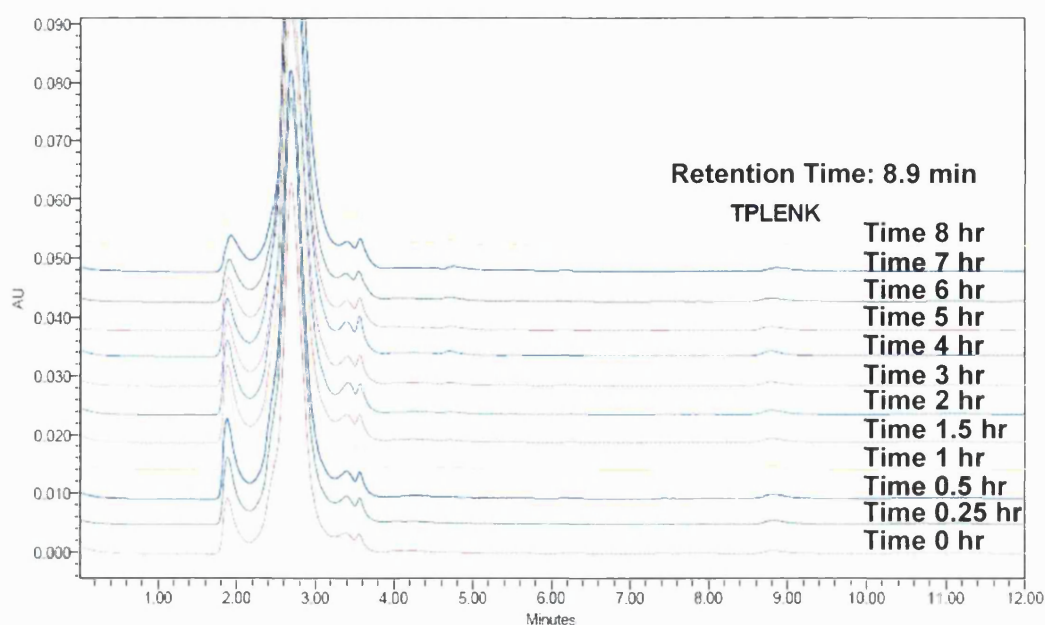


Figure 4.14: HPLC chromatograms of TPLENK in 50% rat Brain Homogenate over time

Table 4.10: Stability of lipidic pro-drug (TPLENK) in 50% Brain Homogenate

Time (Hours)	TPLENK %	SD TPLENK	Leucine ^[5] - Enkephalin (L) %	SD L
0	80.64	20.8	0	0
0.08	73.85	5.3	0	0
0.25	90.24	13.1	0	0
0.5	96.66	24.29	0	0
1	99.4	24.47	0	0
1.5	81.97	25.72	0	0
2	81.41	19.41	0	0
3	77.01	17.4	0	0
4	93.36	21	0.01	0.01
5	95.19	11.86	0	0
6	98.27	17.88	0	0
7	99.18	12.76	0.03	0.01
8	95.48	18.1	1.01	0.23

4.5 Discussion-Conclusions

An ideal drug candidate needs to have specific druglike properties, including chemical and enzymatic stability, solubility, low clearance by the liver or kidney, permeation across biological membranes, potency, and safety, while being patient friendly by having minimal frequency of dosing, pleasant taste/odor if designed for oral administration or causing minimal pain upon parenteral administration. The clinical development of peptide drugs in oral dosage forms has been limited by their unfavorable physicochemical properties, which restrict their intestinal permeation and by their metabolic lability to proteolytic enzymes leading to rapid clearance from the systemic circulation (Wang et al. 1999; Adessi and Soto 2002; Mahato et al. 2003; Liederer and Borchardt 2005). A prodrug strategy is employed in many cases to overcome these biopharmaceutical problems by synthesizing prodrugs with improved cell permeation characteristics and increased stability to hydrolytic enzymes (Borchardt 1999). Therefore, conversion to the parent drug is critical for the prodrug approach to be successful involving metabolism by enzymes that are distributed throughout the body by hydrolysis or oxidation by cytochrome P450s (Liederer and Borchardt 2006).

When designing a strategy for the delivery of a peptide orally, assessment of the stability of the peptide in simulated gastrointestinal conditions (pH and enzymes) is vital. Both parent peptide and prodrug were stable in simulated gastric fluid (in the absence of pepsin) for up to 3 hours in the presence or absence of GCPQ with at least 92% of the peptides remaining intact (Figures 4.3 and 4.4). Pepsin can preferentially cleave a hydrophobic, preferably aromatic, residue (e.g. Phenylalanine) in either sides of the peptide chain or also at the free carboxyl side of a Leucine (Sweeney and Walker 1993). The degradation of TPLENK was rapid in rat intestinal washings (pH 6.6) (Figure 4.6) possibly due to esterase activity in the homogenate combined with brush border enzyme degradation of the Tyr⁵-Gly⁴ bond mostly by Aminopeptidase N which is the major enzyme for the degradation of enkephalin peptides (Dodda-Kashi and Lee 1986). Acylation with short chains of the phenolic -OH of enkephalin analogs (e.g. DADLE) has been shown to increase the hydrolytic rate in the presence of Carboxypeptidase A (attacking the Phe-Leu bond) and can also provide an explanation for the faster rate of hydrolysis of the prodrug in the presence of intestinal wash

(Fredholt et al. 2000). Endopeptidases and especially α -Chymotrypsin that cleaves peptide bonds near hydrophobic amino acids may be responsible for the fast hydrolytic rate of both parent peptide and prodrug in intestinal washes at near optimum pH (6.6). Protection provided by GCPQ to esterases and brush border enzyme activity (Figure 4.6) could be attributed to the physical protection to enzymatic attack of the peptide within agglomerates and /or reduction of enzyme activity in the presence of GCPQ. A large proportion of the peptidases associated with the brush-border membranes are metalloproteases requiring divalent metal ions for their activity, like aminopeptidase N and trypsin (Woodley 1994; Bernkop-Schnurch et al. 1997). Chitosan has been shown to act as a chelator binding divalent ions like Zn^{2+} (required for Aminopeptidase N enzymatic activity) (Bernkop-Schnurch et al. 1997; Tang and Hon 2000). Furthermore, it is possible that pepsin and chymotrypsin are positively charged species and cannot bind to GCPQ particles that are also positively charged (Uchegbu et al. 2004; Ubaidulla et al. 2007). However, the exact mechanism by which GCPQ protects against enzymatic degradation is not fully elucidated, but an increased intestinal stability in the presence of GCPQ can thus allow for increased amounts of the peptides being available for absorption within the jejunum and the ileum.

Brain, liver and plasma were chosen as the most relevant biological media for stability studies due to their importance in bioconversion of prodrugs and in the case of brain also as the site of pharmacological effects of this prodrug. Liver and plasma homogenates illustrated significant esterase specific activity as indirectly determined by the rates of p-nitrophenyl butyrate hydrolysis (Figures 4.9 and 4.11, p: 223, 225). Based on the effect of the potent esterase B inhibitor paraoxon, the esterase isoenzymes present in the biological media were characterised into type B and type A/C (not paraoxon inhibited). The relative amount of esterases of type A/C were only 3.8 %, 9.5% and 49.9% of the total amount of esterases present in rat plasma, liver and brain homogenates respectively (Figures 4.9 and 4.11, p: 223, 225) which correlated well with previous studies by Liederer et al that reported approximately 6%, 1% and 45% for rat plasma, liver and brain homogenates respectively (Liederer and Borchardt 2005) taking into consideration interspecies variability.

TPLENK showed more favourable brain to plasma stability in homogenates and reasonable stability in liver homogenates to allow for *in vivo* bioconversion of the pro-

drug. The stability of the prodrug in brain homogenates is partly justifiable by the low esterase specific activity of the brain homogenates (versus the plasma and liver homogenates as well as previously reported values for brain homogenates) in rat (Liederer and Borchardt 2005). Testing lower concentration ($<12.5\ \mu\text{M}$) of the lipidic peptide with the homogenate or increasing the amount of brain homogenate used (thus increasing the amount of available esterases free for hydrolysis) would be needed before assuming the lipidic prodrug is stable in brain homogenate and quantifying its half-life in this medium. However, increased esterase specific activity of the biological media does not necessarily correlate with higher rates of hydrolysis always (Liederer and Borchardt 2005).

Esterase activity in the brain is associated with both the soluble and membrane-bound compartment of nerve tissue with esterases in the water-soluble fractions of nerve tissue [which are resistant to organophosphorous inhibitors such as di-isopropyl fluorophosphate (DFP)] being classified as type A/C esterases (Aldridge 1953), while membrane-bound esterases, that are inhibited by DFP, are classed as type B esterases (Rumsby et al. 1973). In addition, since esterases B are the predominant enzymes in the liver and plasma, it is likely that the lipidic prodrug is a better substrate for type B membrane bound esterases than esterases A/C (paraaxon inhibited). Further studies are required, however, on assessment of the stability of the lipidic prodrug in the presence and absence of paraaxon to validate this. It is also important to keep in mind that the specific esterase activity in humans is less than in rodents and that esterases of the type A/C are the predominant enzymes in humans (Liederer and Borchardt 2005). However, other enzymes besides esterases, such as cytochrome P450, are proficient in cleaving esters and can contribute *in vitro* and *in vivo* to the bioconversion of ester prodrugs. Endo- and exopeptidases can also affect the metabolism of the prodrugs. Furthermore, it has to be noted that separate enzymes may be involved in the hydrolysis of short and long chain ester substrates in the brain with long chain esters being hydrolysed by lipase (lipoprotein lipase EC 3.1.1.34) (Rumsby et al. 1973; Eckel and Robbins 1984) present in endothelial cells.

A prodrug designed to enhance lipophilicity / membrane permeation for drug delivery to the CNS will require the prodrug activation to occur after the prodrug has crossed the BBB, so as bioconversion will give rise to the more polar active compound that can

elicit its pharmacological effects that would not be able to cross the BBB if it was released immediately before reaching the target organ. Our studies do not support brain bioconversion of the lipidic pro-drug at least in the rat, but possible bioconversion of the parent peptide in plasma and liver that then can be transported and cross the biological barrier at the site of action to elicit its antinociceptive effects. However, further studies in other species like the mouse and the guinea pig (closer esterase profile to humans (Liederer and Borchardt 2005)) need also to be conducted.

As hydrolysis of ester bonds is sensitive to steric hindrance (Buchwald and Bodor 1999) and TPLENK is bioconverted to Leucine^[5]-Enkephalin, addition of the palmitic tail on the free hydroxyl group of Leucine^[5]-Enkephalin does not abolish enzymatic attack indicating a flexible conformation of the prodrug depending on the environment and available metabolic pathways in the body for its clearance.

One problem with ester prodrugs is the difficulty in predicting their rates of bioconversion and, thus, their pharmacological or toxicological effects especially when one is trying to use animal data to predict the prodrug's bioconversion in humans. Species differences can generally result from the existence of different types of esterases in biological media and differences in their respective substrate specificities (Liederer and Borchardt 2005). Even within one species, the rate of hydrolysis is not always predictable for the same reasons (Hosokawa et al. 1995) with bioconversion being affected by various factors such as age, gender, and disease (Liederer and Borchardt 2006).

To summarise, the lipidised prodrug of Leucine^[5]-Enkephalin, TPLENK, has been shown to be able to be bioconverted *ex vivo* to the parent peptide probably mainly by type B esterases in the presence of rat plasma and liver homogenates with short half lives of ~73 and ~44 minutes respectively. The prodrug showed good stability in a low pH environment (simulated gastric fluid) for up to 3 hours at 37°C and in rat brain homogenates up to 8 hours. The use of GCPQ (1:5 w/w peptide:polymer ratio) enhanced significantly the stability of both peptides in rat intestinal wash.

Chapter 5

***In Vivo* Pharmacokinetic & Pharmacodynamic Studies**

5.0 Preface

No longer considered a static, impenetrable barrier, the dynamic regulatory functions of the BBB have become increasingly apparent, which is particularly evident for the transport of peptides across the BBB. Interactions of peptides with the endothelial cells composing the BBB could lead to endocytosis and eventually transcytosis of peptides. Part of the scepticism concerning the ability of peptides to cross the BBB probably could be explained by the lack of appropriate and sensitive methods for quantification of the relatively tiny amounts in blood that reaches the brain parenchyma in intact form (Kastin and Pan 2003). For insulin, only about 0.05% of the injected amount reaches the brain (Banks and Kastin 1998) and this low amount cannot be explained by rapid transport out of the brain (Cashion et al. 1996). For opiates, it was shown that peripheral injection of a Methionine^[51]-Enkephalin analog causes electroencephalogram changes that can be reversed by an opiate antagonist that crosses the BBB, but not by one which only acts peripherally, establishing that even small amounts of peptide crossing the BBB can be active (Kastin et al. 1991). Morphine, although not a peptide, is often misleadingly thought of as entering the brain freely. However, only about 0.02% of the injected dose is found in the brain (Advokat and Gulati 1991; Banks and Kastin 1994). In general, only a small portion of peripherally delivered peptide reaches the brain parenchyma, but this small amount is often sufficient to affect physiological functions and modulate neuroendocrine and behavioural responses (Kastin and Pan 2003). Thus, the study of both the pharmacokinetics as well as the pharmacodynamics after dosing is crucial to identify doses and formulations that not only cross the BBB but the amount delivered are adequate to elicit a pharmacological response.

Leucine^[51]-Enkephalin is a derivative neuropeptide of proteolytic cleavage of the propeptides Prodynorphin and Proenkephalin and acts by binding preferentially to δ -opioid receptors in the brain (Summers and Hayes 1981; Strand 1999). Different neuropeptides probably use different routes and mechanisms for penetration, and neuropeptides and their analogs cross the BBB to varying degrees. Neuropeptide

transport systems can be saturable and highly stereospecific and most systems are located in the choroid plexus or the capillary bed of the CNS (Strand 1999). Some of these systems transport peptides into the brain, but also out of the brain or bidirectionally (Strand 1999). Enkephalins were demonstrated to be taken up efficiently into the brain, and the involvement of a saturable mechanism for the transport of Leucine^[5]-Enkephalin was shown by an *in situ* vascular brain perfusion technique (Tsuji and Tamai 1998). One system involved in the brain-to-blood transport of neuropeptides, the peptide transport system-1 (PTS-1), transports small peptides with an N-terminal tyrosine such as the tetrapeptides Tyr-Pro-Leu-Gly-NH₂ and Tyr-Pro-Trp-Gly-NH₂ which have antiopiate and antidepressant properties, and the analgesic peptides Methionine^[5]-Enkephalin and Leucine^[5]-Enkephalin and Dynorphin. However, PTS-1 transports only in the direction of brain-to-blood lacking a blood-to-brain, or influx, component. Thus, Leucine^[5]-Enkephalin, which is transported in both directions, probably uses another transport system for influx.

Since most peptide and polypeptides are large hydrophilic molecules that have slow and limited penetration across the BBB, traditional techniques such as the Brain Uptake Index (BUI) method (Oldendorf 1971) are not appropriate and have led to the misconception that “circulating peptides do not effectively cross the BBB” and that it is unlikely that distribution of peptides in brain will occur after systemic administration (Pardridge 1984). The BUI method measures single-pass uptake from blood over a few seconds and provides an excellent estimate of the rapid uptake of glucose and water by the brain, but is unsuitable for study of slowly penetrating molecules (Davson and Segal 1995).

There are three basic methods to evaluate how much and how fast peptides cross the BBB: (i) IV delivery followed by multiple-time regression analysis (Blasberg et al. 1980; Blasberg et al. 1983; Patlak et al. 1983; Kastin et al. 2001), (ii) *in situ* brain perfusion (Zlokovic et al. 1986; Zlokovic et al. 1987; Zlokovic et al. 1989) and (iii) studies in cultured brain microvessel endothelial cells constituting the *in vitro* BBB (Audus and Borchardt 1987; Abbott et al. 1992; Maresh et al. 2001; Terasaki and Hosoya 2001), all of them requiring that the peptide remain stable during the study period and that it completely cross the endothelial cell barrier (Kastin and Pan 2003). All of the above techniques rely severely on the use of radiolabeled peptides. Thus, a

fragment of the injected/used substance (i.e. in the case of enkephalins, a radiolabeled tyrosine generated by cleavage by aminopeptidases in the plasma and brain which is the predominant enzyme for degradation of Leucine^[51]-Enkephalin (Lund et al. 1998)) could mistakenly appear to represent the intact peptide as measured by radioactivity. However, although some peptides can remain stable in blood for at least 10 minutes after IV administration, their radiolabeled equivalents can be more than 50% degraded in blood within the same time (Kastin and Pan 2003).

Thus, IV administration of the peptide and quantitation of levels in plasma and tissues after the animal is euthanized is probably a more realistic *in vivo* approach. Quantitation is usually done with HPLC or LC-MS, gel electrophoresis (useful for bigger peptides or proteins), radioimmunoassay (RIA) or a combination of the above. For quantitative purposes, LC-MS and RIA would be the most sensitive (concentration in the range of pg mL⁻¹). However, a limitation of this approach is that degradation can occur after passage across the BBB and entry into brain before homogenisation and quantitation, leading to reported values being underestimated. Degradation can also take place at the BBB itself from peptidases present in the capillary endothelial cells (Kastin and Pan 2003).

There are only two approaches today that challenged the long standing belief that neuropeptides are quickly inactivated in the GI tract and therefore are ineffective if administered orally. One of them is a prodrug approach (Wang et al. 2006), while the second one is a delivery approach using polysorbate coated nanoparticles (Das and Lin 2005). Leucine^[51]-Enkephalin was modified at the N-terminal via an amide bond with a novel amine-reacting lipophilic dimethylmaleic anhydride analog, 3, 4-bis (decylthiomethyl)-2, 5- furandione (Wang et al. 2006). However, the lipidised pro-drug had limited brain permeation and produced its analgesic effects by peripheral opioid receptors (Wang et al. 2006). The delivery approach utilised Dalargin as a model peptide, an opioid peptide that does not cross the BBB after intravenous administration, and followed on an earlier report on oral Dalargin delivery using polysorbate coated nanoparticles and achievement of central antinociception which did not provide adequate characterisation of the formulation utilised or stated the dose of peptide administered (Schroeder et al. 1998). Poly (butylcyanoacrylate) nanoparticles, surface-coated with polysorbate-80 and poly(ethylene) glycol 20,000 was shown to be able to

elicit statistical significant antinociception at 60 minutes after oral administration (Das and Lin 2005). Only oral pharmacodynamic studies were reported and the effects was not necessarily more pronounced but rather shortly prolonged (Das and Lin 2005).

The aim of these *in vivo* studies is to assess the IV and oral delivery potential of hydrophilic peptides such as Leucine^[51]-Enkephalin by lipidisation via cleavable ester bond (prodrug formation) and/or encapsulation in GCPQ, a carbohydrate bioavailability enhancer. The pharmacokinetic levels in blood and brain as measured by RIA as well as the pharmacodynamics assessed using the tail-flick bioassay are examined after IV and oral delivery of the polymer formulations of parent peptide and prodrug (TPLENK) compared to the parent peptide and placebo as controls.

5.1 Radioimmunoassays

Radioimmunoassays are designed to utilise the competition, between peptides tagged with radioisotopes (the antigen) and unlabeled peptide in the sample, for binding to a limited number of antibodies generated against that peptide (Gill et al. 2003). After incubating the unlabeled specimens and standards (samples of known concentration of pure peptide) with assay reagents (antibody, radiolabeled peptide, buffer, and stabilisers), the amount of radiolabeled peptide bound to the antibody is measured (Gill et al. 2003). The more unlabeled peptide present in the mixture, the less radiolabeled peptide will be bound to the antibody. The standards provide a calibration for the amount of bound radiolabeled peptide across a range of known peptide concentrations, thereby allowing the interpretation of the assay results in terms of clinically relevant peptide levels (Gill et al. 2003).

The accuracy of the RIA depends on the ability to separate antibody-bound from unbound reagents, particularly the radiolabeled antigen being measured (Gill et al. 2003). A variety of methods can be used to separate bound from unbound peptide after the competitive binding has occurred, with the most common involving precipitation of the bound antibody and separation from the unbound reagents by centrifugation (Figure 5.1) (Gill et al. 2003).

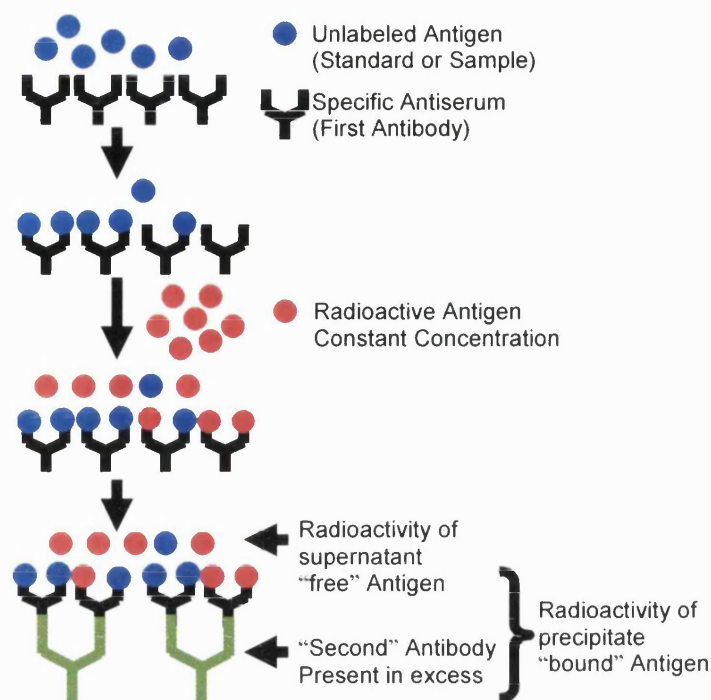


Figure 5.1: Competitive radioimmunoassay.

Achieving a measurement as close as possible to the true value depends on four complementary characteristics of immunoassays: sensitivity, specificity, precision and accuracy. Sensitivity describes quantitatively either the minimum measurable difference in peptide concentrations or the minimum peptide concentration that can be measured [limit of detection (LOD)], is system-dependent and a function of the antibody's affinity for the peptide as well as the error associated with repeated measurements (Gill et al. 2003). For competitive immunoassays that have a negative dose-response curve, the lower 95% confidence limit of replicate determinations of a "zero" dose standard is equivalent to the limit of detection (Figure 5.2) (Gill et al. 2003). Generally, the maximum measurable concentration is defined based upon acceptable between-assay variance and this concentration is chosen as the highest point on the standard curve (Gill et al. 2003). Specificity is the degree to which an immunoassay measures only the target peptide and is dependent on the ability of the antibodies to discriminate among antigens, but also on the extent to which measurements are free from interference by nonantigenic materials in the specimen can lead to overestimation (Gill et al. 2003). Precision, a measure of reproducibility of repeated measurements, is based upon repeated measurements of stable aliquots of the same specimen. The variance associated with the

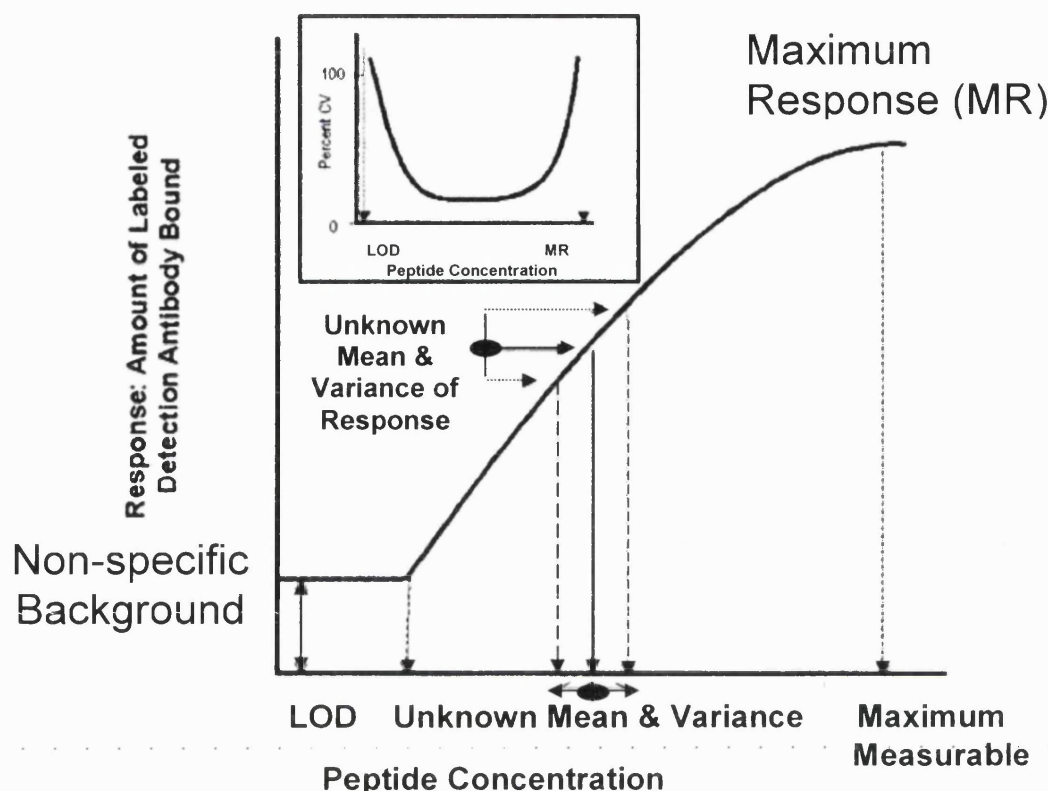


Figure 5.2: Principles of Immunoassay. Insert: The coefficient of variation (CV) defined as the standard deviation expressed as a percentage of the mean of replicated measurements, is used to represent variance. CV of repeated measurements is not uniform across the dose-response curve and at very low or very high concentrations of peptide, there is no dose-response relationship, and the CV approaches infinity (due to the sigmoidal shape of the RIA standard curve). A CV of 20% is generally accepted. Reproduced from (Gill et al. 2003).

dose-response curve is most often the largest source of error, especially at both extremes of the standard curve (Gill et al. 2003). Accuracy describes how closely the obtained measurements are with the actual mass of the peptide present in the specimen. Specificity is the most significant factor contributing to inaccuracy (Gill et al. 2003). Peptide isoforms and metabolites can often contribute to a lack of specificity and thus inaccuracy (Gill et al. 2003). Interference by serum or tissue components often limits accuracy by masking immunoreactivity of the antigens or by reducing the affinity or availability of the antibodies upon which the assay depends (Gill et al. 2003).

Most peptides can be labelled easily for RIA. The simplest approach consist of an oxidation reaction with chloramine-T, which incorporates one or more molecules of iodine (usually ^{125}I , 60.1 days half-life) to a peptide containing tyrosyl and/or histidyl residues (Benoit et al. 1987). Whenever a sensitive RIA is required, the highest specific activity per peptide molecule normally using a high-specific activity isotope such as ^{125}I without altering its capacity to react with the antibody is required (Benoit et al. 1987).

A gamma counter apparatus is used to measure the radioactivity of ^{125}I in the standards and samples analysed after precipitation in the end of the RIA procedure. The sensor, called a scintillator, consists of a transparent crystal, usually phosphor, which fluoresces when struck by ionizing radiation. A sensitive photomultiplier tube (PMT) measures the light from the crystal. The PMT is attached to an electronic amplifier and other electronic equipment to count and possibly quantify the amplitude of the signals produced by the photomultiplier, which is proportional to the intensity of the scintillation and thus the energy of the radiation which produced it. For any given isotope the radiation shows a continuous distribution of energies, or spectrum, with a characteristic maximum for each specific isotope.

Measurements of peptides in brain extracts, plasma or tissue perfusates needs special controls in each situation (Benoit et al. 1987). Even if the first antibody in the RIA has been extensively characterised, cross-reactive substances may still lead to overestimation of the actual contents (Benoit et al. 1987). Other substances unrelated to the antigenic determinant can modify substantially the antigen-antibody reaction or the precipitation of the immune complex (Table 5.1) (Benoit et al. 1987). In rare cases, an extract may even contain proteins or salts that increase the binding of the antigen to the antibody, leading to underestimation or false negative results (Benoit et al. 1987). However, when the RIA has been validated, the results are generally accurate (Benoit et al. 1987). Thus, the extraction step itself is most important, and the optimal extraction procedure may vary among different peptides.

Table 5.1: Sources of Artifacts in RIA Determinations of tissues and body tissues

- | |
|--|
| <ul style="list-style-type: none">• Degradation of labelled antigen by unextracted enzymes• Cross-reactivity with structurally related substances• Variations in binding caused by: Salts, Lipids, Excess protein• Limited buffering capacity of buffer solutions• “Block Effects” in large assays• Interassay variability• Nonparallelism• Poor recoveries• Unsuspected heterogeneity of immunoreactive material caused by multiple molecular forms• Degradation of precursor and formation de novo of peptides during extraction. |
|--|

5.2 Animal Models of Nociception & the Tail-Flick Bioassay

Pain in animals was defined as an aversive sensory experience caused by actual or potential tissue damage/injury that elicits progressive motor and vegetative reactions, results in learned avoidance behaviour, and may modify species specific behaviour, including social behaviour (Zimmermann 1986) and is one of the outputs of the nociceptive system, which itself is a component of the overall homeostatic control systems, and is divided in acute and chronic pain. An accurate assessment of pain in animals is difficult especially in the light of absence of vocal responses or other presentation of physical signs or overt behaviours (Le Bars et al. 2001).

Animal pain tests have been developed primarily for the screening of potential analgesic drugs. In this context, the most important characteristic of a test is that it correctly identifies compounds that are analgesic in pathophysiological pain in humans and correctly eliminates compounds without activity (Franklin and Abbott 1989). The use of pain tests was stimulated by the discovery of the endogenous opioids (Franklin and Abbott 1989).

Antinociceptive animal models can be classified by the nature of the nociceptive stimulus i.e. thermal, electrical, mechanical, or chemical and by the nature of the response, which may involve defining the responses as a function of their increasing complexity from spinal reflexes (e.g. tail flick test) to elaborate, learned behaviours that presumably involve the higher levels of the CNS (e.g. shock titration) (Franklin and Abbott 1989). Effectively, the sensitivity and selectivity of pain tests is affected by the

nature of the stimulus and response but also from the general environment in which the test is carried out. The characteristics of pain tests are affected firstly by the sensory modality of the pain stimulus and secondly by whether the stimulus produces tissue injury or evokes a response that avoids injury (Franklin and Abbott 1989). In humans and in animals, experimental studies of the mechanisms underlying acute pain necessitate the use of appropriate stimuli to provoke the sensation, and have to be quantifiable, reproducible and non-invasive (Le Bars et al. 2001). Electrical and thermal stimuli can meet these requirements.

The application of electrical stimuli produce synchronised afferent signals (Le Bars et al. 2001). However, they are not natural type of stimulus like those encountered by an animal in its normal environment and more importantly, intense electrical stimuli excite in a non differential fashion all peripheral fibers, including large diameter fibers, which are not directly implicated in nociception, as well as fine A δ and C fibers, which mediate sensations of cold and hot as well as nociceptive information (Le Bars et al. 2001). On the other hand, the application of noxious mechanical stimulus can be progressive or coarse. Responses produced by noxious mechanical stimuli are graded in relation to the intensity and/or duration of the stimulus, from reflexes up through vocalisations ultimately to complex motor behaviours (Le Bars et al. 2001). The disadvantage of the application of mechanical stimuli is that they are not specific, difficult to apply to freely moving animals and likely to produce changes in tissues (sensitisation or actual lesions) (Le Bars et al. 2001). Chemical stimulation involving the administration of algogenic agents represents a slow, or even very slow, form of stimulation (Le Bars et al. 2001). Chemical stimuli differ from other stimuli as they are progressive, of longer duration and have an inescapable character once they have been applied, and thus, as a result typical reflexes, which necessitate a minimum level of synchronisation of activity in primary afferent nerves, are not produced by these stimuli (Le Bars et al. 2001).

Thermal stimuli are more selective in the way they stimulate cutaneous receptors, exciting specific categories of peripheral axons, including thermosensitive and nociceptive fibers (Le Bars et al. 2001). The use of radiant lamps or contact thermodes have a slow speed of cutaneous heating (<10°C/sec), which results in an asynchronous activation of peripheral and central neurons (Le Bars et al. 2001).

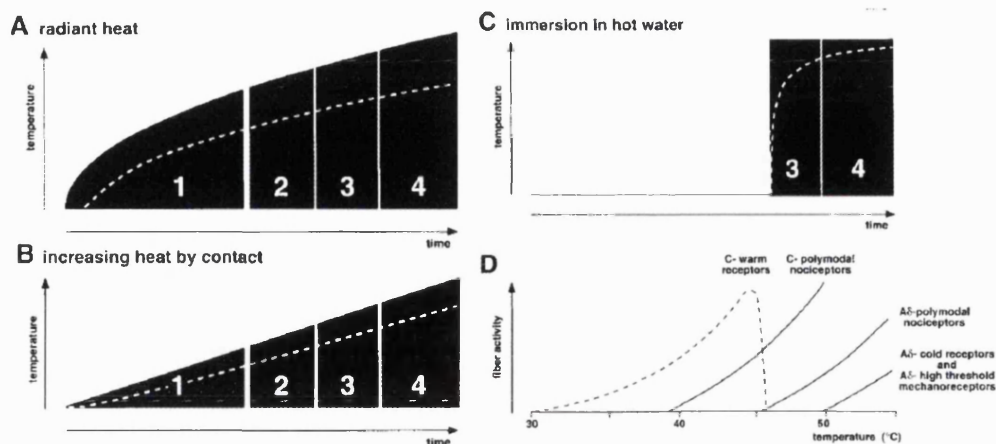


Figure 5.3: Skin and within temperature increase versus time and cutaneous receptors evoked by different temperatures. A: Skin temperature increases in proportion to the square root of the time when subjected to a constant power heat source. The increase is more gradual deep within the skin (white broken line). B: Increase in temperature can be proportional to time when contact thermode is used. Within the skin the increase in temperature is more gradual and dependent on the rate of heating by the thermode. C: Immersing the tail in hot, soaking water, the temperature of the skin interface almost immediately achieves the temperature of the bath, if the bath has an adequate thermostatic control and the water is agitated. The increase in temperature within the skin will be smoother and more gradual. D: Fiber activity evoked in cutaneous receptors by different temperatures applied to the skin. When the temperature is gradually increased from the normal value for the skin (around 30°C with an ambient temperature of 20°C) to within the noxious range, there is a successive activation of thermoreceptors and then C and A δ -polymodal nociceptors. At the highest temperatures, high-threshold mechanoreceptors and cold receptors are also activated. Periods 1-4 can be defined as activation of 1: thermoreceptors, 2: thermoreceptors and C-polymodal nociceptors, 3: C and A δ -polymodal nociceptors and 4: polymodal nociceptors, high-threshold mechanoreceptors and cold receptors. Adapter from (Le Bars et al. 2001)

However, the immersion of an animal's tail in a thermostatic and stirred bath allows for a more rapid, although not instantaneous, increase in skin temperature (Figure 5.3) (Hardy et al. 1965). Thermal stimuli tests involve a short duration of skin stimulation. They do not involve visceral or musculoskeletal tissues, and measure the response time to a stimulus of increasing intensity with the assumption that this reaction time is related to the threshold. The most common variation of the radiant heat tail-flick test is the tail-immersion test. The mouse is confined in a restrainer and the whole tail is dipped in 55-60°C water (stimulation of minimal surface area) maintained by a circulating waterbath (Franklin and Abbott 1989). The response was 1-3 slow movements followed by rapid, continuous tail movements and sometimes a squeak (Franklin and Abbott 1989). There is growing body of evidence to suggest that reflex or avoidance responses, evoked by thermal stimuli, are very sensitive to opioid agonists (and antagonists) that stimulate μ -

receptors as well as aspirin and acetaminophen in mice, but are insensitive to agonists that act as κ -receptors which are more effective against noxious chemical and mechanical stimuli (Franklin and Abbott 1989).

The tail-flick response is a spinal reflex, at least in its shorter latency form, and it persists after section or cold block of upper part of the spinal cord (Le Bars et al. 2001). As with all reflexes, it is subject to control by supraspinal structures (Mitchell and Hellon 1977). The tail-flick reflex may not always be purely spinal, notably when the heating slope is slower and there is an increase in reaction time. It is possible that the response is mediated by a spino-bulbo-spinal circuit or a learning process (Le Bars et al. 2001). Excluding animals with longer baseline reaction times than 5 seconds and using the tail-flick immersion test that increases the temperature very quickly can avoid this. Another interesting observation made by D'Amour and Smith is that the blocking of the tail-flick by morphine was "quantal" or absolute in the sense that, for a given dose, animals either responded or did not respond (before the cut-off time), but that although the proportion of nonresponding animals increased with the dose of the analgesic, those that continued to respond always showed a reaction time close to that of the controls (D'Amour and Smith 1941). However, an all-or-none analgesic effect has not been reported for humans (Miller 1948).

Acclimatisation of the experimental animals to the testing environment that would be carefully controlled is imperative. Stress can markedly attenuate responses to noxious stimuli (Franklin and Abbott 1989). Stress results in increases in core temperature and consequently the temperature of the tail (Le Bars et al. 2001). If animals are not adapted to the laboratory before testing begins, the increase in responsiveness to nociceptive stimulation caused by the decline in stress may be interpreted as tolerance to the effect of the experimental treatment (Franklin and Abbott 1989). Thermoregulation in rodents (that do not sweat) occurs through the tail and to a lesser extent by the paws. The dissipation of heat is regulated at the level of the tail by abrupt variations of blood-flow in a system of arteriovenous anastomoses; this flow can increase by a factor of 35 when the arteriovenous anastomoses are open and tail skin temperature may increase by as much as 10°C (Figure 5.4) (Le Bars et al. 2001). Thus, a positive correlation between room temperature and the cutaneous temperature of the tail, and a negative correlation of each of these and the tail-withdrawal reaction time exists (Le Bars et al. 2001).

Finally, timing of the experimental procedures can affect the results as circadian rhythms are likely to interfere with measurements taken during various tests of nociception (Miller 1948).

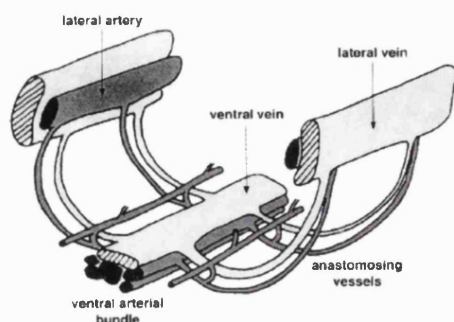


Figure 5.4: Vascularisation of the mouse tail.
From (Young and Dawson 1982)

5.3 Materials and Methods

5.3.1 Animals

ICR (CD-1) male outbred mice (Pharmacokinetic studies: 17-24g, 4 weeks old, Pharmacodynamic studies: 22-28g, 4-5 weeks old, Harlan, Oxon, UK) were used. The animals were housed in groups of 5 in plastic cages in controlled laboratory conditions with ambient temperature and humidity maintained at $\sim 22^{\circ}\text{C}$ and 60% with a 12-hour light and dark cycle (lights on at 7:00 and off at 19:00). Food and water were available *ad libitum* and the animals acclimatised for 5-7 days prior to any experiment in the Animal House, School of Pharmacy, University of London (London, UK). Animals were fasted overnight for oral delivery experiments. Animals for pharmacokinetic studies were only used once and were acclimatised at the testing environment for at least 1 hour prior to testing. Animals for the tail-flick test were acclimatised at the testing environment for at least 20 hours prior to testing (lights off at 20:00 and on at 8:00, ambient temperature at $\sim 22^{\circ}\text{C}$ and humidity at $\sim 60\%$). All experiments were performed in accordance with the recommendations and policies of the Home Office (Animals Scientific Procedures Act 1986, UK) and the Ethics Committee of the School of Pharmacy, University of London guidelines for the care and use of laboratory animals.

Syringes (Terumo, 6%, Luer) were attached to 26G x 5/8 inches (0.45 mm x 16 mm, BD Microlance™ 3) for intravenous administration and to 19-20G commercial gavage needles (2-3 cm long) for oral administration.

5.3.2 Formulations

Pharmacokinetic studies included a combination of the following arms: (i) Placebo: Sodium Chloride 0.9% (IV studies) or H₂O (Oral studies), (ii) Leucine^[5]-Enkephalin (L), (iii) Leucine^[5]-Enkephalin and GCPQ (LG) and (iv) Palmitoyl Tyrosyl Leucine^[5]-Enkephalin (TPLENK) and GCPQ (PG). The dose administered corresponded to 10 or 25 mg Kg⁻¹ and 14.3 mg Kg⁻¹ of mouse body weight after intravenous administration and 25 or 70 mg Kg⁻¹ and 37.5 or 100 mg Kg⁻¹ after oral gavage for Leucine^[5]-Enkephalin (L and LG) and TPLENK (PG) respectively. Pharmacodynamic studies included all the above four arms and the dose administered corresponded to 14 mg Kg⁻¹ and 20 mg Kg⁻¹ of mouse body weight after intravenous administration and 70 mg Kg⁻¹ and 100 mg Kg⁻¹ after oral gavage for Leucine^[5]-Enkephalin (L and LG) and TPLENK (PG) respectively. Sodium chloride 0.9% was used as the disperse phase for the IV formulations and double de-ionised filtered (0.2µm, 33mm Millex GP syringe driven filter unit, PES membrane for sterilisation of aqueous solutions) water (pH 6.4) for the oral formulations. Final formulation concentration was 5 or 3 mg mL⁻¹ for IV and 5 or 15mg mL⁻¹ for the peptides with a ratio of peptide to polymer to be 1: 2.3 w/w and 1: 5 w/w for IV and oral administration respectively. All formulations were prepared by vortexing (WhirliMixer, Fisherbrand) and then by probe sonication (MSE Soniprep 150) with the instrument set at 50% of its maximum output for 15 minutes on ice. The formulations were left overnight in the fridge and prior to IV administration were filtered (0.8µm, 13mm, Acrodisc Syringe Filter, Supor Low Protein Binding Non-Pyrogenic Membrane, PALL Life Sciences). A clear filtrate was obtained for Leucine^[5]-Enkephalin and Leucine^[5]-Enkephalin and GCPQ and a translucent for TPLENK and GCPQ. Oral formulations were not filtered. Administered volume was set to a maximum of 0.2 ml per mouse of formulations administered intravenously or orally. Administered volume was adjusted based on HPLC quantitation of LENK and TPLENK after filtration and the body weight of each animal. The maximum volume was dosed for placebo (NaCl, H₂O) receiving mice.

Table 5.2: Study Design and Formulations for *in vivo* studies.

Route	Arms	P: P Ratio (w/w)	C (mg/ml)	Filtered	Appearance	L Dose (mg/kg)	Animals (n)
Pharmacokinetics:							
IV	NaCl		0	0.22 μ m	Clear	0	4
	L	1 to 2.3	5	0.22 μ m	Clear	25	4
	LG	1 to 2.3	5	0.22 μ m	Clear	25	4
IV	LG	1 to 2.3	3	0.8 μ m	Clear	10	4
	PG	1 to 2.3	3	0.8 μ m	Translucent	14.3 \equiv 10	4
IV	LG	1 to 2.3	3	0.8 μ m	Clear	8.9	4
	PG	1 to 2.3	3	0.8 μ m	Translucent	12.75 \equiv 8.9	4
PO	H ₂ O			-		0	4
	L	1 to 2.3	5	-	Clear	25	4
	LG	1 to 2.3	5	-	Clear, yellow Translucent, cream	25	4
	PG	1 to 2.3	5	-		37.5 \equiv 25	4
PO	H ₂ O		0	-	Clear	0	4
	L	1 to 5	15	-	Clear	70	4
	LG	1 to 5	15	-	Clear, yellow, v. viscous	70	4
	PG	1 to 5	15	-	Opaque, cream, viscous	100 \equiv 70	4
Pharmacodynamics:							
IV	NaCl		0	0.8 μ m	Clear	0	8
	L	1 to 2.3	3	0.8 μ m	Clear	14	8
	LG	1 to 2.3	3	0.8 μ m	Clear	14	8
	PG	1 to 2.3	3	0.8 μ m	Translucent	20 \equiv 14	8
PO	H ₂ O		0	-	Clear	0	16
	L	1 to 5	15	-	Clear	70	16
	LG	1 to 5	15	-	Clear, yellow, v. viscous	70	16
	PG	1 to 5	15	-	Opaque, cream, viscous	100 \equiv 70	16

Key: P:P: Peptide to Polymer (GCPQ), C: Peptide Concentration, n: number of animals per arm, IV: Intravenous, PO: Oral, L: Leucine^[5]-Enkephalin, LG: Leucine^[5]-Enkephalin & GCPQ, PG: TPLENK & GCPQ, \equiv : signifies the weight in mg of molar equivalent doses

The particle size and distribution of freshly filtered polymer dispersions with Leucine^[5]-Enkephalin (LENK) [3 or 5 mg mL⁻¹] or Palmitoylated Leucine^[5]-Enkephalin (TPLENK) [3mg mL⁻¹] prepared for IV pharmacokinetic and pharmacodynamic studies were determined by photon correlation spectroscopy (PCS) (Malvern Zetasizer 3000HS, Malvern Instruments, UK) at 25°C at a wavelength of 633nm and the data analysed using the *Contin* method of data analysis. Polymer solutions were left for 30 min at room temperature (25°C) before particle sizing was done. The accuracy of the instrument was assessed using on drop of latex beads (polystyrene, mean size: 0.1 µm, Sigma Co., UK) in 50 mM sodium chloride (dispersed phase). All measurements were performed in triplicate. Results are expressed as Zave, the mean hydrodynamic diameter ($\langle Rh \rangle = \frac{1}{2} Zave$), along with their polydispersity index.

The morphological examination of the nanoparticles was studied with TEM. A drop of the filtered IV formulations was placed on Formvar[®]/Carbon Coated Grid (F196/100 3.05mm, Mesh 300, Tab Labs Ltd, England). Excess sample was filtered off with No. 1 Whatman Filter paper and negatively stained with 1% aqueous Uranyl Acetate. Imaging was carried out under a FEI CM120 BioTwin Transmission Electron Microscope (TEM) (Ex. Philips, Eindhoven, Netherlands). Digital Images were captured using an AMT (digital) camera.

Examination of the oral particulate formulations was done with scanning electron microscopy (SEM). Fresh samples were mounted on a standard SEM sample holder and were fixed on a brass/aluminium stub using double sided carbon impregnated adhesive discs. The sample was then sputtered coated with a conducting gold-palladium (10 nm, 60% gold-palladium) coating using a SEM coating system for 2 minutes at 30 mA (Emitech K550 Sputter Coater, Emitech Limited, Ashford, UK, Deposition range: 0-50 mA, Deposition rate: 0-25 nm/min, Sputter timer: 0-4 min, Vacuum Pump: 85 lit/min, room temperature) before viewed and photographed under a range of magnifications under high vacuum using Philips XL 30 ESEM FEG scanning electron microscope (School of Pharmacy, University of London).

The peptide formulations (10 µL) were diluted to a total of 180 µL with mobile phase and analysed by reversed phase high-performance liquid chromatography on a reversed phase Waters Sunfire C18 column (5µm, 4.6mm X 250mm) with a guard column

attached [Waters Sunfire C18 (5 μ m, 4.6mm X 10mm)], using a Waters TM 515 HPLC pump connected to a Water TM 717 plus Autosampler with a Waters TM 486 Tunable Absorbance Detector. The mobile phase consisted of 82% 50mM acetate buffer and 18% acetonitrile (pH 5.8). Unless otherwise indicated, samples were detected at 280nm. Flow rate was set at 1mL min⁻¹ at 35°C for analytical runs and the injection volume at 40 μ L. The retention time was 11.5 minutes for Leucine^[5]-Enkephalin and 14.0 minutes for TPLENK and the lowest detection limit is 1 μ g ml⁻¹ and 10 μ g ml⁻¹ respectively. Empower software I was utilised for obtaining the results.

5.3.3 Biological Sample Handling and Extraction

Blood samples (0.4 - 0.8mls per mouse) were collected into a chilled syringe (Terumo, 6%, Luer syringe attached to 25G x 5/8 inches (0.5 mm x 16 mm, BD MicrolanceTM 3) and transferred into an evacuated sterile spray coated with tripotassium ethylenediamin tetraacetic acid (K3, 3.6mg) medical grade PET tubes (3 x 75mm K3E Vacutainer ©, BD Biosciences, UK) and maintained on ice (4°C) till centrifugation. There is no dilution effect in spray coated tubes. Plasma was obtained as the supernatant after centrifugation of blood samples at 1,600 g or 4800rpm for 15 minutes at 4°C with a Hermle Z323 centrifuge (Hermle Laborteschink GmbH, Germany) and was pipetted into 1.5 mL centrifuge tubes and stored at -80°C for later use.

Brain tissue minus the cerebellum (0.25-0.35g) recovered from mice were immediately frozen in liquid nitrogen (-80°C) till they were homogenised. The brain weight was recorded for each individual animal. After thawing, tissues were boiled for 10 minutes in 30 volumes of a mixture of 1M of acetic acid (99-100%, VWR International), 0.02M of hydrochloric acid (36%, VWR International) and 0.1% 2-mercaptoethanol (\geq 99.0%, Fluka) (De Ceballos et al. 1991; Ahmed et al. 1994; Wu et al. 2005). The tissues were homogenised with 80 strokes per minute for half a minute with a glass 3 mL homogeniser (Jencons-PLS, England). The homogenate was transferred in 15 mL centrifuge tubes and was centrifuged to remove any debris at 9,000 rpm for 20 minutes at 4°C with a Hermle Z323 centrifuge (Hermle Laborteschink GmbH, VWR, UK). The pellet was discarded and the supernatant stored in glass 14 mL vials was frozen (-20°C) and lyophilised. The lyophilised samples were stored at -80°C for later use.

The lyophilised brain homogenate samples were reconstituted with 1 mL of Buffer A (1% Trifluoroacetic acid, 99.5% Acros Organics, Fischer Scientific) vortexed and centrifuged at 13,000 rpm for 20 minutes (MicroCentaur, MSE, London, UK). 100 μ L of plasma after thawing and a 100 μ L of Buffer A were centrifuged at 13,000 rpm for 20 minutes (MicroCentaur, MSE, London, UK) to acidify the plasma sample and remove interfering proteins. C18 silica solid phase extraction columns (Waters SEP-PAK, 200 mg C18, Bachem, UK) were equilibrated with 1 mL of Buffer B [60% Acetonitrile (\geq 99.9% Fischer Scientific), 1% Trifluoroacetic acid and 39% distilled water) and washed with 9 mL of Buffer A. 300 μ L of the supernatant of the reconstituted brain homogenate and the supernatant of the plasma without the pellet were loaded onto the equilibrated column. Then, the columns were washed with 6 mL of Buffer A and the washings were discarded. The peptides were eluted with 3 mL of Buffer B and collected in a 5 mL polypropylene tube (Sarstedt, UK). The eluates were dried under a stream of Nitrogen at 30°C using a sample concentrator (Dri-Block DB-3, Techne Sample Concentrator). The samples were then kept at -20°C until they were used for RIA quantitation.

5.3.4 Radioimmunoassay

Quantitation of the amount of Leucine^[5]-Enkephalin was according to the manufacturer's protocol (S-2118, Bachem, UK). The kit is based on the principle of competitive radioimmunoassay and it is 100% specific for Leucine^[5]-Enkephalin. Sensitivity of the assay is 9 pg per tube for Leucine^[5]-Enkephalin and the intra-assay variance is \leq 5%. An aliquot of samples or standards (100 μ L) diluted in RIA buffer (Y-1050) was incubated with 100 μ L of specific rabbit antiserum for 22 hours at 4°C. [¹²⁵I]-Tyr-Leucine^[5]-Enkephalin was added (100 μ L) and the samples and standards were left for a further 22 hours at 4°C to achieve appropriate sensitivity. The working tracer solutions were counted to be between ~12,000 – 12,500 cpm / 100 μ L after dilution with RIA buffer (Manufacturers recommended range between C_{100} = 10,000-15,000 cpm). After incubation, goat-anti-rabbit IgG (Immunoglobulin G) (100 μ L) was added as a secondary antibody followed by normal rabbit serum (100 μ L) and left for 90 minutes at room temperature. Addition of 500 μ L of RIA buffer followed and the standards and samples were centrifuged at 1700g for 20 minutes. The radioactivity of the precipitate (bound labelled antigen) and of supernatant (free labelled antigen) are counted by a

Perkin-Elmer (Packard) Cobra II Gamma Counter (Model E5002) (Rayne Building, University College London, UK) for 1 minute.

5.3.5 Tail-Flick Bioassay

Antinociception was assessed in mice using the tail flick warm water bioassay (D'Amour and Smith 1941; Mogil et al. 1999). The protruding distal part of the tail (~4-5cm) of confined mice in a Plexiglas restrainer was immersed in circulating warm water maintained at $55^{\circ}\text{C} \pm 0.1^{\circ}\text{C}$ (Tjolsen and Hole 1993; Polt et al. 1994) by a thermostatically controlled water bath (W14, Grant Instruments, Cambridge Ltd, Herts, UK). Before any experiment was performed the temperature was checked using a thermometer (Gallenkamp, Griffin, THL-333-020L, 76 mm x 1mm, UK). The response latency times, in centiseconds, recorded for each mouse to withdraw its tail by a “sharp flick” were recorded using a digital stopwatch capable of measuring $1/100^{\text{th}}$ of a second. The first sign of a rapid tail flick will be taken as the behavioural endpoint which followed in most cases 1-3 slow tail movements. Three separate withdrawal latency determinations (separated by $\geq 20\text{sec}$) were averaged (Polt et al. 1994) and individual time points were at least 10 minutes apart. The tail of the mice were wiped dry immediately after testing to prevent the hot water from clinging to the tail producing erythema. Mice not responding within 5 sec will be excluded for further testing (Baseline cut-off = 5 seconds) and the baseline latency was measured for all mice 2 hours prior testing. Maximum possible cut-off was set to 10 seconds to avoid unnecessary damage to the tail (Tjolsen and Hole 1993). A maximum score will be assigned (100%) to animals not responding within 10 seconds. The response times were then converted to percentage of maximum possible effect (% MPE) by a method reported previously (Polt et al. 1994) with the following equation:

$$\% \text{ MPE} = \frac{(\text{Test Latency} - \text{Baseline Latency}) \times 100}{10 - \text{Baseline Latency}} \quad (\text{Equation 5.1})$$

Thus, if Test Latency is i.e. 9.8 seconds (or 980 centiseconds) and the Baseline Latency is 2.20 seconds (or 220 centiseconds) the % MPE was found to be

$$\% \text{ MPE} = \frac{(9.8 - 2.20) \times 100}{10 - 2.20} = \frac{760}{7.8} = 97.44\%$$

Data are presented as the mean \pm SEM for groups of 8 mice per arm of intravenous delivery studies or 16 mice per arm of oral delivery studies. Data are also presented in the quantal form of the tail flick test (number of mice that exhibited maximum latencies to thermal stimuli) which ensures no false positive responses (D'Amour and Smith 1941). An analgesic responder was defined as one whose response tail flick latency was two or more times the value of the baseline latency (Shimoyama et al. 1997).

5.3.6 Statistical Analysis

All pharmacokinetic results were expressed as mean \pm standard error (SEM: SD / \sqrt{n} , where SD is the standard deviation and n is the number of animals). The Student's t-test (Microsoft Excel) was used to assess any statistically difference among the means for the two arms of the studies. A p-value less than 0.05 was considered as a representation of significant difference. All tail-flick results were expressed as mean \pm standard error. A one-way ANOVA test using Minitab 16 was done to assess any statistically difference among the means of % MPE for the different arms of the study. A post-hoc analysis (Tukey's Test) was performed to determine the groups, which show significant difference. In each case, a p-value less than 0.05 was considered as a representation of significant difference. Plasma half-life calculations were performed by assuming expodential decay in Origin 6.

5.4 Results

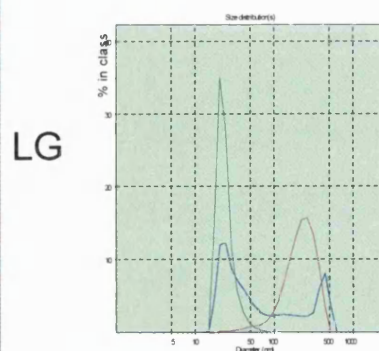
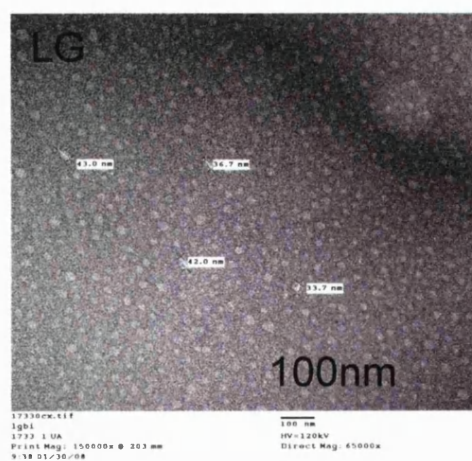
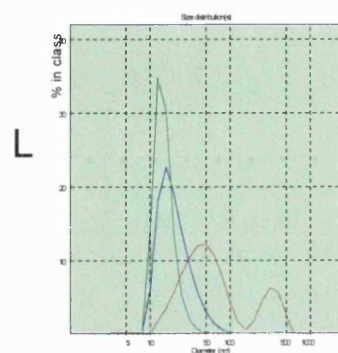
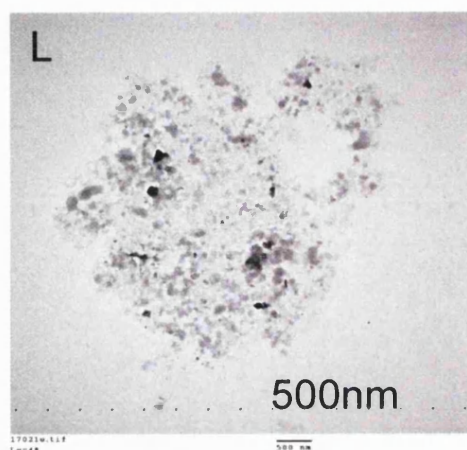
Table 5.3 summarises the mean particle size, polydispersity and HPLC peptide content for all formulations used *in vivo* studies. HPLC calibration curve equations used for extrapolation of peptide content in the formulation (after filtration in the case of IV formulations) were:

$$y = 8280.4x + 30884 \quad (r^2 = 0.9934) \text{ for Leucine}^{151}\text{-Enkephalin} \quad (\text{Equation 5.2})$$

and $y = 1449.2x + 6000.6$ ($r^2 = 0.9942$) TPLENK

(Equation 5.3)

respectively. TEM images for IV formulations and SEM images of the oral formulations are shown (Figure 5.5).



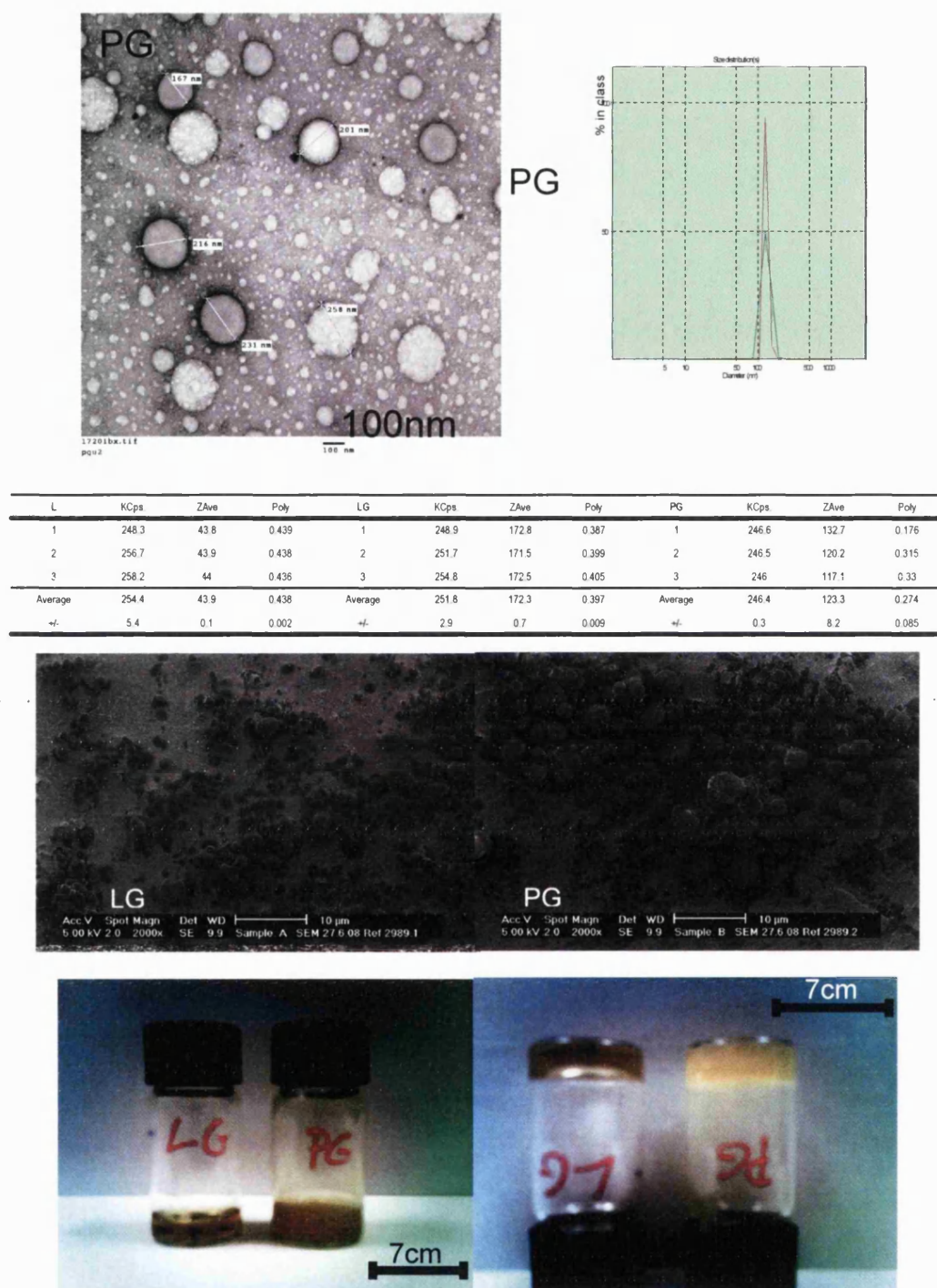


Figure 5.5: Top Right: Negative stained TEM images for L (5 mg mL⁻¹), LG and PG (3 mg mL⁻¹, 1: 2.3 w/w peptide to GCPQ) in NaCl 0.9% (L & LG filtered through 0.22µm and PG through 0.8 µm). Top Left: Mean particle size of above formulations along with their mean distributions (red: intensity, blue: volume, green: number) from PCS after filtration (triplicates). Bottom: SEM images and macroscopic appearance of LG and PG unfiltered formulations for oral administration (Bar: 10µm and 7cm).

Table 5.3: Formulations characterisation results for *in vivo* studies.

Route	Arms	L Dose (mg/kg)	GCPQ P%: Q%	C (mg/ ml)	Filte -red	Zave (nm)	Polydi- spersity	HPLC Reco- vered %	Vol (μL)
Pharmacokinetics:									
IV	NaCl	0	N/A	0	0.22 μm				
	L	25	N/A	5	0.22 μm	43.9	0.438	75	120-160
	LG	25	18.7:8.3	5	0.22 μm	159.7	0.89	95	95-125
IV	LG	10	18.7:8.3	3	0.8 μm	172.3	0.397	75	80-110
	PG	14.3 ≡ 10	18.7:8.3	3	0.8 μm	123.3	0.274	40	195-200
IV	LG	8.9	17.5:14.4	3	0.8 μm	192.2	0.599	98	55-75
	PG	12.75 ≡ 8.9	17.5:14.4	3	0.8 μm	191.7	0.329	58	130-180
PO	H ₂ O	0	N/A	0	-				
	L	25	N/A	5	-			100	90-120
	LG	25	24.5:8.1	5	-			99	90-120
	PG	37.5 ≡ 25	24.5:8.1	5	-			98	135-185
PO	H ₂ O	0	N/A	0	-				
	L	70	N/A	15	-			100	85-115
	LG	70	18.6:10.4	15	-			99	90-115
	PG	100 ≡ 70	18.6:11.2	15	-			99	120-165
Pharmacodynamics:									
IV	NaCl	0	N/A	0	0.8 μm				
	L	14	N/A	3	0.8 μm			82	125-160
	LG	14	19.5:7.9	3	0.8 μm	103.5	0.845	77	135-170
	PG	20 ≡ 14	18.0:11.8	3	0.8 μm	162.9	0.692	70	205-210
PO	H ₂ O	0	N/A	0					
	L	70	N/A	15				100	105-130
	LG	70	18.0:11.8	15				99	105-130
	PG	100 ≡ 70	18.6:10:4	15				98	150-190

Key; Vol: Administered Volume, P%: Palmitoylation, Q: Quaternisation, C: Peptide Concentration, N/A: Not applicable, IV: Intravenous, PO: Oral, L: Leucine^[6]-Enkephalin, LG: Leucine^[6]-Enkephalin & GCPQ, PG: TPLENK & GCPQ, ≡: signifies the weight in mg of molar equivalent doses

Calibration graphs for RIA quantitation were plotted based on the gamma counter readings using Microsoft Excel (Figure 5.6) to show the relationship of amount of unlabelled antigen added to the ratio of bound and free labelled antigen of the tested standards. The concentration of unknown antigen in test sample was extrapolated from the calibration graph for every kit.

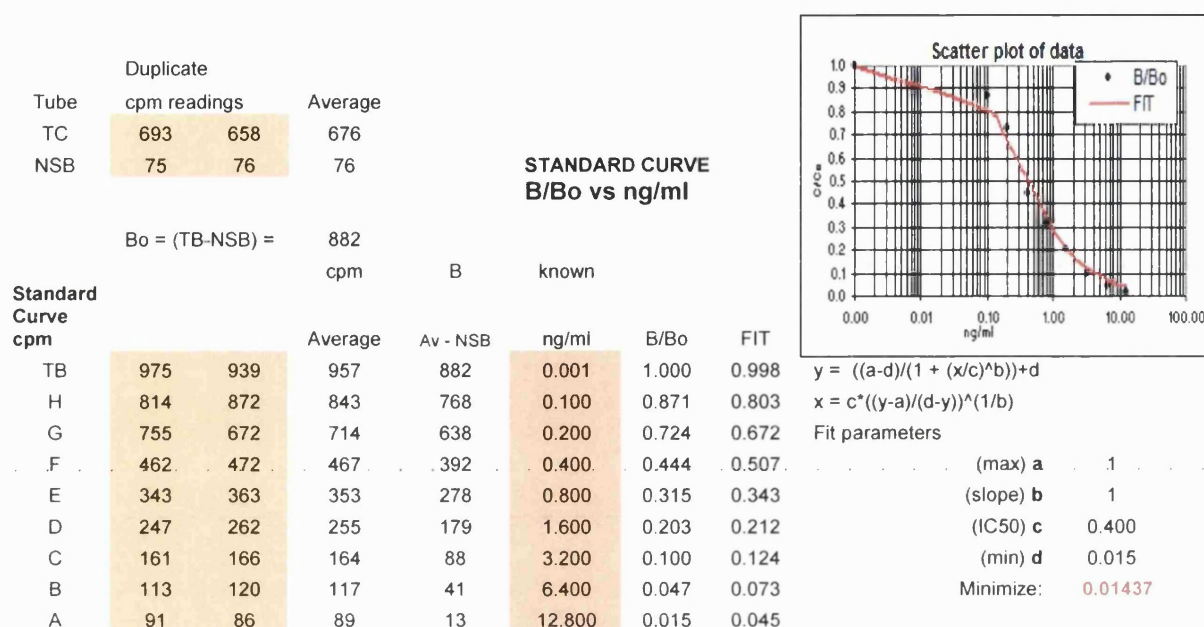


Figure 5.6: Example of RIA standard curve plotted in Microsoft Excel used for extrapolation of concentrations of samples [B: Bound tracer concentration, B₀: Value of B when no unlabeled antigen is added to tracer, T_B: Total binding, T_C: Total counts (total number of cpm added to each RIA tube), NSB: Nonspecific binding].

The preliminary pharmacokinetics of L, LG, PG formulations following IV and oral administration was studied in mice. A molar equivalent dose of TPLENK was used for the IV and oral studies (Table 5.2). Since the original radioimmunoassay was developed specifically for Leucine¹⁵¹-Enkephalin, when analysing TPLENK samples only the amount of TPLENK bioconverted *in vivo* to Leucine¹⁵¹-Enkephalin was quantified. For calculation of the % of dose of Leucine¹⁵¹-Enkephalin in plasma per animal, the total amount of plasma per animal was needed and 31.5 µL of plasma per g of animal weight was accepted (Pinkerton et al. 1970; He et al. 2002). Similarly, the brain minus the cerebellum of each animal was weighed and the weight used for % of dose of Leucine¹⁵¹-Enkephalin in brain. Results are shown as % of Leucine¹⁵¹-Enkephalin

administered dose and as concentration recovered from plasma ($\text{ng } 10^{-1}\text{mL}^{-1}$) or from brain tissue in (ng g^{-1}). There was no recovery of Leucine¹⁵¹-Enkephalin after placebo doses administration. No statistical significant difference was obtained between IV

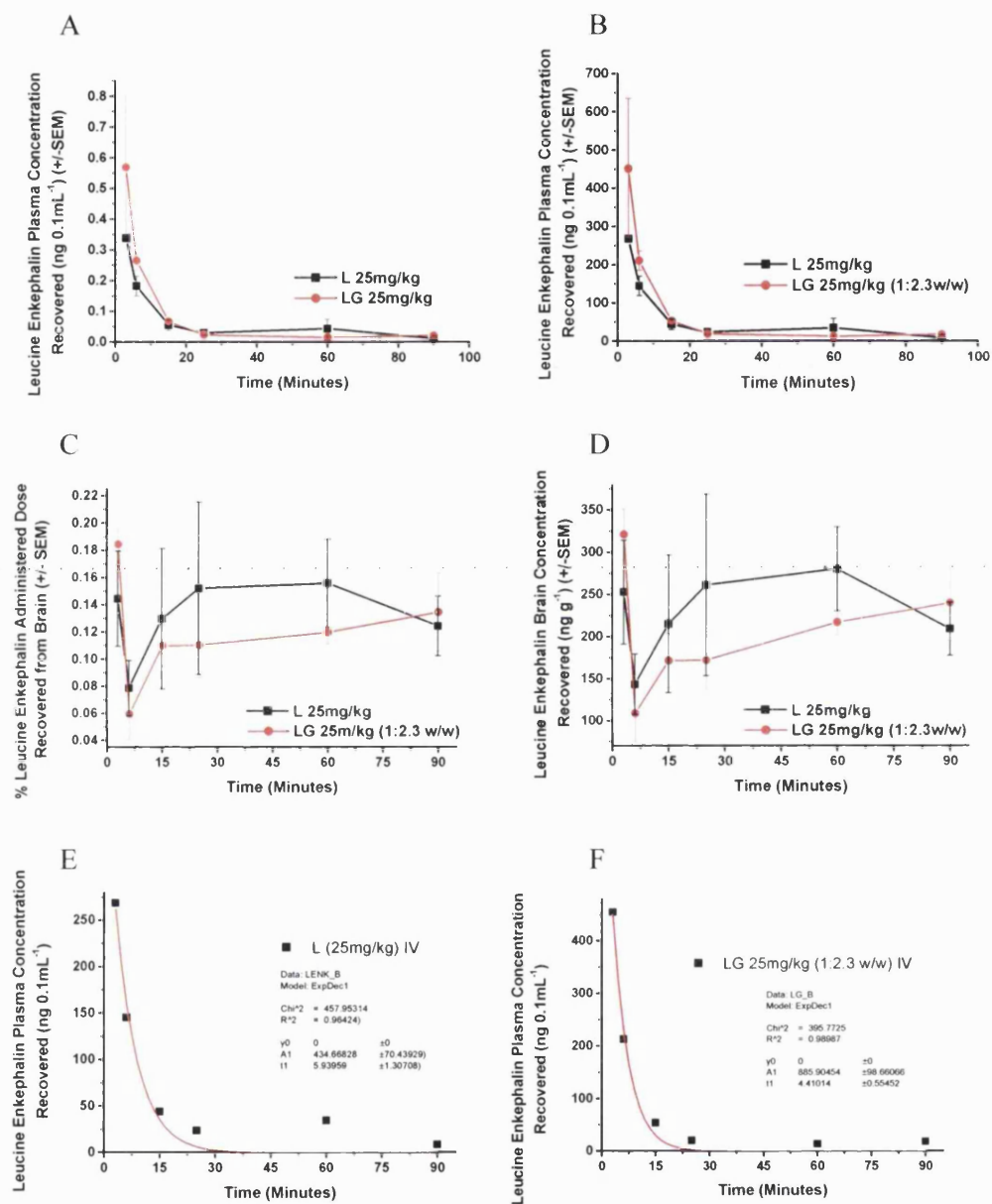


Figure 5.7: Intravenous Study: **A, B:** Leucine¹⁵¹-Enkephalin recovered as % of dose and concentration ($\text{ng } 0.1\text{mL}^{-1}$) in plasma respectively. **C, D:** Leucine¹⁵¹-Enkephalin recovered as % of dose and concentration (ng g^{-1}) in brain respectively. **E, F:** Expodential decay (first order) fitted curves for calculation of Leucine¹⁵¹-Enkephalin half-life in the absence and presence of GCPQ respectively.

administration of the nanoparticulate formulation of Leucine^[5]-Enkephalin to the peptide alone (Figure 5.7, Table 5.4). However, the plasma half-life was increased by 1.4 fold when the nanoparticulate formulation was used (Figure 5.7 E, F). The plasma half-life was increased by 3.2 fold when the nanoparticulate formulation of the lipidic peptide (PG) was used versus the nanoparticulate formulation of Leucine^[5]-Enkephalin (LG) and the AUC₍₀₋₂₄₀₎ in the brain was increased by 1.5 fold

Table 5.4: Summary of % of dose and concentration of Leucine^[5]-Enkephalin recovered after IV administration (n=4) of L and LG (25mg kg⁻¹) in plasma and brain samples quantified using RIA (Student's t-test, p-values significant: p≤0.05) (PG AUC (0-240):

% Dose Leucine Enkephalin Administered Dose Recovered from Plasma (±SEM) (n=4)						Recovered
Time (Minutes)	3	6	15	25	60	90
L	0.1249	0.024405	0.007752	0.003982	0.00587	0.001458
L SEM	0.077609	0.004492	0.002408	0.001009	0.00427	0.001119
LG	0.074266	0.037545	0.010826	0.003614	0.002109	0.002959
LG SEM	0.026621	0.005346	0.001522	0.000227	0.000517	0.001153
p-value	0.573123	0.110321	0.329064	0.743265	0.444554	0.385925
Leucine Enkephalin Concentration (ng/0.1mL) Recovered from Plasma (±SEM) (n=4)						
Time (Minutes)	3	6	15	25	60	90
L	268.6768	145.0453	43.82338	23.54326	34.23391	8.456761
L SEM	8.650489	25.57392	14.0253	6.117501	24.40597	6.548926
LG	454.2688	212.9142	53.75909	19.81642	12.94406	17.62768
LG SEM	182.8451	25.46159	6.999737	1.557863	3.310872	6.321233
p-value	0.384998	0.109055	0.557593	0.592042	0.448888	0.352598
% Dose Leucine Enkephalin Administered Dose Recovered from Brain (±SEM) (n=4)						
Time (Minutes)	3	6	15	25	60	90
L	0.144402	0.078678	0.1296	0.152044	0.155819	0.124401
L SEM	0.03491	0.02038	0.051675	0.063215	0.032355	0.021893
LG	0.184649	0.059913	0.110365	0.110732	0.120255	0.135023
LG SEM	0.011888	0.018695	0.015526	0.023485	0.00868	0.028418
p-value	0.341264	0.522919	0.741704	0.574779	0.357365	0.777767
Leucine Enkephalin Concentration (ng/g) Recovered from Brain (±SEM) (n=4)						
Time (Minutes)	3	6	15	25	60	90
L	252.8849	143.4403	215.141	261.1518	280.06	209.1433
L SEM	61.57782	35.99944	81.68801	107.4796	49.79841	31.33436
LG	321.5581	109.4882	172.2887	172.6711	217.3834	240.2502
LG SEM	29.65055	33.85053	32.07763	34.34129	15.19284	44.24384
p-value	0.367903	0.517784	0.651502	0.481225	0.302667	0.589186

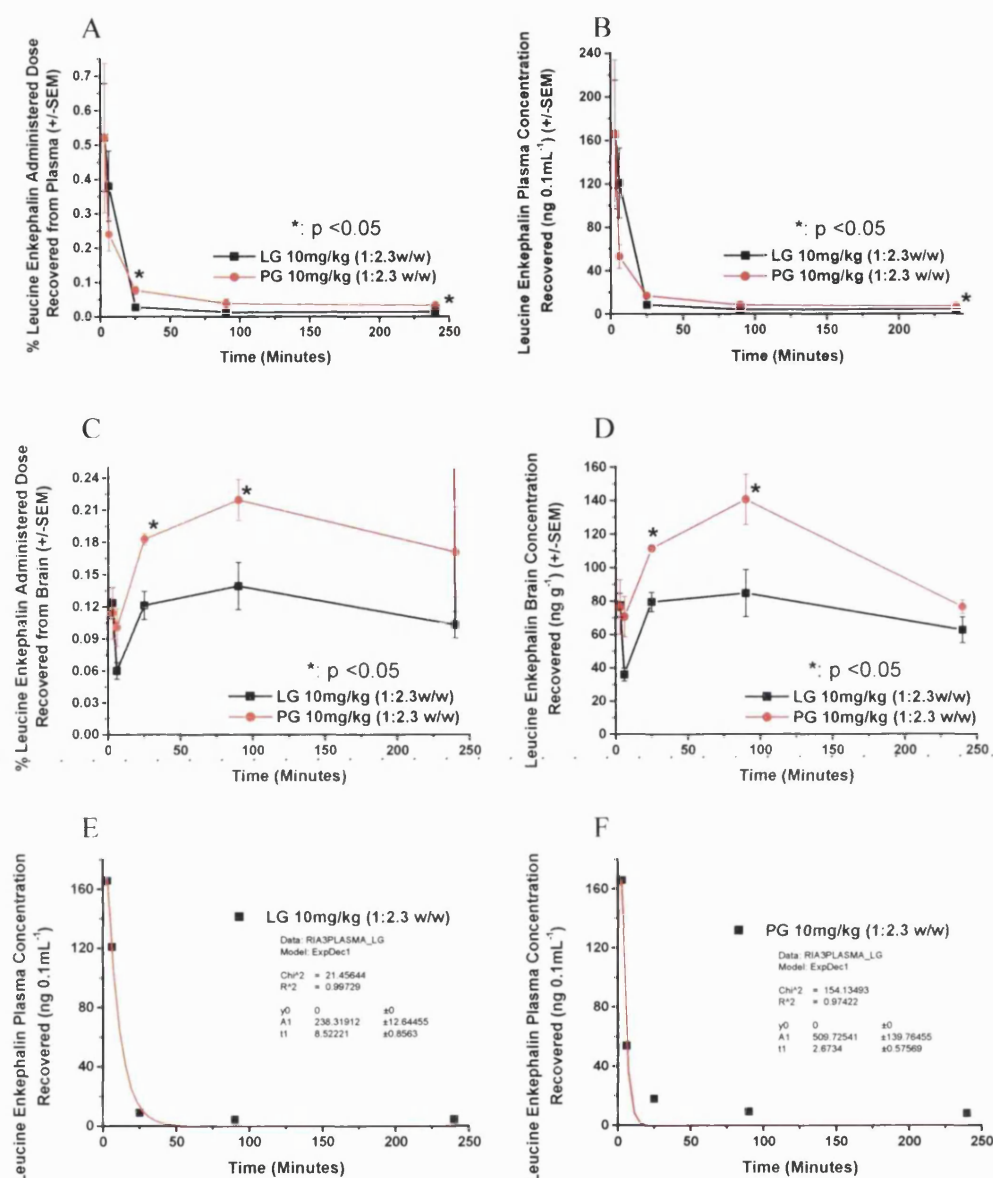


Figure 5.8: Intravenous study: **A, B:** Leucine¹⁵¹-Enkephalin recovered as % of dose and concentration (ng 0.1mL⁻¹) in plasma respectively. **C, D:** Leucine¹⁵¹-Enkephalin recovered as % of dose and concentration (ng g⁻¹) in brain respectively. **E, F:** Exponential decay (first order) fitted curves for calculation of Leucine¹⁵¹-Enkephalin or TPLENK half-life in the presence of GCPQ respectively.

(26435.2 ng g⁻¹ min vs LG AUC (0-240): 17644.5 ng g⁻¹ min, Figure 5.8, Table 5.5). Repeating the IV study of the nanoparticulate formulation of TPLENK to nanoparticulate formulation of the parent peptide (with a slightly lower dose) gave a similar increase (1.4 fold) in AUC₍₀₋₂₄₀₎ (PG AUC₍₀₋₂₄₀₎: 398.2 ng g⁻¹ min vs LG AUC

(0-240): 289.1 ng g⁻¹ min, Figure 5.9, Table 5.6). Statistical significant plasma and brain levels were achieved for the nanoparticulate formulation of the lipidic peptide at 25 (p = 0.023) and 240 (p = 0.017) minutes in plasma and 25 (p = 0.012) and 90 (p = 0.033) minutes in brain (Figure 5.8, Table 5.5).

Table 5.5: Summary of % of dose and concentration of Leucine^[5]-Enkephalin recovered after IV administration (n=4) of LG and PG (10mg kg⁻¹) in plasma and brain samples quantified using RIA (Student's t-test, p-values significant: p≤0.05)

% Dose Leucine Enkephalin Administered Dose Recovered from Plasma (+/-SEM) (n=4)					
Time (Minutes)	3	6	25	90	240
LG	0.522106	0.380899	0.027749	0.01312	0.013849
LG SEM	0.156816	0.101665	0.001677	0.003777	0.001657
PG	0.522848	0.242655	0.08004	0.041575	0.035502
PG SEM	0.216587	0.047992	0.012364	0.013986	0.004921
p-value	0.997883	0.28218	0.02307	0.132542	0.016749

Leucine Enkephalin Concentration (ng/0.1mL) Recovered from Plasma (+/-SEM) (n=4)					
Time (Minutes)	3	6	25	90	240
LG	165.7479	120.9205	8.809048	4.164991	4.396662
LG SEM	49.78298	32.27449	0.532278	1.199079	0.525951
PG	165.9836	53.92333	17.78675	9.238801	7.889324
PG SEM	68.75776	10.66485	2.747665	3.107947	1.093528
p-value	0.997883	0.126844	0.204671	0.204671	0.041178

% Dose Leucine Enkephalin Administered Dose Recovered from Brain (+/-SEM) (n=4)					
Time (Minutes)	3	6	25	90	240
LG	0.123679	0.059958	0.12144	0.139332	0.103056
LG SEM	0.014557	0.007792	0.013074	0.021938	0.01221
PG	0.114482	0.101161	0.183418	0.22001	0.171274
PG SEM	0.02412	0.017773	0.00521	0.019197	0.042035
p-value	0.76732	0.099099	0.012132	0.033125	0.204009

Leucine Enkephalin Concentration (ng/g) Recovered from Brain (+/-SEM) (n=4)					
Time (Minutes)	3	6	25	90	240
LG	77.47556	35.98262	79.47912	84.70911	62.50861
LG SEM	7.115212	3.824911	5.753296	14.01518	7.711346
PG	76.55465	70.75672	111.5095	140.8147	76.28106
PG SEM	16.23113	12.12868	1.420124	15.09783	4.084158
p-value	0.997702	0.058765	0.008599	0.034672	0.180893

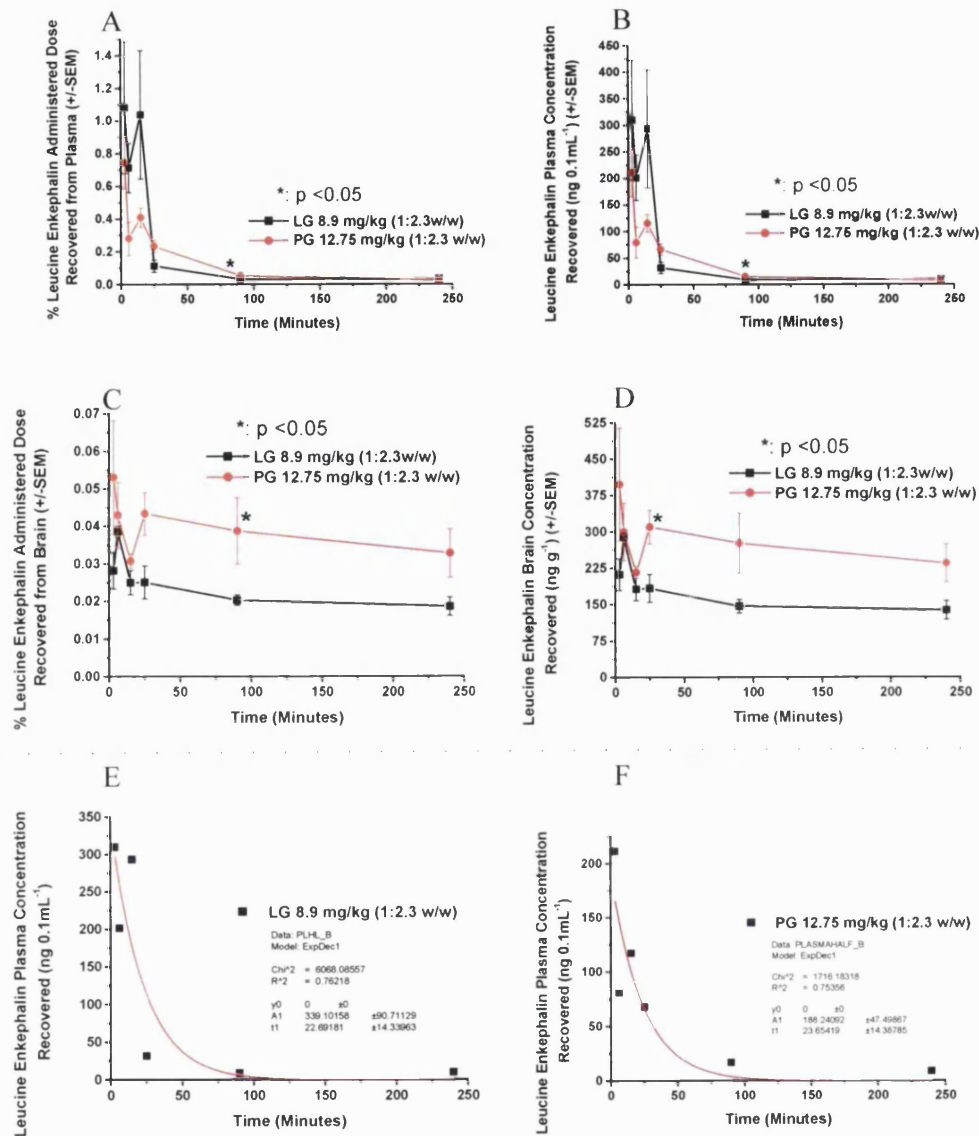


Figure 5.9: Intravenous study: **A, B:** Leucine^[51]-Enkephalin recovered as % of dose and concentration (ng 0.1mL⁻¹) in plasma respectively. **C, D:** Leucine^[51]-Enkephalin recovered as % of dose and concentration (ng g⁻¹) in brain respectively. **E, F:** Exponential decay (first order) fitted curves for calculation of Leucine^[51]-Enkephalin or TPLENK half-life in the presence of GCPQ respectively.

Table 5.6: Summary of % of dose and concentration of Leucine^[5]-Enkephalin recovered after IV administration (n=4) of LG and PG (8.9 mg kg⁻¹) in plasma and brain samples quantified using RIA (Student's t-test, p-values significant: p≤0.05).

% Dose Leucine Enkephalin Administered Dose Recovered from Plasma (+/-SEM) (n=4)						
Time (Minutes)	3	6	15	25	90	240
LG	1.0821062	0.7128262	1.0382154	0.1123503	0.0309886	0.0344865
LG SEM	0.4028596	0.1504708	0.393215	0.0373308	0.0009447	0.0066537
PG	0.7485385	0.2864151	0.4148543	0.2400507	0.058616	0.0305612
PG SEM	0.1566838	0.1019945	0.0587704	0.0372538	0.0053878	0.0014351
p-value	0.4845254	0.0632181	0.211067	0.0517679	0.012947	0.6013868
Leucine Enkephalin Concentration (ng/0.1mL) Recovered from Plasma (+/-SEM) (n=4)						
Time (Minutes)	3	6	15	25	90	240
LG	310.01402	201.40169	293.33704	31.743406	8.755516	9.7438073
LG SEM	112.06821	42.513975	111.09885	10.547436	0.2669292	1.879942
PG	211.49184	80.923627	117.2128	67.823848	16.561351	8.6347448
PG SEM	44.269397	28.817504	16.604959	10.525665	1.5222598	0.4054798
p-value	0.4604081	0.0632181	0.211067	0.0517679	0.012947	0.6013868
% Dose Leucine Enkephalin Administered Dose Recovered from Brain (+/-SEM) (n=4)						
Time (Minutes)	3	6	15	25	90	240
LG	0.0281832	0.0386106	0.0249959	0.0250851	0.0203179	0.0186066
LG SEM	0.0048747	0.0014189	0.0032093	0.0043885	0.0014127	0.0024378
PG	0.0531983	0.043075	0.0307883	0.0434812	0.0388316	0.0328338
PG SEM	0.0151585	0.0088078	0.0019199	0.0056725	0.0088366	0.0064288
p-value	0.1987497	0.6496135	0.183233	0.0450273	0.1259544	0.1101216
Leucine Enkephalin Concentration (ng/g) Recovered from Brain (+/-SEM) (n=4)						
Time (Minutes)	3	6	15	25	90	240
LG	211.78986	289.07844	181.90243	183.53174	146.43155	137.78148
LG SEM	32.954469	7.6991436	23.4654	28.538399	13.885312	19.358858
PG	398.18902	300.19446	216.72168	310.32858	276.36921	234.28262
PG SEM	116.29602	59.354459	11.786248	34.759324	62.277778	38.914478
p-value	0.2083077	0.8641482	0.249181	0.0316323	0.1262331	0.0844618

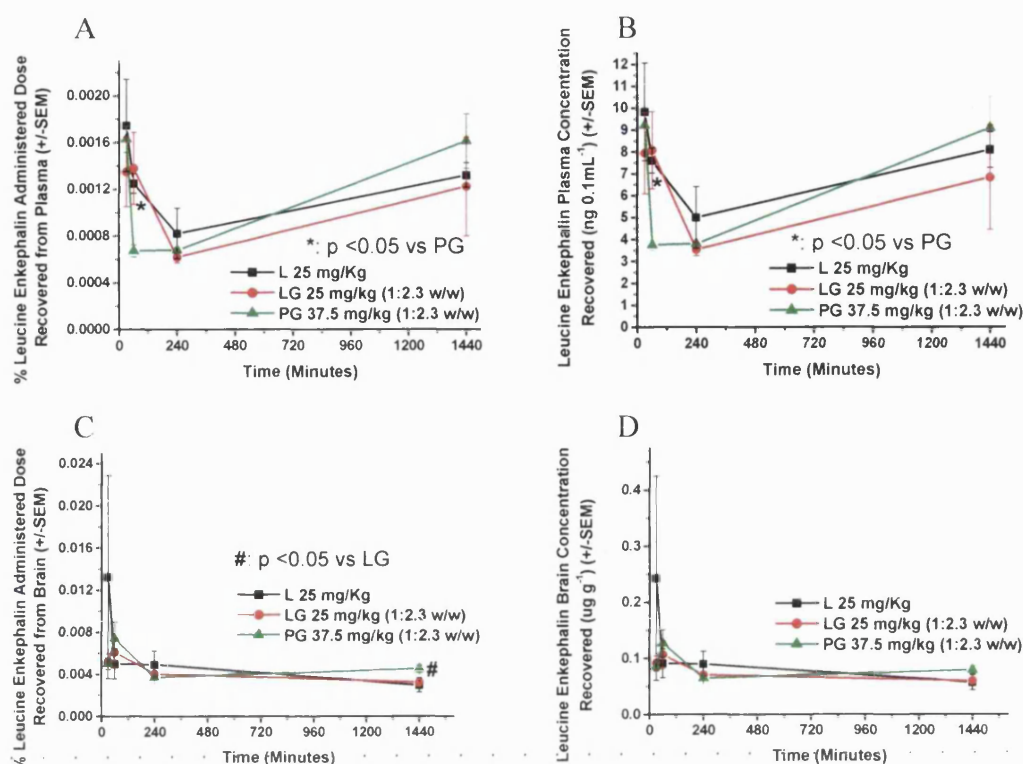


Figure 5.10: Oral Study: **A, B**: Leucine¹⁵¹-Enkephalin recovered as % of dose and concentration (ng 0.1mL⁻¹) in plasma respectively. **C, D**: Leucine¹⁵¹-Enkephalin recovered as % of dose and concentration (μg g⁻¹) in brain respectively.

The concentration of Leucine¹⁵¹-Enkephalin following oral administration peaked at 30 minutes for L and PG formulations (L: 9.8 ng 10⁻¹mL⁻¹ and PG: 9.2 ng 10⁻¹mL⁻¹) and 1 hour for LG (8.1 ng 10⁻¹mL⁻¹) in plasma and at 30 minutes for Leucine¹⁵¹-Enkephalin formulation (L: 0.243 μg g⁻¹) and at 1 hour for LG and PG formulations (LG: 0.107 μg g⁻¹, PG: 0.127 μg g⁻¹) in the brain tissue (Figure 5.10, Table 5.7). The only statistically significantly different plasma levels were achieved for Leucine¹⁵¹-Enkephalin versus the nanoparticulate formulation of the lipidic peptide (PG) at 1 hour (p = 0.004) in plasma.

Table 5.7: Summary of % of dose and concentration of Leucine^[5]-Enkephalin recovered after oral administration (n=4) of L and LG (25 mg kg⁻¹) and PG (37.5mg kg⁻¹) in plasma and brain samples quantified using RIA (Student's t-test, p-values significant: p≤0.05).

% Dose Leucine Enkephalin Administered Dose Recovered from Plasma (+/-SEM) (n=4)					% Dose Leucine Enkephalin Administered Dose Recovered from Brain (+/-SEM) (n=4)				
Time (Minutes)	30	60	240	1440	Time (Minutes)	30	60	240	1440
L	0.0017478	0.0012514	0.0008211	0.0013181	L	0.0132306	0.0049898	0.0049473	0.0029719
L SEM	0.0003955	8.432E-05	0.000218	0.0001064	L SEM	0.0096271	0.0014253	0.0012718	0.0006715
LG	0.00135	0.0013814	0.0006159	0.0012169	LG	0.0051843	0.006061	0.0040369	0.0032237
LG SEM	0.0002981	0.0003096	4.612E-05	0.0004237	LG SEM	0.0007559	0.0013549	0.0001741	0.000286
PG	0.0016293	0.0006723	0.0006768	0.0016147	PG	0.0049684	0.0073878	0.0036653	0.0044909
PG SEM	0.0001143	5.145E-05	2.499E-05	0.0002326	PG SEM	0.0005545	0.0015538	0.0001668	0.0003637
p-value					p-value				
L vs LG	0.4525019	0.6994482	0.3925611	0.8244122	L vs LG	0.4366207	0.6055864	0.5047649	0.7418542
LG vs PG	0.4153668	0.0645727	0.2897834	0.4419717	LG vs PG	0.8255188	0.5436451	0.1741791	0.0337983
PG vs L	0.7831394	0.0010877	0.5351	0.2903337	PG vs L	0.4244492	0.2987805	0.3561254	0.0938232

Leucine Enkephalin Concentration (ng/0.1mL) Recovered from Plasma (+/-SEM) (n=4)					Leucine Enkephalin Concentration (µg/g) Recovered from Brain (+/-SEM) (n=4)				
Time (Minutes)	30	60	240	1440	Time (Minutes)	30	60	240	1440
L	9.833385	7.6063727	5.0050363	8.1060087	L	0.242805	0.0913839	0.0902512	0.0570216
L SEM	2.2376067	0.5748181	1.4060867	0.8142462	L SEM	0.1817101	0.0257506	0.0225078	0.0136683
LG	7.9398172	8.0796186	3.5439576	6.8343239	LG	0.0917916	0.1069771	0.070373	0.0596029
LG SEM	1.8592397	1.7626406	0.2981414	2.3839768	LG SEM	0.012662	0.0244974	0.0031199	0.0049625
PG	9.2090464	3.7465376	3.79578	9.0962093	PG	0.0856497	0.1267106	0.0645611	0.079055
PG SEM	0.8460317	0.2283801	0.1022349	1.4288532	PG SEM	0.0083053	0.0240835	0.0026042	0.0073014
p-value					p-value				
L vs LG	0.540013	0.8123217	0.3786115	0.642338	L vs LG	0.4673413	0.6762519	0.4438965	0.8682133
LG vs PG	0.5665712	0.0898955	0.4724895	0.4534035	LG vs PG	0.7012543	0.586557	0.2041515	0.0758484
PG vs L	0.8074949	0.003581	0.4534912	0.5746153	PG vs L	0.4509138	0.3552107	0.3373387	0.2193996

The concentration of Leucine^[5]-Enkephalin following oral administration peaked at 1 hour for L and LG formulations (L: 29.3 ng 10⁻¹mL⁻¹ and LG: 26.6 ng 10⁻¹mL⁻¹) and 30 minutes for PG (17.1 ng 10⁻¹mL⁻¹) in plasma and at 4 hours in the brain tissue for all three formulations (L: 0.695 µg g⁻¹, LG: 1.090 µg g⁻¹, PG: 1.098 µg g⁻¹). The AUC₍₀₋₁₄₄₀₎ in the plasma was increased by 1.2 and 1.3 fold for the nanoparticulate formulations of LENK and TPLENK respectively (LG AUC₍₀₋₁₄₄₀₎: 16547.7 ng g⁻¹ min and PG AUC₍₀₋₁₄₄₀₎: 18216.0 ng g⁻¹ min versus L AUC₍₀₋₁₄₄₀₎: 13768.5 ng g⁻¹ min, Figure 5.11, Table 5.8). The AUC₍₀₋₁₄₄₀₎ in the brain was increased by 1.7 fold for both nanoparticulate formulations (LG and PG) (LG AUC₍₀₋₁₄₄₀₎: 1000.9 µg g⁻¹ min and PG

AUC₍₀₋₁₄₄₀₎: 984.8 $\mu\text{g g}^{-1} \text{ min}$ versus L AUC₍₀₋₁₄₄₀₎: 595.2 $\mu\text{g g}^{-1} \text{ min}$, Figure 5.11, Table 5.8). Statistically significantly different plasma and brain levels were achieved: for the nanoparticulate formulation of the lipidic peptide (PG) versus Leucine^[51]-Enkephalin at 4 hours ($p = 0.001$) in plasma and 1 hour ($p = 0.006$), 4 hours ($p = 0.017$) and 24 hours ($p = 0.019$) minutes in brain and versus LG at 4 hours ($p = 0.013$) in plasma; for the nanoparticulate formulation of Leucine^[51]-Enkephalin (LG) at 4 hours ($p = 0.030$) and 24 hours ($p = 0.013$) minutes in brain.

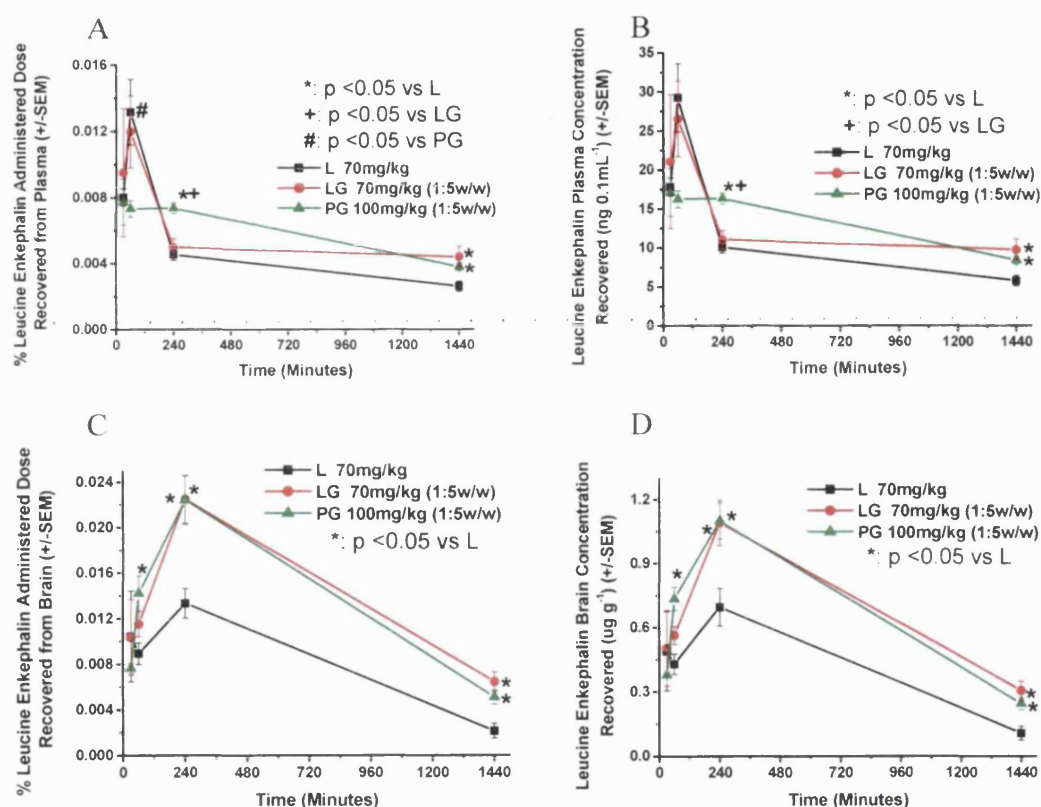


Figure 5.11: Oral Study: **A, B:** Leucine^[51]-Enkephalin recovered as % of dose and concentration ($\text{ng } 0.1\text{mL}^{-1}$) in plasma respectively. **C, D:** Leucine^[51]-Enkephalin recovered as % of dose and concentration ($\mu\text{g g}^{-1}$) in brain respectively.

Table 5.8: Summary of % of dose and concentration of Leucine^[5]-Enkephalin recovered after oral administration (n=4) of L and LG (70mg kg⁻¹) and PG (100mg kg⁻¹) in plasma and brain samples quantified using RIA (Student's t-test, p-values significant: p≤0.05).

% Dose Leucine Enkephalin Administered Dose Recovered from Plasma (+/-SEM) (n=4)					% Dose Leucine Enkephalin Administered Dose Recovered from Brain (+/-SEM) (n=4)				
Time (Minutes)	30	60	240	1440	Time (Minutes)	30	60	240	1440
L	0.008019	0.013164	0.004545	0.002596	L	0.010416	0.008924	0.013341	0.002132
L SEM	0.000515	0.00197	0.000332	0.000308	L SEM	0.003983	0.000947	0.001304	0.000655
LG	0.009485	0.011951	0.004964	0.004373	LG	0.010306	0.011494	0.022467	0.006387
LG SEM	0.003865	0.002169	0.000535	0.00061	LG SEM	0.003321	0.001103	0.002112	0.000854
PG	0.007692	0.007281	0.007333	0.003762	PG	0.007577	0.014172	0.022385	0.005032
PG SEM	0.001394	0.000493	0.000319	0.000227	PG SEM	0.000454	0.001544	0.00213	0.000623
p-value					p-value				
L vs LG	0.719807	0.693454	0.529985	0.040512	L vs LG	0.983784	0.127609	0.01037	0.007481
LG vs PG	0.677807	0.08056	0.00895	0.384016	LG vs PG	0.446505	0.20786	0.979191	0.247062
PG vs L	0.833299	0.027444	0.00092	0.022552	PG vs L	0.505331	0.027454	0.011079	0.018372
Leucine Enkephalin Concentration (ng/0.1mL) Recovered from Plasma (+/-SEM) (n=4)					Leucine Enkephalin Concentration (ng/g) Recovered from Brain (+/-SEM) (n=4)				
Time (Minutes)	30	60	240	1440	Time (Minutes)	30	60	240	1440
L	17.8194	29.25279	10.09892	5.76904	L	0.489058	0.428628	0.694883	0.105691
L SEM	1.14516	4.377709	0.738523	0.683646	L SEM	0.18495	0.047341	0.08848	0.031797
LG	21.07799	26.55855	11.03183	9.718276	LG	0.504117	0.563176	1.090202	0.303242
LG SEM	8.58899	4.821082	1.189512	1.354588	LG SEM	0.176008	0.042063	0.106865	0.043996
PG	17.09321	16.17989	16.29602	8.360811	PG	0.376787	0.732811	1.097522	0.241579
PG SEM	3.098703	1.095453	0.70883	0.505344	PG SEM	0.014149	0.054367	0.085424	0.028031
p-value					p-value				
L vs LG	0.731089	0.693583	0.534643	0.05404	L vs LG	0.954885	0.078421	0.030336	0.012779
LG vs PG	0.686374	0.11815	0.013132	0.40327	LG vs PG	0.52235	0.051126	0.959146	0.289446
PG vs L	0.837298	0.054355	0.000926	0.025043	PG vs L	0.587268	0.005802	0.016983	0.01887

Leucine^[5]-Enkephalin causes central analgesic effects in the brain with slight preference for δ -opioid receptor. Occurrence of central analgesic effects would prove the brain targeting of LENK-GCPQ particulate formulation and TPLENK-GCPQ particulate formulation in accordance with the preliminary pharmacokinetic data. LENK and physiologic sodium chloride (NaCl 0.9%) (pH 7.4) have been used as controls. LENK alone was used in order to observe the equipotent effect of this peptide in the same dose as in the particulate formulation and NaCl as a placebo to rule out the plausible effects of endogenously produced neuropeptides during antinociception testing.

Table 5.9: Tail Flick Bioassay summary of % Antinociception and Standard Error for different time points after IV administration in CD-1 mice (n = 8 / arm).

Time (Minutes)	Leucine Enkephalin (L)	SEM L	Leucine Enkephalin & GCPQ (LG)	SEM LG	PTLENK & GCPQ (PG)	SEM PG	NaCl	SEM NaCl
15	14.68649	11.32654	8.57482	6.95895	22.39985	11.01022	-6.24672	1.69086
25	21.1611	10.12007	18.46864	5.87792	40.53095	13.86995	0.03268	2.46079
45	6.64971	4.41094	24.74681	9.93288	63.17826	11.88423	0.27294	5.90708
60	21.15813	7.46451	52.33869	16.5511	62.876	17.33179	-2.26883	6.07352
90	3.16714	7.79669	56.0967	14.78388	61.18867	18.41156	0.31928	3.48786
120	12.70779	13.38113	50.16879	14.9031	73.48876	11.89332	-4.07166	3.75245
150	15.40307	9.92394	40.50673	13.16384	51.48884	12.6954	3.53267	5.62704
180	17.87253	13.95296	41.48998	7.94828	42.33692	12.82953	-6.38716	3.43098
210	12.32664	8.6689	24.96747	8.64481	22.10904	11.12288	-6.02787	3.41969

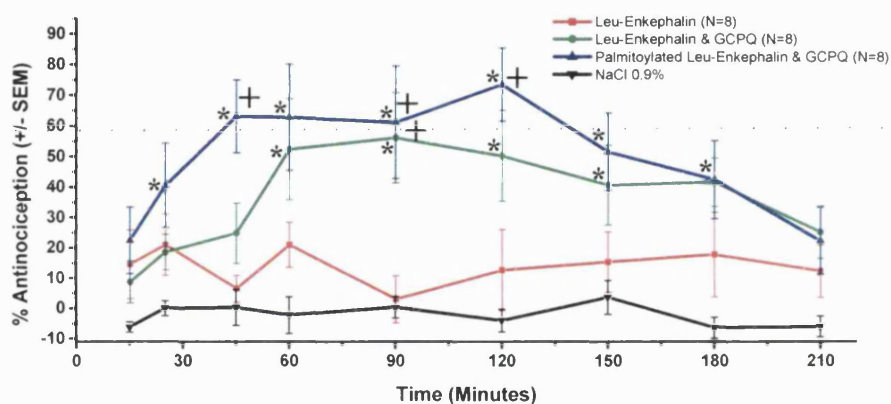


Figure 5.12: Tail Flick Bioassay; Top: Placebo/NaCl (black) Leucine^[5]-Enkephalin 14mg Kg⁻¹ (red), Leucine^[5]-Enkephalin: GCPQ 14mg Kg⁻¹ (1:2.3 w/w) (green), and Palmitoyl Tyrosyl Leucine^[5]-Enkephalin (TPLENK): GCPQ 20 mg Kg⁻¹ (blue) % Antinociception (Mean % MPE ± SEM) at equivalent doses after IV administration to CD-1 Mice (n=8), (ANOVA Statistically different groups: *:p<0.05 vs NaCl, +: p<0.05 vs Leucine^[5]-Enkephalin).

Average baseline latency for intravenously dosed animals was determined to be 1.84 ± 0.62 (Mean ± SD) sec. Maximal possible latencies were reached for none, none, four and four mice out of 8 for NaCl (0%), L (0%), LG (50%) and PG (50%) respectively (Figure 5.12). The number of analgesic responders defined as one whose response was 2 or more times the value of the baseline latency were none, three, eight and eight out of 8

for NaCl (0%), L (37.5%), LG (100%) and PG (100%) respectively (Figure 5.12). Typical Straub Tail effect characterised by erect tails at time points of high % MPE was observed. Statistically significant differences ($p < 0.05$) were observed between PG versus NaCl (25, 45, 60, 90, 120, 150, 180 minutes, $p = 0.036, <0.0001, 0.005, 0.001, <0.0001, 0.014, 0.007$ respectively), PG versus L (45, 90, 120 minutes, $p = <0.0001, 0.001, <0.0001$ respectively), LG versus NaCl (60, 90, 120, 180 minutes, $p = 0.005, 0.001, <0.0001, 0.007$ respectively), LG versus L (90 minutes, $p = 0.001$) but not between Leucine^[5]-Enkephalin (L) versus NaCl or PG versus LG at all time points (Table 5.9, Figure 5.12).

Table 5.10: Tail Flick Bioassay summary of % Antinociception and Standard Error for different time points after oral administration in CD-1 mice ($n = 16$ / arm).

Time (Minutes)	Leucine Enkephalin (L)	SEM L	Leucine Enkephalin & GCPQ (LG)	SEM LG	PTLENK & GCPQ (PG)	SEM PG	H ₂ O	SEM H ₂ O
30	-10.609311	2.511134	4.1083419	1.412297	10.70264	5.12298	-9.25246	3.031974
60	-5.768922	3.003939	13.8027946	2.562807	37.37973	7.926511	-2.21878	2.615753
90	0.03365426	3.826422	45.2582904	8.912382	46.31852	8.16213	-1.9164	4.471152
120	9.1510636	4.646787	57.5765857	6.783871	62.06339	10.65815	0.56005	3.445308
150	20.8660911	9.306315	54.8981231	8.019285	63.12523	9.611573	-7.2813	2.988494
180	22.6053814	8.294781	56.7562668	8.75993	67.13502	9.443008	-6.39638	3.507817
240	29.0419674	9.400221	51.4759776	9.587627	69.75987	8.844893	-3.11512	4.002311
360	19.860263	6.575041	44.1163574	9.380468	73.31767	7.524339	-5.79867	2.492713
480	6.46511125	6.133546	29.9943619	7.700225	62.09644	8.816509	-8.67098	3.665189
1440	1.2427257	2.982931	3.77772218	2.476439	2.425277	3.182452	-5.91745	3.242234

Average baseline latency for orally dosed animals was determined to be 2.33 ± 0.70 (Mean \pm SD) sec. Maximal possible latencies were reached for none, one, six and nine mice out of 16 for H₂O (0%), L (6.25%), LG (37.5%) and PG (56.25%) respectively (Figure 5.13). The number of analgesic responders defined as one whose response was 2 or more times the value of the baseline latency were none, five, thirteen and fifteen out of 16 for H₂O (0%), L (31.25%), LG (81.25%) and PG (93.75%) respectively (Figure 5.13). Statistically significant differences ($p < 0.05$) were observed between PG versus H₂O (30, 60, 90, 120, 150, 180, 240, 360, 480 minutes, $p = <0.0001$ for all time points), PG versus L (90, 120, 150, 180, 240, 360, 480 minutes, $p = <0.0001$ for all time points), PG versus LG (60, 360, 480 minutes, $p = <0.0001$ at all time points), LG versus H₂O (30, 90, 120, 150, 180 minutes, $p = <0.0001$ for all time points), and LG versus L (60, 360, 480 minutes, $p = <0.001$ for all time points) (Table 5.10 , Figure 5.13).

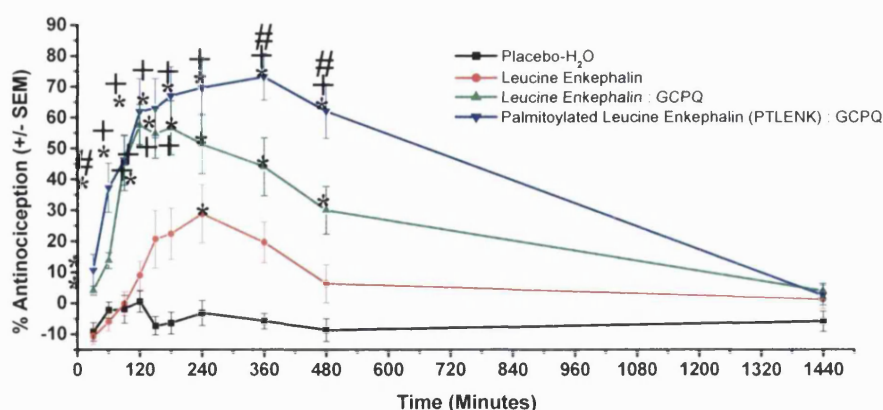


Figure 5.13: Tail Flick Bioassay; Placebo/H₂O (black) Leucine^[51]-Enkephalin 70mg Kg⁻¹ (red), Leucine^[51]-Enkephalin: GCPQ 70mg Kg⁻¹ (1:5 w/w) (green), and Tyrosyl Palmitate Leucine^[51]-Enkephalin (TPLENK): GCPQ 100 mg Kg⁻¹ (1:5 w/w) (blue) % Antinociception (Mean % MPE \pm SEM) at equivalent doses after oral administration to CD-1 Mice (n=16); (ANOVA Statistically different groups: *:p<0.05 vs H₂O, +:p<0.05 vs Leucine^[51]-Enkephalin, #:p<0.05 vs Leucine^[51]-Enkephalin: GCPQ).

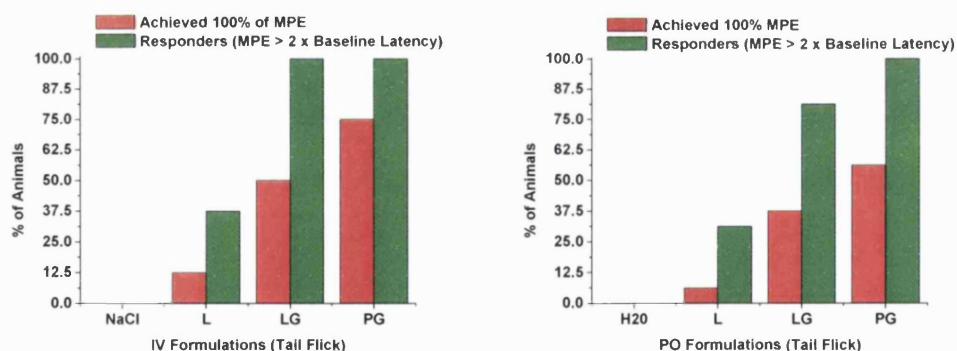


Figure 5.14: Quantal form and % of analgesic responders of tail-flick bioassay after IV (n=8) (left) and oral (n=16) (right) administration.

5.4 Discussion-Conclusions

The BBB is a critical element in the regulation of the constancy of the internal environment of the brain, which is imperative for optimal neuronal functions. However, due to the presence of this barrier consisting of epithelia-like tight junctions lining the brain capillary endothelium more than 98% of all new potential CNS active drugs for the treatment of neurological conditions do not cross the BBB (Pardridge 1998). In the area of brain delivery of drugs and macromolecules, there have been a number of approaches to overcome the BBB, such as osmotic opening of tight junctions, usage of pro-drugs, and carrier systems like targeted antibodies, liposomes and nanoparticles (Witt and Davis 2006). However, the majority of formulations created by these strategies are either directly administered in the CNS through intrathecal administration or if they are delivered systemically they utilise an invasive route (intravenous or intraperitoneal). Surface coated nanoparticles with polysorbate 80 is a single study that was shown to be able to increase the analgesic effects of peptides to the CNS after oral administration, although toxic effects of polysorbate on the integrity of the BBB are postulated after IV administration as polysorbate 80 is able to modulate tight junctions (Kreuter 2001). This is the first study today to deliver orally a small hydrophilic peptide, Leucine^[5]-Enkephalin, to the CNS at statistical significant greater amounts that were adequate to elicit an enhanced and prolonged pharmacodynamic response with a combined approach that utilised a carbohydrate amphiphilic CNS bioavailability enhancer, GCPQ, and the use of a lipidised bioreversible peptide pro-drug, Palmitoyl Tyrosyl Leucine^[5]-Enkephalin (TPLENK).

The pharmacokinetic *in vivo* studies comparing Leucine^[5]-Enkephalin with the nanoparticulate formulation of Leucine^[5]-Enkephalin illustrated a trend for increased brain uptake of the peptide, however the results were not statistically different (Figure 5.7, Table 5.4). An interesting observation is that at 6 minutes after intravenous administration of the peptide alone, there is a decrease in the brain amounts of the peptide recovered that then increases with time at least up to 60 minutes post-dose. This observation could be explained by a saturable transport process for the opioid peptide. Zlokovic et al (1988) illustrated that during single passage of enkephalins through the choroid plexus circulation, unidirectional uptake at the blood-tissue interface of the

blood-CSF barrier that consists of two components: a saturable component, which represents uptake of the intact peptide by the choroid epithelium, and a non-saturable component, which reflects enzymatic degradation of the peptide in the blood and/or at the barrier, with a liberation of the N-terminal tyrosyl residue (Zlokovic et al. 1988). Transport mechanism for Leucine^[5]-Enkephalin requires the intact molecule, since the tetrapeptide without its C-terminal amino acid has no effect on the transport of Leucine^[5]-Enkephalin, and the tetrapeptide without the N-terminal amino acid causes only a small to moderate inhibition (Zlokovic et al. 1987). Furthermore, although the N-terminal part of the molecule was more important for transport activity, the transport system is specific to Leucine^[5]-Enkephalin (Zlokovic et al. 1987). In our studies, the amount of the peptide retrieved from the brain was increasing up to 90 minutes post-intravenous administration in the case of the nanoparticulate formulation which is consistent with the pharmacodynamic observations of a statistical significant antinociception effect at 90 minutes (Figure 5.12). Thus, the above observations can be attributed to protection from enzymatic hydrolysis and longer circulation times conferred by the use of GCPQ.

Comparing the nanoparticulate formulations of Leucine^[5]-Enkephalin and the lipidic pro-drug, TPLENK, after intravenous administration (Figure 5.8, Table 5.5) an increase in the plasma half-life was achieved (if one assumes first order exponential decay of the peptide) and statistically significant greater amounts in plasma at 25 minutes and brain at 25 and 90 minutes after IV administration. The brain AUC₍₀₋₂₄₀₎ was increased by 1.4-1.5 fold when the nanoparticulate formulation of the pro-drug was used compared to the nanoparticulate formulation of the parent peptide. A similar decrease in brain levels at 6 minutes was observed in this study as well indicating a saturable transport mechanism for Leucine^[5]-Enkephalin. However, the effect was less significant when the pro-drug nanoparticulate formulation was administered. Carrier-mediated transport of enkephalins in the CNS has been demonstrated also at the blood side of the BBB (Zlokovic et al. 1987), at the CSF side of the blood-CSF barrier (Begley and Chain 1981), from brain to blood (Banks et al. 1986), and by the choroid plexus (Huang and Lajtha 1978; Zlokovic et al. 1988). Bidirectional facilitated diffusion at the blood-CNS barriers and/or increased enzymatic stability of the pro-drug in plasma and/or brain could attribute for the above increased levels. However, further *in vivo* studies on the kinetics of transport with the use of a radiolabeled tracer of both parent peptide and pro-

drug in the absence and presence of an excess unlabeled peptide are required to support this hypothesis. Furthermore, the sustained increased and pharmacologically active levels present in the brain up to 2 hours as supported by the tail-flick observations (Figure 5.12) and up to 90 minutes as supported by the pharmacokinetic studies could be attributed to a controlled-release profile, increased stability to plasma enzymatic degradation and better transport of the lipidic prodrug in the blood conferred by the use of the carbohydrate amphiphilic polymer allowing for increased bioavailable amounts of the parent peptide at the site of action (brain). In the case that hydrolysis of the ester pro-drug is taking place in the brain that should not lead to toxic by-products as palmitic acid is the most prominent fatty acid in nervous tissue (Alberghina 1998) and enkephalin and its other enzymatically produced peptide sequences are naturally present and can be eliminated by the CNS normal pathways.

Unfortunately, due to limitations in the number of analysed samples with the same radioimmunoassay kit (would only allow for 3 time points per arm of study of 4 animals) and the absence of documented IV doses along with brain levels in pharmacokinetic studies, a study that examined both nanoparticulate formulations and the peptide alone was not performed with the same Leucine^[51]-Enkephalin dose in order to examine both nanoparticulate formulations (parent peptide and pro-drug) to the parent peptide alone. However, the statistically significant increased antinociception provided for both the nanoparticulate formulations versus the peptide alone illustrates the bioavailability enhancing capacity of the use of the carbohydrate polymer. Transport of the nanoparticles across the BBB cannot be excluded, but further studies need to confirm this either *in vitro* (brain endothelial cells) or *in vivo* (imaging studies).

An important point to mention is that the radioimmunoassay kit is 100% specific for Leucine^[51]-Enkephalin, the amount quantified in plasma and brain for the lipidic pro-drug is the amount of the pro-drug that is bioconverted to Leucine^[51]-Enkephalin *in vivo* by plasma or brain esterases. This can explain the difference in the lower plasma levels of the pro-drug to the higher brain levels and the increased elicited antinociception. Studying the effect of extreme pH conditions on the stability of the pro-drug can elicit a pH range and conditions (e.g. time) where the pro-drug can be converted to the parent peptide *in vitro*. Thus, the amount of TPLENK in biological *in vivo* samples collected from the pharmacokinetic studies could be converted *in vitro* to the parent peptide,

allowing for a more direct representation of the pro-drug in plasma and brain. However, the sensitivity of the radioimmunoassay to Leucine^[5]-Enkephalin in known amounts treated *in vitro* before quantification needs to be studied to avoid any reduced specificity of the assay. The use of enzyme inhibitors in the homogenisation media for the brain tissues as pepstatin (soluble in DMSO, added in a dose of 20 mg L⁻¹) and bacitracin (50 mg L⁻¹) can avoid any degradation of Leucine^[5]-Enkephalin and the pro-drug in the case enzymes were not denatured due to the low acidic pH of the homogenisation media (Benoit et al. 1987) along with mercaptoethanol that protected the peptides from oxidation (De Ceballos et al. 1991).

Delivering the peptide alone or the polymer formulations of the peptide alone and the pro-drug orally was shown to lead to statistically significant increases in plasma and brain bioavailability. Peak plasma concentrations were reached at one hour post-oral administration for the peptide and the polymer formulation of the peptide. Plasma levels of Leucine^[5]-Enkephalin alone and with GCPQ followed a similar trend, while the GCPQ formulation of TPLENK showed a different pattern with sustainable levels of the parent peptide in plasma that were statistically different at 4 hours, probably due to increased enzymatic stability and/or increased transport across the intestinal membrane. On the other hand, the polymer pro-drug formulation were significantly higher earlier in the brain (1 hour) and remained significant at the peak time for Leucine^[5]-Enkephalin alone or with GCPQ (4 hours) (Figure 5.11, Table 5.8), which is also supported by the tail-flick results (Figure 5.13). The oral dose successfully delivered was double the dose of dalargin delivered orally in the study by Das et al (2005), but this can be attributable to the increased enzymatic stability primarily to aminopeptidase N of dalargin due to the presence of a D-alanine which is the main enzyme involved in enkephalin degradation in the gut, the plasma, and the brain (Dodda-Kashi and Lee 1986; Zlokovic et al. 1988; Hussain et al. 1990; Das and Lin 2005). However, lower Leucine^[5]-Enkephalin doses than 70 mg kg⁻¹ (but >25mg kg⁻¹) have not been studied.

Protection from enzymatic degradation of the peptides in the gastrointestinal tract is another explanation for the increased plasma and brain bioavailability and it was illustrated in simulated *in vitro* gastric and intestinal experiments (Figures 4.3 and 4.6). A large proportion of the peptidases associated with the brush-border membranes are metalloproteases requiring divalent metal ions for their activity, like aminopeptidase N

and trypsin (Woodley 1994; Bernkop-Schnurch et al. 1997). Aminopeptidase N requires Zn^{2+} for enzymatic activity and is regarded as the most abundant peptide on the brush-border intestinal membrane for Leucine^[5]-Enkephalin degradation (Dodda-Kashi and Lee 1986). Chitosan has been shown to act as a chelator binding divalent ions like Zn^{2+} (Bernkop-Schnurch et al. 1997; Tang and Hon 2000) providing protection to peptides from enzymatic degradation, which can attribute to an increase in available amounts of peptides for transport.

A ratio of polymer to peptide of 1 to 5 (w/w) was chosen for the oral studies as a GCPQ was shown previously to increase the plasma bioavailability of cyclosporine A when administered with the same ratio after oral administration in rats (Le and Uchegbu 2006). However, at this polymer to peptide ratio, the viscosity of the resulting oral formulations taking into consideration the maximum volume allowed for oral dosing to a mouse according to good practise (0.2ml) increased significantly (Figure 5.5). Furthermore, the formulations shear-thinned when stress (vortexing) was applied probably due to breakage of formed intermolecular bonds within polymer chains and illustrated hysteresis and time-dependent shear-thickening when the stress was removed, typical of thixotropic materials. Along with the increase in viscosity, an increase in particle size was observed for the formulation (Figure 5.5 TEM images (1:2.3 w/w ratio, peptide concentration 3 mg ml⁻¹) versus the SEM images (1:5 w/w ratio, peptide concentration 15mg mL⁻¹). However, the increase in viscosity was less significant in the case of the palmitoylated peptide (increased mass of peptide was available), indicating a destabilising effect caused by the presence of this peptide in the close packing and formation of a gel network within polymer chains through hydrophobic interactions (Uchegbu et al. 2001). The increase in viscosity can be explained by the volume fraction and maximum volume fraction as described by the Krieger-Dougherty equation:

$$\eta / \eta_{\text{medium}} = [1 - \phi / \phi_m]^{-[\eta] \phi_m} \quad (\text{Equation 5.4})$$

where η is the viscosity of the suspension, η_{medium} is the viscosity of the medium, ϕ is the volume fraction of solids in the suspension, ϕ_m is the maximum volume fraction in the suspension and $[\eta]$ is the intrinsic viscosity of the medium which is 2.5 for spheres (Hill 2008). Volume fractions are useful alternatives to mole fractions and

express relative amounts of various components in mixtures that there is a large disparity between sizes of various molecules. As the volume fraction of solids in the system increases, the particles become more closely packed together, and it becomes more difficult to move freely (Figure 5.15) (Hill 2008). Thus, particle-particle interactions increase and resistance to flow (viscosity) increases (Hill 2008). When the volume fraction increases to the near maximum for the sample, the viscosity rises very steeply (Hill 2008). Volume fraction also affects the nature of the relationship between shear rate and viscosity. Increasing volume fraction leads to shear-thinning behaviour (Hill 2008). The lower viscosity of the palmitoylated peptide formulation can be also attributed to the higher polydispersity of the system compared to that of Leucine^[5]-Enkephalin in the same concentration and peptide to polymer ratio. As the particle size distribution increases, this allows for a closer packing arrangement of particles (smaller particles in the gaps between bigger particles), increasing the maximum volume fraction (ϕ_m) (Hill 2008). Based on the Krieger-Dougherty equation, when the ϕ_m increases, the viscosity η decreases, allowing for more free flowing particles (self-lubrication). However, whether this increased overall viscosity of the oral polymer formulation is ideal for delivery (increased mucoadhesion and transit time) and protection of the peptide in the GI tract or it hinders release of the peptide needs to be assessed by a combination of rheological and release studies in physiological relevant media along with *in vivo* studies.

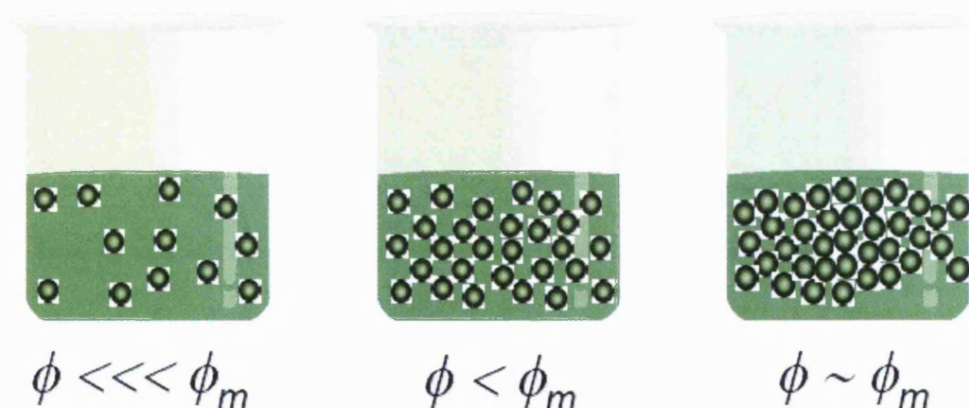


Figure 5.15: Packing of particles when the volume fraction approaches the volume fraction maximum. Reproduced from (Hill 2008).

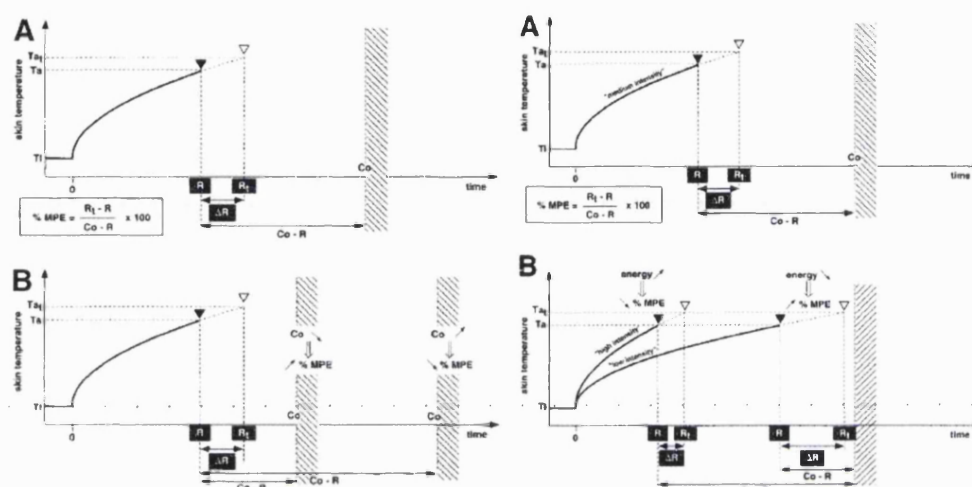
The tail-flick bioassay was chosen to assess antinociception after IV and oral administration. Thermal pain was preferred from inflammatory pain caused by chemical agents as used in the oral study by Wang et al (2006), because it is more natural for the animal and it refers to acute pain compared to chronic pain. Furthermore, analgesics will be much more efficient when the stimulus produces weaker and less synchronous neuronal activity as it is likely to happen during the subcutaneous or intraperitoneal administration of relatively weak algogenic agents (having being chosen for ethical reasons and to minimise stress) as in the case of the formalin or writhing test (Le Bars et al. 2001). The use of placebos in the tail flick bioassay (water for the oral studies and sodium chloride for the IV studies which were the dispersion media for the formulations) as controls rules out the plausible endogenous production of antinociceptive neuropeptides during the stressful and repetitive testing conditions. No testing was performed before 15 minutes after dose administration to avoid increasing excessively stress levels of the animals and room temperature and humidity levels were controlled in the testing environment, to minimise errors in the experiment due to tail temperature fluctuations.

The majority of antinociceptive tests define a limit on the duration of exposure to pain stimulus (the cut-off time) to avoid damage to the tissue (Le Bars et al. 2001). To correct for erroneous interpretation of normal response latency times to latency caused by analgesics, the results are normalised as percentages of the maximum possible effects (MPE %) that is also arbitrarily chosen and calculated by the following equation (Harris and Pierson 1964):

$$\% \text{ MPE} = \frac{\text{Reaction time after treatment (Rt)} - \text{Control reaction time (R)}}{\text{Cut-off time (Co)} - \text{Control reaction time (R)}} \quad (\text{Equation 5.5})$$

Reducing the cutoff time can improve the efficiency of a substance. However, the comparison between analgesic compounds under the same conditions will still remain valid. Furthermore, the percentage of the maximum possible effect will vary with the energy of the thermal response. When the calorific energy is increased, the temperature increases more rapidly with the inescapable consequence of a decrease of difference in reaction time ($\Delta R = R_t - R$), an increase in $Co - R$, and hence a decrease in their ratio, the %

MPE (Figure 5.16) (Le Bars et al. 2001). In our study, the consistently short control reaction times in all groups and the fact that only two animals were excluded for having a baseline reaction time of higher than 5 seconds along with the placebo reaction times indicate that the caloric transfer and intensity of applied stimulus achieved was adequate for valid assessment of the analgesic compounds and assessment of full responders (quantal form of the tail flick), and responders.



The calculation of the percentage of the MPE of a treatment that alters a reaction time is dependent on the predetermined cut-off time. In these diagrams, the occurrence of the control reaction is represented by a black triangle and that of the reaction after treatment, by an open triangle. Note that the treatment increases the measured reaction time by ΔR . **A.** Calculation of the index. **B.** Example of how the choice of the cut-off time determines the index. Note that the % MPE is negatively correlated with the cut-off time. % MPE, the percentage of the maximum possible effect; R, measured control reaction time; R_1 , measured reaction time after treatment; Co, cut-off time.

The calculation of the percentage of the MPE of a treatment that alters a reaction time is dependent on the intensity of applied stimulus. In these diagrams, the occurrence of the control reaction is represented by a black triangle and that of the reaction after treatment, by an open triangle. Note that the treatment increases the measured reaction time by ΔR . **A.** Calculation of the index. **B.** The intensity of the stimulus energy determines the index. The % MPE is negatively correlated with stimulus intensity for simply physical reasons. With a powerful stimulus, the temperature increases rapidly, which results in a decrease in ΔR and an increase in (Co-R) decreases, and thus, the ratio between them is greater. % MPE, the percentage of the maximum possible effect; R, measured control reaction time; R_1 , measured reaction time after treatment; Co, cut-off time.

Figure 5.16: Effect of predetermined cut-off time (left) and intensity of applied stimulus (right) on the % MPE calculated for the tail-flick test. Reproduced from (Le Bars et al. 2001)

In the quantal form of the tail flick test, only morphine-like analgesics are detected and there are virtually no false positive responses, while in this form the test fails to detect agonist-antagonist analgesics and non-steroidal anti-inflammatory agents (NSAIDs) (Franklin and Abbott 1989). The tail-flick test can be made more sensitive by reducing the stringency of the above criterion, and calling any increase in latencies time analgesia. However, with these modifications the tail flick test detects agonist-

antagonist analgesics, but also shows false positives responses to a variety of agents that are not analgesics (Taber 1973; Franklin and Abbott 1989). In our study, the nanoparticulate formulations of Leucine^[5]-Enkephalin and the lipidic pro-drug provided more analgesic responders that achieved 100% of the MPE and more responders (achieving increased or equal double latency times to their respective baseline latency) (Figure 5.14).

Another interesting observation of the tail-flick studies was the presence of typical Straub tail effect at points of high % MPE with the nanoparticulate IV formulations. The Straub tail reaction in mice is an S-shaped dorsiflexion of the mouse tail and is long known as a sensitive and specific effect of morphine. It is based on a contraction of the sacro-coccygeal dorsalis muscles, which in the case of morphine is induced by a long-lasting stimulation of the muscles motor innervation at the level of lumbosacral spinal cord (Stoiber et al. 2000). Thus, this observation which is a typical index of opiate activation and involves both central and peripheral components of the nervous system (Srimal et al. 1965; Buckett 2008), provides further evidence for the successful delivery of the peptide to the site of action and its receptor in adequate pharmacological amounts.

To summarise, the present study is the first study to achieve oral delivery of the labile small hydrophilic linear peptide Leucine^[5]-Enkephalin orally to the CNS proven by pharmacokinetics as well as pharmacodynamic studies. The use of a carbohydrate bioavailability enhancer alone or with the use of a bioreversible pro-drug strategy, allowed for enhanced and prolonged antinociceptive effects. We hypothesise that the increase in brain bioavailability following the strategy adopted is due to: (i) an increase in plasma levels of Leucine^[5]-Enkephalin leading to an increase in brain levels of Leucine^[5]-Enkephalin and (ii) the lipophilic prodrug promoting passage of the peptide across the blood-brain barrier.

Chapter 6

Conclusions & Future Work

6.0 Conclusions

The World Health Organisation has indicated that CNS disorders are the major medical challenge of the 21st century, yet treatments for most CNS disorders are either inadequate or absent due to the BBB (Ohlsen 2007), which is composed of a layer of extremely tightly packed epithelial cells, saturated with enzymes designed to protect the brain from entrance of noxious substances via the bloodstream. The incidence of CNS disorders is increasing with rising average lifespan, while on the other hand the compounds with a molecular weight greater than 600-800 Da are naturally limited by the BBB, eliminating potentially active compounds / biologicals from entering the CNS and leading to a higher failure rate for CNS drug development. Bioavailability is essentially independent of molecular mass with agents of less than 800 Da, however, bioavailability decreases sharply when the molecular mass increases beyond 600-800 Da (Donovan et al. 1990). Thus, there is an imperative need for non-invasive delivery platforms for the delivery of biopharmaceuticals and active compounds for the treatment of CNS disorders like multiple sclerosis, Parkinson's disease, Alzheimer's disease and dementias, mental illnesses, schizophrenia, sleep disorders and addictions.

The majority of administered drugs use invasive routes and are either administered directly to the CNS via intracerebral or intrathecal administration or by systemic administration approaches involving osmotic opening of the BBB, endogenous transporters for carrier mediated uptake [e.g. monoclonal antibody and drug conjugates or monoclonal antibody and particle conjugates (Pardridge 2007; Pardridge 2008)], inhibition of ABC cassette transporters e.g. P-glycoprotein (de Vries et al. 2007), cationisation of peptides/drugs or coating with cationised albumin for adsorptive mediated endocytosis (Kumagai et al. 1987) and finally the use of polysorbate 80 coated poly(butylcyanoacrylate) nanoparticles (Kreuter et al. 1995). The use of monoclonal antibodies limits the amounts of drugs / biomacromolecules able to be transported across the BBB and their success has not yet been validated in a clinical setting.

Cationisation, a non-specific approach, has the potential to deliver greater amounts, however concerns over immunogenicity and toxicity of the compounds have been raised (Bergmann et al. 1984; Pardridge et al. 1989). P-glycoprotein is not unique in the BBB and its inhibition can potentially lead to altered metabolism of other drugs / compounds and toxicological concerns. Poly (butylcyanoacrylate) [PBCA] nanoparticles represent the only successful example of *in vivo* delivery of peptides to the brain after intravenous and oral delivery based solely on the assessment of the peptide's pharmacodynamic response. However, the effect was short-lived and was not statistically different from positive controls after 60 minutes post-intravenous injection and after 2 hours after oral administration (Kreuter 2001; Das and Lin 2005). Furthermore, enhanced transport of these nanoparticles may also involve tight junction modulation (Kreuter 2001) or P-gp inhibition (Woodcock et al. 1992).

Based on the above and the metabolic instability and physicochemical nature of biomacromolecules, the present study focused on the oral delivery of hydrophilic biomacromolecules to the CNS by utilising a novel lipidic ester prodrug approach that will increase the lipophilicity of small hydrophilic compounds for the delivery of drugs/biomacromolecules across the BBB that would be formulated with a carbohydrate bioavailability enhancer with a proven record of increasing CNS activity.

Creation of a prodrug is a useful approach for overcoming biological barriers like the intestinal barrier and the BBB by altering the physicochemical properties of the parent drug / biomacromolecule to avoid enzymatic inactivation and to allow more of the active compound to reach the desired site of action. Peptide lipidisation involves the blocking of polar functional moieties on the peptide backbone with groups that greatly enhance the lipid solubility of the peptide. Keeping in mind that rate of passive diffusion across the biological membrane will increase exponentially with increasing lipophilicity when the water solubility is not compromised (Hu 2005), there is promise for the design of lipidic pro-drugs to achieve a balance between hydrophilicity and lipophilicity that can be used for oral delivery of peptides (Fredholt et al. 2000; Wang et al. 2006) to the CNS (Batrakova et al. 2005).

TPLENK is a novel prodrug of a small linear labile peptide Leucine^[5]-Enkephalin, a delta selective endogenous opioid neuropeptide, that is synthesised by palmitoylation of

the free phenolic hydroxy moiety of tyrosine. The synthetic protocol can be scaled up and automated as well as applied directly to other CNS active peptides. Incorporation of labile lipid motifs into LENK will enhance the lipophilic character of the neuropeptide and contribute to cellular uptake with minimal alteration of the native sequence and conformation. The use of GCPQ can counteract the reduction in hydrophilicity and reduced dissolution that can potentially limit the flux of the lipidised peptide across biological barriers or the transport in biological fluids. Furthermore, the increase in molecular weight of the endogenous peptide after modification remains small (239 Da added) yielding TPLENK that has a total molecular weight within the range of molecular weights (150-800 Da) of compounds found to be useful for the treatment of CNS diseases.

TPLENK can act as an amphiphile as revealed by TEM studies forming dense networks of fibres in excess of 1 μ m long and a diameter of 10-15 nm in an aqueous environment. The presence of the palmitic tail is long enough to favour thermodynamically the formation of an extensive nanofibre network with the self-assembly process mediated possibly via weak intermolecular bonds, such as van der Waals bonds, electrostatic interactions, hydrogen bonds and aromatic stacking interactions combined together to form intact and well-ordered supramolecular structures. Addition of a palmitic tail on the phenolic hydroxyl moiety of LENK leads to a highly constrained tyrosine derivative, which may have an increased δ -opioid selectivity by stabilisation of the lipidic tail via hydrophobic interactions to unique residues thought to be present in the hydrophobic pocket attributed to the δ -opioid receptor. However, the latter needs to be proven by further studies.

GCPQ is a low molecular weight amphiphilic CNS carbohydrate bioavailability enhancer (Qu et al. 2006) and has been used to deliver both parent peptides and amphiphilic prodrugs after IV or oral administration. Formulations were created via self-assembly in aqueous media with peptide to polymer weight ratio of 1:5 yielding better encapsulation efficiencies. This formulation was chosen for oral delivery studies. A ratio of 1: 2.3 w/w was selected for IV administration due to the low viscosity and smaller mean particle size of this formulation. Such parameters are desired when administering drugs via the intravenous route. Liquid stability studies of TPLENK and GCPQ (1:2.3 w/w) were shown to be stable for up to 5 weeks when stored between 2-

8°C as demonstrated by HPLC and photon correlation spectroscopy, although the polydispersity increased gradually indicative of aggregation processes. On the other hand, freeze-dried formulations of TPLENK and GCPQ (1:2.3 w/w) remained stable for up to 6 months at least in terms of mean particle size, polydispersity and peptide content, while appearing as a fluffy, porous network with the peptide being dispersed in the polymer matrix. No shrinkage was observed from the sides of the container and the reconstitution with sterile water was almost instantaneous providing a clear, colourless polymeric dispersion, with GCPQ possibly acting as a cryoprotectant.

Both parent peptide and prodrug were stable in simulated gastric fluid (in the absence of pepsin) for up to 3 hours at 37°C in the presence or absence of GCPQ (1:5 w/w ratio) with at least 92 % of the peptides remaining intact after 3 hours. Although protection of a phenolic moiety, which is susceptible to rapid and extensive pre-systemic metabolism, will limit first-pass intestinal and hepatic metabolism (Rautio et al. 2008), TPLENK showed rapid degradation in the presence of rat intestinal washings (pH 6.6) possibly due to esterase activity in the homogenate combined with brush border enzyme degradation by Aminopeptidase N (Dodda-Kashi and Lee 1986) or an increase in the hydrolytic rate of Carboxypeptidase A (Fredholt et al. 2000). However, the stability of the amphiphilic prodrug as well as the parent peptide was greatly enhanced by the use of GCPQ (1:5 w/w ratio), but the exact mechanism responsible for this enzymatic protection is not clear.

TPLENK, has been shown to be able to be bioconverted *ex vivo* to the parent peptide probably mainly by type B membrane bound esterases in the presence of rat plasma and liver homogenates with short half lives of ~73 and ~44 minutes respectively. However, TPLENK showed more favourable brain to plasma stability in homogenates and was stable in rat brain homogenates up to 8 hours. The stability of the prodrug in brain homogenates is partly justifiable by the low esterase specific activity of the brain homogenates in rat in combination with a smaller ratio of type B esterases in brain homogenates, however further studies are required.

The present study is the first study to demonstrate the oral delivery of the labile small hydrophilic linear peptide Leucine^[51]-Enkephalin to the CNS via both pharmacokinetics as well as pharmacodynamics data. The use of GCPQ, a carbohydrate bioavailability

enhancer, alone or with the use of a novel bioreversible pro-drug strategy, allowed for enhanced and prolonged central antinociceptive effects.

Preliminary pharmacokinetic data after IV administration ($n = 4$) of LENK suggest a trend towards a longer brain and plasma half-life for LENK in the presence of GCPQ although data was not statistically significant ($p > 0.05$). The plasma half-life of LENK on intravenous (IV) administration was increased 1.4 fold when the nanoparticulate formulation was used and by 3.2 fold when TPLENK was administered with GCPQ. More importantly, the brain AUC of LENK was increased almost 2-fold by lipidisation of the peptide and encapsulation of the lipid prodrug within GCPQ aggregates after intravenous administration. TPLENK was converted into LENK *in vivo* after IV and oral administration. The use of TPLENK: GCPQ increased the half life of LENK in the plasma after IV (peptide: polymer; 1:2.3 w/w ratio) and oral (peptide: polymer; 1:5 w/w ratio) and almost doubled the plasma AUC of LENK when compared to the administration of LENK alone. GCPQ increased the plasma half life of LENK on oral administration and doubled the AUC of LENK in the brain (Figure 5.11). The oral administration of LENK: GCPQ (1:5 w/w ratio) and TPLENK: GCPQ (1:5 w/w ratio) resulted in a significant increase in LENK central analgesic activity with the timing of the highest % antinociception achieved correlating well with the pharmacokinetic data. GCPQ peptide formulations yielded the most animals reaching the maximum possible effect as indicative by the quantal form of the tail-flick bioassay that identifies only morphine-like analgesics with the majority of the animals tested classified as analgesic responders (>80% in all cases).

To summarise, GCPQ enhances the brain bioavailability and central analgesic effects of Leucine^[5]-Enkephalin (LENK) after oral administration. Additionally, the use of TPLENK, a novel lipophilic ester prodrug, which is converted to Leucine^[5]-Enkephalin by plasma and liver esterases also enhances the brain bioavailability and central analgesic effects of LENK on intravenous and oral administration. We hypothesise that the increase in brain bioavailability and pharmacodynamic effects following the oral administration of LENK : GCPQ is due to an increased absorption of LENK caused by the oral absorption enhancer GCPQ. The increased brain bioavailability and central analgesic effects of TPLENK are due to the lipophilic prodrug (TPLENK) promoting

passage of the drug across the blood-brain barrier and possible pharmacodynamic activity from the intact lipidic prodrug.

6.1 Future work

Although the presented results provided the proof of concept and answer some of the questions regarding this novel approach for the delivery of hydrophilic macromolecules to the CNS, further research questions stemmed out of this work.

We hypothesised that the central pharmacological effects were elicited by bioconversion of TPLENK to the parent peptide and transport of Leucine^[5]-Enkephalin across the BBB. However, transport of TPLENK across the BBB and binding to opioid receptors cannot be ruled out especially as addition of the palmitic tail does not alter significantly the required pharmacophore. Identification of the IC₅₀ (inhibitory concentration) for TPLENK for different types of opioid receptors is required and if TPLENK binds to opioid receptors, its selectivity profile (μ/δ ratio) would need to be identified in the guinea pig ileum assay (rich in μ receptors) and in the mouse vas deferens assay (rich in δ receptors) and compared to LENK under the same experimental conditions. Conformation of TPLENK would also need to be studied further combining X-ray powder diffraction data and NMR studies (i.e. combining the d-spacings from X-ray diffraction with the distances between atoms and torsional angles identified via NMR studies). Circular dichroism can also help to quantify the peptide helicity and thus in identifying whether the peptide assumes α -helix, β -sheet or a mixture structure.

Studying the biodistribution of both peptides in the body is important and can be done either via iodination or via the use of a fluorescent dye and confocal microscopy of the tissues. Iodination of the free amide terminus using the Bolton-Hunter reagent or using tritiated leucine for synthesising LENK and then TPLENK is possible and can provide useful evidence regarding the amount of the peptide being absorbed orally and across the BBB compared to a group of animals receiving only the radioactive tracer (e.g. I¹²⁵). These results can also be compared with the distribution of fluorescent peptides (created by a fluorescent dye attached to the free N terminal of the peptides) and confocal microscopy. A combination of tritiated peptides and iodinated polymer (again via the

free amine terminus) can provide a good estimation of the biodistribution and clearance of the formulation as a whole.

Studying the *in vitro* bioconversion of TPLENK amounts in biological samples to Leucine^[5]-Enkephalin can provide for a method to directly quantify the amount of TPLENK in plasma using the radioimmunoassay for quantification. The development of a combined RP-HPLC (especially if equipped with a photodiode array detector) or capillary electrophoresis and mass-spectrometry method for the analysis of *in vivo* pharmacokinetic samples can yield a second sensitive technique to validate the results obtained with the radioimmunoassay. Microdialysis studies can help in quantifying the amount of the unbound free peptides available in the CSF and blood that would be available to cause central analgesic effects.

Furthermore, creating a dose-response curve using the tail-flick bioassay after oral administration can provide information on the smallest dose that maintains central activity and optimal formulation for oral delivery in terms of viscosity in combination with rheological experiments and release studies in simulated gastric fluid.

Toxicological studies would also need to be conducted *in vivo* after oral administration of the formulations and equivalent amount of polymer alone by assessing well-being based on clinical signs, survival, food consumption, weight increase, haematological changes and organ weights and histology changes in healthy animals over time versus controls in a blinded study design. Cell transport studies and toxicity of the peptides and formulations in Caco-2 cells can provide information regarding the permeability of the peptides and a possible mechanism for the enhanced bioavailability observed along with studies using bovine brain endothelial cell lines co-cultured with astrocytes as a model for the permeability and transport across the BBB.

Stability of TPLENK in the presence and absence of paraoxon needs to be further assessed and will confirm whether type B esterases are important for TPLENK's hydrolysis in the rat. Stability assessments using a mouse model would also be beneficial in order to correlate the *in vitro* findings with the available *in vivo* data. Keeping in mind that humans have a lower amount of esterases specific activity, studies at least in human plasma can provide more relevant information. Furthermore, varying

the amount of peptide to enzyme ratio in the brain homogenate studies can possibly allow for a faster hydrolytic rate than can be used for identifying its half-life in these media.

Studying and controlling the conditions that drive molecular self-assembly of TPLENK in aqueous environment could provide information on how a small amphipathic peptide with the potential to create nanotubes of ordered structure can be used for the delivery of other small biomacromolecules as a delivery device. Isothermal titration calorimetry studies in an isotonic and physiologic pH buffer can be conducted to identify a critical micelle concentration by measuring the enthalpy changes. Isothermal calorimetry can also be used to assess the membrane binding potential of TPLENK and LENK (for comparison) by injecting the peptide into a calorimeter filled with buffer and small unilamellar vesicles or conducting the studies in the reverse.

.....

Finally, the use of GCPQ as a cryoprotectant for peptide therapeutic agents can be explored further.

Publications

1. A. Lalatsa, A. G. Schächlein, and I. F. Uchegbu (2009) Carbohydrate Nanoparticles for Peptide Delivery to the Central Nervous System. Science Manuscript in preparation
2. A. Lalatsa, A. G. Schächlein, and I. F. Uchegbu (2009) Oral Peptide Delivery to the Central Nervous System: Opioid Peptides and the Blood-Brain Barrier. Int. J. Pharm. Manuscript in preparation
3. A. Lalatsa, A. G. Schächlein, and I. F. Uchegbu. Blood-Brain Barrier Session Podium Presentation: “Carbohydrate Amphiphiles Enable Oral Peptide Delivery to the Central Nervous System”. 36th Annual Meeting of the Controlled Release Society, Auditorium 12, Bella Center, New York (21th July 2009, 4:45-5:00) Abstract 4441-1
4. A. Lalatsa, A. G. Schächlein, and I. F. Uchegbu. Poster: “Carbohydrate Nanoparticles for Peptide Delivery to the Central Nervous System”, 5th Annual bioProcessUK Conference, Thistle Hotel, Brighton (26-27th November 2008)
5. A. Lalatsa, A. G. Schächlein, and I. F. Uchegbu. Drug Delivery and Design I Session Podium Presentation: Carbohydrate Nanoparticles for Peptide Delivery to the Central Nervous System. Globalization of Pharmaceuticals Education Network GPEN 2008 Meeting, Promotiezaal Hallen, Katholieke Universiteit, Leuven, Belgium (10th September 2008, 09:10-09:30) Abstract PD-W-02
6. A. Lalatsa, A. G. Schächlein, and I. F. Uchegbu. Peptide Delivery Session Podium Presentation: “Carbohydrate Nanoparticles for Peptide Delivery to the Central Nervous System”. 35th Annual Meeting of the Controlled Release Society, Trianon Ballroom, Hilton New York, New York (14th July 2008, 5:00-5:20) Abstract 3279
7. A. Lalatsa, A. G. Schächlein, and I. F. Uchegbu. Poster: “Carbohydrate Nanoparticles for Peptide Delivery to the Central Nervous System”, 1st Lilly Lecture, School of Pharmacy, Univ. of London (16th May 2007)

3. Podium:

Carbohydrate Amphiphiles Enable Oral Peptide Delivery to the Central Nervous System

Aikaterini Lalatsa¹, Andreas G. Schätzlein¹, Ijeoma F. Uchegbu¹¹The Nanomedicines Research Centre, Department of Pharmaceutics, The School of Pharmacy, University of London, 29-39 Brunswick Square, London, WC1N 1AX, U.K.
aikaterini.lalatsa@pharmacy.ac.uk

ABSTRACT SUMMARY:

Quaternary Ammonium Palmitoyl Glycol Chitosan (GCPQ) enhances the brain bioavailability and central analgesic effects of Leucine⁵-Enkephalin (LENK) after oral administration. Additionally, the use of TPLENK, a novel lipophilic ester prodrug, which is converted to LENK by plasma and liver esterases also enhances the brain bioavailability and central analgesic effects of LENK on oral administration. We hypothesise that the increase in brain bioavailability and pharmacodynamic effects following the oral administration of GCPQ - LENK is due to an increased absorption of LENK caused by the oral absorption enhancer GCPQ. The increased brain bioavailability and central analgesic effects of TPLENK are due to the lipophilic prodrug (TPLENK) promoting passage of the drug across the blood-brain barrier and possible pharmacodynamic activity from the intact lipidic prodrug.

Bioconversion of TPLENK was assessed also utilizing rat plasma and liver homogenates [5,6].

A radioimmunoassay (RIA, Bachem) was used for peptide quantification in plasma & brain [7] after oral administration. The tail flick bioassay was used to assess the central analgesic effects.

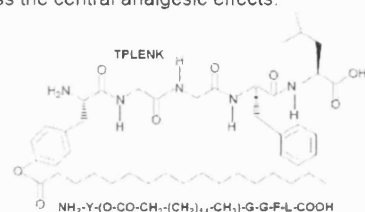


Figure 1: Structure of the lipophilic prodrug - TPLENK

RESULTS AND DISCUSSION:

Palmitoylation of the free hydroxyl group of LENK was achieved successfully, as illustrated by ESI-MS, MALDI and NMR [3]. Total synthetic yield was 88% for LENK & 60% for TPLENK. Purification of both peptides was carried out with semi-preparative RP-HPLC.

Both peptides are stable for up to 3 hours in SGF in the absence of pepsin with 94% of the peptides remaining. LENK was more stable than TPLENK in rat intestinal wash media with $68.9 \pm 1.6\%$ and $17.8 \pm 0.7\%$ LENK and TPLENK recovered after 4 hours respectively. The stability of TPLENK in rat intestinal wash was greatly enhanced by the addition of GCPQ with $66 \pm 0.89\%$ of TPLENK recovered after 4 hours in the presence of GCPQ compared to $17.8 \pm 0.7\%$ in the absence of GCPQ. Apparent half-lives ($t_{1/2}$) for the disappearance of TPLENK were ~ 73 and ~ 44 minutes approximately in plasma and liver homogenates respectively as calculated from pseudo first-order rate constants obtained by linear regression of log drug concentration versus time plots [3].

GCPQ increased the plasma half life of LENK on oral administration (Figure 2a) and doubled the AUC of LENK in the brain (Figure 2b). TPLENK was converted into LENK in vivo and the use of GCPQ - TPLENK increased the half life of LENK in the plasma and doubled the AUC of LENK when compared to the administration of LENK alone (Figure 2b). The oral administration of GCPQ - LENK and GCPQ - TPLENK resulted in a significant increase in LENK central analgesic activity (Figure

INTRODUCTION:

Peptides are of tremendous clinical value for the treatment of many central nervous system (CNS) disorders. Many existing peptide pharmaceuticals are rendered ineffective after oral administration or are unable to cross the blood-brain barrier (BBB) mainly due to their hydrophilicity, size and charge. The current project is aimed at enhancing the oral bioavailability of water soluble peptides, e.g. Leucine⁵-Enkephalin (LENK) by lipidisation and/or encapsulation in Quaternary Ammonium Palmitoyl Glycol Chitosan (GCPQ) [1]. LENK is an endogenous opioid neuropeptide with a blood half-life of approximately 3 minutes in man [2]. A lipophilic prodrug, palmitoylated Leucine Enkephalin (TPLENK), comprising a cleavable ester bond susceptible to blood esterases was synthesized and characterised [3].

EXPERIMENTAL METHODS:

Standard solid-phase peptide synthesis of LENK (YGGFL) was carried out on an automated peptide synthesizer and the free hydroxyl group of LENK was esterified using the active N-hydroxysuccinimide ester of palmitic acid to produce the lipophilic prodrug TPLENK (Figure 1) [3]. ESI-MS, MALDI, NMR, & analytical/preparative RP-HPLC were utilised for peptide characterization and purification.

Gut stability of LENK & TPLENK was assessed in Simulated Gastric Fluid (SGF) devoid of pepsin and rat intestinal wash [4] with RP-HPLC quantification.

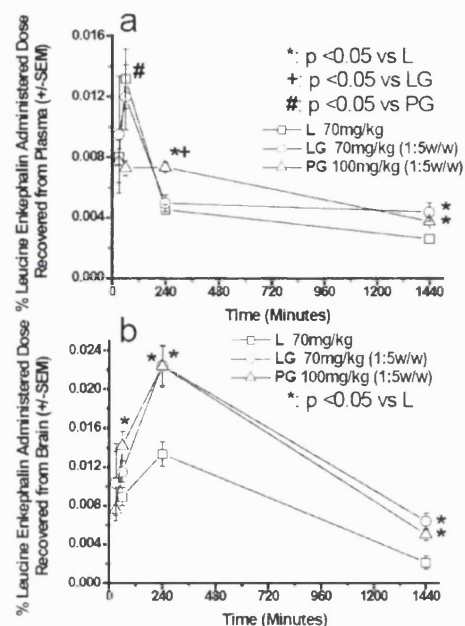


Figure 2: Plasma (a) and brain (b) pharmacokinetic data after the oral administration of the equivalent of 70 mg kg^{-1} LENK. % of LENK dose recovered after the oral administration of LENK (square), GCPQ - LENK (circle) and GCPQ - TPLENK (triangle) formulations to CD-1 Mice ($n=4$)

3). The timing of the highest % antinociception achieved correlates well with the pharmacokinetic data. 94% of the animals that received GCPQ - TPLENK were found to be analgesic responders (Figure 3b).

CONCLUSION:

The present study is the first study to demonstrate the oral delivery of the labile small hydrophilic linear peptide Leucine⁶-Enkephalin to the CNS via both pharmacokinetics as well as pharmacodynamics data. The use of GCPQ, a carbohydrate bioavailability enhancer, alone or with the use of a novel bioreversible pro-drug strategy, allowed for enhanced and prolonged central antinociceptive effects.

ACKNOWLEDGEMENTS:

Financial support from the Engineering and Physical Sciences Research Council (EPSRC) and the School of Pharmacy, University of London is greatly acknowledged.

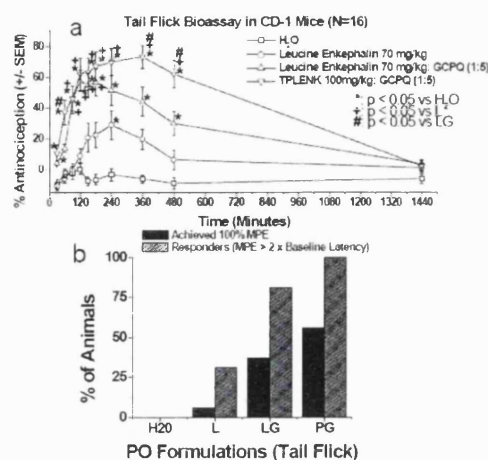


Figure 3: Central analgesic effects as demonstrated using the Tail Flick Bioassay after the oral administration of 70 mg kg^{-1} equivalent of LENK. a) Water (square), LENK (circle), GCPQ - LENK (up triangle), GCPQ - TPLENK (down triangle), % antinociception achieved in CD-1 mice ($n=16$). * = $p < 0.05$ versus H_2O , + = $p < 0.05$ versus LENK, # = $p < 0.05$ versus GCPQ - LENK. b) black bars = % of animals achieving maximum possible response (MPE, lag time for removal of tail from noxious stimuli was truncated at 10sec), grey bar = % of animals which achieved a lag time for removal of tail from a noxious stimuli that was at least twice their baseline value), ($n=16$).

REFERENCES:

1. Qu, X.; et al. *Biomacromolecules*. 2006, 7, (12), 3452-9.
2. Hussain, M.A.; et al. *Drug Metab. Dispos.* 1990, 18, (3), 288-291.
3. Lalatsa, A.; et al. 35th Annual Meeting of the Controlled Release Society. 2008, Abstract, 3279.
4. Cheng, W. S.; et al. *Pharm. Res.* 2007, 24, (1), 99-110.
5. Ouyang, H.; et al. *Pharm. Res.* 2002, 19, (6), 794-801.
6. Liederer, B.M.; R.T. Borchardt. *J. Pharm. Sci.* 2005, 94, (10), 2198-206.
7. De Ceballos, M.L.; et al. *Neuropeptides*. 1991, 20, (3), 201-209.

4. Poster:

Carbohydrate Nanoparticles for Peptide Delivery to the Central Nervous System

A. Lalatsa¹, A.G. Schätzlein¹, I.F. Uchegbu¹¹ The Nanomedicines Research Centre, Department of Pharmaceutics, The School of Pharmacy, University of London, 29-39, Brunswick Square, U.K., WC1N 1AX.

Aim: The current project is aimed at enhancing the bioavailability of water soluble peptides, e.g. Leucine⁵-Enkephalin (LENK) by lipidisation and/or encapsulation in a carbohydrate bioavailability enhancer, Quaternary Ammonium Palmitoyl Glycol Chitosan (GCPQ) [1]. LENK is an endogenous opioid neuropeptide. A lipophilic prodrug, palmitoylated Leucine Enkephalin (TPLENK), comprising a cleavable ester bond susceptible to blood esterases was synthesised and characterised.

Methods: Standard solid-phase peptide synthesis of LENK was carried out and the free hydroxyl group of LENK was esterified. Bioconversion of TPLENK was assessed utilising rat plasma and liver homogenates. A radioimmunoassay was used for peptide quantitation in plasma and brain and the tail flick bioassay was performed to assess the pharmacodynamic response after intravenous administration.

Results - Conclusions: The lipophilic prodrug was converted into the LENK by plasma and liver esterases with apparent half-lives for the disappearance of the pro-drug of ~73 and ~44 minutes in plasma and liver homogenates respectively. The plasma half-life of LENK on intravenous administration was increased from 5 minutes to 9 minutes (Figure 1). More importantly the brain AUC of LENK was increased almost 2-fold by lipidisation of the peptide and encapsulation of the lipid prodrug within GCPQ nanoparticles, while maintaining its pharmacological activity (Figure 2). We hypothesise that the increase in brain bioavailability following the strategy adopted is due to: (i) an increase in plasma levels of LENK leading to an increase in brain levels of LENK and (ii) the lipophilic prodrug promoting passage of the drug across the blood-brain barrier, with GCPQ enabling the lipid prodrug to be transported in the blood to the blood-brain barrier.

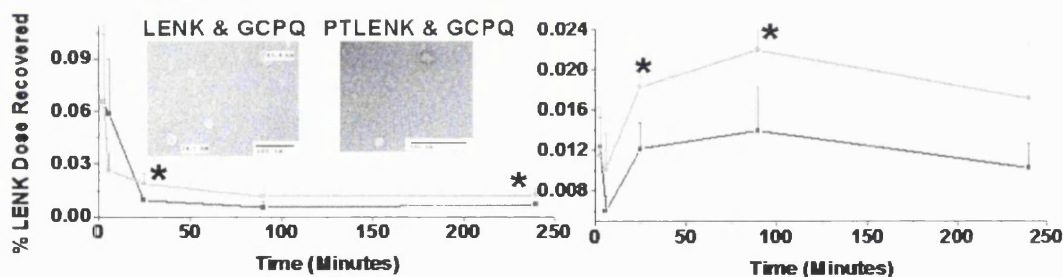


Figure 1 Pharmacokinetic Data: Plasma (left panel) and Brain (right panel) % of LENK dose recovered after IV administration of LENK:GCPQ (red) and TPLENK:GCPQ (green) formulations to CD-1 Mice (n=4), (*:p<0.05). TEM images at 3mg/ml (right panel). The disperse phase was NaCl 0.9%.

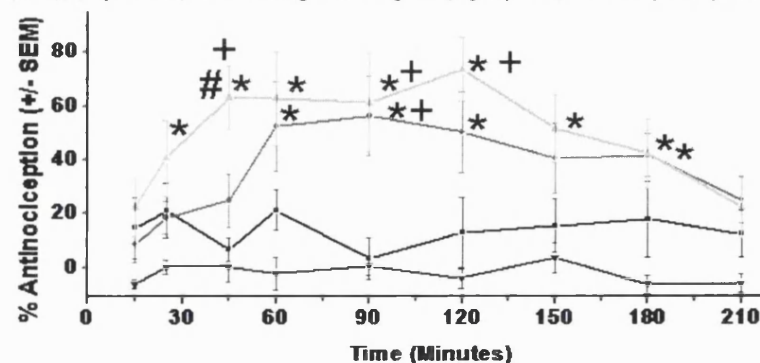


Figure 2 Tail Flick Bioassay: LENK (black), LENK:GCPQ (red), TPLENK:GCPQ (green) and Placebo/NaCl (blue) % Antinociception at equivalent doses after IV administration to CD-1 Mice (n=8), (ANOVA Statistically different groups: *:p<0.05 vs NaCl, +: p<0.05 vs LENK, #: p<0.05 vs LENK:GCPQ).

References:

1. Qu, X., et al., *Carbohydrate-based micelle clusters which enhance hydrophobic drug bioavailability by up to 1 order of magnitude*. *Biomacromolecules*, 2006. 7(12): p. 3452-9.

5. Podium:

Carbohydrate Nanoparticles for Peptide Delivery to the Central Nervous System

A. Lalatsa¹, A.G. Schätzlein¹, I.F. Uchegbu¹¹ The Nanomedicines Research Centre, Department of Pharmaceutics, The School of Pharmacy, University of London, 29-39, Brunswick Square, U.K., WC1N 1AX.

Aim: The current project is aimed at enhancing the bioavailability of water soluble peptides, e.g. Leucine^[5]-Enkephalin (LENK) by lipidisation and/or encapsulation in a carbohydrate bioavailability enhancer, Quaternary Ammonium Palmitoyl Glycol Chitosan (GCPQ). LENK is an endogenous opioid neuropeptide with a blood half-life of 3 minutes in man. A lipophilic prodrug, palmitoylated Leucine Enkephalin (TPLENK), comprising a cleavable ester bond susceptible to blood esterases was synthesised and characterised.

Methods: Standard solid-phase peptide synthesis of LENK was carried out and the free hydroxyl group of LENK was esterified. ESI-MS, MALDI, NMR, & analytical/preparative HPLC were utilised for peptide characterisation and purification. Bioconversion of TPLENK was assessed utilising rat plasma and liver homogenates. A radioimmunoassay was used for peptide quantitation in plasma and brain and the tail flick bioassay was performed to assess the pharmacodynamic response after intravenous administration.

Results: The lipophilic prodrug was converted into the parent drug by plasma and liver esterases with apparent half-lives for the disappearance of the pro-drug of ~73 and ~44 minutes in plasma and liver homogenates respectively. The plasma half-life of LENK on intravenous administration was increased from 5 minutes to 9 minutes (Figure 1). More importantly the brain AUC of LENK was increased almost 2-fold by lipidisation of the peptide and encapsulation of the lipid prodrug within GCPQ nanoparticles. We hypothesise that the increase in brain bioavailability following the strategy adopted is due to: (i) an increase in plasma levels of LENK leading to an increase in brain levels of LENK and (ii) the lipophilic prodrug promoting passage of the drug across the blood-brain barrier, with GCPQ enabling the lipid prodrug to be transported in the blood to the blood-brain barrier.

Conclusions: A novel method for the creation of a lipophilic ester pro-drug of Leucine-Enkephalin was established. In vivo testing revealed that the intravenous injection of the lipophilic prodrug encapsulated within a chitosan amphiphile increased the brain AUC by 2 fold when compared to the peptide alone. Further studies on the pharmacodynamics are planned.

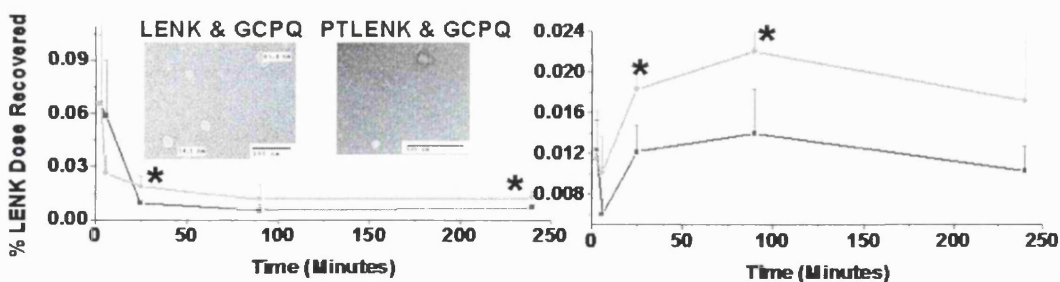


Figure 1 Pharmacokinetic Data: Plasma (left panel) and Brain (right panel) % of LENK dose recovered after IV administration of LENK:GCPQ (red) and TPLENK:GCPQ (green) formulations to CD-1 Mice (n=4), (*:p < 0.05). TEM images at 3mg/ml (right panel). The disperse phase was NaCl 0.9%.

6. Podium:

Carbohydrate Nanoparticles for Peptide Delivery to the Central Nervous System

Aikaterini Lalatsa¹, Andreas G. Schätzlein¹, Ijeoma F. Uchegbu¹¹The Nanomedicines Research Centre, Department of Pharmaceutics, The School of Pharmacy, University of London, 29-39, Brunswick Square, London, U.K., WC1N 1AX
aikaterini.lalatsa@pharmacy.ac.uk

ABSTRACT SUMMARY:

Quaternary Ammonium Palmitoyl Glycol Chitosan (GCPQ) enhances the *in vitro* stability of both Leucine-Enkephalin (LENK) and TPLENK, a novel lipophilic ester prodrug, which can be converted to LENK by esterases. GCPQ showed a tendency to increase the blood and brain residence time of this neuropeptide.

INTRODUCTION:

Peptides are of tremendous clinical value for the treatment of many central nervous system (CNS) disorders. Many existing peptide pharmaceuticals are rendered ineffective after oral administration or are unable to cross the blood-brain barrier (BBB) mainly due to their hydrophilicity, size and charge. The current project is aimed at enhancing the bioavailability of water soluble peptides, e.g. Leucine [5]-Enkephalin (LENK) by lipidisation and/or encapsulation in Quaternary Ammonium Palmitoyl Glycol Chitosan (GCPQ) [1]. LENK is an endogenous opioid neuropeptide with a blood half-life of approximately 3 minutes in man [2, 3]. A lipophilic prodrug, palmitoylated Leucine Enkephalin (TPLENK), comprising a cleavable ester bond susceptible to blood esterases was synthesized and characterised. Additionally, the brain delivery of LENK in the presence of GCPQ was assessed.

EXPERIMENTAL METHODS:

Standard solid-phase peptide synthesis of LENK (YGGFL) was carried out on an automated peptide synthesizer and the free hydroxyl group of LENK was esterified using the active N-hydroxysuccinimide ester of palmitic acid (Figure 1). ESI-MS, MALDI, NMR & analytical/preparative RP-HPLC were utilised

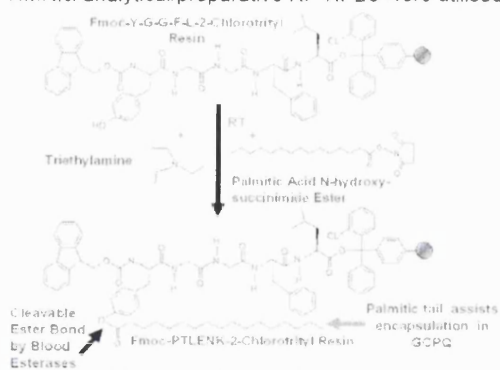


Figure 1: Rationale of TPLENK synthesis.

Figure 2: Negative ESI-MS & ¹H NMR in DMSO (5.35mM) of TPLENK.

for peptide characterization and purification.

Gut stability of LENK & TPLENK was assessed in Simulated Gastric Fluid (SGF) devoid of pepsin and rat intestinal wash [4] with RP-HPLC quantification. Bioconversion of TPLENK was assessed also utilizing rat plasma and liver homogenates [5, 6].

A radioimmunoassay (RIA, Bachem) was used for peptide quantitation in plasma & brain [7] after intravenous (IV) administration.

RESULTS AND DISCUSSION:

Palmitoylation of the free hydroxyl group of LENK was achieved successfully, as illustrated by ESI-MS, MALDI and NMR (Figure 2). Total synthetic yield was 88% for LENK & 60% for TPLENK. Purification of both peptides was carried out with semi-preparative RP-HPLC.

Both peptides are stable for up to 3 hours in SGF in the absence of pepsin with 94% of the peptides remaining. Stability of the lipophilic pro-drug in rat intestinal wash was greatly enhanced by the addition of GCPQ with 66 ± 0.89 % of TPLENK recovered after 2 hours in the presence of GCPQ compared to 17.8 ± 0.7% in the absence of GCPQ. Apparent half-

lives ($t_{1/2}$) for the disappearance of the lipophilic pro-drug were ~ 73 and ~ 44 minutes approximately in plasma and liver homogenates respectively as calculated from pseudo first-order rate constants obtained by linear regression of log drug concentration versus time plots (Figure 3).

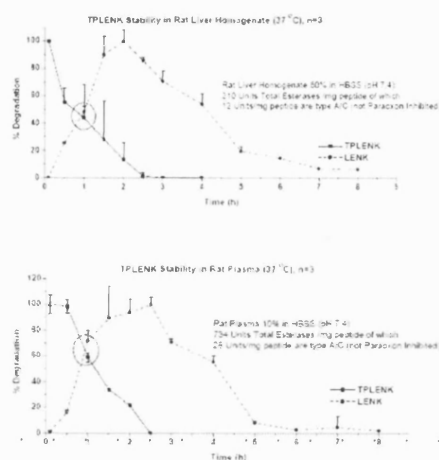


Figure 3: Stability of LENK & TPLENK in rat plasma and liver homogenates.

Aggregates of 160nm were present in the free LENK formulation, while the GCPQ-LENK formulation presented as a homogeneous dispersion of 44nm particles (Figure 4).

Preliminary pharmacokinetic data after IV administration ($n = 4$) of LENK suggest a trend towards a longer brain and plasma half-life for LENK in the presence of GCPQ although data was not statistically significant ($p > 0.05$) (Figure 5). Further studies will assess LENK concentrations in plasma & brain homogenates after IV and oral administration. The pharmacokinetic and pharmacodynamic profile of TPLENK in the presence and absence of GCPQ will be also studied.

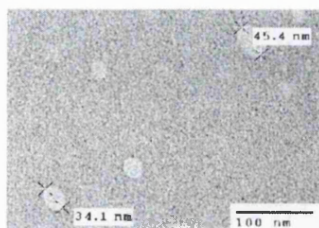


Figure 4: TEM images of LENK & GCPQ formulation used for IV studies.

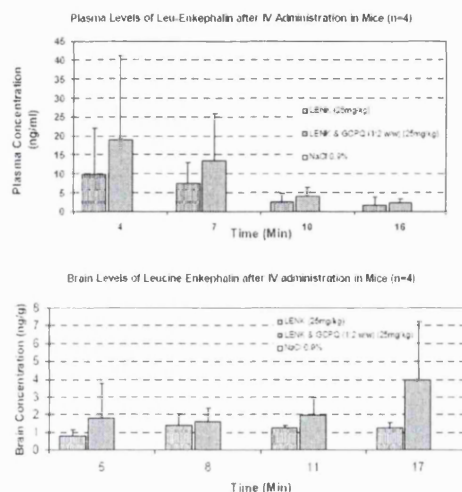


Figure 5: Plasma & Brain Concentration of LENK after IV administration ($p > 0.05$). The disperse phase was 0.9% NaCl.

CONCLUSION:

A novel method for the creation of a lipophilic ester prodrug of Leucine-Enkephalin was established. Stability of the parent peptide and the pro-drug was good in simulated gastric fluid and enhanced for the lipophilic pro-drug in rat intestinal wash by the presence of GCPQ. Preliminary in vivo testing indicates that LENK tended to have a longer plasma and brain half-life in the presence of GCPQ. Further studies on the pharmacokinetics and pharmacodynamics of the lipophilic ester prodrug are planned.

REFERENCES:

1. Qu, X., *et al.* *Biomacromolecules*. **7**(12): 3452 (2006)
2. Hussain, M.A., *et al.* *Drug Metab. Dispos.* **18**(3): 288 (1990)
3. Sokolov, O.Y., *et al.* *Bull. Exp. Biol. Med.* **137**(4): 342 (2004)
4. Cheng, W., S. *et al.* *Pharm. Res.* **24**(1): 99 (2007)
5. Ouyang, H., *et al.* *Pharm. Res.* **19**(6): 794 (2002)
6. Liederer, B.M. and R.T. Borchardt. *J. Pharm. Sci.* **94**(10): 2198 (2005)
7. De Ceballos, M.L., *et al.* *Neuropeptides*. **20**(3): 201 (1991)

ACKNOWLEDGEMENTS:

Financial support from the Engineering and Physical Sciences Research Council (EPSRC) and the School of Pharmacy, University of London is greatly acknowledged.

References

- (BP), British Pharmacopoeia. (2007). Appendix 1A. B. Pharmacopoeia. Norwich, UK, TSO. IV: A61.
- (FDA), Food and Drug Administration. (2001, 8th March 2001). Guidance for Industry Retrieved on the 25th December, 2008, from <http://www.fda.gov/CDER/GUIDANCE/3618fnl.htm>.
- (NC-IUBMB), National Committee of the International Union of Biochemistry and Molecular Biology. (2008). "Enzyme Nomenclature: Recommendations of the Nomenclature Committee of the International Union of Biochemistry and Molecular Biology on the Nomenclature and Classification of Enzymes by Reactions they Catalyse."
- Abbott, N. J. (2002). "Astrocyte-endothelial interactions and blood-brain barrier permeability." *J Anat* **200**(6): 629-38.
- Abbott, N. J., C. C. Hughes, et al. (1992). "Development and characterisation of a rat brain capillary endothelial culture: towards an in vitro blood-brain barrier." *J Cell Sci* **103** (Pt 1): 23-37.
- Abbott, N. J., L. Ronnback, et al. (2006). "Astrocyte-endothelial interactions at the blood-brain barrier." *Nat Rev Neurosci* **7**(1): 41-53.
- Abbruscato, T. J., S. A. Thomas, et al. (1997). "Brain and spinal cord distribution of biphalin: correlation with opioid receptor density and mechanism of CNS entry." *J Neurochem* **69**(3): 1236-45.
- Abbruscato, T. J., S. A. Williams, et al. (1996). "Blood-to-central nervous system entry and stability of biphalin, a unique double-enkephalin analog, and its halogenated derivatives." *J Pharmacol Exp Ther* **276**(3): 1049-57.
- Aburi, M. and P. E. Smith (2002). "A conformational analysis of leucine enkephalin as a function of pH." *Biopolymers* **64**(4): 177-88.
- Adessi, C. and C. Soto (2002). "Converting a peptide into a drug: strategies to improve stability and bioavailability." *Curr Med Chem* **9**(9): 963-78.
- Adibi, S. A. (1971). "Intestinal transport of dipeptides in man: relative importance of hydrolysis and intact absorption." *J Clin Invest* **50**(11): 2266-75.
- Adibi, S. A. and Y. S. Kim (1981). Peptide absorption and hydrolysis. *Physiology of the Gastrointestinal Tract*. L. R. Johnson. New York, Raven Press: 10736-95.
- Adibi, S. A. and D. W. Mercer (1973). "Protein digestion in human intestine as reflected in luminal, mucosal, and plasma amino acid concentrations after meals." *J Clin Invest* **52**(7): 1586-94.
- Adler, S. G., H. Wang, et al. (1983). "Electrical charge. Its role in the pathogenesis and prevention of experimental membranous nephropathy in the rabbit." *J Clin Invest* **71**(3): 487-99.
- Advokat, C. and A. Gulati (1991). "Spinal transection reduces both spinal antinociception and CNS concentration of systemically administered morphine in rats." *Brain Res* **555**(2): 251-8.
- Ahmed, M., A. Bjurholm, et al. (1994). "Extraction of neuropeptides from joint tissue for quantitation by radioimmunoassay. A study in the rat." *Peptides* **15**(2): 317-22.
- Ajdary, S., F. Dobakhti, et al. (2007). "Oral administration of BCG encapsulated in alginate microspheres induces strong Th1 response in BALB/c mice." *Vaccine* **25**(23): 4595-601.
- Alberghina, M. (1998). Chapter 25: Fatty acid and lipid intermediate transport.

- Introduction to the Blood-Brain Barrier: Methodology, biology, and pathology. W. M. Pardridge. Cambridge, UK, Cambridge University Press: 227-237.
- Albericio, F. (2000). "Orthogonal protecting groups for N(alpha)-amino and C-terminal carboxyl functions in solid-phase peptide synthesis." Biopolymers **55**(2): 123-39.
- Albericio, F. and L. A. Carpino (1997). "Coupling reagents and activation." Methods Enzymol **289**: 104-26.
- Albert, A. (1958). "Chemical aspects of selective toxicity." Nature **182**(4633): 421-2.
- Aldridge, W. N. (1953). "Serum esterases. I. Two types of esterase (A and B) hydrolysing p-nitrophenyl acetate, propionate and butyrate, and a method for their determination." Biochem J **53**(1): 110-7.
- Aldridge, W. N. (1952). "Serum Esterases." Biochem J **53**: 110-117.
- Alexander, B., X. Li, et al. (2000). "A quantitative evaluation of the permeability of the blood brain barrier of portacaval shunted rats." Metab Brain Dis **15**(2): 93-103.
- Allemann, E., J. Leroux, et al. (1998). "Polymeric nano- and microparticles for the oral delivery of peptides and peptidomimetics." Adv Drug Deliv Rev **34**(2-3): 171-189.
- Almeida, A. J. and E. Souto (2007). "Solid lipid nanoparticles as a drug delivery system for peptides and proteins." Adv Drug Deliv Rev **59**(6): 478-90.
- Al-Obeidi, F., A. M. Castrucci, et al. (1989). "Potent and prolonged acting cyclic lactam analogues of alpha-melanotropin: design based on molecular dynamics." J Med Chem **32**(12): 2555-61.
- Alyautdin, R., D. Gothier, et al. (1995). "Analgesic activity of the hexapeptide dalargin adsorbed on the surface of polysorbate 80-coated poly(butyl cyanoacrylate) nanoparticles. ." Eur. J. Pharm. Biopharm. **41**: 44-48.
- Amand, L.-E. and C. J. Tullin. "The theory of FTIR. Application examples from measurement at the 12MW circulating fluidised bed boiler at Chalmers. ." Retrieved 27th October, 2008, from http://www.entek.chalmers.se/~leam/ftir/ftir_pdf/own_pub/theory_ftir.pdf.
- Amodeo, P., F. Naider, et al. (1998). "Conformational sampling of bioactive conformers: a low-temperature NMR study of ¹⁵N-Leu-enkephalin." J Pept Sci **4**(4): 253-65.
- Andersson, L., L. Blomberg, et al. (2000). "Large-scale synthesis of peptides." Biopolymers **55**(3): 227-50.
- Anon. (2007). "Chapter: 7 Light Scattering." Retrieved 2nd July, 2007, from http://www.ias.ac.in/initiat/sci_ed/resources/chemistry/LightScat.pdf.
- Armstrong, D. and R. Zidovetzki. (2004). "Helical Wheel Projections." Retrieved 25th November, 2008, from <http://rzlab.ucr.edu/scripts/wheel/wheel.cgi?sequence=ABCDEFGHIIJLKMNOP&submit=Submit>.
- Artursson, P., T. Lindmark, et al. (1994). "Effect of chitosan on the permeability of monolayers of intestinal epithelial cells (Caco-2)." Pharm Res **11**(9): 1358-61.
- Asada, H., T. Douen, et al. (1995). "Absorption characteristics of chemically modified-insulin derivatives with various fatty acids in the small and large intestine." J Pharm Sci **84**(6): 682-7.
- Ashcroft, A. E. (2008). "An Introduction to Mass Spectrometry." Retrieved 10th October, 2008.

- Aspden, T. J., J. D. Mason, et al. (1997). "Chitosan as a nasal delivery system: the effect of chitosan solutions on in vitro and in vivo mucociliary transport rates in human turbinates and volunteers." *J Pharm Sci* **86**(4): 509-13.
- Atherton, E., D. L. J. Clive, et al. (1975). "Polyamide supports for polypeptide synthesis." *J Am Chem Soc* **97**: 6584.
- Attwood, T. K. and J. B. Findlay (1994). "Fingerprinting G-protein-coupled receptors." *Protein Eng* **7**(2): 195-203.
- Aubry, A., N. Birlirakis, et al. (1989). "A crystal molecular conformation of leucine-enkephalin related to the morphine molecule." *Biopolymers* **28**(1): 27-40.
- Audus, K. L. and R. T. Borchardt (1987). "Bovine brain microvessel endothelial cell monolayers as a model system for the blood-brain barrier." *Ann N Y Acad Sci* **507**: 9-18.
- Audus, K. L., P. J. Chikhale, et al. (1992). "Brain uptake of drugs: The influence of chemical and biological factors." *Adv Drug Res* **23**: 3-64.
- Avdeef, A. (2001). "Physicochemical profiling (solubility, permeability and charge state)." *Curr Top Med Chem* **1**(4): 277-351.
- Badkar, A. V., A. M. Smith, et al. (2007). "Transdermal delivery of interferon alpha-2B using microporation and iontophoresis in hairless rats." *Pharm Res* **24**(7): 1389-95.
- Bai, J. P. F. (1994). "The regional differences in the mucosal-cell lysosomal proteases within the rat small intestine." *Int. J. Pharm.* **107**: 133-140.
- Bak, A., O. S. Gudmundsson, et al. (1999). "Acyloxyalkoxy-based cyclic prodrugs of opioid peptides: evaluation of the chemical and enzymatic stability as well as their transport properties across Caco-2 cell monolayers." *Pharm Res* **16**(1): 24-9.
- Banks, J. F., Jr. and C. M. Whitehouse (1996). "Electrospray ionization mass spectrometry." *Methods Enzymol* **270**: 486-519.
- Banks, W. A. and A. J. Kastin (1994). "Opposite direction of transport across the blood-brain barrier for Tyr-MIF-1 and MIF-1: comparison with morphine." *Peptides* **15**(1): 23-9.
- Banks, W. A. and A. J. Kastin (1998). "Differential permeability of the blood-brain barrier to two pancreatic peptides: insulin and amylin." *Peptides* **19**(5): 883-9.
- Banks, W. A., A. J. Kastin, et al. (1986). "Entry of DSIP peptides into dog CSF: role of physicochemical and pharmacokinetic parameters." *Brain Res Bull* **17**(2): 155-8.
- Banks, W. A., A. J. Kastin, et al. (1986). "Carrier-mediated transport of enkephalins and N-Tyr-MIF-1 across blood-brain barrier." *Am J Physiol* **251**(4 Pt 1): E477-82.
- Barlos, K. and D. Gatos (1999). "9-Fluorenylmethyloxycarbonyl/ tbutyl-based convergent protein synthesis." *Biopolymers* **51**(4): 266-78.
- Barlos, K., D. Gatos, et al. (1989). "Darstellung geschützter peptid-fragmente unter einatz substituierter triphenylmethyl-harze." *Tetrahedron Lett* **30**(30): 3943-3946.
- Barlos, K., D. Gatos, et al. (1991). "Application of 2-chlorotrityl resin in solid phase synthesis of (Leu15)-gastrin I and unsulfated cholecystokinin octapeptide. Selective O-deprotection of tyrosine." *Int J Pept Protein Res* **38**(6): 555-61.
- Batrakova, E. V., D. W. Miller, et al. (2001). "Pluronic P85 enhances the delivery of digoxin to the brain: in vitro and in vivo studies." *J Pharmacol Exp Ther* **296**(2): 551-7.

- Batrakova, E. V., S. V. Vinogradov, et al. (2005). "Polypeptide point modifications with fatty acid and amphiphilic block copolymers for enhanced brain delivery." Bioconjug Chem **16**(4): 793-802.
- Batrakova, E. V., Y. Zhang, et al. (2004). "Effects of pluronic P85 on GLUT1 and MCT1 transporters in the blood-brain barrier." Pharm Res **21**(11): 1993-2000.
- Beavis, R. C. and B. T. Chait (1996). "Matrix-assisted laser desorption ionization mass-spectrometry of proteins." Methods Enzymol **270**: 519-51.
- Beavis, R. C., T. Chaudhary, et al. (1992). "a-Cyano-4-hydroxycinnamic acid as a matrix for matrixassisted laser desorption mass spectrometry." Org. Mass Spectrom. **27**(2): 156-158.
- Beckett, A. H. and A. F. Casy (1954). "Synthetic Analgesics: stereochemical considerations. ." J. Pharm. Pharmacol. **6**: 986-1001.
- Begley, D. J. (1996). "The blood-brain barrier: principles for targeting peptides and drugs to the central nervous system." J Pharm Pharmacol **48**(2): 136-46.
- Begley, D. J. (2004). "ABC transporters and the blood-brain barrier." Curr Pharm Des **10**(12): 1295-312.
- Begley, D. J. (2004). "Delivery of therapeutic agents to the central nervous system: the problems and the possibilities." Pharmacol Ther **104**(1): 29-45.
- Begley, D. J. (2004). Efflux mechanisms in the central nervous system: a powerful influence on drug distribution within the brain. Blood-spinal Cord and Brain Barriers in Health and Disease. H. S. Sharma and J. Westman. San Diego, Elsevier: 83-97.
- Begley, D. J. and M. W. Brightman (2003). Structural and functional aspects of the blood-brain barrier. Peptide transport and Delivery into the Central Nervous System. Progress in Drug Research. L. P.-T. Prokai, K. Basel, Switzerland, Birkhauser Verlag. **61**: 39-78.
- Begley, D. J. and D. G. Chain (1981). "Clearance of 3H-Tyr-leucine-enkephalin from rabbit cerebrospinal fluid." J. Physiol. (Lond.) **319**: 40-41P.
- Behnam, B. A. and C. M. Deber (1984). "Evidence for a folded conformation of methionine- and leucine-enkephalin in a membrane environment." J Biol Chem **259**(23): 14935-40.
- Behrens, I., A. I. Pena, et al. (2002). "Comparative uptake studies of bioadhesive and non-bioadhesive nanoparticles in human intestinal cell lines and rats: the effect of mucus on particle adsorption and transport." Pharm Res **19**(8): 1185-93.
- Bencharit, S., C. L. Morton, et al. (2003). "Crystal structure of human carboxylesterase 1 complexed with the Alzheimer's drug tacrine: from binding promiscuity to selective inhibition." Chem Biol **10**(4): 341-9.
- Benoit, J. P., N. Faisant, et al. (2000). "Development of microspheres for neurological disorders: from basics to clinical applications." J Control Release **65**(1-2): 285-96.
- Benoit, R., N. Ling, et al. (1987). Chapter 2: Peptides: Strategies for Antibody production and Radioimmunoassays. Neuromethods. A. A. Boulton, G. B. Baker and P. Q. J. Clifton, New Jersey, The Humana Press Inc. **6**: 43-72.
- Beranova-Giorgianni, S. and D. M. Desiderio (1997). "Fast atom bombardment mass spectrometry of synthetic peptides." Methods Enzymol **289**: 478-99.
- Bergmann, F., R. Segal, et al. (1957). "A new type of esterase in hog-kidney extract." Biochem J **67**(3): 481-6.
- Bergmann, P., R. Kacenenbogen, et al. (1984). "Plasma clearance, tissue

- distribution and catabolism of cationized albumins with increasing isoelectric points in the rat." *Clin Sci (Lond)* **67**(1): 35-43.
- Bernkop-Schnurch, A. (1998). "The use of inhibitory agents to overcome the enzymatic barrier to perorally administered therapeutic peptides and proteins." *J Control Release* **52**(1-2): 1-16.
- Bernkop-Schnurch, A., C. Paikl, et al. (1997). "Novel bioadhesive chitosan-EDTA conjugate protects leucine enkephalin from degradation by aminopeptidase N." *Pharm Res* **14**(7): 917-22.
- Bernkop-Schnurch, A., Y. Pinter, et al. (2005). "The use of thiolated polymers as carrier matrix in oral peptide delivery--proof of concept." *J Control Release* **106**(1-2): 26-33.
- Bernstein, G. (2008). "Delivery of insulin to the buccal mucosa utilizing the RapidMist system." *Expert Opin Drug Deliv* **5**(9): 1047-55.
- Betz, A. L., J. A. Firth, et al. (1980). "Polarity of the blood-brain barrier: distribution of enzymes between the luminal and antiluminal membranes of brain capillary endothelial cells." *Brain Res* **192**(1): 17-28.
- Bewley, T. A. and C. H. Li (1983). "Evidence for tertiary structure in aqueous solutions of human beta-endorphin as shown by difference absorption spectroscopy." *Biochemistry* **22**(11): 2671-5.
- Bickel, U., T. Yoshikawa, et al. (2001). "Delivery of peptides and proteins through the blood-brain barrier." *Adv Drug Deliv Rev* **46**(1-3): 247-79.
- Bilsky, E. J., R. D. Eggleton, et al. (2000). "Enkephalin glycopeptide analogues produce analgesia with reduced dependence liability." *J Med Chem* **43**(13): 2586-90.
- Blasberg, R. G., J. D. Fenstermacher, et al. (1983). "Transport of alpha-aminoisobutyric acid across brain capillary and cellular membranes." *J Cereb Blood Flow Metab* **3**(1): 8-32.
- Blasberg, R. G., J. Gazendam, et al. (1980). "Quantitative autoradiographic studies of brain edema and a comparison of multi-isotope autoradiographic techniques." *Adv Neurol* **28**: 255-70.
- Blasi, P., S. Giovagnoli, et al. (2007). "Solid lipid nanoparticles for targeted brain drug delivery." *Adv Drug Deliv Rev* **59**(6): 454-77.
- Blomberg, D., P. Kreye, et al. (2006). "Synthesis and biological evaluation of leucine enkephalin turn mimetics." *Org Biomol Chem* **4**(3): 416-23.
- Bodanszky, M. (1955). "Synthesis of peptides by aminolysis of nitrophenyl esters." *Nature* **175**(4459): 685.
- Bodor, N. and P. Buchwald (1999). "Recent advances in the brain targeting of neuropharmaceuticals by chemical delivery systems." *Adv Drug Deliv Rev* **36**(2-3): 229-254.
- Bodor, N. and P. Buchwald (2003). "Brain-targeted drug delivery: experiences to date." *Am. J. Drug Targ* **1**: 13-26.
- Bodor, N. and P. Buchwald (2006). Targeting of neuropharmaceuticals by chemical delivery systems. *Blood-Brain Interfaces: From Ontogeny to Artificial Barriers*. R. Dermietzel, D. C. Spray and M. Nedergaard. Weinheim, Wiley-VCH Verlag GmbH & Co, KGaA.
- Bodor, N., L. Prokai, et al. (1992). "A strategy for delivering peptides into the central nervous system by sequential metabolism." *Science* **257**(5077): 1698-700.
- Bodor, N., E. Shek, et al. (1975). "Delivery of a quaternary pyridinium salt across the blood-brain barrier by its dihydropyridine derivative." *Science* **190**(4210): 155-6.

- Borchardt, R. T. (1999). "Optimizing oral absorption of peptides using prodrug strategies." *J Control Release* **62**(1-2): 231-8.
- Borm, P. J., D. Robbins, et al. (2006). "The potential risks of nanomaterials: a review carried out for ECETOC." *Part Fibre Toxicol* **3**: 11.
- Bourland, J. A., D. K. Martin, et al. (1997). "Carboxylesterase-mediated transesterification of meperidine (Demerol) and methylphenidate (Ritalin) in the presence of [2H6]ethanol: preliminary in vitro findings using a rat liver preparation." *J Pharm Sci* **86**(12): 1494-6.
- Brewster, M. E., K. S. Estes, et al. (1988). "Improved delivery through biological membranes. 32. Synthesis and biological activity of brain-targeted delivery systems for various estradiol derivatives." *J Med Chem* **31**(1): 244-9.
- Brightman, M. (1992). Ultrastructure of brain endothelium. *Physiology and Pharmacology of the Blood-Brain Barrier. Handbook of Experimental Pharmacology*. M. W. B. Bradbury. Berlin, Springer-Verlag: 1-22.
- Brightman, M. W. and T. S. Reese (1969). "Junctions between intimately apposed cell membranes in the vertebrate brain." *J Cell Biol* **40**: 648-677.
- Broadwell, R. D., B. J. Balin, et al. (1988). "Transcytotic pathway for blood-borne protein through the blood-brain barrier." *Proc Natl Acad Sci U S A* **85**(2): 632-6.
- Broccardo, M., V. Erspamer, et al. (1981). "Pharmacological data on dermorphins, a new class of potent opioid peptides from amphibian skin." *Br J Pharmacol* **73**(3): 625-31.
- Brownless, J. and C. H. Williams (1993). "Peptidases, peptides and the mammalian blood-brain barrier." *J. Neurochem* **60**: 1089-96.
- Brownson, E. A., T. J. Abbruscato, et al. (1994). "Effect of peptidases at the blood brain barrier on the permeability of enkephalin." *J Pharmacol Exp Ther* **270**(2): 675-80.
- Buchwald, P. and N. Bodor (1998). "Octanol-water partition of nonzwitterionic peptides: predictive power of a molecular size-based model." *Proteins* **30**(1): 86-99.
- Buchwald, P. and N. Bodor (1999). "Quantitative structure-metabolism relationships: steric and nonsteric effects in the enzymatic hydrolysis of noncongener carboxylic esters." *J. Med. Chem.* **42**: 5160-8.
- Buckett, W. R. (2008). "Laboratory testing of new drugs for morphine-like drug dependence." *Addiction* **62**(3-4): 387-90.
- Builders, P. F., O. O. Kunle, et al. (2008). "Preparation and evaluation of mucinated sodium alginate microparticles for oral delivery of insulin." *Eur J Pharm Biopharm.*
- Bundgaard, H. and J. Moss (1990). "Prodrugs of peptides. 6. Bioreversible derivatives of thyrotropin-releasing hormone (TRH) with increased lipophilicity and resistance to cleavage by the TRH-specific serum enzyme." *Pharm Res* **7**(9): 885-92.
- Burdick, D. J. and J. T. Stults (1997). "Analysis of peptide synthesis products by electrospray ionization mass spectrometry." *Methods Enzymol* **289**: 499-519.
- Buscher, H. H., R. C. Hill, et al. (1976). "Evidence for analgesic activity of enkephalin in the mouse." *Nature* **261**(5559): 423-5.
- Butt, A. M., H. C. Jones, et al. (1990). "Electrical resistance across the blood-brain barrier in anaesthetized rats: a developmental study." *J Physiol* **429**: 47-62.
- Calvo, P., B. Gouritin, et al. (2001). "Long-circulating PEGylated polycyanoacrylate nanoparticles as new drug carrier for brain delivery." *Pharm Res* **18**(8): 1157-

66.

- Campbell, B. J., L. J. Forrester, et al. (1984). "Beta-lactamase activity of purified and partially characterized human renal dipeptidase." J Biol Chem **259**(23): 14586-90.
- Carpino, L. A. (1957). "Oxidative Reactions of Hydrazines. IV. Elimination of Nitrogen from 1,1-Disubstituted-2-arenesulfonhydrazides1-4." J Am Chem Soc **79**: 4427.
- Carrigan, C. N. and B. Imperiali (2005). "The engineering of membrane-permeable peptides." Anal Biochem **341**(2): 290-8.
- Cashion, M. F., W. A. Banks, et al. (1996). "Sequestration of centrally administered insulin by the brain: effects of starvation, aluminum, and TNF-alpha." Horm Behav **30**(3): 280-6.
- Castro, B., J. R. Dormoy, et al. (1975). "Reactifs de couplage peptidique I (1) - l'hexafluorophosphate de benzotriazolyl N-oxytrisdimethylamino phosphonium (B.O.P.)." Tetrahedron Lett **16**(14): 1219.
- Castro, B., J. R. Dormoy, et al. (1977). J. Chem. Res. (S): 182.
- Center, A. (2008). "Electron Microscope: The Electron Microscope in Biology." Retrieved 24th November 2008, from <http://www.hei.org/research/aemi/emt.htm>.
- Cereijido, M., I. Meza, et al. (1981). "Occluding junctions in cultured epithelial monolayers." Am J Physiol **240**(3): C96-102.
- Cereijido, M., O. Ruiz, et al. (1993). The paracellular pathway. Biological Barriers to Protein Delivery. K. L. Audus and T. Raub. New York, NY, Plenum Press: 3-21.
- Chaki, K., S. Sakurada, et al. (1990). "N-terminal tetrapeptide of dermorphin and D-Arg-substituted tetrapeptides: inactivation process of the antinociceptive activity by peptidase." Life Sci **46**(23): 1671-8.
- Chakrabarti, S. and A. A. Sima (1990). "The presence of anionic sites in basement membranes of cerebral capillaries." Microvasc Res **39**: 123-127.
- Chan, L. M., S. Lowes, et al. (2004). "The ABCs of drug transport in intestine and liver: efflux proteins limiting drug absorption and bioavailability." Eur J Pharm Sci **21**(1): 25-51.
- Chandrasekhar, I., W. F. van Gunsteren, et al. (2006). "Orientation and conformational preference of leucine-enkephalin at the surface of a hydrated dimyristoylphosphatidylcholine bilayer: NMR and MD simulation." J Am Chem Soc **128**(1): 159-70.
- Chapman, J. R. (1996). Mass Spectrometry: Ionisation Methods and Instrumentation. Methods in Molecular Biology, Volume 61: Protein and Peptide Analysis by Mass Spectrometry. J. R. Chapman. Totowa, NJ, Humana Press Inc. **61**: 1-28.
- Chaturvedi, K., K. H. Christoffers, et al. (2000). "Structure and regulation of opioid receptors." Biopolymers **55**(4): 334-46.
- Chen, C. and G. M. Pollack (1998). "Altered disposition and antinociception of [D-penicillamine(2,5)] enkephalin in mdrla-gene-deficient mice." J Pharmacol Exp Ther **287**(2): 545-52.
- Cheng, W., S. Satyanarayanajois, et al. (2007). "Aqueous-soluble, non-reversible lipid conjugate of salmon calcitonin: synthesis, characterization and in vivo activity." Pharm Res **24**(1): 99-110.
- Cheng, W. P., A. I. Gray, et al. (2006). "Polyelectrolyte nanoparticles with high drug loading enhance the oral uptake of hydrophobic compounds."

- Biomacromolecules 7(5): 1509-20.
- Chikhale, E. G., K. Y. Ng, et al. (1994). "Hydrogen bonding potential as a determinant of the in vitro and in situ blood-brain barrier permeability of peptides." Pharm Res 11(3): 412-9.
- Chiou, G. C. and C. Y. Chuang (1989). "Improvement of systemic absorption of insulin through eyes with absorption enhancers." J Pharm Sci 78(10): 815-8.
- Chornet, E. and S. Dumitriu (1998). "Inclusion and release of proteins from polysaccharide-based polyion complexes." Adv Drug Deliv Rev 31(3): 223-246.
- Claridge, T. D. W. (2009). High-resolution NMR techniques in Organic Chemistry. Oxford, U. K., Elsevier.
- Conradi, R. A., P. S. Burton, et al. (1996). Physico-chemical and biological factors that influence a drug's cellular permeability by passive diffusion. Lipophilicity in Drug Action and Toxicology. V. Pliska, H. Testa and H. Van de Waterbeemd. VCH, Weinheim: 233-250.
- Conradi, R. A., A. R. Hilgers, et al. (1991). "The influence of peptide structure on transport across Caco-2 cells." Pharm Res 8(12): 1453-60.
- Conradi, R. A., A. R. Hilgers, et al. (1992). "The influence of peptide structure on transport across Caco-2 cells. II. Peptide bond modification which results in improved permeability." Pharm Res 9(3): 435-9.
- Coppi, G., M. Bondi, et al. (2008). "Toxicity and gut associated lymphoid tissue translocation of polymyxin B orally administered by alginate/chitosan microparticles in rats." J Pharm Pharmacol 60(1): 21-6.
- Corbett, A. D., G. Henderson, et al. (2006). "75 years of opioid research: the exciting but vain quest for the Holy Grail." Br J Pharmacol 147 Suppl 1: S153-62.
- Cortesi, R., R. Argnani, et al. (2006). "Cationic liposomes as potential carriers for ocular administration of peptides with anti-herpetic activity." Int J Pharm 317(1): 90-100.
- Coste, J., D. Le-Nguyen, et al. (1990). "PyBOP®: A new peptide coupling reagent devoid of toxic by-product." Tetrahedron Lett 31(2): 205.
- Couvreur, P. and F. Puisieux (1993). "Nano-and microparticles for the delivery of polypeptides and proteins." Adv Drug Deliv Rev 10: 141-62.
- Crampton, R. F., M. T. Lis, et al. (1973). "Sites of maximal absorption and hydrolysis of two dipeptides by rat small intestine in vivo." Clin Sci 44(6): 583-94.
- Crooks, S. L. and L. J. Charles (2000). Overview of Combinational Chemistry. London, John Wiley & Sons, Inc.
- Damge, C., C. Michel, et al. (1990). "Nanocapsules as carriers for oral peptide delivery." J. Control. Release 13: 233-239.
- D'Amour, F. E. and D. L. Smith (1941). "A method for determining loss of pain sensation." JPET 72: 74-79.
- Das, D. and S. Lin (2005). "Double-coated poly (butylcynanoacrylate) nanoparticulate delivery systems for brain targeting of dalargin via oral administration." J Pharm Sci 94(6): 1343-53.
- David, J. H. and H. Peck (1993). Analytical Biochemistry. London?, Langman Scientific & Technical.
- Davson, H. and M. B. Segal (1995). Physiology of the CSF & Blood-Brain Barriers. New York, USA, CRC Press.
- De Ceballos, M. L., M. D. Taylor, et al. (1991). "Isocratic Reverse-Phase HPLC Separation and RIA Used in the Analysis of Neuropeptides in Brain Tissue."

- Neuropeptides **20**: 201-9.
- de Vries, N. A., J. Zhao, et al. (2007). "P-glycoprotein and breast cancer resistance protein: two dominant transporters working together in limiting the brain penetration of topotecan." Clin Cancer Res **13**(21): 6440-9.
- Deguchi, Y., Y. Miyakawa, et al. (2003). "Blood-brain barrier transport of a novel micro 1-specific opioid peptide, H-Tyr-D-Arg-Phe-beta-Ala-OH (TAPA)." J Neurochem **84**(5): 1154-61.
- Deguchi, Y., Y. Naito, et al. (2004). "Blood-brain barrier permeability of novel [D-arg2]dermorphin (1-4) analogs: transport property is related to the slow onset of antinociceptive activity in the central nervous system." J Pharmacol Exp Ther **310**(1): 177-84.
- Delie, F. and M. J. Blanco-Prieto (2005). "Polymeric particulates to improve oral bioavailability of peptide drugs." Molecules **10**(1): 65-80.
- Desai, M. P., V. Labhasetwar, et al. (1996). "Gastrointestinal uptake of biodegradable microparticles: effect of particle size." Pharm Res **13**(12): 1838-45.
- Deshpande, M. S. (1994). "Formation of carbon-carbon bond on solid support: Application of the stille reaction." Tetrahedron Lett **35**(31): 5613.
- Dixon, D. and D. Harden. (2008, 22nd October 2008). "Molecular Modeling." Retrieved 22th October, 2008, from <http://chemistry.gsu.edu/glactone/modeling/MMintro.html>.
- Dixon, M. and E. C. Webb (1979). Enzymes. New York, Academic Press.
- Dodané, V., M. Amin Khan, et al. (1999). "Effect of chitosan on epithelial permeability and structure." Int J Pharm **182**(1): 21-32.
- Dodda-Kashi, S. D. and V. H. L. Lee (1986). "Enkephalin hydrolysis in homogenates of various absorptive mucosae of the albino rabbit: Similarities in rates and involvement of aminopeptidases" Life Sci. **38**: 2019-28
- Domard, A., M. Rinaudo, et al. (1986). "New method for the quaternisation of chitosan." Int. J. Biol. Macromol. **8**: 105-7.
- Donovan, M. D., G. L. Flynn, et al. (1990). "Absorption of polyethylene glycols 600 through 2000: the molecular weight dependence of gastrointestinal and nasal absorption." Pharm Res **7**(8): 863-8.
- Dore-Duffy, P. (2003). "Isolation and characterization of cerebral microvascular pericytes." Methods Mol Med **89**: 375-82.
- Doyle, K. P., T. Yang, et al. (2008). "Nasal administration of osteopontin peptide mimetics confers neuroprotection in stroke." J Cereb Blood Flow Metab **28**(6): 1235-48.
- Doyle, L. A. and D. D. Ross (2003). "Multidrug resistance mediated by the breast cancer resistance protein BCRP (ABCG2)." Oncogene **22**(47): 7340-58.
- Drasar, B. S. and M. J. Hill (1974). Human intestinal flora. London, Academic Press: 54-167.
- Drewe, J., G. Fricker, et al. (1993). "Enteral absorption of octreotide: absorption enhancement by polyoxyethylene-24-cholesterol ether." Br J Pharmacol **108**(2): 298-303.
- Du Vigneaud, V., C. Ressler, et al. (1953). "The synthesis of an octapeptide amide with the hormonal activity of Oxytocin." J Am Chem Soc **75**: 4879.
- Duncan, R. (1992). "Drug-polymer conjugates: potential for improved chemotherapy." Anticancer Drugs **3**(3): 175-210.
- Eckel, R. H. and R. J. Robbins (1984). "Lipoprotein lipase is produced, regulated, and functional in rat brain." Proc Natl Acad Sci U S A **81**(23): 7604-7.

- Egleton, R. D., E. J. Bilsky, et al. (2005). "Biosian glycopeptides penetrate the blood-brain barrier." *Tetrahedron Asymmetry* **16**: 65-75.
- Egleton, R. D. and T. P. Davis (1999). "Transport of the delta-opioid receptor agonist [D-penicillamine^{2,5}] enkephalin across the blood-brain barrier involves transcytosis." *J Pharm Sci* **88**(4): 392-7.
- Egleton, R. D., S. A. Mitchell, et al. (2000). "Improved bioavailability to the brain of glycosylated Met-enkephalin analogs." *Brain Res* **881**(1): 37-46.
- Eguchi, M. (2004). "Recent advances in selective opioid receptor agonists and antagonists." *Med Res Rev* **24**(2): 182-212.
- Ejendal, K. F. and C. A. Hrycyna (2005). "Differential sensitivities of the human ATP-binding cassette transporters ABCG2 and P-glycoprotein to cyclosporin A." *Mol Pharmacol* **67**(3): 902-11.
- Ekrami, H. M., A. R. Kennedy, et al. (1995). "Water-soluble fatty acid derivatives as acylating agents for reversible lipidization of polypeptides." *FEBS Lett* **371**(3): 283-6.
- Elmagbari, N. O., R. D. Egleton, et al. (2004). "Antinociceptive structure-activity studies with enkephalin-based opioid glycopeptides." *J Pharmacol Exp Ther* **311**(1): 290-7.
- Emerich, D. F., M. A. Tracy, et al. (1999). "Biocompatibility of poly (DL-lactide-co-glycolide) microspheres implanted into the brain." *Cell Transplant* **8**(1): 47-58.
- Erickson, R. H., Y. Suzuki, et al. (1992). "Rat intestinal angiotensin-converting enzyme: purification, properties, expression, and function." *Am J Physiol* **263**(4 Pt 1): G466-73.
- Farkas, E. and P. G. Luiten (2001). "Cerebral microvascular pathology in aging and Alzheimer's disease." *Prog Neurobiol* **64**(6): 575-611.
- Fei, Y. J., Y. Kanai, et al. (1994). "Expression cloning of a mammalian proton-coupled oligopeptide transporter." *Nature* **368**(6471): 563-6.
- Feng, S. S., L. Mu, et al. (2004). "Nanoparticles of biodegradable polymers for clinical administration of paclitaxel." *Curr Med Chem* **11**(4): 413-24.
- Fenstermacher, J., P. Gross, et al. (1988). "Structural and functional variations in capillary systems within the brain." *Ann N Y Acad Sci* **529**: 21-30.
- Fields, G. B. (1997). *Methods in Enzymology. Solid-Phase Peptide Synthesis*. London, Academic Press.
- Fields, G. B. and R. L. Noble (1990). "Solid phase peptide synthesis utilizing 9-fluorenylmethoxycarbonyl amino acids." *Int J Pept Protein Res* **35**(3): 161-214.
- Fisher, J. F., A. W. Harrison, et al. (1991). "Peptide to glycopeptide: glycosylated oligopeptide renin inhibitors with attenuated in vivo clearance properties." *J Med Chem* **34**(10): 3140-3.
- Fix, J. A. (1996). "Strategies for delivery of peptides utilizing absorption-enhancing agents." *J Pharm Sci* **85**(12): 1282-5.
- Fjellestad-Paulsen, A., C. Soderberg-Ahlm, et al. (1995). "Metabolism of vasopressin, oxytocin, and their analogues in the human gastrointestinal tract." *Peptides* **16**(6): 1141-7.
- Florence, A. T. and D. Attwood Chapter 11. Peptides, proteins, and other biopharmaceuticals. *Physicochemical Principles of Pharmacy*.
- Florence, A. T., A. M. Hillery, et al. (1995). "Nanoparticles as carriers for oral peptide absorption: studies on particle uptake and fate." *J. Control. Release* **36**: 39-46.

- Franklin, K. B. J. and F. V. Abbott (1989). Techniques for Assessing the Effects of Drugs on Nociceptive Responses. Neuromethods 13: Psychopharmacology. A. A. Boulton, G. B. Baker and A. J. Greensham. Clifton, New Jersey, Humana Press Inc. : 145-216.
- Franklin, T. J. and G. A. Snow (1985). Biochemistry of Antimicrobial Action. London, Chapman & Hall.
- Fredholt, K., C. Adrian, et al. (2000). "Chemical and enzymatic stability as well as transport properties of a Leu-enkephalin analogue and ester prodrugs thereof." J Control Release **63**(3): 261-73.
- Frokjaer, S. and D. E. Otzen (2005). "Protein drug stability: a formulation challenge." Nat Rev Drug Discov **4**(4): 298-306.
- Fu, X., Z. Song, et al. (2004). A Predictive Model for Blood-Brain Barrier Penetration. Internet Electronic Conference of Molecular Design.
- Furuse, M., K. Fujita, et al. (1998). "Claudin-1 and -2: novel integral membrane proteins localizing at tight junctions with no sequence similarity to occludin." J Cell Biol **141**(7): 1539-50.
- Furuse, M., T. Hirase, et al. (1993). "Occludin: a novel integral membrane protein localizing at tight junctions." J Cell Biol **123**(6 Pt 2): 1777-88.
- Gawne, G., G. Kenner, et al. (1969). "Acyloxyphosphonium salts as acylating agents. Synthesis of peptides." J Am Chem Soc **91**: 5669.
- Gentry, C. L., R. D. Egleton, et al. (1999). "The effect of halogenation on blood-brain barrier permeability of a novel peptide drug." Peptides **20**(10): 1229-38.
- Geology, D. o. (2002). "Philips PW3040 X-ray Diffractometer with X'Pert Software". Retrieved 24th August, 2008, from <http://departments.colgate.edu/geology/instruments/xrd.htm>.
- Gesellchen, P. D., C. J. Parli, et al. (1981). A novel method for analysis of the in vivo stability of opioid peptides. Peptides: synthesis, structure, function. D. H. Rich and E. Gross. Rockford, Pierce: 637-40.
- Gessner, A., C. Olbrich, et al. (2001). "The role of plasma proteins in brain targeting: species dependent protein adsorption patterns on brain-specific lipid drug conjugate (LDC) nanoparticles." Int J Pharm **214**(1-2): 87-91.
- Ghosh, M. K. and A. K. Mitra (1992). "Enhanced delivery of 5-iodo-2'-deoxyuridine to the brain parenchyma." Pharm Res **9**(9): 1173-6.
- Gill, S., F. J. Hayes, et al. (2003). Issues in Endocrine Immunoassays. Handbook of Diagnostic Endocrinology. J. E. Hall and L. K. Nieman. Totowa, New Jersey, Humana Press, Inc.: 1-21.
- Gonzalvo, M. C., F. Gil, et al. (1997). "Inhibition of paraoxonase activity in human liver microsomes by exposure to EDTA, metals and mercurials." Chem Biol Interact **105**(3): 169-79.
- Gottesman, M. M. and I. Pastan (1993). "Biochemistry of multidrug resistance mediated by the multidrug transporter." Annu Rev Biochem **62**: 385-427.
- Graham, W. H., E. S. Carter, 2nd, et al. (1992). "Conformational analysis of Met-enkephalin in both aqueous solution and in the presence of sodium dodecyl sulfate micelles using multidimensional NMR and molecular modeling." Biopolymers **32**(12): 1755-64.
- Gray, R. A., D. G. Vander Velde, et al. (1994). "Delta-sleep-inducing peptide: solution conformational studies of a membrane-permeable peptide." Biochemistry **33**(6): 1323-31.
- Greene, D. L., V. S. Hau, et al. (1996). "Enkephalin analog prodrugs: assessment of in vitro conversion, enzyme cleavage characterization and blood-brain barrier

- permeability." *J Pharmacol Exp Ther* **277**(3): 1366-75.
- Gref, R., Y. Minamitake, et al. (1994). "Biodegradable long-circulating polymeric nanospheres." *Science* **263**(5153): 1600-3.
- Gregoriadis, G. (2006). *Liposome Technology: Liposome preparation and related techniques*. London, Taylor & Francis, Inc. .
- Greig, N. H., P. L. Stahle, et al. (1990). "High-performance liquid chromatographic analysis of chlorambucil tert.-butyl ester and its active metabolites chlorambucil and phenylacetic mustard in plasma and tissue." *J Chromatogr* **534**: 279-86.
- Guggi, D., C. E. Kast, et al. (2003). "In vivo evaluation of an oral salmon calcitonin-delivery system based on a thiolated chitosan carrier matrix." *Pharm Res* **20**(12): 1989-94.
- Gutte, B. and R. B. Merrifield (1971). "The synthesis of ribonuclease A." *J Biol Chem* **246**(6): 1922-41.
- Guy, C. A. and G. B. Fields (1997). "Trifluoroacetic acid cleavage and deprotection of resin-bound peptides following synthesis by Fmoc chemistry." *Methods Enzymol* **289**: 67-83.
- Habgood, M. D., D. J. Begley, et al. (2000). "Determinants of passive drug entry into the central nervous system." *Cell Mol Neurobiol* **20**(2): 231-53.
- Hansen, D. W., Jr., A. Stapelfeld, et al. (1992). "Systemic analgesic activity and delta-opioid selectivity in [2,6-dimethyl-Tyr1,D-Pen2,D-Pen5]enkephalin." *J Med Chem* **35**(4): 684-7.
- Hardebo, J. E. and J. Kahrstrom (1985). "Endothelial negative surface charge areas and blood-brain barrier function." *Acta Physiol Scand* **125**(3): 495-9.
- Hardy, J. D., J. A. Stolwijk, et al. (1965). "Skin temperature and cutaneous pain during warm water immersion." *J Appl Physiol* **20**(5): 1014-21.
- Harel, M., A. Aharoni, et al. (2004). "Structure and evolution of the serum paraoxonase family of detoxifying and anti-atherosclerotic enzymes." *Nat Struct Mol Biol* **11**(5): 412-9.
- Harris, L. S. and A. K. Pierson (1964). "Some Narcotic Antagonists in the Benzomorphan Series." *J Pharmacol Exp Ther* **143**: 141-8.
- Hashimoto, M., K. Takada, et al. (1989). "Synthesis of palmitoyl derivatives of insulin and their biological activities." *Pharm Res* **6**(2): 171-6.
- Hawkins, B. T. and T. P. Davis (2005). "The blood-brain barrier/neurovascular unit in health and disease." *Pharmacol Rev* **57**(2): 173-85.
- He, L., C. P. Vicente, et al. (2002). "Heparin cofactor II inhibits arterial thrombosis after endothelial injury." *J Clin Invest* **109**(2): 213-9.
- Hill, A. (2008). *Introducing some of the relationships between rheology & particle properties*. Malvern-Materials Characterisation Seminar, School of Pharmacy, University of London, Malvern Instruments.
- Hillenkamp, F., M. Karas, et al. (1991). "Matrix-assisted laser desorption/ionization mass spectrometry of biopolymers." *Anal Chem* **63**(24): 1193A-1203A.
- Hirano, S., H. Seino, et al. (1989). "Biocompatibility of chitosan by oral and intravenous administration." *Polym. Eng. Sci.* **59**: 897-901.
- Hoet, P. H., I. Bruske-Hohlfeld, et al. (2004). "Nanoparticles - known and unknown health risks." *J Nanobiotechnology* **2**(1): 12.
- Horan, P. J., A. Mattia, et al. (1993). "Antinociceptive profile of biphalin, a dimeric enkephalin analog." *J Pharmacol Exp Ther* **265**(3): 1446-54.
- Hosokawa, M., T. Endo, et al. (1995). "Interindividual variation in carboxylesterase levels in human liver microsomes." *Drug Metab Dispos* **23**(10): 1022-7.

- Hu, L. (2005). Prodrug Approaches to Drug Delivery. Drug Delivery: Principles and Applications. B. Wang, T. J. Siahaan and R. Soltero. New Jersey, John Wiley & Sons, Inc.: 125-165.
- Huang, J. T. and A. Lajtha (1978). "The accumulation of (3H) enkephalinamide (2-D-alanine-5-methioninamide) in rat brain tissues." Neuropharmacology **17**(12): 1075-9.
- Huang, J. T., M. Mannik, et al. (1984). "In situ formation of immune complexes in the choroid plexus of rats by sequential injection of a cationized antigen and unaltered antibodies." J Neuropathol Exp Neurol **43**(5): 489-99.
- Hughes, J., T. W. Smith, et al. (1975). "Identification of two related pentapeptides from the brain with potent opiate agonist activity." Nature **258**(5536): 577-80.
- Hussain, M. A., S. M. Rowe, et al. (1990). "Inhibition of leucine enkephalin metabolism in rat blood, plasma and tissues in vitro by an aminoboronic acid derivative." Drug Metab Dispos **18**(3): 288-91.
- Hussain, M. A., A. B. Shenvi, et al. (1989). "The use of alpha-aminoboronic acid derivatives to stabilize peptide drugs during their intranasal absorption." Pharm Res **6**(2): 186-9.
- Hutchinson, F. G. and B. J. A. Furr (1990). "Bioderadable polymer systems for the sustained release of polypeptides." J. Control. Release **13**: 279-94.
- Ireland, R. E. (1969). Organic synthesis. NJ, Prentice Hall.
- Iwanaga, K., S. Ono, et al. (1999). "Application of surface-coated liposomes for oral delivery of peptide: effects of coating the liposome's surface on the GI transit of insulin." J Pharm Sci **88**(2): 248-52.
- Iwanaga, K., S. Ono, et al. (1997). "Oral delivery of insulin by using surface coating liposomes: Improvement of stability of insulin in GI tract " Int. J. Pharm. **157**: 73-80.
- Jaehde, U., R. Masereeuw, et al. (1994). "Quantification and visualization of the transport of octreotide, a somatostatin analogue, across monolayers of cerebrovascular endothelial cells." Pharm Res **11**(3): 442-8.
- Janes, K. A., P. Calvo, et al. (2001). "Polysaccharide colloidal particles as delivery systems for macromolecules." Adv Drug Deliv Rev **47**(1): 83-97.
- Jennewein, H. M., F. Waldeck, et al. (1974). "The absorption of tetragastrin from different sites in rats and dogs." Arzneimittelforschung **24**(8): 1225-8.
- Jmol. (2008). "The 20 Amino Acids." Retrieved on the 15th August, 2008, from http://www.ecosci.jp/amino/amino2j_e.html.
- Jorgensen, W. L., D. S. Maxwell, et al. (1996). "Development and Testing of the OPLS All-Atom Force Field on Conformational Energetics and Properties of Organic Liquids." J. Am. Chem. Soc. **118**(45): 11225-36.
- Juhasz, P., C. E. Costello, et al. (1993). "Matrix-assisted laser desorption ionization mass spectrometry with 2-(4-hydroxyphenylazo)benzoic acid matrix." J. Am. Soc. Mass Spectrom. **4**(5): 399-409.
- Kacem, K., P. Lacombe, et al. (1998). "Structural organization of the perivascular astrocyte endfeet and their relationship with the endothelial glucose transporter: a confocal microscopy study." Glia **23**(1): 1-10.
- Kahns, A. H., A. Buur, et al. (1993). "Prodrugs of peptides. 18. Synthesis and evaluation of various esters of desmopressin (dDAVP)." Pharm Res **10**(1): 68-74.
- Kalyanasundaram, K. and J. K. Thomas (1977). "Environmental effects on the vibronic band intensities in pyrene monomer fluorescence & their application

- to studies of micellar systems." *J. Am. Chem. Soc.* **99**: 2039-44.
- Kane, B. E., B. Svensson, et al. (2006). "Molecular recognition of opioid receptor ligands." *Aaps J* **8**(1): E126-37.
- Kante, B., P. Couvreur, et al. (1982). "Toxicity of polyalkylcyanoacrylate nanoparticles I: Free nanoparticles." *J Pharm Sci* **71**(7): 786-90.
- Karas, M., D. Bachman, et al. (1987). "Matrix-assisted ultraviolet laser desorption of non-volatile compounds." *Int. J. Mass Spectrom. Ion Proc.* **78**: 53-68.
- Karas, M. and F. Hillenkamp (1988). "Laser desorption ionization of proteins with molecular masses exceeding 10,000 daltons." *Anal Chem* **60**(20): 2299-301.
- Kastin, A. J., V. Akerstrom, et al. (2001). "Validity of multiple-time regression analysis in measurement of tritiated and iodinated leptin crossing the blood-brain barrier: meaningful controls." *Peptides* **22**(12): 2127-36.
- Kastin, A. J. and W. Pan (2003). Peptide transport across the blood-brain barrier. *Progress in Drug Research*. L. Prokai and K. Prokai-Tatrai. Basel, Switzerland, Birkhauser Verlag. **61**: 81-100.
- Kastin, A. J., M. A. Pearson, et al. (1991). "EEG evidence that morphine and an enkephalin analog cross the blood-brain barrier." *Pharmacol Biochem Behav* **40**(4): 771-4.
- Kawachi, I., T. Fujieda, et al. (2001). "Purification and properties of extracellular chitinases from the parasitic fungus *Isaria japonica*." *J Biosci Bioeng* **92**(6): 544-9.
- Kebarle, P. and L. Tang (1993). *Anal.Chem.* **65**: 972A.
- Kelder, J., P. D. Grootenhuis, et al. (1999). "Polar molecular surface as a dominating determinant for oral absorption and brain penetration of drugs." *Pharm Res* **16**(10): 1514-9.
- Kim, B. Y., J. H. Jeong, et al. (2005). "Bioadhesive interaction and hypoglycemic effect of insulin-loaded lectin-microparticle conjugates in oral insulin delivery system." *J Control Release* **102**(3): 525-38.
- Kim, Y. S., W. Birtwhistle, et al. (1972). "Peptide hydrolases in the brush-border and soluble fractions of small intestinal mucosa of ra and man." *J. Clin. Invest.* **51**: 1419-1430.
- Kisel, M. A., L. N. Kulik, et al. (2001). "Liposomes with phosphatidylethanol as a carrier for oral delivery of insulin: studies in the rat." *Int J Pharm* **216**(1-2): 105-14.
- Knapp, R. J., E. Malatynska, et al. (1995). "Molecular biology and pharmacology of cloned opioid receptors." *Faseb J* **9**(7): 516-25.
- Knapp, R. J., S. D. Sharma, et al. (1991). "[D-Pen2,4'-125I-Phe4,D-Pen5]enkephalin: a selective high affinity radioligand for delta opioid receptors with exceptional specific activity." *J Pharmacol Exp Ther* **258**(3): 1077-83.
- Kniesel, U. and H. Wolburg (2000). "Tight junctions of the blood-brain barrier." *Cell Mol Neurobiol* **20**(1): 57-76.
- Knipp, G. T., D. G. Vander Velde, et al. (1997). "The effect of beta-turn structure on the passive diffusion of peptides across Caco-2 cell monolayers." *Pharm Res* **14**(10): 1332-40.
- Kotze, A. F., H. L. Luessen, et al. (1997). "N-trimethyl chitosan chloride as a potential absorption enhancer across mucosal surfaces: in vitro evaluation in intestinal epithelial cells (Caco-2)." *Pharm Res* **14**(9): 1197-202.
- Kotze, A. F., M. M. Thanou, et al. (1999). "Enhancement of paracellular drug transport with highly quaternized N-trimethyl chitosan chloride in neutral

- environments: in vitro evaluation in intestinal epithelial cells (Caco-2)." J Pharm Sci **88**(2): 253-7.
- Kovacs, J., L. Kisfaludy, et al. (1967). "On the optical purity of peptide active esters prepared by N,N'-dicyclohexylcarbodiimide and "complexes" of N,N'-dicyclohexylcarbodiimide-pentachlorophenol and N,N'-dicyclohexylcarbodiimide-pentafluorophenol." J Am Chem Soc **89**(1): 183-4.
- Krauland, A. H., D. Guggi, et al. (2004). "Oral insulin delivery: the potential of thiolated chitosan-insulin tablets on non-diabetic rats." J Control Release **95**(3): 547-55.
- Kreuter, J. (1995). "Nanoparticulate systems in drug delivery and targeting." J Drug Target **3**(3): 171-3.
- Kreuter, J. (2001). "Nanoparticulate systems for brain delivery of drugs." Adv Drug Deliv Rev **47**(1): 65-81.
- Kreuter, J., R. N. Alyautdin, et al. (1995). "Passage of peptides through the blood-brain barrier with colloidal polymer particles (nanoparticles)." Brain Res **674**(1): 171-4.
- Kreuter, J., V. E. Petrov, et al. (1997). "Influence on the type of surfactant on the analgesic effects induced by the peptide dalargin after its delivery across the blood-brain barrier using surfactant-coated nanoparticles. ." J. Control. Rel. **40**: 81-87.
- Kreuter, J., P. Ränge, et al. (2003). "Direct evidence that polysorbate-80-coated poly(butylcyanoacrylate) nanoparticles deliver drugs to the CNS via specific mechanisms requiring prior binding of drug to the nanoparticles." Pharm Res **20**(3): 409-16.
- Kreuter, J., D. Shamenkov, et al. (2002). "Apolipoprotein-mediated transport of nanoparticle-bound drugs across the blood-brain barrier." J Drug Target **10**(4): 317-25.
- Kroll, R. A. and E. A. Neuwelt (1998). "Outwitting the blood-brain barrier for therapeutic purposes: osmotic opening and other means." Neurosurgery **42**(5): 1083-99; discussion 1099-100.
- Kumagai, A. K., J. B. Eisenberg, et al. (1987). "Absorptive-mediated endocytosis of cationized albumin and a beta-endorphin-cationized albumin chimeric peptide by isolated brain capillaries. Model system of blood-brain barrier transport." J Biol Chem **262**(31): 15214-9.
- La Du, B. N. (1992). Human serum paraoxonase / arylesterase. Pharmacogenetics of drug metabolism. W. Kalow. New York, Pergamon Press, Inc.: 51-91.
- Lambert, D. M., M. Geurts, et al. (1995). "Simple derivatives of amino acid neurotransmitters. Anticonvulsant evaluation of derived amides, carbamates and esters of glycine and beta-alanine." J. Pharm Belg. **50**: 194-203.
- Lang, V. B., P. Langguth, et al. (1997). "Structure-permeation relations of met-enkephalin peptide analogues on absorption and secretion mechanisms in Caco-2 monolayers." J Pharm Sci **86**(7): 846-53.
- Langguth, P., V. Bohner, et al. (1997). "The challenge of proteolytic enzymes in intestinal peptide delivery." J Control Release **46**: 39-57.
- Lavalle, S. M., P. W. Finn, et al. (2000). "A randomised kinematics-based approach to pharmacophore-constrained conformational search and database screening." J. Computational Chem. **21**(9): 731-47.
- Le Bars, D., M. Gozariu, et al. (2001). "Animal models of nociception." Pharmacol Rev **53**(4): 597-652.
- Le, H. T. B. and I. F. Uchegbu (2006). Self-Assembling Amphiphiles Increase the

- Dissolution and Absorption of Hydrophobic Drugs. 4th International Nanomedicines & Drug Delivery Symposium (NanoDDS' 06), Omaha, Nebraska.
- Lee, K. C., S. Y. Chae, et al. (2009). "Intrapulmonary potential of polyethylene glycol-modified glucagon-like peptide-1s as a type 2 anti-diabetic agent." Regul Pept **152**(1-3): 101-7.
- Lee, V. H. L. (1990). "Protease inhibitors and penetration enhances as approaches to modify peptide absorption." J Control Release **13**: 213-223.
- Lee, V. H. L., S. Dodda-Kashi, et al. (1991). Oral route of peptide and protein drug delivery. Peptide and Protein Drug Delivery. V. H. L. Lee. New York, Marcel Dekker, Inc: 691-738.
- Lee, Y. H. and P. J. Sinko (2000). "Oral delivery of salmon calcitonin." Adv Drug Deliv Rev **42**(3): 225-38.
- Lehr, C. M., J. A. Bouwstra, et al. (1992). "In vitro evaluation of mucoadhesive properties of chitosan and some other natural polymers." Int J Pharm **78**: 43-48.
- Lennernas, H. and E. Lundgren (2004). "Intestinal and blood-brain drug transport: beyond involvement of a single transport function." Drug Discovery Today: Technologies **1**(4): 417-22.
- Levin, V. A. (1980). "Relationship of octanol/water partition coefficient and molecular weight to rat brain capillary permeability." J Med Chem **23**(6): 682-4.
- Lewiś, P. N., F. A. Momany, et al. (1973). "Chain reversals in proteins." Biochim Biophys Acta **303**(2): 211-29.
- Li, H., J. H. Song, et al. (2003). "Polyethylene glycol-coated liposomes for oral delivery of recombinant human epidermal growth factor." Int J Pharm **258**(1-2): 11-9.
- Liang, M., N. M. Davies, et al. (2008). "Increasing entrapment of peptides within poly(alkyl cyanoacrylate) nanoparticles prepared from water-in-oil microemulsions by copolymerization." Int J Pharm **362**(1-2): 141-6.
- Liang, R., Y. J. Fei, et al. (1995). "Human intestinal H⁺/peptide cotransporter. Cloning, functional expression, and chromosomal localization." J Biol Chem **270**(12): 6456-63.
- Liao, S., J. Alfaro-Lopez, et al. (1998). "De novo design, synthesis, and biological activities of high-affinity and selective non-peptide agonists of the delta-opioid receptor." J Med Chem **41**(24): 4767-76.
- Liederer, B. M. and R. T. Borchardt (2005). "Stability of oxymethyl-modified coumarinic acid cyclic prodrugs of diastereomeric opioid peptides in biological media from various animal species including human." J Pharm Sci **94**(10): 2198-206.
- Liederer, B. M. and R. T. Borchardt (2006). "Enzymes involved in the bioconversion of ester-based prodrugs." J Pharm Sci **95**(6): 1177-95.
- Lim, S. B., I. Rubinstein, et al. (2008). "Freeze drying of peptide drugs self-associated with long-circulating, biocompatible and biodegradable sterically stabilized phospholipid nanomicelles." Int J Pharm **356**(1-2): 345-50.
- Lin, Y. H., C. H. Chang, et al. (2009). "Development of pH-responsive chitosan/heparin nanoparticles for stomach-specific anti-Helicobacter pylori therapy." Biomaterials.
- Lipinski, C. A., F. Lombardo, et al. (2001). "Experimental and computational approaches to estimate solubility and permeability in drug discovery and

- development settings." *Adv Drug Deliv Rev* **46**(1-3): 3-26.
- Lipkowski, A. W., A. M. Konecka, et al. (1982). "Double enkephalins." *Pol J Pharmacol Pharm* **34**(1-3): 69-71.
- Lipkowski, A. W., A. M. Konecka, et al. (1982). "Double-enkephalins--synthesis, activity on guinea-pig ileum, and analgesic effect." *Peptides* **3**(4): 697-700.
- Lis, H. and N. Sharon (1993). "Protein glycosylation. Structural and functional aspects." *Eur J Biochem* **218**(1): 1-27.
- Liu, Y., W. L. Lu, et al. (2005). "Pharmacodynamics and pharmacokinetics of recombinant hirudin via four non-parenteral routes." *Peptides* **26**(3): 423-30.
- Lloyd-Williams, P., F. Albericio, et al. (1997). *Chemical Approaches to the Synthesis of Peptides and Proteins*. New York, CRC Press.
- Lord, J. A., A. A. Waterfield, et al. (1977). "Endogenous opioid peptides: multiple agonists and receptors." *Nature* **267**(5611): 495-9.
- Lucangioli, S. E., E. Kenndler, et al. (2003). "Relation between retention factors of immunosuppressive drugs in microemulsion electrokinetic chromatography with biosurfactants and octanol-water partition coefficients." *J Pharm Biomed Anal* **33**(5): 871-8.
- Lumbierres, M., J. M. Palomo, et al. (2005). "Solid-phase synthesis of lipidated peptides." *Chemistry* **11**(24): 7405-15.
- Lumbierres, M., J. M. Palomo, et al. (2006). "Solid-phase synthesis of palmitoylated and farnesylated lipopeptides employing the fluoride-labile PTMSEL linker." *Tetrahedron Lett* **47**: 2671-74.
- Lund, L., A. Bak, et al. (1998). "The enzymatic degradation and transport of leucine-enkephalin and 4-imidazolidinone enkephalin prodrugs at the blood-brain barrier." *Int. J. Pharmaceutics* **172**: 97-101.
- Lundin, P. D., M. Bojrup, et al. (1997). "Enhancing effects of monohexanoin and two other medium-chain glyceride vehicles on intestinal absorption of desmopressin (dDAVP)." *J Pharmacol Exp Ther* **282**(2): 585-90.
- Lundin, S. and P. Artursson (1990). "Absorption of vasopressin analogue, 1-deamino-8-D-arginine-vasopressin (dDAVP), in human intestinal epithelial cell line, Caco-2." *Int. J. Pharm.* **64**(2-3): 181-6.
- Lundin, S., N. Pantzar, et al. (1991). "Differences in transport rate of oxytocin and vasopressin analogues across proximal and distal isolated segments of the small intestine of the rat." *Pharm Res* **8**(10): 1274-80.
- Lutsiak, M. E., G. S. Kwon, et al. (2002). "Analysis of peptide and lipopeptide content in liposomes." *J Pharm Pharm Sci* **5**(3): 279-84.
- Mackness, M. I., H. M. Thompson, et al. (1987). "Distinction between 'A'-esterases and arylesterases. Implications for esterase classification." *Biochem J* **245**(1): 293-6.
- Macromodel (1999). *Macromodel Interactive Molecular Modeling System Version 7.0 User Manual*. NY, Schrodinger Inc.
- Mahato, R. I., A. S. Narang, et al. (2003). "Emerging trends in oral delivery of peptide and protein drugs." *Crit Rev Ther Drug Carrier Syst* **20**(2-3): 153-214.
- Mann, M. and M. Wilm (1995). "Electrospray mass spectrometry for protein characterization." *Trends Biochem Sci* **20**(6): 219-24.
- Mant, C. T., L. H. Kondejewski, et al. (1997). "Analysis of synthetic peptides by high-performance liquid chromatography." *Methods Enzymol* **289**: 426-69.
- Marastoni, M., S. Salvadori, et al. (1987). "Synthesis and activity profiles of new dermorphin-(1-4) peptide analogues." *J Med Chem* **30**(9): 1538-42.

- Maresh, G. A., L. M. Maness, et al. (2001). "In vitro demonstration of a saturable transport system for leptin across the blood-brain barrier." *Life Sci* **69**(1): 67-73.
- Matthews, D. M. and J. W. Payne (1980). "Transmembrane transport of small peptides." *Curr. Top. Membr. Transp.* **14**: 331-4125.
- McClean, S., E. Prosser, et al. (1998). "Binding and uptake of biodegradable poly-DL-lactide micro- and nanoparticles in intestinal epithelia." *Eur J Pharm Sci* **6**(2): 153-63.
- Medzihradsky, K. (2003). "Josef Rudinger Memorial Lecture 2002. The chemistry of the opioid receptor binding sites." *J Pept Sci* **9**(6): 333-53.
- Meek, J. L. (1980). "Prediction of peptide retention times in high-pressure liquid chromatography on the basis of amino acid composition." *Proc Natl Acad Sci U S A* **77**(3): 1632-6.
- Meirovitch, E. and H. Meirovitch (1996). "New theoretical methodology for elucidating the solution structure of peptides from NMR data. II. Free energy of dominant microstates of Leu-enkephalin and population-weighted average nuclear Overhauser effects intensities." *Biopolymers* **38**(1): 69-88.
- Meldal, M. (1997). "Properties of solid supports." *Methods Enzymol* **289**: 83-104.
- Mergler, M., R. Nyfeler, et al. (1988). "Peptide synthesis by a combination of solid-phase and solution methods II synthesis of fully protected peptide fragments on 2-methoxy-4-alkoxy-benzyl alcohol resin." *Tetrahedron Lett* **29**(32): 4009-4012.
- Merrifield, B. (1997). "Concept and early development of solid-phase peptide synthesis." *Methods Enzymol* **289**: 3-13.
- Merrifield, B. R. (1963). "Solid Phase Peptide Synthesis. I. The Synthesis of a Tetrapeptide." *J Am Chem Soc* **85**: 2149.
- Merrifield, R. B., L. D. Vizioli, et al. (1982). "Synthesis of the antibacterial peptide cecropin A (1-33)." *Biochemistry* **21**(20): 5020-31.
- Merskey, H., D. G. Albe-Fessard, et al. (1979). "Pain terms: a list with definitions and notes on usage." *Pain* **6**: 249-252.
- Mertsch, K. and J. Maas (2002). "Blood-brain barrier penetration & drug development from an industrial point of view." *Curr. Med. Chem.-Central Nervous System Agents* **2**: 187-201.
- Metia, P. K. and A. K. Bandyopadhyay (2008). "In vitro evaluation of novel mucoadhesive buccal tablet of oxytocin prepared with Diospyros peregrina fruit mucilages." *Yakugaku Zasshi* **128**(4): 603-9.
- Miller, L. C. (1948). "A critique of analgesic testing methods." *Ann N Y Acad Sci* **51**: 34-50.
- Minato, S., K. Iwanaga, et al. (2003). "Application of polyethyleneglycol (PEG)-modified liposomes for oral vaccine: effect of lipid dose on systemic and mucosal immunity." *J Control Release* **89**(2): 189-97.
- Minn, A., R. D. S. El-Bacha, et al. (2000). Drug metabolism in the brain: benefits and risks. *The Blood-brain Barrier and Drug Delivery to the CNS*. D. J. Begley, M. W. B. Bradbury and J. Kreuter. New York, Dekker: 145-170.
- Misra, A., S. Ganesh, et al. (2003). "Drug delivery to the central nervous system: a review." *J Pharm Pharm Sci* **6**(2): 252-73.
- Mitchell, D. and R. F. Hellon (1977). "Neuronal and behavioural responses in rats during noxious stimulation of the tail." *Proc R Soc Lond B Biol Sci* **197**(1127): 169-94.
- Mizuma, T., A. Koyanagi, et al. (2000). "Intestinal transport and metabolism of

- glucose-conjugated kyotorphin and cyclic kyotorphin: metabolic degradation is crucial to intestinal absorption of peptide drugs." Biochim Biophys Acta **1475**(1): 90-8.
- Mizuno, N., T. Niwa, et al. (2003). "Impact of drug transporter studies on drug discovery and development." Pharmacol Rev **55**(3): 425-61.
- Mogil, J. S., S. G. Wilson, et al. (1999). "Heritability of nociception I: responses of 11 inbred mouse strains on 12 measures of nociception." Pain **80**(1-2): 67-82.
- Mohamadi, F., N. Richards, et al. (1990). "MacroModel—an integrated software system for modeling organic and bioorganic molecules using molecular mechanics." J. Comput. Chem. **11**: 440-67.
- Mollica, A., P. Davis, et al. (2006). "Synthesis and biological activity of the first cyclic biphalin analogues." Bioorg Med Chem Lett **16**(2): 367-72.
- Moore, W. T. (1997). "Laser desorption mass spectrometry." Methods Enzymol **289**: 520-42.
- Morley, J. S. (1980). "Structure-activity relationships of enkephalin-like peptides." Annu Rev Pharmacol Toxicol **20**: 81-110.
- Morley, J. S. (1983). "Chemistry of opioid peptides." Br Med Bull **39**(1): 5-10.
- Mosberg, H. I., R. Hurst, et al. (1983). "Bis-penicillamine enkephalins possess highly improved specificity toward delta opioid receptors." Proc Natl Acad Sci U S A **80**(19): 5871-4.
- Mu, Y., H. Kamada, et al. (1999). "Bioconjugation of laminin peptide YIGSR with poly(styrene co-maleic acid) increases its antimetastatic effect on lung metastasis of B16-BL6 melanoma cells." Biochem Biophys Res Commun **255**(1): 75-9.
- Muranishi, S. (1990). "Absorption enhancers." Crit Rev Ther Drug Carrier Syst **7**(1): 1-33.
- Nagy, Z., H. Peters, et al. (1983). "Charge-related alterations of the cerebral endothelium." Lab Invest **49**(6): 662-71.
- Naha, P. C., V. Kanchan, et al. (2008). "Improved bioavailability of orally delivered insulin using Eudragit-L30D coated PLGA microparticles." J Microencapsul **25**(4): 248-56.
- Namjoshi, S., Y. Chen, et al. (2008). "Enhanced transdermal delivery of a dipeptide by dermaportation." Biopolymers **90**(5): 655-62.
- Naughton, M. A. and F. Sanger (1961). "Purification and specificity of pancreatic elastase." Biochem J **78**: 156-63.
- Negri, L., R. Lattanzi, et al. (1999). "Dermorphin and deltorphin glycosylated analogues: synthesis and antinociceptive activity after systemic administration." J Med Chem **42**(3): 400-4.
- Neuwelt, E. A. (2004). "Mechanisms of disease: the blood-brain barrier." Neurosurgery **54**(1): 131-40; discussion 141-2.
- Neuwelt, E. A. and E. P. Frenkel (1989). The Challenge of the Blood-Brain Barrier. Implications of the Blood-Brain Barrier and its manipulation. E. A. Neuwelt. New York Plenum Publisher Corporation. **1**: 19.
- Neuwelt, E. A. and S. I. Rapoport (1984). "Modification of the blood-brain barrier in the chemotherapy of malignant brain tumors." Fed Proc **43**(2): 214-9.
- Nizri, G. and S. Magdassi (2005). "Solubilization of hydrophobic molecules in nanoparticles formed by polymer-surfactant interactions." J Colloid Interface Sci **291**(1): 169-74.
- Noble, L., A. I. Gray, et al. (1999). "A non-covalently cross-linked chitosan based hydrogel." Int J Pharm **192**(2): 173-82.

- Novabiochem, E. B., Inc. (2006). "2-Chlorotrityl chloride resin (100-200 mesh), 1% DVB." Retrieved 3rd June, 2006, from <http://www.merckbiosciences.co.uk/Products/ProductDisplay.asp?catno=01-64-0114&>.
- Ogawa, T., M. Araki, et al. (2003). "Synthesis and antinociceptive activity of orally active opioid peptides: improvement of oral bioavailability by esterification." *Chem Pharm Bull (Tokyo)* **51**(7): 759-71.
- Ohlsen, R. (2007, 2009). "Drug Delivery Technology: Revolutionizing CNS Therapies." Retrieved 27th January, 2009, from <http://www.pharmavision.co.uk/article95-drugdeliverytechnologyrevolutionizingcnsstherapies.php>.
- Okamoto, K. (2008). "Review: MALDI Mass Spectrometry of Synthetic Polymers." Retrieved 24th November, 2008, from http://www.tytlabs.co.jp/english/review/rev413epdf/e413_029okamoto.pdf.
- Okumu, F. W., G. M. Pauletti, et al. (1997). "Effect of restricted conformational flexibility on the permeation of model hexapeptides across Caco-2 cell monolayers." *Pharm Res* **14**(2): 169-75.
- Oldendorf, W. H. (1971). "Brain uptake of radiolabeled amino acids, amines, and hexoses after arterial injection." *Am J Physiol* **221**(6): 1629-39.
- Oldendorf, W. H., M. E. Cornford, et al. (1977). "The large apparent work capability of the blood-brain barrier: a study of the mitochondrial content of capillary endothelial cells in brain and other tissues of the rat." *Ann Neurol* **1**(5): 409-17.
- Olivier, J. C., L. Fenart, et al. (1999). "Indirect evidence that drug brain targeting using polysorbate 80-coated polybutylcyanoacrylate nanoparticles is related to toxicity." *Pharm Res* **16**(12): 1836-42.
- Oliyai, R. and V. J. Stella (1993). "Prodrugs of peptides and proteins for improved formulation and delivery." *Annu Rev Pharmacol Toxicol* **33**: 521-44.
- Ouyang, H., F. Tang, et al. (2002). "A modified coumarinic acid-based cyclic prodrug of an opioid peptide: its enzymatic and chemical stability and cell permeation characteristics." *Pharm Res* **19**(6): 794-801.
- Paakkari, P., I. Paakkari, et al. (1993). "Dermorphin analog Tyr-D-Arg2-Phe-sarcosine-induced opioid analgesia and respiratory stimulation: the role of mu 1-receptors?" *J Pharmacol Exp Ther* **266**(2): 544-50.
- Palomo, C., J. M. Aizpurua, et al. (2007). "Synthesis of beta-lactam scaffolds for ditopic peptidomimetics." *Org Lett* **9**(1): 101-4.
- Pandey, R. and G. K. Khuller (2006). "Oral nanoparticle-based antituberculosis drug delivery to the brain in an experimental model." *J Antimicrob Chemother* **57**(6): 1146-52.
- Pardridge, W. M. (1984). "Transport of nutrients and hormones through the blood-brain barrier." *Fed Proc* **43**(2): 201-4.
- Pardridge, W. M. (1991). *Peptide Drug Delivery to the Brain*. New York, Raven Press Ltd.
- Pardridge, W. M. (1992). "Opioid peptide drug development: transport of opioid chimeric peptides through the blood-brain barrier." *NIDA Res Monogr* **120**: 153-68.
- Pardridge, W. M. (1998). "CNS drug design based on principles of blood-brain barrier transport." *J Neurochem* **70**(5): 1781-92.
- Pardridge, W. M. (2001). Drug targeting, drug discovery, and brain drug development. . *Brain Drug Targeting-The Future of Brain Drug*

- Development. W. M. Pardridge. Cambridge, University Press: 1-12.
- Pardridge, W. M. (2005). "The blood-brain barrier: bottleneck in brain drug development." *NeuroRx* **2**(1): 3-14.
- Pardridge, W. M. (2007). "Blood-brain barrier delivery of protein and non-viral gene therapeutics with molecular Trojan horses." *J Control Release* **122**(3): 345-8.
- Pardridge, W. M. (2008). "Re-engineering biopharmaceuticals for delivery to brain with molecular Trojan horses." *Bioconjug Chem* **19**(7): 1327-38.
- Pardridge, W. M., R. J. Boado, et al. (1995). "Vector-mediated delivery of a polyamide ("peptide") nucleic acid analogue through the blood-brain barrier in vivo." *Proc Natl Acad Sci U S A* **92**(12): 5592-6.
- Pardridge, W. M., D. Triguero, et al. (1989). "Transport of histone through the blood-brain barrier." *J Pharmacol Exp Ther* **251**(3): 821-6.
- Pardridge, W. M., D. Triguero, et al. (1990). "Beta-endorphin chimeric peptides: transport through the blood-brain barrier in vivo and cleavage of disulfide linkage by brain." *Endocrinology* **126**(2): 977-84.
- Patlak, C. S., R. G. Blasberg, et al. (1983). "Graphical evaluation of blood-to-brain transfer constants from multiple-time uptake data." *J Cereb Blood Flow Metab* **3**(1): 1-7.
- Pauletti, G. M., R. T. Borchardt, et al. (1997). "Improvement of oral peptide bioavailability: Peptidomimetics and prodrug strategies." *Adv Drug Deliv Rev* **27**(2-3): 235-256.
- Pauletti, G. M., S. Gangwar, et al. (1996). "Structural requirements for intestinal absorption of peptide drugs." *J. Control. Release* **41**: 3-17.
- Pauletti, G. M., F. W. Okumu, et al. (1997). "Effect of size and charge on the passive diffusion of peptides across Caco-2 cell monolayers via the paracellular pathway." *Pharm Res* **14**(2): 164-8.
- Peters, T. J. (1970). "The subcellular localization of di- and tri-peptide hydrolase activity in guinea-pig small intestine." *Biochem J* **120**(1): 195-203.
- Pinkerton, P. H., R. M. Bannerman, et al. (1970). "Iron metabolism and absorption studies in the X-linked anaemia of mice." *Br J Haematol* **18**(2): 211-28.
- Pinto Reis, C., R. J. Neufeld, et al. (2006). "Nanoencapsulation II. Biomedical applications and current status of peptide and protein nanoparticulate delivery systems." *Nanomedicine* **2**(2): 53-65.
- Plattner, J. J., P. A. Marcotte, et al. (1988). "Renin inhibitors. Dipeptide analogues of angiotensinogen utilizing a structurally modified phenylalanine residue to impart proteolytic stability." *J Med Chem* **31**(12): 2277-88.
- Pollay, M. (1987). "Blood-Brain Barrier: Review of clinical aspects." *Contemp. Neurosurg* **9**: 1-6.
- Polt, R., F. Porreca, et al. (1994). "Glycopeptide enkephalin analogues produce analgesia in mice: evidence for penetration of the blood-brain barrier." *Proc Natl Acad Sci U S A* **91**(15): 7114-8.
- Powell, M. F., T. Stewart, et al. (1993). "Peptide stability in drug development. II. Effect of single amino acid substitution and glycosylation on peptide reactivity in human serum." *Pharm Res* **10**(9): 1268-73.
- Prego, C., D. Torres, et al. (2006). "Chitosan-PEG nanocapsules as new carriers for oral peptide delivery. Effect of chitosan pegylation degree." *J Control Release* **111**(3): 299-308.
- Prescott, L. and M. W. Brightman (1998). Circumventricular organs of the brain. Introduction to the Blood-brain Barrier: Methodology, Biology, and Pathology. W. M. Pardridge. UK:, Cambridge University Press: 270-276.

- Preston, J. E. (2001). "Ageing choroid plexus-cerebrospinal fluid system." Microsc Res Tech **52**(1): 31-7.
- Prokai, L., X.-D. Ouyang, et al. (1994). "Chemical delivery system to transport amide to the central nervous system." J. Am. Chem. Soc. **116**: 2643-4.
- Prokai, L., K. Prokai-Tatrai, et al. (2000). "Targeting drugs to the brain by redox chemical delivery systems." Med Res Rev **20**(5): 367-416.
- Pugh, K. C., E. J. York, et al. (1992). "Effects of resin swelling and substitution on solid phase synthesis." Int J Pept Protein Res **40**(3-4): 208-13.
- Qu, X., V. V. Khutoryanskiy, et al. (2006). "Carbohydrate-based micelle clusters which enhance hydrophobic drug bioavailability by up to 1 order of magnitude." Biomacromolecules **7**(12): 3452-9.
- Quattrin, T. (2006). "Inhaled insulin: a novel and non-invasive way for insulin administration?" Curr Drug Saf **1**(2): 151-8.
- Quellec, P., R. Gref, et al. (1998). "Protein encapsulation within polyethylene glycol-coated nanospheres. I. Physicochemical characterization." J Biomed Mater Res **42**(1): 45-54.
- Quinn, D. M. (1987). "Acetylcholinesterase: Enzyme structure, reaction dynamics, and virtual transition states." Chem. Rev. **87**: 955-79.
- Quinn, D. M., K. Shirai, et al. (1982). "Lipoprotein lipase catalyzed hydrolysis of water-soluble p-nitrophenyl esters. Inhibition by apolipoprotein C-II." Biochemistry **21**(26): 6872-9.
- Raeissi, S. and K. L. Audus (1989). "In-vitro characterization of blood-brain barrier permeability to delta sleep-inducing peptide." J Pharm Pharmacol **41**(12): 848-52.
- Ramadas, M., W. Paul, et al. (2000). "Lipoinulin encapsulated alginate-chitosan capsules: intestinal delivery in diabetic rats." J Microencapsul **17**(4): 405-11.
- Rapoport, S. I. (2000). "Osmotic opening of the blood-brain barrier: principles, mechanism, and therapeutic applications." Cell Mol Neurobiol **20**(2): 217-30.
- Rasmussen, G. J. and H. Bundgaard (1991). "Prodrugs of peptides. 15. 4-Imidazolidinone prodrug derivatives of enkephalins to prevent aminopeptidase-catalysed metabolism in plasma and absorptive mucosae." Int. J. Pharm. **76**: 113-122.
- Rautio, J., H. Kumpulainen, et al. (2008). "Prodrugs: design and clinical applications." Nat Rev Drug Discov **7**(3): 255-70.
- Reches, M. and E. Gazit (2006). "Designed aromatic homo-dipeptides: formation of ordered nanostructures and potential nanotechnological applications." Phys Biol **3**(1): S10-9.
- Reches, M. and E. Gazit (2006). "Molecular Self Assembly of Peptide Nanostructures: Mechanism of Association and Potential Uses." Current Nanoscience **2**: 105-111.
- Reddy, K. R. (2000). "Controlled-release, pegylation, liposomal formulations: new mechanisms in the delivery of injectable drugs." Ann Pharmacother **34**(7-8): 915-23.
- Reis, C. P., F. J. Veiga, et al. (2008). "Nanoparticulate biopolymers deliver insulin orally eliciting pharmacological response." J Pharm Sci.
- Rennels, M. L., T. F. Gregory, et al. (1983). "Innervation of capillaries by local neurons in the cat hypothalamus: a light microscopic study with horseradish peroxidase." J Cereb Blood Flow Metab **3**(4): 535-42.
- Rinova, M. and M. Lebl (1996). "Molecular Diversity and Libraries of Structures: Synthesis and Screening." Collect Czech, Chem. Commun. **61**(2): 171-231.

- Roemer, D. and J. Pless (1979). "Structure activity relationship of orally active enkephalin analogues as analgesics." Life Sci **24**(7): 621-4.
- Romanowski, M., X. Zhu, et al. (1997). "Interaction of a highly potent dimeric enkephalin analog, biphalin, with model membranes." Biochim Biophys Acta **1329**(2): 245-58.
- Roseman, M. A. (1988). "Hydrophobicity of the peptide C=O...H-N hydrogen-bonded group." J Mol Biol **201**(3): 621-3.
- Rossomando, E. F. (1987). Application of HPLC to the Assay of Enzymatic Activities. High Performance Liquid Chromatography in Enzymatic Analysis: Applications to the Assay of Enzymatic Activity. New York, John Wiley & Sons, Inc.: 1-14.
- Rubas, W., M. E. Cromwell, et al. (1996). "Flux measurements across Caco-2 monolayers may predict transport in human large intestinal tissue." J Pharm Sci **85**(2): 165-9.
- Rumsby, M. G., H. M. Getliffe, et al. (1973). "On the association of non-specific esterase activity with central nerve myelin preparations." J Neurochem **21**(4): 959-67.
- Saffran, M., C. Bedra, et al. (1988). "Vasopressin: a model for the study of effects of additives on the oral and rectal administration of peptide drugs." J Pharm Sci **77**(1): 33-8.
- Salahuddin, T. S., B. B. Johansson, et al. (1988). "Structural changes in the rat brain after carotid infusions of hyperosmolar solutions. An electron microscopic study." Acta Neuropathol (Berl) **77**(1): 5-13.
- Salamat-Miller, N. and T. P. Johnston (2005). "Current strategies used to enhance the paracellular transport of therapeutic polypeptides across the intestinal epithelium." Int J Pharm **294**(1-2): 201-16.
- Sang Yoo, H. and T. Gwan Park (2004). "Biodegradable nanoparticles containing protein-fatty acid complexes for oral delivery of salmon calcitonin." J Pharm Sci **93**(2): 488-95.
- Sargent, D. F. and R. Schwyzer (1986). "Membrane lipid phase as catalyst for peptide-receptor interactions." Proc Natl Acad Sci U S A **83**(16): 5774-8.
- Sarin, V. K., S. B. H. Kent, et al. (1984). "A general approach to the quantitation of synthetic efficiency in solid-phase peptide synthesis as a function of chain length." J Am Chem Soc **106**: 7845.
- Sasaki, Y., M. Matsui, et al. (1985). "The analgesic activity of D-Arg2-dermorphin and its N-terminal tetrapeptide analogs after subcutaneous administration in mice." Neuropeptides **5**(4-6): 391-4.
- Sato, T. and M. Hosokawa (1998). "The mammalian carboxylesterases: from molecules to functions." Annu Rev Pharmacol Toxicol **38**: 257-88.
- Schipper, N. G. M., S. Olsson, et al. (1997). "Chitosan as absorption enhancers for poorly absorbable drugs 2: mechanism of absorption enhancement." Pharm Res **14**: 923-930.
- Schipper, N. G. M., K. M. Varum, et al. (1996). "Chitosan as absorption enhancers for poorly absorbable drugs 1: influence of molecular weight and degree of acetylation on drug transport across human intestinal epithelial (Caco-2) cells." Pharm Res **13**: 1686-92.
- Schipper, N. G. M., K. M. Varum, et al. (1999). "Chitosan as absorption enhancers for poorly absorbable drugs 3: influence of mucus on absorption enhancement." Eur. J. Pharm. Sci. **8**(4): 335-343.
- Schlageter, K. E., P. Molnar, et al. (1999). "Microvessel organization and structure

- in experimental brain tumors: microvessel populations with distinctive structural and functional properties." *Microvasc Res* **58**(3): 312-28.
- Schroder, E. and K. Lubke (1965). *"Methods of Peptide Synthesis"*. New York, Raven Press.
- Schroeder, U., P. Sommerfeld, et al. (1998). "Efficacy of oral dalargin-loaded nanoparticle delivery across the blood-brain barrier." *Peptides* **19**(4): 777-80.
- Schwyzler, R., M. Feurer, et al. (1955). "Über aktivierte Ester. III. Umsetzungen aktivierter Ester von Aminosäure- und Peptid-Derivaten mit Aminen und Aminosäureestern." *Helv. Chim. Acta* **38**(1): 83-91.
- Sciences, P. L. a. A. (2005). "FT-IR Spectroscopy Attenuated Total Reflectance (ATR)." *Technical Note-FTIR Spectroscopy* Retrieved 27th October, 2008, from http://las.perkinelmer.com/content/TechnicalInfo/TCH_FTIRATR.pdf.
- Sedlakova, R., R. R. Shivers, et al. (1999). "Ultrastructure of the blood-brain barrier in the rabbit." *J Submicrosc Cytol Pathol* **31**(1): 149-61.
- Seifert, W. E., Jr. and R. M. Caprioli (1996). "Fast atom bombardment mass spectrometry." *Methods Enzymol* **270**: 453-86.
- Sereda, T. J., C. T. Mant, et al. (1995). "Selectivity due to conformational differences between helical and non-helical peptides in reversed-phase chromatography." *J Chromatogr A* **695**(2): 205-21.
- Sharma, P., M. V. Varma, et al. (2005). "Absorption enhancement, mechanistic and toxicity studies of medium chain fatty acids, cyclodextrins and bile salts as peroral absorption enhancers." *Farmaco* **60**(11-12): 884-93.
- Shaw, J. S., L. Miller, et al. (1982). "Selective antagonists at the opiate delta-receptor." *Life Sci* **31**(12-13): 1259-62.
- Sheehan, J. C. and G. P. Hess (1955). "A New Method of Forming Peptide Bonds." *J Am Chem Soc* **77**: 1067.
- Shenderovich, M. D., S. Liao, et al. (2000). "A three-dimensional model of the delta-opioid pharmacophore: comparative molecular modeling of peptide and nonpeptide ligands." *Biopolymers* **53**(7): 565-80.
- Shimoyama, N., M. Shimoyama, et al. (1997). "d-Methadone is antinociceptive in the rat formalin test." *J Pharmacol Exp Ther* **283**(2): 648-52.
- Shimura, T., S. Tabata, et al. (1992). "In-vivo blood-brain barrier transport of a novel adrenocorticotrophic hormone analogue, ebiratide, demonstrated by brain microdialysis and capillary depletion methods." *J Pharm Pharmacol* **44**(7): 583-8.
- Sieber, P. and B. Iselin (1968). "[Peptide synthesis under application of the 2-(p-diphenyl)-isopropylloxycarbonyl (Dpoc)-amino protection groups]." *Helv Chim Acta* **51**(4): 622-32.
- Silk, D. B., J. A. Nicholson, et al. (1976). "Relationships between mucosal hydrolysis and transport of two phenylalanine dipeptides." *Gut* **17**(11): 870-6.
- Simone, E. A., T. D. Dziubla, et al. (2009). "Loading PEG-catalase into filamentous and spherical polymer nanocarriers." *Pharm Res* **26**(1): 250-60.
- Sixt, M., B. Engelhardt, et al. (2001). "Endothelial cell laminin isoforms, laminins 8 and 10, play decisive roles in T cell recruitment across the blood-brain barrier in experimental autoimmune encephalomyelitis." *J Cell Biol* **153**(5): 933-46.
- Smith, D. and J. F. Griffin (1978). "Conformation of [Leu5]enkephalin from X-ray diffraction: features important for recognition at opiate receptor." *Science* **199**(4334): 1214-6.
- So, T., H. O. Ito, et al. (1999). "Extended blood half-life of monomethoxypolyethylene glycol-conjugated hen lysozyme is a key

- parameter controlling immunological tolerogenicity." *Cell Mol Life Sci* **55**(8-9): 1187-94.
- Soares, A. F., A. Carvalho Rde, et al. (2007). "Oral administration of peptides and proteins: nanoparticles and cyclodextrins as biocompatible delivery systems." *Nanomed* **2**(2): 183-202.
- Sogorb, M. A. and E. Vilanova (2002). "Enzymes involved in the detoxification of organophosphorus, carbamate and pyrethroid insecticides through hydrolysis." *Toxicol Lett* **128**(1-3): 215-28.
- Sorensen, M., B. Steenberg, et al. (1997). "The effect of beta-turn structure on the permeation of peptides across monolayers of bovine brain microvessel endothelial cells." *Pharm Res* **14**(10): 1341-8.
- Spadaccini, R. and P. A. Temussi (2001). "Natural peptide analgesics: the role of solution conformation." *Cell Mol Life Sci* **58**(11): 1572-82.
- Spatola, A. F., H. Saneii, et al. (1986). "Structure-activity relationships of enkephalins containing serially replaced thiomethylene amide bond surrogates." *Life Sci* **38**(14): 1243-9.
- Sprimal, R. C., K. D. Jaitly, et al. (1965). "Effect of muscle relaxants on the straub tail phenomenon." *Jap. J. Pharmacol.* **15**: 323.
- Still, W. C., K. Tempczyk, et al. (1990). "Semianalytical treatment of solvation for molecular mechanics and dynamics." *J. Am. Chem. Soc.* **112**(16): 6127-30.
- Stoiber, W., A. M. Sanger, et al. (2000). "Different modes of action of morphine and epibatidine in Straub tail reactions in mice." *Arzneimittelforschung* **50**(8): 683-7.
- Strand, F. L. (1999). *Neuropeptides : regulators of physiological processes (Cellular and molecular Neuroscience)*. London, MIT Press.
- Strand, F. L. (1999). *Neuropeptides: Regulators of Physiological Processes*. London, Massachusetts Institute of Technology, The MIT press.
- Strous, G. J. and J. Dekker (1992). "Mucin-type glycoproteins." *Crit Rev Biochem Mol Biol* **27**(1-2): 57-92.
- Stults, J. T. (1995). "Matrix-assisted laser desorption/ionization mass spectrometry (MALDI-MS)." *Curr Opin Struct Biol* **5**(5): 691-8.
- Sugimoto, M., M. Morimoto, et al. (1998). "Preparation and characterisation of water-soluble chitin and chitosan derivatives." *Carbohydr. Polym.* **36**: 49-59.
- Summers, M. C. and R. J. Hayes (1981). "The interaction of N alpha-alkylenkephalins with opiate receptors. Tissue-dependent shifts in the opiate activity of methionine-enkephalin following N alpha-alkylation." *J Biol Chem* **256**(10): 4951-6.
- Suzuki, H. and Y. Sugiyama (2002). "Single nucleotide polymorphisms in multidrug resistance associated protein 2 (MRP2/ABCC2): its impact on drug disposition." *Adv Drug Deliv Rev* **54**(10): 1311-31.
- Sweeney, P. J. and J. M. Walker (1993). *Enzymes of Molecular Biology. Enzymes of Molecular Biology*. M. M. Burrell. Totowa, NJ, Humana Press. **16**: 290-91.
- Swenson, E. S., W. B. Milisen, et al. (1994). "Intestinal permeability enhancement: structure-activity and structure-toxicity relationships for nonylphenoxypolyoxyethylene surfactant permeability enhancers." *Pharm Res* **11**(10): 1501-4.
- Taber, R. I. (1973). "Predictive value of analgesic assays in mice and rats." *Adv Biochem Psychopharmacol* **8**(0): 191-211.
- Tagami, M., Y. Nara, et al. (1990). "Ultrastructural changes in cerebral pericytes and

- astrocytes of stroke-prone spontaneously hypertensive rats." *Stroke* **21**(7): 1064-71.
- Takano, M., R. Yumoto, et al. (2006). "Expression and function of efflux drug transporters in the intestine." *Pharmacol Ther* **109**(1-2): 137-61.
- Takaori, K., J. Burton, et al. (1986). "The transport of an intact oligopeptide across adult mammalian jejunum." *Biochem Biophys Res Commun* **137**(2): 682-7.
- Takayama, K., M. Hirata, et al. (1990). "Effect of interpolymer complex formation on bioadhesive property and drug release phenomenon of compressed tablet consisting of chitosan and sodium hyaluronate." *Chem Pharm Bull (Tokyo)* **38**(7): 1993-7.
- Takeuchi, H., H. Yamamoto, et al. (1996). "Enteral absorption of insulin in rats from mucoadhesive chitosan-coated liposomes." *Pharm Res* **13**(6): 896-901.
- Tang, L.-G. and D. N.-S. Hon (2000). "Chelation of chitosan derivatives with Zinc ions. II. Association complexes of Zn⁺² onto O, N-carboxymethyl chitosan." *J. Applied Polymer Sci.*: 1476-85.
- Tauzin, B. (2006). *Biotechnology Medicines in Development*. Washington, DC, Pharmaceutical Research and Manufacturers Association.
- Terasaki, T., K. Hirai, et al. (1989). "Absorptive-mediated endocytosis of a dynorphin-like analgesic peptide, E-2078 into the blood-brain barrier." *J Pharmacol Exp Ther* **251**(1): 351-7.
- Terasaki, T. and K. Hosoya (2001). "Conditionally immortalized cell lines as a new in vitro model for the study of barrier functions." *Biol Pharm Bull* **24**(2): 111-8.
- Terasaki, T., S. Takakuwa, et al. (1992). "Absorptive-mediated endocytosis of an adrenocorticotrophic hormone (ACTH) analogue, ebiratide, into the blood-brain barrier: studies with monolayers of primary cultured bovine brain capillary endothelial cells." *Pharm Res* **9**(4): 529-34.
- Tewa-Tagne, P., S. Briancon, et al. (2006). "Spray-dried microparticles containing polymeric nanocapsules: formulation aspects, liquid phase interactions and particles characteristics." *Int J Pharm* **325**(1-2): 63-74.
- Thanou, M., S. Henderson, et al. (2007). "N-sulfonato-N,O-carboxymethylchitosan: a novel polymeric absorption enhancer for the oral delivery of macromolecules." *J Control Release* **117**(2): 171-8.
- Thanou, M., J. C. Verhoef, et al. (2001). "Chitosan and its derivatives as intestinal absorption enhancers." *Adv Drug Deliv Rev* **50 Suppl 1**: S91-101.
- Thanou, M., J. C. Verhoef, et al. (2001). "Intestinal absorption of octreotide using trimethyl chitosan chloride: studies in pigs." *Pharm Res* **18**(6): 823-8.
- Thieriet, N., F. Guibe, et al. (2000). "Solid-phase peptide synthesis in the reverse (N → C) direction." *Org Lett* **2**(13): 1815-7.
- Thomas, S. A., T. J. Abbruscato, et al. (1997). "The entry of [D-penicillamine-2,5]enkephalin into the central nervous system: saturation kinetics and specificity." *J Pharmacol Exp Ther* **280**(3): 1235-40.
- Thwaites, D. T., B. H. Hirst, et al. (1993). "Passive transepithelial absorption of thyrotropin-releasing hormone (TRH) via a paracellular route in cultured intestinal and renal epithelial cell lines." *Pharm Res* **10**(5): 674-81.
- Tjolsen, A. and K. Hole (1993). "The tail-flick latency is influenced by skin temperature." *AAPS J* **2**: 107-111.
- Tomatis, R., M. Marastoni, et al. (1997). "Synthesis and pharmacological activity of deltorphin and dermorphin-related glycopeptides." *J Med Chem* **40**(18): 2948-52.

- Toniolo, C. (1990). "Conformationally restricted peptides through short-range cyclizations." *Int J Pept Protein Res* **35**(4): 287-300.
- Torchilin, V. P. (2005). "Recent advances with liposomes as pharmaceutical carriers." *Nat Rev Drug Discov* **4**(2): 145-60.
- Troster, S. D. and J. Kreuter (1988). "Contact angles of surfactants with a potential to alter the body distribution of colloidal drug carriers on poly(methyl methacrylate) surfaces." *Int. J. Pharm.* **45**: 91-100.
- Troster, S. D., U. Muller, et al. (1990). "Modification of the body distribution of poly(methyl methacrylate) nanoparticles in rats by coating with surfactants." *Int. J. Pharm.* **61**: 85-100.
- Tsai, Y. J., A. Rottero, et al. (1997). "Synthesis and purification of NB1-palmitoyl insulin." *J Pharm Sci* **86**(11): 1264-8.
- Tsuji, A. (2005). "Small molecular drug transfer across the blood-brain barrier via carrier-mediated transport systems." *NeuroRx* **2**(1): 54-62.
- Tsuji, A. and I. Tamai (1996). "Carrier-mediated intestinal transport of drugs." *Pharm Res* **13**(7): 963-77.
- Tsuji, A. and I. Tamai (1998). Blood-brain barrier transport of drugs. *Introduction to the Blood-Brain Barrier: Methodology, biology, and pathology*. W. M. Pardridge. Cambridge, UK, Cambridge University Press: 243.
- Tsuji, A. and I. I. Tamai (1999). "Carrier-mediated or specialized transport of drugs across the blood-brain barrier." *Adv Drug Deliv Rev* **36**(2-3): 277-290.
- Tsutsumi, Y., M. Onda, et al. (2000). "Site-specific chemical modification with poly(ethylene glycol) of recombinant immunotoxin anti-Tac(Fv)-PE38 (LMB-2) improves antitumor activity and reduces animal toxicity and immunogenicity." *Proc Natl Acad Sci U S A* **97**(15): 8548-53.
- Tsuzuki, N., T. Hama, et al. (1991). "Adamantane as a brain-directed drug carrier for poorly absorbed drug: antinociceptive effects of [D-Ala²]Leu-enkephalin derivatives conjugated with the 1-adamantane moiety." *Biochem Pharmacol* **41**(4): R5-8.
- Ubaidulla, U., R. K. Khar, et al. (2007). "Development and characterization of chitosan succinate microspheres for the improved oral bioavailability of insulin." *J Pharm Sci* **96**(11): 3010-23.
- Ubaidulla, U., R. K. Khar, et al. (2007). "Development and in-vivo evaluation of insulin-loaded chitosan phthalate microspheres for oral delivery." *J Pharm Pharmacol* **59**(10): 1345-51.
- Uchegbu, I. F., L. Sadiq, et al. (2001). "Quaternary ammonium palmitoyl glycol chitosan--a new polysoap for drug delivery." *Int J Pharm* **224**(1-2): 185-99.
- Uchegbu, I. F., L. Sadiq, et al. (2004). "Gene transfer with three amphiphilic glycol chitosans--the degree of polymerisation is the main controller of transfection efficiency." *J Drug Target* **12**(8): 527-39.
- Uchiyama, T., A. Kotani, et al. (1998). "Effects of various protease inhibitors on the stability and permeability of [D-Ala²,D-Leu⁵]enkephalin in the rat intestine: comparison with leucine enkephalin." *J Pharm Sci* **87**(4): 448-52.
- Uchiyama, T., A. Kotani, et al. (2000). "Development of novel lipophilic derivatives of DADLE (leucine enkephalin analogue): intestinal permeability characteristics of DADLE derivatives in rats." *Pharm Res* **17**(12): 1461-7.
- Ukai, M., T. Kobayashi, et al. (1995). "Attenuation of memory with Tyr-D-Arg-Phe-beta-Ala-NH₂, a novel dermorphin analog with high affinity for mu-opioid receptors." *Eur J Pharmacol* **287**(3): 245-9.
- van der Merwe, S. M., J. C. Verhoef, et al. (2004). "Trimethylated chitosan as

- polymeric absorption enhancer for improved peroral delivery of peptide drugs." *Eur J Pharm Biopharm* **58**(2): 225-35.
- van der Spoel, D. and H. J. Berendsen (1997). "Molecular dynamics simulations of Leu-enkephalin in water and DMSO." *Biophys J* **72**(5): 2032-41.
- van Gunsteren, W. F., D. Bakowies, et al. (2006). "Biomolecular modeling: Goals, problems, perspectives." *Angew Chem Int Ed Engl* **45**(25): 4064-92.
- Van Hoogdalem, E. J., A. G. De Boer, et al. (1988). "Rectal absorption enhancement of rate-controlled delivered ampicillin sodium by sodium decanoate in conscious rats." *Pharm Weekbl Sci* **10**(2): 76-9.
- van Hoogdalem, E. J., A. G. de Boer, et al. (1989). "Intestinal drug absorption enhancement: an overview." *Pharmacol Ther* **44**(3): 407-43.
- Vehaskari, V. M., C. T. Chang, et al. (1984). "The effects of polycations on vascular permeability in the rat. A proposed role for charge sites." *J Clin Invest* **73**(4): 1053-61.
- Veronesi, M. C., D. J. Kubek, et al. (2007). "Intranasal delivery of a thyrotropin-releasing hormone analog attenuates seizures in the amygdala-kindled rat." *Epilepsia* **48**(12): 2280-6.
- Virden, A. (2008). *Laser Diffraction Particle Sizing* Malvern Materials Characterisation Seminar, School of Pharmacy, University of London, Malvern.
- Walker, C. H. and M. I. Mackness (1983). "Esterases: problems of identification and classification." *Biochem Pharmacol* **32**(22): 3265-9.
- Wang, B., K. Nimkar, et al. (1999). "Synthesis and evaluation of the physicochemical properties of esterase-sensitive cyclic prodrugs of opioid peptides using coumarinic acid and phenylpropionic acid linkers." *J Pept Res* **53**(4): 370-82.
- Wang, J., D. Chow, et al. (2003). "Reversible lipidization for the oral delivery of salmon calcitonin." *J Control Release* **88**(3): 369-80.
- Wang, J., D. J. Hogenkamp, et al. (2006). "Reversible lipidization for the oral delivery of leu-enkephalin." *J Drug Target* **14**(3): 127-36.
- Wang, W. (1996). "Oral protein drug delivery." *J Drug Target* **4**(4): 195-232.
- Wang, W. (2006). Polymer Characterization techniques. *Polymers in Drug Delivery*. I. F. Uchegbu and A. G. Schatzlein. London, Taylor & Francis Group: 23-34.
- Wang, W., J. Jiang, et al. (1999). "Prodrug approaches to the improved delivery of peptide drugs." *Curr Pharm Des* **5**(4): 265-87.
- Wang, W., A. M. McConaghy, et al. (2001). "Controls on polymer molecular weight may be used to control the size of palmitoyl glycol chitosan polymeric vesicles." *Langmuir* **17**: 631-6.
- Wang, Y. C., Y. C. Wu, et al. (2007). "Structure-activity relationships of Leu-Enkephalin analog with (4-Carboxamido)phenylalanine substituted for tyrosine: a molecular dynamics study." *Biopolymers* **86**(3): 231-9.
- Washington, U. o. (2009, 3rd March 2009). "Biostructure 431: Neuroanatomy." Retrieved 15th May 2009, from <http://bstr431.biostr.washington.edu/syl/09lab02/09lab02.htm>.
- Watt, I. M. (1997). *The Principles and Practice of Electron Microscopy*. Cambridge, Cambridge University Press.
- Weber, S. J., T. J. Abbruscato, et al. (1993). "Assessment of an in vitro blood-brain barrier model using several [Met⁵]enkephalin opioid analogs." *J Pharmacol Exp Ther* **266**(3): 1649-55.
- Weber, S. J., D. L. Greene, et al. (1992). "Whole body and brain distribution of

- [3H]cyclic [D-Pen2,D-Pen5] enkephalin after intraperitoneal, intravenous, oral and subcutaneous administration." *J Pharmacol Exp Ther* **263**(3): 1308-16.
- Weber, S. J., D. L. Greene, et al. (1991). "Distribution and analgesia of [3H][D-Pen2, D-Pen5]enkephalin and two halogenated analogs after intravenous administration." *J Pharmacol Exp Ther* **259**(3): 1109-17.
- Weindl, A. (1973). Neuroendocrine aspects of circumventricular organs. *Frontiers in Neuroendocrinology*. W. F. Ganong and L. Martini. New York, Oxford University Press: 3-32.
- Wellings, D. A. and E. Atherton (1997). "Standard Fmoc protocols." *Methods Enzymol* **289**: 44-67.
- Werle, M., H. Takeuchi, et al. (2008). "Modified chitosans for oral drug delivery." *J Pharm Sci*.
- Wermuth, C. G. (2006). *Pharmacophores: historical perspective and viewpoint from a medicinal chemist*, Wiley-VCH.
- Werring, D. J., D. Brassat, et al. (2000). "The pathogenesis of lesions and normal-appearing white matter changes in multiple sclerosis: a serial diffusion MRI study." *Brain* **123** (Pt 8): 1667-76.
- Whitaker, J. R., F. Menger, et al. (1966). "The kinetics of some carboxypeptidase A and acetylcarboxypeptidase A catalyzed hydrolyses." *Biochemistry* **5**(1): 386-92.
- White, J. S. and D. C. White (1997). *Source book of enzymes*. New York, CRC Press LLC.
- Wieland, T., W. Schafer, et al. (1951). *Liebigs Ann. Chem.* **573**: 99.
- Williams, C. A. (1998). "Application of photon correlation spectroscopy to a macromolecular system." Retrieved 29th November 2008, 2008, from <http://www.wooster.edu/physics/JrIS/Files/Williams.pdf>.
- Williams, D. H. and I. Fleming (1995). *Spectroscopic Methods in Organic Chemistry*. London, The McGraw-Hill Companies.
- Wilmot, C. M. and J. M. Thornton (1990). "Beta-turns and their distortions: a proposed new nomenclature." *Protein Eng* **3**(6): 479-93.
- Witt, K. A. and T. P. Davis (2006). "CNS Drug Delivery: Opioid peptides and the Blood-Brain Barrier." *AAPS J.* **8**(1): E76-88.
- Witt, K. A., T. J. Gillespie, et al. (2001). "Peptide drug modifications to enhance bioavailability and blood-brain barrier permeability." *Peptides* **22**(12): 2329-43.
- Witt, K. A., J. D. Huber, et al. (2002). "Pluronic p85 block copolymer enhances opioid peptide analgesia." *J Pharmacol Exp Ther* **303**(2): 760-7.
- Witt, K. A., J. D. Huber, et al. (2001). "Pharmacodynamic and pharmacokinetic characterization of poly(ethylene glycol) conjugation to met-enkephalin analog [D-Pen2, D-Pen5]-enkephalin (DPDPE)." *J Pharmacol Exp Ther* **298**(2): 848-56.
- Witt, K. A., C. A. Slate, et al. (2000). "Assessment of stereoselectivity of trimethylphenylalanine analogues of delta-opioid [D-Pen(2),D-Pen(5)]-enkephalin." *J Neurochem* **75**(1): 424-35.
- Wolber, G., T. Seidel, et al. (2008). "Molecule-pharmacophore superpositioning and pattern matching in computational drug design." *Drug Discov Today* **13**(1-2): 23-9.
- Wolburg, H., K. Wolburg-Buchholz, et al. (2001). "Claudin-1, claudin-2 and claudin-11 are present in tight junctions of choroid plexus epithelium of the

- mouse." *Neurosci Lett* **307**(2): 77-80.
- Wong, V. and B. M. Gumbiner (1997). "A synthetic peptide corresponding to the extracellular domain of occludin perturbs the tight junction permeability barrier." *J Cell Biol* **136**(2): 399-409.
- Woodcock, D. M., M. E. Linsenmeyer, et al. (1992). "Reversal of multidrug resistance by surfactants." *Br J Cancer* **66**(1): 62-8.
- Woodley, J. F. (1994). "Enzymatic barriers for GI peptide and protein delivery." *Crit Rev Ther Drug Carrier Syst* **11**(2-3): 61-95.
- Wu, Q., K. Hultenby, et al. (2005). "Tissue levels of leu-enkephalin in rats with adjuvant arthritis." *J Neuroimmunol* **158**(1-2): 34-9.
- Wu, Y., W. Yang, et al. (2005). "Chitosan nanoparticles as a novel delivery system for ammonium glycyrrhizinate." *Int J Pharm* **295**(1-2): 235-45.
- Wu, Z. H., Q. N. Ping, et al. (2004). "Hypoglycemic efficacy of chitosan-coated insulin liposomes after oral administration in mice." *Acta Pharmacol Sin* **25**(7): 966-72.
- Wyatt (1998). *ASTRA for Windows User's Guide for the DAWN DSP and miniDAWN Light Scattering Instruments Version 4.70*. Santa Barbara, US, Wyatt Technology Corporation
- Wyatt. (1999, 15th June 1999). "Light Scattering for the Masses: Dn/dc with an Optilab." Retrieved 24th November, 2008.
- Xing, L., C. Dawei, et al. (2003). "Oral colon-specific drug delivery for bee venom peptide: development of a coated calcium alginate gel beads-entrapped liposome." *J Control Release* **93**(3): 293-300.
- Yamabe, K., Y. Kato, et al. (2003). "Potentiality of double liposomes containing salmon calcitonin as an oral dosage form." *J Control Release* **89**(3): 429-36.
- Yamamoto, A. (1998). "[Improvement of intestinal absorption of peptide and protein drugs by chemical modification with fatty acids]." *Nippon Rinsho* **56**(3): 601-7.
- Yenice, I., M. C. Mocan, et al. (2008). "Hyaluronic acid coated poly-epsilon-caprolactone nanospheres deliver high concentrations of cyclosporine A into the cornea." *Exp Eye Res* **87**(3): 162-7.
- Yeung, D. T., D. Josse, et al. (2004). "Structure/function analyses of human serum paraoxonase (HuPON1) mutants designed from a DFPase-like homology model." *Biochim Biophys Acta* **1702**(1): 67-77.
- Yokohama, S., K. Yamashita, et al. (1984). "Absorption of thyrotropin-releasing hormone after oral administration of TRH tartrate monohydrate in the rat, dog and human." *J Pharmacobiodyn* **7**(2): 101-11.
- Yoshioka, M., R. H. Erickson, et al. (1987). "Role of rat intestinal brush-border membrane angiotensin-converting enzyme in dietary protein digestion." *Am J Physiol* **253**(6 Pt 1): G781-6.
- Young, A. A. and N. J. Dawson (1982). "Evidence for on-off control of heat dissipation from the tail of the rat." *Can J Physiol Pharmacol* **60**(3): 392-8.
- Yu, J., E. R. Butelman, et al. (1997). "Dynorphin A (1-8) analog, E-2078, crosses the blood-brain barrier in rhesus monkeys." *J Pharmacol Exp Ther* **282**(2): 633-8.
- Zenker, D., D. Begley, et al. (2003). "Human blood-derived macrophages enhance barrier function of cultured primary bovine and human brain capillary endothelial cells." *J Physiol* **551**(Pt 3): 1023-32.
- Zervas, L., D. Borovas, et al. (1963). "New Methods in Peptide Synthesis. I. Tritylsulfonyl and o-Nitrophenylsulfonyl Groups as N-Protecting Groups1,2." *J Am Chem Soc* **85**: 3660.

- Zhang, X., A. A. Chentoufi, et al. (2009). "A genital tract peptide epitope vaccine targeting TLR-2 efficiently induces local and systemic CD8⁺ T cells and protects against herpes simplex virus type 2 challenge." Mucosal Immunol 2(2): 129-43.
- Zimmermann, M. (1986). Behavioural investigations of pain in animals. Assessing Pain in Farm Animals. I. J. H. Duncan and Y. Molony. Bruxelles, Office for Official Publications of the European Communities: 16-29.
- Ziv, E., O. Lior, et al. (1987). "Absorption of protein via the intestinal wall. A quantitative model." Biochem Pharmacol 36(7): 1035-9.
- Zlokovic, B. V. (2004). "Clearing amyloid through the blood-brain barrier." J Neurochem 89(4): 807-11.
- Zlokovic, B. V., D. J. Begley, et al. (1986). "Measurement of solute transport across the blood-brain barrier in the perfused guinea pig brain: method and application to N-methyl-alpha-aminoisobutyric acid." J Neurochem 46(5): 1444-51.
- Zlokovic, B. V., M. N. Lipovac, et al. (1987). "Transport of leucine-enkephalin across the blood-brain barrier in the perfused guinea pig brain." J Neurochem 49(1): 310-5.
- Zlokovic, B. V., J. B. Mackic, et al. (1989). "Kinetic analysis of leucine-enkephalin cellular uptake at the luminal side of the blood-brain barrier of an in situ perfused guinea-pig brain." J Neurochem 53(5): 1333-40.
- Zlokovic, B. V., M. B. Segal, et al. (1988). "Unidirectional uptake of enkephalins at the blood-tissue interface of the blood-cerebrospinal fluid barrier: a saturable mechanism." Regul Pept 20(1): 33-44.